NEURAL CONTROL OF ENERGY HOMEOSTASIS AND ENERGY HOMEOSTASIS REGULATION OF BRAIN FUNCTION

EDITED BY: Lionel Carneiro, Virginie Aubert and Claude Knauf
PUBLISHED IN: Frontiers in Neuroscience

frontiers Research Topics

frontiers

ISSN 1664-8714
ISBN 978-2-88976-003-9
DOI 10.3389/978-2-88976-003-9

About Frontiers

Frontiers is more than just an open-access publisher of scholarly articles: it is a pioneering approach to the world of academia, radically improving the way scholarly research is managed. The grand vision of Frontiers is a world where all people have an equal opportunity to seek, share and generate knowledge. Frontiers provides immediate and permanent online open access to all its publications, but this alone is not enough to realize our grand goals.

Frontiers Journal Series

The Frontiers Journal Series is a multi-tier and interdisciplinary set of open-access, online journals, promising a paradigm shift from the current review, selection and dissemination processes in academic publishing. All Frontiers journals are driven by researchers for researchers; therefore, they constitute a service to the scholarly community. At the same time, the Frontiers Journal Series operates on a revolutionary invention, the tiered publishing system, initially addressing specific communities of scholars, and gradually climbing up to broader public understanding, thus serving the interests of the lay society, too.

Dedication to Quality

Each Frontiers article is a landmark of the highest quality, thanks to genuinely collaborative interactions between authors and review editors, who include some of the world's best academicians. Research must be certified by peers before entering a stream of knowledge that may eventually reach the public - and shape society; therefore, Frontiers only applies the most rigorous and unbiased reviews.
Frontiers revolutionizes research publishing by freely delivering the most outstanding research, evaluated with no bias from both the academic and social point of view. By applying the most advanced information technologies, Frontiers is catapulting scholarly publishing into a new generation.

What are Frontiers Research Topics?

Frontiers Research Topics are very popular trademarks of the Frontiers Journals Series: they are collections of at least ten articles, all centered on a particular subject. With their unique mix of varied contributions from Original Research to Review Articles, Frontiers Research Topics unify the most influential researchers, the latest key findings and historical advances in a hot research area! Find out more on how to host your own Frontiers Research Topic or contribute to one as an author by contacting the Frontiers Editorial Office: frontiersin.org/about/contact

NEURAL CONTROL OF ENERGY HOMEOSTASIS AND ENERGY HOMEOSTASIS REGULATION OF BRAIN FUNCTION

Topic Editors:
Lionel Carneiro, The Ohio State University, United States
Virginie Aubert, Loyola University Chicago, United States
Claude Knauf, Université Toulouse III Paul Sabatier, France

Citation: Carneiro, L., Aubert, V., Knauf, C., eds. (2022). Neural Control of Energy Homeostasis and Energy Homeostasis Regulation of Brain Function. Lausanne: Frontiers Media SA. doi: 10.3389/978-2-88976-003-9

Table of Contents

frontiers | Frontiers in Neuroscience

EDITORIAL
published: 01 April 2022
doi: 10.3389/fnins.2022.872296

Editorial: Neural Control of Energy Homeostasis and Energy Homeostasis Regulation of Brain Function

Lionel Carneiro[1]*, *Claude Knauf*[2,3] and *Virginie Mansuy-Aubert*[4]

[1] Department of Biological Chemistry and Pharmacology, Ohio State University, Columbus, OH, United States, [2] Université Paul Sabatier, Toulouse III, INSERM U1220, Institut de Recherche en Santé Digestive (IRSD), CHU Purpan, Toulouse, France, [3] International Research Project (IRP), European Lab "NeuroMicrobiota", Toulouse, France, [4] Department of Cell and Molecular Physiology, Stritch School of Medicine, Loyola University Chicago, Maywood, IL, United States

Keywords: obesity, diabetes, neurological disorders, nutrition, gut brain axis

Editorial on the Research Topic

Neural Control of Energy Homeostasis and Energy Homeostasis Regulation of Brain Function

In recent years, research related to metabolic disorders has led to numerous discoveries linking metabolic control, and age-related diseases including cognitive deficiencies. It is now established that glucose homeostasis dysregulations are risk factors for dementia, but also Alzheimer and Parkinson's diseases or even mood disorders. Thus, nutritional approaches have been proven successful on cognitive improvement in people with neurological disorders (Carneiro and Pellerin). Altogether, these observations indicate that energy homeostasis regulation is of great importance for normal brain function. Consequently, recent attention has grown in order to decipher the mechanisms lying beneath the interplay between metabolism and brain activity. For instance, a stress response involves a regulatory loop from brain to periphery that involves the hypothalamus. Interestingly, the hypothalamus is well known for its contribution to metabolic regulations such as body weight or blood glucose among others. Blood glucose is an internal parameter described as affected by stress hormones such as cortisol. Thus, the development of a new system able to regulate energy levels in hypercortisolism represents a significant advance in the management of disorders such as Cushing's disease. Hence helping to improve brain activity by lowering specific symptoms such as fatigue and disturbed sleep (Fekri Azgomi et al.).

In accordance with a brain function dependence on energetic status, Das et al. demonstrate an interplay between brain energy metabolism and cognitive dysfunction in Alzheimer's disease (AD). In their article, the authors developed a highly sensitive system to measure brain energy metabolism in early stages of AD. Such tool would be of help for an early diagnosis of the disease. Moreover, it could contribute to a better management of AD as well. In addition, their work supports a key role of brain energy metabolism on AD, and hence, supports a role for the energy balance in neurological disorders (Das et al.). In this regard, a key role of nutrient sensing in brain function in addition to energy homeostasis would not be surprising. Accordingly, the results provided by Garcia et al.,

OPEN ACCESS

Edited and reviewed by:
Gilles Mithieux,
Centre National de la Recherche Scientifique (CNRS), France

***Correspondence:**
Lionel Carneiro
lionel.carneiro@inserm.fr

Specialty section:
This article was submitted to Neuroenergetics, Nutrition and Brain Health, a section of the journal Frontiers in Neuroscience

Received: *09 February 2022*
Accepted: *03 March 2022*
Published: *01 April 2022*

Citation:
Carneiro L, Knauf C and Mansuy-Aubert V (2022) Editorial: Neural Control of Energy Homeostasis and Energy Homeostasis Regulation of Brain Function. Front. Neurosci. 16:872296. doi: 10.3389/fnins.2022.872296

studying the cell types involved in the palatability of food are of great interest. Indeed, the authors demonstrate the role of GABAergic neurons of the lateral hypothalamic area on the coding of palatability. In fact, the results provided indicate that these GABAergic neurons display activity changes in response to differences in palatability. Furthermore, the activation of these neurons stimulates food intake of food with the highest palatability (Garcia et al.). The results presented by Garcia et al., also highlight the importance of hedonism on food ingestion. By so, this study supports the role of a psychological aspect on brain control of metabolism. This role is further described in the innovative view of the phantom limbs experience applied to people following a bariatric surgery (Gautron). In his article Gautron describes how subjects undergoing a bypass surgery still experience satiation while the surgery is associated with a complete denervation. Indeed, the stimulation of mechanoreceptors of the stomach are necessary to induce satiation. Therefore, Gautron present a new hypothesis on changes in nerve distribution to preserve the satiation response. Although still hypothetic, this review supports the existence of a complex interplay between biological, bioenergetics and psychological aspects in metabolic regulations. In fact, data obtained from bariatric surgery have highlighted the key role of gut-brain axis in physiology. The gut is the first organ to sense nutrients and thus, is the first organ involved in metabolic control. The development of gut-brain axis research has also contributed to a better understanding of the link between brain function and energy homeostasis. Indeed, in addition to the nervous connections between the gut and the brain (An et al.), it is now established that products of gut metabolism are also linked with brain activity. Among these signals, SCFA and ketone bodies are the most studied. However, many other could be also involved.

Interestingly, this close relationship between brain function and energy homeostasis partly accounts for the increased risk of neurological disorders in diabetic people. On the other hand, Niu et al., present data showing behavioral side effects of the use of oxytocin for body weight management. Hence, it appears important to pursue research efforts to better understand the mechanisms involved in the relationship between cognition and metabolism. A better knowledge of this relationship would be important to address the side effects in the current therapies used. In fact, this dual effect of oxytocin in weight management and prosocial behavior could represent a promising research track for both metabolic and cognitive research fields.

The link between brain function and energy homeostasis regulating circuits within the brain is assessed in the study of Li et al. In their study the authors describe a link between binge eating and stress response. In fact, the authors showed that the reward system in BEPs rats overcame the homeostasis and stress response systems. This work supports an interplay between, stress, reward and energy homeostasis regulation. Moreover, it appears that those systems are capable of regulating each other (Li et al.). In accordance with that, the work of Perissinotti et al. showing the involvement of TRPC channel on the POMC expressing neurons depolarization supports the need to dig deeper on the neural control of metabolism. This study first demonstrates that TRPC alone can induce a POMC expressing neurons excitability. Furthermore, they also report the role of t-type channels in such POMC neurons excitability. Altogether their work brings up a putatively new protein involved in obesity development including t-type channels and KLHL1. Both proteins participate in the sensitivity to leptin of POMC expressing neurons. Thus, although POMC neurons have been identified decades ago, Perissinotti et al., studies indicate that the complete understanding of the function of these neurons are far to be completely elucidated (Perissinotti, Martínez-Hernández, and Piedras-Rentería; Perissinotti, Martínez-Hernández, He, et al.). Furthermore, the study of early developmental organization of neural circuits should also help understand the complexes interplay between different brain regions and brain functions. Thus, Lanzillo et al. provide interesting data describing the ontogeny of the BNST projections to the hypothalamus. Such work highlights the early link between stress response systems and metabolic control ones. Since the BNST is well known for mechanisms disturbed in psychiatric disorders, this suggests a putative early link between metabolism and brain disorders (Lanzillo et al.).

Altogether, these recent researches highlight the numerous gaps still existing on the understanding of neural control of energy homeostasis. Therefore, more research is needed to completely decipher the mechanisms at play. In this aspect, studies on models such as fish could help identify new mechanisms involved in metabolic control and brain function (Soengas). Eventually, one could expect to better apprehend the link between metabolism and neurological function.

Overall, the publications presented in this Research Topic support a link between brain control of energy homeostasis and brain activity. It also shows that despite extensive work made in recent years, several mechanisms are yet to be discovered. In particular, the mechanisms linking energy homeostasis and brain function are far to be clearly identified. In fact, a large number of studies indicate a clear relationship between neuronal disorders and metabolism. Therefore, metabolic studies aiming at addressing the impact on brain disorders as well as studies looking at brain disorders impact on metabolic control are still needed. Finally, such researches could help to better treat both metabolic and neuronal disorders.

AUTHOR CONTRIBUTIONS

All authors listed have made a substantial, direct, and intellectual contribution to the work and approved it for publication.

ACKNOWLEDGMENTS

We are thankful to all the authors of the articles published in this Research Topic for their contributions and the reviewers for their rigorous evaluations. We also thank the Editorial Board of the Frontiers Journals for their support.

Conflict of Interest: The authors declare that the research was conducted in the absence of any commercial or financial relationships that could be construed as a potential conflict of interest.

Publisher's Note: All claims expressed in this article are solely those of the authors and do not necessarily represent those of their affiliated organizations, or those of the publisher, the editors and the reviewers. Any product that may be evaluated in this article, or claim that may be made by its manufacturer, is not guaranteed or endorsed by the publisher.

frontiers in Neuroscience

ORIGINAL RESEARCH
published: 21 January 2021
doi: 10.3389/fnins.2020.608047

Lateral Hypothalamic GABAergic Neurons Encode and Potentiate Sucrose's Palatability

*Aketzali Garcia, Alam Coss, Jorge Luis-Islas, Liliana Puron-Sierra, Monica Luna, Miguel Villavicencio and Ranier Gutierrez**

Laboratory of Neurobiology of Appetite, Department of Pharmacology, CINVESTAV, Mexico City, Mexico

Sucrose is attractive to most species in the animal kingdom, not only because it induces a sweet taste sensation but also for its positive palatability (i.e., oromotor responses elicited by increasing sucrose concentrations). Although palatability is such an important sensory attribute, it is currently unknown which cell types encode and modulate sucrose's palatability. Studies in mice have shown that activation of GABAergic LHA^{Vgat+} neurons evokes voracious eating; however, it is not known whether these neurons would be driving consumption by increasing palatability. Using optrode recordings, we measured sucrose's palatability while VGAT-ChR2 transgenic mice performed a brief access sucrose test. We found that a subpopulation of LHA^{Vgat+} neurons encodes palatability by increasing (or decreasing) their activity as a function of the increment in licking responses evoked by sucrose concentrations. Optogenetic gain of function experiments, where mice were able to choose among available water, 3% and 18% sucrose solutions, uncovered that opto-stimulation of LHA^{Vgat+} neurons consistently promoted higher intake of the most palatable stimulus (18% sucrose). In contrast, if they self-stimulated near the less palatable stimulus, some VGAT-ChR2 mice preferred water over 18% sucrose. Unexpectedly, activation of LHA^{Vgat+} neurons increased quinine intake but only during water deprivation, since in sated animals, they failed to promote quinine intake or tolerate an aversive stimulus. Conversely, these neurons promoted overconsumption of sucrose when it was the nearest stimulus. Also, experiments with solid foods further confirmed that these neurons increased food interaction time with the most palatable food available. We conclude that LHA^{Vgat+} neurons increase the drive to consume, but it is potentiated by the palatability and proximity of the tastant.

Keywords: LHA GABA neurons, feeding circuit, palatability, sucrose, taste

OPEN ACCESS

Edited by:
Lionel Carneiro, The Ohio State University, United States

Reviewed by:
Chad L. Samuelsen, University of Louisville, United States
Patricia M. Di Lorenzo, Binghamton University, United States

****Correspondence:***
Ranier Gutierrez
ranier@cinvestav.mx
orcid.org/0000-0002-9688-0289

Specialty section:
This article was submitted to Neuroenergetics, Nutrition and Brain Health, a section of the journal Frontiers in Neuroscience

Received: *18 September 2020*
Accepted: *02 December 2020*
Published: *21 January 2021*

Citation:
Garcia A, Coss A, Luis-Islas J, Puron-Sierra L, Luna M, Villavicencio M and Gutierrez R (2021) Lateral Hypothalamic GABAergic Neurons Encode and Potentiate Sucrose's Palatability. Front. Neurosci. 14:608047. doi: 10.3389/fnins.2020.608047

INTRODUCTION

The lateral hypothalamic area (LHA) has been regarded as the "feeding center" since its lesion results in hypophagia and subsequent death (Anand and Brobeck, 1951; Teitelbaum and Epstein, 1962). It is part of a neural circuit related to feeding and reward (Delgado and Anand, 1953; Olds and Milner, 1954) as rats are willing to press a lever to deliver electrical intracranial self-stimulation (ICSs), and if food is available, it also promotes feeding (Delgado and Anand, 1953; Mendelson, 1967; Mogenson and Stevenson, 1967; Coons and Cruce, 1968). Moreover, if a sweet tastant is

available, the rate of electrical ICSs is further increased, whereas bitter compounds decreased them (Phillips and Mogenson, 1968; Poschel, 1968), suggesting an interaction between ICSs and taste palatability. In this regard, and because of its connections with different cortical and subcortical gustatory regions (Simerly, 2004; Berthoud and Münzberg, 2011), the LHA is anatomically located to receive, process, and broadcast taste palatability information (Ferssiwi et al., 1987; Berridge and Valenstein, 1991). Pioneering electrophysiological studies have recorded gustatory-evoked responses in the LHA (Schwartzbaum, 1988; Yamamoto et al., 1989). One recent and elegant study uncovered two functional populations of LHA neurons: one activated by palatable tastants, e.g., sucrose, and another by aversive tastants, like quinine (Li et al., 2013). However, the genetic identity of the LHA cell type(s) involved in processing palatability-related information remains elusive, and to unveil their identity is the goal of this study.

The LHA is currently viewed as a hub of various cell types (Stuber and Wise, 2016), grossly divided into two larger populations related to feeding: the glutamatergic ($LHA^{Vglut2+}$) and GABAergic (LHA^{Vgat+}) neurons (Gutierrez et al., 2020). Activation of $LHA^{Vglut2+}$ neurons leads to reduced food intake and is aversive (Jennings et al., 2013). In contrast, stimulation of LHA^{Vgat+} neurons is rewarding and produces voracious eating of both foods with nutritional value (Jennings et al., 2015; Navarro et al., 2016) and those without calories, even gnawing behavior toward the cork, an irrelevant biological stimulus (Navarro et al., 2016). Moreover, LHA^{Vgat+} neurons enhance the salience of the nearest stimulus and induce reward via stimulation of their projections to the ventral tegmental area (VTA) (Nieh et al., 2016). In addition, the evoked feeding is mediated by modulation of terminals reaching a region adjacent to the locus coeruleus (Marino et al., 2020). On the contrary, inhibition of GABAergic LHA^{Vgat+} cell somas is aversive and stops feeding (Jennings et al., 2015; Navarro et al., 2016). However, the role of LHA^{Vgat+} neurons in processing sucrose's palatability remains to be determined.

This study identified a new role of LHA^{Vgat+} neurons in encoding and enhancing sucrose's oromotor palatability responses. Sucrose's palatability was defined as the enhancement of hedonically positive oromotor responses triggered by increasing sucrose concentrations (Berridge and Grill, 1983; Spector et al., 1998; Villavicencio et al., 2018). Specifically, oromotor responses include an increase in lick rate and bout size. Thus, it should not be confused with a conscious hedonic feeling of pleasant taste that humans experience (Grill and Berridge, 1985; Sclafani, 1991; Berridge and Kringelbach, 2008). We found that opto-stimulation of LHA GABAergic neurons increases the consumption of the most palatable and proximal tastant. They accomplish this by potentiating the palatability of nearby gustatory stimuli. For aversive stimuli, the effect of these neurons is different. In a single bottle test, we found that water deprivation increased the tolerance for bitter compounds and gated a window of opportunity where the activation of GABAergic neurons is sufficient to temporarily reassign the negative hedonic value of quinine and promote its intake. Nevertheless, in a three-option preference test, mice failed to develop a quinine preference when sucrose was available under these neurons' activation, thus, demonstrating that activation of GABAergic neurons does not merely trigger indiscriminate oromotor tongue movements; rather, the animals' evoked consummatory behavior largely depends on their internal state and on the palatability of the stimulus. Moreover, optogenetic activation of LHA^{Vgat+} neurons evoked many hallmark behaviors resembling those seen in LHA electrical stimulation. In this regard, and consistent with their positive role in palatability, our results could indirectly explain why electrical ICSs are further facilitated by the presence of sweet solutions (Phillips and Mogenson, 1968; Poschel, 1968). We also found that LHA^{Vgat+} neurons are the common neural substrate for both reward and feeding since after repeated self-stimulation, the more the VGAT-ChR2 mice opto-self-stimulated, the stronger the laser-induced licking they exhibited. We conclude that a subpopulation of GABAergic LHA^{Vgat+} neurons combines stimulus proximity and palatability-related information to enhance nearby energy-rich foods' palatability and further increase consummatory behaviors.

MATERIALS AND METHODS

Animal Subjects

We used 42 VGAT-ChR2-EYFP mice (number ID 014548; Jackson Laboratory, Sacramento, CA, USA) and 25 wild-type (WT) littermates, which served as controls. Mice were from both sexes between 8 and 16 weeks old, and they were individually housed in their home cages and maintained in a temperature-controlled ($22 \pm 1^{\circ}C$) room with 12:12 h light–dark cycle. Unless otherwise mentioned, chow food (PicoLab Rodent Diet 20, MO, USA) and water were available *ad libitum*. For experiments with water restriction, after each behavioral session, mice were allowed to drink water for 1 h daily. All procedures were performed with the approval of the CINVESTAV Animal Care and Use Committee. One session per day was conducted between 11:00 a.m. and 2:00 p.m.

Surgical Procedures

All mice were anesthetized with ketamine (100 mg/kg, i.p.) and xylazine (8 mg/kg, i.p.), and then placed into a stereotaxic apparatus (Stoelting, IL, USA). Lidocaine (0.05 ml) was administered subcutaneously under the head's skin as a local analgesic, and ophthalmic ointment (hydrocortisone, neomycin, and polymyxin-B) was applied periodically to maintain eye lubrication. The antibiotic enrofloxacin (0.4 ml/kg) was injected for 3 days after surgery.

For experiments with opto-stimulation of LHA^{Vgat+} cell somas, a single multimode optical fiber with a 200-μm core diameter and with 0.39 NA (FT200UMT; Thorlabs, NJ, USA) was implanted unilaterally targeting the LHA using the following coordinates: AP: −1.25 mm, ML: ±1 mm, DV: −4.9 mm, from bregma. For electrophysiology recordings, a custom-made optrode was unilaterally implanted counterbalanced across hemispheres (AP: −1.25 mm, ML: ±1 mm, from bregma; DV: −5.2 mm ventral to dura). The optrode comprises an array of 16 tungsten wires formvar coated (35 μm diameter) surrounding and protruding 1 mm from the single multimode optical fiber

tip. No significant differences were found between hemispheres, so data were pooled together (data not shown). All experiments began 7 days after surgery to allow recovery.

Histology and Immunofluorescence

Mice were sacrificed by an overdose of pentobarbital (150 mg/kg) and perfused with PBS, followed by 4% paraformaldehyde. Brains were fixed overnight in 4% paraformaldehyde and gradually replaced in a gradient of concentrations of sucrose (until 30%). For histology, brain slides (40 μm) were cut with a cryostat (Thermo Scientific HM525 NX), and images were taken with a Nikon Eclipse E200 microscope and a Progress Gryphax microscope camera, using a 10× objective. For immunofluorescence, free-floating brain slides (40 μm) were blocked with 1% BSA and 0.2% Triton in PBS for 30 min. They were then washed with 0.2% Triton in PBS three times every 10 min, followed by incubation with the following primary antibodies: mouse anti-GAD 67 primary antibody (Millipore, Mab5406, 1:1,000 dilution), and rabbit anti-GFP primary antibody (Invitrogen, A11122, 1:1,000 dilution). Incubation took place overnight at 4°C. The next day, brain slides were washed with 0.2% Triton in PBS three times every 10 min, and then incubated with the secondary antibodies Alexa 647 goat anti-mouse (Invitrogen, A21235, 1:500 dilution), and Alexa 488 donkey anti-rabbit (Invitrogen, A21206, 1:500 dilution) during 90 min at room temperature. Afterward, we applied DAPI to stain the nuclei. Brain slides were put on slides with a mounting medium for fluorescence (Vectashield), and images were taken with a Leica confocal microscope using a 63× objective.

Gustatory Stimuli

Sucrose of reagent-grade chemical quality (Sigma-Aldrich, Mexico City, Mexico) was used in the following concentrations: 0 (water only), 3, 10, and 18 wt%. Reagent-grade quinine hydrochloride dihydrate (QHCl) was also used at 0.04 wt% (Sigma-Aldrich, Mexico City, Mexico). Artificial saliva contained the following (in mM): 4 NaCl, 10 KCl, 6 $NaHCO_3$, 6 $KHCO_3$, 0.5 $CaCl_2$, 0.5 $MgCl_2$, 0.24 K_2HPO_4, and 0.24 KH_2PO_4 (Zocchi et al., 2017). We added 0.05 mM HCl to adjust pH to 7. The solutions were dissolved in distilled water, maintained under refrigeration, and used at room temperature. We also used 20 mg chocolate pellets (Bio-Serv, NJ, USA), chow food (PicoLab Rodent Diet 20, MO, USA), a high-fat diet with 45% kcal% fat (Research Diets, NJ, USA), granulated sugar cube, and cork.

Electrophysiology

Neural activity was recorded using a Multichannel Acquisition Processor System (Plexon, Dallas TX, USA) interfaced with Med Associates to simultaneously record behavioral events (Gutierrez et al., 2010). Extracellular voltage signals were first amplified by an analog head-stage (Plexon, HST/16o25-GEN2-18P-2GP-G1), then amplified and sampled at 40 kHz. Raw signals were band-pass filtered from 154 Hz to 8.8 kHz and digitalized at 12 bits resolution. Only single neurons with action potentials with a signal to noise ratio of 3:1 were analyzed (Gutierrez et al., 2010). Action potentials were isolated online using a voltage–time threshold window, and three principal components contour templates algorithm. Furthermore, off-line spike sorting was performed (Plexon Offline Sorter), and only single units with stable waveforms across the session were included in the analyses (Gutierrez et al., 2010) (see **Supplementary Figure 1**). Also, to verify waveform stability, we correlated the waveform's shapes recorded in the brief access test and the optotagging session.

Optogenetic Stimulation

A 473-nm laser intensity was modulated by a DPSS system (OEM laser, UT, USA). Laser pulses were synchronized with behavioral events with Med Associates Inc. software and TTL signal generator (Med Associates Inc., VT, USA). The patch cord's optical power was at 15 mW, and it was measured with an optical power meter (PM20A, Thorlabs, NJ, USA). However, we delivered between 10 and 12.6 mW at the fiber optic tip, depending on each fiber's efficiency. Unless otherwise mentioned, the laser was turned on by 2 s (at 50 Hz) and 4 s off, with 10 ms pulse width and a duty cycle of 50%.

Parameters of Stimulation for LHA GABAergic Neurons

To explore the best stimulation parameters for LHA GABAergic neurons, mice were implanted with an optrode in LHA and placed in a custom-made box with dimensions of 18 × 13 × 7.5 cm. With no food available, the laser was turned on at different frequencies—0, 2.5, 5, 10, 20, and 50 Hz semirandomly, while the animals' neural activity was recorded for 20 min. We used a Kruskal–Wallis test to compare firing rates during the baseline (from −1 to −0.04 s) against the activity during laser presentation (from 0 to 2 s) aligned (time = 0 s) to laser onset for all frequencies tested. Neurons that significantly increased their firing rate during the laser stimulation were named "activated," and neurons that decreased their activity were named "inhibited."

Neural Activity Recording During a Brief Access Test and Palatability-Related Responses

We used a brief access test in water-deprived mice while the LHA activity was recorded for 30 min. We employed a licking spout consisting of independent stainless-steel needles (20-gauge) cemented together with dental acrylic at the sipper tube's tip (Villavicencio et al., 2018). Each needle was connected to a solenoid valve (Parker, Ohio, USA) by a silicon tube. The drop (∼2 μl) was calibrated before starting the session, using a pressurized control system. The trial structure was as follows: At the beginning of the task, the sipper was extended in lick position. To start a new trial, each mouse was required to introduce its head into the central port and then elicited a dry lick to start the reward epoch (7 s). During this period, a tastant's drop was delivered every lick. The sipper was retracted for 3 s as intertrial interval (ITI), and then re-extended in a lick position into the central port. Tastant solutions (artificial saliva, water, sucrose 3%, and sucrose 18%) were delivered in a semirandom order.

To identify neurons whose firing rate correlated with palatability-induced oromotor responses, we used a best-window analysis based on a previous study (Villavicencio et al., 2018).

This method has been used to detect palatability-related activity in a brief access test. Briefly, during each recording session, a palatability index (PI) was calculated. The PI reflects the overall appetitive oromotor responses elicited by each tastant delivered in the session. It was computed by averaging the lick rate during the entire reward epoch, including all the trials per session. In mice, the PI takes values between 0 and 8 Hz for sucrose stimuli (Glendinning et al., 2005): 0 Hz means animals ultimately rejected a solution in all trials, whereas 8 Hz indicates they licked continuously during the entire reward epoch, thus reflecting a greater palatability response elicited by the tastant. Then, the firing rate was calculated for a variety of time centers (from 0.25 to 6.75 s with 0.5 s steps) and multiple window sizes (from 0.5 to 7 s, 0.5 s steps), such that each window was estimated as the center $\pm$ (window size/2). We identified the windows where the mean firing rate was significantly different for at least one tastant delivered (i.e., tastants, using a Kruskal–Wallis test at an alpha of 0.05). Next, we computed Pearson's correlation coefficient (r; the alpha level at 0.05) between both the PI and the firing rate on a trial-by-trial basis. The window with the largest absolute Pearson's correlation coefficient was selected as the "best window." Thus, for the "best window" and each statistical test (i.e., Kruskal–Wallis test and Pearson's correlation coefficient), a permutation assay was used for multiple-testing correction. This analysis was accomplished by shuffling the different tastants delivered 20,000 times (using the Matlab function "shuffle"). A corrected p-value was obtained using the following formula $p = (k + 1)/(n + 1)$, where k is when a permuted distribution leads to a p-value smaller than the original p-value and n is the number of repetitions. Only time windows with $p < 0.05$ in both tests (Kruskal–Wallis and Pearson correlation) were considered statistically significant. Thus, the "best window" is where the firing rate maximally correlated with the oromotor responses (the lick rate) elicited by sucrose's palatability on a trial-by-trial basis. Importantly, results were qualitatively similar if we used the lick bout size rather than the lick rate to compute the PI. A lick bout was defined as the collection of at least two rhythmic licks separated by a pause $\geq$500 ms during the reward epoch. The bout size was the time difference (in seconds) between the last and first lick in the bout (Gutierrez et al., 2006).

To evaluate whether palatability-related neurons dynamically track the changes in lick rate across the session, we computed the lick rate in the reward epoch as a function of trial types [artificial saliva (AS), water, sucrose 3%, and sucrose 18%], divided into blocks of 10th percentile of trials each. We verified that every block across the session has the same number of trials.

Optotagging Task

Once the brief access test was finished, each mouse was tested in the optotagging task. For this task, we removed the licking spout from the behavioral box. Over the session (15 min), the laser was turned on (at 50 Hz) during 2 or 7 s, followed by 10 s off.

Laser-activated neurons (pLHA^{Vgat}) were detected by using two methods: 1) a Kruskal–Wallis to compare firing rates during a baseline (from -1 to -0.04 s) against the activity during the presentation of laser (from 0 to 2 s, aligned to laser onset) and 2) CUMSUM statistic (Gutierrez et al., 2006) to obtain the first bin (1 ms resolution) after the first laser pulse that significantly increased the firing rate above baseline (from -20 to 0 ms). Only neurons showing a significant value in both tests were considered laser-activated pLHA^{Vgat}. From the population of pLHA^{Vgat} neurons, we identified two types of populations: (1) ChR2-expressing cells LHA^{Vgat+} or early neurons: these neurons were those with an action potential evoked within $\leq$15 ms latency (Buonomano, 2003), measured by a CUMSUM statistic; and (2) laser-activated late neurons: these were those with an action potential occurring after >15 ms latency. Also, to classify non-LHA^{Vgat} neurons, we used the Kruskal–Wallis test as described above. Neurons with no significant modulation were classified as "unmodulated."

Open Loop Stimulation With One Option

The front panel of an operant conditioning chamber (Med Associates Inc., VT, USA) was equipped with a central port and a sipper, where individual licks were registered by a contact lickometer (Med Associates Inc., VT, USA). To determine the best stimulation parameters to induce feeding behavior, a group of naive mice had free access to sucrose 10% solution. For open loop stimulation, mice were opto-stimulated by alternating blocks of 5 min "off" and 5 min "on" across a 40-min session (Nieh et al., 2016). During opto-stimulated blocks, the laser was turned "on" regardless of the mice's behavior and spatial position in the chamber. A different opto-stimulation frequency (0, 2.5, 5, 10, 20, and 50 Hz) was delivered daily. The laser-bound feeding index was measured as the number of licks in a 2.5-s window from laser onset divided by the total licks in the session, hereafter named laser-bound feeding, and it was plotted as a function of laser frequency.

Prestimulation Task

A group of naive mice was placed in an operant conditioning chamber with a central port. A door blocked the access to the sipper during the first 15 min (prestimulation period). Each mouse was opto-stimulated with all prestimulation protocols (0, 5, 10, and 15 min) following a Latin square design. Then, the door was opened, and a 10% sucrose solution was available during the next 15 min. During the prestimulation period, the laser was turned on for 2 s and off for 4 s.

Open Loop Stimulation With Three Options

To determine whether opto-stimulation of LHA GABAergic neurons drives the intake with a bias toward the most palatable stimulus available, a new group of naive mice was tested in an open loop stimulation task (alternating 5 min no-laser and 5 min "on" (2 s on, 4 s off) blocks across a 40-min session). The operant chamber was equipped with three ports, where mice had free access to water (central sipper), a 3% sucrose solution (left sipper), and an 18% sucrose solution (right sipper). Lateral sippers were counterbalanced across animals. This task comprises four baseline sessions (with no photostimulation, data not shown), and 11 test sessions were pooled together. The number of licks given to the sipper filled with sucrose 18%, across the 11 sessions, was also plotted.

For this experiment, we video tracked the mouse's distance and head angle relative to each of the three sippers. The sippers' position and the animal's three anatomical points, the nose, the neck, and the tail's base, were extracted using the DeepLabCut Python package (Mathis et al., 2018; Nath et al., 2019). We define the mouse position as the coordinates (x and y) for the nose, whereas the head direction was a two-dimensional vector going from the neck to the nose. For each video frame, the distance to each sipper was calculated (in pixels), as well as the angle between the head direction and position of each sipper (in degrees). An angle of 0° means the mouse is looking at the sipper, and 180° means the mouse is facing the opposite direction. For distance measuring, 100 pixels correspond to ∼6 cm. The mouse position and direction were extracted from the train of the stimulation's first laser pulse, and the following 6-s window was analyzed to find out if the mice initiated a licking behavior at any of the three sippers. Then, we built a two-dimensional array containing the probability of licking any sipper given the mouse's distance and angle during the first laser of each opto-stimulation train.

Open Loop Stimulation in an Open Field With Chow, High-Fat Diet, or Granulated Sugar Cube

A new group of animals was placed in the circular arena's center (50 cm in diameter). Three or two food plates were equidistant to each other, and each contained either chow, high-fat diet, or granulated sugar cube. Mice were opto-stimulated by alternating 5 min block with no-laser and 5 min laser block across the session (20 min). In open loop, the laser was turned "on" regardless of the mice's behavior and spatial position in the arena. All sessions were recorded and analyzed with Bonsai software (https://open-ephys.org/bonsai). We calculated the mouse's centroid at each frame and used that information to create a heatmap of its position. The distance of the mouse's centroid from each stimulus was computed. A food interaction occurred when the distance was below 60 mm, and the animal stayed there for at least 1 s. Food plates were weighed at the beginning and end of each session.

Closed-Loop Stimulation With Three Options

To evaluate whether activation of LHA^{Vgat+} neurons induces preference for the most proximal stimulus, we used a closed-loop stimulation protocol (in the same mice from Open loop stimulation with three options), over 11 additional sessions (40 min each). As noted above, mice were placed in an operant conditioning chamber with three ports (water, central sipper; 3% sucrose solution, left sipper; 18% sucrose solution, right sipper). Photostimulation was delivered when the subject made a head entry in the central port (containing a sipper filled with water), laser was turned on by 2 s followed by a time out of 4 s (where the laser could not be reactivated), and after this, a new laser onset (2 s "on") occurred when mice performed a new head entry. Thus, in this experiment, the less palatable stimuli (water) was the nearest to opto-self-stimulation. During photostimulation, sucrose preference index was measured as the number of licks of 18% sucrose divided by the total licks for sucrose 18% + water. Values higher than 0.5 indicate sucrose preference.

To evaluate the laser-bound feeding development across the sessions, we correlated laser-bound feeding during open loop stimulation sessions vs. closed-loop stimulation for the first three and the last five sessions.

TABLE 1 | Protocol used for closed-loop stimulation with the central port stimulus replaced.

Stimuli in the central port	Sessions tested
Water	Last 5 sessions of the closed loop (**Figure 7**)
Extinction (no opto-stimulation)	4
Water	3
Empty sipper	3
Water	3
0.04% Quinine	4
Airpuff	4
Unavoidable airpuff	3
Sucrose 18% (water was placed in the sucrose 18% port)	4

Closed Loop in an Open Field

In a circular arena, four stimuli were located equidistant to each other: wood cork, chow, chocolate pellets, or a sipper filled with a 10% sucrose solution. During the session, a homemade computer vision program tracked in real-time the position of the subject. Each mouse needs to enter the designated area to receive opto-self-stimulation (2 s laser on and 4 s off). Mice need to leave and re-enter the designated area to begin a new trial. Only one designated area was used per session, and it remained in the same position for up to three or four consecutive sessions. Each session's duration was 40 min (mice were the same as those used in previous task).

Closed-Loop Stimulation With Different Options in the Central Port

For the same group of mice used in Closed-loop with three options, on subsequent days, the central port's stimulus was replaced across 28 sessions, following the protocols described in **Table 1**.

Closed-Loop Stimulation Task With One Option

Mice were put in a smaller and custom-made box with 18 × 13 × 7.5 cm internal dimensions. The front wall was equipped with one single sipper and a contact lickometer with a V shape to register individual licks. First, mice were tested, for 3 days, with a 0.04% quinine solution under sated state (fed mice) and then for three more days under a 23-h water-deprived condition, each session lasting 20 min. Then, mice were tested for 2 days with a sipper filled with 18% sucrose, in a sated state, and then two more days in a water-deprived condition. Opto-self-stimulation (2 s on with a time out of 4 s, where the laser could not be activated)

TABLE 2 | Protocol for opto-self-stimulation in a brief access test.

Laser on	Time on (2) (s)	No. of sessions (30 min each)
All trials	2	6
Water trials	2	3
Sucrose 3% trials	2	3
Sucrose 18% trials	2	3
All trials	7	4
Water trials	7	3
Sucrose 3% trials	7	3
Sucrose 18% trials	7	3
Mock laser (sucrose 3% trials)*	7	3

**For mock laser sessions, mice were connected to a false fiber optic, whereas the real laser was glued outside the skull to emit blue light.*

was delivered when mice made a head entry in the central port. Water-deprived mice had access to *ad libitum* water for 1 h after the session ended.

Opto-Self-Stimulation During a Brief Access Test

To evaluate whether activation of GABAergic neurons enhances oromotor palatability responses, we performed a brief access test with a new group of mice over 31 sessions. The behavioral setup conditions were the same as described above, and as tastant solutions, we used water, sucrose 3%, and sucrose 18% (delivered in a semirandom order). The trial structure was similar, but this time to start a new trial, each mouse was required to introduce its head into the central port to turn "on" the laser. Then, a dry lick was elicited to start the reward epoch (7 s). Each head entry triggers the laser onset for 2 s "on" (or in different sessions for 7 s "on"; see **Table 2**). At the end of the session, mice had access to *ad libitum* water for 1 h. Protocols are described in **Table 2**.

In addition, to verify that LHA GABAergic neurons were capable of sustained activation over 7 s of opto-stimulation, we plotted the peristimulus time histograms (PSTH) of pLHA^{Vgat}, non-LHA^{Vgat}, and unmodulated neurons using the same method previously described.

Data Analysis

All data analysis was performed using MATLAB (The MathWorks Inc., Natick, MA) and GraphPad Prism (La Jolla, CA, USA). We used the mean ± SEM and the α level at 0.05.

RESULTS

Initially, we determined the optimal stimulation parameters to activate LHA GABAergic neurons. This was accomplished by implanting an optrode in naive mice that constitutively expressed ChR2, fused with an enhanced yellow fluorescent protein (EYFP) in GABAergic neurons expressing the gene for the vesicular γ-aminobutyric acid transporter (hereafter referred to as VGAT-ChR2 mice) (Zhao et al., 2011; **Figures 1A,B**). We found that a laser stimulation of 50 Hz (10 ms width) evoked the strongest LHA neuronal responses (**Figures 1C–F**; Gigante et al., 2016). Unless otherwise mentioned, this frequency was used for all subsequent experiments.

LHA Neurons Encode Sucrose's Oromotor Palatability Responses

In rats, previous electrophysiological studies suggest that ensembles of LHA neurons process palatability-related information (Norgren, 1970; Schwartzbaum, 1988; Yamamoto et al., 1989; Li et al., 2013). Based on these results, we then asked whether LHA neurons could provide information about sucrose's palatability using a behavioral task with only palatable stimuli (i.e., AS, water, sucrose 3 wt%, and sucrose 18 wt%). To this end, taste responses were recorded from a total of 284 LHA neurons, while VGAT-ChR2 mice performed a brief access test (**Figure 2A**). To uncover palatability-responsive neurons, we analyzed neuronal activity using a previously described "best-window analysis" (Villavicencio et al., 2018) (see section Materials and Methods). This strategy detects the optimal interval, where the firing rate best correlates with the sucrose's PI computed as the average lick rate (or bout size), on a session-by-session basis, evoked by each gustatory stimulus in the reward epoch (**Figure 2B**; one-way ANOVA, $F_{(3,108)} = 10.35$, $p < 0.0001$; **Supplementary Figure 2A**; one-way ANOVA, $F_{(3,108)} = 2.926$, $p < 0.05$). **Figure 2C** depicts the responses of two representative LHA neurons: As expected, we found one whose activity increased as the sucrose concentration increased (positive Pearson's correlation, $r = 0.87$; **Figure 2C**, *left*), and the other was negatively associated with palatability oromotor responses evoked by sucrose ($r = -0.64$; **Figure 2C**, *right*). **Figure 2D** shows the normalized activity exhibiting either positive (59/284 neurons, 21%) or negative correlations (76/284, 27%) with the PI. Also, qualitatively similar results were found using the bout size to compute the PI (**Supplementary Figure 2B**). Thus, these data confirmed that the LHA mice's neurons exhibit palatability-related responses, and this activity can be either correlated or anticorrelated with the sucrose solution's PI.

Dynamic Tracking of Palatability Over the Entire Course of a Behavioral Session

Having demonstrated that LHA neurons encode sucrose's palatability-induced oromotor responses, we then explored whether LHA palatability-related neurons can dynamically adjust their responses to track the changes in sucrose's palatability across the session when the animals would approach satiation. We found that the lick rate declined across the session as a function of sucrose's palatability (**Figure 2E**; RM ANOVA, main effect of stimuli, $F_{(3,402)} = 163.7$, $p < 0.0001$; effect of time, $F_{(9,1206)} = 100.4$, $p < 0.0001$; and stimuli by time interaction, $F_{(27,3,618)} = 16.54$, $p < 0.0001$). Briefly, early in the session, animals licked more for all stimuli, but as the session progressed, the lick rate declined, especially for AS and water but not for sucrose (3 and 18%), indicating that they tracked palatability responses rather than satiety (**Figure 2E**). Similar to what we have shown in the nucleus accumbens shell (NAcSh) (Villavicencio

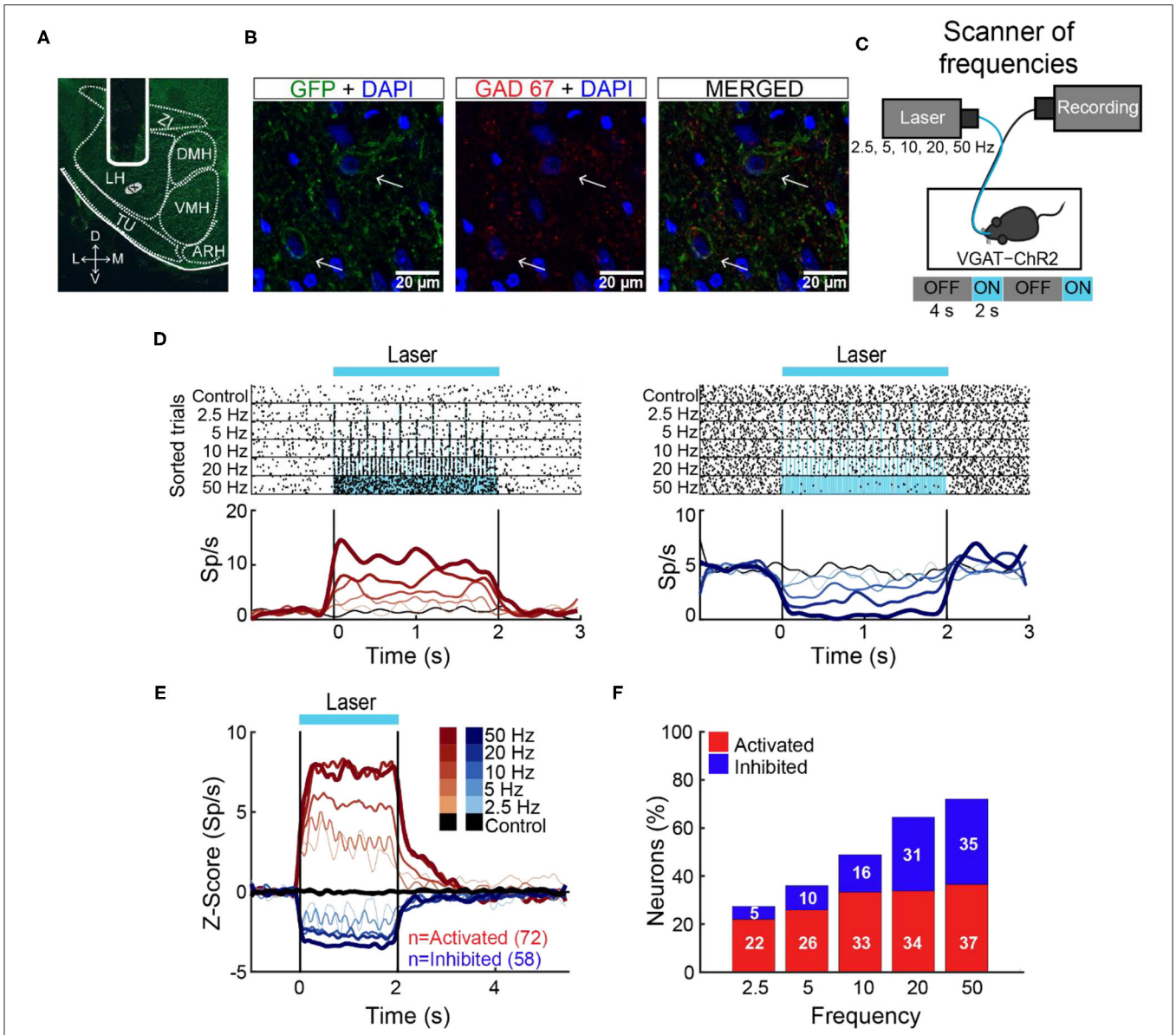

FIGURE 1 | The 50-Hz stimulation evoked the largest LHA neuronal responses. **(A)** Representative location of an optrode in LHA of VGAT-ChR2 mice. **(B)** Confocal images from LHA immunostained for GFP (green), GAD67 (red), and DAPI (blue). Arrows indicate the colocalization of ChR2-EYFP and GAD67 (see merged). **(C)** Schematic of optrode recordings in LHA during control trials (with no-laser) and opto-stimulation at 2.5, 5, 10, 20, and 50 Hz delivered randomly. In each trial, the laser had a cycle of 2 s on and 4 s off. **(D)** Representative raster plots of two neurons recorded in LHA. The first one was activated (left panel), and the second inhibited (right panel) during opto-stimulation. Spiking responses were aligned (time = 0 s) to the first laser pulse. Black ticks depict action potentials and blue marks laser pulses. Below are the corresponding PSTHs (firing rates, Sp/s). Red and blue ascending gradients indicate the frequency of stimulation [see **(E)** for the color bar]. Black trace represents activity during control trials without laser. Vertical black lines indicate laser onset (time = 0 s) and offset (time = 2 s), respectively. **(E)** Normalized *Z* score population responses of LHA neurons recorded from $n = 5$ VGAT-ChR2 mice. Red and blue colors depict activated or inhibited responses, respectively, relative to baseline (−1 to 0 s) and thickness, and gradient colors indicate higher stimulation frequencies. Black trace illustrates neural activity during control trials for all recorded neurons ($n = 186$). **(F)** Percentage of neurons recruited as a function of stimulation frequency.

et al., 2018), a brain region that sends outputs to LHA and is involved in feeding and also contains palatability-related neurons (O'Connor et al., 2015; Villavicencio et al., 2018), we also found that the LHA neuron's firing rate (either increasing or decreasing neurons) adjusts across the session to reflect sucrose's palatability (**Figure 2F**). These data indicate that within the session, as the animals approach satiety, the responses of the palatability-related neurons tracked the rapid decline in the lick rate mainly for the two less palatable stimuli (i.e., AS and water) but not for the higher sucrose concentration (sucrose 3 and 18%), suggesting these neurons are tracking palatability and no satiety.

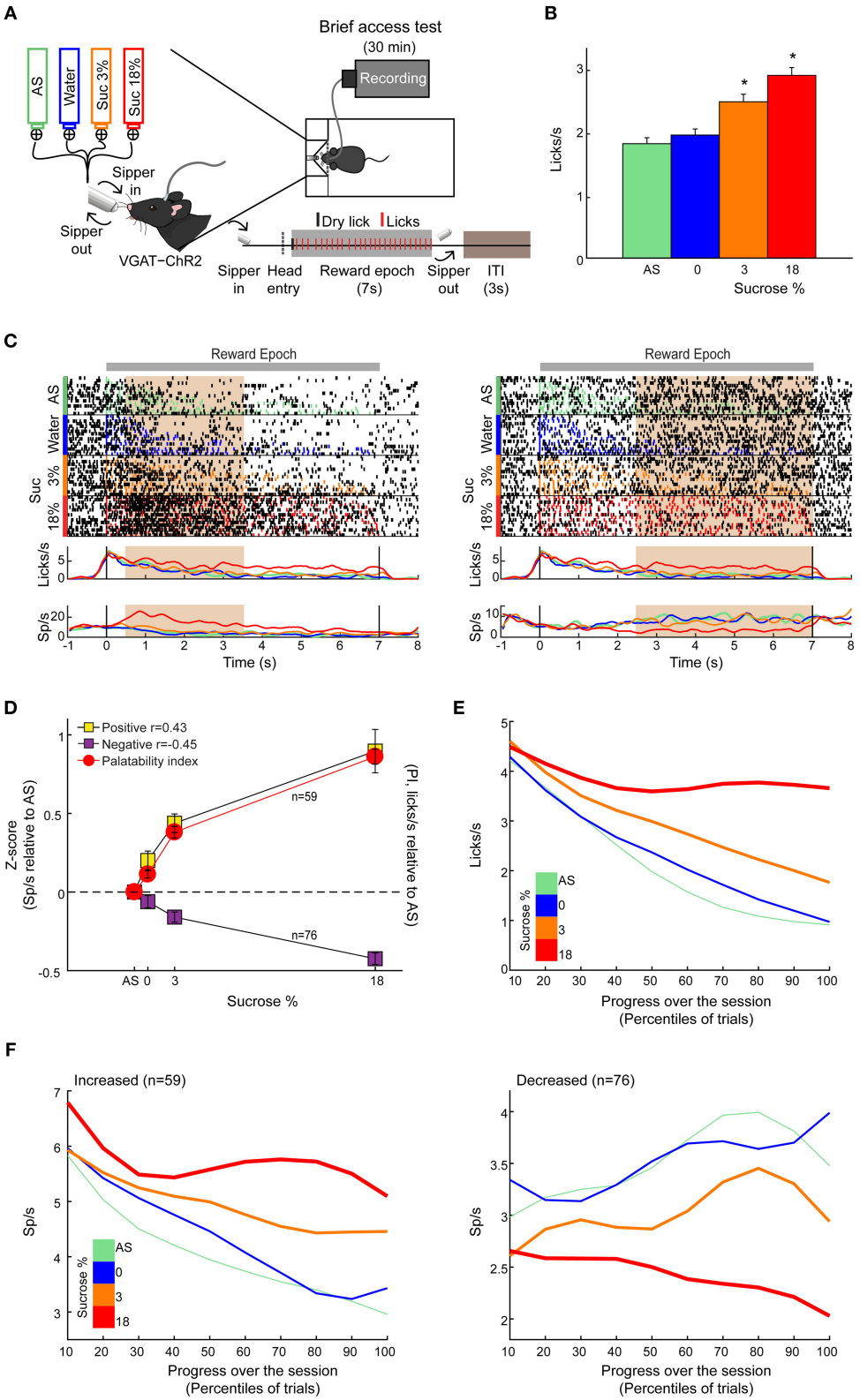

FIGURE 2 | LHA neurons process palatability-related information. **(A)** Brief access taste setup depicting a behavioral box equipped with a computer-controlled retractile sipper that for each lick independently delivers a drop of artificial saliva (AS), water, sucrose 3%, or 18% concentrations. After a head entry (dashed line), the first dry lick (black line) enables the 7-s reward epoch. During this period, in each lick (red), a drop of the four tastants was randomly delivered. After the reward epoch,

(Continued)

FIGURE 2 | the sipper was retracted for an intertrial interval (ITI) of 3 s and then re-extended to start a new trial. **(B)** Average lick rate during the entire reward epoch, reflecting greater palatability as a function of sucrose concentration. * Indicates significant difference ($p < 0.05$) among the stimuli. Using one-way ANOVA followed by the Holm–Sidak test. **(C)** Representative raster plot of two LHA neurons recorded while mice performed a brief access test. Spikes are plotted as black ticks, whereas licks for each tastant are color-coded (green, AS; blue, water; orange, sucrose 3%; red, sucrose 18%). Below are the corresponding peristimulus time histograms (PSTHs) of lick rate (licks/s) and firing rate (spikes/s; Sp/s) as a function of trial type. Neuronal responses were aligned (time = 0 s) to the first rewarded lick. The brown rectangles depict the "best" window with the maximum Pearson correlation coefficient between firing rates and sucrose's palatability index (PI). The left and right raster plots displayed two neurons with a positive and negative correlation, respectively. **(D)** Z score normalized activity (relative to AS trials) for LHA neurons with either positive or negative correlation against PI (red circles). **(E)** Population PSTHs of the lick rates given in the reward epoch as a function of trial type, divided into blocks of 10th percentiles of trials each. **(F)** Population PSTHs of the firing rate during the reward epoch of the palatability-related neurons across the session for each trial type. The *left panel* depicts neurons that fired more to higher sucrose concentrations [positive sucrose's palatability correlation; **(D)** yellow], whereas the *right panel* illustrates neurons with decreasing firing rates as the sucrose concentration increased [i.e., negative correlation with sucrose's palatability; **(D)** purple].

A Subpopulation of Opto-Identified LHA^{Vgat+} Neurons Encodes Sucrose's Palatability

To identify LHA^{Vgat+} neurons from our recordings, we opto-stimulated the same mice recorded in the brief access test seen in **Figure 2**. We verified the stability of the waveforms between tasks (i.e., brief access test and optotagging), and we only included single units with stable waveforms in the analysis (see section Materials and Methods; **Supplementary Figure 1**). **Figure 3A** displays the setup and the normalized (Z score) activity of laser-activated neurons (48%; 137/284) (for details, see section Materials and Methods). Since these neurons may include ChR2-expressing cells and other LHA neurons modulated by indirect polysynaptic feedback of afferent fibers from other areas in the brain (Nieh et al., 2015), we decided to name them putative LHA^{Vgat} (pLHA^{Vgat}) neurons. Note that pLHA^{Vgat} neurons comprise the ensemble recruited by the optogenetic stimulation of LHA GABAergic neurons, suggesting they convey similar information. Therefore, we next evaluated whether pLHA^{Vgat} neurons were correlated with sucrose's palatability. In total, 50% (69/137) of laser-activated neurons exhibited responses that were significantly palatability related; specifically, 34% showed a positive correlation (46 out of 137), whereas 17% (23 out of 137) had a negative correlation with sucrose's palatability (**Figure 3B**; positive vs. negative chi-square test$_{(1,274)} = 10.25$, $p < 0.01$). **Figure 3C** shows the population activity of pLHA^{Vgat} neurons with either a positive (yellow) or negative (purple) Pearson's correlation coefficients with the PI (red). Furthermore, from all recorded LHA neurons that encode sucrose-induced oromotor palatability responses with a positive correlation ($n = 59$, see **Figure 2D**), we found that more than 78% (46/59) belonged to the pLHA^{Vgat} (**Figure 3D**). In contrast, only 30% (23/76) of pLHA^{Vgat} neurons were negative palatability related (**Figure 3D**; positive vs. negative chi-square test$_{(1,135)} = 30.25$, $p < 0.0001$). Similar results were found when we analyzed the laser-activated late neurons (hereafter named late neurons) from the pLHA^{Vgat} population. These neurons exhibited a delayed laser-evoked action potential with a slow latency (>15 ms), $n = 66$ (see **Supplementary Figure 3A**). We compared the proportion of late neurons against all palatability-responsive neurons recorded in the LHA and found that 41% (24/59) belonged to the positive palatability-related population, and only 8% (6/76) were negative palatability-related neurons (**Supplementary Figures 3B,C**; chi-square test$_{(1,135)} = 20.65$, $p < 0.0001$). Thus, pLHA^{Vgat} encode sucrose's palatability with a biased toward positive correlations.

To confirm the identity of LHA^{Vgat+} neurons, we searched for neurons in which a brief pulse of light evoked an action potential with an early latency (≤15 ms) that would reflect the expression of ChR2 in their somas (Buonomano, 2003). In total, from the pLHA^{Vgat} population, 52% (71/137) neurons exhibited an early response to blue light (**Figures 3E,F**), suggesting that these pLHA^{Vgat} neurons were LHA^{Vgat+} neurons. We found that over half of the identified LHA^{Vgat+} neurons, 55% (39/71), were involved in encoding sucrose's oromotor palatability, and the remaining (45%) were unmodulated by sucrose. From the LHA neurons related to sucrose's oromotor palatability, 31% of LHA^{Vgat+} neurons positively correlated with sucrose's palatability (22/71), and 24% were anticorrelated (17/71) (**Figure 3G**; positive vs. negative chi-square test$_{(1,142)} = 0.88$, $p = 0.34$). The LHA^{Vgat+} neuronal responses with positive and negative Pearson's correlation coefficients with lick-related palatability responses are seen in **Figure 3H**. Once again, we compared the proportion of opto-identified LHA^{Vgat+} neurons against all palatability-responsive neurons recorded in the LHA. We found a trend to encode sucrose's palatability in a positive rather than negative manner. That is, 37% (22/59) of LHA^{Vgat+} neurons belonged to the positive palatability-related population, whereas only 22% (17/76) were negative palatability-related neurons (**Figure 3I**; positive vs. negative chi-square test$_{(1,135)} = 3.59$, $p = 0.057$). Altogether, these data suggest that LHA^{Vgat+} neurons tend to encode sucrose's palatability in a positive rather than in a negative manner. More importantly, our data agree with the idea that the LHA^{Vgat+} neurons comprised heterogeneous subpopulations with different functional responses (Jennings et al., 2015).

Non-LHA^{Vgat} Neurons Negatively Encode Sucrose's Palatability

In contrast, we found that 25% of the LHA neurons exhibited a laser-induced inhibition (70/284, non-LHA^{Vgat} neurons, **Figure 3J**, blue trace), and the remaining 27% (77/284) were unmodulated during blue light stimulation (**Figure 3J**, black trace). Unlike pLHA^{Vgat} neurons, only 7% (5 out of 70) of the non-LHA^{Vgat} neurons showed a positive correlation, whereas the vast majority, 36% (25 out of 70), had a negative correlation with sucrose's palatability (**Figures 3K,L**; positive vs. negative chi-square test$_{(1,140)} = 16.97$, $p < 0.0001$). These results

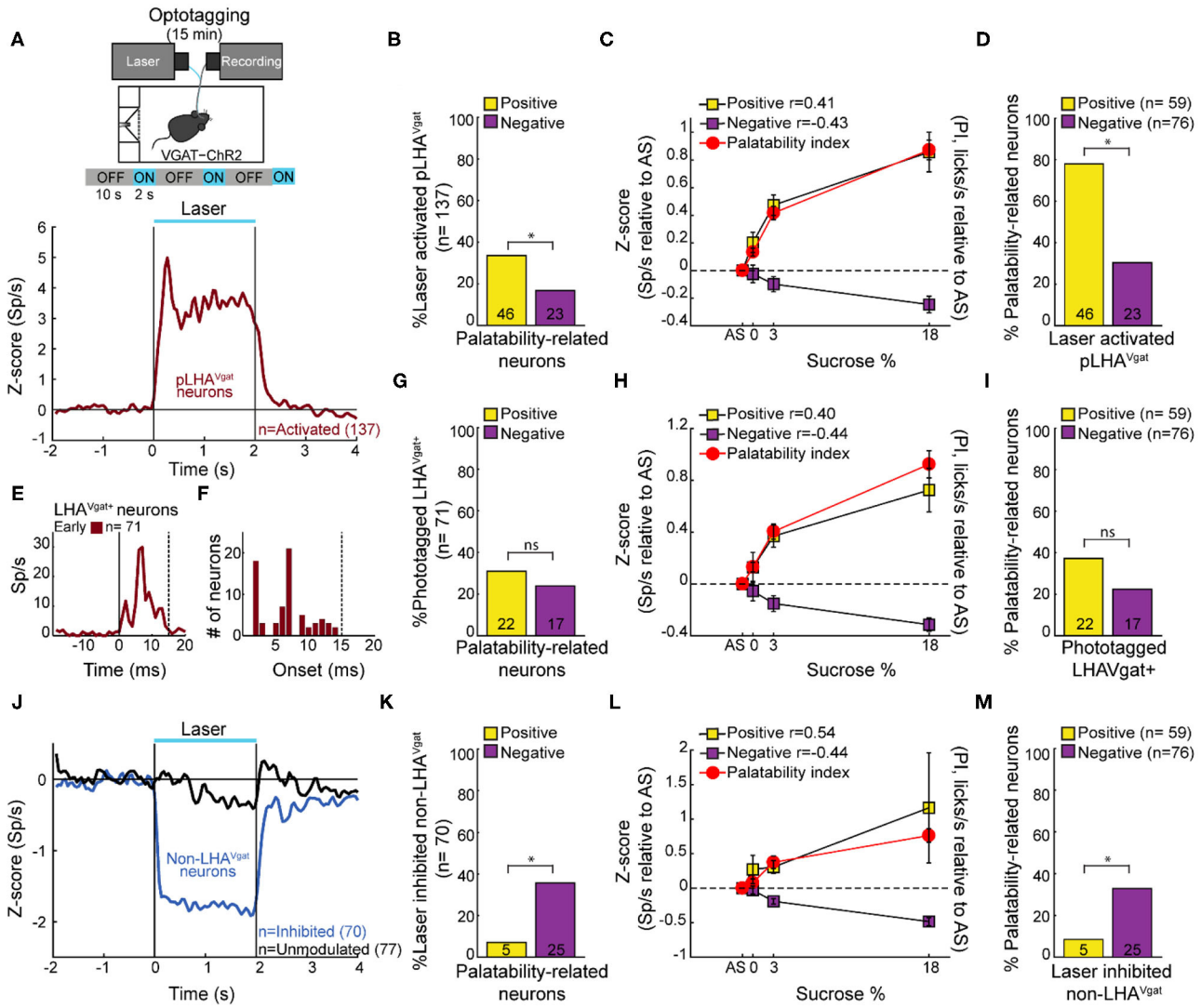

FIGURE 3 | A subpopulation of LHA^{Vgat+} neurons encodes sucrose's palatability. **(A)** To confirm the LHA^{Vgat+} neurons' identity after the brief access test, we performed laser opto-stimulation in a cycle 2 s on (at 50 Hz) and 10 s off over 15 min session. In this phase, mice had no access to the sipper (*above panel*). *Below*, the normalized *Z* score population activity of all 284 LHA neurons recorded from three VGAT-ChR2 mice. Responses were aligned to the laser onset (time = 0 s), relative to baseline (−1 to 0 s) activity. The red line depicts the responses of activated putative pLHA^{Vgat} neurons. **(B)** Percentage of laser-activated pLHA^{Vgat+} neurons whose activity (in the brief access test) also positively or negatively correlates with sucrose's PI. *$p < 0.01$, chi-square. **(C)** *Z* score activity (relative to AS) for all activated pLHA^{Vgat} neurons and its correlation with the sucrose's PI. **(D)** Percentage of positive or negative laser-activated palatability-related neurons. *$p < 0.0001$, chi-square. **(E)** PSTH of identified (opto-tagged) LHA^{Vgat+} neurons exhibiting early evoked responses (i.e., ChR2 expressing cells). **(F)** Histogram of opto-tagged LHA^{Vgat+} neurons with evoked early responses (latencies <15 ms) from laser onset. **(G–I)** The same conventions as in **(B–D)**, but for opto-tagged LHA^{Vgat+} neurons encoding sucrose's palatability. **(J–M)** Non-LHA^{Vgat} neurons that negatively encode sucrose's palatability. **(J)** Blue and black traces correspond to inhibited (non-LHA^{Vgat+} neurons) and unmodulated responses, respectively. Same conventions as in **(A)**. **(K–M)** The same conventions as in **(B–D)**. *$p < 0.001$, chi-square.

suggest that non-LHA^{Vgat} neurons (perhaps glutamatergic Vglut2 neurons) preferentially encode sucrose's palatability with negative correlations (**Figure 3M**; positive vs. negative chi-square test$_{(1,135)} = 11.46$, $p < 0.001$).

Activation of LHA^{Vgat+} Neurons Drives Sucrose Intake

If a subpopulation of LHA GABAergic neurons preferentially encodes sucrose's palatability by increasing firing rates, its optogenetic stimulation should promote increased sucrose intake. To characterize its impact on sucrose intake, we used an open loop optogenetic stimulation involving 5-min blocks with laser and no-laser stimulation, while naive VGAT-ChR2 mice had *ad lib* access to a sipper filled with sucrose 10% (**Figure 4A**). We analyzed the intake as a function of laser frequency (**Figure 4B**; two-way ANOVA, frequency by blocks interaction, $F_{(35,96)} = 2.268$, $p < 0.01$); a *post hoc* test uncovered that in the first three blocks with laser, 50 Hz stimulation induced a significant increase

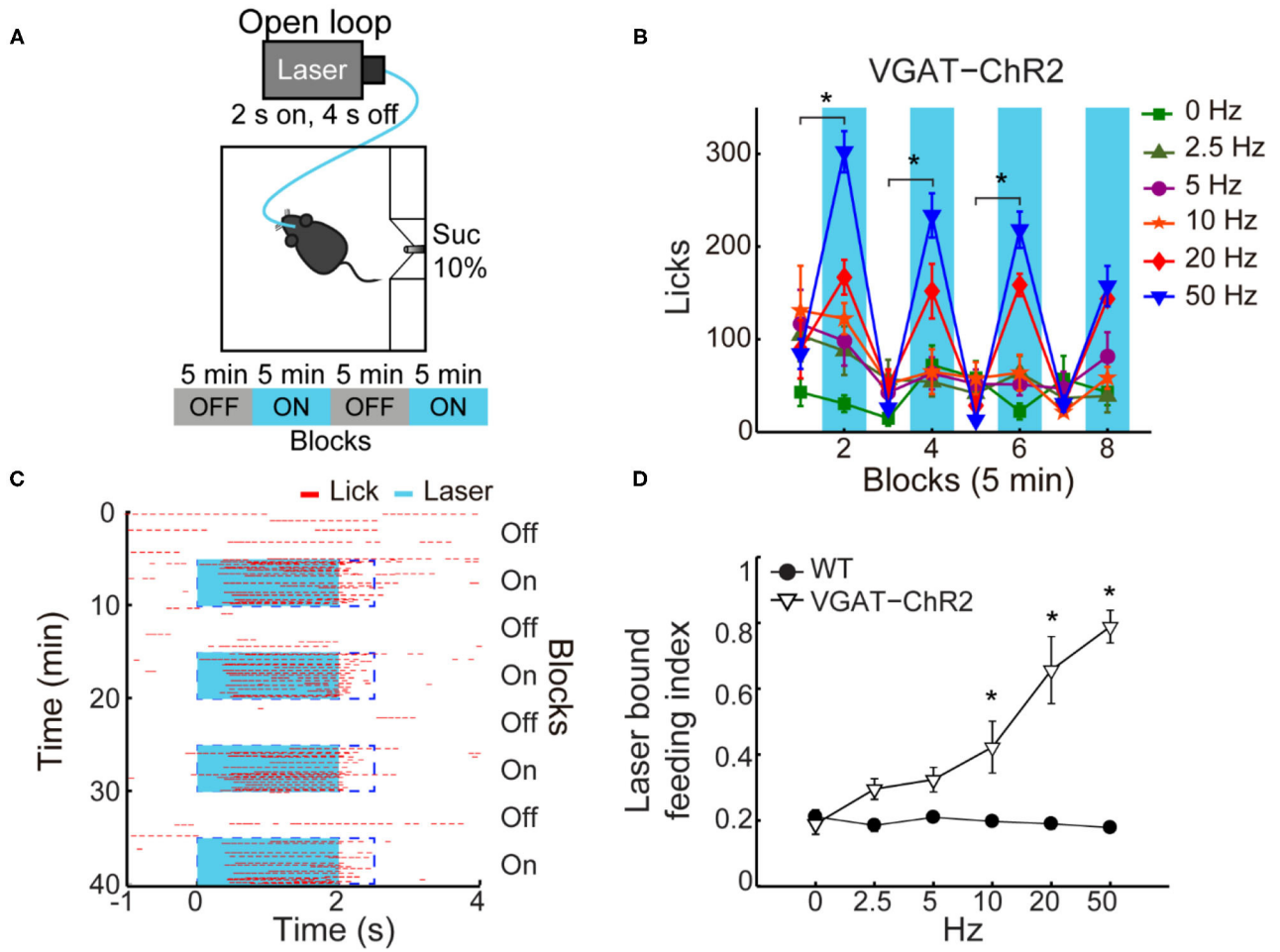

FIGURE 4 | In sated VGAT-ChR2 mice, 50 Hz stimulation of LHA^{Vgat+} neurons induced the greatest intake of sucrose. **(A)** Behavioral setup for open loop stimulation, where the laser was turned on regardless of the mice's behavior. The box was equipped with a central sipper, where mice had free access to 10% sucrose. Open loop stimulation comprised 5 min block without laser followed by opto-stimulation for 5 min, in a cycle 2 s on and 4 s off, during a 40-min session. VGAT-ChR2 ($n = 3$) and WT ($n = 5$) mice received stimulation of only one of the following frequencies in ascending order per session: 0, 2.5, 5, 10, 20, and 50 Hz. **(B)** Opto-stimulation of LHA^{Vgat+} neurons induced sucrose (10%) intake in a frequency-dependent manner that peaked at 50 Hz. * Denotes statistically significant difference ($p < 0.001$) between non-laser and laser-stimulated blocks at 50 Hz. Besides mice being sated, the lower intake at 0 Hz could be due to the lack of experience drinking in the novel box. **(C)** Representative raster plot of open loop stimulation from a VGAT-ChR2 mouse at 50 Hz. Lick responses (red ticks) were aligned to laser onset (blue rectangles, opto-stimulation period). The laser-bound index was the number of licks within 2.5 s from laser onset (dashed blue rectangles) divided by total licks. **(D)** The laser-bound feeding index of VGAT-ChR2 increased as a function of the laser frequency. *Indicates significant difference from WT mice ($p < 0.01$). Using a two-way ANOVA followed by the Holm–Sidak test. In this and other figures, data represent mean ± SEM.

in sucrose intake (**Figure 4B**; blocks 2, 4, and 6) compared with the previous blocks of no-laser (**Figure 4B**; $p < 0.001$; blocks 1, 3, and 5). **Figure 4C** shows a raster plot for licking responses of a representative open loop session. At 50 Hz, we found that feeding (licking) was elicited within a 0.72 ± 0.03-s latency from laser onset, and it abruptly stopped (0.27 ± 0.1 s) after laser offset (see blue dash rectangles). VGAT-ChR2 mice exhibited an increase in the laser-bound feeding as the laser frequency increased (**Figure 4D**; two-way ANOVA, group by frequency interaction, $F_{(5,36)} = 12.86$, $p < 0.0001$). Thus, to induce sucrose intake, LHA^{Vgat+} neurons require continued activation. Our data then confirmed that 50 Hz is the best stimulation frequency to drive neuronal responses and sucrose intake.

LHA^{Vgat+} Neurons Do Not Induce a Persistent Hunger State

A previous study showed that brief optogenetic stimulation of "hunger-inducing" AgRP neurons in the arcuate nucleus before food availability promotes consummatory behavior that persists for several minutes in the absence of continued AgRP neuron activation (Burnett et al., 2016; Chen et al., 2016). Based on this study, we tested whether the prestimulation of LHA^{Vgat+} neurons could evoke a similar hunger state. Unlike AgRP neurons (Burnett et al., 2016; Chen et al., 2016), prestimulation of LHA^{Vgat+} neurons failed to evoke and sustain subsequent sucrose intake (see **Supplementary Figure 4**; two-way ANOVA, group by prestimulation protocol, $F_{(3,56)} = 0.50$, $p = 0.68$). Our

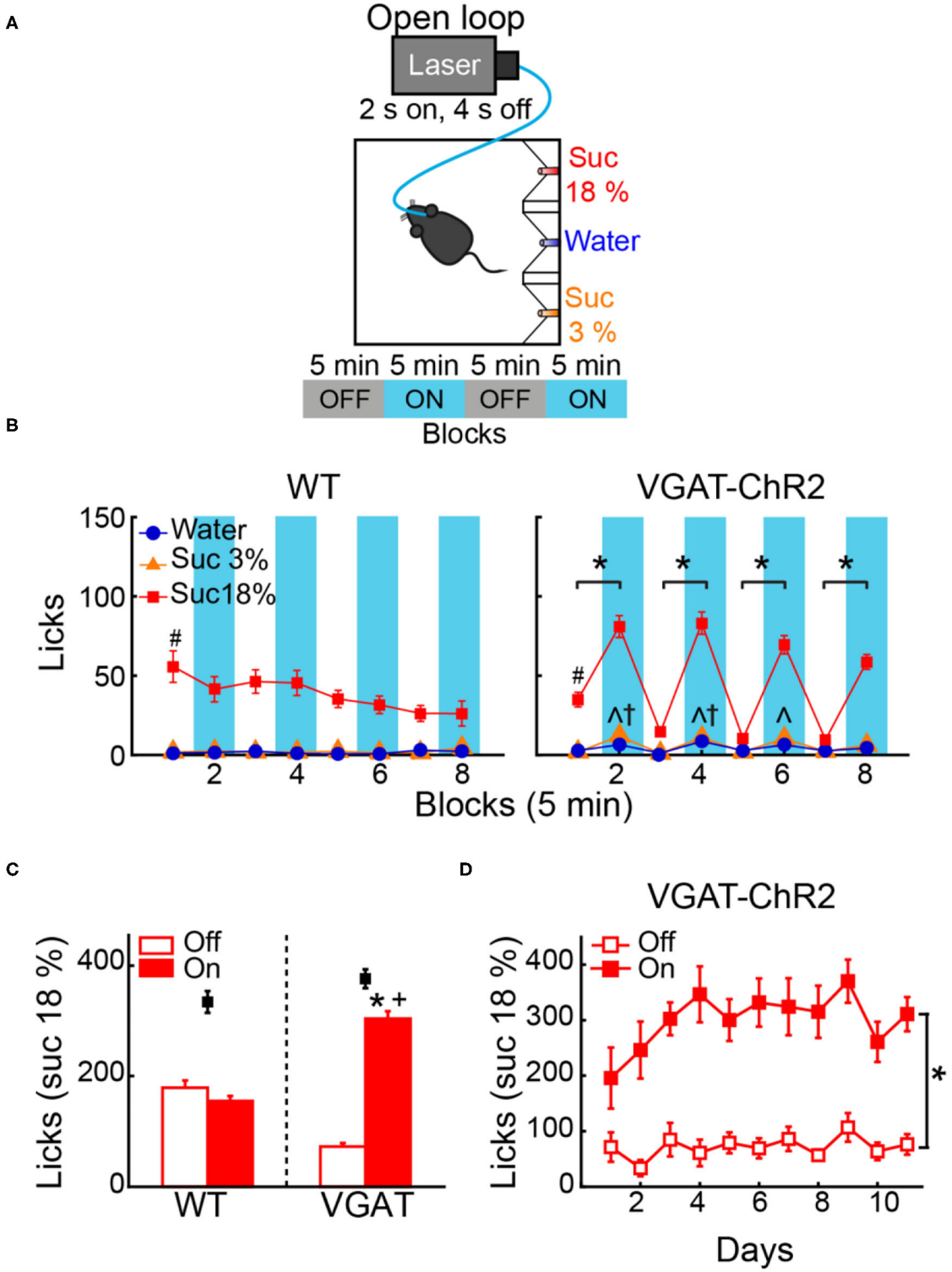

FIGURE 5 | Open loop stimulation of LHA^{Vgat+} neurons biases consumption toward the most palatable tastant and reinforces intake during opto-stimulation. **(A)** Behavioral protocol. Sated mice ($n = 6$ WT and $n = 12$ VGAT-ChR2) were located in an operant box equipped with three ports. The left port contained sucrose 18%, the central port water, and the right port sucrose 3%, counterbalanced across individuals. For details of the open loop, see **Figure 4A**. **(B)** *Left and right panels*, number of licks for each gustatory stimulus for WT and VGAT-ChR2 mice. Note that the VGAT-ChR2 mice increased consumption of the most palatable stimulus available (sucrose 18%) mainly in opto-stimulated blocks (blue rectangles), while it decreased intake in blocks without laser. **(C)** Mean licks for sucrose 18%, during blocks with laser on and off from WT and VGAT-ChR2 mice. Black squares show the total licks given for each group. **(D)** Licks for sucrose 18% during blocks with or

(Continued)

FIGURE 5 | without laser across days. *Indicates a significant difference ($p < 0.0001$) between laser and no-laser blocks. $^{\#}p < 0.0001$ statistically significant difference between sucrose 18% and the other stimuli. $^{\wedge}p < 0.01$ between WT and VGAT-ChR2 for sucrose 3%; $^{\dagger}p < 0.01$ higher intake of water of VGAT-ChR2 compared with WT; $^{+}p < 0.0001$ higher consumption of VGAT-ChR2 compared with WT for sucrose 18% during blocks with laser. Using a two-way ANOVA and RM ANOVA followed by the Holm–Sidak test.

results suggest that feeding occurs while LHA^{Vgat+} neurons are active (**Figure 4C**), but they do not induce a persistent hunger state as AgRP neurons do (Chen et al., 2016).

Open Loop Activation of LHA^{Vgat+} Neurons Drives Intake of the Highest Sucrose Concentration Available

To test whether activation of LHA^{Vgat+} neurons promotes the intake of the most palatable available stimulus, naive WT and VGAT-ChR2 mice were opto-stimulated in an open loop protocol, with access to three adjacent ports containing water, sucrose 3%, or sucrose 18% (**Figure 5A**). As expected, both WT and VGAT-ChR2 mice preferred sucrose 18% over water, and sucrose 3% (**Figure 5B**; WT: two-way ANOVA main effect tastants; $F_{(2,1,560)} = 543.3$, $p < 0.0001$; VGAT-ChR2: $F_{(2,3,144)} = 983$, $p < 0.0001$). However, we found that sated VGAT-ChR2 mice increased their intake of 18% sucrose mainly during the laser-activated blocks compared with controls (**Figure 5B**, *right*; two-way ANOVA group by laser block interaction $F_{(7,1,568)} = 31.86$, $p < 0.0001$) and rarely licked in the absence of stimulation (**Figure 5C**). In this regard, VGAT-ChR2 mice seem to counteract the evoked sucrose intake by voluntarily restraining consumption in the no-laser blocks (blocks 3, 5, and 7), resulting in no significant differences between groups in the total intake of 18% sucrose (**Figure 5C**, see black squares; unpaired Student's *t*-test, $t_{(196)} = 1.512$, $p = 0.1320$). A between-days analysis revealed that the evoked 18% sucrose intake began from the first stimulation day (**Figure 5D**; RM ANOVA laser blocks, $F_{(1,22)} = 64.64$, $p < 0.0001$), although sucrose consumption ramps up throughout the days (**Figure 5D**; RM ANOVA main effect days, $F_{(10,220)} = 2.169$, $p < 0.05$). This suggests that LHA^{Vgat+} neurons, rather than inducing hunger *per se*, induced a learning process that potentiates the intake of the most palatable stimulus and confines consumption mainly in the presence of opto-stimulation.

The small increase in water and sucrose 3% intake observed during opto-stimulation of LHA^{Vgat+} neurons could be explained by random stimulation near those tastants (**Figure 5B**, *right panel*). Accordingly, we found in laser blocks 2, 4, and 6 a significant increase in water and sucrose 3% in the VGAT-ChR2 mice compared with the WT mice that completely neglected those tastants (**Figure 5B**, $^{\wedge}p < 0.05$ for sucrose 3%; $^{\dagger}p < 0.05$ for water). We hypothesize that this additional intake can be attributed to trials where laser activation occurred near these less palatable stimuli. To answer this, we employed a videography analysis (**Figures 6A,B**). When opto-stimulation occurred in the distance minor to 50 pixels (∼3 cm, see section Materials and Methods) relative to sucrose 3% or water ports, the licking probability increased significantly after opto-stimulation (**Figure 6B**; sucrose 3%: $F_{(9,155)} = 29.33$, $p < 0.0001$; water: one-way ANOVA; $F_{(9,153)} = 12.74$, $p < 0.0001$). The angle of the head was less informative (**Figures 6C,D**; sucrose 3%: $F_{(17,147)} = 0.71$, $p = 0.78$; water: one-way ANOVA; $F_{(17,145)} = 0.96$, $p = 0.49$; sucrose 18%: one-way ANOVA; $F_{(17,153)} = 0.49$, $p = 0.95$). Conversely, since mice are naturally attracted to the most palatable tastant, they spent more time near the lateral port with 18% sucrose, increasing their overconsumption (**Figure 6C**, **Supplementary Video 1**). Moreover, we observed that for the sucrose 18% port, even when the mouse position was twice as far (i.e., 6 cm) from the sucrose 18% port, the licking probability increased significantly (**Figure 6B**, *right panel*; one-way ANOVA, $F_{(9,161)} = 82.87$, $p < 0.0001$). These data are consistent with a study showing that opto-stimulation of LHA^{Vgat+} neurons promotes the intake of the nearest stimulus (Nieh et al., 2016) but further demonstrates that the most palatable stimulus has nearly twice the distance of attraction than the other less palatable options.

Open Loop Activation of LHA^{Vgat+} Neurons Also Increases the Time Spent and Drives the Intake of the Most Palatable Solid Food Available

We also explored whether LHA GABA neurons could induce the intake of the most palatable solid food available. Thus, using an open loop protocol, we opto-stimulate these neurons while mice choose among different solid foods. We found that optogenetic activation of LHA^{Vgat+} neurons increased the time spent near the most palatable food available. VGAT-ChR2 mice spent more time near the high-fat diet than the granulated sugar cube or the chow food pellet, relative to the WT group. Also, the intake of transgenic mice was higher for high-fat diet than the other food stimuli (see **Supplementary Figure 5**, **Supplementary Video 2**; time spent: one-way ANOVA, $F_{(5,306)} = 38.52$, $p < 0.0001$; intake: one-way ANOVA, $F_{(5,282)} = 68.76$, $p < 0.0001$); however, both WT and VGAT-ChR2 mice consumed similar amounts of high-fat diet ($p = 0.0985$), perhaps because it is a highly palatable food. When mice were able to choose between a sugar cube and a chow pellet, now the activation of these neurons increased the time spent and consumption of sugar cube over chow (see **Supplementary Figure 6**, **Supplementary Video 3**; time spent: one-way ANOVA, $F_{(3,96)} = 16.13$, $p < 0.0001$; intake: one-way ANOVA, $F_{(3,92)} = 13.65$, $p < 0.0001$). Our data suggest that open loop stimulation of LHA GABAergic neurons promotes the attraction to and the intake of the most palatable food available.

Closed-Loop Stimulation of LHA^{Vgat+} Neurons Drives the Intake of the Nearest Appetitive Stimuli

To further test the idea that LHA^{Vgat+} neurons could induce a preference for a proximal (but less palatable) stimulus over a distal one with higher hedonic value, we used a closed-loop

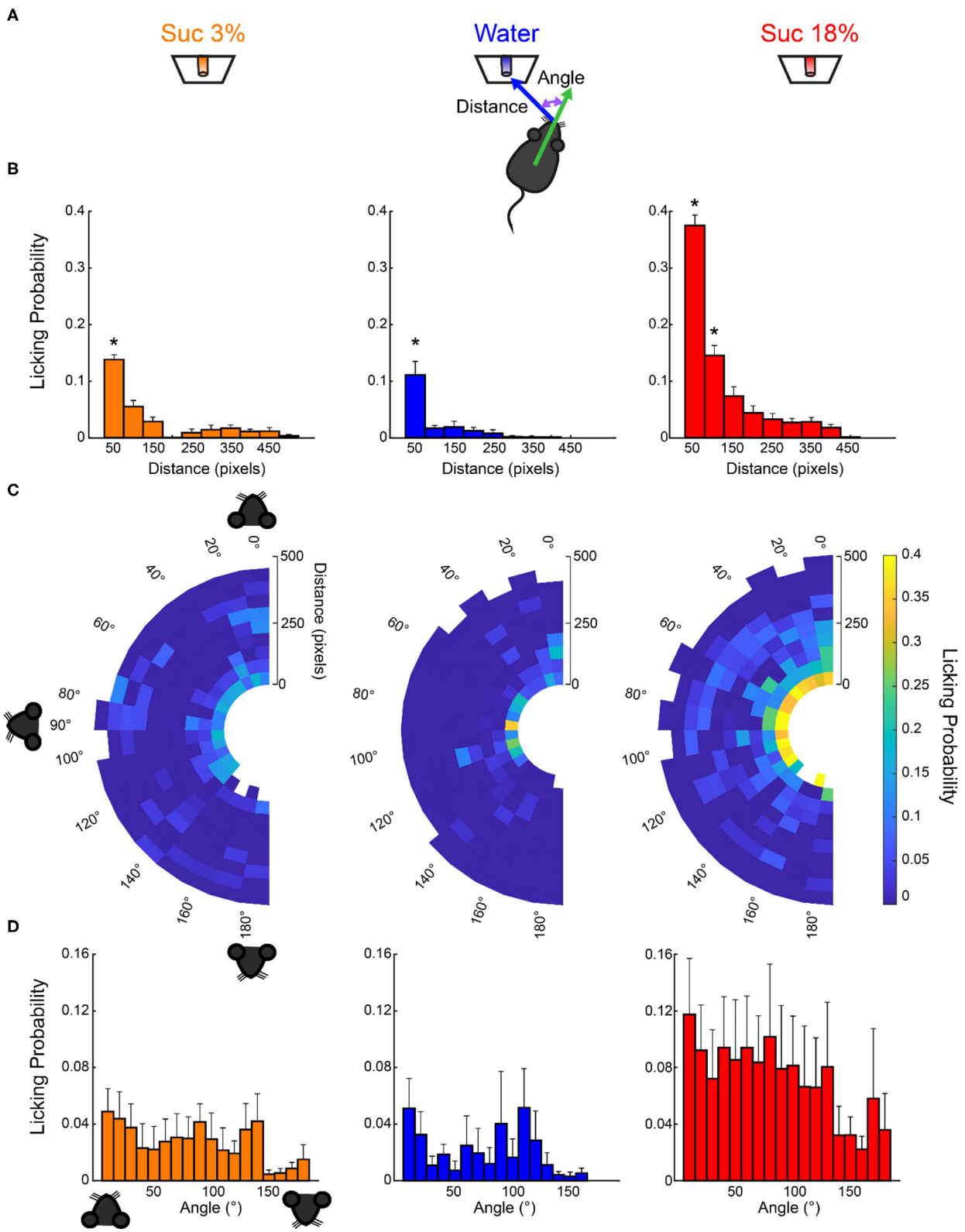

FIGURE 6 | Licking probability increased as a function of distance. **(A)** Schematics for video tracking (see *Materials and Methods*). We calculated the distance and the head angle between the mouse's nose and each of the three sippers containing sucrose 3%, water, or sucrose 18% for each laser onset. **(B)** It depicts the probability that laser onset evoked licking as a function of the mouse's distance relative to each sipper. **(C)** Polar plots depict the licking probability after laser onset, given the

(Continued)

FIGURE 6 | distance and angle of the mouse relative to a licking sipper. At the onset of each laser stimulation, we computed the head angle and distance relative to each sipper, and in the following 6-s window, we tally if the mouse licked to any sipper. We normalized by dividing the number of times licking was elicited by the number of first lasers occurring on those coordinates. The drawing of the mice's head illustrates that if a mouse was facing toward the sipper, the angle is 0°, in a perpendicular position (90°), or 180° if it was looking in the opposite direction. **(D)** The probability of licking after laser onset vs. the angle between the head direction and the sipper. * Indicates significantly different ($p < 0.001$) from all other distances. One-way ANOVA followed by the Holm–Sidak test.

stimulation protocol. That is, the same mice (from **Figure 5**) were photostimulated, but here the laser was triggered by each head entry in the central port (i.e., opto-self-stimulation). This closed-loop configuration guarantees that stimulation only occurs proximal to water, the least palatable stimulus of the three in the box (**Figure 7A**, *right*). We found that activation of LHA^{Vgat+} neurons is rewarding since transgenic mice visited the central port significantly more and performed a higher number of opto-self-stimulations than the WT mice (**Figure 7B**; unpaired Student's *t* test, $t_{(196)} = 12$, $p < 0.0001$). Surprisingly, the total number of licks in the session seen in **Figure 7C** shows that during closed-loop stimulation, the VGAT-ChR2 mice explored and consumed more water than the WT mice (two-way ANOVA group by tastants interaction, $F_{(2,585)} = 13.09$, $p < 0.0001$, *post hoc* test at water, $p < 0.0001$). Note that in both open loop and closed-loop protocols, the WT and VGAT-ChR2 mice exhibited, at the end of the session, similar number of licks for 18 wt% sucrose (**Figure 7C**; two-way ANOVA group by protocol interaction, $F_{(1,391)} = 2.172$, $p = 0.1414$). That is, the total licks for sucrose 18% were not significantly different between groups, suggesting that these neurons do not interfere with the overall attractiveness of sucrose. However, by counting the number of licks given when the laser was turned on (in a 2.5-s window from laser onset—see **Figure 7D**), we uncovered a striking change in preference. As noted, in the open loop, the VGAT-ChR2 mice exhibited a higher preference for sucrose 18 wt%, over both sucrose 3 wt% and water. Now, in the closed-loop protocol, the same transgenic mice consumed more water compared with WT (two-way ANOVA group by tastants interaction, $F_{(2,585)} = 12.18$, $p < 0.0001$, *post hoc* test at water, $p < 0.0001$), and the consumption of water was about the same as sucrose 18% ($p = 0.8731$, n.s.; **Figure 7D**). The increase in water intake was selective to the photostimulation window since the transgenic mice only drank sucrose 18%, and neglected water when the laser was turned off (see arrow in **Figure 7E**; two-way ANOVA group by tastants interaction, $F_{(2,585)} = 64.16$, $p < 0.0001$, *post hoc* test at water vs. sucrose 18%, $p < 0.0001$). Thus, LHA^{Vgat+} neurons could promote water intake, but only when it is the nearest stimulus. The sucrose preference index (**Figure 7F**) showed that during the open loop, all VGAT-ChR2 mice preferred sucrose 18% over water (**Figure 7F**; values >0.5 and near to 1), whereas in the closed-loop protocol, when water was the nearest stimulus, most mice ($n = 9$ out of 12) significantly diminished their sucrose preference (**Figure 7F**, see the drop in preference index; paired Student's *t*-test, $t_{(58)} = 7.98$, $p < 0.0001$). From these nine animals, six exhibited a higher preference for water over sucrose 18% (preference index values <0.5; **Supplementary Video 4**). **Figure 7G** shows the color-coded location of fiber optic tips in each VGAT-ChR2 mice plotted in **Figure 7F**. However, the location of the optical fibers does not explain the variability in preference. Perhaps the variability is due to different behavioral strategies used by each mouse. Nevertheless, the large variability in the drop of sucrose preference resembles the findings with sweet-induced facilitation by electrical ICSs (Poschel, 1968). These data suggest that LHA^{Vgat+} neurons drive consummatory behavior by integrating the stimulus proximity and hedonic value.

After Repeated Stimulation, the Correlation Between Laser-Bound Feeding and Self-Stimulation Strengthens

Previous studies have shown that after repeated LHA bulk stimulation (either electrically or with optogenetic targeting all cell types together), subjects switched from exhibiting stimulus-bound feeding to only self-stimulating, indicating that LHA-evoked feeding and reward could represent two distinct processes (Gigante et al., 2016; Urstadt and Berridge, 2020). Consequently, we explored whether laser-bound feeding changed after repeated optogenetic stimulation. In contrast to previous studies, we observed that laser-bound feeding induced by LHA^{Vgat+} neurons strengthened across sessions (**Figure 8A**, first 3 days: $r = 0.12$, $p = 0.69$; last 5 stimulation days: $r = 0.63$, $p < 0.05$), and after repeated stimulation, both opto-self-stimulation and laser-bound feeding exhibited a robust correlation (**Figure 8B**, first 3 days: $r = 0.42$, $p = 0.16$; last 5 days: $r = 0.61$, $p < 0.05$), suggesting that LHA-evoked feeding (licking) involves a learning process (Sharpe et al., 2017) and that LHA GABAergic neurons are a common neural substrate for feeding and reward.

The "Stimulus Proximity Effect" Is Not Restricted to Liquid Tastants, and It Also Occurs With Chocolate and Chow Pellets

The "proximity effect" evoked by LHA^{Vgat+} neurons was not restricted to liquid tastants; it also applied to solid foods. In a real-time place preference arena with four stimuli (**Figure 9A**), when chocolate pellets or chow food was the designated food near opto-self-stimulation of LHA^{Vgat+} neurons, mice also increased the time spent near those foods (**Figure 9B**; pellet: one-way ANOVA; $F_{(4,145)} = 99.05$, $p < 0.0001$; chow, $F_{(4,145)} = 182$, $p < 0.0001$) as well as their intake (**Figure 9C**; pellet: unpaired Student's *t* test, $t_{(68)} = 3.234$, $p < 0.05$; chow: unpaired Student's *t* test, $t_{(68)} = 3.651$, $p < 0.05$) (see **Supplementary Video 5**). Thus, these LHA GABAergic neurons reinforced the approach and exploration to any, if not the most appetitive stimulus, that happened to be proximal to the opto-stimulation.

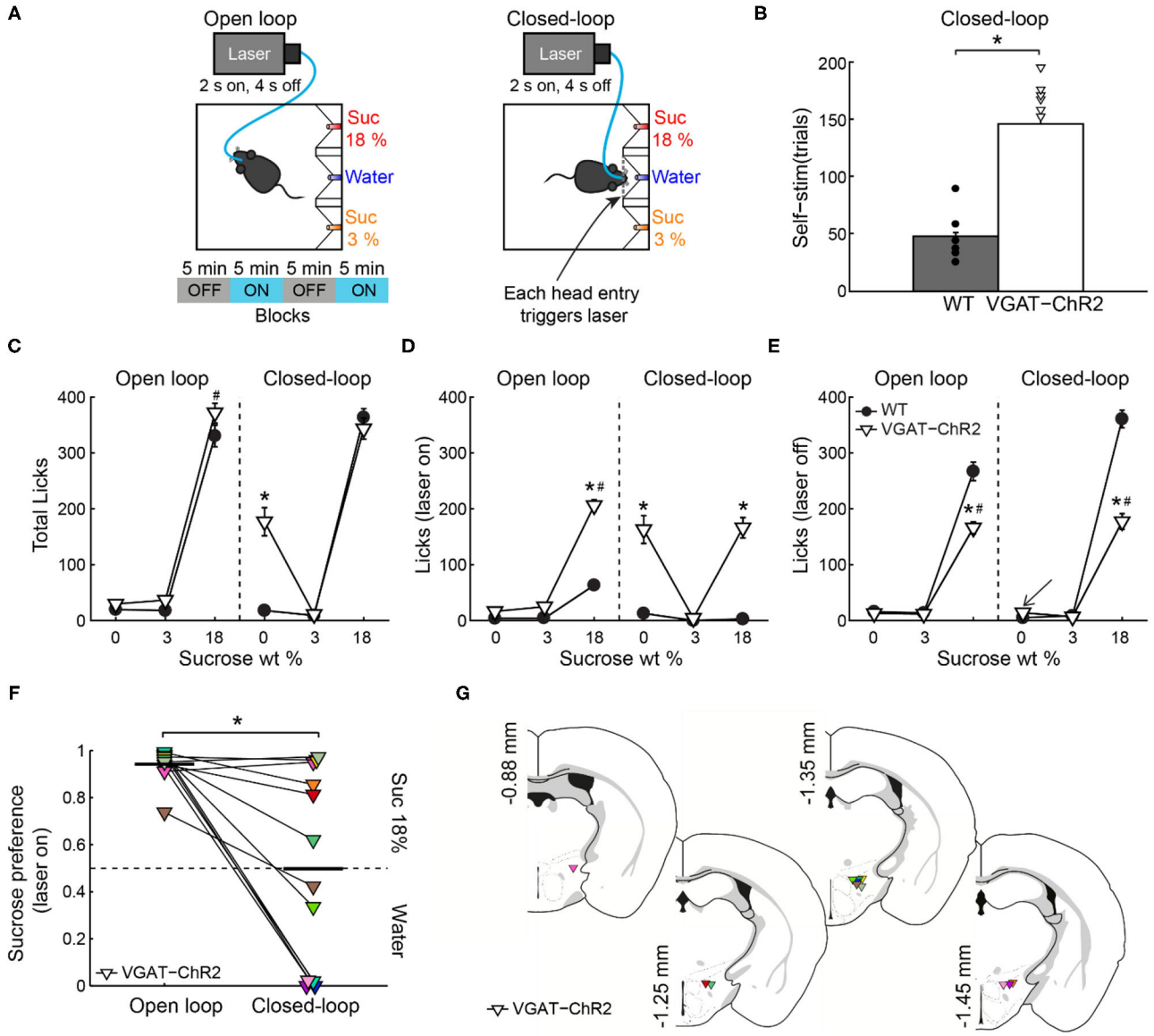

FIGURE 7 | If stimulation occurred near the less palatable stimulus, LHA^{Vgat+} neurons induced water intake despite sucrose. **(A)** For the open loop stimulation, the laser was activated (2 s on, 4 s off) regardless of behavior and mice position. The same mice and conventions as in **Figure 5A**. In the closed-loop configuration, the laser was triggered by a head entry in the central port. **(B)** The number of laser activations during the closed-loop protocol. The VGAT-ChR2 mice self-stimulate more than the WT mice. Each dot and triangle represent a single mouse. Unpaired *t*-test. **(C)** The total number of licks given for each stimulus during the entire session. In the open loop, both mice groups licked more sucrose 18% than water or sucrose 3%. However, in the closed-loop configuration, the VGAT-ChR2 consumed more water (0% sucrose) than the WT mice. **(D)** The number of licks evoked during 2.5 s after laser onset for each gustatory stimulus. **(E)** The number of licks when laser was turned off for each gustatory stimulus. **(F)** The water–sucrose 18% preference index from VGAT-ChR2 mice during photostimulation was defined as the number of 18% sucrose licks divided by the total licks for sucrose 18% + water. Thus, values higher than 0.5 indicate sucrose 18%, and values lower than 0.5 indicate preference for water. Some VGAT-ChR2 mice preferred water over sucrose. The horizontal black lines indicate mean preference in both stimulation protocols. Paired *t*-test. **(G)** Fiber optic location in the LHA of VGAT-ChR2 mice. *$p < 0.0001$ indicates a significant difference from WT mice and stimulation protocols. #$p < 0.0001$ between sucrose 18% and the other stimuli. Two-way ANOVA followed by the Holm–Sidak test.

LHA^{Vgat+} Neurons' Activation Is Rewarding

In the same WT and VGAT-ChR2 mice tested in the closed-loop configuration seen in **Figure 7**, we went on to show that mice visited the central water port to opto-self-stimulate. To do this, we performed extinction sessions with the laser disconnected (**Figure 10A**). We observed a rapid decrease in the number of opto-self-stimulations (**Figure 10B**; extinction phase, gray shadow). As expected, self-stimulation rapidly recovered when the laser was turned on again (**Figure 10**, see water after extinction). Thus, LHA^{Vgat+} neurons convey

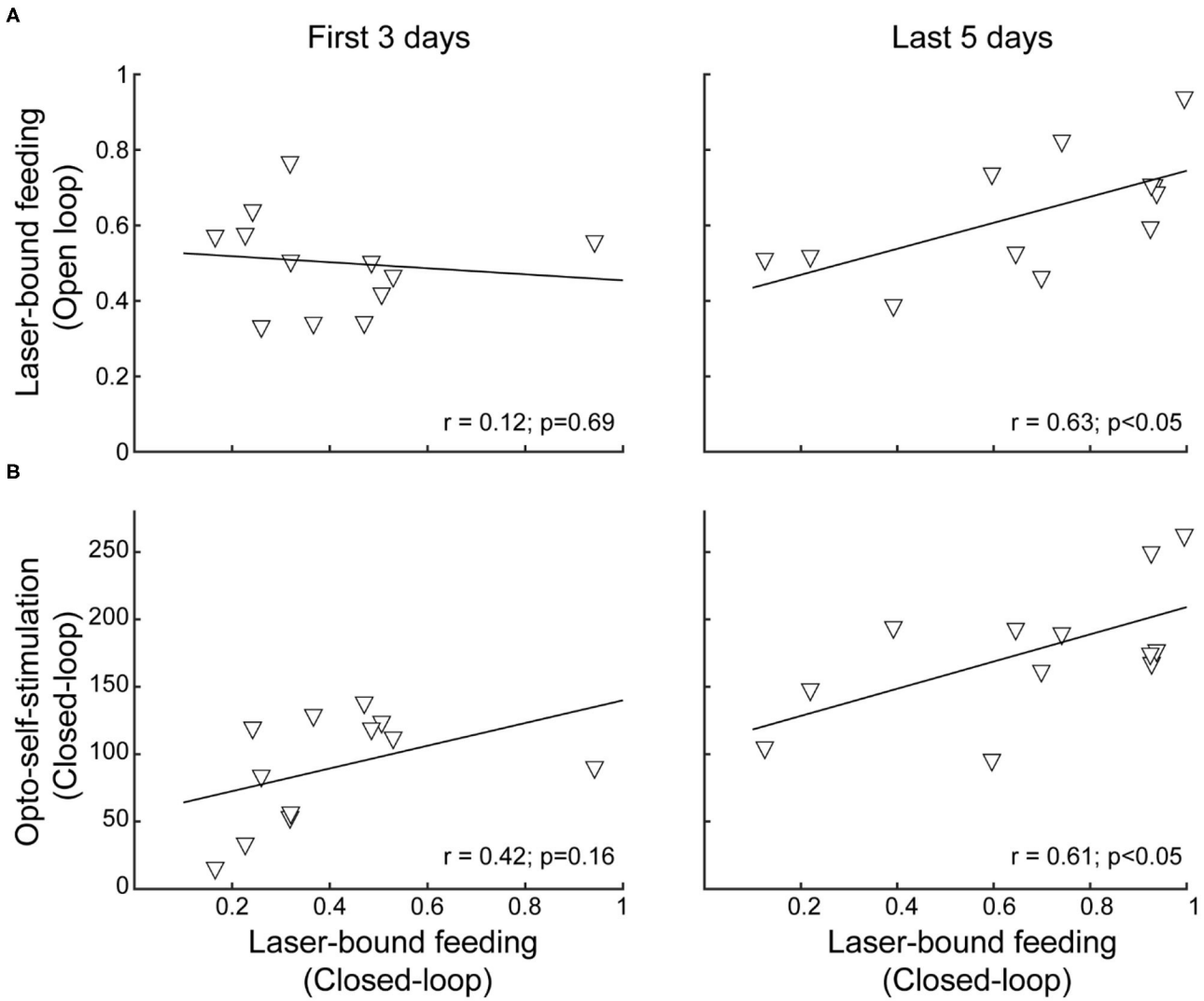

FIGURE 8 | After repeated activation of LHA^{Vgat+} neurons, laser-bound feeding (in open vs. closed loop) strengthened and exhibited a positive correlation. **(A)** Scatter plots showing the relationship between laser-bound feeding (licks given during the 2.5 s window from laser onset relative to total licks in the session) in both open loop and closed-loop tasks during the first 3 days (*left panel*) and the last 5 days of opto-stimulation of open loop vs. opto-self-stimulation of the closed-loop protocols (*right panel*). **(B)** Likewise, after repeated activation, both opto-self-stimulations and laser-bound feeding (licking) showed a significant correlation. Scatter depicting the average number of opto-self-stimulations vs. the laser-bound feeding observed in the closed-loop protocol.

a hedonically positive, rewarding signal (Jennings et al., 2015).

LHA^{Vgat+} Neurons Also Promote Licking an Empty Sipper

A previous study demonstrated that chemogenetic activation of LHA^{Vgat+} neurons increased gnawing to non-edible cork (Navarro et al., 2016). In the absence of other stimuli but cork, we also observed gnawing behavior in some mice, although we did not systematically study stereotypy (see **Supplementary Video 6**). Instead, we further explored this idea by replacing water, in the central port, with an empty sipper (**Figure 10**, empty sipper). Transgenic mice continued opto-self-stimulating at the same pace as if water were still present in the central port. LHA^{Vgat+} stimulation evoked licking an empty sipper compared with WT mice (**Figure 10C**, unpaired Student's *t*-test, $t_{(40)} = 2.532$, $p < 0.05$). Thus, LHA^{Vgat+} neurons evoke an imminent urge to express consummatory behavior even in the form of dry licking an empty sipper, a non-biological relevant stimulus, but only when it is the nearest stimulus to photostimulation. This effect is perhaps also mediated by an increase in the rewarding value of appetitive oromotor responses *per se*.

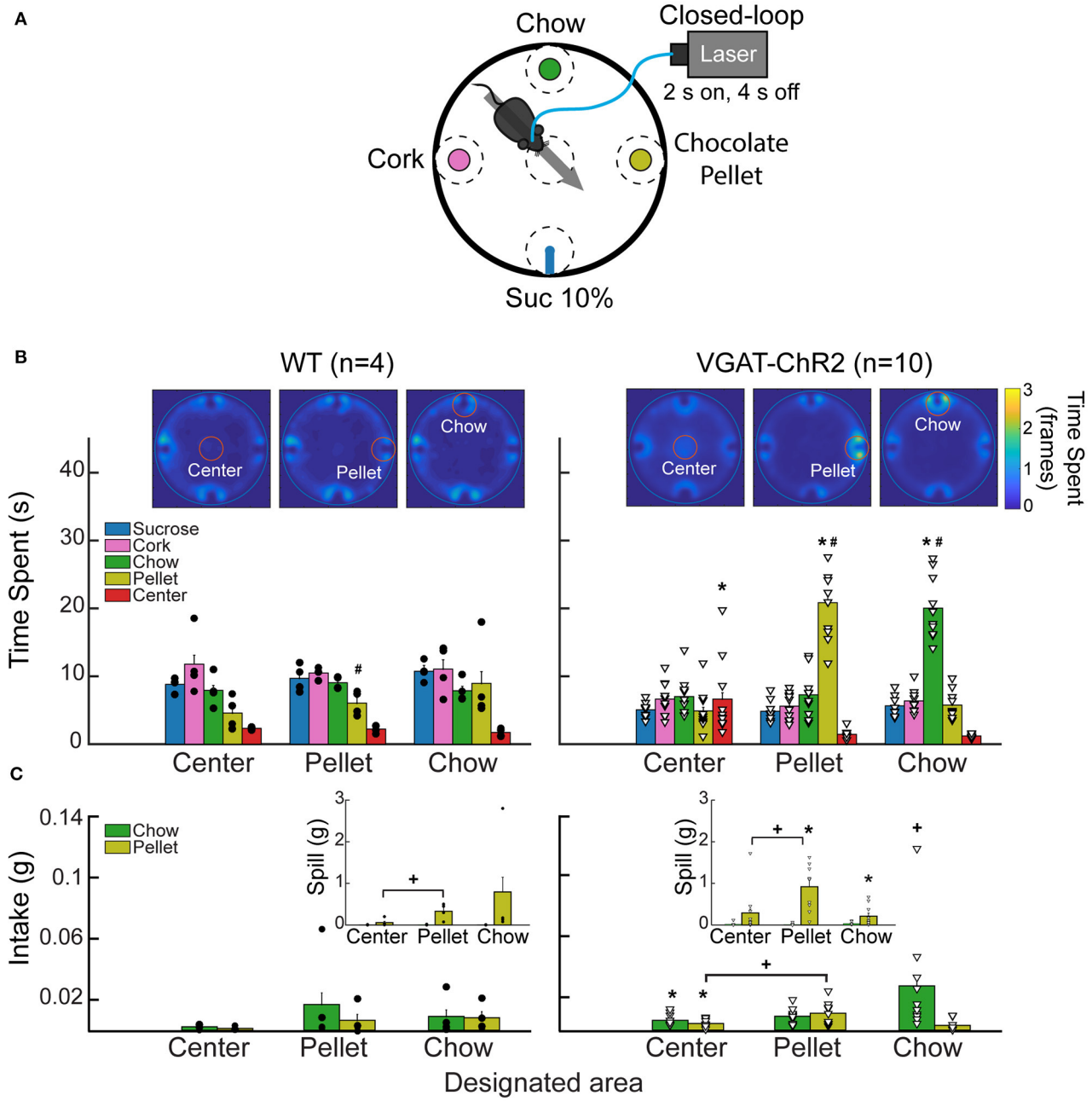

FIGURE 9 | Stimulation of LHA^{Vgat+} neurons is rewarding and biases the approach toward the nearest stimulus. **(A)** Different stimuli (plates containing cork, chow, chocolate pellets, or a sipper filled with 10% liquid sucrose) were presented simultaneously in a circular arena. In this task, when mice cross a designated area (dashed circles), the laser was turned on (2 s on; 4 s off) in a 40-min session. Thus, a mouse had to leave and re-enter the designated area to receive a new opto-self-stimulation. Only one designated area was used per session, and it remained in the same position for up to three or four consecutive sessions. **(B)** Heatmap and time spent from a representative WT (left panel) and VGAT-ChR2 mice (right panel), when the designated area was either the center, the pellet, or the chow (see red circles for the currently designated zone). The color bar indicates the number of frames the subject was detected in a given pixel; higher values indicate it remained in the same place for a longer time. *Below*, bar graphs depict the time spent in seconds exploring the designated area (within a radius of 5 cm). Each dot and triangle represent a single individual. Though mice normally avoid exploring the center of an open field, opto-self-stimulation in the center zone increased the time transgenic mice spent exploring it, compared with WT. Transgenic mice spent more time exploring the chocolate pellets and the chow food when they were in the designated zones. **(C)** Intake of chocolate pellet and chow. Activation of LHA^{Vgat+} neurons in the center zone increased chocolate pellets and chow consumption compared with the WT. *Inset*: Spill from chocolate pellets and chow. *Indicates statistically significant difference ($p < 0.05$) from the WT. $^{+}p < 0.05$ shows a significant increase in intake and spill during the session that a designated area was opto-self-stimulated relative to the sessions where the center was opto-self-stimulated. Unpaired Student's *t*-test. $^{\#}p < 0.01$ indicates a significant difference between designated area opto-stimulated and the other open field areas. One-way ANOVA followed by the Holm–Sidak test. See **Supplementary Video 5**.

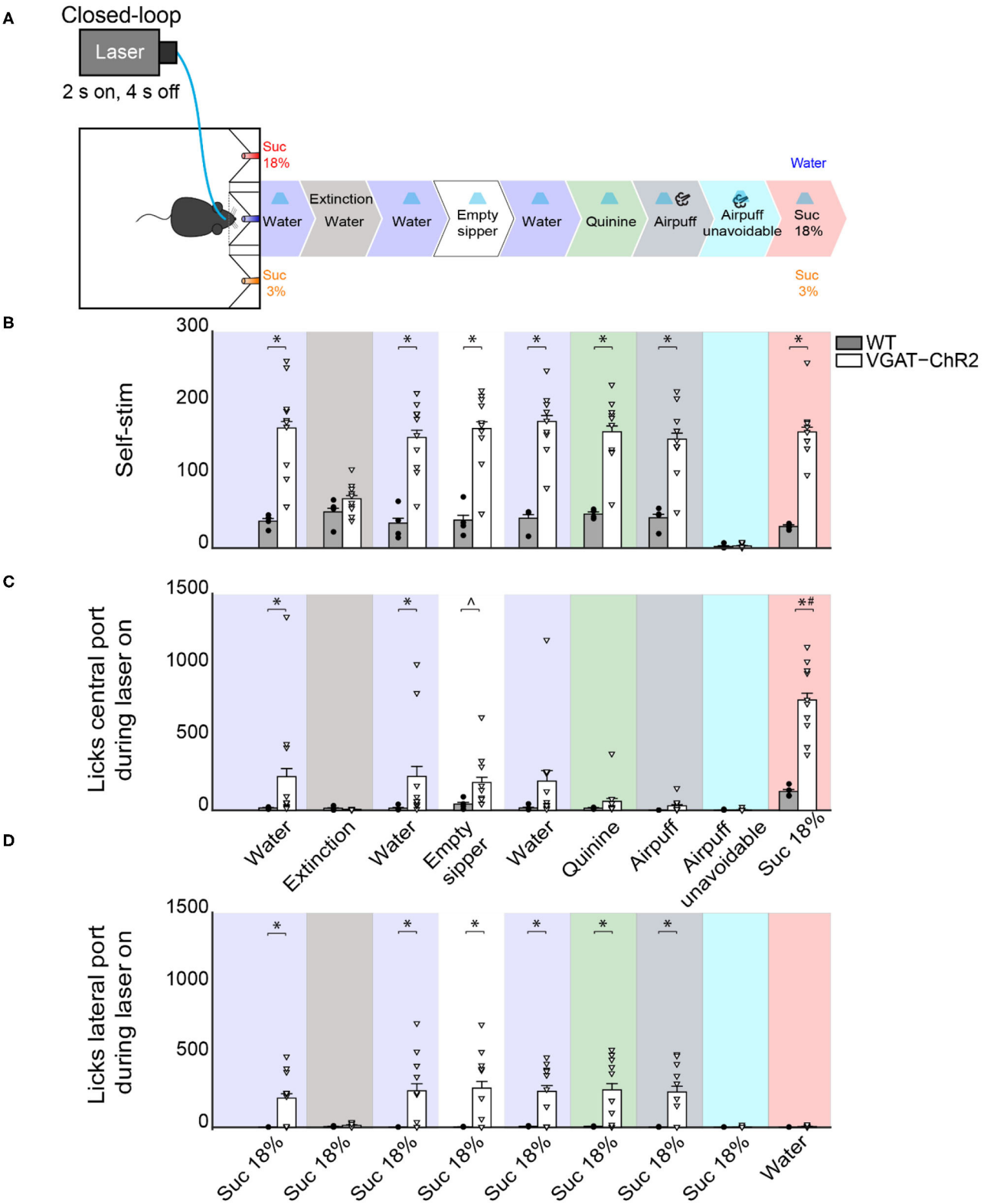

FIGURE 10 | Activating LHA^{Vgat+} neurons does not induce the intake of a bitter tastant, nor an unavoidable aversive stimulus, but it increases sucrose consumption. **(A)** Schematic of behavioral setup showing stimuli delivered at the central port. The water stimulus in the central port was replaced by an empty sipper, quinine, or airpuff. In all phases, head entry in the central port triggered the laser, except in the airpuff unavoidable condition, where the first lick delivered both the laser and the

(Continued)

FIGURE 10 | airpuff. Finally, the airpuff in the central port was replaced by sucrose 18%. **(B)** The number of opto-self-stimulations given for each stimulus. The VGAT-ChR2 mice performed more self-stimulations than WT, except during extinction sessions and when the airpuff was unavoidable. **(C)** The number of licks given to the central port. The licks in the central port decreased when an aversive stimulus was present, such as quinine or airpuffs. In contrast, a non-edible stimulus such as an empty sipper elicited more licks from VGAT-ChR2 mice ($p < 0.05$). Moreover, when sucrose 18% was in the central port, the VGAT-ChR2 group increased its consumption substantially compared with the WT. **(D)** The number of licks in the lateral port containing sucrose 18% during opto-self-stimulation. The intake of the lateral port of sucrose 3% is not shown because it was neglectable. Each dot and triangle represent a single individual. ^Denotes statistically significant difference ($p < 0.0001$) from WT. Unpaired Student's *t*-test. *$p < 0.05$ relative to the WT group. #$p < 0.05$ between sucrose 18% from other stimuli delivered at the central port. Two-way ANOVA followed by the Holm–Sidak test.

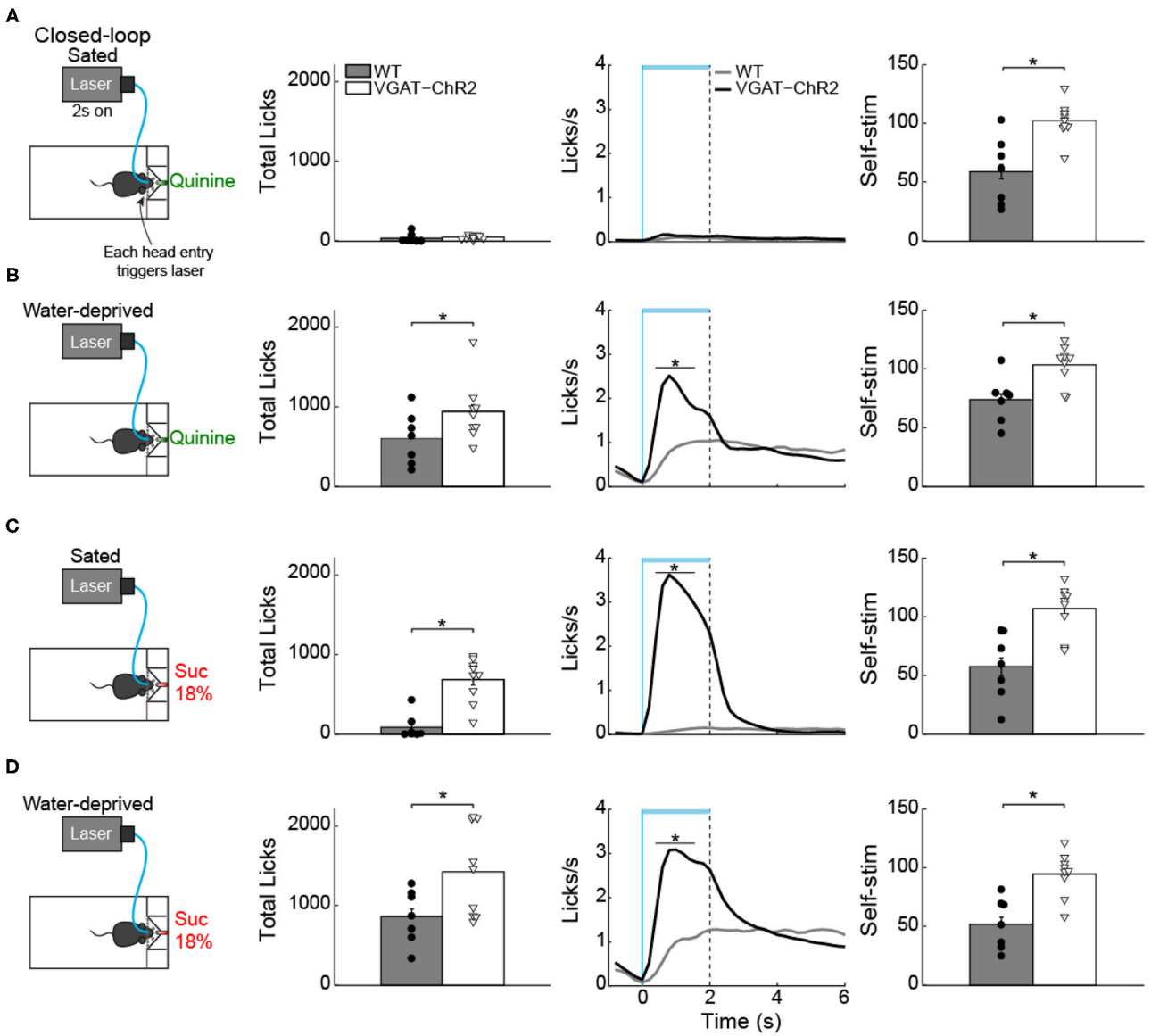

FIGURE 11 | Water deprivation gates a time window where activation of LHA GABAergic neurons increases quinine intake. **(A)** Sated mice had free access to one sipper filled with quinine. The laser was turned "on" in a closed-loop protocol (*left panel*). Each head entry triggers 2-s laser "on" followed by a 4-s time out with no-laser. In sated VGAT-ChR2 mice, activation of these neurons did not increase quinine intake (*central panel* shows the PSTH of the lick rates aligned to laser onset) (time = 0 s). Although sated transgenic mice do not lick for quinine, they continued opto-self-stimulating (*right panel*). **(B)** Water-deprived transgenic mice consumed more quinine than WT mice (*central panel*) when the laser was turned on (horizontal blue line). **(C,D)** Total licks, PSTH of the lick rate (*central panels*), and number of opto-self-stimulations of 18% sucrose during sated and water deprivation conditions (*right panel*). The horizontal blue line indicates opto-self-stimulation window. The vertical blue line indicates the laser onset, and the black dashed line the laser offset. *$p < 0.01$ indicates significant differences compared with WT mice according to an unpaired Student's *t*-test.

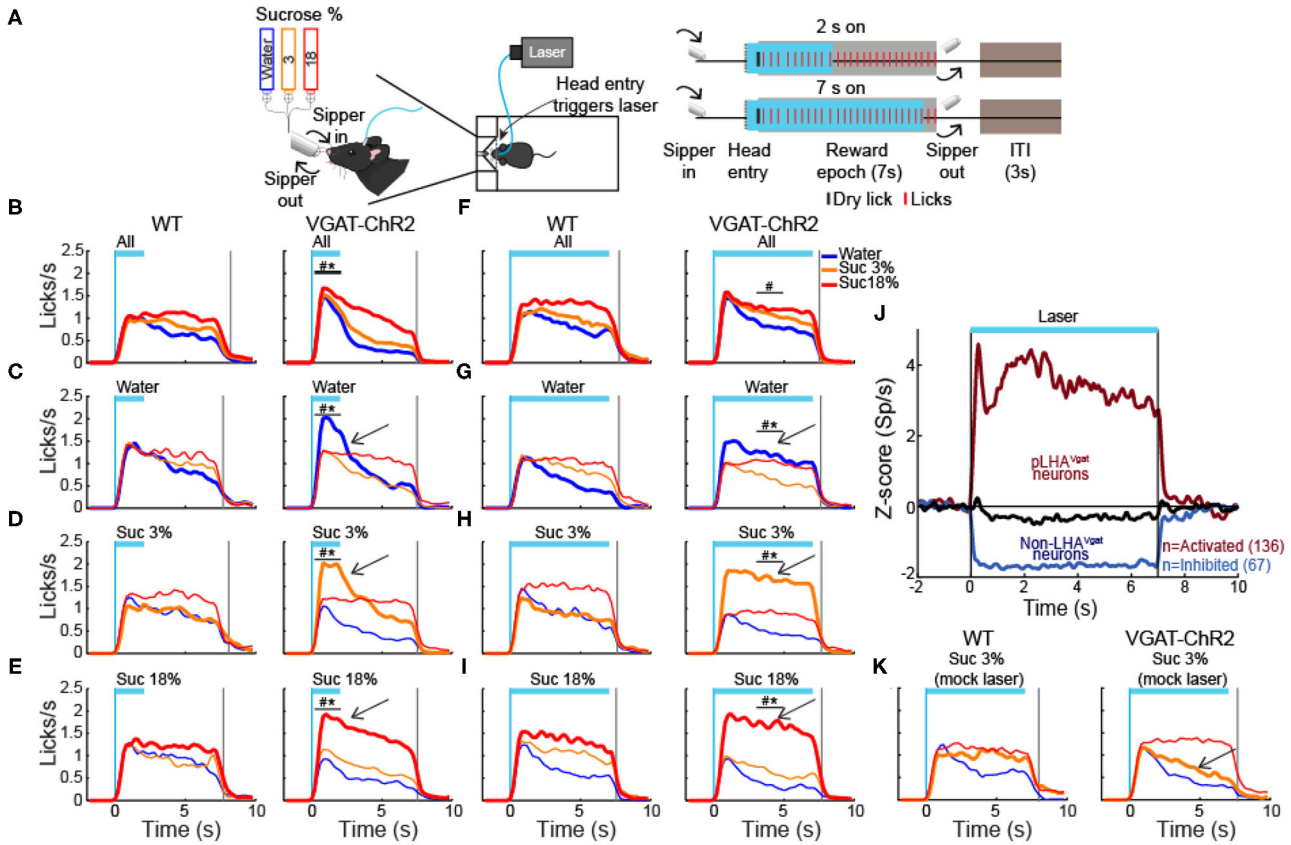

FIGURE 12 | Activation of LHA GABA neurons enhances water and sucrose's palatability. **(A)** Closed-loop stimulation during the brief access test. *Left panel*, behavioral setup. The box contained a sipper that delivered an ~2 μl drop of either water, sucrose 3%, or 18% per lick. *Right panel*, schematics of the structure of a trial. A head entry in the port (dashed vertical line) triggered opto-self-stimulation, at 50 Hz, in some sessions for 2 s and others for 7 s (blue rectangles). The reward epoch begins with the first dry lick on the sipper (black tick) and always lasts 7 s (gray rectangles). During the reward epoch, a drop of tastant was delivered in each lick (red marks). At the end of the reward epoch, the sipper was retracted, and an intertrial interval (ITI) of 3 s began. **(B–E)** Data of closed loop for 2 s stimulation in the reward epoch. PSTH of lick rate of WT (left panel) and VGAT-ChR2 mice (*right panel*) aligned (time = 0 s) to laser onset. Opto-self-stimulation was delivered during all trials **(B)** or during only water trials (**C**, see arrow), or sucrose 3% **(D)**, or 18% **(E)**. **(F–I)** Licking responses but during 7 s opto-self-stimulation. Same conventions as in **(B–E)**. The vertical blue line indicates laser onset and the gray line the end of the reward epoch. The horizontal blue line indicates opto-self-stimulation window. *Indicates significant difference ($p < 0.05$) from the WT group. #$p < 0.05$ among the stimuli. Two-way ANOVA followed by the Holm–Sidak test. **(J)** Normalized *Z* score population activity of 284 neurons recorded in LHA in VGAT-ChR2 mice ($n = 3$). The laser was turned on for 7 s at 50 Hz. Neuronal responses were aligned to laser onset (time = 0 s). Red and blue colors indicate activated or inhibited laser-evoked responses, relative to baseline (−1 to 0 s). Black trace illustrates neurons unmodulated by the laser. **(K)** Mock laser stimulation did not affect palatability responses. PSTH of licking responses, opto-self-stimulation was delivered along with sucrose 3% trials during 7 s (arrow). Note that both groups increased the lick rate as a function of palatability; the same conventions as in **(B–E)**. To elicit mock laser stimulation, mice were connected to a mock fiber optic (with no-laser connected), whereas the real fiber was glued outside the mice's head to emit blue light.

When Sucrose Is Available, Activation of LHA^{Vgat+} Neurons Neither Promotes Intake of an Aversive Bitter Tastant nor Tolerance of Punishment, but It Further Increases Sucrose Consumption

To explore whether the "stimulus proximity effect" was also applied to aversive stimuli, we replaced the central stimulus (water) with aversive stimuli, including quinine (a tastant that humans experience as bitter taste) or airpuffs (**Figure 10A**). Upon quinine presentation, the number of licks given in the central port sharply decreased (**Figure 10C**, green), but transgenic mice continued to self-stimulate and go to the lateral port to lick for sucrose 18% (**Figure 10D**, green). We obtained similar results to those in quinine stimulation during the airpuff delivery phase (**Figure 10D**, dark gray). Under this condition, transgenic mice completely stopped self-stimulation (**Figure 10B**, cyan) and aborted 18% sucrose intake from the lateral port (**Figure 10D**, cyan). These results suggest that, in sated mice, LHA^{Vgat+} neurons did not induce quinine intake nor increase tolerance to airpuffs.

Finally, we explored whether proximity to the most palatable tastant further facilitated its overconsumption. Thus, we exchanged the position of water and sucrose 18%. When sucrose 18% was delivered in the central port, transgenic mice greatly overconsumed it (**Figure 10C**, pink). The intake of sucrose 18%

was higher than for all the other tastants tested previously ($p < 0.0001$). These results collectively suggest that activation of LHA^{Vgat+} neurons is rewarding and promotes increased consumption of the nearest stimulus even if it is not the most palatable (e.g., water and empty sipper). If the nearest stimulus happens to be the most palatable (i.e., sucrose 18%), then LHA GABA neurons further facilitated its consumption.

LHA GABA Neurons Increased Quinine Intake but Only in Water-Deprived Mice

Having demonstrated that in the presence of sucrose, activation of these neurons failed to increase quinine intake (**Figure 10C**, green), with a new group of naive mice, we then explored whether LHA^{Vgat+} neurons could induce quinine intake when it was the only option. As expected, in sated mice, we found that activation of LHA^{Vgat+} neurons did not affect quinine intake compared with WT (**Figure 11A**; unpaired Student's *t*-test, $t_{(46)} = 0.9925$, $p = 0.3262$). Surprisingly, it promoted a higher quinine intake when transgenic mice were water-deprived (**Figure 11B**; unpaired Student's *t*-test, $t_{(46)} = 2.958$, $p < 0.01$), specifically during the photostimulation window (**Figure 11B**; unpaired Student's *t*-test, $t_{(46)} = 4.473$, $p < 0.0001$), suggesting that activation of these neurons is sufficient to increase the acceptance of bitter tastants but only during water deprivation. In contrast, we found that regardless of homeostatic needs, activation of these neurons increased sucrose 18% intake relative to WT mice (**Figures 11C,D**; unpaired Student's *t*-test, $t_{(30)} = 6.933$, $p < 0.0001$; unpaired Student's *t*-test, $t_{(30)} = 3.183$, $p < 0.01$).

Activation of LHA^{Vgat+} Neurons Enhances Palatability

We next explored whether, at equal stimulus distance, these neurons could enhance palatability responses. To do this, in a new group of water-deprived mice, we employed a brief access test again. In this task, we delivered gustatory stimuli water, sucrose 3%, and sucrose 18% from the same sipper tube, but in different trials. **Figure 12A** displays the trial's structure (same conventions as in **Figure 2**). We found that both groups increased their licking rate as a function of sucrose's concentration, reflecting its palatability (**Figure 12B**; two-way ANOVA main effect of tastants, $F_{(2,174)} = 9.101$, $p < 0.001$). However, during the 2 s of laser stimulation, the VGAT-ChR2 mice exhibited a greater lick rate for all three tastants. After the laser was turned "off," these mice abruptly stopped licking for water and sucrose 3% compared with the WT group (**Figure 12B**, *right panel*; two-way ANOVA group by tastants interaction, $F_{(2,174)} = 5.293$, $p < 0.01$). Moreover, when stimulation was paired with water trials, transgenic mice selectively increased their lick rate to water relative to WT (**Figure 12C**, blue line and arrow; two-way ANOVA group by tastants interaction, $F_{(2,84)} = 6.009$, $p < 0.01$), even surpassing licking responses evoked by the most palatable sucrose 18%. A similar enhancement of oromotor responses was observed by pairing sucrose 3% trials with LHA^{Vgat+} opto-self-stimulation (**Figure 12D**, orange; two-way ANOVA group by tastants interaction, $F_{(2,84)} = 16.72$, $p < 0.0001$). Likewise, the laser-bound feeding (licking rate) was strongest when sucrose 18% was paired with the optogenetic stimulation (**Figure 12E**, red, see arrow; two-way ANOVA group by tastants interaction, $F_{(2,84)} = 16.49$, $p < 0.0001$).

Finally, we show that palatability responses could be artificially extended as long as LHA^{Vgat+} neurons were continuously activated. For this, we photostimulated them for up to 7 s. We observed a similar enhancement pattern, maintained for the duration of opto-stimulation (see **Figures 12F–I**, arrows; all trials: two-way ANOVA main effect of tastants, $F_{(2,114)} = 12.53$, $p < 0.0001$; water trials: two-way ANOVA group by tastants interaction, $F_{(2,84)} = 9.850$, $p < 0.001$; sucrose 3% trials: two-way ANOVA group by tastants interaction, $F_{(2,84)} = 33.47$, $p < 0.0001$; sucrose 18% trials: two-way ANOVA group by tastants interaction, $F_{(2,84)} = 8.360$, $p < 0.001$), suggesting that LHA^{Vgat+} neurons can adjust the enhancement of oromotor palatability responses by simply sustaining its neuronal activity. We verified that using optrode recordings, 7-s optogenetic stimulation produced sustained LHA^{Vgat+} neuronal responses (**Figure 12J**). Moreover, transgenic mice did not merely use the light as a cue to guide behavior since laser stimulation with a mock optical fiber failed to increase licking (**Figure 12K**; two-way ANOVA group by tastants interaction, $F_{(2,54)} = 1.619$, $p = 0.207$). In sum, our data demonstrate that activation of LHA^{Vgat+} neurons triggers a reinforcing signal that amplifies the positive hedonic value of proximal stimuli, promoting overconsumption.

DISCUSSION

LHA has historically been viewed as a critical center for feeding (Anand and Brobeck, 1951; Delgado and Anand, 1953; Teitelbaum and Epstein, 1962), although it also processes sucrose's palatability-related information (Norgren, 1970; Ono et al., 1986; Li et al., 2013). In addition to nutritive value, sucrose's palatability is the affective or hedonic attribute of sweetness that determines whether to like it or not (Grill and Berridge, 1985). Despite the importance of palatability to promote overconsumption, the specific LHA cell type(s) identity involved in processing sucrose's palatability has remained elusive. Our results demonstrated that a subpopulation of LHA^{Vgat+} GABAergic neurons encodes sucrose's palatability by exhibiting two opposite modulatory patterns, either correlating positively or negatively with the palatability index, with a bias toward a positive correlation. Furthermore, opto-stimulation of LHA^{Vgat+} cell somas promoted the approach and intake of the most palatable tastant available. In contrast, opto-self-stimulation promoted increased liquid intake of the less attractive and proximal stimuli, despite having more palatable but distal tastants available. These findings show that LHA^{Vgat+} neurons compute and/or combine, at least, two types of information: one related to stimulus proximity and the other to palatability that results in enhancing stimulus saliency (Nieh et al., 2016). Experiments with solid food also unveiled that transgenic mice spent more time near the most palatable food available. More importantly, among the many other functions already ascribed to these neurons [see below and Nieh et al. (2016)], our data uncovered a new

function of LHA^{Vgat+} neurons as physiological potentiators of sucrose-induced oromotor palatability responses.

Previous studies have shown that the LHA^{Vgat+} population contains many subpopulations with different functional responses, with at least one ensemble responding to appetitive (approach) and others to consummatory behaviors (Jennings et al., 2015). Furthermore, activation of these neurons is rewarding, induces voracious eating (Jennings et al., 2015; Navarro et al., 2016), and promotes interaction of the nearest stimulus (either objects or other mice) (Nieh et al., 2016), suggesting that they play a role in multiple motivated behaviors. However, it is also known that LHA connects and receives direct inputs from multiple cortical and subcortical gustatory regions (Simerly, 2004; Berthoud and Münzberg, 2011), and some electrophysiological studies report that LHA neurons respond to gustatory stimuli—in particular to tastant palatability (Norgren, 1970; Ono et al., 1986; Schwartzbaum, 1988; Yamamoto et al., 1989; Karádi et al., 1992). As noted in rodents, palatability is operationally defined as the enhancement of hedonically positive oromotor responses induced by stimulating the tongue with ascending sucrose concentrations (Berridge and Grill, 1983; Spector et al., 1998; Villavicencio et al., 2018). Specifically, these hedonically positive oromotor responses may include an increase in the lick rate or the bout size. In agreement with this definition, we found that a subpopulation of LHA palatability-related neurons tracked licking oromotor-related responses by increasing or decreasing their activity in a sucrose concentration-dependent manner. Within a session, LHA neurons tracked the sucrose's palatability rather than satiety or hunger signals. We showed that these LHA^{Vgat+} neurons could function as enhancers of sucrose's palatability. Optogenetic activation of these neurons can also enhance water's palatability if it is the nearest stimulus. We found an increased lick rate for water during these neurons' activation as if the animal were sampling a high sucrose concentration. Moreover, their activation promotes the intake of liquid sucrose (or solid granulated sugar cube). These neurons also increased the consumption of other more palatable stimuli like high-fat pellets (see **Supplementary Figure 5**; **Supplementary Video 2**), similar to the other GABAergic neurons but in the zona incerta (Zhang and van den Pol, 2017). Thus, our data demonstrate that activation of LHA GABAergic drives the intake of the most palatable stimulus available in the animal's environment.

Although activation of LHA^{Vgat+} promotes substantial feeding behavior, it has become clear that LHA^{Vgat+} neurons are not directly involved in evoking hunger (Burnett et al., 2016; Navarro et al., 2016; Marino et al., 2020), as AgRP neurons in the arcuate do (Chen et al., 2016). In this regard, and unlike AgRP neurons, prestimulation of LHA GABAergic neurons did not trigger a sustained sucrose intake in the absence of continuous activation (**Supplementary Figure 4**). Thus, to induce a consummatory behavior, these neurons are required to remain active. Moreover, and in agreement with these findings, we found that the intake induced by LHA^{Vgat+} neurons conveys a positive valence signal that combines both stimulus proximity and palatability-related information. Thus, these neurons enhance the saliency of nearby hedonically positive stimuli, whether those stimuli are sapid chemicals, as we show, or social cues, as in the approach behavior toward juvenile or female intruders and new objects (Nieh et al., 2016).

It is important to highlight that opto-self-activation of LHA^{Vgat+} neurons resembles many hallmark behaviors evoked by LHA electrical stimulation. In particular, our results could shed some light on why, at low-intensity electrical currents, lever pressing to deliver ICSs only occurs if food (or sucrose) is in close proximity (Mendelson, 1967; Coons and Cruce, 1968; Valenstein et al., 1968; Valenstein and Phillips, 1970). Consistent with its role in enhancing sucrose's palatability, a subpopulation of GABAergic neurons could indirectly explain why sweet tastants further potentiate the rate of LHA electrical ICSs (Poschel, 1968). We concluded that a subpopulation of LHA^{Vgat+} neurons could account for many, if not all, of these electrically induced phenomena. Also, we found differences between unspecific LHA stimulation and our targeted LHA^{Vgat+} stimulation. Unlike electrical LHA stimulation, we found that the laser-bound feeding was observed in all tested VGAT-ChR2 mice ($n = 31$, **Figures 4–12**). In contrast, to the high variability found in rats exhibiting LHA electrically induced feeding, one study reported that only 12 of 34 rats showed stimulus-bound feeding (Valenstein and Cox, 1970). Similarly, a large variability was observed when unspecific bulk optogenetic stimulation activated *all* cell types found in LHA, simultaneously (Urstadt and Berridge, 2020). These studies reported that after repeated LHA stimulation (either electrically or with optogenetics), some subjects switched from exhibiting stimulus-bound feeding to only self-stimulating, suggesting that these two processes were flexible and not correlated (Gigante et al., 2016; Urstadt and Berridge, 2020). In contrast, we found that repeated stimulation of LHA^{Vgat+} neurons increases laser-induced feeding (licking). Likewise, the correlation between optogenetic self-stimulation and laser-bound feeding increases over stimulation days (**Figure 8**). That is, the more the animals self-stimulated, the stronger the evoked laser-bound licking was. Thus, LHA^{Vgat+} neurons are the common neural substrate for evoking both feeding and reward, though it was recently shown that they do it by using two projection pathways: reward via a VTA projection and feeding via the peri-locus coeruleus nuclei (Marino et al., 2020).

Given that LHA is involved in reward and aversion (Ono et al., 1986), we next tested whether LHA^{Vgat+} neurons could promote bitter tastants' intake. We found that opto-stimulation of LHA^{Vgat+} neurons failed to promote quinine intake, a bitter tastant, or tolerance of an aversive airpuff when sucrose was also available. Thus, these neurons play a minimal role in increasing the preference for a proximal but aversive stimulus over distal sucrose. Furthermore, in sated mice and using a single bottle test, these neurons also failed to increase quinine intake. Unexpectedly, during water deprivation, a copious quinine consumption was observed. These results demonstrate that the consummatory drive induced by the activation of GABAergic neurons largely depends on the palatability of the stimulus and the animal's internal state. These results agree with previous findings that chemogenetic inhibition of LHA^{Vgat+} neurons did not alter the quinine rejection responses. Thus, in sated mice, these neurons are not necessary to express hedonically negative responses induced by bitter tastants (Fu et al., 2019).

However, they did not explore their sufficiency. Our results showed that water deprivation temporarily gated LHA^{Vgat+} neurons to promote quinine intake and further demonstrated that their activation is sufficient to increase acceptance of an aversive tastant during water deprivation.

The LHA comprises multiple heterogeneous and overlapping populations based on the expression of genetic markers for neuropeptides, receptors, and proteins involved in the synthesis and vesicular packaging of neurotransmitters (Bonnavion et al., 2016; Mickelsen et al., 2019). Thus, the LHA^{Vgat+} population can be further subdivided into GABA neurons expressing leptin receptor (LepRb) (Leinninger et al., 2009; Mickelsen et al., 2019), or the neuropeptide galanin (Gal), or neurotensin (Nts) (Qualls-Creekmore et al., 2017; Kurt et al., 2019; Mickelsen et al., 2019). It is known that the activation of LHA GABA-LepRb is rewarding (Giardino et al., 2018), similar to LHA^{Vgat+} neurons. Likewise, LHA GABA-Gal-expressing neurons are related to food reward behavior, but unlike LHA^{Vgat+}, these neurons do not promote food consumption (Qualls-Creekmore et al., 2017). From these subpopulations, only the LHA GABA-Nts neurons recapitulate some (but not all) of the behavioral effects reported here. Unlike LHA^{Vgat+} neurons, a previous study found that LHA GABA-Nts neurons do not increase chow intake. Instead, they promote the liquid intake of palatable tastants (water, NaCl, and sucrose). In sated mice, chemogenetic activation of GABA-Nts increased the intake of bitter quinine, albeit with lower magnitude, when it was the only liquid available to eat with chow food, a marked contrast to our findings with broad LHA GABAergic neurons' activation, although they did not explore quinine intake in the absence of chow food or water-deprived mice. However, they performed a two-bottle test and found that GABA-Nts neurons increased water intake over quinine, suggesting that activation of these neurons is not involved in driving mice's preference for bitter tastants, similar to what we found for the LHA^{Vgat+} population. Also, similar to our findings, activation of LHA GABA-Nts induced water drinking, which was further facilitated if the solution was sucrose (Kurt et al., 2019). Thus, it will be interesting to determine the role that LHA GABA-Nts neurons play in encoding and potentiating sucrose's palatability. It follows that the LHA contains nested functions encoded in each subpopulation (or cell types) that are then recruited selectively to exert a more refined control over feeding and reward.

A caveat of this study is that we employed bacterial artificial chromosomes (BAC) transgenic strain mouse, VGAT-ChR2, that constitutively expressed ChR2 in GABAergic neurons expressing the gene for the VGAT (Zhao et al., 2011). In this model, we cannot rule out the unintended activation of GABAergic terminals from distal regions (Thoeni et al., 2020), which also occurs with classic electrical stimulation. Nevertheless, in the more specific transgenic model, the Vgat-ires-Cre mice, a similar feeding-bound behavior for chow food has been found (Marino et al., 2020), as we have shown here (see chow in **Figures 9B,C**; **Supplementary Video 5**). Moreover, the VGAT-ChR2 transgenic model affords important advantages such as a consistent expression of ChR2 (Zeng and Madisen, 2012) and heritable transgene expression patterns across experimental cohorts (Ting and Feng, 2013), which increased reproducibility across animals tested. It is also a more selective model to characterize GABAergic neurons (excluding the glutamatergic component) and their effects recapitulating classical effects observed with electrical LHA stimulation (Delgado and Anand, 1953; Phillips and Mogenson, 1968).

In summary, here, we found that at least a subpopulation of LHA^{Vgat+} neurons could be an important hub that links stimulus proximity and palatability-related information to potentiate the palatability of nearby energy-rich foods, especially those containing sucrose.

DATA AVAILABILITY STATEMENT

The datasets presented in this article are available on request to the corresponding author. Requests to access the datasets should be directed to Ranier Gutierrez, ranier@cinvestav.mx.

ETHICS STATEMENT

The animal study was reviewed and approved by CINVESTAV Animal Care and Use Committee.

AUTHOR CONTRIBUTIONS

AG, AC, JL-I, and RG designed the research. AG, AC, JL-I, LP-S, and ML performed the research. MV contributed unpublished analytic tools. AG, AC, JL-I, and RG analyzed the data, AG and RG wrote the paper. All authors reviewed and approved the manuscript for publication.

FUNDING

This project was supported in part by Productos Medix 3247, Cátedra Marcos Moshinky, fundación Miguel Alemán Valdés, CONACyT Grants Fronteras de la Ciencia 63, and Problemas Nacionales 464 (to RG).

ACKNOWLEDGMENTS

Aketzali Garcia had a CONACyT doctoral fellowship, and data in this work is part of her doctoral dissertation in the Posgrado en Ciencias Biomédicas of the Universidad Nacional Autónoma de México. We want to thank Martin Vignovich and Professor Sidney A. Simon for helpful comments in an early version of this manuscript. We thank Mario Gil Moreno for building homemade optrode, and the valuable help of Juan de Dios Rodriguez-Callejas during the acquisition of confocal microscope images is also acknowledged. We also thank Ricardo Gaxiola, Victor Manuel García Gómez, and Fabiola Hernandez Olvera for invaluable animal care. This manuscript has been released as a preprint at Biorxiv (Garcia et al., 2020).

SUPPLEMENTARY MATERIAL

The Supplementary Material for this article can be found online at: https://www.frontiersin.org/articles/10.3389/fnins.2020.608047/full#supplementary-material

REFERENCES

Anand, B. K., and Brobeck, J. R. (1951). Localization of a "feeding center" in the hypothalamus of the rat. *Proc. Soc. Exp. Biol. Med.* 77, 323–324.

Berridge, K. C., and Grill, H. J. (1983). Alternating ingestive and aversive consummatory responses suggest a two-dimensional analysis of palatability in rats. *Behav. Neurosci.* 97, 563–573.

Berridge, K. C., and Kringelbach, M. L. (2008). Affective neuroscience of pleasure: reward in humans and animals. *Psychopharmacology* 199, 457–480. doi: 10.1007/s00213-008-1099-6

Berridge, K. C., and Valenstein, E. S. (1991). What psychological process mediates feeding evoked by electrical stimulation of the lateral hypothalamus? *Behav. Neurosci.* 105, 3–14. doi: 10.1037//0735-7044.105.1.3

Berthoud, H.-R., and Münzberg, H. (2011). The lateral hypothalamus as integrator of metabolic and environmental needs: from electrical self-stimulation to opto-genetics. *Physiol. Behav.* 104, 29–39. doi: 10.1016/j.physbeh.2011.04.051

Bonnavion, P., Mickelsen, L. E., Fujita, A., de Lecea, L., and Jackson, A. C. (2016). Hubs and spokes of the lateral hypothalamus: cell types, circuits and behaviour. *J. Physiol.* 594, 6443–6462. doi: 10.1113/JP271946

Buonomano, D. V. (2003). Timing of neural responses in cortical organotypic slices. *Proc. Natl. Acad. Sci. U.S.A.* 100, 4897–4902. doi: 10.1073/pnas.0736909100

Burnett, C. J., Li, C., Webber, E., Tsaousidou, E., Xue, S. Y., Brüning, J. C., et al. (2016). Hunger-driven motivational state competition. *Neuron* 92, 187–201. doi: 10.1016/j.neuron.2016.08.032

Chen, Y., Lin, Y.-C., Zimmerman, C. A., Essner, R. A., and Knight, Z. A. (2016). Hunger neurons drive feeding through a sustained, positive reinforcement signal. *Elife* 5:e18640. doi: 10.7554/eLife.18640

Coons, E. E., and Cruce, J. A. (1968). Lateral hypothalamus: food current intensity in maintaining self-stimulation of hunger. *Science* 159, 1117–1119. doi: 10.1126/science.159.3819.1117

Delgado, J. M., and Anand, B. K. (1953). Increase of food intake induced by electrical stimulation of the lateral hypothalamus. *Am. J. Physiol.* 172, 162–168. doi: 10.1152/ajplegacy.1952.172.1.162

Ferssiwi, A., Cardo, B., and Velley, L. (1987). Gustatory preference-aversion thresholds are increased by ibotenic acid lesion of the lateral hypothalamus in the rat. *Brain Res.* 437, 142–150. doi: 10.1016/0006-8993(87)91535-6

Fu, O., Iwai, Y., Narukawa, M., Ishikawa, A. W., Ishii, K. K., Murata, K., et al. (2019). Hypothalamic neuronal circuits regulating hunger-induced taste modification. *Nat. Commun.* 10:4560. doi: 10.1038/s41467-019-12478-x

Garcia, A., Coss, A., Luis-Islas, J., Puron-Sierra, L., Luna, M., Villavicencio, M., et al. (2020). Lateral Hypothalamic GABAergic neurons encode and potentiate sucrose's palatability. *bioRxiv [Preprint]*. doi: 10.1101/2020.06.30.180646

Giardino, W. J., Eban-Rothschild, A., Christoffel, D. J., Li, S.-B., Malenka, R. C., and de Lecea, L. (2018). Parallel circuits from the bed nuclei of stria terminalis to the lateral hypothalamus drive opposing emotional states. *Nat. Neurosci.* 21, 1084–1095. doi: 10.1038/s41593-018-0198-x

Gigante, E. D., Benaliouad, F., Zamora-Olivencia, V., and Wise, R. A. (2016). Optogenetic activation of a lateral hypothalamic-ventral tegmental drive-reward pathway. *PLoS ONE* 11:e0158885. doi: 10.1371/journal.pone.0158885

Glendinning, J. I., Chyou, S., Lin, I., Onishi, M., Patel, P., and Zheng, K. H. (2005). Initial licking responses of mice to sweeteners: effects of tas1r3 polymorphisms. *Chem. Senses* 30, 601–614. doi: 10.1093/chemse/bji054

Grill, H. J., and Berridge, K. C. (1985). "Taste reactivity as a measure of the neural control of palatability," in *Progress in Psychobiology and Physiological Psychology* (Orlando, FL: Academic Press), 1–54.

Gutierrez, R., Carmena, J. M., Nicolelis, M. A. L., and Simon, S. A. (2006). Orbitofrontal ensemble activity monitors licking and distinguishes among natural rewards. *J. Neurophysiol.* 95, 119–133. doi: 10.1152/jn.00467.2005

Gutierrez, R., Fonseca, E., and Simon, S. A. (2020). The neuroscience of sugars in taste, gut-reward, feeding circuits, and obesity. *Cell. Mol. Life Sci.* 77, 3469–3502. doi: 10.1007/s00018-020-03458-2

Gutierrez, R., Simon, S. A., and Nicolelis, M. A. (2010). Licking-induced synchrony in the taste-reward circuit improves cue discrimination during learning. *J. Neurosci.* 30, 287–303. doi: 10.1523/JNEUROSCI.0855-09.2010

Jennings, J. H., Rizzi, G., Stamatakis, A. M., Ung, R. L., and Stuber, G. D. (2013). The inhibitory circuit architecture of the lateral hypothalamus orchestrates feeding. *Science* 341, 1517–1521. doi: 10.1126/science.1241812

Jennings, J. H., Ung, R. L., Resendez, S. L., Stamatakis, A. M., Taylor, J. G., Huang, J., et al. (2015). Visualizing hypothalamic network dynamics for appetitive and consummatory behaviors. *Cell* 160, 516–527. doi: 10.1016/j.cell.2014.12.026

Karádi, Z., Oomura, Y., Nishino, H., Scott, T. R., Lénárd, L., and Aou, S. (1992). Responses of lateral hypothalamic glucose-sensitive and glucose-insensitive neurons to chemical stimuli in behaving rhesus monkeys. *J. Neurophysiol.* 67, 389–400. doi: 10.1152/jn.1992.67.2.389

Kurt, G., Woodworth, H. L., Fowler, S., Bugescu, R., and Leinninger, G. M. (2019). Activation of lateral hypothalamic area neurotensin-expressing neurons promotes drinking. *Neuropharmacology* 154, 13–21. doi: 10.1016/j.neuropharm.2018.09.038

Leinninger, G. M., Jo, Y.-H., Leshan, R. L., Louis, G. W., Yang, H., Barrera, J. G., et al. (2009). Leptin acts via leptin receptor-expressing lateral hypothalamic neurons to modulate the mesolimbic dopamine system and suppress feeding. *Cell Metab.* 10, 89–98. doi: 10.1016/j.cmet.2009.06.011

Li, J. X., Yoshida, T., Monk, K. J., and Katz, D. B. (2013). Lateral hypothalamus contains two types of palatability-related taste responses with distinct dynamics. *J. Neurosci.* 33, 9462–9473. doi: 10.1523/JNEUROSCI.3935-12.2013

Marino, R. A. M., McDevitt, R. A., Gantz, S. C., Shen, H., Pignatelli, M., Xin, W., et al. (2020). Control of food approach and eating by a GABAergic projection from lateral hypothalamus to dorsal pons. *Proc. Natl. Acad. Sci. U.S.A.* doi: 10.1073/pnas.1909340117

Mathis, A., Mamidanna, P., Cury, K. M., Abe, T., Murthy, V. N., Mathis, M. W., et al. (2018). DeepLabCut: markerless pose estimation of user-defined body parts with deep learning. *Nat. Neurosci.* 21, 1281–1289. doi: 10.1038/s41593-018-0209-y

Mendelson, J. (1967). Lateral hypothalamic stimulation in satiated rats: the rewarding effects of self-induced drinking. *Science* 157, 1077–1079. doi: 10.1126/science.157.3792.1077

Mickelsen, L. E., Bolisetty, M., Chimileski, B. R., Fujita, A., Beltrami, E. J., Costanzo, J. T., et al. (2019). Single-cell transcriptomic analysis of the lateral hypothalamic area reveals molecularly distinct populations of inhibitory and excitatory neurons. *Nat. Neurosci.* 22, 642–656. doi: 10.1038/s41593-019-0349-8

Mogenson, G. J., and Stevenson, J. A. (1967). Drinking induced by electrical stimulation of the lateral hypothalamus. *Exp. Neurol.* 17, 119–127. doi: 10.1016/0014-4886(67)90139-2

Nath, T., Mathis, A., Chen, A. C., Patel, A., Bethge, M., and Mathis, M. W. (2019). Using DeepLabCut for 3D markerless pose estimation across species and behaviors. *Nat Protoc.* 14, 2152–2176. doi: 10.1038/s41596-019-0176-0

Navarro, M., Olney, J. J., Burnham, N. W., Mazzone, C. M., Lowery-Gionta, E. G., Pleil, K. E., et al. (2016). Lateral hypothalamus GABAergic neurons modulate consummatory behaviors regardless of the caloric content or biological relevance of the consumed stimuli. *Neuropsychopharmacology* 41, 1505–1512. doi: 10.1038/npp.2015.304

Nieh, E. H., Matthews, G. A., Allsop, S. A., Presbrey, K. N., Leppla, C. A., Wichmann, R., et al. (2015). Decoding neural circuits that control compulsive sucrose seeking. *Cell* 160, 528–541. doi: 10.1016/j.cell.2015.01.003

Nieh, E. H., Vander Weele, C. M., Matthews, G. A., Presbrey, K. N., Wichmann, R., Leppla, C. A., et al. (2016). Inhibitory input from the lateral hypothalamus to the ventral tegmental area disinhibits dopamine neurons and promotes behavioral activation. *Neuron* 90, 1286–1298. doi: 10.1016/j.neuron.2016.04.035

Norgren, R. (1970). Gustatory responses in the hypothalamus. *Brain Res.* 21, 63–77. doi: 10.1016/0006-8993(70)90021-1

O'Connor, E. C., Kremer, Y., Lefort, S., Harada, M., Pascoli, V., Rohner, C., et al. (2015). Accumbal D1R neurons projecting to lateral hypothalamus authorize feeding. *Neuron* 88, 553–564. doi: 10.1016/j.neuron.2015.09.038

Olds, J., and Milner, P. (1954). Positive reinforcement produced by electrical stimulation of septal area and other regions of rat brain. *J. Comp. Physiol. Psychol.* 47, 419–427. doi: 10.1037/h0058775

Ono, T., Nakamura, K., Nishijo, H., and Fukuda, M. (1986). Hypothalamic neuron involvement in integration of reward, aversion, and cue signals. *J. Neurophysiol.* 56, 63–79. doi: 10.1152/jn.1986.56.1.63

Phillips, A. G., and Mogenson, G. J. (1968). Effects of taste on self-stimulation and induced drinking. *J. Comp. Physiol. Psychol.* 66, 654–660. doi: 10.1037/h0026523

Poschel, B. P. H. (1968). Do biological reinforcers act via the self-stimulation areas of the brain? *Physiol. Behav.* 3, 53–60. doi: 10.1016/0031-9384(68)90031-0

Qualls-Creekmore, E., Yu, S., Francois, M., Hoang, J., Huesing, C., Bruce-Keller, A., et al. (2017). Galanin-Expressing GABA neurons in the lateral hypothalamus modulate food reward and noncompulsive locomotion. *J. Neurosci*. 37, 6053–6065. doi: 10.1523/JNEUROSCI.0155-17.2017

Schwartzbaum, J. S. (1988). Electrophysiology of taste, feeding and reward in lateral hypothalamus of rabbit. *Physiol. Behav*. 44, 507–526. doi: 10.1016/0031-9384(88)90313-7

Sclafani, A. (1991). "The hedonics of sugar and starch," in *The Hedonics of Taste* (New York, NY: Lawrence Erlbaum Associates, Inc), 59–87.

Sharpe, M. J., Marchant, N. J., Whitaker, L. R., Richie, C. T., Zhang, Y. J., Campbell, E. J., et al. (2017). Lateral hypothalamic gabaergic neurons encode reward predictions that are relayed to the ventral tegmental area to regulate learning. *Curr. Biol.* 27, 2089–2100.e5. doi: 10.1016/j.cub.2017.06.024

Simerly, R. B. (2004). "Anatomical substrates of hypothalamic integration," in *The Rat Nervous System* (Burlington: Academic Press).

Spector, A. C., Klumpp, P. A., and Kaplan, J. M. (1998). Analytical issues in the evaluation of food deprivation and sucrose concentration effects on the microstructure of licking behavior in the rat. *Behavi. Neurosci.* 112, 678–694.

Stuber, G. D., and Wise, R. A. (2016). Lateral hypothalamic circuits for feeding and reward. *Nat. Neurosci.* 19, 198–205. doi: 10.1038/nn.4220

Teitelbaum, P., and Epstein, A. N. (1962). The lateral hypothalamic syndrome: recovery of feeding and drinking after lateral hypothalamic lesions. *Psychol. Rev*. 69, 74–90.

Thoeni, S., Loureiro, M., O'Connor, E. C., and Lüscher, C. (2020). Depression of accumbal to lateral hypothalamic synapses gates overeating. *Neuron* 107, 158–172.e4. doi: 10.1016/j.neuron.2020.03.029

Ting, J. T., and Feng, G. (2013). Development of transgenic animals for optogenetic manipulation of mammalian nervous system function: progress and prospects for behavioral neuroscience. *Behav. Brain Res.* 255, 3–18. doi: 10.1016/j.bbr.2013.02.037

Urstadt, K. R., and Berridge, K. C. (2020). Optogenetic mapping of feeding and self-stimulation within the lateral hypothalamus of the rat. *PLoS ONE* 15:e0224301. doi: 10.1371/journal.pone.0224301

Valenstein, E. S., and Cox, V. C. (1970). Influence of hunger, thirst, and previous experience in the test chamber on stimulus-bound eating and drinking. *J. Comp. Physiol. Psychol.* 70, 189–199. doi: 10.1037/h0028708

Valenstein, E. S., Cox, V. C., and Kakolewski, J. W. (1968). Modification of motivated behavior elicited by electrical stimulation of the hypothalamus. *Science* 159, 1119–1121. doi: 10.1126/science.159.3819.1119

Valenstein, E. S., and Phillips, A. G. (1970). Stimulus-bound eating and deprivation from prior contact with food pellets. *Physiol. Behav.* 5, 279–282. doi: 10.1016/0031-9384(70)90099-5

Villavicencio, M., Moreno, M. G., Simon, S. A., and Gutierrez, R. (2018). Encoding of sucrose's palatability in the nucleus accumbens shell and its modulation by exteroceptive auditory cues. *Front. Neurosci.* 12:265. doi: 10.3389/fnins.2018.00265

Yamamoto, T., Matsuo, R., Kiyomitsu, Y., and Kitamura, R. (1989). Response properties of lateral hypothalamic neurons during ingestive behavior with special reference to licking of various taste solutions. *Brain Res*. 481, 286–297. doi: 10.1016/0006-8993(89)90805-6

Zeng, H., and Madisen, L. (2012). Mouse transgenic approaches in optogenetics. *Prog. Brain Res*. 196, 193–213. doi: 10.1016/B978-0-444-59426-6.00010-0

Zhang, X., and van den Pol, A. N. (2017). Rapid binge-like eating and body weight gain driven by zona incerta GABA neuron activation. *Science* 356, 853–859. doi: 10.1126/science.aam7100

Zhao, S., Ting, J. T., Atallah, H. E., Qiu, L., Tan, J., Gloss, B., et al. (2011). Cell type-specific channelrhodopsin-2 transgenic mice for optogenetic dissection of neural circuitry function. *Nat. Methods* 8, 745–752. doi: 10.1038/nmeth.1668

Zocchi, D., Wennemuth, G., and Oka, Y. (2017). The cellular mechanism for water detection in the mammalian taste system. *Nat. Neurosci.* 20, 927–933. doi: 10.1038/nn.4575

Conflict of Interest: The authors declare that the research was conducted in the absence of any commercial or financial relationships that could be construed as a potential conflict of interest.

frontiers in Neuroscience

HYPOTHESIS AND THEORY
published: 01 February 2021
doi: 10.3389/fnins.2021.626085

The Phantom Satiation Hypothesis of Bariatric Surgery

*Laurent Gautron**

Department of Internal Medicine, Center for Hypothalamic Research, The University of Texas Southwestern Medical Center, Dallas, TX, United States

The excitation of vagal mechanoreceptors located in the stomach wall directly contributes to satiation. Thus, a loss of gastric innervation would normally be expected to result in abrogated satiation, hyperphagia, and unwanted weight gain. While Roux-en-Y-gastric bypass (RYGB) inevitably results in gastric denervation, paradoxically, bypassed subjects continue to experience satiation. Inspired by the literature in neurology on phantom limbs, I propose a new hypothesis in which damage to the stomach innervation during RYGB, including its vagal supply, leads to large-scale maladaptive changes in viscerosensory nerves and connected brain circuits. As a result, satiation may continue to arise, sometimes at exaggerated levels, even in subjects with a denervated or truncated stomach. The same maladaptive changes may also contribute to dysautonomia, unexplained pain, and new emotional responses to eating. I further revisit the metabolic benefits of bariatric surgery, with an emphasis on RYGB, in the light of this *phantom satiation hypothesis*.

Keywords: neurology, autonomic nervous system, vagus, gastroenterology, appetite, nociception, vagotomy

OPEN ACCESS

Edited by:
Lionel Carneiro, The Ohio State University, United States

Reviewed by:
Timothy H. Moran, Johns Hopkins University, United States
Jens Juul Holst, University of Copenhagen, Denmark

***Correspondence:**
Laurent Gautron
laurent.gautron@utsouthwestern.edu

Specialty section:
This article was submitted to Neuroenergetics, Nutrition and Brain Health, a section of the journal Frontiers in Neuroscience

Received: *04 November 2020*
Accepted: *06 January 2021*
Published: *01 February 2021*

Citation:
Gautron L (2021) The Phantom Satiation Hypothesis of Bariatric Surgery. Front. Neurosci. 15:626085. doi: 10.3389/fnins.2021.626085

INTRODUCTION

Satiation in Health and Obesity

A wide range of sensations can be evoked from the gastrointestinal (GI) tract including, but not limited to, pain and warmth (Cervero, 1994; Mulak et al., 2008). However, the sensation that is most frequently experienced in healthy subjects is satiation (Stevenson et al., 2015). Satiation corresponds to the sensation of epigastric fullness (without pain) which accompanies meal termination (Benelam, 2009; Bellisle et al., 2012). In the human literature, the term of satiation also commonly refers to the subjective feeling of satisfaction toward the end of a meal (Benelam, 2009; Bellisle et al., 2012). Because satiation directly leads to meal termination, it is a contributing factor to maintaining a normal feeding behavior (de Graaf et al., 2004). To avoid confusion, I will refrain from using the term of *fullness* because it is inconsistently used to refer either to the feeling of gastric distention or to the persistent lack of hunger between meals, which should correctly be referred to as *satiety* (Bellisle et al., 2012; Andermann and Lowell, 2017). The mechanical deformation of the GI tract is a primary event responsible for satiation. Interestingly, as early as 1911, studies in conscious humans with externalized fistulas established that a feeling of gastric distension can specifically arise from the mechanical deformation of the GI muscularis (but not of its mucosa) (Hertz, 1911; Boring, 1915; Wolf and Wolff, 1943; Nathan, 1981). Likewise, human subjects fed by parenteral means, for which nutrients bypass the GI tract, often complain of not feeling satiation to the same extent as after eating and drinking (Stratton and Elia, 1999). Satiation can be assessed in human

subjects during the ingestion of a test meal either by quantifying food intake or by assessing self-reported appetite levels (Benelam, 2009). Admittedly, there are technical difficulties in measuring self-reported levels of satiation in humans including considerable variability between individuals (Bellisle et al., 2012; Gibbons et al., 2019; Nielsen et al., 2019; Gero, 2020). While this article is primarily concerned with human biology, I will consider laboratory animal and human studies in parallel. In laboratory animals, food intake can be measured *post hoc* as an indirect indicator of satiation and appetite levels. For example, the inflation of a gastric balloon in rats significantly reduces spontaneous food intake and leads to early meal termination (Geliebter et al., 1986; Phillips and Powley, 1998).

Satiation can be modulated by many factors including nutritional, sociocultural, genetic, and environmental factors. It is beyond the scope of this article to examine all the physiological factors that influence satiation and additional information on the topic can be found in review articles (Warwick, 1996; Benelam, 2009; Keenan et al., 2015; Hetherington et al., 2018; Kral et al., 2018; Rogers, 2018; Gibbons et al., 2019; Thornhill et al., 2019). However, obesity deserves a special mention. Subjects with a weaker satiation response to fatty foods are predisposed to excessive weight gain and obesity (Blundell et al., 2005) and children who spontaneously eat larger meals tend to gain more weight (Syrad et al., 2016). On the other hand, currently available human data are inherently correlative and complicated by the fact that obtaining accurate measurements of caloric intake and energy expenditure remains challenging. In laboratory animals, many studies have shown that meal size increases in response to a high-fat diet (Farley et al., 2003; Melhorn et al., 2010; la Fleur et al., 2014; Treesukosol and Moran, 2014). The observed increase in meal size tends to occur soon after switching animals to a high-fat diet when they are not yet obese, consistent with the view that diminished satiation may precede excessive weight gain. However, considering the wide range of nutritional and environmental factors that can modulate satiation, the mechanisms responsible for altered satiation in obesity are not known with certainty. One possible mechanism may involve altered gut-brain communication with reduced sensitivity to postprandial cues (Kentish et al., 2012). Another non-exclusive possibility may involve exaggerated hedonic responses to an obesogenic diet (Berthoud, 2012; Licholai et al., 2018).

Brief Overview of the Neurobiology of Satiation

Vagal Afferents

The vagus nerve is a mixed nerve containing both efferent and afferent fibers (Berthoud and Neuhuber, 2019). The latter correspond to the vagal neurons carrying sensory information from the GI tract to the brainstem. Vagal afferents responding to stimuli arising from the GI tract are specifically connected to the medial portion of the nucleus of the solitary tract (Saper, 2002). The stomach itself is innervated by two gastric branches of the subdiaphragmatic vagus nerve that enter the gastric wall at the level of the lower esophageal sphincter before sending smaller offshoots throughout most of the muscularis and mucosa (Wang and Powley, 2007). Within the periphery, afferent endings responding to mechanical events are highly enriched in the muscularis at the levels of the stomach and upper intestines (Ozaki et al., 1999; Fox et al., 2000; Williams et al., 2016). At least two types of specialized vagal terminals known as intramuscular arrays and intraganglionic laminar endings are involved in detecting mechanical events in the stomach (Berthoud et al., 1997; Fox et al., 2000; Powley et al., 2016). In addition to the stomach wall, these specialized vagal mechanoreceptors are present at lower densities in the esophagus and duodenum (Wang and Powley, 2000; Wang et al., 2012). Electrophysiological recordings have established that vagal mechanoreceptors rapidly and linearly respond to the application of varied mechanical stimuli to the stomach wall including stretch and tension (Peles et al., 2003; Kentish et al., 2014). Gastric distension suppresses feeding in a vagally-dependent manner in rats (Phillips and Powley, 1998) and, furthermore, mutant mice lacking vagal mechanoreceptors eat larger meals (Fox et al., 2001; Fox, 2006). Conversely, the selective excitation of vagal mechanoreceptors supplying the muscularis elicits meal termination in genetically engineered mice (Bai et al., 2019). As a remark, the same study found that selective mucosal afferents stimulation does not modify feeding. Hence, there is ample evidence that vagal mechanoreceptors supplying the stomach wall are both required and sufficient for eliciting satiation. At the same time, the sensory integration of postprandial cues at the level of vagal afferents is more complex than often appreciated. In particular, mechanoreceptors activity is modulated by many chemical signals including, most notably, the gut peptide cholecystokinin (CCK) (Gibbs and Smith, 1977; Schwartz et al., 1995; Williams et al., 2016). Thus, the excitability of mechanoreceptors is modulated by numerous factors and researchers are just beginning to understand how GI signals are integrated at the level of vagal endings (Egerod et al., 2019). Finally, communication between the stomach and the brain involves more than just vagal afferents, but also a complex network of enteric and spinal neurons (Furness, 2006; Udit and Gautron, 2013; Sharkey et al., 2018; Spencer et al., 2018). Although subsets of spinal afferents respond to a wide range of noxious and innocuous stimuli in the GI tract (Grundy, 1988; Spencer et al., 2016), their contribution to the postprandial regulation of feeding is not well-known (Berthoud and Neuhuber, 2019).

Central Viscerosensory Circuits

It is without saying that satiation requires more than the excitation of vagal mechanoreceptors. Vagal afferents are connected, in a multisynaptic manner, to brain networks encompassing integrative cortices and subcortical areas (Min et al., 2011; Hays et al., 2013; Andermann and Lowell, 2017; Cao et al., 2017; Ly et al., 2017). Based on both animal studies and human brain imaging, the regions involved in relaying information of vagal origin to the cortex include, beyond the nucleus of solitary tract, the parabrachial nucleus, and ventrobasal thalamus (Saper, 2000, 2002; Craig, 2002). Without entering into details, the aforementioned brain relays have been linked to the regulation of satiation and meal size in

laboratory animals (Dossat et al., 2013; Alhadeff et al., 2014; Cavanaugh et al., 2015; Campos et al., 2016; Zafra et al., 2017). As early as in the 1930's, studies showed that the electrical stimulation of the vagus nerve altered cortical electrograms (Bailey and Bremer, 1938; O'Brien et al., 1971; Ito and Craig, 2003). Among integrative cortices involved in the processing of gastric distension, vagal information is the insular cortex (Saper, 2002). For instance, based on electrical stimulation experiments in conscious subjects, the stimulation of the human insular cortex causes sensations that are secondary to changes in the GI motility (Pool, 1954). Likewise, many recent brain-imaging studies have described altered activity in the insular cortex in association with the feeling of epigastric distension in humans (Tataranni et al., 1999; Ladabaum et al., 2007; Wang et al., 2008). Importantly, neurons of the insular cortex responding to different visceral territories (stomach, heart, etc.) and sensory modalities (stretch, taste, etc.) are topographically organized (Saper, 2002). There are also insular neurons that can respond to multiple sensory modalities of viscerosensory origin (Saper, 2002). In turn, insular neurons modulate GI functions (Levinthal and Strick, 2020). In summary, one can rightfully conceive the stomach wall as a sensory organ connected to a viscerosensitive neural network specialized in responding to gastric volumetric changes (**Figure 1**). A detailed knowledge of these brain circuits is not needed to understand the hypothesis described later, and more information can be found elsewhere (Saper, 2002; Mulak et al., 2008; de Araujo et al., 2012; Frank et al., 2016; Andermann and Lowell, 2017).

SATIATION WITHOUT A VAGUS NERVE

Experimental and Clinical Vagotomies

Vagotomy is a procedure that consists in denervating vagally-innervated organs to varying extents (Phillips and Powley, 1998). A deafferentation is a procedure consisting of interrupting or

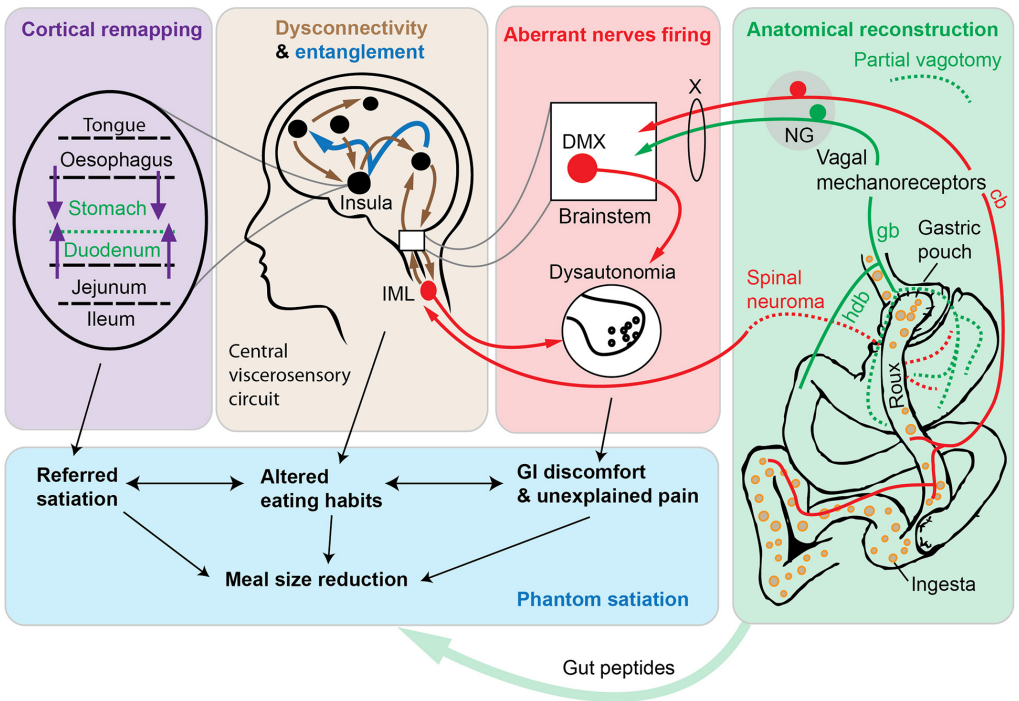

FIGURE 1 | Schematic diagram depicting the phantom satiation hypothesis. According to the observations presented in this article, the metabolic benefits of Roux-en-Y gastric bypass (RYGB) are mediated, at least in part, by a combination of aberrant changes in a complex viscerosensory neural circuit. A key event following RYGB surgery is an unintentional gastric denervation (green box). Available data indicate that RYGB is associated with a gastric denervation (green dotted lines indicate axotomized axons of vagal or spinal origins). The duodenum itself can be conceived as a functionally denervated, in the sense that duodenal afferents cease to be directly stimulated by nutrients and mechanical stimuli. According to our hypothesis, partial vagotomy leads to widespread maladaptive changes in peripheral nerves (red box and arrows) and in central viscerosensory circuits (brown box and arrows). In particular, in animal models of bariatric surgery, sympathetic, parasympathetic, and nociceptive nerves behave as if they were hyperresponsive to a meal (red arrows). At the central level, altered connectivity in many cortical and subcortical areas has been reported after RYGB using brain imaging technologies in human subjects. In addition, the entanglement of viscerosensory modalities (dark blue arrows) may further participate to abnormal emotional and sensory responses to eating. Finally, the remapping of insular cortices involved in gastrointestinal territories representation is likely to occur (purple box and arrows), thereby contributing to viscerosensory anomalies and referred sensations. This neurobiological model, directly inspired by the literature on phantom limbs, predicts that subjects with RYGB may experience exaggerated satiation. Ultimately, reduced meal size and perturbed eating patterns (blue box), among other postprandial anomalies, may contribute to weight loss. Hence, the "phantom satiation" hypothesis reinterprets bariatric surgery as a type of injury—that is to say a procedure that inflicts irreversible anatomical and functional damage—even if an injury with evident long-term health benefits. Abbreviations: cb, celiac branch; deaf., deafferentation; DMX, dorsal motor nucleus of the vagus; gb, gastric branch; hdb, hepato-duodenal branch. NG, nodose ganglion; IML, intermediolateral column; X, vagus nerve.

destroying the afferent fibers contained in a specific nerve or organ, while minimally interfering with motor fibers (Walls et al., 1995). The regrowth of vagal terminals after vagotomy is possible in rats, but takes weeks and is incomplete (Phillips and Powley, 1998; Powley et al., 2005a). From their inability to feel completely satiated, one would expect vagotomized animals to ingest larger meals and overeat. In laboratory animals, vagotomies can result in increased meal size, hyperphagia, and loss of responsiveness to pharmacological CCK (Smith et al., 1981; Walls et al., 1995; Phillips and Powley, 1998; Schwartz et al., 1999; Sclafani et al., 2003; Powley et al., 2005a). At the same time, vagotomy-induced overeating is often transient, presumably due to compensatory changes at the central level (Walls et al., 1995; Chavez et al., 1997; Phillips and Powley, 1998; Zafra et al., 2003; Reidelberger et al., 2014). Instead, in normal-weight animals, long-term vagotomy and deafferentation have been reported to result in animals eating smaller meals, with some degree of anorexia and weight loss (Mordes et al., 1979; Sclafani and Kramer, 1985; Kraly et al., 1986; Erecius et al., 1996; Leonhardt et al., 2004; Powley et al., 2005a; McDougle et al., 2020). Interestingly, eating smaller meals post-vagotomy is often compensated by more frequent meals, further suggesting significant brain adaptations (Powley et al., 2005a). Likewise, in varied models of rodent obesity, vagotomy, and deafferentation have repeatedly been shown to reduce feeding and body weight gain (Cox and Powley, 1981; Ferrari et al., 2005; Powley et al., 2005a; Stearns et al., 2012; Dezfuli et al., 2018).

It must be stressed that truncal and gastric vagotomies used to be safely performed in human subjects suffering from ulcers, with or without obesity (Gortz et al., 1990; Wills and Grusendorf, 1993). In vagotomized subjects, dumping syndrome, malaise, anemia, and digestive issues commonly occur. However, the latter side effects were usually treatable and not directly correlated with weight loss in many patients (Faxen et al., 1979; Irving et al., 1985; Wills and Grusendorf, 1993). Instead, vagotomy has been reported to induce weight-loss with reduced food intake and modified food preference in obese subjects (Kral, 1978; Gortz et al., 1990). In fact, vagotomized patients often self-reported a lack of hunger (Sheiner et al., 1980; Kral et al., 2009; Plamboeck et al., 2013). The time needed for severed axons to recolonize the human stomach and become functional is unknown. Because peptic ulcers rarely reoccur after vagotomy (Jordan and Thornby, 1987; Popiela et al., 1993), it is unlikely that regrown vagal axons become functional again. Of note, humans treated with truncal vagotomy often received a pyloroplasty to prevent gastric stasis. Pyloroplasty itself exerts profound effects on appetite and food intake that are closely resembling those of bariatric surgery (Fraser et al., 1983; Chang et al., 2001; Dezfuli et al., 2018; Harada et al., 2018). Nonetheless, subsets of patients with selective gastric vagotomy without pyloroplasty also showed long-term weight loss with some degree of dysphagia, early satiety and nausea (Jordan and Thornby, 1987).

Unintentional Surgical Vagotomy

Certain types of obesity surgeries including, most notably, Roux-en-Y gastric bypass (RYGB) result in a partial and unintentional vagotomy. RYGB is a surgery that consists in dividing the stomach into a small pouch and reconnecting it to the jejunum (Stefater et al., 2012). In bypassed subjects, food travels from the pouch to the lower intestines without traversing the stomach remnant and duodenum (called Roux limb) (**Figure 1**). Several investigators suggested that RYGB must be accompanied by gastric denervation (Powley et al., 2005b; Berthoud, 2008; Stylopoulos and Aguirre, 2009). Our own experimental data have confirmed that bypassed mice show vagal denervation at the levels of the gastric pouch, the bypassed stomach, and sites of clipping and anastomosis (Gautron et al., 2013). In contrast, vagal innervation remained largely intact in animals that were unoperated on or sham-operated on. In agreement with our observations, RYGB surgery in rats also causes rapid neuronal damage in vagal afferents (Minaya et al., 2019). It is also likely that the construction of a gastric pouch inevitably results in some degree of spinal deafferentation. It is striking that many of the aforementioned effects of RYGB are recapitulated in vagotomized subjects (Brolin et al., 1994; Laurenius et al., 2012; Stano et al., 2017). Moreover, bypassed individuals reach satiation more quickly than expected and independently of side effects such as dumping syndrome and related symptoms such as nausea, cramps, and dizziness (Halmi et al., 1981; Nguyen et al., 2016). Hence, RYGB has a direct impact on the innervation of the stomach, which in turn may actively play a role in the metabolic actions and side effects of gastric bypass. Of note, since food travels directly into the jejunum of bypassed individuals, this new configuration can be conceived as a *functional duodenal vagotomy*, in the sense that duodenal afferents cease to be directly stimulated by nutrients and mechanical stimuli during the postprandial phase (**Figure 1**). Thus, RYGB is likely to result in a partial loss of sensory input from the upper GI tract including stomach and duodenum. Although counterintuitive, when we consider the literature on intentional and unintentional vagotomies as a whole, it appears that vagotomized animals and human subjects eat less than they did prior to surgery.

Paradox of Satiation With Vagotomy

It has often been argued, with good reasons, that vagotomies, especially when vagal (motor) efferents are involved, are difficult to interpret because of secondary dysmotility, malaise, and dyspepsia (Sclafani et al., 1981; McDougle et al., 2020). At the same time, the latter factors could not entirely account for reduced food intake and weight loss (Mordes et al., 1979; Sclafani and Kramer, 1985). It is also true that vagotomies are not entirely specific or complete (Browning et al., 2013a) and that experiments consisting of administering exogenous gut peptides, including CCK, lack in physiological relevance (French et al., 1993; Baldwin et al., 1998). Hence, there are numerous unresolved difficulties and discrepancies in the vagotomy literature. Technical and interpretation difficulties aside, one would expect vagotomized individuals to be unable to fully experience satiation and eat more (McDougle et al., 2020). On top of that, the rebound hyperphagia in individuals losing weight when dieting is not seen in bypassed and vagotomized subjects or animals (Berthoud, 2008; Hao et al., 2016). Importantly, bypassed animals are able to overeat upon a metabolic restriction (Stefater et al., 2010; Lutz and Bueter, 2014). This indicates that RYGB does not prevent animals from

experiencing hunger but rather produces a state of exacerbated satiation. Thus, subjects with a gastric vagotomy or a truncated stomach likely continue to experience postprandial satiation, if not at exaggerated levels. At first glance, *satiation without a gastric vagus* is a phenomenon that challenges our current understanding of gut-brain communication. RYGB is associated with profound anatomical and physiological changes, the number of which could contribute to perturbate normal eating patterns (Hankir et al., 2018; Sandoval, 2019). For instance, it is possible that RYGB-associated elevated gut peptides secretion contributes to enhanced satiation, among other metabolic improvements. Nonetheless, experts in the field have not reached a consensus on what exactly contributes to altering eating behavior after bariatric surgery (Hao et al., 2016; Sandoval, 2019). For example, RYGB is effective in numerous mouse models lacking key hormones and gut peptides (Mokadem et al., 2014; Morrison et al., 2016; Hao et al., 2018; Boland et al., 2019). Below, I will propose a novel and complementary explanation based on adaptations in viscerosensory circuits.

THE PHANTOM SATIATION HYPOTHESIS

Overview of Phantom Limbs Phenomena

Is it always the case that the denervation or removal of a body part results in a loss of sensation from this body part? The field of neurology teaches us the contrary. Indeed, many amputees continue to feel the presence of their lost limb, a phenomenon described as *phantom limb* (Ramachandran et al., 2009; Collins et al., 2018; Makin and Flor, 2020). Even though phantom pain syndromes have been first described 500 years ago (Keil, 1990), the treatment of phantom limb syndromes has remained challenging up to this day (Alviar et al., 2016). Briefly, the sensations that can be evoked from a phantom limb can be either non-painful (e.g., tingling), or excruciatingly painful, and spontaneous or consecutive to the stimulation of other body parts (referred sensations) (Aglioti et al., 1994; Ramachandran et al., 2009; Collins et al., 2018). In other words, phantom sensations are sensations felt from a body part that is either missing and/or denervated. The prevalence of phantom pain is estimated at 50–80% of all amputees (Dijkstra et al., 2002). To the best of our knowledge, there is no definitive consensus on how to explain phantom sensations (Ortiz-Catalan, 2018). Among commonly cited reasons for phantom sensations is that damaged sensory fibers in the stump (or neuroma) remain chronically irritated. Their erratic firing may evoke sensations and pain interpreted as originating from the missing body part (Collins et al., 2018). Another explanation involves localized cortical remapping (Flor et al., 2013). The idea behind cortical remapping is that the somatosensory cortical area corresponding to the amputated body part is "invaded" by adjacent cortical areas representing other body parts. Hence, stimuli applied to other body parts may evoke sensations from what is perceived as the missing limb (Hunter et al., 2003). In parallel, maladaptive remodeling of the cortices would contribute to evoking unsolicited pain along with a distorted body representation (Remple et al., 2004). Other researchers have also proposed that large-scale functional changes in brain connectivity beyond the cortex cause phantom sensations (Makin et al., 2013). Lastly, according to a recent theory, amputation renders the neural circuits not normally connected to the missing body part prone to stochastic entanglement with one another (Ortiz-Catalan, 2018). Broadly speaking, the term of entanglement corresponds to the linking of brain networks that do not normally fire together, thereby resulting in unexplained sensations. A combination of all of the above hypotheses, rather than a single mechanism, is likely to account for the emergence of the variety of phantom sensations encountered in amputees.

Phantom Internal Organs

Understandingly, the literature on phantom sensations focused on limbs, but phantom sensations from internal organs have also been occasionally reported (Roldan and Lesnick, 2014). These organs include the eyes (Andreotti et al., 2014), rectum (Ovesen et al., 1991), kidney (Roldan and Lesnick, 2014), pelvic organs (Dorpat, 1971), and breast (Di Noto et al., 2013; Bjorkman et al., 2017). Of note, Dorpat (1971) already discussed the case of what is called "phantom stomach sensations" but without mentioning satiation itself. In particular, this author mentioned patients complaining of persisting ulcers symptoms after vagotomy or gastrectomy, in spite of their ulcers being healed or removed. Dorpat added that human subjects typically do not experience the feeling of "having an internal organ," but rather of having sensations normally associated with the functioning of the organ in question. For example, subjects without a rectum sometimes experience the feeling of defecation (Dorpat, 1971; Ovesen et al., 1991). Inspired by the above literature, I would like to propose that satiation continue to arise after gastrectomy or gastric vagotomy due to phantom sensations, which I called the *phantom satiation hypothesis*. Before explaining it, let us note that our hypothesis is speculative and not to be confused with *phantom fullness* that has been used to refer to fullness not correlated with caloric content in healthy individuals (Camps et al., 2016). According to the hypothesis presented here, phantom sensations of satiation are evoked when food is traversing GI segments above and below the denervated or truncated stomach, including the esophagus and lower intestines (**Figure 1**).

PREDICTIONS AND CONSISTENCY WITH THE LITERATURE

Meal Size Reduction

If the hypothesis is correct, phantom satiation should durably influence food intake regulation among bypassed subjects. Accordingly, bypassed individuals report altered experience of hunger and fullness in a qualitative manner (Halmi et al., 1981; Miras and le Roux, 2013). Moreover, bypassed human subjects eat smaller meals for at least two years post-surgery (Laurenius et al., 2012). Overall, reduction in caloric intake over a long period is an important determinant of weight loss after RYGB in humans (Kenler et al., 1990; Odstrcil et al., 2010; Miller et al., 2014). Similarly, meal size reduction was reported in bypassed laboratory animals (Zheng et al., 2009;

Mathes et al., 2015; Washington et al., 2016). Several authors postulated that restricting the stomach volume is sufficient to explain a reduced food intake and meal size (Warde-Kamar et al., 2004; Langer et al., 2006). However, others have well explained that gastric capacity is not correlated with reduced feeding after bariatric surgery (Stefater et al., 2012; Sandoval, 2019; Evers et al., 2020). As discussed earlier, gastric vagotomy also causes a reduction in feeding without restricting gastric capacity. Therefore, early satiation in bypassed subjects is highly unlikely to occur because of gastric restriction *per se*, but rather due to changes in the neural circuits normally involved in detecting volumetric changes of the stomach.

Correlation With Vagal Trauma and Irreversibility

While surgeons pay attention not to damage nerves during bariatric surgery, axons near sites of surgical incision will inevitably be severed. Another prediction is that the degree to which bariatric surgery alters feeding behavior and body weight should be correlated with the trauma to the vagus nerve across different types of bariatric surgeries. For instance, different types of obesity surgeries differently modify the stomach anatomy (Stefater et al., 2012). The two types of surgeries that affect the anatomy of the stomach (and therefore its innervation) the most are RYGB and vertical sleeve gastrectomy (VSG) (Stefater et al., 2010; Kizy et al., 2017). The degree of vagal damage after VSG is poorly defined, but is expected to be extensive along the sites of gastric resection. Interestingly, RYGB and VSG reduce feeding to a comparable extent in humans and rats (Chambers et al., 2011; Stemmer et al., 2013; Yousseif et al., 2014). However, RYGB and VSG exert much more marked effects on feeding behavior than does gastric banding (Korner et al., 2006; Scholtz et al., 2014). One big difference is that gastric banding theoretically does not damage the stomach anatomy or its innervation. Likewise, surgeries associated with incision of gastric tissue produce greater weight loss and reduction of feeding than surgeries only consisting of reducing stomach capacity in the rat (Evers et al., 2020). Following the same idea, because the stomach is more richly innervated than lower GI segments, surgical operation of the lower intestines should affect feeding to a lesser extent. For instance, duodenal-jejunal exclusion, a procedure that leaves the stomach intact, is significantly less effective at reducing feeding or body weight in animals and humans (Geloneze et al., 2009; Kindel et al., 2011; Alvarez et al., 2020). In further support of our model, adding gastric vagotomy to gastrectomy does not produce further weight-loss in laboratory rodents (Hankir et al., 2016; Dezfuli et al., 2018). This is logical considering that gastric vagotomy already occurred in bypassed subjects.

Irreversibility

Without proper treatment, phantom pain can persist for years in amputees. This may be because the neural changes brought about by an amputation are hardly reversible. RYGB is a complicated procedure that cannot easily be reversed in a laboratory animal. However, reversal of RYGB is performed in patients with severe complications such intractable vomiting, malnutrition or chronic pain (Moon et al., 2015; Shah and Gislason, 2020). As one would expect, reversal of RYGB is often followed by some degree of weight regain consecutive to the correction of the debilitating symptoms (Moon et al., 2015; Shah and Gislason, 2020). When weight regain is observed, most patients do not regain their pre-RYGB weight (Shoar et al., 2016) and, furthermore, a subset of patients never regains any weight. This agrees with the view that the metabolic benefits of RYGB persist to some extent after reversal. Hence, the loss of gastric innervation is a factor that correlate well with the known course of clinical outcomes after bariatric surgery.

Indiscriminate Weight-Loss in the Non-obese

Our hypothesis implies that a trauma to the upper GI tract will invariably cause weight-loss even in non-obese individuals. Because bariatric surgery is overwhelmingly prescribed for clinically obese subjects, the literature on the impact of bariatric surgery in non-obese is limited. One study in non-obese rats demonstrated significant weight loss after RYGB and VSG (Xu et al., 2015). In contrast, a recent study showed that RYGB did not cause sustained weight loss in the non-obese mouse (Mumphrey et al., 2019). However, RYGB was performed in adolescent mice while they were still growing at a rapid pace. In humans, there is increasing interested in using bariatric surgery to treat diabetic patients without obesity. Several clinical studies have clearly indicated that weight-loss follows RYGB and VSG in non-obese or mildly obese subjects (Cohen et al., 2012; Noun et al., 2016; Ferraz et al., 2019). It is also noteworthy that gastrectomy done in non-obese subjects with gastric cancer also results in sustained weight loss, loss of appetite and abdominal discomfort (Adachi et al., 1999; Laffitte et al., 2015). Notably, surgical reconstruction after various gastrectomies often include Roux-en-Y like procedures, which means that their effects on rate of intestinal nutrient entry and gut hormone secretion will be similar. Hence, gastrectomy and various gastric surgeries indiscriminately causes sustained weight loss.

Weight Loss and Brain Lesions

In the proposed model, phantom satiation arises following GI denervation and ensuing maladaptive brain changes. One would expect lesions in brain regions involved in processing vagal sensory information including, but not limited to the insula, to be associated with satiation and weight loss. While there is little literature on satiation and brain lesions, neurologists have reported that strokes often cause important weight loss in subsets of patients (Scherbakov et al., 2019). The impact of stroke on body weight differ between patients presumably due to differences in the brain regions affected by the stroke. Taste deficits sometimes manifest alongside post-stroke weight loss (Scherbakov et al., 2011; Dutta et al., 2013), indicating that lesions in viscerosensory brain sites cause weight loss. In one particular clinical case, a patient with a lesion in the left posterior insular cortex, a region that receives general viscerosensory input, showed involuntary weight loss with sustained appetite loss over one year (Mak et al., 2005). We do not dispose of enough evidence to say

that exaggerated satiation is responsible for weight loss after brain lesion in humans. Nonetheless, it was repeatedly observed that experimental lesions of viscerosensory relays in non-obese rats including, most notably, the parabrachial and dorsovagal complexes can result in sustained weight loss with depressed ingestive behaviors (Hill and Almli, 1983; Hyde and Miselis, 1983; Kott et al., 1984; Kenney et al., 1989; Dayawansa et al., 2011). In agreement with the hypothesis presented in this article, the aforementioned observations strongly support the idea that derangements in the integrity of key brain sites involved in GI viscerosensory processing can cause weight loss with reduced food intake. In fact, deep brain stimulation for the treatment of human obesity is an active area of research (Nangunoori et al., 2016; Formolo et al., 2019), but is almost entirely focused on brain regions involved in energy balance and reward. Based on the hypothesis presented here, modulating brain regions directly involved in satiation, including the insula and parabrachial complex, may also be considered as an appropriate strategy against obesity.

POTENTIAL MECHANISMS LEADING TO PHANTOM SATIATION

Nerves Injury and Adaptations

Gastric Neuroma

The mechanisms underlying *phantom satiation* are unknown. Nonetheless, I could invoke the same combination of peripheral and central adaptations described in the case of phantom limbs (**Figure 1**). The neuroma theory postulates that the disorganized growth of damaged nerve terminals at the site of injury can cause phantom sensations including, but not limited to, unexplained pain (Buch et al., 2020). Our group previously reported the presence of dystrophic and damaged vagal terminals in the stomach of the bypassed mouse (Gautron et al., 2013). Dystrophic terminals may correspond to degenerating and/or regrowing axons. Of note, a generalized and persistent decrease in excitability occurs after axotomy of vagal sensory neurons (Scherbakov et al., 2019). Hence, gastric vagal fibers severed during surgery probably become hyporesponsive. As explained before, the vagal supply to the lower GI tract remains largely intact after RYGB (Gautron et al., 2013). In contrast to gastric afferents, the excitability of intact vagal fibers located in the coeliac branches supplying the lower intestines may be enhanced (**Figure 1**). Specifically, several experimental studies showed that neuronal activation in the nucleus of the solitary tract is greater in RYGB and VSG animals after eating a test meal (Chambers et al., 2012; Mumphrey et al., 2016). Intrajejunal nutrients cause greater satiating effects in bypassed rats (Bachler et al., 2018). The latter findings indicate that vagal afferents that supply the lower intestines behave as if they were hyperresponsive to a meal. What causes the enhanced activity of intestinal vagal fibers is uncertain. Many factors come to mind including rapid gastric emptying, undigested food, excessive gut peptide secretion, altered microbiome, or perturbed vago-vagal reflexes (Sandoval, 2019).

The stomach is also densely innervated by spinal sensory axons traveling through the splanchnic plexus (Spencer et al., 2016). As mentioned before, RYGB surgery is likely to cause spinal endings located in the stomach to be interrupted and damaged. Spinal afferents are critical in visceral nociception (Saper, 2000; Spencer et al., 2016, 2018), but whether irritated spinal endings contribute to a gastric neuroma after bariatric surgery remains to be determined. The hyperexcitability of spinal nociceptors around sites of surgical anastomosis may be one logical explanation of phantom pain, even though no direct evidence is currently available to support this view. Moreover, it is possible that a loss of gastric vagal signaling is indirectly changing the activity of spinal afferent pathways. For example, the electrical stimulation of the vagus nerve produces analgesia by recruiting the antinociceptive descending pathway (Randich and Gebhart, 1992; Janig et al., 2000). Conversely, vagotomy has been associated with hyperalgesia in association with widespread changes in pro-nociceptive pathways stimuli (Ammons et al., 1983; Khasar et al., 1998; Furuta et al., 2009, 2012). Unexplained pain is a key feature of phantom phenomena. In the context of obesity surgery, painful complications with a known etiology can arise (e.g., hernia, adhesion, dumping syndrome) (Iannelli et al., 2006). However, bypassed patients can experience unexplained pain not related to the complications of surgery (Groven et al., 2010; Alsulaimy et al., 2017). For instance, bypassed patients have anecdotally reported feeling general aching all over the body or sharp pain in the stomach area (Groven et al., 2010). At least two studies focusing entirely on the prevalence of post-bariatric chronic abdominal pain revealed that approximately 7% of bypassed patients report pain of unknown etiology (Pierik et al., 2017; Mala and Hogestol, 2018). If unexplained pain is reflective of phantom pain, then the incidence of phantom pain is admittedly much lower after RYGB than after limb amputation. On the other hand, unexplained pain may have been underreported in the literature. According to one study, mild or intermittent pain not requiring a medical follow-up may be present in 80–95% of RYGB patients (Abdeen and le Roux, 2016). Interestingly, persistent abdominal pain occurs in subsets of RYGB patients after reversal to a normal anatomy (Shoar et al., 2016). At the same time, internal organs are less heavily innervated by spinal afferents than limbs and one would expect phantom pain from the upper GI tract to be less severe than in the case of phantom pain from a limb. Finally, it must be noted that the literature on visceral pain after bariatric surgery is still very limited.

Dysautonomia

Vagal and spinal afferents are connected in a multisynaptic manner to a complex circuit that exerts a descending excitatory or inhibitory influence on varied autonomic reflexes and sensory pathways (Saper, 2000; Craig, 2002; Travagli et al., 2003; Berthoud et al., 2006). For instance, altered vagal afferents activity may directly modulate vagal efferents pathways in a reflex manner (Travagli et al., 2003). One study also showed that RYGB in the rat leads to both changes in morphology and membrane excitability of vagal (motor) efferents consistent with hyperexcitability (Browning et al., 2013b). Both spinal and

vagal afferents also play an important role in modulating the sympathetic outflow to cardiovascular and metabolic viscera (Craig, 2002; Madden et al., 2017; Sabbatini et al., 2017; Rajendran et al., 2019). In particular, the vagus nerve exerts a tonic inhibition on sympathetically-driven thermogenesis in obese rat (Madden and Morrison, 2016). Similarly, vagal afferent signaling is involved in modulating the activity of splanchnic nerves, several of which provide sympathetic innervation to the GI tract, adrenals, and spleen (Sabbatini et al., 2017; Komegae et al., 2018). In other words, gastric vagotomy is likely to cause dysautonomia, a condition in which the parasympathetic and sympathetic outflows to viscera are perturbed (**Figure 1**). Interestingly, one study recently demonstrated that RYGB significantly elevated the basal activity of sympathetic fibers located in the mouse splanchnic nerve (Ye et al., 2020). The same study also found that splanchnic denervation prevented weight-loss and increase in energy expenditure that normally accompanies RYGB in laboratory animals (Ye et al., 2020). In summary, emerging evidence suggests widespread anatomical and functional changes in sensory and autonomic pathways following RYGB (**Figure 1**). It must be stressed that cortical and sub-cortical brain regions are linked with autonomic preganglionic and viscerosensory areas by bidirectional neural pathways (Saper et al., 1976; Goto and Swanson, 2004). There is also functional evidence that higher-order brain regions exert top-down excitatory influence on presynaptic vagal terminals (Browning, 2019). Therefore, the aforementioned changes in central circuits and peripheral nerves should be seen as intertwined rather than independent and parallel events (**Figure 1**). Overall, researchers are just beginning to understand how peripheral neurons are perturbed after bariatric surgery.

Brain Plasticity and Maladaptive Changes

Cortical Remapping

Cortical plasticity has been studied in the context of injuries to somatosensory rather than viscerosensory nerves (Mogilner et al., 1993; Nordmark and Johansson, 2020). Nonetheless, structural and functional changes are likely to occur after bariatric surgery in viscerosensory cortical areas involved in evoking satiation. In particular, after a partial loss of sensory input from the upper GI tract, the area normally representing the denervated region may be taken over by adjacent areas representing nearby innervated GI segments, a phenomenon known as cortical remapping (**Figure 1**). Whether cortical remapping occurs after bariatric surgery remains unknown. Nerve injury can lead to altered synaptic biology in the mouse insular cortex (Qiu et al., 2014). Surgeries such as mastectomy and hysterectomy are suspected to trigger cortical remapping (Di Noto et al., 2013). Thus, one would expect to see structural and functional changes in the insular cortex and connected integrative cortices after invasive bariatric surgeries including, most notably, RYGB. Nonetheless, studies on cortical remapping in relation to internal organs, in general, and the GI tract, in particular, are very few. If cortical remapping occurs after RYGB, it could explain what I would like to call *referred satiation*. When food is traversing their esophagus and lower intestines in bypassed subjects with truncated and denervated stomach, they may experience a feeling of satiation reminiscent of that normally evoked by gastric distension. This is because the postprandial stimulation of the cortical areas representing the esophagus and lower intestines is interpreted as originating from the stomach after cortical remapping (**Figure 1**). Perhaps, cortical remapping could explain the exaggerated postprandial neuronal activation and satiation observed in response to jejunum nutrients infusion (Chambers et al., 2012; Mumphrey et al., 2016; Bachler et al., 2018).

Brain Dysconnectivity and Neural Entanglement

The altered functional connectivity of long-range subcortical areas involved in viscerosensitivity and nociception may occur (**Figure 1**). In particular, RYGB has been repeatedly associated with altered functional connectivity in response to food image or food ingestion (Frank et al., 2014; Hunt et al., 2016; Olivo et al., 2017; Baboumian et al., 2019). In the case of food image, brain activity was comparable in normal-weight and RYGB subjects, thus making it difficult to distinguish the contribution of body weight from that of the bypass surgery (Frank et al., 2014). However, in response to food ingestion, brain activity in RYGB patients was significantly different from both normal-weight and obese individuals and weight loss by diet (Hunt et al., 2016; Baboumian et al., 2019). Brain areas differently activated after RYGB encompassed structures distributed across the neuraxis including the hypothalamus, brainstem, hippocampus, and cortex. This suggests that the surgery itself is responsible for the reported changes in brain functions. Many neuroimaging findings in RYGB subjects were often associated with self-reported exaggerated fullness and lower levels of appetite with altered food preferences (Ochner et al., 2011; Hunt et al., 2016; Zoon et al., 2018; Baboumian et al., 2019). Similar brain imaging observations made after VSG (Cerit et al., 2019). Furthermore, widespread structural and functional changes across the brain also take place after RYGB (Rullmann et al., 2018) and VSG (Michaud et al., 2020). Without proving our hypothesis, the above observations are compatible with the idea that large-scale neuroplasticity and maladaptive changes, in both the brain and peripheral nerves, may account for the persistence of satiation and other food-related sensations and emotional responses (**Figure 1**).

If one applies the stochastic entanglement theory to viscerosensory brain networks (Ortiz-Catalan, 2018), cortical and subcortical regions normally involved in evoking satiation may transition to a state of instability after loss of sensory inputs. When in such a state, neurons belonging to separate viscerosensory modalities may eventually become *entangled* and fire together. The direct result of such a state of viscerosensory entanglement may be postprandial sensations and emotional responses that differ from before surgery. Accordingly, bariatric patients often report new sensations and emotional responses to eating (Hillersdal et al., 2017). Clinicians are also becoming increasingly aware of the risk of new food-related behaviors after bariatric surgery, including anorectic-like behaviors (Opozda et al., 2016; Watson et al., 2020). Because of its stochastic nature (Ortiz-Catalan, 2018), entanglement should be associated with a

variability of outcomes after RYGB, both in terms of metabolic benefits (e.g., maximal weigh loss) and side effects (e.g., severity of nausea). In spite of receiving the same surgery, heterogeneity of outcomes among RYGB patients is a well-documented phenomenon (King et al., 2020). This inherent variability in outcomes has complicated the task of determining which exact physiological parameters drive weight-loss in bypassed humans (e.g., feeding vs. energy expenditure). Similarly, in subsets of bypassed subjects, the entanglement of viscerosensory circuits may not occur, potentially leading to failure to lose weight. Certain individuals fail to lose weight after RYGB, often due to excessive eating and psychological issues (Dykstra et al., 2014), with a failure rate estimated at 15–20% (Elnahas et al., 2014; Sima et al., 2019). At first glance, individuals who do not reduce eating after obesity surgery contradict our hypothesis, since the same anatomical changes and degree of trauma to the vagus nerve exist in unresponsive individuals. However, it is noteworthy that phantom sensations, although common in amputees, are not always present. Why certain individuals will not develop phantom sensations, or only temporarily, remains unclear (Ortiz-Catalan, 2018). Perhaps, failure to lose weight after bariatric surgery is related to genetic polymorphisms affecting the neural circuits involved in appetite regulation. A good example is the melanocortin-4-receptor (MC4R), a brain and vagal receptor involved in appetite regulation (Cone, 2006; Gautron et al., 2010). Impaired MC4R signaling in both humans and animals is associated with resistance to RYGB-induced weight loss (Hatoum et al., 2012; Zechner et al., 2013). Gene variations involved in neurotransmitters and gut peptides signaling have also been linked to the outcome of RYGB (Matzko et al., 2012; Novais et al., 2016). This further underscores the critical role that the nervous system plays in the metabolic outcome of obesity surgeries. Alternatively, the entanglement theory may also account for the occasional failure of RYGB. While it remains a speculative theory, the idea of entanglement of viscerosensory functions fits remarkably well with a large body of clinical observations pertinent to bypassed subjects.

PHANTOM SATIATION AND WEIGHT-LOSS

Does Satiation Account for Weight-Loss After RYGB?

One question to ask is whether phantom satiation can contribute to sustained weight loss. It has been argued that reduced meal size in bypassed laboratory animals is unlikely to drive weight loss because, unlike in humans, they tend to consume the same number of daily calories as experimental controls over the long term (Zechner et al., 2013; Mokadem et al., 2014; Arble et al., 2018). In fact, bypassed animals progressively eat more meals in a compensatory manner (Zheng et al., 2009). Instead, a combination of elevated energy expenditure and malabsorption contribute to weight loss in animal models of bariatric surgery (Bueter et al., 2010; Li et al., 2015; Ye et al., 2020). Many biological and technical factors may possibly account for species differences in the outcome of bariatric surgery (Sandoval, 2019). In particular, the anatomical organization of viscerosensory circuits may differ between primates and rodents (Craig, 2002). Moreover, metabolic regulation differs in significant ways between humans and laboratory rodents (Even et al., 2017). Here, I suggest that phantom satiation can partially contribute to weight loss, even in the case of unchanged total daily food intake. Indeed, emerging evidence points to the fact that meal size and feeding timing contribute to the etiology of human obesity, independent of changes in total food intake (Berg et al., 2009; Mattson et al., 2014; Baron et al., 2017; McHill et al., 2017). Moreover, inherent circadian variations in central and peripheral metabolic pathways exist (Hatori et al., 2012; Cedernaes et al., 2019). Remarkably, constraining laboratory rodents to eating small intermittent meals is sufficient to prevent hyperphagia and diet-induced obesity even in association with unchanged daily caloric intake (Licholai et al., 2018). Hence, it is plausible that phantom satiation, by constraining meal size and patterns throughout the day, may contribute to weight loss (**Figure 1**). Our hypothesis is focused on satiation and feeding behavior but, by no means, excludes the contribution of altered energy expenditure to the health benefits of bariatric surgery. In fact, food intake and energy expenditure are more intertwined than often considered. For example, the simple act of sham feeding (chewing followed by spitting) can raise energy expenditure in human subjects (LeBlanc and Cabanac, 1989; LeBlanc and Soucy, 1996). The latter phenomenon has been described as a *cephalic thermic response to food*. Thus, it may be that eating smaller meals more often throughout the day also augments thermogenesis and energy expenditure. That said, gastric denervation cannot account for the entirety of the metabolic effects of bariatric surgery because gastric vagotomy alone is less effective than RYGB. However, this could also be because vagotomy alone does not entirely recapitulate the impact of RYGB on the non-vagal components of the stomach innervation. Lastly, the hypothesis described in this article deliberately focused on satiation because it is a well-known function of vagal signaling in the upper GI tract (Bai et al., 2019). Nonetheless, the vagus nerve is involved in modulating food-related sensations and feelings other than satiation including, but not limited to, food reward, appetition, learned taste avoidance, food preference, and nausea (Sclafani and Kramer, 1985; Labouesse et al., 2012; Sclafani and Ackroff, 2012; Horn, 2014; Behary and Miras, 2015; Hankir et al., 2017; Han et al., 2018; Shechter and Schwartz, 2018; Qu et al., 2019; Sandoval, 2019; Fernandes et al., 2020; Zhang et al., 2020). It is therefore conceivable that phantom sensations arising after bariatric surgery may include phantom nausea and discomfort, as well as taste disturbance and modified food preferences. In apparent agreement with this view, food preference after bariatric surgery shifts away from caloric and fatty food (Chambers et al., 2012; Nielsen et al., 2019). Furthermore, using direct measurements of food intake, human studies showed that weight loss is correlated with a marked reduced preference for caloric food after bariatric surgery, but only in certain individuals (Sondergaard Nielsen et al., 2018). However, food preferences are not significantly changed by surgery in most patients (Sondergaard Nielsen et al., 2018) and, consequently, are unlikely

to play a major role in the metabolic outcomes of either RYGB or VSG in humans.

As a side note, RYGB and VSG rapidly improves glucose homeostasis in both human subjects and laboratory animals (Bojsen-Moller, 2015; Arble et al., 2018). At first glance, the hypothesis described in this article does not seem relevant to glucose metabolism because the anti-diabetic actions of these surgeries occur independently of weight-loss and reduced feeding (Chambers et al., 2011; Laferrere and Pattou, 2018; Evers et al., 2020). On the other hand, eating smaller meals may contribute to improve glucose metabolism after RYGB in human subjects (Stano et al., 2017). Moreover, peripheral nerves are known to play a modulatory role in glucose metabolism (Gardemann et al., 1992; Cardin et al., 2001; Razavi et al., 2006). For instance, gastric vagotomy alone alters glucose homeostasis in humans (Akiyama et al., 1984; Galewski et al., 1995; Plamboeck et al., 2013) and, furthermore, an intact innervation to the portal vein is required for the anti-diabetic actions of RYGB in mice (Troy et al., 2008). Therefore, the hypothesis described in this article may also be relevant to glucose metabolism after bariatric surgery.

Mimicking Phantom Satiation: A New Weight-Loss Treatment?

The second question to ask is whether the phantom satiation hypothesis could help design a new weight-loss treatment. I concur with the view that a better understanding of the biological changes taking place after bariatric surgery may lead to the discovery of a novel and less invasive weight loss treatment (Browning and Hajnal, 2014; Pucci and Batterham, 2019; Gimeno et al., 2020). If the *phantom satiation* hypothesis is correct, the biological changes that accompany bariatric surgeries are highly complex and widespread across the body all the way up to integrative cortices (**Figure 1**). This level of complexity may render difficult finding alternative strategy to bariatric surgery, especially by pharmacological means. With this in mind, a successful alternative to bariatric surgery may consist in permanently silencing the nerves to the upper GI tract, by device- or surgery-assisted means. In support of this view, obese patients are already eligible for an FDA-approved vagal neuromodulation procedure termed vBloc (Shikora et al., 2015; Apovian et al., 2017). Neuromodulatory devices can be laparoscopically implanted and electrodes attached to each vagal trunk near the gastro-oesophaeal junction. The stimulation at the high frequency of at least 500 Hz inhibits the axonal conduction of both motor and sensory neurons (Camilleri et al., 2008; Waataja et al., 2011). Its mechanisms of action remain mysterious and one recent modeling study indicates that vBloc is more likely to excite than inhibit vagal afferents (Pelot et al., 2017). On the other hand, new data in rats also indicate that electrodes chronically attached to the vagus nerve produce significant damage to vagal efferent axons (Somann et al., 2018). Patients can expect an average excess weight loss of 22% over 18 months, which is admittedly not as effective as RYGB. However, vBloc differs in significant ways from bariatric surgery. First, vBloc only stimulates the vagus nerve in an intermittent manner and, secondly, leaves spinal nerves untouched. Regardless of technical details, the *phantom satiation* hypothesis predicts that an effective alternative strategy to bariatric surgery would consist in mimicking, as closely as possible, the patterns of denervation and dysautonomia observed after RYGB. In the anticipation of side effects, such an alternative strategy should ideally be easily reversible and adjustable in strength.

CONCLUDING REMARKS

To paraphrase Dr. David Horrobin, a hypothesis that is wrong will attract no following and disappear (Horrobin, 2000). If proven right, however, it can be the beginning of new fields of knowledge. As of today, the *phantom satiation* hypothesis appears consistent with a large body of literature and provides a complementary explanation to already existing hypotheses on how GI surgeries modify metabolism and behaviors. Many researchers have stressed the key role played by the brain and peripheral nerves in the outcome of bariatric surgery (Powley et al., 2005b; Browning and Hajnal, 2014; Lasselin et al., 2014; Li and Richard, 2017; Hankir et al., 2018; Sinclair et al., 2018; Sandoval, 2019; Nota et al., 2020; Ye et al., 2020). Specifically, they have proposed that microbial, hormonal, inflammatory and autonomic changes may contribute, perhaps synergistically, to alter brain functions after bariatric surgery. In turn, altered brain activity may contribute to modified energy expenditure with or without altered food intake. Together, the *phantom satiation* hypothesis and related neurocentric hypotheses of bariatric surgery invite us to consider the GI tract not merely as a receptacle for food but as a complex sensory organ. Nonetheless, the present hypothesis differs from other theories that convey the idea that bariatric surgery "corrects" biological derangements brought about by obesity. Yes, bariatric surgery is genuinely effective, but it should not be touted as a "corrective procedure," considering that its mechanisms remain uncertain. In particular, available data suggest that vagal and GI functions remain largely normal in obesity (Lieverse et al., 1994; Klatt et al., 1997; Bluemel et al., 2017). In other words, bariatric surgery is done on an otherwise healthy GI tract, which inevitably deteriorates, rather than improves, its functions. The best evidence is that gut peptide secretion in bypassed subjects is very high compared to that of normal-weight subjects (Laferrere et al., 2007; Dirksen et al., 2013). Furthermore, the intestinal mucosa of bypassed human subjects and animals becomes abnormally hypertrophic (le Roux et al., 2010; Mumphrey et al., 2015). Hence, if the *phantom satiation* hypothesis is correct, bariatric surgery is not a procedure that returns obese individuals to some hypothetical state of "normalcy" but rather that profoundly disrupts normal GI viscerosensory and endocrine functions (**Figure 1**). To be clear, the phantom satiation hypothesis should not be interpreted as if humoral mechanisms are irrelevant to the outcome of bariatric surgery. In particular, the receptors for many gut peptides are expressed in brain regions involved in viscerosensory functions (Honda et al., 1993; Zigman et al., 2006; Graham et al., 2020). It is therefore conceivable that excessive gut peptides secretion after bariatric surgery may contribute to exacerbate

the aforementioned brain maladaptive changes observed after vagal damage. Hence, further understanding of the mechanisms underlying bariatric surgery will likely require a multidisciplinary and integrated approach beyond the traditional boundaries of the academic disciplines of endocrinology and metabolism. In particular, one area in need of further research is how bariatric surgeries perturbate interoceptive, nociceptive, and autonomic pathways.

DATA AVAILABILITY STATEMENT

The original contributions presented in the study are included in the article/supplementary material, further inquiries can be directed to the corresponding author.

AUTHOR CONTRIBUTIONS

LG wrote the manuscript entirely and generated the figure.

FUNDING

This work supported by internal funds at the University of Texas Southwestern Medical Center.

ACKNOWLEDGMENTS

The idea behind this article occurred to me while watching the animated movie "I lost my body."

REFERENCES

Abdeen, G., and le Roux, C. W. (2016). Mechanism underlying the weight loss and complications of roux-en-y gastric bypass. review. *Obes. Surg.* 26, 410–421. doi: 10.1007/s11695-015-1945-7

Adachi, Y., Suematsu, T., Shiraishi, N., Katsuta, T., Morimoto, A., Kitano, S., et al. (1999). Quality of life after laparoscopy-assisted billroth i gastrectomy. *Ann. Surg.* 229, 49–54. doi: 10.1097/00000658-199901000-00006

Aglioti, S., Bonazzi, A., and Cortese, F. (1994). Phantom lower limb as a perceptual marker of neural plasticity in the mature human brain. *Proc. Biol. Sci.* 255, 273–278. doi: 10.1098/rspb.1994.0039

Akiyama, H., Ohdate, K., Iwasaki, M., Yoshioka, S., Kameya, S., and Izima, N. (1984). Effects of selective vagotomy with or without drainage on glucose tolerance test. *Jpn. J. Surg.* 14, 15–22. doi: 10.1007/bf02469597

Alhadeff, A. L., Hayes, M. R., and Grill, H. J. (2014). Leptin receptor signaling in the lateral parabrachial nucleus contributes to the control of food intake. *Am. J. Physiol. Regul. Integr. Comp. Physiol.* 307, R1338–R1344.

Alsulaimy, M., Punchai, S., Ali, F. A., Kroh, M., Schauer, R., Brethauer, S. A., et al. (2017). The utility of diagnostic laparoscopy in post-bariatric surgery patients with chronic abdominal pain of unknown etiology. *Obes. Surg.* 27, 1924–1928. doi: 10.1007/s11695-017-2590-0

Alvarez, R., Sandoval, D. A., and Seeley, R. J. (2020). A rodent model of partial intestinal diversion: a novel metabolic operation. *Surg. Obes. Relat. Dis.* 16, 270–281. doi: 10.1016/j.soard.2019.10.026

Alviar, M. J., Hale, T., and Dungca, M. (2016). Pharmacologic interventions for treating phantom limb pain. *Cochrane Database Syst. Rev.* 10:CD006380.

Ammons, W. S., Blair, R. W., and Foreman, R. D. (1983). Vagal afferent inhibition of primate thoracic spinothalamic neurons. *J. Neurophysiol.* 50, 926–940. doi: 10.1152/jn.1983.50.4.926

Andermann, M. L., and Lowell, B. B. (2017). Toward a wiring diagram understanding of appetite control. *Neuron* 95, 757–778. doi: 10.1016/j.neuron.2017.06.014

Andreotti, A. M., Goiato, M. C., Pellizzer, E. P., Pesqueira, A. A., Guiotti, A. M., Gennari-Filho, H., et al. (2014). Phantom eye syndrome: a review of the literature. *Sci. World J.* 2014:686493.

Apovian, C. M., Shah, S. N., Wolfe, B. M., Ikramuddin, S., Miller, C. J., Tweden, K. S., et al. (2017). Two-year outcomes of vagal nerve blocking (Vbloc) for the treatment of obesity in the recharge trial. *Obes. Surg.* 27, 169–176. doi: 10.1007/s11695-016-2325-7

Arble, D. M., Evers, S. S., Bozadjieva, N., Frikke-Schmidt, H., Myronovych, A., Lewis, A., et al. (2018). Metabolic comparison of one-anastomosis gastric bypass, single-anastomosis duodenal-switch, Roux-En-Y Gastric bypass, and vertical sleeve gastrectomy in rat. *Surg. Obes. Relat. Dis.* 14, 1857–1867. doi: 10.1016/j.soard.2018.08.019

Baboumian, S., Pantazatos, S. P., Kothari, S., McGinty, J., Holst, J., and Geliebter, A. (2019). Functional magnetic resonance imaging (FMRI) of neural responses to visual and auditory food stimuli pre and post Roux-En-Y Gastric Bypass (Rygb) and Sleeve Gastrectomy (Sg). *Neuroscience* 409, 290–298. doi: 10.1016/j.neuroscience.2019.01.061

Bachler, T., Geary, N., Bueter, M., Leeners, B., Rehfeld, J. F., Lutz, T. A., et al. (2018). Rygb increases the satiating effect of intrajejunal lipid infusions in female rats. *Appetite* 131, 94–99. doi: 10.1016/j.appet.2018.08.020

Bai, L., Mesgarzadeh, S., Ramesh, K. S., Huey, E. L., Liu, Y., Gray, L. A., et al. (2019). Genetic identification of vagal sensory neurons that control feeding. *Cell* 179, 1129–1143e23.

Bailey, P., and Bremer, F. (1938). A sensory cortical representaiton of the vagus nerve: with a note on the effects of low blood pressure on the cortical electrogram. *J. Neurophysiol.* 1, 405–412. doi: 10.1152/jn.1938.1.5.405

Baldwin, B. A., Parrott, R. F., and Ebenezer, I. S. (1998). Food for thought: a critique on the hypothesis that endogenous cholecystokinin acts as a physiological satiety factor. *Prog. Neurobiol.* 55, 477–507. doi: 10.1016/s0301-0082(98)00005-7

Baron, K. G., Reid, K. J., Kim, T., Horn, L. Van, Attarian, H., Wolfe, L., et al. (2017). Circadian timing and alignment in healthy adults: associations with bmi, body fat, caloric intake and physical activity. *Int. J. Obes. (Lond.)* 41, 203–209. doi: 10.1038/ijo.2016.194

Behary, P., and Miras, A. D. (2015). Food preferences and underlying mechanisms after bariatric surgery. *Proc. Nutr. Soc.* 74, 419–425. doi: 10.1017/s0029665115002074

Bellisle, F., Drewnowski, A., Anderson, G. H., Westerterp-Plantenga, M., and Martin, C. K. (2012). Sweetness, satiation, and satiety. *J. Nutr.* 142, 1149S–1154S.

Benelam, B. (2009). Satiation, satiety and their effects on eating behaviour. *Nutr. Bull.* 34, 126–173. doi: 10.1111/j.1467-3010.2009.01753.x

Berg, C., Lappas, G., Wolk, A., Strandhagen, E., Toren, K., Rosengren, A., et al. (2009). Eating patterns and portion size associated with obesity in a swedish population. *Appetite* 52, 21–26. doi: 10.1016/j.appet.2008.07.008

Berthoud, H. R. (2008). The vagus nerve, food intake and obesity. *Regul. Pept.* 149, 15–25. doi: 10.1016/j.regpep.2007.08.024

Berthoud, H. R. (2012). The neurobiology of food intake in an obesogenic environment. *Proc. Nutr. Soc.* 71, 478–487. doi: 10.1017/s0029665112000602

Berthoud, H. R., and Neuhuber, W. L. (2019). Vagal mechanisms as neuromodulatory targets for the treatment of metabolic disease. *Ann. N.Y. Acad. Sci.* 1454, 42–55. doi: 10.1111/nyas.14182

Berthoud, H. R., Patterson, L. M., Neumann, F., and Neuhuber, W. L. (1997). Distribution and structure of vagal afferent intraganglionic laminar endings (Igles) in the rat gastrointestinal tract. *Anat. Embryol. (Berl.)* 195, 183–191. doi: 10.1007/s004290050037

Berthoud, H. R., Sutton, G. M., Townsend, R. L., Patterson, L. M., and Zheng, H. (2006). Brainstem mechanisms integrating gut-derived satiety signals and descending forebrain information in the control of meal size. *Physiol. Behav.* 89, 517–524. doi: 10.1016/j.physbeh.2006.08.018

Bjorkman, B., Lund, I., Arner, S., and Hyden, L. C. (2017). The meaning and consequences of amputation and mastectomy from the perspective of pain and suffering. *Scand. J. Pain* 14, 100–107. doi: 10.1016/j.sjpain.2016.09.012

Bluemel, S., Menne, D., Milos, G., Goetze, O., Fried, M., Schwizer, W., et al. (2017). Relationship of body weight with gastrointestinal motor and sensory

function: studies in anorexia nervosa and obesity. *BMC Gastroenterol.* 17:4. doi: 10.1186/s12876-016-0560-y

Blundell, J. E., Stubbs, R. J., Golding, C., Croden, F., Alam, R., Whybrow, S., et al. (2005). Resistance and susceptibility to weight gain: individual variability in response to a high-fat diet. *Physiol. Behav.* 86, 614–622. doi: 10.1016/j.physbeh.2005.08.052

Bojsen-Moller, K. N. (2015). Mechanisms of improved glycaemic control after Roux-En-Y Gastric bypass. *Dan. Med. J.* 62:B5057.

Boland, B., Mumphrey, M. B., Hao, Z., Gill, B., Townsend, R. L., Yu, S., et al. (2019). The PYY/Y2r-deficient mouse responds normally to high-fat diet and gastric bypass surgery. *Nutrients* 11:585. doi: 10.3390/nu11030585

Boring, E. G. (1915). The sensations of the alimentary canal. *Am. J. Psychol.* 26, 1–57. doi: 10.2307/1412877

Brolin, R. E., Robertson, L. B., Kenler, H. A., and Cody, R. P. (1994). Weight loss and dietary intake after vertical banded gastroplasty and Roux-En-Y Gastric bypass. *Ann. Surg.* 220, 782–790. doi: 10.1097/00000658-199412000-00012

Browning, K. N. (2019). Stress-induced modulation of vagal afferents. *Neurogastroenterol. Motil.* 31:e13758.

Browning, K. N., Babic, T., Holmes, G. M., Swartz, E., and Travagli, R. A. (2013a). A critical re-evaluation of the specificity of action of perivagal capsaicin. *J. Physiol.* 591(Pt 6), 1563–1580. doi: 10.1113/jphysiol.2012.246827

Browning, K. N., Fortna, S. R., and Hajnal, A. (2013b). Roux-En-Y Gastric Bypass reverses the effects of diet-induced obesity to inhibit the responsiveness of central vagal motoneurones. *J. Physiol.* 591, 2357–2372. doi: 10.1113/jphysiol.2012.249268

Browning, K. N., and Hajnal, A. (2014). The effects of bariatric surgery: will understanding its mechanism render the knife unnecessary? *Expert Rev. Gastroenterol. Hepatol.* 8, 1–4. doi: 10.1586/17474124.2014.846214

Buch, N. S., Qerama, E., Brix Finnerup, N., and Nikolajsen, L. (2020). Neuromas and postamputation pain. *Pain* 161, 147–155. doi: 10.1097/j.pain.0000000000001705

Bueter, M., Lowenstein, C., Olbers, T., Wang, M., Cluny, N. L., Bloom, S. R., et al. (2010). Gastric bypass increases energy expenditure in rats. *Gastroenterology* 138, 1845–1853. doi: 10.1053/j.gastro.2009.11.012

Camilleri, M., Toouli, J., Herrera, M. F., Kulseng, B., Kow, L., Pantoja, J. P., et al. (2008). Intra-abdominal vagal blocking (Vbloc therapy): clinical results with a new implantable medical device. *Surgery* 143, 723–731. doi: 10.1016/j.surg.2008.03.015

Campos, C. A., Bowen, A. J., Schwartz, M. W., and Palmiter, R. D. (2016). Parabrachial CGRP neurons control meal termination. *Cell Metab.* 23, 811–820. doi: 10.1016/j.cmet.2016.04.006

Camps, G., Mars, M., de Graaf, C., and Smeets, P. A. (2016). Empty calories and phantom fullness: a randomized trial studying the relative effects of energy density and viscosity on gastric emptying determined by MRI and satiety. *Am. J. Clin. Nutr.* 104, 73–80. doi: 10.3945/ajcn.115.129064

Cao, J., Lu, K. H., Powley, T. L., and Liu, Z. (2017). Vagal nerve stimulation triggers widespread responses and alters large-scale functional connectivity in the rat brain. *PLoS One* 12:e0189518. doi: 10.1371/journal.pone.0189518

Cardin, S., Jackson, A., Edgerton, D. S., Neal, D. W., Coffey, C. S., and Cherrington, A. D. (2001). Effect of vagal cooling on the counterregulatory response to hypoglycemia induced by a low dose of insulin in the conscious dog. *Diabetes* 50, 558–564. doi: 10.2337/diabetes.50.3.558

Cavanaugh, A. R., Schwartz, G. J., and Blouet, C. (2015). High-fat feeding impairs nutrient sensing and gut brain integration in the caudomedial nucleus of the solitary tract in mice. *PLoS One* 10:e0118888. doi: 10.1371/journal.pone.0118888

Cedernaes, J., Huang, W., Ramsey, K. M., Waldeck, N., Cheng, L., Marcheva, B., et al. (2019). Transcriptional basis for rhythmic control of hunger and metabolism within the AGRP neuron. *Cell Metab.* 29, 1078–1091 e5.

Cerit, H., Davidson, P., Hye, T., Moondra, P., Haimovici, F., Sogg, S., et al. (2019). Resting-state brain connectivity predicts weight loss and cognitive control of eating behavior after vertical sleeve gastrectomy. *Obesity (Silver Spring)* 27, 1846–1855. doi: 10.1002/oby.22607

Cervero, F. (1994). Sensory innervation of the viscera: peripheral basis of visceral pain. *Physiol. Rev.* 74, 95–138. doi: 10.1152/physrev.1994.74.1.95

Chambers, A. P., Jessen, L., Ryan, K. K., Sisley, S., Wilson-Perez, H. E., Stefater, M. A., et al. (2011). Weight-independent changes in blood glucose homeostasis after gastric bypass or vertical sleeve gastrectomy in rats. *Gastroenterology* 141, 950–958. doi: 10.1053/j.gastro.2011.05.050

Chambers, A. P., Wilson-Perez, H. E., McGrath, S., Grayson, B. E., Ryan, K. K., D'Alessio, D. A., et al. (2012). Effect of vertical sleeve gastrectomy on food selection and satiation in rats. *Am. J. Physiol. Endocrinol. Metab.* 303, E1076–E1084.

Chang, T. M., Chan, D. C., Liu, Y. C., Tsou, S. S., and Chen, T. H. (2001). Long-term results of duodenectomy with highly selective vagotomy in the treatment of complicated duodenal ulcers. *Am. J. Surg.* 181, 372–376. doi: 10.1016/s0002-9610(01)00580-3

Chavez, M., Kelly, L., York, D. A., and Berthoud, H. R. (1997). Chemical lesion of visceral afferents causes transient overconsumption of unfamiliar high-fat diets in rats. *Am. J. Physiol.* 272(5 Pt 2), R1657–R1663.

Cohen, R. V., Pinheiro, J. C., Schiavon, C. A., Salles, J. E., Wajchenberg, B. L., and Cummings, D. E. (2012). Effects of Gastric bypass surgery in patients with type 2 diabetes and only mild obesity. *Diabetes Care* 35, 1420–1428. doi: 10.2337/dc11-2289

Collins, K. L., Russell, H. G., Schumacher, P. J., Robinson-Freeman, K. E., O'Conor, E. C., Gibney, K. D., et al. (2018). A review of current theories and treatments for phantom limb pain. *J. Clin. Invest.* 128, 2168–2176. doi: 10.1172/jci94003

Cone, R. D. (2006). Studies on the physiological functions of the melanocortin system. *Endocr. Rev.* 27, 736–749. doi: 10.1210/er.2006-0034

Cox, J. E., and Powley, T. L. (1981). Prior vagotomy blocks vmh obesity in pair-fed rats. *Am. J. Physiol.* 240, E573–E583.

Craig, A. D. (2002). How do you feel? Interoception: the sense of the physiological condition of the body. *Nat. Rev. Neurosci.* 3, 655–666. doi: 10.1038/nrn894

Dayawansa, S., Peckins, S., Ruch, S., and Norgren, R. (2011). Parabrachial and hypothalamic interaction in sodium appetite. *Am. J. Physiol. Regul. Integr. Comp. Physiol.* 300, R1091–R1099.

de Araujo, I. E., Geha, P., and Small, D. M. (2012). Orosensory and homeostatic functions of the insular taste cortex. *Chemosens. Percept.* 5, 64–79. doi: 10.1007/s12078-012-9117-9

de Graaf, C., Blom, W. A., Smeets, A., Stafleu, A., and Hendriks, H. F. (2004). Biomarkers of satiation and satiety. *Am. J. Clin. Nutr.* 79, 946–961.

Dezfuli, G., Gillis, R. A., Tatge, J. E., Duncan, K. R., Dretchen, K. L., Jackson, G., et al. (2018). Subdiaphragmatic vagotomy with pyloroplasty ameliorates the obesity caused by genetic deletion of the melanocortin 4 receptor in the mouse. *Front. Neurosci.* 12:104. doi: 10.3389/fnins.2018.00104

Di Noto, P. M., Newman, L., Wall, S., and Einstein, G. (2013). The hermunculus: what is known about the representation of the female body in the brain? *Cereb. Cortex* 23, 1005–1013. doi: 10.1093/cercor/bhs005

Dijkstra, P. U., Geertzen, J. H., Stewart, R., and van der Schans, C. P. (2002). Phantom pain and risk factors: a multivariate analysis. *J. Pain Symptom Manage.* 24, 578–585.

Dirksen, C., Damgaard, M., Bojsen-Moller, K. N., Jorgensen, N. B., Kielgast, U., Jacobsen, S. H., et al. (2013). Fast pouch emptying, delayed small intestinal transit, and exaggerated gut hormone responses after Roux-En-Y Gastric bypass. *Neurogastroenterol. Motil.* 25, 346–e255.

Dorpat, T. L. (1971). Phantom sensation of internal organs. *Compr. Psychiatry* 12, 27–35. doi: 10.1016/0010-440x(71)90053-8

Dossat, A. M., Diaz, R., Gallo, L., Panagos, A., Kay, K., and Williams, D. L. (2013). Nucleus accumbens Glp-1 receptors influence meal size and palatability. *Am. J. Physiol. Endocrinol. Metab.* 304, E1314–E1320.

Dutta, T. M., Josiah, A. F., Cronin, C. A., Wittenberg, G. F., and Cole, J. W. (2013). Altered taste and stroke: a case report and literature review. *Top Stroke Rehabil.* 20, 78–86. doi: 10.1310/tsr2001-78

Dykstra, M. A., Switzer, N. J., Sherman, V., Karmali, S., and Birch, D. W. (2014). Roux En Y Gastric bypass: how and why it fails? *Surg. Curr. Res.* 4:165.

Egerod, K. L., Schwartz, T. W., and Gautron, L. (2019). The molecular diversity of vagal afferents revealed. *Trends Neurosci.* 42, 663–666. doi: 10.1016/j.tins.2019.08.002

Elnahas, A. I., Jackson, T. D., and Hong, D. (2014). Management of failed laparoscopic Roux-En-Y Gastric bypass. *Bariatr. Surg. Pract. Patient Care* 9, 36–40.

Erecius, L. F., Dixon, K. D., Jiang, J. C., and Gietzen, D. W. (1996). Meal patterns reveal differential effects of vagotomy and tropisetron on responses to indispensable amino acid deficiency in rats. *J. Nutr.* 126, 1722–1731. doi: 10.1093/jn/126.6.1722

Even, C., Virtue, S., Morton, N. M., Fromentin, G., and Semple, R. K. (2017). Editorial: are rodent models fit for investigation of human obesity and related diseases? *Front. Nutr.* 4:58. doi: 10.3389/fnut.2017.00058

Evers, S. S., Lewis, A. G., Tong, C., Shao, Y., Alvarez, R., Ridelman, E., et al. (2020). The unconventional role for gastric volume in the response to bariatric surgery for both weight loss and glucose lowering. *Ann. Surg.* 271, 1102–1109. doi: 10.1097/sla.0000000000003240

Farley, C., Cook, J. A., Spar, B. D., Austin, T. M., and Kowalski, T. J. (2003). Meal pattern analysis of diet-induced obesity in susceptible and resistant rats. *Obes. Res.* 11, 845–851. doi: 10.1038/oby.2003.116

Faxen, A., Rossander, L., and Kewenter, J. (1979). The effect of parietal cell vagotomy and selective vagotomy with pyloroplasty on body weight and dietary habits. a prospective randomized study. *Scand. J. Gastroenterol.* 14, 7–11. doi: 10.3109/00365527909179839

Fernandes, A. B., Alves da Silva, J., Almeida, J., Cui, G., Gerfen, C. R., Costa, R. M., et al. (2020). Postingestive modulation of food seeking depends on vagus-mediated dopamine neuron activity. *Neuron* 106, 778–788 e6.

Ferrari, B., Arnold, M., Carr, R. D., Langhans, W., Pacini, G., Bodvarsdottir, T. B., et al. (2005). Subdiaphragmatic vagal deafferentation affects body weight gain and glucose metabolism in obese male zucker (Fa/Fa) rats. *Am. J. Physiol. Regul. Integr. Comp. Physiol.* 289, R1027–R1034.

Ferraz, A. A. B., de Sa, V. C. T., Santa-Cruz, F., Siqueira, L. T., Silva, L. B., and Campos, J. M. (2019). Roux-En-Y Gastric bypass for nonobese patients with uncontrolled type 2 diabetes: a long-term evaluation. *Surg. Obes. Relat. Dis.* 15, 682–687. doi: 10.1016/j.soard.2019.02.006

Flor, H., Diers, M., and Andoh, J. (2013). The neural basis of phantom limb pain. *Trends Cogn. Sci.* 17, 307–308. doi: 10.1016/j.tics.2013.04.007

Formolo, D. A., Gaspar, J. M., Melo, H. M., Eichwald, T., Zepeda, R. J., Latini, A., et al. (2019). Deep brain stimulation for obesity: a review and future directions. *Front. Neurosci.* 13:323. doi: 10.3389/fnins.2019.00323

Fox, E. A. (2006). A genetic approach for investigating vagal sensory roles in regulation of gastrointestinal function and food intake. *Auton Neurosci.* 12, 9–29. doi: 10.1016/j.autneu.2006.03.005

Fox, E. A., Phillips, R. J., Martinson, F. A., Baronowsky, E. A., and Powley, T. L. (2000). Vagal afferent innervation of smooth muscle in the stomach and duodenum of the mouse: morphology and topography. *J. Comp. Neurol.* 428, 558–576. doi: 10.1002/1096-9861(20001218)428:3<558::aid-cne11>3.0.co;2-m

Fox, E. A., Phillips, R. J., Martinson, F. A., Baronowsky, E. A., and Powley, T. L. (2001). C-Kit mutant mice have a selective loss of vagal intramuscular mechanoreceptors in the forestomach. *Anat. Embryol. (Berl.)* 204, 11–26. doi: 10.1007/s004290100184

Frank, S., Heinze, J. M., Fritsche, A., Linder, K., von Feilitzsch, M., Konigsrainer, A., et al. (2016). Neuronal food reward activity in patients with type 2 diabetes with improved glycemic control after bariatric surgery. *Diabetes Care* 39, 1311–1317. doi: 10.2337/dc16-0094

Frank, S., Wilms, B., Veit, R., Ernst, B., Thurnheer, M., Kullmann, S., et al. (2014). Altered brain activity in severely obese women may recover after Roux-En Y Gastric bypass surgery. *Int. J. Obes. (Lond.)* 38, 341–348. doi: 10.1038/ijo.2013.60

Fraser, A. G., Brunt, P. W., and Matheson, N. A. (1983). A comparison of highly selective vagotomy with truncal vagotomy and pyloroplasty–one surgeon's results after 5 years. *Br. J. Surg.* 70, 485–488. doi: 10.1002/bjs.1800700811

French, S. J., Murray, B., Rumsey, R. D., Sepple, C. P., and Read, N. W. (1993). Is cholecystokinin a satiety hormone? correlations of plasma cholecystokinin with hunger, satiety and gastric emptying in normal volunteers. *Appetite* 21, 95–104. doi: 10.1016/0195-6663(93)90002-2

Furness, J. B. (2006). The organisation of the autonomic nervous system: peripheral connections. *Auton Neurosci.* 130, 1–5. doi: 10.1016/j.autneu.2006.05.003

Furuta, S., Matsumoto, K., Horie, S., Suzuki, T., and Narita, M. (2012). Subdiaphragmatic vagotomy induces a functional change in visceral adelta primary afferent fibers in rats. *Synapse* 66, 369–371. doi: 10.1002/syn.20991

Furuta, S., Shimizu, T., Narita, M., Matsumoto, K., Kuzumaki, N., Horie, S., et al. (2009). Subdiaphragmatic vagotomy promotes nociceptive sensitivity of deep tissue in rats. *Neuroscience* 164, 1252–1262. doi: 10.1016/j.neuroscience.2009.09.021

Galewski, D., Schwille, O., Rumenapf, G., Scheele, J., Kissler, H., and Steinlein, R. (1995). Proximal gastric vagotomy: effects of two surgical modifications on oral and intravenous glucose tolerance in the conscious rat. *Physiol. Behav.* 57, 813–819. doi: 10.1016/0031-9384(94)00331-x

Gardemann, A., Puschel, G. P., and Jungermann, K. (1992). Nervous control of liver metabolism and hemodynamics. *Eur. J. Biochem.* 207, 399–411. doi: 10.1111/j.1432-1033.1992.tb17063.x

Gautron, L., Lee, C., Funahashi, H., Friedman, J., Lee, S., and Elmquist, J. (2010). Melanocortin-4 receptor expression in a vago-vagal circuitry involved in postprandial functions. *J. Comp. Neurol.* 518, 6–24. doi: 10.1002/cne.22221

Gautron, L., Zechner, J. F., and Aguirre, V. (2013). Vagal innervation patterns following Roux-En-Y Gastric bypass in the mouse. *Int. J. Obes. (Lond.)* 37, 1603–1607. doi: 10.1038/ijo.2013.48

Geliebter, A., Westreich, S., Gage, D., and Hashim, S. A. (1986). Intragastric balloon reduces food intake and body weight in rats. *Am. J. Physiol.* 251(4 Pt 2), R794–R797.

Geloneze, B., Geloneze, S. R., Fiori, C., Stabe, C., Tambascia, M. A., Chaim, E. A., et al. (2009). Surgery for nonobese type 2 diabetic patients: an interventional study with duodenal-jejunal exclusion. *Obes. Surg.* 19, 1077–1083. doi: 10.1007/s11695-009-9844-4

Gero, D. (2020). Challenges in the interpretation and therapeutic manipulation of human ingestive microstructure. *Am. J. Physiol. Regul. Integr. Comp. Physiol.* 318, R886–R893.

Gibbons, C., Hopkins, M., Beaulieu, K., Oustric, P., and Blundell, J. E. (2019). Issues in measuring and interpreting human appetite (satiety/satiation) and its contribution to obesity. *Curr. Obes. Rep.* 8, 77–87. doi: 10.1007/s13679-019-00340-6

Gibbs, J., and Smith, G. P. (1977). Cholecystokinin and satiety in rats and rhesus monkeys. *Am. J. Clin. Nutr.* 30, 758–761. doi: 10.1093/ajcn/30.5.758

Gimeno, R. E., Briere, D. A., and Seeley, R. J. (2020). Leveraging the gut to treat metabolic disease. *Cell Metab.* 31, 679–698. doi: 10.1016/j.cmet.2020.02.014

Gortz, L., Bjorkman, A. C., Andersson, H., and Kral, J. G. (1990). Truncal vagotomy reduces food and liquid intake in man. *Physiol. Behav.* 48, 779–781. doi: 10.1016/0031-9384(90)90226-t

Goto, M., and Swanson, L. W. (2004). Axonal projections from the parasubthalamic nucleus. *J. Comp. Neurol.* 469, 581–607. doi: 10.1002/cne.11036

Graham, D. L., Durai, H. H., Trammell, T. S., Noble, B. L., Mortlock, D. P., Galli, A., et al. (2020). A novel mouse model of glucagon-like peptide-1 receptor expression: a look at the brain. *J. Comp. Neurol.* 528, 2445–2470. doi: 10.1002/cne.24905

Groven, K. S., Raheim, M., and Engelsrud, G. (2010). "My quality of life is worse compared to my earlier life": living with chronic problems after weight loss surgery. *Int. J. Qual. Stud. Health Well-being* 5:4.

Grundy, D. (1988). Speculations on the structure/function relationship for vagal and splanchnic afferent endings supplying the gastrointestinal tract. *J. Auton Nerv. Syst.* 22, 175–180. doi: 10.1016/0165-1838(88)90104-x

Halmi, K. A., Mason, E., Falk, J. R., and Stunkard, A. (1981). Appetitive Behavior after Gastric Bypass for Obesity. *Int. J. Obes.* 5, 457–464.

Han, W., Tellez, L. A., Perkins, M. H., Perez, I. O., Qu, T., Ferreira, J., et al. (2018). A neural circuit for gut-induced reward. *Cell* 175, 665–678 e23.

Hankir, M. K., Patt, M., Patt, J. T., Becker, G. A., Rullmann, M., Kranz, M., et al. (2016). Suppressed fat appetite after Roux-En-Y gastric bypass surgery associates with reduced brain mu-opioid receptor availability in diet-induced obese Male rats. *Front Neurosci* 10:620. doi: 10.3389/fnins.2016.00620

Hankir, M. K., Seyfried, F., Hintschich, C. A., Diep, T. A., Kleberg, K., Kranz, M., et al. (2017). Gastric bypass surgery recruits a gut Ppar-alpha-striatal D1r pathway to reduce fat appetite in obese rats. *Cell Metab.* 25, 335–344. doi: 10.1016/j.cmet.2016.12.006

Hankir, M. K., Seyfried, F., Miras, A. D., and Cowley, M. A. (2018). Brain feeding circuits after Roux-En-Y Gastric bypass. *Trends Endocrinol. Metab.* 29, 218–237. doi: 10.1016/j.tem.2018.01.009

Hao, Z., Leigh Townsend, R., Mumphrey, M. B., Gettys, T. W., Yu, S., Munzberg, H., et al. (2018). Roux-En-Y Gastric bypass surgery-induced weight loss and metabolic improvements are similar in TGR5-deficient and wildtype mice. *Obes. Surg.* 28, 3227–3236. doi: 10.1007/s11695-018-3297-6

Hao, Z., Mumphrey, M. B., Townsend, R. L., Morrison, C. D., Munzberg, H., Ye, J., et al. (2016). Reprogramming of defended body weight after Roux-En-Y Gastric bypass surgery in diet-induced obese mice. *Obesity (Silver Spring)* 24, 654–660. doi: 10.1002/oby.21400

Harada, K., Yoshida, N., Baba, Y., Nakamura, K., Kosumi, K., Ishimoto, T., et al. (2018). Pyloroplasty may reduce weight loss 1 year after esophagectomy. *Dis. Esophagus.* 31:3.

Hatori, M., Vollmers, C., Zarrinpar, A., DiTacchio, L., Bushong, E. A., Gill, S., et al. (2012). Time-restricted feeding without reducing caloric intake prevents metabolic diseases in mice fed a high-fat diet. *Cell Metab* 15, 848–860. doi: 10.1016/j.cmet.2012.04.019

Hatoum, I. J., Stylopoulos, N., Vanhoose, A. M., Boyd, K. L., Yin, D. P., Ellacott, K. L., et al. (2012). Melanocortin-4 receptor signaling is required for weight loss after gastric bypass surgery. *J. Clin. Endocrinol. Metab.* 97, E1023–E1031.

Hays, S. A., Rennaker, R. L., and Kilgard, M. P. (2013). Targeting plasticity with vagus nerve stimulation to treat neurological disease. *Prog. Brain Res.* 207, 275–299. doi: 10.1016/b978-0-444-63327-9.00010-2

Hertz, A. F. (1911). *The Sensibility of the Alimentary Canal*. Oxford: Oxford University Press.

Hetherington, M. M., Blundell-Birtill, P., Caton, S. J., Cecil, J. E., Evans, C. E., Rolls, B. J., et al. (2018). Understanding the science of portion control and the art of downsizing. *Proc. Nutr. Soc.* 77, 347–355. doi: 10.1017/s0029665118000435

Hill, D. L., and Almli, C. R. (1983). Parabrachial nuclei damage in infant rats produces residual deficits in gustatory preferences/aversions and sodium appetite. *Dev. Psychobiol.* 16, 519–533. doi: 10.1002/dev.420160608

Hillersdal, L., Christensen, B. J., and Holm, L. (2017). Changing tastes: learning hunger and fullness after gastric bypass surgery. *Sociol Health Illn* 39, 474–487. doi: 10.1111/1467-9566.12504

Honda, T., Wada, E., Battey, J. F., and Wank, S. A. (1993). Differential gene expression of Cck(a) and Cck(B) receptors in the rat brain. *Mol. Cell Neurosci.* 4, 143–154.

Horn, C. C. (2014). Measuring the nausea-to-emesis continuum in non-human animals: refocusing on gastrointestinal vagal signaling. *Exp. Brain Res.* 232, 2471–2481. doi: 10.1007/s00221-014-3985-y

Horrobin, D. F. (2000). Why is speculation so awful? *BMJ* 321, 571–572. doi: 10.1136/bmj.321.7260.571/a

Hunt, K. F., Dunn, J. T., le Roux, C. W., Reed, L. J., Marsden, K., Patel, A. G., et al. (2016). Differences in regional brain responses to food ingestion after roux-en-y gastric bypass and the role of gut peptides: a neuroimaging study. *Diabetes Care* 39, 1787–1795. doi: 10.2337/dc15-2721

Hunter, J. P., Katz, J., and Davis, K. D. (2003). The effect of tactile and visual sensory inputs on phantom limb awareness. *Brain* 126(Pt 3), 579–589. doi: 10.1093/brain/awg054

Hyde, T. M., and Miselis, R. R. (1983). Effects of area postrema/caudal medial nucleus of solitary tract lesions on food intake and body weight. *Am. J. Physiol.* 244, R577–R587.

Iannelli, A., Facchiano, E., and Gugenheim, J. (2006). Internal hernia after laparoscopic roux-en-y gastric bypass for morbid obesity. *Obes. Surg.* 16, 1265–1271. doi: 10.1381/096089206778663689

Irving, A. D., Smith, G., and Coubrough, H. (1985). Long-term metabolic effects of truncal vagotomy and gastrojejunostomy for chronic duodenal ulcer. *Clin. Nutr.* 4, 129–133. doi: 10.1016/0261-5614(85)90017-2

Ito, S., and Craig, A. D. (2003). Vagal input to lateral area 3a in cat cortex. *J. Neurophysiol.* 90, 143–154. doi: 10.1152/jn.01054.2002

Janig, W., Khasar, S. G., Levine, J. D., and Miao, F. J. (2000). The role of vagal visceral afferents in the control of nociception. *Prog. Brain Res.* 122, 273–287. doi: 10.1016/s0079-6123(08)62145-7

Jordan, P. H. Jr., and Thornby, J. (1987). Should it be parietal cell vagotomy or selective vagotomy-antrectomy for treatment of duodenal ulcer? a progress report. *Ann. Surg.* 205, 572–590. doi: 10.1097/00000658-198705000-00017

Keenan, G. S., Brunstrom, J. M., and Ferriday, D. (2015). Effects of meal variety on expected satiation: evidence for a 'perceived volume'. *Heuristic. Appetite* 89, 10–15. doi: 10.1016/j.appet.2015.01.010

Keil, G. (1990). [So-called initial description of phantom pain by ambroise pare. "Chose Digne D'admiration Et Quasi Incredible": the "Douleur Es Parties Mortes Et Amputees"]. *Fortschr. Med.* 108, 62–66.

Kenler, H. A., Brolin, R. E., and Cody, R. P. (1990). Changes in eating behavior after horizontal gastroplasty and Roux-En-Y gastric bypass. *Am. J. Clin. Nutr.* 52, 87–92. doi: 10.1093/ajcn/52.1.87

Kenney, N. J., Kott, J. N., Tomoyasu, N., Bhatia, A. J., Ruiz, A. S., and McDowell, M. M. (1989). Body weight of rats following area postrema ablation: effect of early force-feeding. *Am. J. Physiol.* 256(4 Pt 2), R939–R945.

Kentish, S., Li, H., Philp, L. K., O'Donnell, T. A., Isaacs, N. J., Young, R. L., et al. (2012). Diet-induced adaptation of vagal afferent function. *J. Physiol.* 590(Pt 1), 209–221. doi: 10.1113/jphysiol.2011.222158

Kentish, S. J., O'Donnell, T. A., Frisby, C. L., Li, H., Wittert, G. A., and Page, A. J. (2014). Altered gastric vagal mechanosensitivity in diet-induced obesity persists on return to normal chow and is accompanied by increased food intake. *Int. J. Obes. (Lond.)* 38, 636–642. doi: 10.1038/ijo.2013.138

Khasar, S. G., Miao, F. J., Janig, W., and Levine, J. D. (1998). Vagotomy-induced enhancement of mechanical hyperalgesia in the rat is sympathoadrenal-mediated. *J. Neurosci.* 18, 3043–3049. doi: 10.1523/jneurosci.18-08-03043.1998

Kindel, T. L., Martins, P. J., Yoder, S. M., Jandacek, R. J., Seeley, R. J., D'Alessio, D. A., et al. (2011). Bypassing the duodenum does not improve insulin resistance associated with diet-induced obesity in rodents. *Obes.(Silver Spring)* 19, 380–387. doi: 10.1038/oby.2010.263

King, W. C., Hinerman, A. S., and Courcoulas, A. P. (2020). Weight regain after bariatric surgery: a systematic literature review and comparison across studies using a large reference sample. *Surg. Obes. Relat. Dis.* 16, 1133–1144. doi: 10.1016/j.soard.2020.03.034

Kizy, S., Jahansouz, C., Wirth, K., Ikramuddin, S., and Leslie, D. (2017). Bariatric surgery: a perspective for primary care. *Diabetes Spectr.* 30, 265–276. doi: 10.2337/ds17-0034

Klatt, S., Pieramico, O., Guthner, C., Ditschuneit, H. H., Glasbrenner, B., Beckh, K., et al. (1997). Proximal gastric motility functions are normal in severe obesity. *Digestion* 58, 115–119. doi: 10.1159/000201433

Komegae, E. N., Farmer, D. G. S., Brooks, V. L., McKinley, M. J., McAllen, R. M., and Martelli, D. (2018). Vagal afferent activation suppresses systemic inflammation via the splanchnic anti-inflammatory pathway. *Brain Behav. Immun.* 73, 441–449. doi: 10.1016/j.bbi.2018.06.005

Korner, J., Inabnet, W. I, Conwell, M., Taveras, C., Daud, A., Olivero-Rivera, L., et al. (2006). Differential effects of gastric bypass and banding on circulating gut hormone and leptin levels. *Obes. (Silver Spring)* 14, 1553–1561. doi: 10.1038/oby.2006.179

Kott, J. N., Ganfield, C. L., and Kenney, N. J. (1984). Area postrema/nucleus of the solitary tract ablations: analysis of the effects of hypophagia. *Physiol. Behav.* 32, 429–435. doi: 10.1016/0031-9384(84)90258-0

Kral, J. G. (1978). Vagotomy for treatment of severe obesity. *Lancet* 1, 307–308. doi: 10.1016/s0140-6736(78)90074-0

Kral, J. G., Paez, W., and Wolfe, B. M. (2009). Vagal nerve function in obesity: therapeutic implications. *World J. Surg.* 33, 1995–2006. doi: 10.1007/s00268-009-0138-8

Kral, T. V. E., Moore, R. H., Chittams, J., Jones, E., O'Malley, L., and Fisher, J. O. (2018). Identifying behavioral phenotypes for childhood obesity. *Appetite* 127, 87–96. doi: 10.1016/j.appet.2018.04.021

Kraly, F. S., Jerome, C., and Smith, G. P. (1986). Specific postoperative syndromes after total and selective vagotomies in the rat. *Appetite* 7, 1–17. doi: 10.1016/s0195-6663(86)80038-1

la Fleur, S. E., Luijendijk, M. C., van der Zwaal, E. M., Brans, M. A., and Adan, R. A. (2014). The snacking rat as model of human obesity: effects of a free-choice high-fat high-sugar diet on meal patterns. *Int. J. Obes. (Lond.)* 38, 643–649. doi: 10.1038/ijo.2013.159

Labouesse, M. A., Stadlbauer, U., Weber, E., Arnold, M., Langhans, W., and Pacheco-Lopez, G. (2012). Vagal afferents mediate early satiation and prevent flavour avoidance learning in response to intraperitoneally infused exendin-4. *J. Neuroendocrinol.* 24, 1505–1516. doi: 10.1111/j.1365-2826.2012.02364.x

Ladabaum, U., Roberts, T. P., and McGonigle, D. J. (2007). Gastric fundic distension activates fronto-limbic structures but not primary somatosensory cortex: a functional magnetic resonance imaging study. *Neuroimage* 34, 724–732. doi: 10.1016/j.neuroimage.2006.07.033

Laferrere, B., Heshka, S., Wang, K., Khan, Y., McGinty, J., Teixeira, J., et al. (2007). Incretin levels and effect are markedly enhanced 1 month after Roux-En-Y Gastric bypass surgery in obese patients with type 2 diabetes. *Diabetes Care* 30, 1709–1716. doi: 10.2337/dc06-1549

Laferrere, B., and Pattou, F. (2018). Weight-independent mechanisms of glucose control after Roux-En-Y Gastric bypass. *Front Endocrinol (Lausanne)* 9:530. doi: 10.3389/fendo.2018.00530

Laffitte, A. M., Polakowski, C. B., and Kato, M. (2015). Early oral re-feeding on oncology patients submitted to gastrectomy for gastric cancer. *Arq. Bras. Cir. Dig.* 28, 200–203. doi: 10.1590/s0102-67202015000300014

Langer, F. B., Bohdjalian, A., Felberbauer, F. X., Fleischmann, E., Reza Hoda, M. A., Ludvik, B., et al. (2006). Does gastric dilatation limit the success of sleeve gastrectomy as a sole operation for morbid obesity? *Obes. Surg.* 16, 166–171. doi: 10.1381/096089206775565276

Lasselin, J., Magne, E., Beau, C., Ledaguenel, P., Dexpert, S., Aubert, A., et al. (2014). Adipose inflammation in obesity: relationship with circulating levels of inflammatory markers and association with surgery-induced weight loss. *J. Clin. Endocrinol. Metab.* 99, E53–E61.

Laurenius, A., Larsson, I., Bueter, M., Melanson, K. J., Bosaeus, I., Forslund, H. B., et al. (2012). Changes in eating behaviour and meal pattern following Roux-En-Y Gastric bypass. *Int. J. Obes. (Lond.)* 36, 348–355. doi: 10.1038/ijo.2011.217

le Roux, C. W., Borg, C., Wallis, K., Vincent, R. P., Bueter, M., Goodlad, R., et al. (2010). Gut hypertrophy after gastric bypass is associated with increased glucagon-like peptide 2 and intestinal crypt cell proliferation. *Ann. Surg.* 252, 50–56. doi: 10.1097/sla.0b013e3181d3d21f

LeBlanc, J., and Cabanac, M. (1989). Cephalic postprandial thermogenesis in human subjects. *Physiol. Behav.* 46, 479–482. doi: 10.1016/0031-9384(89)90024-3

LeBlanc, J., and Soucy, J. (1996). Interactions between postprandial thermogenesis, sensory stimulation of feeding, and hunger. *Am. J. Physiol.* 271(4 Pt 2), R936–R940.

Leonhardt, M., Hrupka, B. J., and Langhans, W. (2004). Subdiaphragmatic vagal deafferentation fails to block the anorectic effect of hydroxycitrate. *Physiol. Behav.* 82, 263–268. doi: 10.1016/j.physbeh.2004.03.021

Levinthal, D. J., and Strick, L. (2020). Multiple areas of the cerebral cortex influence the stomach. *Proc. Natl. Acad. Sci. U.S.A.* 117, 13078–13083. doi: 10.1073/pnas.2002737117

Li, W., Baraboi, E. D., Cluny, N. L., Roy, M. C., Samson, P., Biertho, L., et al. (2015). Malabsorption plays a major role in the effects of the biliopancreatic diversion with duodenal switch on energy metabolism in rats. *Surg. Obes. Relat. Dis.* 11, 356–366. doi: 10.1016/j.soard.2014.07.020

Li, W., and Richard, D. (2017). Effects of bariatric surgery on energy homeostasis. *Can. J. Diabetes* 41, 426–431. doi: 10.1016/j.jcjd.2017.05.002

Licholai, J. A., Nguyen, K. P., Fobbs, W. C., Schuster, C. J., Ali, M. A., and Kravitz, A. V. (2018). Why do mice overeat high-fat diets? How high-fat diet alters the regulation of daily caloric intake in mice. *Obesity (Silver Spring)* 26, 1026–1033. doi: 10.1002/oby.22195

Lieverse, R. J., Jansen, J. B., Masclee, A. M., and Lamers, C. B. (1994). Satiety effects of cholecystokinin in humans. *Gastroenterology* 106, 1451–1454. doi: 10.1016/0016-5085(94)90397-2

Lutz, T. A., and Bueter, M. (2014). The physiology underlying Roux-En-Y Gastric bypass: a status report. *Am. J. Physiol. Regul Integr Comp Physiol* 307, R1275–R1291.

Ly, H. G., Dupont, P., Van Laere, K., Depoortere, I., Tack, J., and Oudenhove, L. Van (2017). Differential brain responses to gradual intragastric nutrient infusion and gastric balloon distension: a role for gut peptides? *Neuroimage* 144(Pt A), 101–112. doi: 10.1016/j.neuroimage.2016.09.032

Madden, C. J., and Morrison, S. F. (2016). A high-fat diet impairs cooling-evoked brown adipose tissue activation via a vagal afferent mechanism. *Am. J. Physiol. Endocrinol. Metab.* 311, E287–E292.

Madden, C. J., Santos da Conceicao, E. P., and Morrison, S. F. (2017). Vagal afferent activation decreases brown adipose tissue (Bat) sympathetic nerve activity and bat thermogenesis. *Temperature (Austin)* 4, 89–96. doi: 10.1080/23328940.2016.1257407

Mak, Y. E., Simmons, K. B., Gitelman, D. R., and Small, D. M. (2005). Taste and olfactory intensity perception changes following left insular stroke. *Behav. Neurosci.* 119, 1693–1700. doi: 10.1037/0735-7044.119.6.1693

Makin, T. R., and Flor, H. (2020). Brain (Re)organisation following amputation: implications for phantom limb pain. *Neuroimage* 218:116943. doi: 10.1016/j.neuroimage.2020.116943

Makin, T. R., Scholz, J., Filippini, N., Henderson Slater, D., Tracey, I., and Johansen-Berg, H. (2013). Phantom pain is associated with preserved structure and function in the former hand area. *Nat. Commun.* 4:1570.

Mala, T., and Hogestol, I. (2018). Abdominal pain after roux-en-y gastric bypass for morbid obesity. *Scand. J. Surg.* 107, 277–284. doi: 10.1177/1457496918772360

Mathes, C. M., Bohnenkamp, R. A., le Roux, C. W., and Spector, A. C. (2015). Reduced sweet and fatty fluid intake after Roux-En-Y Gastric bypass in rats is dependent on experience without change in stimulus motivational potency. *Am. J. Physiol. Regul. Integr. Comp. Physiol.* 309, R864–R874.

Mattson, M. P., Allison, D. B., Fontana, L., Harvie, M., Longo, V. D., Malaisse, W. J., et al. (2014). Meal frequency and timing in health and disease. *Proc. Natl. Acad. Sci. U.S.A.* 111, 16647–16653.

Matzko, M. E., Argyropoulos, G., Wood, G. C., Chu, X., McCarter, R. J., Still, C. D., et al. (2012). Association of ghrelin receptor promoter polymorphisms with weight loss following Roux-En-Y gastric bypass surgery. *Obes. Surg.* 22, 783–790. doi: 10.1007/s11695-012-0631-2

McDougle, M., Quinn, D., Diepenbroek, C., Singh, A., de la Serre, C., and de Lartigue, G. (2020). Intact vagal gut-brain signaling prevents hyperphagia and excessive weight gain in response to high-fat high-sugar diet. *Acta Physiol. (Oxf)* e13530.

McHill, A. W., Phillips, A. J., Czeisler, C. A., Keating, L., Yee, K., Barger, L. K., et al. (2017). Later circadian timing of food intake is associated with increased body fat. *Am. J. Clin. Nutr.* 106, 1213–1219.

Melhorn, S. J., Krause, E. G., Scott, K. A., Mooney, M. R., Johnson, J. D., Woods, S. C., et al. (2010). Acute exposure to a high-fat diet alters meal patterns and body composition. *Physiol. Behav.* 99, 33–39. doi: 10.1016/j.physbeh.2009.10.004

Michaud, A., Dadar, M., Pelletier, M., Zeighami, Y., Garcia-Garcia, I., Iceta, S., et al. (2020). Neuroanatomical changes in white and grey matter after sleeve gastrectomy. *Neuroimage* 213, 116696. doi: 10.1016/j.neuroimage.2020.116696

Miller, G. D., Norris, A., and Fernandez, A. (2014). Changes in Nutrients and food groups intake following laparoscopic Roux-En-Y gastric bypass (RYGB). *Obes. Surg.* 24, 1926–1932. doi: 10.1007/s11695-014-1259-1

Min, D. K., Tuor, U. I., and Chelikani, K. (2011). Gastric distention induced functional magnetic resonance signal changes in the rodent brain. *Neuroscience* 179, 151–158. doi: 10.1016/j.neuroscience.2011.01.051

Minaya, D. M., Di Lorenzo, P. M., Hajnal, A., and Czaja, K. (2019). Rouxeny gastric bypass surgery triggers rapid dna fragmentation in vagal afferent neurons in rats. *Acta Neurobiol. Exp. (Wars)* 79, 432–444. doi: 10.21307/ane-2019-040

Miras, A. D., and le Roux, C. W. (2013). Mechanisms underlying weight loss after bariatric surgery. *Nat. Rev. Gastroenterol. Hepatol.* 10, 575–584. doi: 10.1038/nrgastro.2013.119

Mogilner, A., Grossman, J. A., Ribary, U., Joliot, M., Volkmann, J., Rapaport, D., et al. (1993). Somatosensory Cortical Plasticity in Adult Humans Revealed by Magnetoencephalography. *Proc Natl Acad Sci U S A* 90, 3593–3597. doi: 10.1073/pnas.90.8.3593

Mokadem, M., Zechner, J. F., Margolskee, R. F., Drucker, D. J., and Aguirre, V. (2014). Effects of Roux-En-Y Gastric bypass on energy and glucose homeostasis are preserved in two mouse models of functional glucagon-like peptide-1 deficiency. *Mol. Metab.* 3, 191–201. doi: 10.1016/j.molmet.2013.11.010

Moon, R. C., Frommelt, A., Teixeira, A. F., and Jawad, M. A. (2015). Indications and outcomes of reversal of Roux-En-Y Gastric bypass. *Surg. Obes Relat Dis* 11, 821–826.

Mordes, J. P., el Lozy, M., Herrera, M. G., and Silen, W. (1979). Effects of vagotomy with and without pyloroplasty on weight and food intake in rats. *Am. J. Physiol.* 236, R61–R66.

Morrison, C. D., Hao, Z., Mumphrey, M. B., Townsend, R. L., Munzberg, H., Ye, J., et al. (2016). Roux-En-Y Gastric bypass surgery is effective in fibroblast growth factor-21 deficient mice. *Mol. Metab.* 5, 1006–1014. doi: 10.1016/j.molmet.2016.08.005

Mulak, A., Kahane, P., Hoffmann, D., Minotti, L., and Bonaz, B. (2008). Brain mapping of digestive sensations elicited by cortical electrical stimulations. *Neurogastroenterol. Motil.* 20, 588–596. doi: 10.1111/j.1365-2982.2007.01066.x

Mumphrey, M. B., Hao, Z., Leigh Townsend, R., Qualls-Creekmore, E., Yu, S., Lutz, T. A., et al. (2019). Gastric bypass surgery in lean adolescent mice prevents diet-induced obesity later in life. *Sci. Rep.* 9:7881.

Mumphrey, M. B., Hao, Z., Townsend, R. L., Patterson, L. M., and Berthoud, H. R. (2015). Sleeve gastrectomy does not cause hypertrophy and reprogramming of intestinal glucose metabolism in rats. *Obes. Surg.* 25, 1468–1473. doi: 10.1007/s11695-014-1547-9

Mumphrey, M. B., Hao, Z., Townsend, R. L., Patterson, L. M., Munzberg, H., Morrison, C. D., et al. (2016). Eating in mice with gastric bypass surgery causes exaggerated activation of brainstem anorexia circuit. *Int. J. Obes. (Lond.)* 40, 921–928. doi: 10.1038/ijo.2016.38

Nangunoori, R. K., Tomycz, N. D., Oh, M. Y., and Whiting, D. M. (2016). Deep brain stimulation for obesity: from a theoretical framework to practical application. *Neural. Plast* 2016:7971460.

Nathan, W. (1981). Gastric sensation: report of a case. *Pain* 10, 259–262. doi: 10.1016/0304-3959(81)90202-5

Nguyen, N. Q., Debreceni, T. L., Burgstad, C. M., Neo, M., Bellon, M., Wishart, J. M., et al. (2016). Effects of fat and protein preloads on pouch emptying, intestinal transit, glycaemia, gut hormones, glucose absorption, blood pressure and gastrointestinal symptoms after Roux-En-Y Gastric bypass. *Obes. Surg.* 26, 77–84. doi: 10.1007/s11695-015-1722-7

Nielsen, M. S., Schmidt, J. B., le Roux, C. W., and Sjodin, A. (2019). Effects of Roux-En-Y Gastric bypass and sleeve gastrectomy on food preferences and potential mechanisms involved. *Curr. Obes. Rep.* 8, 292–300. doi: 10.1007/s13679-019-00354-0

Nordmark, F., and Johansson, R. S. (2020). Disinhibition of human primary somatosensory cortex after median nerve transection and reinnervation. *Front. Hum. Neurosci.* 14:166. doi: 10.3389/fnhum.2020.00166

Nota, M. H. C., Vreeken, D., Wiesmann, M., Aarts, E. O., Hazebroek, E. J., and Kiliaan, A. J. (2020). Obesity affects brain structure and function- rescue by bariatric surgery? *Neurosci. Biobehav. Rev.* 108, 646–657. doi: 10.1016/j.neubiorev.2019.11.025

Noun, R., Slim, R., Nasr, M., Chakhtoura, G., Gharios, J., Antoun, N. A., et al. (2016). Results of laparoscopic sleeve gastrectomy in 541 consecutive patients with low baseline body mass index (30-35 Kg/M(2)). *Obes. Surg.* 26, 2824–2828. doi: 10.1007/s11695-016-2224-y

Novais, F., Weber, T. K., Lemke, N., Verlengia, R., Crisp, A. H., Rasera-Junior, I., et al. (2016). Gene polymorphisms as a predictor of body weight loss after Roux-En-Y Gastric bypass surgery among obese women. *Obes. Res. Clin. Pract.* 10, 724–727. doi: 10.1016/j.orcp.2016.07.002

O'Brien, J. H., Pimpaneau, A., and Albe-Fessard, D. (1971). Evoked cortical responses to vagal, laryngeal and facial afferents in monkeys under chloralose anaesthesia. *Electroencephalogr. Clin. Neurophysiol.* 31, 7–20. doi: 10.1016/0013-4694(71)90285-9

Ochner, C. N., Kwok, Y., Conceicao, E., Pantazatos, S. P., Puma, L. M., Carnell, S., et al. (2011). selective reduction in neural responses to high calorie foods following gastric bypass surgery. *Ann. Surg.* 253, 502–507. doi: 10.1097/sla.0b013e318203a289

Odstrcil, E. A., Martinez, J. G., Santa Ana, C. A., Xue, B., Schneider, R. E., Steffer, K. J., et al. (2010). The contribution of malabsorption to the reduction in net energy absorption after long-limb Roux-En-Y gastric bypass. *Am. J. Clin. Nutr.* 92, 704–713. doi: 10.3945/ajcn.2010.29870

Olivo, G., Zhou, W., Sundbom, M., Zhukovsky, C., Hogenkamp, P., Nikontovic, L., et al. (2017). Resting-state brain connectivity changes in obese women after roux-en-y gastric bypass surgery: a longitudinal study. *Sci. Rep.* 7:6616.

Opozda, M., Chur-Hansen, A., and Wittert, G. (2016). Changes in problematic and disordered eating after gastric bypass, adjustable gastric banding and vertical sleeve gastrectomy: a systematic review of pre-post studies. *Obes. Rev.* 17, 770–792. doi: 10.1111/obr.12425

Ortiz-Catalan, M. (2018). The stochastic entanglement and phantom motor execution hypotheses: a theoretical framework for the origin and treatment of phantom limb pain. *Front. Neurol.* 9:748. doi: 10.3389/fneur.2018.00748

Ovesen, P., Kroner, K., Ornsholt, J., and Bach, K. (1991). Phantom-related phenomena after rectal amputation: prevalence and clinical characteristics. *Pain* 44, 289–291. doi: 10.1016/0304-3959(91)90099-j

Ozaki, N., Sengupta, J. N., and Gebhart, G. F. (1999). Mechanosensitive properties of gastric vagal afferent fibers in the rat. *J. Neurophysiol.* 82, 2210–2220. doi: 10.1152/jn.1999.82.5.2210

Peles, S., Petersen, J., Aviv, R., Policker, S., Abu-Hatoum, O., Ben-Haim, S. A., et al. (2003). Enhancement of antral contractions and vagal afferent signaling with synchronized electrical stimulation. *Am. J. Physiol. Gastrointest. Liver Physiol.* 285, G577–G585.

Pelot, N. A., Behrend, C. E., and Grill, W. M. (2017). Modeling the response of small myelinated axons in a compound nerve to kilohertz frequency signals. *J. Neural Eng.* 14:046022. doi: 10.1088/1741-2552/aa6a5f

Phillips, R. J., and Powley, T. L. (1998). Gastric volume detection after selective vagotomies in rats. *Am. J. Physiol.* 274, R1626–R1638.

Pierik, A. S., Coblijn, U. K., de Raaff, C. A. L., van Veen, R. N., van Tets, W. F., and van Wagensveld, B. A. (2017). Unexplained abdominal pain in morbidly obese patients after bariatric surgery. *Surg. Obes. Relat. Dis.* 13, 1743–1751. doi: 10.1016/j.soard.2017.05.027

Plamboeck, A., Veedfald, S., Deacon, C. F., Hartmann, B., Wettergren, A., Svendsen, L. B., et al. (2013). The effect of exogenous GLP-1 on food intake is lost in male truncally vagotomized subjects with pyloroplasty. *Am. J. Physiol. Gastrointest. Liver Physiol.* 304, G1117–G1127.

Pool, J. L. (1954). The visceral brain of man. *J. Neurosurg.* 11, 45–63. doi: 10.3171/jns.1954.11.1.0045

Popiela, T., Turczynowski, W., Karcz, D., Legutko, J., and Zajac, A. (1993). Long-term results of highly selective vagotomy in the treatment of duodenal ulcer patients using the intra-operative endoscopic congo red test to identify the parietal cell antrum-corpus borderline. *Hepatogastroenterology* 40, 267–271.

Powley, T. L., Chi, M. M., Baronowsky, E. A., and Phillips, R. J. (2005a). Gastrointestinal tract innervation of the mouse: afferent regeneration and meal patterning after vagotomy. *Am. J. Physiol. Regul. Integr. Comp. Physiol.* 289, R563–R574.

Powley, T. L., Chi, M. M., Schier, L. A., and Phillips, R. J. (2005b). Obesity: should treatments target visceral afferents? *Physiol. Behav.* 86, 698–708. doi: 10.1016/j.physbeh.2005.08.059

Powley, T. L., Hudson, C. N., McAdams, J. L., Baronowsky, E. A., and Phillips, R. J. (2016). Vagal intramuscular arrays: the specialized mechanoreceptor arbors that innervate the smooth muscle layers of the stomach examined in the rat. *J. Comp. Neurol.* 524, 713–737. doi: 10.1002/cne.23892

Pucci, A., and Batterham, R. L. (2019). Mechanisms underlying the weight loss effects of Rygb and Sg: similar, yet different. *J. Endocrinol. Invest.* 42, 117–128. doi: 10.1007/s40618-018-0892-2

Qiu, S., Zhang, M., Liu, Y., Guo, Y., Zhao, H., Song, Q., et al. (2014). Glua1 phosphorylation contributes to postsynaptic amplification of neuropathic pain in the insular cortex. *J. Neurosci.* 34, 13505–13515. doi: 10.1523/jneurosci.1431-14.2014

Qu, T., Han, W., Niu, J., Tong, J., and de Araujo, I. E. (2019). On the roles of the duodenum and the vagus nerve in learned nutrient preferences. *Appetite* 139, 145–151. doi: 10.1016/j.appet.2019.04.014

Rajendran, S., Challis, R. C., Fowlkes, C. C., Hanna, P., Tompkins, J. D., Jordan, M. C., et al. (2019). Identification of peripheral neural circuits that regulate heart rate using optogenetic and viral vector strategies. *Nat. Commun.* 10:1944.

Ramachandran, V. S., Brang, D., and McGeoch, P. D. (2009). Size reduction using mirror visual feedback (MVF) reduces phantom pain. *Neurocase* 15, 357–360. doi: 10.1080/13554790903081767

Randich, A., and Gebhart, G. F. (1992). Vagal afferent modulation of nociception. *Brain Res. Brain Res. Rev.* 17, 77–99. doi: 10.1016/0165-0173(92)90009-b

Razavi, R., Chan, Y., Afifiyan, F. N., Liu, X. J., Wan, X., Yantha, J., et al. (2006). Trpv1+ sensory neurons control beta cell stress and islet inflammation in autoimmune diabetes. *Cell* 127, 1123–1135.

Reidelberger, R., Haver, A., Anders, K., and Apenteng, B. (2014). Role of capsaicin-sensitive peripheral sensory neurons in anorexic responses to intravenous infusions of cholecystokinin, peptide Yy-(3-36), and glucagon-like peptide-1 in rats. *Am. J. Physiol. Endocrinol. Metab.* 307, E619–E629.

Remple, M. S., Jain, N., Diener, P. S., and Kaas, J. H. (2004). Bilateral effects of spinal overhemisections on the development of the somatosensory system in rats. *J. Comp. Neurol.* 475, 604–619. doi: 10.1002/cne.20203

Rogers, J. (2018). Combating excessive eating: a role for four evidence-based remedies. *Obesity (Silver Spring)* 26 Suppl 3, S18–S24.

Roldan, C. J., and Lesnick, J. S. (2014). Phantom organ pain syndrome, a ghostly visitor to the Ed. *Am. J. Emerg. Med.* 32, e1–e2.

Rullmann, M., Preusser, S., Poppitz, S., Heba, S., Hoyer, J., Schutz, T., et al. (2018). Gastric-bypass surgery induced widespread neural plasticity of the obese human brain. *Neuroimage* 172, 853–863. doi: 10.1016/j.neuroimage.2017.10.062

Sabbatini, M., Grossini, E., Molinari, C., Mary, D., Vacca, G., and Cannas, M. (2017). Gastric distension causes changes in heart rate and arterial blood pressure by affecting the crosstalk between vagal and splanchnic systems in anesthetised rats. *Exp. Brain Res.* 235, 1081–1095. doi: 10.1007/s00221-016-4819-x

Sandoval, D. A. (2019). Mechanisms for the metabolic success of bariatric surgery. *J. Neuroendocrinol.* 31:e12708. doi: 10.1111/jne.12708

Saper, C. B. (2000). Pain as a visceral sensation. *Prog. Brain Res.* 122, 237–243. doi: 10.1016/s0079-6123(08)62142-1

Saper, C. B. (2002). The central autonomic nervous system: conscious visceral perception and autonomic pattern generation. *Annu. Rev. Neurosci.* 25, 433–469. doi: 10.1146/annurev.neuro.25.032502.111311

Saper, C. B., Loewy, A. D., Swanson, L. W., and Cowan, W. M. (1976). Direct hypothalamo-autonomic connections. *Brain Res.* 117, 305–312. doi: 10.1016/0006-8993(76)90738-1

Scherbakov, N., Dirnagl, U., and Doehner, W. (2011). Body weight after stroke: lessons from the obesity paradox. *Stroke* 42, 3646–3650. doi: 10.1161/strokeaha.111.619163

Scherbakov, N., Pietrock, C., Sandek, A., Ebner, N., Valentova, M., Springer, J., et al. (2019). Body weight changes and incidence of cachexia after stroke. *J. Cachexia Sarcopenia Muscle* 10, 611–620. doi: 10.1002/jcsm.12400

Scholtz, S., Miras, A. D., Chhina, N., Prechtl, C. G., Sleeth, M. L., Daud, N. M., et al. (2014). Obese patients after gastric bypass surgery have lower brain-hedonic responses to food than after gastric banding. *Gut* 63, 891–902. doi: 10.1136/gutjnl-2013-305008

Schwartz, G. J., Salorio, C. F., Skoglund, C., and Moran, T. H. (1999). , Gut vagal afferent lesions increase meal size but do not block gastric preload-induced feeding suppression. *Am. J. Physiol* .276(6 Pt 2), R1623–R1629.

Schwartz, G. J., Tougas, G., and Moran, T. H. (1995). Integration of vagal afferent responses to duodenal loads and exogenous Cck in rats. *Peptides* 16, 707–711. doi: 10.1016/0196-9781(95)00033-g

Sclafani, A., and Ackroff, K. (2012). Role of gut nutrient sensing in stimulating appetite and conditioning food preferences. *Am. J. Physiol. Regul. Integr. Comp. Physiol.* 302, R1119–R1133.

Sclafani, A., Ackroff, K., and Schwartz, G. J. (2003). Selective effects of vagal deafferentation and celiac-superior mesenteric ganglionectomy on the reinforcing and satiating action of intestinal nutrients. *Physiol. Behav.* 78, 285–294. doi: 10.1016/s0031-9384(02)00968-x

Sclafani, A., Aravich, P. F., and Landman, M. (1981). Vagotomy blocks hypothalamic hyperphagia in rats on a chow diet and sucrose solution, but not on a palatable mixed diet. *J. Comp. Physiol. Psychol.* 95, 720–734. doi: 10.1037/h0077830

Sclafani, A., and Kramer, T. H. (1985). Aversive effects of vagotomy in the rat: a conditioned taste aversion analysis. *Physiol. Behav.* 34, 721–725. doi: 10.1016/0031-9384(85)90370-1

Shah, K., and Gislason, H. (2020). Roux-En-Y Gastric bypass reversal: a novel technique with functional reversal - case series. *Obes. Surg.* 30, 1589–1595. doi: 10.1007/s11695-020-04420-8

Sharkey, K. A., Beck, L., and McKay, D. M. (2018). Neuroimmunophysiology of the gut: advances and emerging concepts focusing on the epithelium. *Nat. Rev. Gastroenterol. Hepatol.* 15, 765–784. doi: 10.1038/s41575-018-0051-4

Shechter, A., and Schwartz, G. J. (2018). Gut-brain nutrient sensing in food reward. *Appetite* 122, 32–35. doi: 10.1016/j.appet.2016.12.009

Sheiner, H. J., Quinlan, M. F., and Thompson, I. J. (1980). Gastric motility and emptying in normal and post-vagotomy subjects. *Gut,* 21, 753–759. doi: 10.1136/gut.21.9.753

Shikora, S. A., Wolfe, B. M., Apovian, C. M., Anvari, M., Sarwer, D. B., Gibbons, R. D., et al. (2015). Sustained weight loss with vagal nerve blockade but not with sham: 18-month results of the recharge trial. *J. Obes.* 2015:365604.

Shoar, S., Nguyen, T., Ona, M. A., Reddy, M., Anand, S., Alkuwari, M. J., et al. (2016). Roux-En-Y Gastric bypass reversal: a systematic review. *Surg. Obes. Relat. Dis.* 12, 1366–1372.

Sima, E., Webb, D. L., Hellstrom, M., and Sundbom, M. (2019). Non-responders after gastric bypass surgery for morbid obesity: peptide hormones and glucose homeostasis. *Obes. Surg.* 29, 4008–4017. doi: 10.1007/s11695-019-04089-8

Sinclair, P., Brennan, D. J., and le Roux, C. W. (2018). Gut adaptation after metabolic surgery and its influences on the brain, liver and cancer. *Nat. Rev. Gastroenterol. Hepatol.* 15, 606–624. doi: 10.1038/s41575-018-0057-y

Smith, G. P., Jerome, C., Cushin, B. J., Eterno, R., and Simansky, K. J. (1981). Abdominal vagotomy blocks the satiety effect of cholecystokinin in the rat. *Science* 213, 1036–1037. doi: 10.1126/science.7268408

Somann, J. P., Albors, G. O., Neihouser, K. V., Lu, K. H., Liu, Z., Ward, M. P., et al. (2018). Chronic cuffing of cervical vagus nerve inhibits efferent fiber integrity in rat model. *J. Neural Eng.* 15:036018. doi: 10.1088/1741-2552/aaa039

Sondergaard Nielsen, M., Rasmussen, S., Just Christensen, B., Ritz, C., le Roux, C. W., Berg Schmidt, J., et al. (2018). Bariatric surgery does not affect food preferences, but individual changes in food preferences may predict weight loss. *Obesity (Silver Spring)* 26, 1879–1887. doi: 10.1002/oby.22272

Spencer, N. J., Hibberd, T. J., Lagerstrom, M., Otsuka, Y., and Kelley, N. (2018). Visceral pain – novel approaches for optogenetic control of spinal afferents. *Brain Res.* 1693(Pt B), 159–164. doi: 10.1016/j.brainres.2018.02.002

Spencer, N. J., Kyloh, M., Beckett, E. A., Brookes, S., and Hibberd, T. (2016). Different types of spinal afferent nerve endings in stomach and esophagus identified by anterograde tracing from dorsal root ganglia. *J. Comp. Neurol.* 524, 3064–3083. doi: 10.1002/cne.24006

Stano, S., Alam, F., Wu, L., Dutia, R., Ng, S. N., Sala, M., et al. (2017). Effect of meal size and texture on gastric pouch emptying and glucagon-like peptide 1 after gastric bypass surgery. *Surg. Obes. Relat. Dis.* 13, 1975–1983. doi: 10.1016/j.soard.2017.09.004

Stearns, A. T., Balakrishnan, A., Radmanesh, A., Ashley, S. W., Rhoads, D. B., and Tavakkolizadeh, A. (2012). Relative contributions of afferent vagal fibers to resistance to diet-induced obesity. *Dig. Dis. Sci.* 57, 1281–1290. doi: 10.1007/s10620-011-1968-4

Stefater, M. A., Perez-Tilve, D., Chambers, A. P., Wilson-Perez, H. E., Sandoval, D. A., Berger, J., et al. (2010). Sleeve gastrectomy induces loss of weight and fat mass in obese rats, but does not affect leptin sensitivity. *Gastroenterology* 138, 2426–2436, 2436.e1–3.

Stefater, M. A., Wilson-Perez, H. E., Chambers, A. P., Sandoval, D. A., and Seeley, R. J. (2012). All bariatric surgeries are not created equal: insights from mechanistic comparisons. *Endocr. Rev.* 33, 595–622. doi: 10.1210/er.2011-1044

Stemmer, K., Bielohuby, M., Grayson, B. E., Begg, D. P., Chambers, A. P., Neff, C., et al. (2013). Roux-En-Y Gastric bypass surgery but not vertical sleeve gastrectomy decreases bone mass in male rats. *Endocrinology* 154, 2015–2024. doi: 10.1210/en.2012-2130

Stevenson, R. J., Mahmut, M., and Rooney, K. (2015). Individual differences in the interoceptive states of hunger, fullness and thirst. *Appetite* 95, 44–57. doi: 10.1016/j.appet.2015.06.008

Stratton, R. J., and Elia, M. (1999). The effects of enteral tube feeding and parenteral nutrition on appetite sensations and food intake in health and disease. *Clin. Nutr.* 18, 63–70. doi: 10.1016/s0261-5614(99)80053-3

Stylopoulos, N., and Aguirre, V. (2009). Mechanisms of bariatric surgery and implications for the development of endoluminal therapies for obesity. *Gastrointest. Endosc.* 70, 1167–1175. doi: 10.1016/j.gie.2009.01.022

Syrad, H., Llewellyn, C. H., Johnson, L., Boniface, D., Jebb, S. A., van Jaarsveld, C. H., et al. (2016). Meal size is a critical driver of weight gain in early childhood. *Sci. Rep.* 6:28368.

Tataranni, A., Gautier, J. F., Chen, K., Uecker, A., Bandy, D., Salbe, A. D., et al. (1999). Neuroanatomical correlates of hunger and satiation in humans using positron emission tomography. *Proc. Natl. Acad. Sci. U.S.A.* 96, 4569–4574. doi: 10.1073/pnas.96.8.4569

Thornhill, K., Charlton, K., Probst, Y., and Neale, E. (2019). Does an increased intake of added sugar affect appetite in overweight or obese adults, when compared with lower intakes? a systematic review of the literature. *Br. J. Nutr.* 121, 232–240. doi: 10.1017/s0007114518003239

Travagli, R. A., Hermann, G. E., Browning, K. N., and Rogers, R. C. (2003). Musings on the wanderer: what's new in our understanding of vago-vagal reflexes? iii. activity-dependent plasticity in vago-vagal reflexes controlling the stomach. *Am. J. Physiol. Gastrointest. Liver Physiol.* 284, G180–G187.

Treesukosol, Y., and Moran, T. H. (2014). Analyses of meal patterns across dietary shifts. *Appetite* 75, 21–29. doi: 10.1016/j.appet.2013.12.004

Troy, S., Soty, M., Ribeiro, L., Laval, L., Migrenne, S., Fioramonti, X., et al. (2008). Intestinal gluconeogenesis is a key factor for early metabolic changes after gastric bypass but not after gastric lap-band in mice. *Cell Metab.* 8, 201–211. doi: 10.1016/j.cmet.2008.08.008

Udit, S., and Gautron, L. (2013). Molecular anatomy of the gut-brain axis revealed with transgenic technologies: implications in metabolic research. *Front. Neurosci.* 7:134. doi: 10.3389/fnins.2013.00134

Waataja, J. J., Tweden, K. S., and Honda, C. N. (2011). Effects of high-frequency alternating current on axonal conduction through the vagus nerve. *J. Neural. Eng.* 8:056013. doi: 10.1088/1741-2560/8/5/056013

Walls, E. K., Wang, F. B., Holst, M. C., Phillips, R. J., Voreis, J. S., Perkins, A. R., et al. (1995). Selective vagal rhizotomies: a new dorsal surgical approach used for intestinal deafferentations. *Am. J. Physiol.* 269(5 Pt 2), R1279–R1288.

Wang, F. B., and Powley, T. L. (2000). Topographic inventories of vagal afferents in gastrointestinal muscle. *J. Comp. Neurol.* 421, 302–324. doi: 10.1002/(sici)1096-9861(20000605)421:3<302::aid-cne2>3.0.co;2-n

Wang, F. B., and Powley, T. L. (2007). Vagal innervation of intestines: afferent pathways mapped with new en bloc horseradish peroxidase adaptation. *Cell Tissue Res.* 329, 221–230. doi: 10.1007/s00441-007-0413-7

Wang, F. B., Young, Y. K., and Kao, C. K. (2012). Abdominal vagal afferent pathways and their distributions of intraganglionic laminar endings in the rat duodenum. *J. Comp. Neurol.* 520, 1098–1113. doi: 10.1002/cne.22812

Wang, G. J., Tomasi, D., Backus, W., Wang, R., Telang, F., Geliebter, A., et al. (2008). Gastric distention activates satiety circuitry in the human brain. *Neuroimage* 39, 1824–1831. doi: 10.1016/j.neuroimage.2007.11.008

Warde-Kamar, J., Rogers, M., Flancbaum, L., and Laferrere, B. (2004). Calorie intake and meal patterns up to 4 years after Roux-En-Y Gastric bypass surgery. *Obes. Surg.*14, 1070–1079. doi: 10.1381/0960892041975668

Warwick, Z. S. (1996). Probing the causes of high-fat diet hyperphagia: a mechanistic and behavioral dissection. *Neurosci. Biobehav. Rev.* 20, 155–161. doi: 10.1016/0149-7634(95)00034-c

Washington, M. C., Mhalhal, T. R., Johnson-Rouse, T., Berger, J., Heath, J., Seeley, R., et al. (2016). Roux-En-Y Gastric bypass augments the feeding responses evoked by gastrin-releasing peptides. *J. Surg. Res.* 206, 517–524. doi: 10.1016/j.jss.2016.08.057

Watson, C., Riazi, A., and Ratcliffe, D. (2020). Exploring the experiences of women who develop restrictive eating behaviours after bariatric surgery. *Obes. Surg.* 30, 2131–2139. doi: 10.1007/s11695-020-04424-4

Williams, E. K., Chang, R. B., Strochlic, D. E., Umans, B. D., Lowell, B. B., and Liberles, S. D. (2016). Sensory neurons that detect stretch and nutrients in the digestive system. *Cell* 166, 209–221. doi: 10.1016/j.cell.2016.05.011

Wills, R. E., and Grusendorf, E. (1993). Vagotomy with laparotomy. *Surg. Technol.* 8–24.

Wolf, S., and Wolff, H. G. (1943). Pain arising from the stomach and mechanisms underlying gastric symptoms. *Res. Pub. Assoc. Res. Nerv. Ment. Dis.* 23, 289–301.

Xu, B., Yan, X., Shao, Y., Shen, Q., Hua, R., Ding, R., et al. (2015). A comparative study of the effect of gastric bypass, sleeve gastrectomy, and duodenal-jejunal bypass on type-2 diabetes in non-obese rats. *Obes, Surg.* 25, 1966–1975. doi: 10.1007/s11695-015-1835-z

Ye, Y., Abu El Haija, M., Morgan, D. A., Guo, D., Song, Y., Frank, A., et al. (2020). Endocannabinoid receptor-1 and sympathetic nervous system mediate the beneficial metabolic effects of gastric bypass. *Cell Rep.* 33: 108270.

Yousseif, A., Emmanuel, J., Karra, E., Millet, Q., Elkalaawy, M., Jenkinson, A. D., et al. (2014). Differential effects of laparoscopic sleeve gastrectomy and laparoscopic gastric bypass on appetite, circulating acyl-ghrelin, peptide YY3-36 and active GLP-1 levels in non-diabetic humans. *Obes. Surg.* 24, 241–252. doi: 10.1007/s11695-013-1066-0

Zafra, M. A., Aguera, A. D., Molina, F., and Puerto, A. (2017). Disruption of re-intake after partial withdrawal of gastric food contents in rats lesioned in the gelatinous part of the nucleus of the solitary tract. *Appetite* 113, 231–238. doi: 10.1016/j.appet.2017.02.040

Zafra, M. A., Molina, F., and Puerto, A. (2003). Effects of perivagal administration of capsaicin on post-surgical food intake. *Auton Neurosci.* 107, 37–44. doi: 10.1016/s1566-0702(03)00128-0

Zechner, J. F., Mirshahi, U. L., Satapati, S., Berglund, E. D., Rossi, J., Scott, M. M., et al. (2013). Weight-independent effects of Roux-En-Y Gastric bypass on glucose homeostasis via melanocortin-4 receptors in mice and humans. *Gastroenterology* 144, 580–590 e7.

Zhang, C., Kaye, J. A., Cai, Z., Wang, Y., Prescott, S. L., and Liberles, S. D. (2020). Area postrema cell types that mediate nausea-associated behaviors. *Neuron* 1–12.

Zheng, H., Shin, A. C., Lenard, N. R., Townsend, R. L., Patterson, L. M., Sigalet, D. L., et al. (2009). Meal patterns, satiety, and food choice in a rat model of Roux-En-Y gastric bypass surgery. *Am. J. Physiol. Regul. Integr. Comp .Physiol.* 297, R1273–R1282.

Zigman, J. M., Jones, J. E., Lee, C. E., Saper, C. B., and Elmquist, J. K. (2006). Expression of ghrelin receptor mrna in the rat and the mouse brain. *J. Comp. Neurol.* 494, 528–548. doi: 10.1002/cne.20823

Zoon, H. F. A., de Bruijn, S. E. M., Jager, G., Smeets, A. M., de Graaf, C., Janssen, I. M. C., et al. (2018). Altered neural inhibition responses to food cues after Roux-En-Y Gastric bypass. *Biol. Psychol.* 137, 34–41. doi: 10.1016/j.biopsycho.2018.06.005

Conflict of Interest: The author declares that the research was conducted in the absence of any commercial or financial relationships that could be construed as a potential conflict of interest.

frontiers in Neuroscience

MINI REVIEW
published: 26 February 2021
doi: 10.3389/fnins.2021.653928

Integration of Nutrient Sensing in Fish Hypothalamus

*José L. Soengas**

Laboratorio de Fisioloxía Animal, Departamento de Bioloxía Funcional e Ciencias da Saúde, Facultade de Bioloxía and Centro de Investigación Mariña, Universidade de Vigo, Vigo, Spain

The knowledge regarding hypothalamic integration of metabolic and endocrine signaling resulting in regulation of food intake is scarce in fish. Available studies pointed to a network in which the activation of the nutrient-sensing (glucose, fatty acid, and amino acid) systems would result in AMP-activated protein kinase (AMPK) inhibition and activation of protein kinase B (Akt) and mechanistic target of rapamycin (mTOR). Changes in these signaling pathways would control phosphorylation of transcription factors cAMP response-element binding protein (CREB), forkhead box01 (FoxO1), and brain homeobox transcription factor (BSX) leading to food intake inhibition through changes in the expression of neuropeptide Y (NPY), agouti-related peptide (AgRP), pro-opio melanocortin (POMC), and cocaine and amphetamine-related transcript (CART). The present mini-review summarizes information on the topic and identifies gaps for future research.

Keywords: fish, food intake regulation, nutrient sensors, transcription factors, hypothalamic integration

OPEN ACCESS

Edited by:
Lionel Carneiro, The Ohio State University, United States

Reviewed by:
Miguel López, University of Santiago de Compostela, Spain
Young-Hwan Jo, Albert Einstein College of Medicine, United States

***Correspondence:**
José L. Soengas
jsoengas@uvigo.es

Specialty section:
This article was submitted to Neuroenergetics, Nutrition and Brain Health, a section of the journal Frontiers in Neuroscience

Received: *15 January 2021*
Accepted: *26 January 2021*
Published: *26 February 2021*

Citation:
Soengas JL (2021) Integration of Nutrient Sensing in Fish Hypothalamus. Front. Neurosci. 15:653928. doi: 10.3389/fnins.2021.653928

INTRODUCTION

Two neuronal populations in the mammalian hypothalamic arcuate nucleus respond to a rise in the levels of circulating metabolites (fatty acid, glucose, and amino acid) (Blouet and Schwartz, 2010; Morton et al., 2014). They respond with decreased expression of agouti-related peptide (AgRP) and neuropeptide Y (NPY) or increased expression of cocaine and amphetamine-related transcript (CART) and pro-opio melanocortin (POMC). These two populations inhibit each other and signal to higher-order neurons in other areas producing other neuropeptides, and food intake changes due to all these interactions.

In fish, AgRP/NPY and POMC/CART neurons are present in the ventral part of *nucleus lateralis tuberis* (NLTv), an analog of arcuate nucleus (Soengas et al., 2018). These neurons connect to other neuronal populations, both in hypothalamic and extra-hypothalamic locations, though their neuropeptide production is mostly unknown (Soengas et al., 2018). The regulation of energy expenditure and food intake relies on detection in vertebrate hypothalamus of changes in nutrient levels through different sensing mechanisms as demonstrated in mammals (Efeyan et al., 2015; Bruce et al., 2017) and fish (Soengas, 2014; Delgado et al., 2017; Soengas et al., 2018). Evidence obtained in rainbow trout (Polakof et al., 2009; Otero-Rodiño et al., 2019b) suggest a relationship between neuropeptide expression and nutrient sensing based on the simultaneous presence in hypothalamic areas of proteins involved in nutrient sensing, such as glucokinase (GCK), and the four neuropeptides. The activation of nutrient sensors enhances the anorexigenic potential (ratio between mRNA abundance of anorexigens and orexigens) through decreased expression of AgRP

and NPY and increased expression of CART and POMC resulting in a decrease in food intake (Delgado et al., 2017; Soengas et al., 2018).

Studies carried out in rainbow trout (Librán-Pérez et al., 2012, 2013, 2014, 2015; Velasco et al., 2016a, 2020; Roy et al., 2020) demonstrated the presence in hypothalamus of fatty acid sensing mechanisms responsive to changes in the levels of long-chain fatty acids like oleate through carnitine palmitoyl transferase-1, mitocondrial ROS production inhibiting ATP-dependent inward rectified potassium channel (K^+_{ATP}), specific fatty acid receptors (FFAR), fatty acid translocase, and lipoprotein lipase. Evidence is also available in other species like grass carp (Li et al., 2016; Tian et al., 2017), Senegalese sole (Conde-Sieira et al., 2015), zebrafish (Liu et al., 2017), Chinese perch (Luo et al., 2020), and blunt snout bream (Dai et al., 2018). Mechanisms are similar to those characterized in mammals (Lipina et al., 2014; Magnan et al., 2015) though fish are also sensitive to polyunsaturated fatty acid like α-linolenate and medium-chain fatty acid like octanoate. Glucose is also sensed in fish hypothalamus. Evidence obtained suggested the presence in rainbow trout (Polakof et al., 2007a,b, 2008a,b,c) and Japanese flounder (Liu et al., 2019) of the canonical mechanism based on GCK, glucose facilitative transporter 2, and K^+_{ATP}. Evidence also supports mechanisms not dependent on GCK like those based on liver X receptor and sweet taste receptor (Otero-Rodiño et al., 2015, 2016, 2017; Balasubramanian et al., 2016). Leucine is the unique branched-chain amino acid (BCAA) whose levels are detected by mammalian hypothalamic amino acid sensing mechanisms (Efeyan et al., 2015; Heeley and Blouet, 2016). In fish, available evidence is restricted to rainbow trout (Comesaña et al., 2018a,b) and Chinese perch (Chen et al., 2021), suggesting the existence of mechanisms based on BCAA metabolism, glutamine metabolism, mechanistic target of rapamycin (mTOR), general control non-derepressible 2 kinase, and taste receptor signaling.

The connection between nutrient-sensing systems and the expression of AgRP/NPY and POMC/CART governing food intake is not clear. In mammals, several transcription factors could be involved (López et al., 2007; Diéguez et al., 2011) including brain homeobox transcription factor (BSX), phosphorylated cAMP response-element binding protein (CREB), and forkhead box01 (FoxO1). Changes in these transcription factors would respond to nutrient-sensing systems through mediation by different signaling pathways (Gao et al., 2013; Morton et al., 2014) including AMP-activated protein kinase (AMPK), mTOR, and protein kinase B (Akt). In the following sections, we will show available knowledge in fish regarding each of these pathways.

SIGNALING PATHWAYS

AMPK

As an energy sensor, AMPK detects lowered cell energy status-eliciting mechanisms to restore energy balance (López, 2017). Thus, when levels of nutrients rise, a decrease occur in the levels and phosphorylation status of AMPK in mammalian hypothalamus, as demonstrated for glucose, leucine, and fatty acid (Diéguez et al., 2011; Fromentin et al., 2012; Oh et al., 2016).

In fish, several studies evaluated AMPK in brain (Zeng et al., 2016; Xu et al., 2018; Abernathy et al., 2019; Yang et al., 2019) but only a few addressed its role in the regulation of feed intake. Thus, in rainbow trout fed a lipid-enriched diet, a decrease occurred in phosphorylation status of hypothalamic AMPKα (Librán-Pérez et al., 2015). This is comparable with that observed in the same species (Kamalam et al., 2012) or in *Megalobrama amblycephala* (Xu et al., 2017) when fed a carbohydrate-enriched diet. Also in rainbow trout, raising levels of nutrients like oleate (Velasco et al., 2016a, 2017b; Blanco et al., 2020), octanoate (Velasco et al., 2017b), glucose (Otero-Rodiño et al., 2017), or β-hydroxybutyrate (Comesaña et al., 2019) also resulted in a decrease in phosphorylation status of AMPKα. The specificity of AMPKα response was supported by the disappearance of responses to oleate in the presence of the AMPKα inhibitor compound C (Velasco et al., 2017b). In contrast to the mammalian model, no changes in phosphorylation status of AMPKα occurred in rainbow trout hypothalamus in response to raised leucine levels (Comesaña et al., 2018a,b, 2020). Changes in AMPK also occurred in liver of fish species under different feeding status including a decrease in refed rainbow trout (Polakof et al., 2011) or an increase in food-deprived zebrafish (Craig and Moon, 2011). A role for hypothalamic AMPKα in food intake control is also supported by the increase observed in hypothalamus of food-deprived rainbow trout (Conde-Sieira et al., 2019). The involvement of AMPK is further supported by the decrease in phosphorylation status of AMPKα observed in rainbow trout hypothalamus under anorectic conditions like treatment with ceramide (Velasco et al., 2016b, 2017a), FFAR agonists (Velasco et al., 2020), or anorectic hormones like CCK (Velasco et al., 2019), GLP-1 (Velasco et al., 2019), or insulin (Blanco et al., 2020). Of the different isoforms of AMPKα, it seems that AMPKα2 is involved in feed intake regulation while AMPKα1 appears to modulate peripheral metabolism (Conde-Sieira et al., 2019).

mTOR

Several studies demonstrate increased mTOR mRNA abundance and phosphorylation status in hypothalamus after a rise in the levels of leucine in mammals (Hu et al., 2016; Pena-Leon et al., 2020). In contrast, the effects of fatty acid or glucose on central mTOR are mostly unknown (André and Cota, 2012). However, the anorectic response induced by leptin treatment increase phosphorylation status of mTOR (Kwon et al., 2016) whereas the orexigenic response induced by ghrelin treatment (André and Cota, 2012) or food deprivation (Ferro Cavalcante et al., 2020) decreased mTOR.

In fish, mTOR was characterized in hypothalamus of several species including rainbow trout (Velasco et al., 2017b; Comesaña et al., 2018a; Blanco et al., 2020) and Japanese sea bass (Liang et al., 2019). In rainbow trout, mTOR levels and phosphorylation status responded with an increase to the presence of nutrients like oleate (Velasco et al., 2017b; Blanco et al., 2020), octanoate (Velasco et al., 2017b), glucose (Blanco et al., 2020), or leucine (Comesaña et al., 2018a,b). The presence of rapamycin blocked

the response to fatty acids in hypothalamus (Velasco et al., 2017b) supporting the specificity of the response. Additional studies relate mTOR to food intake regulation in fish. Thus, increased mTOR occurred under anorectic conditions like feeding a lipid-enriched diet in rainbow trout (Librán-Pérez et al., 2015) and blunt snout bream (Dai et al., 2018) or different treatments in rainbow trout with PYY (Velasco et al., 2018), CCK (Velasco et al., 2019), insulin (Blanco et al., 2020), or ceramide (Velasco et al., 2017a). In other fish species, available information is limited. Thus, in Japanese sea bass, hypothalamic mTOR activation modulates POMC and NPY expression (Liang et al., 2019) whereas in cavefish, CCK treatment increased mTOR levels (Penney and Volkoff, 2014). In liver, mTOR phosphorylation status also changed under different feeding status. mTOR increases after a rise in levels of amino acids (Lansard et al., 2011; Wacyk et al., 2012; Liang et al., 2016; Skiba-Cassy et al., 2016), feeding lipid-enriched diets (Librán-Pérez et al., 2015; Zeng et al., 2016), or refeeding (Lansard et al., 2009; Wade et al., 2014) while a decrease occurred under food deprivation (Craig and Moon, 2011).

Akt

In mammals, Akt levels and phosphorylation status in hypothalamus increased in response to a rise in the concentration of nutrients such as glucose (Chalmers et al., 2014), leucine (Hu et al., 2016), and β-hydroxybutyrate (Park et al., 2011). This response also occurred under anorectic situations in which hypothalamic POMC mRNA abundance increase (Kwon et al., 2016).

In fish, several evidence suggests the involvement of Akt in the hypothalamic mechanisms related to food intake control. Treatment with nutrients activates this signal through increased phosphorylation status, as demonstrated in rainbow trout for oleate (Blanco et al., 2020), octanoate (Velasco et al., 2017b), glucose (Otero-Rodiño et al., 2017), and leucine (Comesaña et al., 2018a). This activation also occurred under anorectic conditions such as treatment with ceramide (Velasco et al., 2016b, 2017a), insulin (Blanco et al., 2020), leptin (Gong et al., 2016), or FFAR agonists (Velasco et al., 2020). A comparable increase occurred in brain when fish were fed diets enriched in carbohydrates, as observed in zebrafish (Jörgens et al., 2015) and rainbow trout (Dai et al., 2014; Jin et al., 2014) or by feeding lipid-enriched diets as demonstrated in rainbow trout (Librán-Pérez et al., 2015) and blunt snout bream (Dai et al., 2018). The response of Akt to the rise in fatty acid levels disappeared in the presence of Akt inhibitor perifosine (Velasco et al., 2017b). Akt involvement in food intake regulation is also supported by the opposed response (decreased phosphorylation status) elicited by the orexigenic ghrelin treatment (Velasco et al., 2017a). In mammals, the activation of Akt signaling in the hypothalamus also resulted in changes in fatty acid metabolism due to the activation of sterol regulatory element-binding protein 1 (SREBP-1) and its target genes ATP citrate synthase (ACLY) and fatty acid synthase (FAS) (Kim et al., 2007). In rainbow trout hypothalamus, enhanced phosphorylation of Akt also occurred in parallel with mRNA abundance of *acly*, *fas*, and *srebp1* (Velasco et al., 2016b). Finally, besides central action, Akt is involved in peripheral responses to changes in feeding *status*. Thus, refeeding enhanced Akt phosphorylation in liver of barramundi (Wade et al., 2014) and rainbow trout (Lansard et al., 2009; Seiliez et al., 2011), and in muscle of Senegalese sole (Borges et al., 2014).

TRANSCRIPTION FACTORS

BSX

The transcription factor BSX interacts with CREB resulting in a parallel increase in the mRNA abundance of *Bsx, Npy*, and *Agrp* in mammalian hypothalamus (Nogueiras et al., 2008; Varela et al., 2011; Lee et al., 2016). Accordingly, *Bsx* decrease under anorectic conditions such as feeding a high-fat diet (Nogueiras et al., 2008) and increase under orexigenic conditions such as food deprivation (Nogueiras et al., 2008) or ghrelin treatment (Lage et al., 2010).

In fish, evidence regarding BSX role in hypothalamus is limited (Cremona et al., 2004; Schredelseker et al., 2020) with a few studies in rainbow trout related to food intake control. In this species, the exposure to oleate (Conde-Sieira et al., 2018) or glucose (Conde-Sieira et al., 2018; Blanco et al., 2020) reduced food intake in parallel with decreased BSX levels. There is no information available for BSX response in fish hypothalamus to the rise in amino acid levels. Other conditions known to decrease food intake in this species also decreased values for BSX as demonstrated by treatment with CCK (Velasco et al., 2019), GLP-1 (Velasco et al., 2019), or FFAR agonists (Velasco et al., 2020). No comparable studies assessed changes in *Bsx* mRNA expression under conditions of raised nutrient levels, not even in mammals. However, indirect evidence is available such as the effects of the treatment with the anorectic hormone leptin in rat resulting in decreased mRNA levels of *Bsx* in arcuate nucleus (Nogueiras et al., 2008) as well as in whole hypothalamus (Gao et al., 2011) in parallel with decreased food intake and *Npy* mRNA levels. In addition, situations in which an orexigenic response occurred (such as those elicited by ghrelin treatment or food deprivation) induced a rise in hypothalamic *Bsx* mRNA abundance (Nogueiras et al., 2008; Lage et al., 2010).

CREB

cAMP response-element binding protein is another transcription factor hypothesized to be involved in the connection between brain metabolism and neuropeptides expression. Accordingly, in mammals, a decrease in CREB levels induced a decrease in mRNA abundance of *Npy* and *Agrp* leading to a decrease in food intake (Belgardt et al., 2009; Blanco de Morentin et al., 2011; Varela et al., 2011). CREB protein abundance decrease when food intake is inhibited enhancing anorexigenic potential through a decrease in mRNA levels of *Npy* and *Agrp* (Fukushima et al., 2015; Kwon et al., 2016) while levels increase under orexigenic situations such as ghrelin treatment (Lage et al., 2010) or food deprivation (Ren et al., 2013).

In fish, available information regarding CREB involvement in food intake regulation is restricted to rainbow trout. In this species, CREB phosphorylation status decreased in response to raised levels of oleate (Velasco et al., 2017b;

Conde-Sieira et al., 2018), octanoate (Velasco et al., 2017b), glucose (Conde-Sieira et al., 2018; Otero-Rodiño et al., 2019a), or leucine (Comesaña et al., 2018a,b). CREB response to fatty acids was abolished by the presence of the CBP-CREB interaction inhibitor (Velasco et al., 2017b). Changes observed in CREB are comparable with those observed under other anorectic situations such as treatment with CCK o GLP-1 (Velasco et al., 2019). Moreover, increased levels of CREB occurred in zebrafish under the orexigenic conditions elicited by food deprivation (Craig and Moon, 2011).

FoxO1

Forkhead box01 is likely involved in the relationship between metabolic changes in hypothalamus and the production of neuropeptides (Gross et al., 2009). Thus, in mammals, situations in which Fox01 increased resulted in an enhancement of *Agrp* mRNA values while those of *Pomc* decreased, changes favoring a decrease in food intake (Belgardt et al., 2009; Blanco de Morentin et al., 2011).

In fish, FoxO1 was characterized in brain in rainbow trout (Conde-Sieira et al., 2018) and turbot (Pan et al., 2019). Increased levels of nutrients enhanced its abundance and phosphorylation status as observed in rainbow trout for oleate (Conde-Sieira et al., 2018; Blanco et al., 2020), octanoate (Velasco et al., 2017b), and glucose (Conde-Sieira et al., 2018; Blanco et al., 2020). The specificity of FoxO1 response to raised levels of fatty acid was supported by its lack of response in the presence of the FoxO1 inhibitor AS1842856 (Velasco et al., 2017b). In contrast, FoxO1 does not appear to respond to changes in the levels of leucine (Comesaña et al., 2018a,b, 2020). Other anorectic conditions also resulted in increased FoxO1 in rainbow trout as observed after treatment with CCK (Velasco et al., 2019), GLP-1 (Velasco et al., 2019), insulin (Blanco et al., 2020), ceramide (Velasco et al., 2016b, 2017a), or FFAR agonists (Velasco et al., 2020). Central changes in FoxO1 are comparable with those occurring in peripheral tissues under different feeding status. Thus, in liver of rainbow trout orexigenic conditions like refeeding decreased FoxO1 levels (Dai et al., 2013) whereas in grass carp adipogenesis (a situation comparable with a rise in nutrient levels) increased FoxO1 in adipocytes (Sun et al., 2017). No prior studies in any other vertebrate species addressed the hypothalamic response of *Foxo1* to changes in nutrient levels. However, changes observed in fish would be comparable with those observed in mammalian hypothalamus under anorectic conditions like feeding a high-fat diet (Yuan et al., 2012) or treatment with insulin or leptin (Diéguez et al., 2011; Kwon et al., 2016). Akt activation is known to induce in mammals the phosphorylation of FoxO1 (Belgardt et al., 2009; Gross et al., 2009), which also result in enhanced CART and POMC expression (Kwon et al., 2016). In fish, a

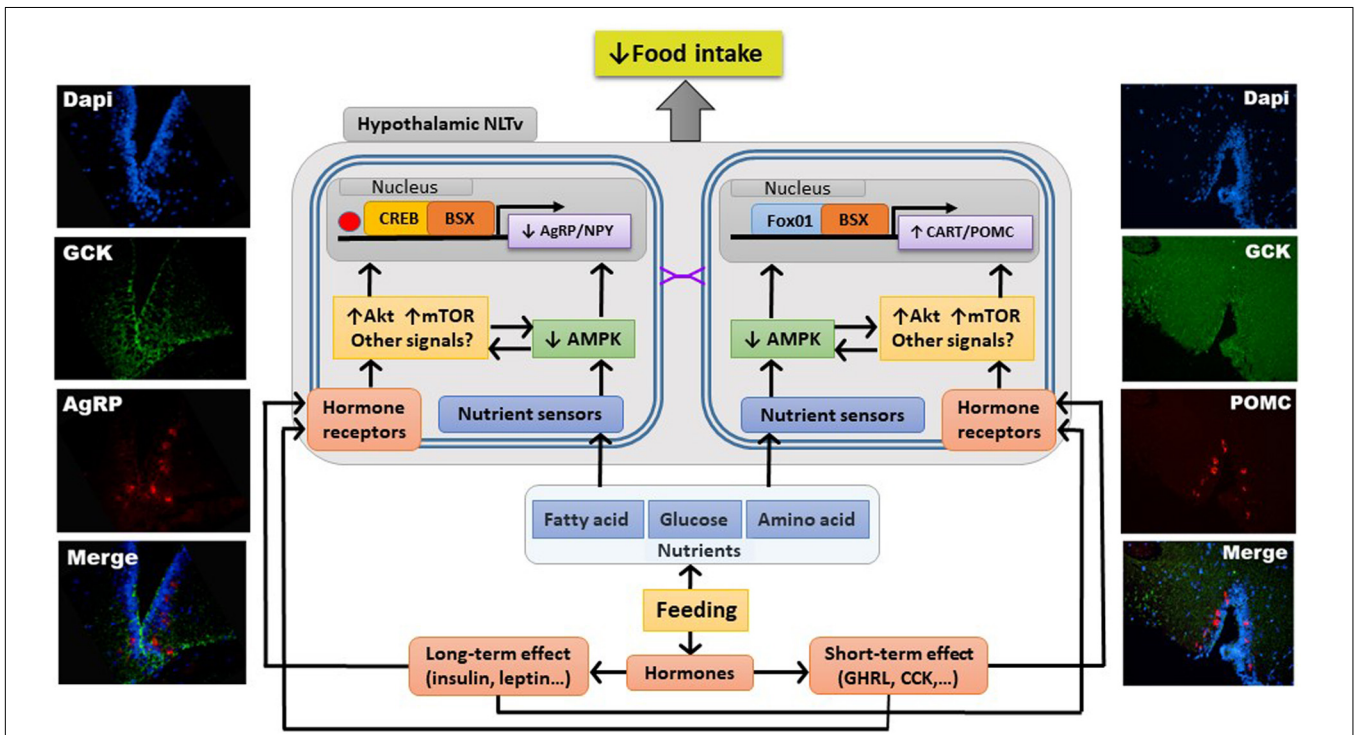

FIGURE 1 | Schematic drawing with a model of processes involved in integration of nutrient-sensing information in fish hypothalamus resulting in homeostatic control of food intake. Left and right panels show pictures showing colocalization of a nutrient-sensing marker [glucokinase (GCK)] with AgRP (left) or POMC (right) in neurons (stained with DAPI) from rainbow trout hypothalamus. Purple symbols, synaptic connection; AgRP, agouti-related peptide; Akt, protein kinase B; AMPK, AMP-activated protein kinase; BSX, brain homeobox transcription factor; CART, cocaine- and amphetamine-related transcript; CCK, cholecystokinin; CREB, cAMP response-element binding protein; FoxO1, forkhead box protein O1; GHRL, ghrelin; mTOR, mechanistic target of rapamycin; NLTv, lateral tuber nucleus pars ventralis; NPY, neuropeptide Y; POMC, pro-opio melanocortin.

simultaneous rise in Akt and FoxO1 occurred in rainbow trout hypothalamus in response to anorectic treatments like oleate (Blanco et al., 2020), octanoate (Velasco et al., 2017b), or insulin (Blanco et al., 2020) but not leucine (Comesaña et al., 2018a). These results allow me to suggest a relationship between Akt and FoxO1 comparable with that suggested in mammals though restricted to several anorectic conditions.

INTERACTION NUTRIENTS-HORMONES

AgRP/NPY and CART/POMC neurons involved in the integration of signals from nutrient sensors also have receptors for hormones like leptin, ghrelin, insulin, CCK, or GLP-1, among others (Blouet and Schwartz, 2010; Morton et al., 2014). The binding of these hormones to their receptors in hypothalamic neurons elicits changes in intracellular signals like AMPK and mTOR. Therefore, the final effect on food intake elicited by changes in neuropeptide expression would result from the interaction on signal transduction of both nutrients and hormones. However, this interaction is mostly unknown, with only some evidence available regarding the interactive effects of leptin or ghrelin on fatty acid sensing (López et al., 2007; Blanco de Morentin et al., 2011; Lockie et al., 2019).

In fish, only two studies carried out in rainbow trout demonstrated interactive effects in hypothalamus between nutrient-sensing mechanisms and hormones such as ghrelin and insulin. The presence of oleate counteracted ghrelin effects on AMPK (Velasco et al., 2016a). In the case of insulin (Blanco et al., 2020), its counteractive effects occurred in the presence of glucose for *bsx* and *mtor* mRNA abundance as well as in the presence of oleate for Akt phosphorylation status, and *foxo1* and *creb1* mRNA abundance. No other studies characterized in fish putative interactions in hypothalamus. However, in rainbow trout treatment with different hormones alter nutrient sensing mechanisms in hypothalamus (Conde-Sieira and Soengas, 2017) as demonstrated for glucosensing (leptin, insulin, ghrelin, nesfatin-1, CCK, and GLP-1) and fatty acid sensing (insulin, ghrelin, PYY, and nesfatin-1). Therefore, it is reasonable to hypothesize the existence of additional interactions through changes in cellular signaling and transcription factors.

CONCLUSION AND PERSPECTIVES

The knowledge available in fish about hypothalamic integration of information of metabolic and endocrine nature eliciting changes in expression of neuropeptides ultimately regulating food intake is limited (Delgado et al., 2017; Soengas et al., 2018). Studies in fish suggest the existence of a network similar in some aspects (but not in others) to that of mammals. In this network, the activation of the nutrient-sensing systems would result in the activation of Akt and mTOR as well as in the inhibition of AMPK. Changes in these signals would result in enhanced levels and phosphorylation status of FoxO1 while decreasing those of CREB and BSX. Finally, these changes in transcription factors would ultimately lead to inhibition of food intake inhibition through changes in neuropeptides (AgRP, NPY, POMC, and CART) expression, as observed in fish hypothalamus under anorectic conditions elicited by raised levels of nutrients. However, the precise mechanisms involved and their interaction with hormones still needs evaluation. A summary of available knowledge is shown in **Figure 1**.

AUTHOR CONTRIBUTIONS

The author confirms being the sole contributor of this work and has approved it for publication.

FUNDING

This study was supported by research grants from the Spanish Agencia Estatal de Investigación and European Fund of Regional Development (PID2019-103969RB-C31) and Xunta de Galicia (Consolidación e estructuración de unidades de investigación competitivas do SUG, ED431B 2019/37).

REFERENCES

Abernathy, O., Kostner, D., Buer, P., Dougherty, M., Schmidtberger, A., Spainhour, R., et al. (2019). Expression of messenger RNA encoding two cellular metabolic regulators, AMP-activated protein kinase (AMPK) and O-GlcNAc transferase (OGT), in channel catfish: their tissue distribution and relationship with changes in food intake. *Comp. Biochem. Physiol. A Mol. Integr. Physiol.* 235, 12–21. doi: 10.1016/j.cbpa.2019.04.023

André, C., and Cota, D. (2012). Coupling nutrient sensing to metabolic homeostasis: the role of the mammalian target of rapamycin complex 1 pathway. *Proc. Nutr. Soc.* 71, 502–510. doi: 10.1017/S0029665112000754

Balasubramanian, M. N., Panserat, S., Dupont-Nivet, M., Quillet, E., Montfort, J., Le Cam, A., et al. (2016). Molecular pathways associated with the nutritional programming of plant-based diet acceptance in rainbow trout following an early feeding exposure. *BMC Genomics* 17:449. doi: 10.1186/s12864-016-2804-1

Belgardt, B. F., Okamura, T., and Brüning, J. C. (2009). Hormone and glucose signalling in POMC and AgRP neurons. *J. Physiol.* 587(Pt 22), 5305–5314. doi: 10.1113/jphysiol.2009.179192

Blanco, A. M., Bertucci, J. I., Soengas, J. L., and Unniappan, S. (2020). *In vitro* insulin treatment reverses changes elicited by nutrients in cellular metabolic processes that regulate food intake in fish. *J. Exp. Biol.* 223(Pt 8), jeb213454. doi: 10.1242/jeb.213454

Blanco de Morentin, P. B., González, C. R., Saha, A. K., Martins, L., Diéguez, C., Vidal-Puig, A., et al. (2011). Hypothalamic AMP-activated protein kinase as a mediator of whole body energy balance. *Rev. Endocr. Metab. Disord.* 12, 127–140. doi: 10.1007/s11154-011-9165-5

Blouet, C., and Schwartz, G. J. (2010). Hypothalamic nutrient sensing in the control of energy homeostasis. *Behav. Brain Res.* 209, 1–12. doi: 10.1016/j.bbr.2009.12.024

Borges, P., Valente, L. M. P., Véron, V., Dias, K., Panserat, S., and Médale, F. (2014). High dietary lipid level is associated with persistent hyperglycaemia and downregulation of muscle Akt-mTOR pathway in Senegalese sole (*Solea senegalensis*). *PLoS One* 9:e102196. doi: 10.1371/journal.pone.0102196

Bruce, K. D., Zsombok, A., and Eckel, R. H. (2017). Lipid processing in the brain: a key regulator of systemic metabolism. *Front. Endocrinol.* 8:60. doi: 10.3389/fendo.2017.00060

Chalmers, J. A., Jang, J. J., and Belsham, D. D. (2014). Glucose sensing mechanisms in hypothalamic cell models: glucose inhibition of AgRP synthesis and secretion. *Mol. Cell. Endocrinol.* 382, 262–270. doi: 10.1016/j.mce.2013.10.013

Chen, K., Zhang, Z., Li, J., Xie, S., Shi, L.-J., He, Y.-H., et al. (2021). Different regulation of branched-chain amino acid on food intake by TOR signaling in Chinese perch (*Siniperca chuatsi*). *Aquaculture* 530:735792. doi: 10.1016/j.aquaculture.2020.735792

Comesaña, S., Conde-Sieira, M., Velasco, C., Soengas, J. L., and Morais, S. (2020). Oral and pre-absorptive sensing of amino acids relates to hypothalamic control of food intake in rainbow trout. *J. Exp. Biol.* 223(Pt 17):jeb221721. doi: 10.1242/jeb.221721

Comesaña, S., Velasco, C., Ceinos, R. M., López Patiño, M. A., Míguez, J. M., Morais, S., et al. (2018a). Evidence for the presence in rainbow trout brain of amino acid-sensing systems involved in the control of food intake. *Am. J. Physiol. Regul. Integr. Comp. Physiol.* 314, R201–R215. doi: 10.1152/ajpregu.00283.2017

Comesaña, S., Velasco, C., Conde-Sieira, M., Míguez, J. M., Soengas, J. L., and Morais, S. (2018b). Feeding stimulation ability and central effects of intraperitoneal treatment of L-leucine, L-valine, and L-proline on amino acid sensing systems in rainbow trout: implication in food intake control. *Front. Physiol.* 9:1209. doi: 10.3389/fphys.2018.01209

Comesaña, S., Velasco, C., Conde-Sieira, M., Otero-Rodiño, C., Míguez, J. M., and Soengas, J. L. (2019). Central treatment of ketone body in rainbow trout alters liver metabolism without apparently altering the regulation of food intake. *Front. Physiol.* 10:1206. doi: 10.3389/fphys.2019.01206

Conde-Sieira, M., Bonacic, K., Velasco, C., Valente, L. M. P., Morais, S., and Soengas, J. L. (2015). Hypothalamic fatty acid sensing in Senegalese sole (*Solea senegalensis*): response to long-chain saturated, monounsaturated, and polyunsaturated (n-3) fatty acids. *Am. J. Physiol. Regul. Integr. Comp. Physiol.* 309, R1521–R1531. doi: 10.1152/ajpregu.00386.2015

Conde-Sieira, M., Capelli, V., Álvarez-Otero, R., Comesaña, S., Liñares-Pose, L., Velasco, C., et al. (2019). Differential role of hypothalamic AMPKα isoforms in fish: an evolutive perspective. *Mol. Neurobiol.* 56, 5051–5066. doi: 10.1007/s12035-018-1434-9

Conde-Sieira, M., Ceinos, R. M., Velasco, C., Comesaña, S., López-Patiño, M. A., Míguez, J. M., et al. (2018). Response of rainbow trout (*Oncorhynchus mykiss*) hypothalamus to glucose and oleate assessed through transcription factors BSX, ChREBP, CREB, and FoxO1. *J. Comp. Physiol. A Neuroethol. Sens. Neural Behav. Physiol.* 204, 893–904. doi: 10.1007/s00359-018-1288-7

Conde-Sieira, M., and Soengas, J. L. (2017). Nutrient sensing systems in fish: impact on food intake regulation and energy homeostasis. *Front. Neurosci.* 10:603. doi: 10.3389/fnins.2016.00603

Craig, P. M., and Moon, T. W. (2011). Fasted zebrafish mimic genetic and physiological responses in mammals: a model for obesity and diabetes? *Zebrafish* 8, 109–117. doi: 10.1089/zeb.2011.0702

Cremona, M., Colombo, E., Andreazzoli, M., Cossu, G., and Broccoli, V. (2004). Bsx, an evolutionary conserved Brain Specific homeoboX gene expressed in the septum, epiphysis, mammillary bodies and arcuate nucleus. *Gene Expr. Patterns* 4, 47–51. doi: 10.1016/S1567-133X(03)00151-0

Dai, W., Panserat, S., Mennigen, J. A., Terrier, F., Dias, K., Seiliez, I., et al. (2013). Post-prandial regulation of hepatic glucokinase and lipogenesis requires the activation of TORC1 signaling in rainbow trout (*Oncorhynchus mykiss*). *J. Exp. Biol.* 216, 4483–4492. doi: 10.1242/jeb.091157

Dai, W., Panserat, S., Terrier, F., Seiliez, I., and Skiba-Cassy, S. (2014). Acute rapamycin treatment improved glucose tolerance through inhibition of hepatic gluconeogenesis in rainbow trout (*Oncorhynchus mykiss*). *Am. J. Physiol. Regul. Integr. Comp. Physiol.* 307, R1231–R1238. doi: 10.1152/ajpregu.00166.2014

Dai, Y.-J., Jiang, G.-Z., Yuan, X.-Y., and Liu, W.-B. (2018). High-fat-diet-induced inflammation depresses the appetite of blunt snout bream (*Megalobrama amblycephala*) through the transcriptional regulation of leptin/mammalian target of rapamycin. *Br. J. Nutr.* 120, 1422–1431. doi: 10.1017/S000711451800288X

Delgado, M. J., Cerdá-Reverter, J. M., and Soengas, J. L. (2017). Hypothalamic integration of metabolic, endocrine, and circadian signals in fish: involvement in the control of food intake. *Front. Neurosci.* 11:354. doi: 10.3389/fnins.2017.00354

Diéguez, C., Vazquez, M. J., Romero, A., López, M., and Nogueiras, R. (2011). Hypothalamic control of lipid metabolism: focus on leptin, ghrelin and melanocortins. *Neuroendocrinology* 94, 1–11. doi: 10.1159/000328122

Efeyan, A., Comb, W. C., and Sabatini, D. M. (2015). Nutrient sensing mechanisms and pathways. *Nature* 517, 302–310. doi: 10.1038/nature14190

Ferro Cavalcante, T. C., de farias campina, R. C., Araújo de Souza, J., Alves Marcelino da Silva, A., and Lopes de Sousa, S. (2020). Hypothalamic peptide and nutrient sensors gene expression in the hypothalamus of neonatal rat. *Brain Res. Bull.* 164, 214–220. doi: 10.1016/j.brainresbull.2020.08.005

Fromentin, G., Darcel, N., Chaumontet, C., Marsset-Baglieri, A., Nadkarni, N., and Tom, D. (2012). Peripheral and central mechanisms involved in the control of food intake by dietary amino acids and proteins. *Nutr. Res. Rev.* 25, 29–39. doi: 10.1017/S0954422411000175

Fukushima, A., Hagiwara, H., Fujioka, H., Kimura, F., Akema, T., and Funabashi, T. (2015). Sex differences in feeding behavior in rats: the relationship with neuronal activation in the hypothalamus. *Front. Neurosci.* 9:88. doi: 10.3389/fnins.2015.00088

Gao, S., Moran, T. H., Lopaschuk, G. D., and Butler, A. A. (2013). Hypothalamic malonyl-CoA and the control of food intake. *Physiol. Behav.* 122, 17–24. doi: 10.1016/j.physbeh.2013.07.014

Gao, S., Zhu, G., Gao, X., Wu, D., Carrasco, P., Casals, N., et al. (2011). Important roles of brain-specific carnitine palmitoyltransferase and ceramide metabolism in leptin hypothalamic control of feeding. *Proc. Natl. Acad. Sci. U.S.A.* 108, 9691–9696. doi: 10.1073/pnas.1103267108

Gong, N., Jönsson, E., and Björnsson, B. T. (2016). Acute anorexigenic action of leptin in rainbow trout is mediated by the hypothalamic Pi3k pathway. *J. Mol. Endocrinol.* 56, 227–238. doi: 10.1530/JME-15-0279

Gross, D. N., Wan, M., and Birnbaum, M. J. (2009). The role of FOXO in the regulation of metabolism. *Curr. Diab. Rep.* 9, 208–214. doi: 10.1007/s11892-009-0034-5

Heeley, N., and Blouet, C. (2016). Central amino acid sensing in the control of feeding behavior. *Front. Endocrinol.* 7:148. doi: 10.3389/fendo.2016.00148

Hu, F., Xu, Y., and Liu, F. (2016). Hypothalamic roles of mTOR complex I: integration of nutrient and hormone signals to regulate energy homeostasis. *Am. J. Physiol. Endocrinol. Metab.* 310, E994–E1002. doi: 10.1152/ajpendo.00121.2016

Jin, J., Médale, F., Kamalam, B. S., Aguirre, P., Véron, V., and Panserat, S. (2014). Comparison of glucose and lipid metabolic gene expressions between fat and lean lines of rainbow trout after a glucose load. *PLoS One* 9:e105548. doi: 10.1371/journal.pone.0105548

Jörgens, K., Stoll, S. J., Pohl, J., Fleming, T. H., Sticht, C., Nawroth, P. P., et al. (2015). High tissue glucose alters intersomitic blood vessels in zebrafish via methylglioxal targeting the VEGF receptor signaling cascade. *Diabetes* 64, 213–225. doi: 10.2337/db14-0352

Kamalam, B. S., Medale, F., Kaushik, S., Polakof, S., Skiba-Cassy, S., and Panserat, S. (2012). Regulation of metabolism by dietary carbohydrate in two lines of rainbow trout divergently selected for muscle fat content. *J. Exp. Biol.* 215, 2567–2578. doi: 10.1242/jeb.070581

Kim, E.-K., Kleman, A. K., and Ronnett, G. V. (2007). Fatty acid synthase gene regulation in primary hypothalamic neurons. *Neurosci. Lett.* 423, 200–204. doi: 10.1016/j.neulet.2007.06.056

Kwon, O., Kim, K. W., and Kim, M.-S. (2016). Leptin signalling pathways in hypothalamic neurons. *Cell. Mol. Life Sci.* 73, 1457–1477. doi: 10.1007/s00018-016-2133-1

Lage, R., Vázquez, M. J., Varela, L., Saha, A. K., Vidal-Puig, A., Nogueiras, R., et al. (2010). Ghrelin effects on neuropeptides in the rat hypothalamus depend on fatty acid metabolism actions on BSX but not on gender. *FASEB J.* 24, 2670–2679. doi: 10.1096/fj.09-150672

Lansard, M., Panserat, S., Plagnes-Juan, E., Dias, K., Seiliez, I., and Skiba-Cassy, S. (2011). L-Leucine, L-Methionine, and L-Lysine are involved in the regulation of intermediary metabolism-related gene expression in rainbow trout hepatocytes. *J. Nutr.* 141, 75–80. doi: 10.3945/jn.110.124511

Lansard, M., Panserat, S., Seiliez, I., Polakof, S., Plagnes-Juan, E., Geurden, I., et al. (2009). Hepatic protein kinase B (Akt)-target of rapamycin (TOR)-signalling pathways and intermediary metabolism in rainbow trout (*Oncorhynchus mykiss*) are not significantly affected by feeding plant-based diets. *Br. J. Nutr.* 102, 1564–1573. doi: 10.1017/S000711450999095X

Lee, B., Lee, S., Lee, S.-K., and Lee, J. W. (2016). The LIM-homeobox transcription factor Isl1 plays crucial roles in the development of multiple arcuate nucleus neurons. *Development* 143, 3763–3773. doi: 10.1242/dev.133967

Li, A., Yuan, X., Liang, X. F., Liu, L., Li, J., Li, B., et al. (2016). Adaptations of lipid metabolism and food intake in response to low and high fat diets in

juvenile grass carp (*Ctenopharyngodon idellus*). *Aquaculture* 457, 43–49. doi: 10.1016/j.aquaculture.2016.01.014

Liang, H., Ren, M., Habte-Tsion, H. M., Ge, X., Xie, J., Mi, H., et al. (2016). Dietary arginine affects growth performance, plasma amino acid contents and gene expressions of the TOR signaling pathway in juvenile blunt snout bream, *Megalobrama amblycephala*. *Aquaculture* 461, 1–8. doi: 10.1016/j.aquaculture.2016.04.009

Liang, X., Han, J., Xue, M., Yu, H., Huang, H., Wu, X., et al. (2019). Growth and feed intake regulation responses to anorexia, adaptation and fasting in Japanese seabass, *Lateolabrax japonicas* when fishmeal is totally replaced by plant protein. *Aquaculture* 498, 528–538. doi: 10.1016/j.aquaculture.2018.09.010

Librán-Pérez, M., Geurden, I., Dias, K., Corraze, G., Panserat, S., and Soengas, J. L. (2015). Feeding rainbow trout with a lipid-enriched diet: effects on fatty acid sensing, regulation of food intake and cellular signaling pathways. *J. Exp. Biol.* 218, 2610–2619. doi: 10.1242/jeb.123802

Librán-Pérez, M., López-Patiño, M. A., Míguez, J. M., and Soengas, J. L. (2013). Oleic acid and octanoic acid sensing capacity in rainbow trout *Oncorhynchus mykiss* is direct in hypothalamus and Brockmann bodies. *PLoS One* 8:e59507. doi: 10.1371/journal.pone.0059507

Librán-Pérez, M., Otero-Rodiño, C., López-Patiño, M. A., Míguez, J. M., and Soengas, J. L. (2014). Central administration of oleate or octanoate activates hypothalamic fatty acid sensing and inhibits food intake in rainbow trout. *Physiol. Behav*. 129, 272–279. doi: 10.1016/j.physbeh.2014.02.061

Librán-Pérez, M., Polakof, S., López-Patiño, M. A., Míguez, J. M., and Soengas, J. L. (2012). Evidence of a metabolic fatty-acid sensing system in the hypothalamus and Brockmann bodies of rainbow trout: implications in food intake regulation. *Am. J. Physiol. Regul. Integr. Comp. Physiol.* 302, R1340–R1350. doi: 10.1152/ajpregu.00070.2012

Lipina, C., Irving, A. J., and Hundal, H. S. (2014). Mitochondria: a possible nexus for the regulation of energy homeostasis by the endocannabinoid system? *Am. J. Physiol. Endocrinol. Metab*. 307, E1–E13. doi: 10.1152/ajpendo.00100.2014

Liu, D., Deng, K., Sampath, W. W. H. A., Gu, Z., Pan, M., Zhang, Y., et al. (2019). Responses of glucosensing system to glucose in Japanese flounder *Paralichthys olivaceus* fed diets with different carbohydrate content. *Comp. Biochem. Physiol. B Biochem. Mol. Biol.* 232, 72–78. doi: 10.1016/j.cbpb.2019.03.001

Liu, H., Xu, Y., Wang, Y., Zhong, S., Wang, M., Lin, P., et al. (2017). Cd36 is a candidate lipid sensor involved in the sensory detection of fatty acid in zebrafish. *Physiol. Behav.* 182, 34–39. doi: 10.1016/j.physbeh.2017.09.015

Lockie, S. H., Stark, R., Mequinion, M., Ch'ng, S., Kong, D., Spanswick, D. C., et al. (2019). Glucose availability predicts the feeding response to ghrelin in male mice, an effect dependent on AMPK in AgRP neurons. *Endocrinology* 159, 3605–3614. doi: 10.1210/en.2018-00536

López, M. (2017). EJE PRIZE 2017: hypothalamic AMPK: a golden target against obesity? *Eur. J. Endocrinol.* 176, R235–R246. doi: 10.1530/EJE-16-0927

López, M., Lelliott, C. J., and Vidal-Puig, A. (2007). Hypothalamic fatty acid metabolism: a housekeeping pathway that regulates food intake. *BioEssays* 29, 248–261. doi: 10.1002/bies.20539

Luo, H., Liang, X.-F., Li, J., Zhang, Y., Xiao, Q., Peng, B., et al. (2020). Effect of long-chain saturated and unsaturated fatty acids on hypothalamic fatty acid sensing in Chinese perch (*Siniperca chuatsi*). *Comp. Biochem. Physiol. B Biochem. Mol. Biol.* 241:110395. doi: 10.1016/j.cbpb.2019.110395

Magnan, C., Levin, B. E., and Luquet, S. (2015). Brain lipid sensing and the neural control of energy balance. *Mol. Cell Endocrinol.* 418(Pt 1), 3–8. doi: 10.1016/j.mce.2015.09.019

Morton, G. J., Meek, T. H., and Schwartz, M. W. (2014). Neurobiology of food intake in health and disease. *Nat. Rev. Neurosci.* 15, 367–378. doi: 10.1038/nrn3745

Nogueiras, R., López, M., Lage, R., Perez-Tilve, D., Pfluger, P., Mendieta-Zerón, H., et al. (2008). Bsx, a novel hypothalamic factor linking feeding with locomotor activity, is regulated by energy availability. *Endocrinology* 149, 3009–3015. doi: 10.1210/en.2007-1684

Oh, Y. T., Oh, H. H., Nguyen, A.-K., Choi, C. S., and Youn, J. H. (2016). Circulating free fatty acids inhibit food intake in an oleate-specific manner in rats. *Physiol. Behav*. 167, 194–201. doi: 10.1016/j.physbeh.2016.09.015

Otero-Rodiño, C., Conde-Sieira, M., Comesaña, S., Álvarez-Otero, R., López-Patiño, M. A., Míguez, J. M., et al. (2019a). Na^+/K^+-ATPase is involved in the regulation of food intake in rainbow trout but apparently not through brain glucosensing mechanisms. *Physiol. Behav*. 209:112617. doi: 10.1016/j.physbeh.2019.112617

Otero-Rodiño, C., Librán-Pérez, M., Velasco, C., López-Patiño, M. A., Míguez, J. M., and Soengas, J. L. (2015). Evidence for the presence of glucosensor mechanisms not dependent on glucokinase in hypothalamus and hindbrain of rainbow trout (*Oncorhynchus mykiss*). *PLoS One* 10:e0128603. doi: 10.1371/journal.pone.0128603

Otero-Rodiño, C., Rocha, A., Sánchez, E., Álvarez-Otero, R., Soengas, J. L., and Cerdá-Reverter, J. M. (2019b). Sensing glucose in the central melanocortin circuits of rainbow trout: a morphological study. *Front. Endocrinol.* 10:254. doi: 10.3389/fendo.2019.00254

Otero-Rodiño, C., Velasco, C., Álvarez-Otero, R., López Patiño, M. A., Míguez, J. M., and Soengas, J. L. (2017). Changes in the levels and phosphorylation status of Akt, AMPK, CREB and FoxO1 in hypothalamus of rainbow trout under conditions of enhanced glucosensing activity. *J. Exp. Biol.* 220, 4410–4417. doi: 10.1242/jeb.165159

Otero-Rodiño, C., Velasco, C., Álvarez-Otero, R., López-Patiño, M. A., Míguez, J. M., and Soengas, J. L. (2016). *In vitro* evidence supports the presence of glucokinase-independent glucosensing mechanisms in hypothalamus and hindbrain of rainbow trout. *J. Exp. Biol*. 219, 1750–1759. doi: 10.1242/jeb.137737

Pan, M., Zhang, Y., Deng, K., Liu, G., Gu, Z., Liu, J., et al. (2019). Forkhead box 01 in turbot *Scophthalmus maximus*: molecular characterization, gene structure, tissue distribution and the role in glucose metabolism. *Gene* 708, 49–56. doi: 10.1016/j.gene.2019.03.065

Park, S., Kim, D. S., and Daily, J. W. (2011). Central infusion of ketone bodies modulates body weight and hepatic insulin sensitivy by modifying hypothalamic leptin and insulin signaling pathways in type 2 diabetic rats. *Brain Res.* 1401, 95–103. doi: 10.1016/j.brainres.2011.05.040

Pena-Leon, V., Perez-Lois, R., and Seoane, L. M. (2020). mTOR pathway is involved in energy homeostasis regulation as a part of the gut-brain axis. *Int. J. Mol. Sci.* 21:5715. doi: 10.3390/ijms21165715

Penney, C. C., and Volkoff, H. (2014). Peripheral injections of cholecystokinin, apelin, ghrelin and orexin in cavefish (*Astyanax fasciatus mexicanus*): effects on feeding and on the brain expression levels of tyrosine hydroxylase, mechanistic target of rapamycin and appetite-related hormones. *Gen. Comp. Endocrinol.* 196, 34–40. doi: 10.1016/j.ygcen.2013.11.015

Polakof, S., Míguez, J. M., Moon, T. W., and Soengas, J. L. (2007a). Evidence for the presence of a glucosensor in hypothalamus, hindbrain, and Brockmann bodies of rainbow trout. *Am. J. Physiol. Regul. Integr. Comp. Physiol.* 292, R1657–R1666. doi: 10.1152/ajpregu.00525.2006

Polakof, S., Míguez, J. M., and Soengas, J. L. (2007b). *In vitro* evidences for glucosensing capacity and mechanisms in hypothalamus, hindbrain, and Brockmann bodies of rainbow trout. *Am. J. Physiol. Regul. Integr. Comp. Physiol.* 293, R1410–R1420. doi: 10.1152/ajpregu.00283.2007

Polakof, S., Míguez, J. M., and Soengas, J. L. (2008a). Changes in food intake and glucosensing function of hypothalamus and hindbrain in rainbow trout subjected to hyperglycemic or hypoglycemic conditions. *J. Comp. Physiol. A Neuroethol. Sens. Neural Behav. Physiol.* 194, 829–839. doi: 10.1007/s00359-008-0354-y

Polakof, S., Míguez, J. M., and Soengas, J. L. (2008b). Dietary carbohydrates induce changes in glucosensing capacity and food intake in rainbow trout. *Am. J. Physiol. Regul. Integr. Comp. Physiol.* 295, R478–R489. doi: 10.1152/ajpregu.00176.2008

Polakof, S., Panserat, S., Craig, P. M., Martyres, D. J., Plagnes-Juan, E., Savari, S., et al. (2011). The metabolic consequences of hepatic AMP-kinase phosphorylation in rainbow trout. *PLoS One* 6:e20228. doi: 10.1371/journal.pone.0020228

Polakof, S., Panserat, S., Plagnes-Juan, E., and Soengas, J. L. (2008c). Altered dietary carbohydrates significantly affect gene expression of the major glucosensing components in Brockmannn bodies and hypothalamus of rainbow trout. *Am. J. Physiol. Regul. Integr. Comp. Physiol.* 295, R1077–R1088. doi: 10.1152/ajpregu.90476.2008

Polakof, S., Rodríguez-Alonso, M., and Soengas, J. L. (2009). Immunohistochemical localization of glucokinase in rainbow trout brain. *Comp. Biochem. Physiol. A Mol. Integr. Physiol.* 153, 352–358. doi: 10.1016/j.cbpa.2009.03.015

Ren, X., Lufty, K., Mangubat, M., Ferrini, M. G., Lee, M. L., Liu, Y., et al. (2013). Alterations in phosphorylated CREB expression in different brain regions following short- and long-term morphine exposure: relationship to food intake. *J. Obes.* 2013:764742. doi: 10.1155/2013/764742

Roy, J., Larroquet, L., Surget, A., Lanuque, A., Sandres, F., Terrier, F., et al. (2020). Impact on cerebral function in rainbow trout fed with plant based omega-3 long chain polyunsaturated fatty acids enriched with DHA and EPA. *Fish Shellfish Immunol.* 103, 409–420. doi: 10.1016/j.fsi.2020.05.044

Schredelseker, T., Veit, F., Dorsky, R. I., and Driever, W. (2020). Bsx is essential for differentiation of multiple neuromodulatory cell populations in the secondary prosencephalon. *Front. Neurosci.* 14:525. doi: 10.3389/fnins.2020.00525

Seiliez, I., Panserat, S., Lansard, M., Polakof, S., Plagnes-Juan, E., Surget, A., et al. (2011). Dietary carbohydrate-to-protein ratio affects TOR signaling and metabolism-related gene expression in the liver and muscle of rainbow trout after a single meal. *Am. J. Physiol. Reg. Integr. Comp. Physiol.* 300, R733–R743. doi: 10.1152/ajpregu.00579.2010

Skiba-Cassy, S., Geurden, I., Panserat, S., and Seiliez, I. (2016). Dietary methionine imbalance alters the transcriptional regulation of genes involved in glucose, lipid and amino acid metabolismin the liver of rainbow trout (*Oncorhynchus mykiss*). *Aquaculture* 454, 56–65. doi: 10.1016/j.aquaculture.2015.12.015

Soengas, J. L. (2014). Contribution of glucose- and fatty acid sensing systems to the regulation of food intake in fish. A review. *Gen. Comp. Endocrinol.* 205, 36–48. doi: 10.1016/j.ygcen.2014.01.015

Soengas, J. L., Cerdá-Reverter, J. M., and Delgado, M. J. (2018). Central regulation of food intake in fish: an evolutionary perspective. *J. Mol. Endocrinol.* 60, R171–R199. doi: 10.1530/JME-17-0320

Sun, J., Xiao, P., Chang, Z. G., Ji, H., Du, Z. Y., and Chen, L. Q. (2017). Forkhead box 01 in grass carp *Ctenopharyngodon idella*: molecular characterization, gene structure, tissue distribution and mRNA expression in insulin-inhibited adipocyte lipolysis. *Comp. Biochem. Physiol. A Mol. Integr. Physiol.* 204, 76–84. doi: 10.1016/j.cbpa.2016.11.011

Tian, J., Liu, W., Gao, W., Wu, F., Yu, L., Lu, X., et al. (2017). Molecular cloning and gene/protein expression of FAT/CD36 from grass carp (*Ctenopharyngodon idella*) and the regulation of its expression by dietary energy. *Fish Physiol. Biochem.* 43, 875–888. doi: 10.1007/s10695-017-0342-7

Varela, L., Vázquez, M. J., Cordido, F., Nogueiras, R., Vidal-Puig, A., Diéguez, C., et al. (2011). Ghrelin and lipid metabolism: key partners in energy balance. *J. Mol. Endocrinol.* 46, R43–R63. doi: 10.1677/JME-10-0068

Velasco, C., Blanco, A. M., Unniappan, S., and Soengas, J. L. (2018). The anorectic effect of central PYY1-36 treatment in rainbow trout (*Oncorhynchus mykiss*) is associated with changes in mRNAs encoding neuropeptides and parameters related to fatty acid sensing and metabolism. *Gen. Comp. Endocrinol.* 267, 137–145. doi: 10.1016/j.ygcen.2018.06.015

Velasco, C., Comesaña, S., Conde-Sieira, M., Míguez, J. M., and Soengas, J. L. (2019). Effects of CCK-8 and GLP-1 on fatty acid sensing and food intake regulation in trout. *J. Mol. Endocrinol.* 62, 101–116. doi: 10.1530/JME-18-0212

Velasco, C., Conde-Sieira, M., Comesaña, S., Chivite, M., Díaz-Rúa, A., Míguez, J. M., et al. (2020). The long-chain fatty acid receptors FFA1 and FFA4 are involved in food intake regulation in fish brain. *J. Exp. Biol.* 223, jeb227330. doi: 10.1242/jeb.227330

Velasco, C., Librán-Pérez, M., Otero-Rodiño, C., López-Patiño, M. A., Míguez, J. M., Cerdá-Reverter, J. M., et al. (2016a). Ghrelin modulates hypothalamic fatty acid-sensing and control of food intake in rainbow trout. *J. Endocrinol.* 228, 25–37. doi: 10.1530/JOE-15-0391

Velasco, C., Librán-Pérez, M., Otero-Rodiño, C., López-Patiño, M. A., Míguez, J. M., and Soengas, J. L. (2016b). Ceramides are involved in regulation of food intake in rainbow trout (*Oncorhynchus mykiss*). *Am. J. Physiol. Regul. Integr. Comp. Physiol.* 311, R658–R668. doi: 10.1152/ajpregu.00201.2016

Velasco, C., Moreiras, G., Conde-Sieira, M., Leao, J. M., Míguez, J. M., and Soengas, J. L. (2017a). Ceramide counteracts the effects of ghrelin on the metabolic control of food intake in rainbow trout. *J. Exp. Biol.* 220(Pt 14), 2563–2576. doi: 10.1242/jeb.159871

Velasco, C., Otero-Rodiño, C., Comesaña, S., Míguez, J. M., and Soengas, J. L. (2017b). Hypothalamic mechanisms linking fatty acid sensing and food intake regulation in rainbow trout. *J. Mol. Endocrinol.* 59, 377–390. doi: 10.1530/JME-17-0148

Wacyk, J., Powell, M., Rodnick, K., Overturf, K., Hill, R., and Hardy, R. (2012). Dietary protein source significantly alters growth performance, plasma variables and hepatic gene expression in rainbow trout (*Oncorhynchus mykiss*) fed amino acid balanced diets. *Aquaculture* 356-357, 223–234. doi: 10.1016/j.aquaculture.2012.05.013

Wade, N. M., Skiba-Cassy, S., Dias, K., and Glencross, B. D. (2014). Postprandial molecular responses in the liver of the barramundi, *Lates calcarifer*. *Fish Physiol. Biochem.* 40, 427–443. doi: 10.1007/s10695-013-9854-y

Xu, C., Li, X.-F., Shi, H.-J., Liu, J., Zhang, L., and Liu, W.-B. (2018). AMP-activated protein kinase α1 in *Megalobrama amblycephala*: molecular charcaterization and the transcriptional modulation by nutrient restriction and glucose and insulin loadings. *Gen. Comp. Endocrinol.* 267, 66–75. doi: 10.1016/j.ygcen.2018.05.030

Xu, C., Liu, W. B., Zhang, D. D., Wang, K. Z., Xia, S. L., and Li, X. F. (2017). Molecular characterization of AMP-activated protein kinase α 2 from herbivorous fish *Megalobrama amblycephala* and responsiveness to glucose loading and dietary carbohydrate levels. *Comp. Biochem. Physiol. A Mol Integr Physiol.* 208, 24–34. doi: 10.1016/j.cbpa.2017.03.008

Yang, S., Wu, H., He, K., Yan, T., Zhou, J., Zhao, L. L., et al. (2019). Response of AMP-activated protein kinase and lactate metabolism of largemouth bass (*Micropterus salmoides*) under acute hypoxic stress. *Sci. Total Env.* 666, 1071–1079. doi: 10.1016/j.scitotenv.2019.02.236

Yuan, M., Pino, E., Wu, L., Kacergis, M., and Soukas, A. A. (2012). Identification of Akt-independent regulation of hepatic lipogenesis by mammalian target of rapamycin (mTOR) complex 2. *J. Biol. Chem.* 287, 29579–29588. doi: 10.1074/jbc.M112.386854

Zeng, L., Liu, B., Wu, C.-W., Lei, J.-L., Xu, M.-Y., Zhu, A.-Y., et al. (2016). Molecular characterization and expression analysis of AMPKα subunit isoform genes from *Scophthalmus maximus* responding to salinity stress. *Fish Physiol. Biochem.* 42, 1595–1607. doi: 10.1007/s10695-016-0243-1

Conflict of Interest: The author declares that the research was conducted in the absence of any commercial or financial relationships that could be construed as a potential conflict of interest.

frontiers in Neuroscience

ORIGINAL RESEARCH
published: 06 April 2021
doi: 10.3389/fnins.2021.641739

Phosphate Brain Energy Metabolism and Cognition in Alzheimer's Disease: A Spectroscopy Study Using Whole-Brain Volume-Coil ^{31}Phosphorus Magnetic Resonance Spectroscopy at 7Tesla

Namrata Das[1], Jimin Ren[2], Jeffrey Spence[1] and Sandra Bond Chapman[1]*

[1] Center for BrainHealth, The University of Texas at Dallas, Dallas, TX, United States, [2] Department of Radiology, Advanced Imaging Research Center, University of Texas Southwestern Medical Center, Dallas, TX, United States

Introduction: Mitochondrial dysfunction is a neurometabolic hallmark signaling abnormal brain energy metabolism (BEM) targeted as a potential early marker of Alzheimer's disease (AD). Advanced imaging technologies, such as ^{31}phosphorus magnetic resonance spectroscopy (^{31}P MRS) at ultra-high-field (UHF) magnetic strength 7T, provide sensitive phosphate-BEM (p-BEM) data with precision. The study's first goal was to develop a methodology to measure phosphate energy and membrane metabolites simultaneously across the whole-brain using volume-coil ^{31}P MRS at 7T in three groups-cognitively normal (CN), amnestic mild cognitive impairment (aMCI), and AD. The second aim investigated whether p-BEM markers in the four brain regions-frontal, temporal, parietal, and occipital were significantly different across the three groups. The final goal examined correspondence between the p-BEM markers and cognition in the three groups.

Methods: Forty-one participants (CN = 15, aMCI = 15, AD = 11) were enrolled and completed cognitive assessment and scan. The cognitive domains included executive function (EF), memory, attention, visuospatial skills, and language. The p-BEM markers were measured using energy reserve index (PCr/t-ATP), energy consumption index (intracellular_Pi/t-ATP), metabolic state indicator (intracellular_Pi/PCr), and regulatory co-factors [magnesium (Mg^{2+}) and intracellular pH].

Results: Thirteen metabolites were measured simultaneously from the whole brain for all three group with high spectral resolution at UHF. In the aMCI group, a lower p-BEM was observed compared to CN group based on two markers, i.e., energy reserve (p = 0.009) and energy consumption (p = 0.05) indices; whereas in AD a significant increase was found in metabolic stress indicator (p = 0.007) and lower Mg^{2+} (p = 0.004) in the temporal lobes compared to aMCI using ANOVA between group analytical approach. Finally, using a linear mixed model, a significant positive correlation was found between Mg^{2+} and cognitive performance of memory (p = 0.013), EF (p = 0.023), and attention (p = 0.0003) in CN but not in aMCI or AD.

Conclusion: To our knowledge, this is the first study to show that it is possible to measure p-BEM *in vivo* with precision at UHF across the three groups. Moreover,

OPEN ACCESS

Edited by:
Lionel Carneiro, The Ohio State University, United States

Reviewed by:
Anne-Karine Bouzier-Sore, Centre National de la Recherche Scientifique (CNRS), France
Jianping Jia, Capital Medical University, China

****Correspondence:***
Namrata Das
Namrata.Das@utdallas.edu

Specialty section:
This article was submitted to Neuroenergetics, Nutrition and Brain Health, a section of the journal Frontiers in Neuroscience

Received: *14 December 2020*
Accepted: *15 February 2021*
Published: *06 April 2021*

Citation:
Das N, Ren J, Spence J and Chapman SB (2021) Phosphate Brain Energy Metabolism and Cognition in Alzheimer's Disease: A Spectroscopy Study Using Whole-Brain Volume-Coil ^{31}Phosphorus Magnetic Resonance Spectroscopy at 7Tesla. Front. Neurosci. 15:641739. doi: 10.3389/fnins.2021.641739

the findings suggest that p-BEM may be compromised in aMCI even before an AD diagnosis, which in future studies should explore to examine whether this energy crisis contributes to some of the earliest neuropathophysiologic changes in AD.

Keywords: phosphate brain energy metabolism, Alzheimer's disease, amnestic mild cognitive impairment, ^{31}phosphorus magnetic resonance spectroscopy, adenosine triphosphate, mitochondria

INTRODUCTION

Neurometabolic abnormalities are now recognized as an important area for understanding the early neuropathophysiologic changes in Alzheimer's disease (AD) of diverse etiology (Barzilai et al., 2012; Lourenço et al., 2015). Mitochondrial dysfunction at the root of many neurometabolic abnormalities is considered a high risk factor in AD (Yamaguchi et al., 1992; Albers and Flint, 2000; Crouch et al., 2005; Atamna and Frey, 2007). Research in the post-mortem brain of AD has shown that accumulation of beta-amyloid (Aβ) protein inside the mitochondria have the potential to alter structural and biochemical functions, accelerating the neurodegeneration process (Cottrell et al., 2001; Baloyannis, 2006; Lin and Beal, 2006). Mitochondria play an essential role in energy metabolism in all organs, especially the brain, due to their high energy requirements (Atamna and Frey, 2007). The observation of mitochondrial alteration in AD supports the postulation that disturbances in brain energy metabolism (BEM) may be a significant risk factor contributing to Aβ and tau deposition as individual's progress from normal aging to transitory stages of AD, i.e., amnestic mild cognitive impairment (aMCI) and AD.

Magnetic resonance spectroscopy (MRS) offers a direct non-invasive imaging methodology to investigate mitochondrial function abnormalities by measuring the concentrations of phosphate energy and membrane metabolites, neuroinflammatory markers, and neurotransmitters in the brain (Ross and Sachdev, 2004). Specifically, ^{31}phosphorus MRS (^{31}P MRS) is used to measure phosphate energy [adenosine triphosphate (ATP), phosphocreatine (PCr), and inorganic phosphate (Pi-extracellular and intracellular)] and membrane phospholipid [phosphoethanolamine (PE), phosphocholine (PC), glycerophosphoethanolamine (GPE), and glycerophosphocholine (GPC)] metabolites along with the assessment of regulatory co-factors magnesium (Mg^{2+}) and brain tissue pH which supports energy metabolism of the brain along with membrane synthesis and degradation. Recent work by Rijpma et al. (2018) using whole-brain volume-coil ^{31}P MRS at 3T in thirty-one (31) participants with mild AD and healthy controls each showed increased PCr signal, PCr/Pi index, and pH in the retrosplenial cortex and hippocampus area of the temporal lobe in AD where early AD molecular changes are known to start. In contrast to alterations in phosphate BEM (p-BEM), the same study did not show any significant difference in the membrane phospholipid index measured using the PE, PC, GPE, and GPC in the brain regions of AD compared to healthy controls. Nonetheless, Rijpma's work at 3-T in AD was one of the first study to apply a methodology to measure phosphate energy and membrane metabolites simultaneously from the whole-brain.

In addition to measuring phosphate metabolites through ^{31}P signal intensities, the ^{31}P-MRS also offers measurements of pH and Mg^{2+} concentration through ^{31}P chemical shifts, based on the high sensitivity of Pi chemical shift δ(Pi) to Pi protonation/deprotonation and the dependence of ATP chemical shift difference δ(α-ATP)–δ(β-ATP) or $\delta_{\alpha-\beta}$ on Mg^{2+} binding to ATP. Mg^{2+} plays a crucial role in regulation of mitochondrial functions as it stimulates over 300 enzymes (Adrasi et al., 2000). Prior research in *in vitro* studies using post-mortem human brains of AD reported reduced Mg^{2+} concentrations in vulnerable brain regions, especially in the hippocampus part of the temporal lobe (Adrasi et al., 2000; Cilliler et al., 2007; Slutsky et al., 2010). However, a knowledge gap exists in investigating the p-BEM, Mg^{2+}, and pH abnormalities in aMCI, i.e., early transitory stage of the AD which is regarded as a heterogeneous and unstable condition as compared to AD and healthy aging. Therefore, it would be informative to include individuals in all three groups, i.e., healthy aging, aMCI, and AD to confirm and better understand those prior research findings from post-mortem AD brains, and to provide *in vivo* references for p-BEM alterations as an early marker of AD etiology and pathology responsible for neurobiological changes due to mitochondrial dysfunction. Whereas the cross-sectional research approach is motivated by evidence from *in vitro* studies of cell-line culture and post-mortem human brain (Atamna and Frey, 2007), there is an urgency in identifying early detectable and potentially treatable p-BEM abnormalities contributing to progressive neurodegeneration in aMCI, since this particular population is at greater risk for developing AD.

Prior to Rijpma's work at 3T, a few studies investigated the relationship between p-BEM and cognition in AD with ^{31}P data acquired from a single brain region at lower magnetic strength. Smith's work using ^{31}P MRS at 1.5-T in seventeen (17) mild to moderate AD and eight (8) healthy controls showed an inverse relationship of PCr/Pi index measured in the frontal lobe with a dementia rating scale (DRS), i.e., lower p-BEM marker was associated with higher DRS severity (Smith et al., 1995). Parallel to Smith's work, another research by group Forlenza et al.'s (2005) using the same magnetic strength over the prefrontal cortex showed an inverse relationship between membrane phospholipid

Abbreviations: AD, Alzheimer's disease; aMCI, amnestic mild cognitive impairment; p-BEM, phosphate brain energy metabolism; ^{31}P MRS, ^{31}Phosphorus MRS; ATP, adenosine triphosphate; PCr, phosphocreatine; Pi, inorganic phosphate; PE, phosphoethanolamine; PC, phosphocholine; GPE, glycerophosphoethanolamine; GPC, glycerophosphocholine; Mg^{2+}, magnesium; Aβ, beta-amyloid; UHF, ultra-high-field; ADNI, Alzheimer disease neuroimaging initiative.

metabolite index with lower cognitive performance measured using the Cambridge Cognitive (CAMCOG) scale subtests in AD (n = 18) compared to healthy controls (n = 16). The CAMCOG scale included cognitive domains of memory, orientation, language, attention, praxis, calculation, abstract thinking, and visual perception. However, the main limitations at lower magnetic strength is the low spectral resolution of these metabolites, restricting the exploration of p-BEM-cognition correspondence in vulnerable brain regions like the temporal lobe compared to other parts of the brain in aMCI and AD. The low spectral resolution and detection sensitivity could be overcome by using ultra-high-field (UHF) magnetic strength at 7T for more accurate measurements of the phosphate metabolites.

At UHF magnetic strength 7T, the first aim of this research was to test the feasibility to acquire high quality whole-brain data for resolving phosphate brain energy and membrane metabolites from each voxel simultaneously across the three cohorts cognitively normal (CN) adults, aMCI, and mild AD using volume-coil ^{31}P MRS. Our second aim was to investigate if p-BEM and membrane phospholipid markers differ across those three groups in the four regions-frontal, temporal, parietal, and occipital bilaterally. The p-BEM markers were measured using the three indices- energy reserve index (PCr/t-ATP), energy consumption index (intracellular_Pi/t-ATP), and metabolic state indicator (intracellular_Pi/PCr), along with regulatory co-factors – magnesium (Mg^{2+}) and pH, separately (definitions of the three indices are cited in our previous publication; Das et al., 2020). Based on the prior study's findings using either ^{18}FDG-PET (Silverman et al., 2001; Mosconi et al., 2010; Mosconi, 2013; Ou et al., 2019) or ^{31}P MRS (Rijpma et al., 2018), which supported reduced respective BEM (glucose or phosphate) in the temporal lobes in MCI and AD, we hypothesized that p-BEM markers-energy reserve, energy consumption indices, and regulatory co-factors (Mg^{2+} and pH), would be lower in the same vulnerable region of the brain and the same population, i.e., aMCI and AD when compared to CN group. The hypothesis of reduced p-BEM in the temporal lobe is the focus of this study because the brain depends on glucose consumption, which is regarded as the primary fuel to generate energy in the form of ATP (Mergenthaler et al., 2013). Moreover, prior 18FDG-PET studies have supported reduced glucose consumption in the temporal lobe, a region vulnerable to the early decline in AD pathology (Mosconi et al., 2010; Ou et al., 2019).

On the other hand, we anticipate that the metabolic state ratio, an indicator of metabolic stress, would be higher in aMCI and mild AD due to increased metabolic neurodegeneration compared to the CN group. Moreover, in congruence with study Rijpma et al.'s (2018), we proposed that the membrane phospholipid index would not be altered across the three groups.

The next aim explored the significant phosphate BEM markers-cognitive correspondence in all the groups. Prior studies using ^{18}FDG-PET (Desgranges et al., 1998; Mosconi et al., 2005; Herholz, 2010; Ou et al., 2019) or ^{31}P MRS at 1.5-T (Smith et al., 1995; Forlenza et al., 2005) have shown a BEM-cognition correspondence across the domain of memory, executive function (EF), attention, visuospatial perception, and language (Hanninen et al., 1996). Therefore, we postulated that there would be a significant association between lower sensitive p-BEM markers and co-factors (Mg^{2+} and pH) separately in the temporal lobe, a vulnerable brain region and lower cognitive performance across the three groups except for metabolic state indicator. The final goal was to compare the sensitivity and specificity of p-BEM markers and cognitive measures to reclassify the individuals in their respective groups correctly. Deep learning model/machine learning applications are rapidly developing to diagnose and predict who converts into AD. A recent application of the deep learning model was on 1,002 Alzheimer's disease Neuroimaging Initiative (ADNI) participants to detect AD in 40 patients in an independent setting. The model showed a sensitivity of 100% and specificity of 82% in predicting the final diagnosis within an average timeline of 75.8 months before the AD diagnosis (Ding et al., 2019). Motivated by this evidence, we aimed to develop a prediction model for reclassifying aMCI and AD group by combining p-BEM markers with cognition.

MATERIALS AND METHODS

Protocol Approvals and Consent

The research on human subjects was approved by the Institutional Review Board (IRB) of The University of Texas Southwestern Medical Center (UTSW#STU 062017-089) and The University of Texas at Dallas (UTD#18-73) to include individuals between the ages of 55-85years in three groups: CN adults, aMCI, and mild AD. Informed consent and HIPPA forms were signed as per the Committee on Human Experimentation's under the Declaration of Helsinki revised in 1981 and useful clinical practice guidelines.

Participants

A total of forty-one participants (15 CN, 15 aMCI, and 11 mild AD) were enrolled in the study using a phone screen, which included questions on demographics, medical history, medicine use, a neuroimaging screening questionnaire, and a memory-screen called Clinical Dementia Rating (CDR) scale. Subjects with a history of substance use, neurological disorders other than AD, psychiatric problems, metal in the body, or left-handers were excluded from the study. CN and aMCI were recruited from the DFW community based on ADNI criteria, and the classification was verified by a clinician and neuroscientist at Center for BrainHealth, UTD. Alzheimer's patients with mild form were recruited from referral either through the local neurologist or from the DFW community after reviewing the individual's medical records from the neurologist. All selected participants were right-handed, native English speakers with a minimum of 12 years of education. Irrespective of gender and ethnic factors, all eligible participants were invited to complete the cognitive screen and assessment.

Characterization of the Participants

The comprehensive ADNI criteria used for enrollment were 1) without subjective memory (CN) or with subjective memory (aMCI and AD) complaints; 2) Clinical Dementia Rating (CDR) scale: A score of zero (0) for CN, half (0.5) for aMCI, and a half or one (0.5 or 1) for mild AD (CDR, Morris, 1993); 3) mini mental status examination (MMSE) (Folstein et al., 1975): 24–30 for CN and aMCI and 20-26 for mild AD and; 4) objective memory status measured by logical memory subtest from Wechsler Memory Scale-III (WMS-III, Wechsler, 1997) with (a) delayed memory recall scores of ≥9 for 16 or more years of education, ≥5 for 8–15 years of educational and ≥3 for 0–7 years of education in CN, or (b) delayed memory recall scores of 8–11 for 16 or more years of education, 4–9 for 8–15 years of educational and 0-6 for 0-7 years of education for aMCI or (c) delayed memory recall scores of ≤8 for 16 or more years of education, ≤4 for 8–15 years of educational and ≤2 for 0—7 years of education for mild AD. In addition to ADNI criteria for the mild AD group, the diagnosis was confirmed by a neurologist. All participants were assessed for signs of depression using the long geriatric depression scale (GDS-long form) form (Yesavage et al., 1982). Individuals with no or mild depression with or without antidepressant medications were enrolled in the study.

Cognitive Screening

A one-hour cognitive screen included vision and hearing test, vitals (blood pressure, pulse rate, weight, and height), and memory screens MMSE and logical memory subtest from Wechsler Memory Scale-III along with two questionnaires – 1. Lawton instrumental daily living activities, 2. Geriatric depression scale-Long form (GDS-long form) was completed at the Center for BrainHealth (CBH), a division of the University of Texas at Dallas (UTD). For eligibility on vision and hearing criteria, visual acuity of 20/50 and 40 dB at 1,000 HZ on the hearing test were the cut-off, respectively.

Cognitive Assessment

Eligible participants on the phone and cognitive screens completed the cognitive assessment of 4-hours divided over 2 days to control for fatigue. The cognitive assessment included measures to investigate the domains of memory (episodic memory), executive function (complex abstraction, innovation, switching and inhibition, conceptual reasoning, working memory, and verbal fluency), attention, visuospatial skills, and language (**Table 1**). The demographics of the participants are presented in **Table 2**.

TABLE 1 | Neurocognitive assessment battery administered across the three groups: cognitively normal, amnestic mild cognitive impairment (aMCI), and mild Alzheimer's disease (AD).

Cognitive Domain	Measures	Description
Executive Function		
1. Complex abstraction	Test of Strategic Learning (TOSL) (Chapman et al., 2002) WAIS-III similarities (Wechsler, 1972)	Assess the ability to condense and synthesize complex information written as a summary from a short complex story. Scores represent a number of abstracted ideas. Assess the ability to think abstractly and to find similarities among words or ideas that may not appear to be similar on the surface.
2. Innovation	Test of Strategic Learning (TOSL) (Chapman et al., 2002)	Assess the ability to construct as many interpretations as possible from a complex short story to measure idea fluency.
3. Inhibition and switching	Trails B (Delis et al., 2001)	Assess the ability to alternate between a number and letter by drawing a continuous line.
4. Conceptual Reasoning	Delis-Kaplan executive function system (DKEFS) card sort (Delis et al., 2001)	Assess the ability to draw similarities between two sets of cards by drawing reasons behind the selection of cards.
5. Working Memory	Digit Span Backwards Test (WMS-III, Wechsler, 1997)	The ability to repeat a series of numbers backward.
6. Fluency: Verbal/Category	Controlled Oral Word Association (COWAT) (Benton et al., 1994; Spreen and Strauss, 1998)	Assess the ability to generate as many words starting with a particular alphabet or a category in one minute.
Memory		
Episodic memory	Memory for facts: Test of Strategic Learning (TOSL) (Chapman et al., 2002) California Verbal Learning Task (Petersen et al., 2001)	Assess the ability to recall details of a complex short story. Assess the ability to recall a list of sixteen (16) words in four categories immediately after the list was read followed by delayed recall after 20 min interval.
Attention	Selective Auditory learning task (Hanten et al., 2007) Digit Span Forward Task (WMS-III, Wechsler, 1997)	Assess the ability to focus and pay attention to high-priority stimulus, while simultaneously blocking or inhibiting unwanted or low-priority information. Assess the ability to pay attention and remember a series of numbers in the same sequence.
Language	Boston Naming Test (Kaplan et al., 1983)	Assess the ability of the individual to say the word associated with the object in the picture.
Visuospatial	Trails A (Delis et al., 2001)	The ability to visually search for numbers in ascending order and draw a continuous line assessing mental flexibility and processing speed.

TABLE 2 | Demographics of the participant enrolled in the study.

	Cognitively normal (CN)	Amnestic Mild Cognitive Impairment (aMCI)	Mild Alzheimer's disease (AD)
Gender	11 Females/4 Males	10 Females/5 Males	6 Females/5 Males
Age (mean ± SD)	63.47 ± 6.13	66.53 ± 6.74	71.73 ± 5.68*
Education	17.83 ± 2.91	17.33 ± 3.21	16.82 ± 3.68
Ethinicty (mean ± SD)	12 Caucasian/2 Asian/1 Hispanic	15 Caucasian	8 Caucasian/2 African American/1 Hispanic
Mini Mental Status Examination (mean ± SD)	29 ± 1.25	28.4 ± 1.404	25 ± 2.90
Clinical Dementia Rating (CDR) scale	0	0.5	0.5 or 1
Body Mass Index BMI (mean ± SD)	24.77 ± 3.19	26.43 ± 5.42	25.22 ± 4.89
Diabetes	1	0	1
Hypertension	1	6	5
Hyperlipidemia	4	7	5
Hypothyroidism	1	4	3

*$p < 0.05$.

Whole-Brain p-BEM Metabolites Data Acquisition Using Volume-Coil ^{31}P Magnetic Resonance Spectroscopy at 7T

The ^{31}P-MRS data were acquired using a human MRI scanner system at 7T (Achieva, Philips Healthcare, Cleveland, OH, United States), in combination with a transmit/receive ^{31}P birdcage volume coil of diameter 23 cm and length 10 cm (Gorten Center, Leiden University Medical Center, Netherlands). The ^{31}P coil was inserted into a cylindrical NOVA ^{1}H transmit/receive head coil for ^{1}H shimming and imaging planning. The participants were positioned head-first, and supine with head posterior rest on a soft cushion and the head positioned in the center of the ^{31}P RF coil. The data acquisitions included a non-localized ^{31}P MRS survey scan with pulse-acquire sequence for evaluation of shimming quality on ^{31}P spectrum, and a 3D MRS imaging scan at an in-plan resolution of 2 × 2 cm^2 reconstructed to 1 × 1 cm^2, slice thickness 2 cm, with 7–9 coronal slices depending on the participants' head size along A-P direction. Other MRS parameters were TR = 0.5 s, TE 0.5 ms, number of average 12, sampling points 2 K, zero-filled to 4 K prior to FT scan time 39 min. **Figures 1** and **2** shows the display of all the phosphorus metabolites.

Phosphate BEM Metabolites Data Analysis

^{31}P MRS raw data were preprocessed using the Philips software package SpecView on the scanner. All the brain slices were preprocessed for zero filings, apodization, Fourier transformation, and phase correction. For baseline correction and spectral fitting, the preprocessed data were post-processed using an in-house MATLAB program at UTSW. The fitting was based on the Voigt lineshape model (a combination of Gaussian and Lorentzian lineshape). Post-processed data was able to resolve thirteen (13) resonance phosphorus peaks of PCr, ATP (α-, β-, and γ-spins), nicotinamide adenine dinucleotide (total NAD), uridine diphosphate glucose (UDPG and its analogs), intracellular and extracellular Pi), five (5) phospholipid metabolites including PE, PC, GPE, GPC, and a macromolecular metabolite peak. The phosphate energy and membrane phospholipid metabolites were measured from each peak's fitting integral. In contrast, the cellular pH and Mg^{2+} concentration were derived from the chemical shift measurements in region summed spectra for the four brain regions of interest- frontal, temporal, parietal, and occipital lobes. For each spectrum, the free intracellular magnesium (Mg^{2+}) concentration was calculated using the chemical shift difference between α- and β-ATP ($\delta_{\alpha-\beta}$ in ppm), whereas pH was calculated from the chemical shift of the corresponding Pi (internal) peaks (δ_{Pi}, in ppm) in reference to PCr (δ_{PCr} = 0ppm) (Das et al., 2020). Total-ATP (t-ATP) signal was calculated by averaging the α-, β-, and γ-ATP resonances. For membrane phospholipid metabolite index/marker, phosphomonoesters (PMEs) was calculated by summation of PE and PC, whereas phosphodiesters (PDEs) by summation of GPE and GPC. Overall, the membrane phospholipid index was calculated by the ratio of PMEs/PDEs.

Statistical Approach

Neurocognitive Measures, p-BEM Markers Along With Regulatory Co-Factors, and Membrane Phospholipid Markers Variations Across the Three Groups

We investigated the relationship between age, education, and gender with individual phosphate energy and membrane phospholipid metabolites. As we found significant inverse relationship of age and gender with the metabolites, all the p-BEM and membrane phospholipid metabolites were adjusted for age, education, and gender. Adjusted p-BEM data was used to calculate the ratios of PCr/t-ATP (reflective of energy reserve), Pi/t-ATP (reflective of energy consumption), Pi/PCr (reflective of a metabolic state), and regulatory co-factors (Mg^{2+} and pH) which were interpreted as BEM markers in the paper along with membrane phospholipid index

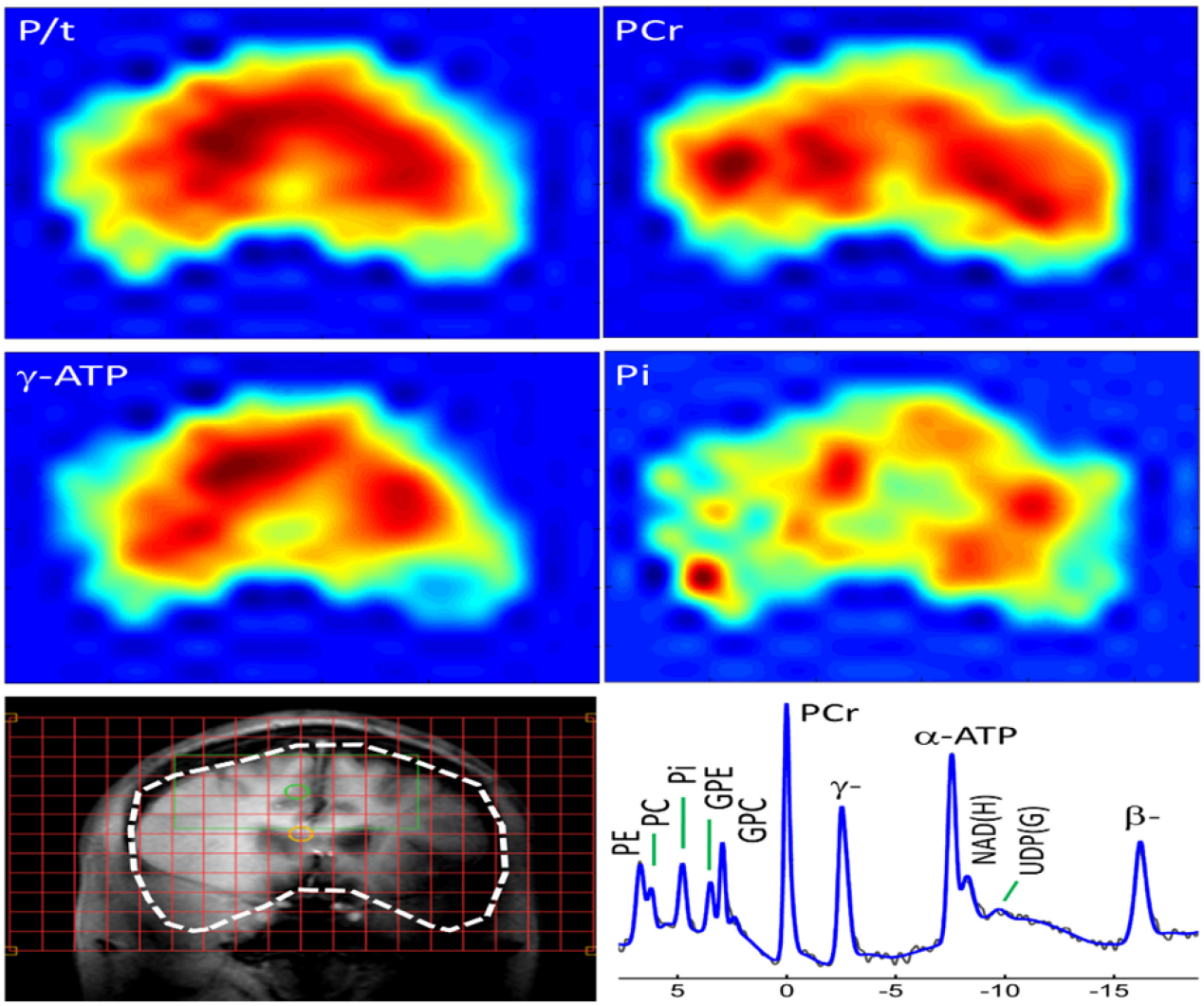

FIGURE 1 | Whole-brain ^{31}P MRS spectral displayed on coronal anatomical images. Total ^{31}P signal from all metabolites; Color maps show the spatial distribution of specific metabolites.

(PMEs/PDEs) (for definition of the terminology refer to our previous publication Das et al., 2020). The BEM markers, membrane phospholipid indices, and regulatory co-factors were transformed into a shifted log scale to symmetrize their respective distributions and reduce high-leverage contributions in individual values regressions. Specifically, those with positive skew coefficients were transformed as $\log(x - a)$, and those with negative skew coefficients were transformed as $-\log(a - x)$, where "x" denotes the specific metabolite's raw score for each participant and "a" denotes the metabolite-specific constant. In addition to the BEM metabolites, all the neurocognitive measures were also adjusted for age, education, and gender. Statistical analyses for the neurocognitive and spectroscopy data were analyzed using R studio 4.1.0 for windows. A one-way analysis of variance (ANOVA) between the group statistical package in R-studio was used to investigate the differences in the three groups with $\alpha = 0.01$ for cognitive measures and $\alpha = 0.10$ for BEM markers, given the exploratory nature of the study. *Post hoc* multiple between-group comparisons using Tukey at $\alpha = 0.05$ for the familywise error rate was performed to identify significant mean differences between the groups.

Phosphate BEM and Regulatory Co-Factors Correspondence With Cognition Across the Three Groups

To navigate the next goal of the research, i.e., any p-BEM–cognition correspondences for which the transformed adjusted BEM and neurocognitive data were scaled to have common variance across the variables. General linear model was used to understand the effect of group and each of the markers or regulatory co-factors on cognition for each pairwise comparison. The model contains each of the indices or regulatory co-factor-by-group interaction on cognitive performance of EF, memory,

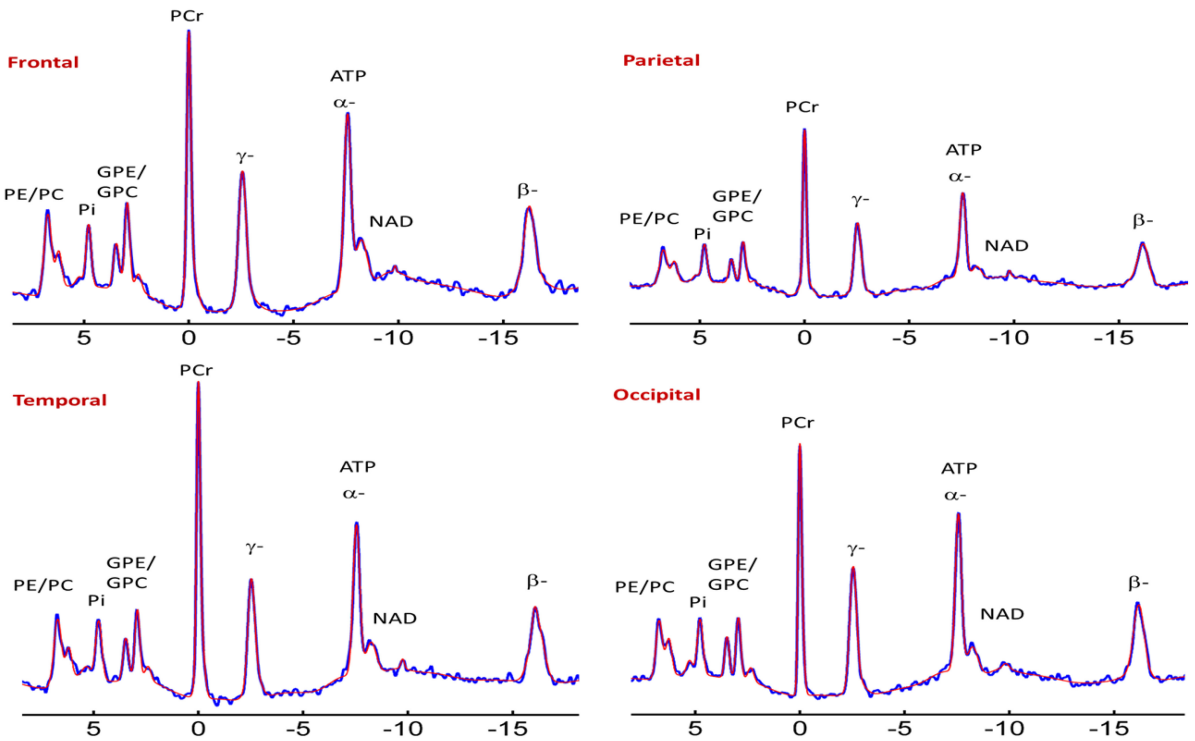

FIGURE 2 | Representative spectra from the frontal, parietal, temporal, and occipital brain areas of a cognitively normal adult. Zero filling to 8,000 data points with 8 Hz vogit lineshape model applied for the display purpose. PE, phosphoethanolamine; PC, phosphocholine; P_i^{in}, inorganic phosphate internal, respectively; GPE, glycerophosphoethanolamine; GPC, glycerophosphocholine; PCr, phosphocreatine; ATP forms: α, β, and δ adenosine triphosphate; NAD, nicotinamide adenine dinucleotide; UDPG, uridine diphosphate glucose.

attention, language, and visuospatial domains in the four brain regions-frontal, temporal, parietal, and occipital separately. All group tests and interaction tests were at $\alpha = 0.05$.

The working linear model used in this work was written as:

$$\text{y\_j} = \text{b0} + \text{b1} * \text{I(group} = \text{aMCI)} + \text{b2} * \text{I(group} = \text{AD)} +$$

$$b3 * \text{x\_j} + \text{b4} * \text{x\_j} * \text{I(group} = \text{MCI)} + \text{b5} * \text{x\_j} *$$

$$\text{I(group} = \text{AD)} + \text{e\_j}, \text{ for j} = 1, \ldots, \text{N subjects.}$$

y_j represents the outcome or dependent variable, i.e., the cognitive performance for the *j*th subject. "*I*" is an indicator function (i.e., 1 if true; 0 otherwise), x_j is one of the indices or pH or Mg^{2+}, e_j is the error term, and the covariates, x_j, are centered at their means. The inclusion of (indices/Mg^{2+}/pH X group) and (indices/Mg^{2+}/pH X mean differences between the group) interaction terms allowed for an in-depth investigation of all the probable effects on the cognitive outcome.

Predictive Model to Assess the Sensitivity, Specificity, Positive Predictive and Negative Predictive Value, and Accuracy of the Data Set

A principal component analysis was used for data reduction as an initial step to develop a predictive model using p-BEM makers and neurocognitive data (**Supplementary Figure 1**). The quadratic discriminant model was applied to the first two principal components that substantially explained much of the variance in the data. The discriminant model was trained using 10-fold cross-validation (CV) framework to obtain estimates of generalization error. For each of the 10-folds of the CV framework, 10% of the data was used as an internal hold-out test to predict the individuals in their respective groups, while the other 90% was used for training the model, including the principal component reduction.

RESULTS

Neurocognitive Measures, p-BEM, Regulatory Co-Factors, and Membrane Phospholipid Markers Variations Across the Three Groups

Neurocognitive Measures Differences Across the Three Group

ANOVA between-group analysis across the three groups showed significant group effects in the five cognitive domains – EF, memory, attention, language, and visuospatial skills *z*-scores. In the executive function category all the subdomains: complex abstraction [similarities: $F(2,38) = 38.87$, $p < 0.001$]; innovation

[TOSL: $F(2,38) = 5.04$, $p = 0.01$]; inhibition and switching [Trails B: $F(2,38) = 50.28$, $p < 0.001$]; conceptual reasoning [DKEFS sort: $F(2,38) = 39.12$, $p < 0.001$]; and fluency [verbal fluency: $F(2,38) = 17.16$, $p < 0.001$); category fluency-animals: $F(2,38) = 10.38$, $p < 0.001$] where significantly lower in mild AD compared to aMCI and CN. The subdomains of complex abstraction and conceptual reasoning performance were significantly reduced in aMCI along with mild AD but not in CN group. For the episodic memory performance [CVLT: immediate recall ($F(2, 38) = 26.6$, $p < 0.001$), short delay recall ($F(2, 38) = 35.82$, $p < 0.001$), long delay recall ($F(2, 38) = 27.76$, $p < 0.001$), intrusions ($F(2, 38) = 8.60$, $p < 0.001$)] was significantly lower in both mild AD and aMCI compared to CN. Similarly, attention domain measured by selective auditory learning test-Trail 1 ($F(2,38) = 51.2$, $p < 0.001$) and digit span forward test ($F(2,38) = 4.077$, $p < 0.025$); language tested using Boston Naming task ($F(2,38) = 22.2$, $p < 0.001$), and visuo-spatial skills assessed using Trails A ($F(2,38) = 16.79$, $p < 0.001$) was significantly lower in mild AD group only (**Supplementary Table 1**).

p-BEM Markers Variations Across the Three Groups

ANOVA between groups analysis showed three significant results. First, in aMCI and mild AD, the energy reserve index (PCr/t_ATP) [$F(2,38) = 15.09$, $p < 0.001$] in the temporal lobe was significantly lowered when compared to CN. Second, in aMCI energy consumption index (intracellular_Pi/t_ATP) [$F(2,38) = 4.82$, $p = 0.01$] of the temporal lobe was significantly lower compared to CN but not in mild AD. Finally, in temporal lobe of mild AD the metabolic state indicator (intracellular_Pi/PCr), [$F(2,38) = 5.68$, $p = 0.007$] was significantly higher when compared to aMCI and CN. The BEM markers in the other brain regions, i.e., frontal, parietal, and occipital were not significantly different across the groups.

The altered p-BEM markers in the temporal lobe in aMCI and mild AD prompted further exploration of which group means difference contributed to the significant effect using Tukey multiple comparisons adjustment. Overall, the results support that the aMCI group could be differentiated from the CN based on two BEM markers: energy reserve index ($t = -0.88$, p.adjusted Tukey = 0.009) and energy consumption index ($t = -0.80$, p.adjusted Tukey = 0.05), respectively. Next, the AD group could be differentiated from the aMCI cohort based on energy reserve index ($t = -0.77$, p.adjusted Tukey = 0.04) and metabolic state indicator ($t = 1.15$, p.adjusted Tukey = 0.007). Finally, all the p-BEM markers differentiated AD from CN [energy reserve index ($t = -1.65$, p.adjusted Tukey < 0.001), energy consumption index ($t = -1.04$, p.adjusted Tukey = 0.018), and metabolic state indicator ($t = 0.95$, p.adjusted Tukey = 0.03).

Regulatory Co-Factors Variations Across the Three Groups

Regulatory co-factor intracellular Mg^{2+} was significantly lower in the temporal lobe in mild AD compared to aMCI and CN [$F(2,38) = 6.48$, $p = 0.0038$]. Moreover, Tukey multiple comparisons adjustment in this model showed a similar pattern as the metabolic state indictor reported above, pointing to a significant mean difference in two specific group comparisons, i.e., AD to CN ($t = -1.03$, p.adusted tukey = 0.015) and AD to aMCI ($t = -1.19$, p.adjusted tukey = 0.004), however, differences between aMCI and CN failed to reach significance ($t = 0.16$, p.adjusted tukey = 0.87). The results from other brain regions were insignificant.

Membrane Phospholipid Marker (PMEs/PDEs) Variations Across the Three Groups

The membrane phospholipid marker (PMEs/PDEs) failed to reach significance across groups in the four brain regions separately [frontal: $F(2,38) = 1.76$, $p = 0.18$; temporal: $F(2,38) = 0.91$, $p = 0.41$; parietal: $F(2,38) = 1.85$, $p = 0.17$; occipital: $F(2,38) = 2.12$, $p = 0.13$]. **Table 3** and **Figure 3** summarizes the findings.

Phosphate BEM-Cognition Correspondence Across the Three Groups

The final step was to investigate the association of significant or sensitive temporal BEM markers – energy reserve index, energy consumption index, metabolic state indicator, and intracellular Mg^{2+} with cognitive domains of executive function, memory, attention, language, and visuospatial skills across the three groups. Overall, a linear mixed model was used to explore the BEM-cognition correspondence. **Figure 4**, **Table 4**, and **Supplementary Table 2**.

Temporal Lobe Energy Reserve Index-Cognition Correspondence

In aMCI, the group-by-temporal lobe energy reserve index interaction effect revealed a significant positive association with EF – verbal fluency z-scores [$F(2,38) = 4.6979$, $p = 0.0156$] in aMCI group ($t = 1.70$, $p = 0.10$), whereas a negative correlation trend was found in mild AD ($t = -1.98$, $p = 0.06$) compared to CN. Moreover, the mild AD group contributed to the significant positive correlation effect by the interaction of energy reserve index and group on EF-inhibition and switching subdomain measured using Trails B z-scores [$F(2, 38) = 7.4030$, $p = 0.002$] compared to aMCI ($t = -1.18$, $p = 0.25$), a negative association with AD ($t = 3.20$, $p = 0.003$) compared to CN.

Temporal Lobe Energy Consumption Index-Cognition Correspondence

In aMCI, the group-by- temporal lobe energy consumption index was strongly associated significantly with EF-verbal fluency z-scores [$F(2,38) = 3.2148$, MS = 1.8657, $p = 0.05$] in AD group compared to aMCI in negative direction ($t = -2.36$, $p = 0.023$). In addition CN group, the main effect of the interaction was also strongly associated with episodic memory-immediate list memory recall z-scores [$F(2,38) = 3.2879$, MS = 1.2066, $p = 0.0491$] whereas the interaction coefficients between the groups where not significant.

Temporal Lobe Metabolic State Indicator-Cognition Correspondence

The group-by-temporal lobe metabolic state indicator effect was significantly inversely associated with EF-innovation subdomain

TABLE 3 | ANOVA analysis of p-BEM markers, Regulatory co-factors (Magnesium and pH), and membrane phospholipid markers in the four brain regions-frontal, temporal, parietal, and occipital across the three cohorts: cognitively normal (CN) adults, amnestic mild cognitive impairment (aMCI), and mild Alzheimer's disease (AD) (*indicates those *F* tests which satisfy FDR = 0.10). Tukey *post hoc* analysis for the significant group difference.

Independent variables	Brain region	ANOVA results *df* = (2,38) F-statistics p-value df = (2,38)		*Post hoc* Tukey multiple comparisons		
				MCI to CN mean difference (p-value)	AD to CN mean difference (p-value)	AD to MCI mean difference (p-value)
BEM indices						
Energy reserve index: PCr/t-ATP	Frontal	0.042	0.96	0.11(0.96)	0.07(0.99)	-0.04(0.99)
	Temporal	15.09	<0.001***	−0.88(0.009)	−1.65(<0.001)	-0.77(0.04)
	Parietal	1.57	0.22	−0.63(0.20)	−0.23(0.83)	0.40(0.56)
	Occipital	0.76	0.47	−0.01(0.999)	−0.44(0.52)	-0.43(0.53)
Energy consumption index: intracellular Pi/t-ATP	Frontal	0.106	0.9	−0.08(0.98)	−0.19(0.89)	-0.11(0.96)
	Temporal	4.82	0.01*	−0.80(0.05)	−1.04(0.018)	-0.24(0.79)
	Parietal	1.87	0.17	−0.44(0.45)	0.29(0.73)	0.73(0.16)
	Occipital	0.003	0.997	0.03(0.99)	0.03(0.99)	0.09(0.99)
Extracellular Pi/t-ATP	Frontal	3.01	0.06*	0.43(0.44)	0.93(0.05)	0.50(0.40)
	Temporal	2.06	0.14	−0.71(0.12)	−0.32(0.69)	0.40(0.56)
	Parietal	0.202	0.82	0.22(0.82)	0.04(0.99)	-0.18(0.89)
	Occipital	2.12	0.13	−0.35(0.59)	0.44(0.49)	0.80(0.11)
Metabolic state indicator: intracellular_Pi/PCr	Frontal	0.126	0.88	−0.07(0.98)	−0.20(0.87)	-0.13(0.95)
	Temporal	5.68	0.007**	−0.21(0.80)	0.95(0.03)	1.15(0.007)
	Parietal	0.76	0.47	0.001(0.999)	0.44(0.52)	0.44(0.53)
	Occipital	0.516	0.60	−0.07(0.98)	0.32(0.71)	0.39(0.60)
Extracellular_Pi/PCr	Frontal	3.27	0.049*	0.47(0.38)	0.96(0.04)	0.49(0.40)
	Temporal	3.44	0.042*	−0.08(0.97)	0.83(0.08)	0.91(0.05)
	Parietal	0.47	0.63	0.34(0.63)	0.07(0.98)	-0.27(0.78)
	Occipital	2.53	0.09*	−0.32(0.64)	0.54(0.34)	0.86(0.076)
Regulatory co-factor						
Intracellular pH	Frontal	1.34	0.26	−0.17(0.24)	−0.17(0.91)	0.42(0.53)
	Temporal	0.25	0.78	−0.03(0.99)	0.23(0.83)	0.27(0.79)
	Parietal	0.27	0.77	0.27(0.75)	0.09(0.97)	-0.17(0.91)
	Occipital	3.40	0.04*	−0.36(0.56)	−0.98(0.03)	-0.62(0.24)
Intracellular magnesium(Mg^{2+})	Frontal	0.61	0.55	−0.34(0.63)	0.05(0.99)	0.39(0.60)
	Temporal	6.48	0.0038**	0.16(0.87)	−1.03(0.015)	-1.19(0.004)
	Parietal	2.03	0.14	−0.14(0.92)	0.61(0.27)	0.75(0.14)
	Occipital	1.50	0.24	−0.03(0.99)	−0.61(0.27)	-0.59(0.30)
Membrane phospholipid indices						
PMEs/PDEs	Frontal	1.76	0.18	−0.11(0.95)	0.59(0.29)	0.69(0.18)
	Temporal	0.91	0.41	−0.27(0.75)	0.27(0.78)	0.54(0.38)
	Parietal	1.85	0.17	0.61(0.22)	0.61(0.27)	0.01(1.00)
	Occipital	2.12	0.13	−0.73(0.11)	−0.32(0.69)	0.41(0.55)

*$p < 0.10$, **$p < 0.01$, ***p.0.001.

z-scores [$F(2,38) = 4.6303$, MS = 3.3063, $p = 0.0164$]. The main effect was attributed by the CN as positive association between the independent and dependent variables compared to aMCI ($t = 2.68$, $p = 0.01$) and mild AD ($t = 2.94$, $p = 0.006$). Additionally to the above results, in aMCI a significant inverse relationship was shown with episodic memory- recognition subdomain [$F(2, 38) = 5.7276$, MS = 4.1099, $p < 0.007$] compared to CN ($t = -2.65$, $p = 0.011$), where a positive correlation was found in AD compared to MCI ($t = 3.08$, $p = 0.004$).

Temporal Lobe Intracellular Mg^{2+}-Cognition Correspondence

The main effect of interaction of group-temporal lobe intracellular Mg^{2+} on EF-complex abstraction [$F(2,38) = 3.2135$, MS = 2.92, $p = 0.05$] compared to aMCI ($t = -2.38$, $p = 0.023$)] and mild AD ($t = -2.39$, $p = 0.02$) compared to CN group. Similarly episodic memory domain-immediate recall [$F(2,38) = 3.6597$, MS = 1,4347, $p = 0.036$] interaction effect was contributed by the aMCI ($t = -2.62$, $p = 0.013$) and mild AD ($t = -2.45$, $p = 0.02$) compared to CN group. Finally, the interaction of group-temporal lobe intracellular Mg^{2+} on attentiotrail 1 domain [$F(2,38) = 8.087$, MS = 1.7004, $p = 0.0012$] was associated with aMCI ($t = -3.99$, $p = 0.003$) and mild AD ($t = -3.39$, $p = 0.002$) compared to CN group.

Predictive Model Results

The principal component reduction and the quadratic discriminant model utilized both the MRS values and neurocognitive data set. For each of the 10 folds, the model was trained on 90% of the data set and tested on hold-out 10% of the data. The cross-validation error was 0.1704 with seven (7) misclassifications out of the 41 individuals data set used

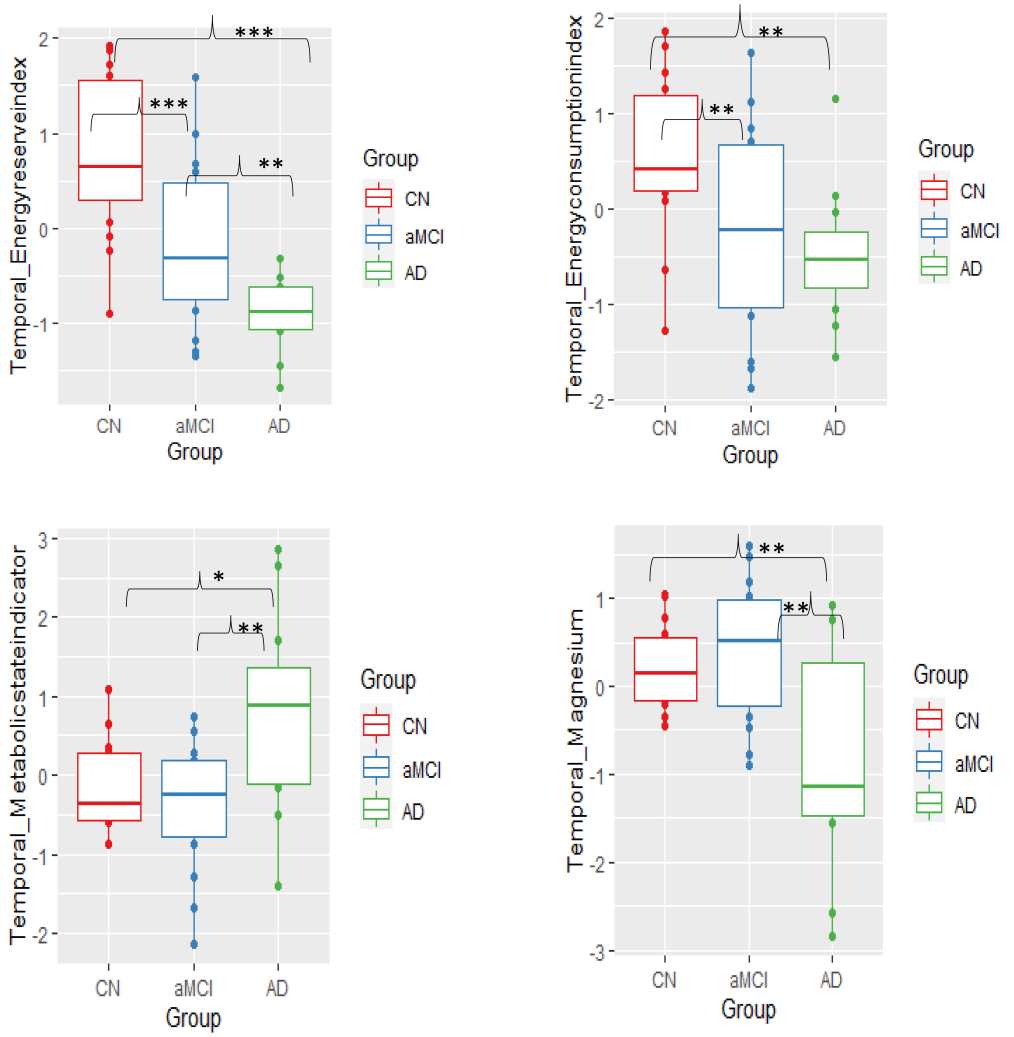

FIGURE 3 | Group mean differences of BEM markers – energy reserve index, energy consumption index, metabolic state, and intracellular pH in the temporal lobe across the three groups-cognitively normal (CN), amnestic mild cognitive impairment (aMCI), and mild Alzheimer's disease (AD) (significant differences $p = 0.10^{*}$, $p = 0.01^{**}$, $p \leq 0.001^{***}$).

in the analysis with a standard error of 0.0513. The respective sensitivity was 73.3% for CN (11 of 15), 80% for aMCI (12 of 15), and 100% for AD (11 of 11), whereas specificity was 88.5% for CN, 84.6% for aMCI, and 100% for AD. The accuracy was 82.9% with the standard error was 0.051. **Table 5** summarizes all the predictive model results.

DISCUSSION

In this pilot work using whole-brain volume-coil ^{31}P MRS at UHF magnetic strength 7T, the first aim was to test the feasibility of measuring phosphate energy and membrane metabolites simultaneously across the three cohorts: CN adults, aMCI, and mild Alzheimer's disease (AD) with precision. With an improved SNR ratio, we supported our hypothesis that at UHF 7T, a distinct peaks of thirteen (13) phosphorus metabolites can be simultaneously acquired from the whole brain consistently across the three populations. Moreover, this research adds on aMCI a transitory, unstable, and heterogeneous group where some are at risk for AD to the existing p-BEM's work that investigated the difference between AD and healthy controls at 3T (Rijpma et al., 2018). aMCI group inclusion in this research fills the gap in knowledge of phosphate BEM alterations in early stage before an AD diagnosis is clinically apparent. In essence, the inclusion of all three groups suggested the viability of studying whole-brain p-BEM application, a window to investigate mitochondrial dysfunction theory which is postulated as an early neurometabolic marker in the pathology of AD from *in vitro* studies (Atamna and Frey, 2007) to *in vivo* using ^{31}P MRS.

The next goal was to investigate whether p-BEM markers and regulatory co-factors (Mg^{2+} and pH) could detect group-level differences across three groups in the four brain regions: frontal, temporal, parietal, and occipital. The work's main aim

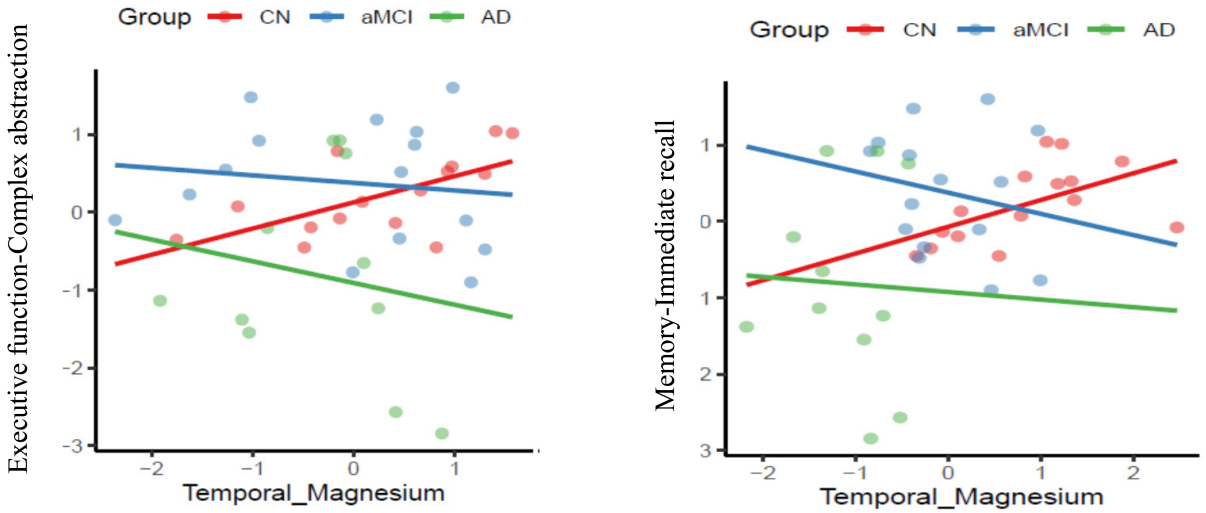

FIGURE 4 | Association of co-factor magnesium (Mg^{2+}) in the temporal brain region with cognitive performance domains of executive function and memory respectively across the three groups-cognitively normal (CN-red color), amnestic mild cognitive impairment (aMCI-blue color) and mild Alzheimer's diseases (AD-green color) ($p \leq 0.05$).

was to examine if measurable p-BEM markers could distinguish the between-group difference of aMCI from CN, one of the most significant challenges facing to develop effective AD diagnosis and treatment. The crucial finding was that the aMCI group was differentiated from CN based on two phosphate BEM markers, specifically, those represented by the energy reserve index and the energy consumption index. Moreover, these significant differences in the two phosphate BEM markers were localized to the temporal lobes bilaterally, the region most commonly vulnerable to early changes in AD's transitory stages (Mosconi et al., 2010; Ou et al., 2019). Furthermore, this research adds to the growing body of evidence on the neurobiological factors at the molecular level in terms of energy metabolism are altered in aMCI and can be detected which are the prime target group for clinical interventions. In sum, the lower energy reserve and energy consumption indices in the aMCI as compared to the CN group suggests that lower phosphate BEM may represent a cellular energy crisis in aMCI, potentially leading to the neurodegeneration process as the disease progress.

Our findings of reduced p-BEM metabolism in the at-risk population could be explained by two theories-mitochondrial dysfunction (Atamna and Frey, 2007) or glucose BEM hypometabolism (Mosconi et al., 2010; Yin et al., 2016), respectively. Mitochondria aids in the replenishing PCr and Pi stores to maintain a continuous supply of energy in the form of ATP. The creatine kinase enzyme controls the release of energy or vice-versa from PCr and Pi (Hettling and van Beek, 2011). Prior work in the post-mortem AD brain has shown decreased creatine kinase activity levels compared to individuals free from any neurodegenerative disorder (David et al., 1998; Aksenov et al., 2000). Thereby, we infer the reduced creatine kinase may potentially disrupt the stores of energy reserve and energy consumption metabolites – PCr and Pi, respectively. Parallel to mitochondrial dysfunction theory, the glucose BEM hypometabolism hypothesis directly affects energy reserve and consumption in the brain as glucose is the brain's primary energy production source (Atamna and Frey, 2007; Mosconi et al., 2010). However, an unanswered question is whether the upstream mitochondrial abnormalities of energy metabolism alter glucose metabolism or if the reverse is true and disruptions in glucose metabolism lead to phosphate BEM changes. Although we cannot answer the direction of the relationship of these markers and glucose metabolism, the study complement prior work on glucose metabolism and *in vitro* mitochondrial dysfunction in aMCI and AD to explore the order of changes further in the *in vivo* setting. This finding is the first evidence suggesting that energy reserve and consumption indices may provide a viable way to measure and identify early p-BEM etiology to explain pathophysiological brain change during a transitory stage of those at-risk for developing AD, namely individuals with aMCI. Therefore, we speculated that the compromised phosphate BEM mechanism leads to an energy crisis, which might be an early biomarker of a degrading brain moving toward dementia.

Additionally, we were also interested in investigating which p-BEM markers and regulatory co-factors could separate mild AD from aMCI. Notably, the p-BEM markers-energy reserve index, metabolic state indicator, and regulatory co-factor Mg^{2+}, mainly in the temporal brain region, separated the two groups. The results supported the hypothesis that the energy reserve index and Mg^{2+} would be lower in mild AD than aMCI. In contrast, the metabolic state indicator marker was higher in mild AD than aMCI. A metabolic state indicator ratio was previously used as a marker to assess mitochondrial function (Chance et al., 1981; Pettegrew et al., 1997; Valkovič et al., 2019). Compared to healthy controls, a higher metabolic status indicated that an organ (e.g., brain or heart) is in metabolic stress due to mitochondrial function abnormalities (Chance et al., 1981;

TABLE 4 | Main effect of BEM and regulatory co-factor (Magnesium^{2+}) interaction with the clinical group on cognitive performance of domains of executive function, memory, attention, visuospatial skills, and language.

Region of interest temporal lobe indices or regulatory co-factor and clinical group effect on cognition	ANOVA between-group results		
	F(df = 2,38)	p-value	Mean squares
Energy reserve index (PCr/t-ATP)			
Executive function	4.6979	0.0156*	2.443
Verbal fluency	7.4030	0.0020**	1.629
A inhibition and switching-Trails B			
Visuospatial domain	3.9816	0.0277*	1.688
Trails A			
Energy consumption index (intracellular_Pi/t_ATP)			
Executive function	3.2148	0.0522*	1.8657
Verbal fluency (A)			
Memory	3.2879	0.0491*	1.2066
Episodic memory	3.8632	0.0305*	2.7135
California Verbal Learning Task (CVLT)			
1. List A-immediate recall			
2. Repetitions			
Metabolic state indicator (intracellular_Pi/PCr)			
Executive function	4.6303	0.0164*	3.3063
Innovation-TOSL			
Memory	5.7276	0.0070**	4.1099
Episodic memory			
California Verbal Learning Task (CVLT)			
Recognition			
Regulatory co-factor-Intracellular Magnesium (Mg^{2+})			
Executive function	3.2135	0.0523*	2.9203
Complex abstraction-TOSL			
Memory			
Episodic memory	3.6597	0.036*	1.4347
California Verbal Learning Task (CVLT)			
List A-immediate recall			
Attention			
Strategic Auditory attention test	8.087	0.0012**	1.7004
Trail 1	3.723	0.034*	2.3072
Trail 2			

Significance $p < 0.05$, $p < 0.01$**, $p < 0.001$***.

Pettegrew et al., 1997; Valkovič et al., 2019). One question that emerges from our findings is why the metabolic state would be higher in mild AD than in aMCI, where neurobiological mechanisms compromised status starts? One possibility could be that the higher metabolic state finding in mild AD may represent metabolic stress due to mitochondrial function alterations in the early AD stages. Specifically, we propose that the turnover rate of energy production and utilization represented by energy reserve and energy consumption indices, which are altered as early as in aMCI, may potentially send a cascade of disruptions to neuronal function leading to higher metabolic stress and cognitive decline as the disease is progressing from aMCI and AD.

A pattern of elevated metabolic state in early AD compared to healthy controls is equivocal given other evidence suggesting the opposite relationship between Pi to PCr ratio (Rijpma et al., 2018). Using ^{31}P MRS at 3T, Rijpma et al. (2018) found a lower metabolic state in individuals with mild AD versus healthy controls in four brain regions (i) right hippocampus of the temporal lobe (ii) left hippocampus of the temporal lobe (iii) anterior cingulate cortex, (iv) retrosplenial cortex. The discrepancy of the higher metabolic state ratio in this study versus lower in the Rijpma study may be due, in part, to at least two different factors. One possible explanation is that the current study investigated metabolism in the temporal lobes entirety. In contrast, the research by Rijpma et al. (2018) only reported the hippocampus's findings within the temporal lobes. Obviously, more focal measurements may be more precise, as it is unclear if the entire temporal lobes metabolic state may be compensating for a lower function in a smaller region (Gould et al., 2006). Another possible explanation for the inconsistent results is that PCr increases with age; therefore, adjusting for age in the data analysis is a crucial step that was not accounted for in Rijpma's study. In the current study to control for age-effects on the phosphate metabolites, all the metabolites were adjusted for age,

TABLE 5 | Prediction model using the discriminant model for classifying the individuals into the group accurately a) confusion matrix b) sensitivity, specificity, positive predictive value (PPV), and negative predictive value (NPV).

a) Confusion matrix

		Group		
Prediction		**CN**	**aMCI**	**AD**
	CN	11	3	0
	aMCI	4	12	0
	AD	0	0	11

b) Sensitivity, specificity, positive predictive value (PPV), and negative predictive value (NPV).

Group	Sensitivity	Specificity	PPV	NPV
CN	0.733	0.885	0.786	0.852
aMCI	0.800	0.846	0.750	0.880
AD	1	1	1	1

gender, and education. Moreover, it is to note that Rijpma's work could motivate efforts toward developing methodologies that allow for BEM markers to be distinguished using lower field MRI strength such as 3T due to these scanners broader availability. To make this possible, further development of radiofrequency (RF) pulses are required so that the higher resolution of metabolites from UHF is measurable using lower magnet strength, e.g., 3-T, for research followed by its clinical application. In sum, we propose that the altered metabolic state indicator may be disrupted, either at a higher or lower level, in mild AD compared to CN and aMCI. More extensive studies are needed to determine if the metabolic state indicator may differentiate aMCI from CN. The small sample size may have precluded such distinctions. The preliminary data support the possibility that alterations in the p-BEM mechanism may contribute to neuronal pathophysiology dysfunction and cognitive decline in AD's early stages.

Finally, intracellular Mg^{2+} was significantly lower in mild AD compared to aMCI and CN. The present work adds to prior work of post-mortem findings of low Mg^{2+} in the brain's vulnerable region using an *in vivo* technique. The use of UHF has enabled to have a high resolution of α- and β-ATP signal, which appeared to be an easy-to-fit singlet they are more complicated as doublet and triplet, respectively, at the lower field at 1.5-T and 3T (Das et al., 2020). Therefore, measuring Mg^{2+} levels precisely could add a new dimension to have a comprehensive approach to understand the role of regulatory co-factors on the p-BEM mechanism, a mitochondrial function.

Overall, this study expanded the knowledge of mitochondrial dysfunction theory from a known BEM marker, i.e., metabolic state indicator, to include two more brain markers, specifically energy reserve and energy consumption indices. Moreover, these two novel brain markers suggest differentiating aMCI from CN based on p-BEM dysfunction theory accounted by the alterations in mitochondrial function observed in the *in vitro* post-mortem AD brain. Overall, we summarize that the dysfunction due to mitochondrial function manifested by changes in energy use and consumption may be disrupted before noticeable metabolic stress is measurable in the brain. The work using UHF is in a nascent stage of development and discovery. Nonetheless, the present results support the viability of investigating p-BEM differences using UHF magnetic strength at 7T as a promising new methodology that may help transfer the knowledge on BEM from *in vitro* to the *in vivo* human brain.

p-BEM-Cognitive Correspondence

Another critical question addressed in this research was the association across the sensitive p-BEM markers of the temporal lobe bilaterally (energy reserve index, energy consumption index, metabolic state indicator, and intracellular Mg^{2+}) and cognitive domains of memory, EF, attention, visuospatial skills, and language in the three groups. In CN, a distinct pattern of higher intracellular Mg^{2+} in the temporal lobe was associated with higher performance in the cognitive domains of memory, EF, and attention. On contrary in aMCI and AD, an inverse relationship was observed across the domains of cognition with Mg^{2+}. A possible explanation of opposite results in CN versus aMCI and mild AD is that Mg^{2+} is one of the regulatory co-factors that regulates BEM mechanisms in the cell to support cognition. In typical biological conditions, as one could speculate in the CN group, Mg^{2+} acts as a co-factor to regulate enzymes such as creatine kinases of BEM mechanism to support neuronal function and cognition, i.e., a direct association between Mg^{2+} and cognitive performance. However, in the compromised brain of aMCI and AD, wherein prior studies have supported low levels of creatine kinase (David et al., 1998; Aksenov et al., 2000) could not compensate for the BEM mechanism despite adequate Mg^{2+} to support cognition. The present findings do not adequately reveal what is happening due to limitations in measuring creatine kinase activity. Future work is needed to expand on the present evidence to explore a possible role of intracellular Mg^{2+} on cognitive performance across the three cohorts.

Prediction Model of MRS and Neurocognitive Measures

The final goal was to develop a prediction model for future applications on the extensive data set. From a theoretical perspective, such approaches will test p-BEM distinction validity by seeking to classify the individuals into their respective groups based on these early molecular changes in the brain vulnerable to the disease. Over the past decade, imaging tools like PET-tau and ^{18}FDG-PET have offered a clinically relevant methodology to investigate early pathological biomarkers internal to cells and predict who will convert to AD in addition to cognition (Koychev et al., 2017; Ding et al., 2019). Therefore, the prediction model approach in this research may help expand the utility of p-BEM characterization across many populations along with neurocognitive measures to improve early detection and prediction as to who will convert to AD in a longitudinal study.

LIMITATIONS

The results are interpreted cautiously due to several limitations. First, the sample size in each cohort was small, making robust conclusions uncertain. Nonetheless, the data showed a promising pattern of altering phosphate BEM markers, a methodology to explore mitochondrial function in transitory stages even before AD's full symptomology. Second, a prior study using either fMRI or PET has focused more on identifying brain areas where disease starts. In this study, investigating the brain's focal vulnerable region was limited due to the larger voxel size. Moreover, the present study reports only relative concentrations of the metabolites in the resting state. Future work is required to be focused on measuring the absolute concentrations of the phosphate metabolites in real-time to understand the rate of turnover of BEM mechanics. Third, as the technological advancements in analyzing partial-volume effects of ^{31}P MRS data were limited, in this study, certain regions of the brain on the border with skull or overlapping regions in a given voxel were excluded, thus following a conservative approach for analysis. To overcome this particular issue, in future studies we are rapidly developing new analytical approaches from the ^{31}P MRS raw data. Fourthly, brain atrophy was not accounted for in the analysis due to the small sample size. Lastly, while we developed a deep learning model with a small study population, the model may not be a robust model for future application to a more extensive data set of BEM markers and neurocognitive measures.

CONCLUSION

To summarize, the present study provides preliminary evidence that phosphate BEM changes may be an early biomarker of AD pathophysiological changes even before the disease symptoms are noticeable. For over a century, AD pathology was associated with the accumulation of β-amyloid and tau, followed by the recent development of glucose metabolism abnormalities contributing to neurodegeneration. However, an unanswered question is if upstream phosphate BEM markers abnormalities cause these known pathological abnormalities cascade. Future directions would further develop this effort to deploy ^{31}P MRS in conjunction with PET-amyloid,-tau, and ^{18}FDG to investigate how abnormal BEM markers modulate the burden of amyloid, tau, and abnormal glucose metabolism in AD neuropathophysiology. Moreover, a longitudinal study is required for tracking p-BEM markers biological mechanisms changes internal to the cell associated with cognitive decline as individuals move from normal aging to the transitory stage of aMCI and AD.

DATA AVAILABILITY STATEMENT

The raw data supporting the conclusions of this article will be made available by the authors, without undue reservation.

ETHICS STATEMENT

The studies involving human participants were reviewed and approved by The University of Texas Southwestern Medical Center. The patients/participants provided their written informed consent to participate in this study.

AUTHOR CONTRIBUTIONS

ND was the principal investigator who played an integral role in developing and implementing the research protocol followed by data collection, analysis and writing the manuscript. JR has been instrumental in the analysis of MRS data along with ND. JS biostatistician was involved in the statistical analytical approach. SC mentored the writing of the manuscript along with research protocol implementation. All authors contributed to the article and approved the submitted version.

FUNDING

The research project was supported by the Dee Wyly Distinguished University Chair at BrainHealth, Aging Mind Foundation, Friends of BrainHealth, Fox Family Foundation, Barbara Wallace and Kelly King Charitable Foundation Trust, the AWARE fund of the Dallas Foundation, and the Golden Rule Family Foundation.

ACKNOWLEDGMENTS

We thank all of the participants in this study and the research team for making this research possible.

SUPPLEMENTARY MATERIAL

The Supplementary Material for this article can be found online at: https://www.frontiersin.org/articles/10.3389/fnins.2021.641739/full#supplementary-material

REFERENCES

Adrasi, I. S., Molnar, Z., and Mako, S. (2000). Disturbances of magnesium concentrations in various brain areas in 'Alzheimer's disease. *Magn. Res.* 13, 189–196.

Aksenov, M., Aksenova, M., Butterfield, D. A., and Markesbery, W. R. (2000). Oxidative modification of creatine kinase BB in 'Alzheimer's disease brain. *J. Neurochem.* 74, 2520–2527. doi: 10.1046/j.1471-4159.2000.0742520.x

Albers, D. S., and Flint, B. M. (2000). ""Mitochondrial dysfunction and oxidative stress in aging and neurodegenerative disease,"," in *Advances in Dementia Research*, eds K. Jellinger, R. Schmidt, and M. Windisch (Vienna: Springer).

Atamna, H., and Frey, W. H. (2007). Mechanisms of mitochondrial dysfunction and energy deficiency in Alzheimer's disease. *Mitochondrion* 7, 297–310. doi: 10.1016/j.mito.2007.06.001

Baloyannis, S. J. (2006). Mitochondrial alterations in 'Alzheimer's disease. *J. Alzheimers Dis.* 9, 119–126. doi: 10.3233/JAD-2006-9204

Barzilai, N., Huffman, D. M., Muzumdar, R. H., and Bartke, A. (2012). The critical role of metabolic pathways in aging. *Diabetes* 61, 1315–1322. doi: 10.2337/db11-1300

Benton, A. L., Hamsher, K., Rey, G. L., and Sivan, A. B. (1994). *Multilingual Aphasia Examination*, 3rd Edn., Iowa City, IA: AJA Associates.

Chapman S. B., Zientz, J., Weiner, M., Rosenberg, R., Frawley, W., Burns, M. H., et al. (2002). Discourse changes in early Alzheimer disease, mild cognitive impairment, and normal aging. *Alzheimer Dis. Assoc. Disord.* 16177–16186. doi: 10.1097/00002093

Chance, B., Eleff, S., Leigh, J. S. Jr., Sokolow, D., and Sapega, A. (1981). Mitochondrial regulation of phosphocreatine/inorganic phosphate ratios in exercising human muscle: a gated ^{31}P NMR study. *Proc. Natl. Acad. Sci. U.S.A.* 78, 6714–6718. doi: 10.1073/pnas.78.11.6714

Cilliler, A. E., Ozturk, S., and Ozbakir, S. (2007). Serum magnesium level and clinical deterioration in 'Alzheimer's disease. *Gerontology* 53, 419–422. doi: 10.1159/000110873

Cottrell, D. A., Blakely, E. L., Johnson, M. A., Ince, P. G., and Turnbull, D. M. (2001). Mitochondrial enzyme-deficient hippocampal neurons and choroidal cells in AD. *Neurology* 57, 260–264. doi: 10.1212/WNL.57.2.260

Crouch, P. J., Blake, R., Duce, J. A., Ciccotosto, G. D., Li, Q. X., Barnham, K. J., et al. (2005). Copper- dependent inhibition of human cytochrome c oxidase by a dimeric conformer of amyloid- beta1–42. *J. Neurosci.* 25, 672–679.

Das, N., Ren, J., Spence, J. S., Rackley, A., and Chapman, S. B. (2020). Relationship of parieto-occipital brain energy phosphate metabolism and cognition using ^{31}P MRS at 7tesla in amnestic mild cognitive impairment. *Front. Aging Neurosci.* 12:222. doi: 10.3389/fnagi.2020.00222

David, S., Shoemaker, M., and Haley, B. E. (1998). Abnormal properties of creatine kinase in 'Alzheimer's disease brain: correlation of reduced enzyme activity and active site photolabeling with aberrant cytosol-membrane partitioning. *Brain Res. Mol. Brain Res.* 54, 276–287. doi: 10.1016/S0169-328X(97)00343-4

Delis, D. C., Kaplan, E., and Kramer, J. H. (2001). *Delis-Kaplan Executive Function System (D-KEFS)*. San Antonio, TX: Psychological Corporation. doi: 10.1037/t15082-000

Desgranges, B., Baron, J. C., de la Sayette, V., Petit-Taboué, M. C., Benali, K., Landeau, B., et al. (1998). The neural substrates of memory systems impairment in Alzheimer's disease. A PET study of resting brain glucose utilization. *Brain* 121, 611–31. doi: 10.1093/brain/121.4.611

Ding, Y., Sohn, J. H., Kawczynski, M. G., Trivedi, H., Harnish, R., Jenkins, N. W., et al. (2019). A deep learning model to predict a diagnosis of alzheimer disease by using 18F-FDG PET of the brain. *Radiology* 290, 456–464. doi: 10.1148/radiol.2018180958

Folstein, M. F., Folstein, S. E., and McHugh, P. R. (1975). "Mini-mental state: a practical method for grading the cognitive state of patients for the clinician. *J. Psychiatr. Res.* 12, 189–198.

Forlenza, O. V., Wacker, P., Nunes, P. V., Yacubian, J., Castro, C. C., Otaduy, M. C. G., et al. (2005). Reduced phospholipid breakdown in 'Alzheimer's brains: a P-31 spectroscopy study. *Psychopharmacology* 180, 359–365.

Gould, R. L., Arroyo, B., Brown, R. G., Owen, A. M., Bullmore, E. T., and Howard, R. J. (2006). Brain mechanisms of successful compensation during learning in Alzheimer disease. *Neurology* 67, 1011–1017. doi: 10.1212/01.wnl.0000237534.31734.1b

Hanten, G., Li, X., Chapman, S. B., Swank, P., Gamino, J., Roberson, G., et al. (2007). Development of verbal selective learning. *Dev. Neuropsychol.* 32, 585–596, doi: 10.1080/87565640701361112

Hanninen, T., Koivisto, K., Reinikainen, K. J., Helkala, E. L., Soininen, H., Mykkänen, L., et al. (1996). Prevalence of ageing-associated cognitive decline in an elderly population. *Age Ageing* 25, 201–205. doi: 10.1093/ageing/25.3.201

Herholz, K. (2010). Cerebral glucose metabolism in preclinical and prodromal Alzheimer's disease. *Expert Rev. Neurother.* 10, 1667–1673. doi: 10.1586/ern.10.136

Hettling, H., and van Beek, J. H. (2011). Analyzing the functional properties of the creatine kinase system with multiscale 'sloppy' modeling. *PLoS Comput. Biol.* 7:e1002130. doi: 10.1371/journal.pcbi.1002130

Kaplan, E., Goodglass, H., Weintraub, S., and Goodglass, H. (1983). *Boston Naming Test*. Philadelphia: Lea & Febiger.

Koychev, I., Gunn, R. N., Firouzian, A., Lawson, J., Zamboni, G., Ridha, B., et al. (2017). PET tau and amyloid-β burden in mild Alzheimer's disease: divergent relationship with age, cognition, and cerebrospinal fluid biomarkers. *J. Alzheimers Dis.* 60, 283–293. doi: 10.3233/JAD-170129

Lin, M., and Beal, M. (2006). Mitochondrial dysfunction and oxidative stress in neurodegenerative diseases. *Nature* 443, 787–795. doi: 10.1038/nature05292

Lourenço, C. F., Ledo, A., Dias, C., Barbosa, R. M., and Laranjinha, J. (2015). Neurovascular and neurometabolic derailment in aging and Alzheimer's disease. *Front. Aging Neurosci.* 7:103. doi: 10.3389/fnagi.2015.00103

Mergenthaler, P., Lindauer, U., Dienel, G. A., and Meisel, A. (2013). Sugar for the brain: the role of glucose in physiological and pathological brain function. *Trends Neurosci.* 36, 587–597. doi: 10.1016/j.tins.2013.07.001

Morris, J. (1993). The Clinical Dementia Rating (CDR): current version and scoring rules. *Neurology* 43, 2412–2414.

Mosconi, L. (2013). Glucose metabolism in normal aging and 'Alzheimer's disease: methodological and physiological considerations for PET studies. *Clin. Transl. Imag.* 1, s40336–s40313. doi: 10.1007/s40336-013-0026-y

Mosconi, L., Berti, V., Glodzik, L., Pupi, A., De Santi, S., and de Leon, M. J. (2010). Pre-clinical detection of 'Alzheimer's disease using FDG-PET, with or without amyloid imaging. *J. 'Alzheimer's Dis.* 20, 843–854. doi: 10.3233/JAD-2010-091504

Mosconi, L., Tsui, W. H., De Santi, S., Li, J., Rusinek, H., Convit, A., et al. (2005). Reduced hippocampal metabolism in MCI and AD: automated FDG-PET image analysis. *Neurology* 64, 1860–1867.

Ou, Y., Xu, W., Li, J., Guo, Y., Cui, M., Chen, K.-L., et al. (2019). FDG-PET as an independent biomarker for Alzheimer's biological diagnosis: a longitudinal study. *Alzheimer's Res. Ther.* 11:57. doi: 10.1186/s13195-019-0512-1

Petersen, R. C., Doody, R., Kurz, A., Mohs, R. C., Morris, J. C., Rabins, P. V., et al. (2001). Current concepts in mild cognitive impairment. *Arch Neurol.* 58, 1985–1992. doi: 10.1001/archneur.58.12.1985

Pettegrew, J. W., McClure, R. J., Keshavan, M. S., Minshew, N. J., Panchalingam, K., and Klunk, W. E. (1997). "31P magnetic resonance spectroscopy studies of developing brain," in *Neurodevelopement & Adult Psychopathology*, eds M. S. Keshavan and R. M. Murray (Cambridge: Cambridge University Press), 71–92.

Rijpma, A., van der Graaf, M., Meulenbroek, O., Olde Rikkert, M., and Heerschap, A. (2018). Altered brain high-energy phosphate metabolism in mild 'Alzheimer's disease: a 3-dimensional ^{31}PMR spectroscopic imaging study. *NeuroImage Clin.* 18, 254–261. doi: 10.1016/j.nicl.2018.01.031

Ross, A. J., and Sachdev, P. S. (2004). Magnetic resonance spectroscopy in cognitive research. *Brain Res. Rev.* 44, 83–102. doi: 10.1016/j.brainresrev.2003.11.001

Silverman, D. H., Small, G. W., Chang, C. Y., Lu, C. S., Kung, De Aburto, M. A., et al. (2001). Positron emission tomography in evaluation of dementia: regional brain metabolism and long-term outcome. *JAMA* 286, 2120–2127. doi: 10.1001/jama.286.17.2120

Slutsky, I., Abumaria, N., Wu, L. J., Huang, C., Zhang, L., Li, B., et al. (2010). Enhancement of learning and memory by elevating brain magnesium. *Neuron* 65, 165–177. doi: 10.1016/j.neuron.2009.12.026

Smith, C. D., Pettigrew, L. C., Avison, M. J., Kirsch, J. E., Tinkhtman, A. J., Schmitt, F. A., et al. (1995). Frontal-lobe phosphorus-metabolism and neuropsychological function in aging and in Alzheimers-disease. *Ann. Neurol.* 38, 194–120.

Spreen, O., and Strauss, E. (1998). *A Compendium of Neuropsychological Tests: Administration, Norms, and Commentary*, 2nd Edn. Oxford University Press.

Valkovič, L., Clarke, W. T., Schmid, A. I., Raman, B., Ellis, J., Watkins, H., et al. (2019). Measuring inorganic phosphate and intracellular pH in the healthy and hypertrophic cardiomyopathy hearts by in vivo 7T 31 P-cardiovascular magnetic resonance spectroscopy. *J. Cardiovasc. Magn. Reson.* 21:19. doi: 10.1186/s12968-019-0529-4.

Wechsler, D. (1972). *Wechsler Adult Intelligence Scale – Administration and Scoring Manual. 2.* San Antonio, TX.

Wechsler, D. (1997). *Wechsler Adult Intelligence Scale –Administration and scoring manual. 3.* San Antonio, TX: The Psychological Association.

Yamaguchi, H., Yamazaki, T., Ishiguro, K., Shoji, M., Nakazato, Y., and Hirai, S. (1992). Ultrastructural localization of Alzheimer amyloid beta/A4 protein precursor in the cytoplasm of neurons and senile plaque-associated astrocytes. *Acta Neuropathol.* 85, 15–22. doi: 10.1007/BF00304629

Yesavage, J. A., Brink, T. L., Rose, T. L., Lum, O., Huang, V., Adey, M., et al. (1982). Development and validation of a geriatric depression screening scale: a preliminary report. *J. Psychiatr. Res.* 17, 37–49.

Yin, F., Sancheti, H., Patil, I., and Cadenas, E. (2016). Energy metabolism and inflammation in brain aging and 'Alzheimer's disease. *Free Radic. Biol. Med.* 100, 108–122. doi: 10.1016/j.freeradbiomed.2016.04.200

Conflict of Interest: The authors declare that the research was conducted in the absence of any commercial or financial relationships that could be construed as a potential conflict of interest.

frontiers in Neuroscience

ORIGINAL RESEARCH
published: 11 June 2021
doi: 10.3389/fnins.2021.679078

TRPC1/5-Ca_V3 Complex Mediates Leptin-Induced Excitability in Hypothalamic Neurons

Paula P. Perissinotti†‡, Elizabeth Martínez-Hernández†‡ and Erika S. Piedras-Rentería‡*

Cell and Molecular Physiology Department and Neuroscience Division of the Cardiovascular Research Institute, Loyola University Chicago, Maywood, IL, United States

OPEN ACCESS

Edited by:
Lionel Carneiro, The Ohio State University, United States

Reviewed by:
Christelle Le Foll, University of Zurich, Switzerland
Céline Cruciani-Guglielmacci, Université Paris Diderot, France

***Correspondence:**
Erika S. Piedras-Rentería
epiedra@luc.edu

†Present address:
Paula P. Perissinotti, Instituto de Fisiología, Biología Molecular y Neurociencias (IFIBYNE, UBA-CONICET), Ciudad Universitaria, Buenos Aires, Argentina
Elizabeth Martínez-Hernández, Department of Physiology and Biophysics, Rush University, Chicago, IL, United States

‡ORCID:
Paula P. Perissinotti
orcid.org/0000-0002-9757-0610
Elizabeth Martínez-Hernández
orcid.org/0000-0002-5004-2239
Erika S. Piedras-Rentería
orcid.org/0000-0001-7983-585X

Specialty section:
This article was submitted to Neuroenergetics, Nutrition and Brain Health, a section of the journal Frontiers in Neuroscience

Received: *10 March 2021*
Accepted: *30 April 2021*
Published: *11 June 2021*

Citation:
Perissinotti PP, Martínez-Hernández E and Piedras-Rentería ES (2021) TRPC1/5-Ca_V3 Complex Mediates Leptin-Induced Excitability in Hypothalamic Neurons. Front. Neurosci. 15:679078. doi: 10.3389/fnins.2021.679078

Leptin regulates hypothalamic $POMC^+$ (pro-opiomelanocortin) neurons by inducing TRPC (Transient Receptor Potential Cation) channel-mediate membrane depolarization. The role of TRPC channels in POMC neuron excitability is clearly established; however, it remains unknown whether their activity alone is sufficient to trigger excitability. Here we show that the right-shift voltage induced by the leptin-induced TRPC channel-mediated depolarization of the resting membrane potential brings T-type channels into the active window current range, resulting in an increase of the steady state T-type calcium current from 40 to 70% resulting in increased intrinsic excitability of POMC neurons. We assessed the role and timing of T-type channels on excitability and leptin-induced depolarization *in vitro* in cultured mouse POMC neurons. The involvement of TRPC channels in the leptin-induced excitability of POMC neurons was corroborated by using the TRPC channel inhibitor 2APB, which precluded the effect of leptin. We demonstrate T-type currents are indispensable for both processes, as treatment with NNC-55-0396 prevented the membrane depolarization and rheobase changes induced by leptin. Furthermore, co-immunoprecipitation experiments suggest that TRPC1/5 channels and $Ca_V3.1$ and $Ca_V3.2$ channels co-exist in complex. The functional relevance of this complex was corroborated using intracellular Ca^{2+} chelators; intracellular BAPTA (but not EGTA) application was sufficient to preclude POMC neuron excitability. However, leptin-induced depolarization still occurred in the presence of either BAPTA or EGTA suggesting that the calcium entry necessary to self-activate the TRPC1/5 complex is not blocked by the presence of BAPTA in hypothalamic neurons. Our study establishes T-type channels as integral part of the signaling cascade induced by leptin, modulating POMC neuron excitability. Leptin activation of TRPC channels existing in a macromolecular complex with T-type channels recruits the latter by locally induced membrane depolarization, further depolarizing POMC neurons, triggering action potentials and excitability.

Keywords: $Ca_V3.1$, $Ca_V3.2$, TRPC channel, hypothalamus, leptin, POMC

Abbreviations: AgRP, agouti-related peptide; AP, action potential, DIV, days *in vitro*; KLHL1, Kelch-like 1; LRb, Leptin receptor; LVA, low-voltage activated; NPY, neuropeptide Y; PIR, post-inhibitory rebound; POMC, proopiomelanocortin positive neurons; TRPC, Transient Receptor Potential Cation; TRPC, Transient Receptor Potential Cation.

INTRODUCTION

Leptin regulates energy homeostasis and serves as a satiety afferent signal in the homeostatic control of adipose tissue mass (Schwartz et al., 2000; Harvey and Ashford, 2003), reducing food intake, increasing energy expenditure and regulating the reward value of nutrient (Ahima and Flier, 2000; Domingos et al., 2011; Williams and Elmquist, 2012). Leptin exerts its physiological action through its specific receptor (LRb), which is highly expressed in hypothalamus and other brain areas (Shioda et al., 1998). Leptin's effects on hypothalamic homeostatic feeding circuits are well established (Kenny, 2011); it negatively modulates orexigenic agouti-related peptide (AgRP)/neuropeptide Y (NPY) neurons by Kv2.1 channel-mediated membrane hyperpolarization (Baver et al., 2014). In contrast, anorexigenic POMC positive neurons are depolarized by leptin (Cowley et al., 2001). This depolarization is mediated via a Jak2-PI3 kinase-PLCγ pathway that ultimately activates TRPC channel activity (Qiu et al., 2010). Similarly, a subset of POMC neurons in the arcuate nucleus responsive to serotonin *via* the 5-HT_{2C} receptor are also activated *via* TRPC channels, suggesting TRPC channels are a common signaling mechanism mediating anorexigenic signaling in the hypothalamus (Sohn et al., 2011). TRPC5 channels are also the molecular mediators of the acute leptin and serotonin effect in POMC neurons (Gao et al., 2017).

The role of TRPC channels in POMC neuron excitability is clearly established; however, it is not known whether their activity alone is sufficient to trigger excitability. Here we used cultured hypothalamic neurons from mice to characterize the role of T-type Ca^{2+} channels and leptin-induced POMC neuron excitability. Our data demonstrate T-type channels are necessary for POMC neuron excitability, by being involved in the excitatory cascade induced by leptin in these neurons. Blockade of either TRPC or T-type channel function prevents the effect of leptin on hypothalamic neuron excitability. Moreover, we demonstrate that: (a) TRPC1 and TRPC5 channels co-immunoprecipitate with T-type channels in the hypothalamus, (b) TRPC-T-type channel complexes exist in a functional microdomain, and (c) TRPC-induced depolarization in these domains triggers neuronal excitability *via* recruitment of T-type channels. Thus, this study confirms T-type channels constitute a target to modulate leptin-activated neurons and their functions, such as energy balance and food intake.

MATERIALS AND METHODS

The animal protocols used in this study were reviewed and approved by an independent Institutional Animal Care and Use Committee (IACUC 2016032). Mixed background (129S1/Sv-Oca2 + Tyr + Kitl + C57BL/6) WT and EGFP-$POMC^{+}$ mice [129S1/Sv-Oca2 + Tyr + Kitl + C57BL/6-Tg(Pomc-EGFP)1Low/J] (The Jackson Laboratory, RRID:IMSR_JAX:009593) were fed on an *ad libitum* standard commercial pellet diet. No exclusion criteria were pre-determined. Altogether, 12 newborn pups were used for hypothalamic cultures (1 pup per cell culture) and 17 adult mice (male) for immunoprecipitation experiments. The study was not pre-registered. Experiments were conducted in the afternoon.

Neuron Cultures

Whole hypothalamus were dissected from newborn mice (postnatal day 0, P0) and cultured as described in Perissinotti et al. (2014). Cells plated at a density of 25,000−35,000/coverslip and kept in a 5% CO_2 humidified atmosphere at 37°C. Newborn pups (no sex determination) were killed by decapitation after cold-induced anesthesia, and their brains rapidly removed prior to hypothalamus dissection; each culture was generated from two independent mice, each plated on 6 coverslips (electrophysiology and ICC data was generated from at least three independent batches of cultures, N = 6 mice). Cryo-anesthesia abolished perception of pain of pups. This method has been validated by Veterinary Services to minimize animal suffering.

Immunocytochemistry (ICC)

WT neurons at 8−11 DIV were prepared as described (Perissinotti et al., 2014). Primary antibody dilutions were: POMC 1:200 (Novus, RRID:AB_791643); AgRP, 1:50 (Sta. Cruz, RRID:AB_2258141), $Ca_V3.1$ 1:200 (Alomone, RRID:AB_2039779) and 1:50 (Millipore, Cat.# MABN464), $Ca_V3.2$ 1:5 (supernatant, NeuroMab, RRID:AB_2069551) and 1:200 (Sta. Cruz, RRID:AB_2259537); TRPC1 (RRID:AB_2040234) 1:100 and TRPC5 (RRID:AB_2040241) 1:120 (Alomone). Secondary antibodies: Alexa-488 Goat anti-mouse (RRID:AB_2633275) and goat anti-rabbit (RRID:AB_143165), −594 goat anti-rabbit (RRID:AB_2762824), and −647 goat anti-chicken (RRID:AB_2762845), 1:2,000 (Molecular Probes, Eugene, OR). Image acquisition was done using a Olympus IX80 microscope, analyzed by deconvolution and processed with ImageJ freeware (NIH) (Schneider et al., 2012).

Immunoprecipitation (IP)

Adult mice (24−30 g) were deeply anesthetized with 2% Isofluorane, then quickly decapitated; whole brains or hypothalamus were isolated according to guidelines of the IACUC. At least two whole brains or two whole hypothalami were needed per n to assess the presence of complexes with $Ca_V3.1$ (α_{1G}) or TRPC1, whereas only one whole brain/one hypothalamus were needed per n for $Ca_V3.2$ (α_{1H}) or TRPC5 complexes; each experiment was replicated three times. Tissues were homogenized using a Bullet blender tissue homogenizer using 0.5 mm zirconium oxide beads (Next Advance) and spun down at 1,300 × g to eliminate debris. A fraction of the supernatant was reserved before immunoprecipitation and stored at −80 C until processing (input); the remaining volume was divided up in equal parts for all experiments. Samples were then processed by addition of the primary antibody and incubation for 1 h at 4°C (antibodies: α1H (Santa Cruz Biotechnology, Inc., Santa Cruz, CA, United States, RRID:AB_2259537), α1G [Millipore, Cat. #MABN464); TRPC5 (Alomone, RRID:AB_2040241)], TRPC1 (Santa Cruz Biotechnology, Inc., Santa Cruz, CA, United States, RRID:AB_2207905), and IgG (Cat. #20008−1−100 and

#20009−1−100, Alpha Diagnostics, San Antonio, TX) and overnight incubation, followed by incubation for 1 h with protein A/G agarose beads (Biovision, Mountain View, CA) on a shaking plate at 4°C. The samples were washed and then precipitated in 0.1 M glycine pH 3.5 and neutralized with 0.5 M Tris·HCl and 1.5 M NaCl pH 7.4 before SDS-PAGE electrophoresis (8%, at 100 V for 90 min) followed by transfer to a PVDF membrane (BioRad). Membranes were washed in Tris-buffered saline (TBS) + Tween (TBST; 0.05% Tween 20), blocked for 1 h in TBST + 5% milk at room temperature, and incubated at 4°C overnight with α1H polyclonal (1:2,000), α1G monoclonal (1:500), TRPC1 monoclonal (1:1,000), or TRPC5 polyclonal (1:1,000) antibody. Incubation with goat anti-rabbit (RRID:AB_1185567) horseradish peroxidase (HRP)- or anti-mouse (RRID:AB_228307) HRP-conjugated secondary antibodies was done at room temperature (1:2,000; Pierce). Blots were exposed to developing agent (Supersignal Femto Dura, Pierce) before analysis with a ChemiDoc MP System (BioRad).

Electrophysiology

Whole-cell patch clamp recordings were performed from cultured hypothalamic neurons from 8 to 11 DIV using an Axopatch 200B amplifier (Axon instruments, Union City, CA) at room temperature. Data were acquired at 1 kHz and digitized at 20 kHz using a Digidata 1322A analog-to-digital converter. Pipettes pulled from borosilicate glass (Warner Instruments, Hamden, CT) had resistances of 3.5–4.5 MΩ when filled with intracellular solutions. Cells with series resistance (R_s) < 20 MΩ were used; R_s was compensated online (>80%). Data was acquired with and analyzed with pClamp 10 software (Molecular Devices). Cell capacitance was measured from a transient current evoked by a 5 mV depolarizing step from a holding potential of -90 mV.

Calcium currents were recorded in an external solution containing (in mM) 5 $CaCl_2$, 140 TEA-Cl, 10 HEPES and 10 glucose (pH 7.4, 300 mOsmol/kgH_2O), using an intracellular solution containing (in mM) 108 $CsMeSO_3$, 4 $MgCl_2$, 10 Cs-EGTA, 9 HEPES, 5 ATP-Mg, 1 GTPLi and 15 phosphocreatine-Tris (pH 7.4, 290 mOsmol/kgH_2O). Voltage control was improved by increasing cell impedance using extracellular TEA and intracellular cesium to block K^+ conductances. I–V curve properties such as its negative slope and reversal potential were monitored for appropriate voltage control. For the study of calcium current properties, we avoided recording from neurons older than 10 DIV because the possibility of space-clamp problems.

Resting membrane potential (RMP) and APs were recorded in external solution containing (in mM) 135 NaCl, 5 KCl, 2 $CaCl_2$, 1 $MgCl_2$, 10 HEPES, 10 glucose (pH 7.4, 300 mosmol/kgH_2O) and intracellular solution containing (in mM) 110 K-gluconate, 20 KCl, 2 $MgCl_2$, 1 EGTA, 10 HEPES, 2 ATP-Mg, 0.25 GTP-Li and 10 phosphocreatine-Tris (pH 7.4, 290 mosmol/kgH_2O). Drugs: NNC-550396 dihydrochloride (Cat. #2268) and Leptin (Cat. #2985) were purchased from Tocris (Bristol, United Kingdom).

Square protocols to obtain I–V curves and T-type steady-state activation and inactivation were done as described in Bean (1985) and Perissinotti et al. (2015).

Current-Voltage Relationships (I–V Curves)

Currents were elicited from a holding potential (V_H) = −90 mV and depolarized for 150 ms to a test potential (V_T) = −70 to + 60 mV, in 10 mV increments.

T-type Current—Rate of Membrane Potential Depolarization Relationship

Different rates of membrane potential depolarization preceding the first action potential were obtained from hypothalamic neurons by changing the rate of current ramp stimulations (20−100 pA/s) in current clamp configuration: 40, 90, 180, 290, or 360 mV/s (V_H = −75 mV). These voltage templates were used in voltage clamp configuration to stimulate calcium currents. The membrane potential was held at a V_H of −50 or −90 mV before clamping the voltage at −75 mV for 10 ms to run the stimulation protocol. The low-voltage activated (LVA) current component contribution was determined by the subtraction method (Bean, 1985): High-voltage activated (HVA) currents obtained at V_H = −50 mV were subtracted from those obtained at V_H = −90 mV (HVA plus LVA currents).

Steady-State Analysis

Steady-state activation (SSA) was analyzed with protocols stepping from V_H = −90 (or −50) mV to V_T = −90 to 0 mV (ΔV = 10 mV) for 12 ms followed by repolarization to −100 mV to evoke inward tail currents. Data were fitted by a single Boltzmann function of the form $I_{max}/[1 + \exp^{(V_{50} - V)/k}] + m$, were I_{max} is maximal current, V_{50} is half-voltage of activation, k is slope factor, and m is baseline. Steady-state inactivation (SSI) was determined by stepping the membrane potential to various pre-pulse voltage levels (V_{pre} = −110 to 0 mV, ΔV = 10 mV) for 1 s before depolarization to a fixed test level (−30 mV) to evoke channel opening. The resulting data were also fitted to a Boltzmann function.

Steady-state current (I_{stst}) was calculated from the formula I = G* (V- $E_{Nernst(ion)}$), where the channel conductance G is multiplied by the channel's open probability (I/I_{max}, SSA) and availability (I/I_{max}, SSI), which were obtained experimentally from the T-type steady state activation (SSA) or inactivation (SSI) curves adjusted to a Boltzmann equation (Bijlenga et al., 2000; Lambert et al., 2014; Rivero-Echeto et al., 2020). Specifically, steady-state current (I_{stst}) was calculated with the steady stated formula Iss (V_T) = G * $I/I_{max,SSA}$ (V_T) * $I/I_{max,SSI}$ (V_T)*(V_T- 50 mV), where V_T is the test voltage, G is the channel conductance (arbitrarily set at 1), $I/I_{max,SSA}$ is the fraction of T-type channels activated at V_T, $I/I_{max,SSI}$ is the fraction of T-type channels available at V_T and 50 mV is the experimentally equilibrium potential for calcium.

Resting Membrane Potential

RMP was recorded in continuous trace mode without current injection for 20 s, and averaged; voltages were corrected for liquid junction potentials.

Input Resistance

Whole cell input resistance (R_{in}) was determined in response to current steps (−80 to 20 pA, stepping each 20 pA). A holding current was applied to set the membrane potential at−60 mV.

Membrane Excitability

AP discharges were triggered by consecutive depolarizing ramps at 20, 40, and 60 pA/s rates for 1.5 s (Balasubramanyan et al., 2006; Lu et al., 2006). A holding current was applied to set the membrane potential at −75 mV. The rheobase was determined as the minimum amount of current required for firing an action potential.

Statistical Analysis

These experiments were exploratory with no pre-determined end-point and no data was excluded from the analyses. No blinding, no randomization, and no sample size calculation were performed. All measurements were done in at least three independent cell cultures. Results are presented as mean ± SEM. The parameter "n" indicates number of cells unless otherwise stated and "N" the number of animals. No test for outliers has been applied. The normality of data distribution was assessed by the Kolmogorov-Smirnov test. Statistical analysis was performed with the Sigma Plot 11 Software. Statistical significance ($P < 0.05$) was determined using either one-way analysis of variance (ANOVA) with Fisher LSD's *post hoc* test for comparisons between multiple groups or an independent-samples *t*-test for comparisons between two groups. Statistical significance ($P < 0.05$) for two proportions was determined using the *Z*-test.

RESULTS

Hypothalamic cultures were studied from 8 to 11 days *in vitro* (DIV). Immunocytochemistry analysis (ICC) showed that POMC and NPY/*AGRP* neurons were present in the culture, with $POMC^+$ neurons (POMC) being the majority (85 vs. 15%, $P < 0.05$, *Z*-test) (**Figures 1A,B**); note that **Figure 1A** figure does not display an average distribution of $POMC^+$ and $AGRP^+$ positive neurons, as it was difficult to find such ratios within the same area during confocal image acquisition. Electrophysiological experiments confirmed 15% of all studied neurons where neither activated nor inhibited by leptin; whereas 80% of all neurons were leptin-activated (**Figures 1C,D**), consistent with the ICC data. In contrast, leptin treatment inhibited 5% of cells, consistent with an NPY phenotype.

The properties of leptin-activated neurons were consistent with POMC neuron responses. As seen in **Figure 2A**, their resting membrane potential (RMP) was slightly depolarized, whereas their input resistance remained unaltered upon application of 100 nM leptin (**Figure 2B**). We assessed the effect of leptin on excitability. Membrane excitability was quantified using depolarizing current ramps (20, 40, and 60 pA/s) from a preset membrane potential of ∼−75 mV to avoid spontaneous tonic firing. To analyze quantitatively the voltage response to the current ramps, three different measurements were calculated: the rheobase, the number of APs triggered, and the rate of membrane potential depolarization preceding the first AP (i.e., the slope of depolarization, $\Delta V/\Delta t$). **Figure 2C** shows an example of neuronal firing evoked in a POMC neuron at ramp rates of 20 pA/s. Leptin treatment on its own decreased the rheobase from 18.4 to 14.1 pA, increased the number of action potentials from 6 to 11 and enhanced the rate of membrane potential depolarization from 30.0 to 65.0 mV/s; according to the leptin-mediated depolarization of the RMP that was observed in **Figure 2A**. The summary of effects of leptin on neurons is depicted in **Figure 2D**. On average, for all tested current ramp rates, leptin decreased the rheobase by ∼25% and increased the rate of membrane potential depolarization between ∼60 and 100%. However, leptin increased the AP number by ∼64% only at ramp rates of 20 pA/s.

T-Type Calcium Currents Are Necessary for the Leptin-Induced Excitability Response

Due to their ability to conduct calcium across the cellular membrane at potentials close to the resting potential, T–type calcium channels are critically important for regulating neuronal excitability (Llinás, 1988; Huguenard, 1996; Perez-Reyes, 2003). Therefore, we were interested in studying the role of T-type calcium currents in the leptin-induced excitability response.

First, we confirmed the presence of $Ca_V3.1$ and $Ca_V3.2$ channels in $POMC^+$ neurons by immunocytochemistry (**Figure 3A**) and characterized the calcium currents present in our cultures, including T-type currents (low-voltage gated, LVA). Analysis of Ca^{2+} currents properties revealed three distinct neuron groups, as seen in the I-V curves depicted in **Figure 3B**. Of all neurons sampled ($n = 28$), 14.3% expressed only high-voltage activated (HVA) currents; 46.4% of neurons expressed both HVA and LVA currents at low levels (LD, $I_{LVApeak} < 6$ -pA/pF), and 39.3% expressed low HVA and high LVA current density levels (HD, $I_{LVApeak}$ from 6 to 20 -pA/pF) (**Figures 3B,C**). Currents elicited by a depolarizing pulse from −90 to −30 mV were confirmed to be T-type by their sensitivity to their specific channel blocker NNC 55-0396 (10 μM, **Figure 3D**).

We next assessed whether T-type channels are part of the cellular pathway of neurons depolarized by leptin. First, we confirmed the presence of TRPC channels in $POMC^+$ neurons in our cultures using immunocytochemistry and western blot analysis (**Figures 4A**, **6**). Membrane excitability in control and leptin-treated neurons was studied before and after the application of the TRPC channel blocker 2-APB (100 μM) or NNC-55-0396 (10 μM) using a ramp rate of 20 pA/s. **Figure 4B** shows representative examples of leptin-treated neurons before and after aforesaid treatments. In control neurons, neither the application of 2-APB nor the addition of NNC-55-0396 affected neuronal membrane excitability *per se* (**Figure 4C**, control, $P > 0.05$, ANOVA). However, in leptin-treated neurons, the effect of leptin was abolished after the addition of 2-APB, resulting in a 24.5 ± 4.3% increase in the rheobase and 48.0 ± 5.3% decrease in the number of spikes, compared to the leptin-treated group, corroborating the role of TRPC channels in the leptin-signaling cascade (**Figure 4C**). Interestingly, the effect of leptin was also prevented solely by the application of the T-type channel blocker NNC-55-0396 (**Figure 4C**, $P < 0.05$, ANOVA). Similarly, both 2-APB and NNC-55-0396 prevented leptin-induced increase

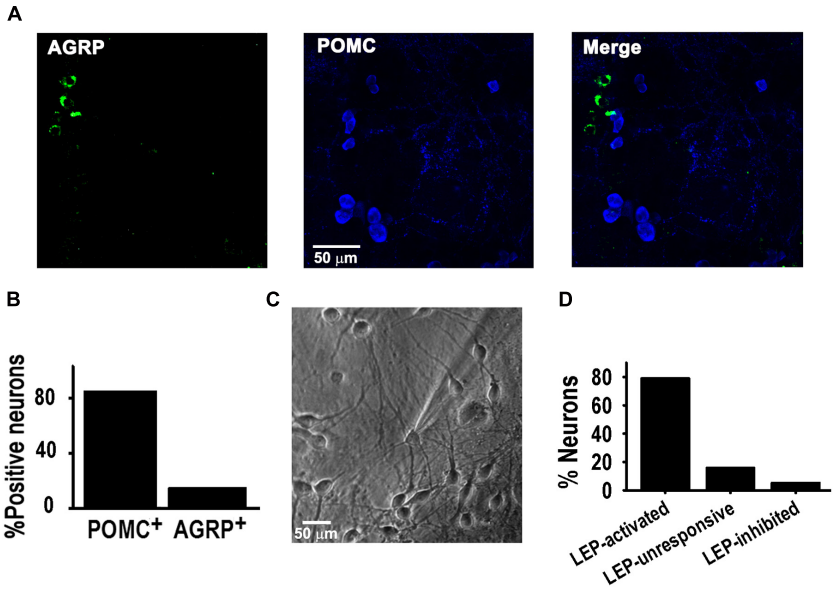

FIGURE 1 | POMC neurons activated by leptin in culture. **(A)** Example of confocal images showing neurons positive for AGRP (green) or POMC (blue) antibodies in hypothalamus culture at 8–10 DIV. **(B)** Percentage of neurons positive for AGRP or POMC antibodies (n = 182). **(C)** Microscopic image of cultured hypothalamic neuron at 8 DIV. **(D)** Percentage of WT neurons activated or inhibited by 100 nM leptin (n = 19), using a 20 pA/s depolarizing ramp stimulus.

of the rate of membrane potential depolarization (**Figure 4D**, $P < 0.05$, ANOVA).

Given that leptin is known to exert direct effects on voltage-gated calcium currents (Takekoshi et al., 2001; Wang et al., 2008), we assessed whether acute incubation with leptin altered T-type LVA currents. As seen in **Figure 5A**, application of 100 nM leptin in the recording chamber for 30 min did not alter the T-type peak current density ($P > 0.05$, t-test, at $V_T = -30$ mV). Furthermore, leptin did not affect either LVA or HVA current-voltage relationships (I-V curve, $P > 0.05$, Two Way RM ANOVA, **Figure 5B**) or the T-type properties of activation or inactivation (not shown), suggesting that the leptin-mediated effect on T-type channels is indirect, likely downstream of TRPC.

So far, our results suggest that T-type calcium currents are as necessary for the leptin-induced excitability response as TRPCs channels. Despite having no direct effect on T-type current density, leptin induced a faster rate of membrane potential depolarization compared to control (**Figure 2D**); which was prevented after blocking TRPC or T-type channels (**Figure 4D**). Faster rates of membrane depolarization induce less T-type current inactivation prior to activation of an action potential (Gutierrez et al., 2001), in fact, the results from **Figures 4C,D** suggest the membrane depolarization rate induced by leptin in response to current ramps of 20 pA/s favors T-type channel recruitment; in contrast, control neurons exhibited slower membrane potential depolarization rates (30.3 ± 2.7 vs. 66.1 ± 4.2 mV/s). The latter conditions favor T-type current inactivation, rendering an inadequate number of available T channels to contribute to the excitability process. Note that NNC-55-0396 did not affect the excitability in control neurons (**Figures 4C,D**). Therefore, we hypothesize that increased T-type channel availability resulting from the faster leptin-induced membrane potential depolarization rate is sufficient to increase membrane excitability and trigger sodium-mediated action potentials in POMC neurons.

In order to evaluate our hypothesis, we first studied whether T-type channels could be recruited by rates of membrane potential depolarization faster than 30 mV/s in control neurons. We assessed the T-type current activation in voltage-clamp configuration in response to increasing rates of membrane potential depolarization preceding the first AP (left panel, **Figure 5C**). Peak currents for each rate of membrane potential depolarization were normalized to the maximally elicited current. Average values were plotted against its respective rate of membrane potential depolarization (slope) and fitted using a Boltzmann equation (right panel, **Figure 5C**). The approximate rate of membrane potential depolarization in response to a ramp rate of 20 pA/s for control (∼30 mV/s, black lines) and leptin-treated (∼70 mV/s, red lines) neurons are shown on the voltage axis of **Figure 5C**. The lines interpolating the Y-axis denote the percentage of non-inactivated I_T that is recruited in response to the respective rate of membrane potential depolarization. In control neurons (black line), only around ∼5% of I_T is available for recruitment by a membrane depolarization rate of ∼30 mV/s. However, membrane depolarization rates similar to those induced by leptin-treatment (∼70 mV/s) would be able to recruit 20% of I_T. Thus, control neurons were stimulated in current-clamp configuration with depolarizing current ramps of 40 pA/s, which produce on average a membrane depolarization rate of 73.8 ± 9.1 mV/s. As seen in **Figure 5D**, NNC-55-0396 not only caused a large increase in the rheobase, but also significantly decreased the number of AP in control neurons.

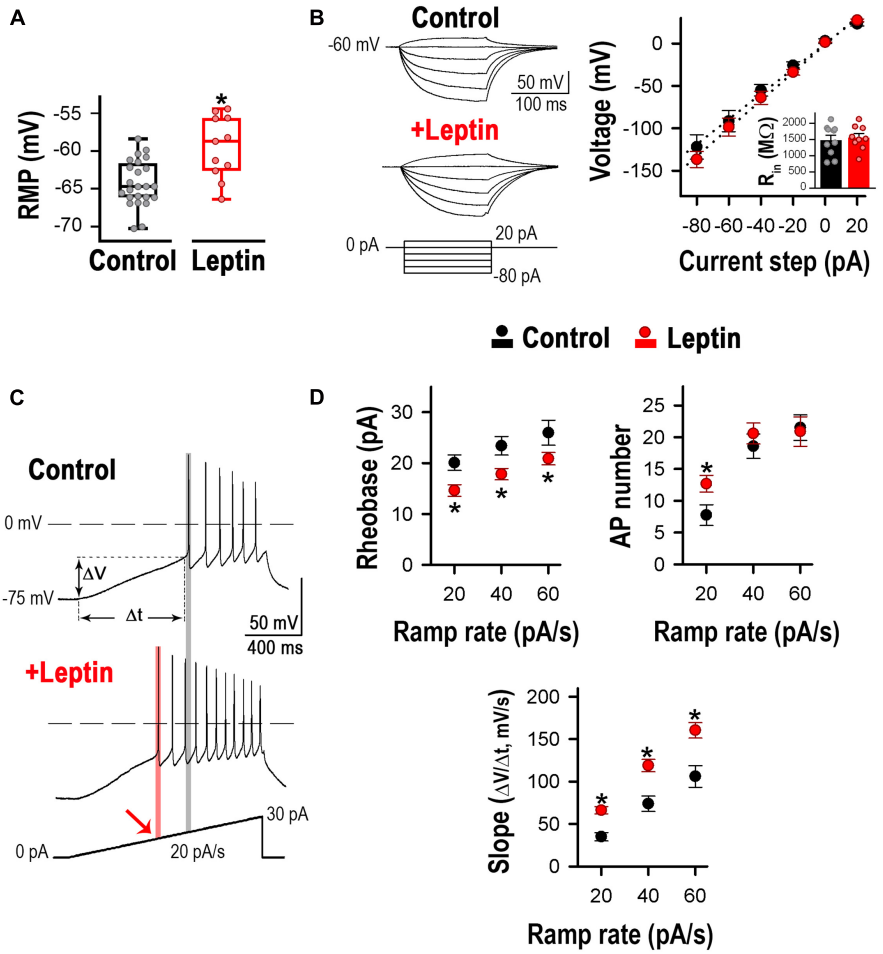

FIGURE 2 | Leptin increases excitability in cultured hypothalamic neurons. **(A)** Leptin application induced a ~6 mV depolarization. Resting membrane potential (RMP) from control (n = 24) and leptin-treated (n = 11) neurons. *Significantly different from control, $P < 0.05$, t-test (t = 3.923, df = 33). **(B)** Input resistance (R_{in}) from control (n = 10) and leptin-treated neurons (n = 9). Representative voltage traces (left) and average voltage-current (V-I) relation (right) in response to 200 ms current steps from –80 to 20 pA (every 20 pA, preset membrane potential = –60 mV). R_{in} was calculated as the slope of the linear regression. No changes in R_{in} were observed between control and leptin treatments ($P > 0.05$, t-test, t = 0.3883, df = 17). **(C)** Examples of neuronal firing in control and leptin-treated neurons elicited from a preset membrane potential of –75 mV by a 20 pA/s ramp. The rheobase is indicated with the gray line in control and the pink line and arrow in leptin-treated neurons. **(D)** Quantification of rheobase (pA), number of action potentials, and rate of membrane potential depolarization (Slope = $\Delta V/\Delta t$, mV/s, see panel **C**) in control (n = 24, 24, 12) and leptin-treated (100 nM, n = 19, 19, 15) neurons in response to 20, 40 and 60 pA/s ramps. *Significantly different from control, $P < 0.05$, t-test. Rheobase: t = 2.744 for 20 pA/s, t = 2.565 for 40 pA/s, t = 1.718 for 60 pA/s, df = 41. AP number: t = 2.257 for 20 pA/s, t = 0.766 for 40 pA/s, t = 0.198, df = 41. Slope: t = 4.030 for 20 pA/s, t = 2.908 for 40 pA/s, t = 2.894 for 60 pA/s, df = 25.

These results confirm that fast rates of membrane depolarization in response to excitatory stimuli recruit enough non-inactivated T-type channels to contribute to the membrane excitability.

Overall, our results show that T-type channel recruitment is necessary in leptin-mediated pathway, likely downstream of TRPC channel activity, as summarized in the cartoon in **Figure 5E**.

T-type Calcium and TRPC1/5 Channels Are Expressed in a Functional Complex

We explored whether TRPC and T-type channels exist in a complex. TRPC1/5 complexes are likely the physiological mediators of leptin's effects in the hypothalamus (Strübing et al., 2001), therefore we assessed whether Ca_V3 channels co-exist with TRPC5 channels in mouse whole brain and hypothalamus samples. **Figure 6A** shows that $Ca_V3.1$ channels co-precipitate with TRPC5 channels (left), and similarly, TRPC5 channels co-precipitate with $Ca_V3.1$ channels (right panel). $Ca_V3.2$ channels also co-precipitate with TRPC5 channels (**Figure 6B**, left), and TRPC5 interact with $Ca_V3.2$ (right). We also determined that TRPC1 is detected in samples co-precipitated with TRPC5 and $Ca_V3.1$ (left) or $Ca_V3.2$ (right) (**Figure 6C**), confirming a TRPC multimer formed by TRPC1/5 is present in the hypothalamus.

Because T-type calcium channels co-exist in a complex with TRPC1/5, it is possible that local membrane depolarization induced by TRPC1/5 channel-mediated cation influx recruits

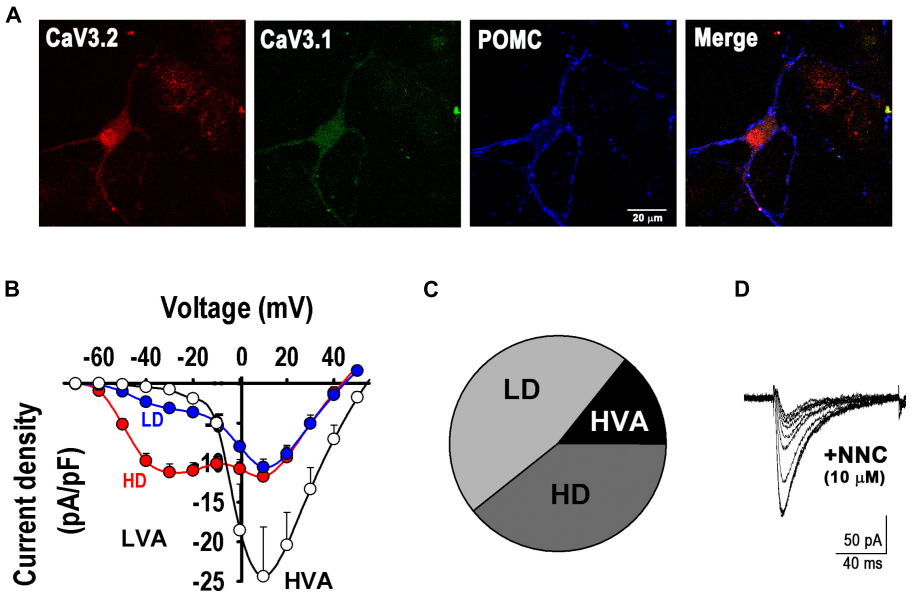

FIGURE 3 | T-type calcium channels in POMC neurons. **(A)** Example of fluorescence images showing the expression of T-type α_{1H} ($Ca_V3.2$, red) and α_{1G} ($Ca_V3.1$, green) channels in a POMC neuron (blue). Bar size, 20 µm. **(B)** I-V curves depict three distinct neuron groups (n = 28): empty circles, neurons expressing only high-voltage activated (HVA) currents; blue circles, neurons expressing low HVA and low LVA current density levels (LD, $I_{LVApeak}$ < 6 -pA/pF); and red circles, neurons expressing low HVA and high LVA current density (HD, $I_{LVApeak}$ from 6 to 20 -pA/pF). **(C)** Pie chart denotes the percentual number of neurons in each group described in **(A)**. **(D)** T-type calcium current blockade by its specific blocker NNC 55-0396 (10 µM); the trace amplitude decrement sequence is shown every 2 min before (larger trace) and during application of the drug.

T-type channel activity. As the ionic selectivity for TRPC1/5 channel complexes is almost 1:1 for Na^+ and Ca^{2+}, Ca^{2+} ions contribute two thirds of the total TRPC1/5-mediated depolarization. Accordingly, chelation of Ca^{2+} influx with a fast chelator that binds Ca^{2+} closer to the mouth's pore (BAPTA-AM, $K_{ON} = 6 \times 10^8$) compared to a slower, global chelator (EGTA-AM, $K_{ON} = 1.5 \times 10^6$) should allow us to discern whether the TRPC1/5 and T-type channels complex function within a microdomain (**Figure 7A**). We incubated cultured hypothalamic neurons with either 10 µM BAPTA-AM or EGTA-AM for 30 min at 37°C prior to whole-cell current clamp to assess excitability. As expected, leptin depolarized the RMP *via* activation of TRPC channels (**Figure 7B**, $P < 0.05$, ANOVA; RMP values for control and leptin-treated neurons have been reproduced from **Figure 2A** for comparison). The depolarizing effect of leptin occurred regardless of incubation with either BAPTA or EGTA (**Figure 7B**, $P < 0.05$, t-test), suggesting that the chelation of calcium does not affect the TRPC1/5 function *per se*. **Figure 7C** shows example traces of APs elicited with a 20 pA/s ramp protocol under control conditions (top trace), and after the addition of 100 nM leptin in the presence of BAPTA (middle) or EGTA (bottom). As expected, the presence of intracellular BAPTA or EGTA did not alter the baseline excitability response compared to control ($P > 0.05$, ANOVA; the rheobase and AP number values for control and leptin-treated neurons have been reproduced in **Figure 7D** from **Figure 4** for comparison). Addition of 100 nM leptin in the presence of EGTA caused the expected increase in excitability ($P < 0.05$, t-test), in contrast with leptin in the presence of internal BAPTA, which did not elicit significant changes in either the number of APs, rheobase or rate of membrane potential depolarization ($P > 0.05$, t-test). Our results suggest that calcium mediates leptin effects on membrane excitability in the proximity of the leptin effector, supporting the idea that TRPC1/5 and T-type channels complex could function within a microdomain.

To further confirm our results, T-type channels were recruited by using depolarizing ramps of 40 pA/s. Neither BAPTA nor EGTA affected membrane excitability in control neurons under those conditions, suggesting no direct effects on the contribution of T-type channels to basal neuronal excitability (**Figure 7E**). However, only BAPTA prevented leptin-mediated effects on membrane excitability (**Figure 7E**) in a similar manner as observed with 20 pA/s depolarizing ramps (**Figure 7D**). These results indicate that the BAPTA effects on membrane excitability were restricted to local leptin-mediated recruitment of T-type channels. The lack of effect of EGTA on membrane excitability confirms that leptin does not depend on a global calcium-dependent mechanism to regulate excitability.

Overall, these results support the hypothesis that Ca^{2+} influx via TRPC1/5 and subsequent depolarization enhances the recruitment of Ca_V3 channels, favoring the generation of APs.

We further studied the physiological relevance of this TRPC1/5-CaV3 complex. As seen in **Figures 2A**, **7B**, the application of leptin induced a ∼6 mV depolarization of RMP. **Figure 7F** (top panel) shows the steady-state activation (SSA) and steady-state inactivation (SSI) properties of T-type current

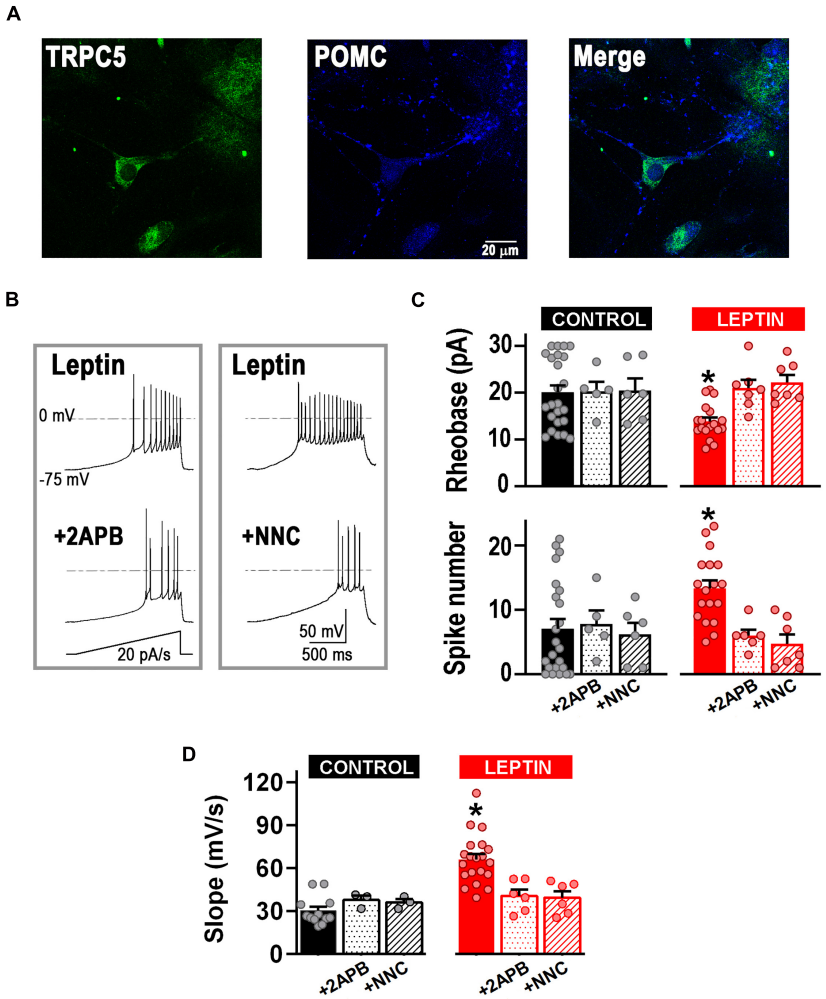

FIGURE 4 | T-type calcium channels are necessary for the leptin-induced excitability response. **(A)** Example of fluorescence images showing the expression of TRPC5 channels (green) in POMC neurons (blue). **(B)** Examples of neuronal firing elicited from a preset membrane potential of –75 mV by a 20 pA/s ramp in leptin-treated neurons before and after the addition of the TRPC channel blocker 2-APB (100 µM) or the T-type channel blocker NNC 55-0396 (10 µM). **(C)** Quantification of rheobase (pA) and number of action potentials in control neurons (n = 24), neurons treated with the TRPC channel blocker 2-APB (100 µM, n = 5), neurons treated with the T-type channel blocker NNC 55–0396 (10 µM, n = 6), neurons treated with leptin (100 nM, n = 18), neurons treated with leptin and 2-APB (n = 5), and neurons treated with leptin and NNC 55-0396 (10 µM, n = 7). *Significantly different from all others, $P < 0.05$, ANOVA, $F_{(5,\ 61)} = 3.786$ (for rheobase), $F_{(5,\ 61)} = 3.856$ (for AP number). **(D)** Quantification of the rate of membrane potential depolarization (slope) in control neurons (n = 12), neurons treated with the TRPC channel blocker 2-APB (100 µM, n = 3), neurons treated with the T-type channel blocker NNC 55-0396 (10 µM, n = 3), neurons treated with leptin (100 nM, n = 20), neurons treated with leptin and 2-APB (n = 6), and neurons treated with leptin and NNC 55-0396 (10 µM, n = 6). *Significantly different from all others, $P < 0.05$, ANOVA, $F_{(5,\ 44)} = 12.77$.

in cultured hypothalamic neurons. The superimposed lines on the graph show the interpolated values of RMP (Y-axis) for control (black lines) and leptin-treated neurons (red lines) pinpointing the non-inactivated (available, SSI) and the activable [open probability (PO), SSA] fractions of T-type channels at the respective resting membrane potentials. We calculated the T-type window current using the fitting parameters of the steady-state activation and inactivation curves (see section "Material and Methods") (Bijlenga et al., 2000; Lambert et al., 2014; Rivero-Echeto et al., 2020), which is shown in turquoise encompassing the region underneath the steady-state curves (**Figure 7F**, top panel). Of note, T-type channels are hardly functional during control conditions, when the 50% of available channels are not highly activable.

Our results show that the leptin-mediated RMP depolarization induces changes in T-type channel availability (SSI) and open probability (SSA) (**Figure 7F**, top panel, red line), leading to a voltage right-shift into the active T-type window current range that results in an increase of the steady state T-type calcium current from 40 to 70%, as better seen in the normalized steady state current graph (**Figure 7F**, bottom panel). These leptin-mediated changes on T-type calcium steady state current ultimately alter the intrinsic excitability of POMC neurons.

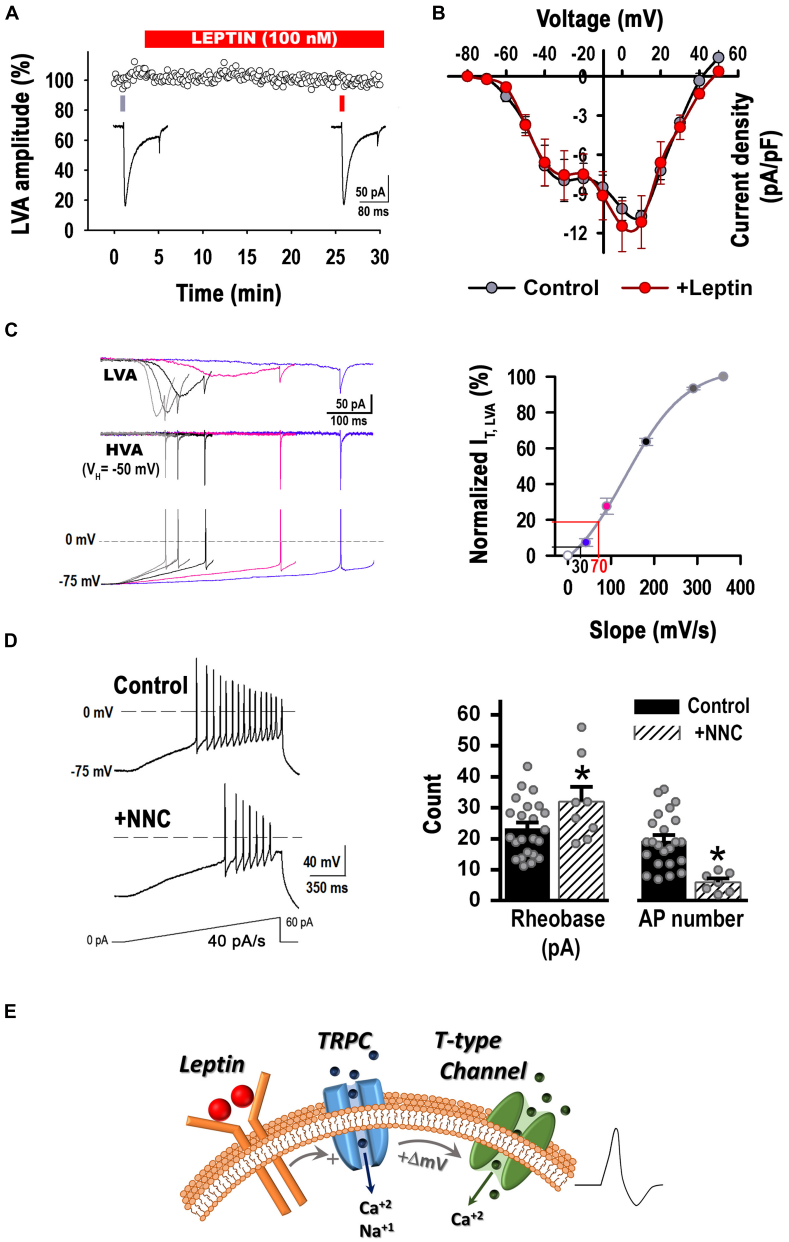

FIGURE 5 | Leptin has no direct effect on T-type current density but increases the membrane depolarization rate favoring T-type channels recruitment. **(A)** Acute incubation with Lep (100 nM) does not alter T-type currents (i.e., LVA currents) elicited by a step voltage from –90 to –30 mV (n = 3). **(B)** I-V curves before and after the application of 100 nM leptin in the recording chamber (n = 8, paired experiments). Currents were elicited by depolarizing voltage steps (ΔV = 10 mV) from a V_H of –90 to 50 mV. There is not a statistically significant difference before and after the addition of leptin [$P > 0.05$, Two Way RM ANOVA, $F_{(1, 55)} = 0.221$]. There is not a statistically significant interaction between the voltage and the treatment [$P > 0.05$, Two Way RM ANOVA, $F_{(11, 55)} = 0.785$]. I-V curves from neurons that expressed LVA current at low and high levels were pooled. **(C) Left:** Average traces of T-type currents elicited by various rates of voltage depolarization preceding the first AP. Stimulation protocols (bottom traces) were obtained from hypothalamic neurons recorded in current clamp configuration during current ramp stimulations (20–100 pA/s), which resulted in the following rates of membrane potential depolarization prior the first AP: 40, 90, 180, 290 or 360 mV/s (V_H = –75 mV). Before stimulation, the membrane potential was held at –90 or –50 mV (V_H) in order to isolate T-type currents. HVA currents recorded from a V_H of –50 mV (middle traces) were subtracted from LVA and HVA currents recorded from a V_H of –90 mV, obtaining the isolated LVA component (top traces). **Right:** Normalized T-type current as function of the membrane depolarization rate (slope) (n = 5). The black line marks the percentage of non-inactivated T-type current recruited by a depolarizing rate of 30 mV/s. The red line marks the percentage of non-inactivated T-type current recruited by a depolarizing rate of 70 mV/s. **(D) Left:** Example of neuronal firing elicited from a preset membrane potential of –75 mV by a 40 pA/s ramp in a control neuron before and after the addition of the T-type channel blocker NNC 55-0396 (10 μM). **Right:** Application of NNC 55-0396 (n = 8) reduced membrane excitability in comparison to control (n = 23) (–75 mV, 40 pA/s ramp). *Significantly different from control, $P < 0.05$, t-test. Rheobase: t = 2.060, df = 29. AP number: t = 3.956, df = 29. **(E)** Updated model of leptin's cellular signaling. Leptin binding to its receptor results in activation of the PI3 kinase signaling pathway and subsequent activation of TRPC channel. TRPC channel activity induces a small but rapid membrane depolarization that recruits T-type channel activity, increasing hypothalamic neuron excitability.

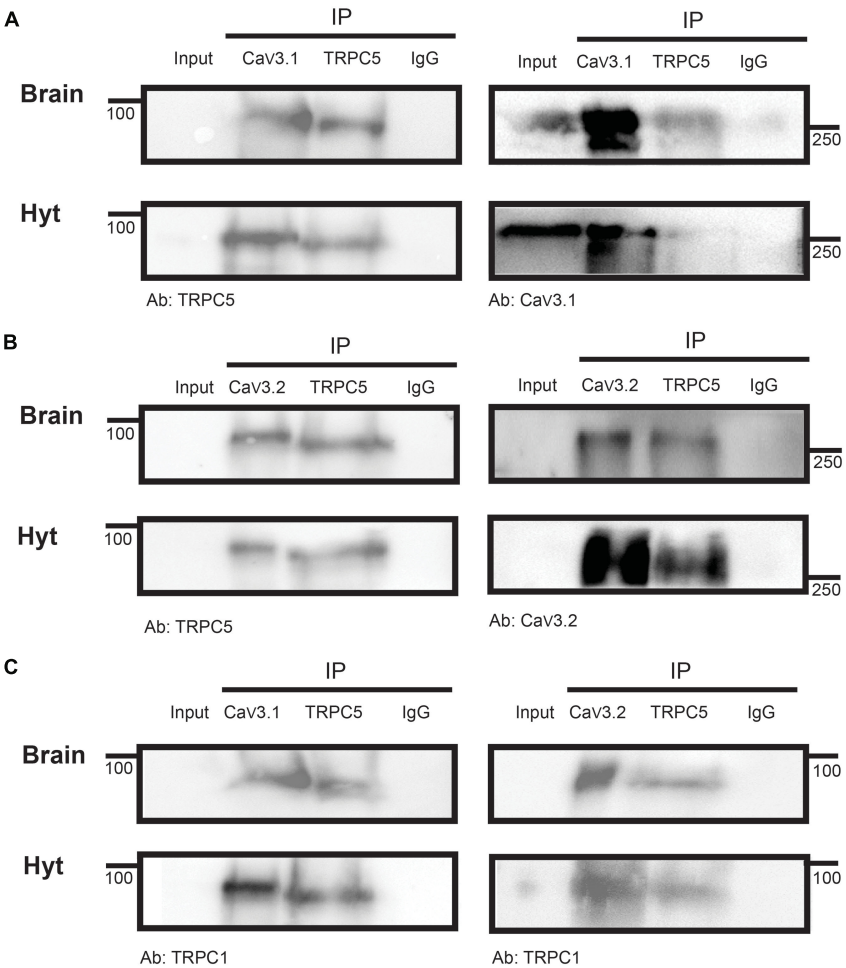

FIGURE 6 | Ca_V3 co-precipitation with TRPC5. Immunoprecipitation of brain and hypothalamus (Hyt) extracts with $Ca_V3.1$ **(A)** or $Ca_V3.2$ **(B)** and TRPC5 in the same samples show their mutual interaction. **(C)** IP of brain and Hyt samples using $Ca_V3.1$ (left) or $Ca_V3.2$ (right) and TRPC5 show their interaction with TRPC1. IgG was used as IP negative control in all cases, (n = 3 for all panels).

DISCUSSION

Neuronal cultures with fully developed synapses (after 7 DIV) are useful for mechanistic studies, as they display an "adult" pattern behavior, including ion channel expression (Schlick et al., 2010). Here we corroborated that our primary $POMC^+$ hypothalamic neurons responded to leptin as expected according to the bibliography. It is well-established that leptin's effect on POMC neurons is mediated by the activation of TRPC channels (Qiu et al., 2010, 2011, 2014), POMC neurons increased in our system their excitability in response to administration of nanomolar levels of leptin and this effect was mediated through the activation of TRPC channels, in line with the literature (Qiu et al., 2010, 2011, 2014). The present work provides additional detail on this mechanism, demonstrating that TRPC and T-type channels coexist in a physical and functional macromolecular complex, whereby, leptin-induced membrane depolarization *via* TRPC channel activity immediately recruits adjacent T-type channels, which further depolarize POMC neurons triggering an increase in intrinsic excitability.

Hyperpolarization-induced removal of T-type channel inactivation allows for their stimulation by small depolarizations near the resting potential, rendering T-type currents optimal for regulating excitability under physiological conditions near resting state; as such, T-type channels help control neuronal excitability in various hypothalamic nuclei (van den Top et al., 2004; Qiu et al., 2006; Bosch et al., 2009; Zhang et al., 2009). T-type channels have a confirmed role linking thalamocortical central regulation of wakefulness and body weight (Uebele et al., 2009), and they have been proposed as potential therapeutic targets for treating obesity (Chemin et al., 2001; Uebele et al., 2009; Chorvat, 2013). T-type antagonists prescribed for epilepsy, depression, obsessive-compulsive disorder and bulimia nervosa can cause loss of appetite as a side effect (Cookson and Duffett, 1998; Traboulsie et al., 2006; Wilfong and Willmore, 2006). Here we establish T-type channels (Ca_V3) as essential mediators of membrane depolarization and neuronal excitability triggered

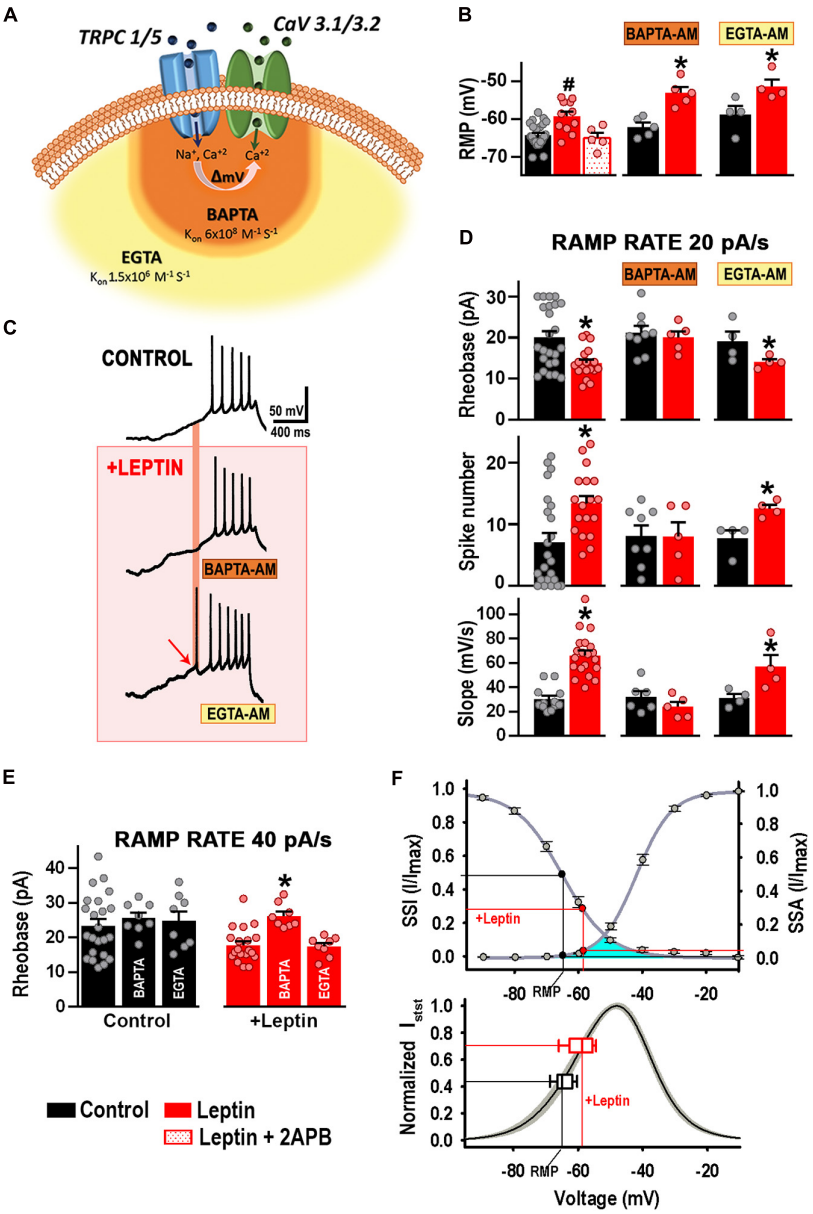

FIGURE 7 | Ca^{2+} influx via TRPC1/5 depolarizes and recruits T-type channels. **(A)** Cartoon depicting T-type calcium channels co-exist in a complex with TRPC1/5. Membrane depolarization induced by TRPC channel-mediated cation influx recruits T-type channel activity. Chelation of Ca^{2+} influx with a fast chelator that binds Ca^{2+} closer to the mouth's pore (BAPTA-AM, $K_{ON} = 6 \times 10^8$) is represented in orange. Chelation of Ca^{2+} influx with a slower chelator (EGTA-AM, $K_{ON} = 1.5 \times 10^6$) is represented in light orange. **(B)** Resting membrane potential (RMP) from control ($n = 24$) and leptin-treated neurons in the absence ($n = 11$) or presence of 2APB ($n = 5$). Values for control and leptin-treated neurons were reproduced from **(A)** for comparison. Cultured hypothalamic neurons were incubated with either 10 μM BAPTA-AM ($n = 5$) or EGTA-AM ($n = 4$) for 30 min at 37°C prior to whole-cell current clamp to assess leptin-mediated effects on the RMP. #Significantly different from others, $P < 0.05$, ANOVA, $F_{(2,\ 37)} = 8.927$. *Significantly different from control, $P < 0.05$, t-test. BAPTA: $t = 4.743$, df = 8. EGTA: $t = 2.579$, df = 6. **(C)** Example traces of APs elicited by a 20 pA/s ramp protocol under control conditions (top trace), and after the addition of 100 nM leptin in the presence of BAPTA (middle) or EGTA (bottom). **(D)** Rheobase, AP number, and slope values elicited by 20 pA/s ramps for each treatment ($n = 4$–24). *Significantly different from control, $P < 0.05$, t-test. Rheobase: $t = 3.285$ (df = 40, control), $t = 0.4757$ (df = 12, BAPTA incubation), $t = 2.019$ (df = 6, EGTA incubation). AP number: $t = 3.065$ (df = 39, control), $t = 0.044$ (df = 11, BAPTA), $t = 3.376$ (df = 6, EGTA). Slope: $t = 6.495$ (df = 30, control), $t = 1.245$ (df = 9, BAPTA incubation), $t = 2.446$ (df = 6, EGTA incubation). **(E)** Rheobase values elicited by 40 pA/s ramps for each treatment ($n = 8$–23). *Significantly different from others, $P < 0.05$, ANOVA, $F_{(2,\ 36)} = 0.2637$ for control neurons, $F_{(2,\ 32)} = 12.36$ for leptin-treated neurons. **(F)** T-type channel availability (SSI) and open probability (SSA) as function of voltage. SSI parameters: $V_{50} = -65.4 \pm 1.0$ mV, k = 7.1 ± 0.5 ($n = 21$). SSA parameters: $V_{50} = -41.8 \pm 0.7$ mV, k = 5.2 ± 0.3 ($n = 22$). Black circles indicate the availability and the open probability of T-type channels) at the indicated RMP. Red circles indicate steady sate properties at depolarized RMP after leptin (100 nM) incubation. Window current, underneath SSA and SSI curves is indicated in turquoise. Window currents were calculated for each recording neuron from the SSA and SSI curves fitted with the Boltzmann function ($n = 18$, see section "Materials and Methods"); SEM is indicated in gray. The steady-state current was normalized to its maximum value (Normalized Isst). Steady-state current at the RMP (empty black box plot) increased after incubation with leptin (empty red box plot).

by activation of the JNK2-PI3K cascade in response to leptin in POMC neurons. Although leptin has many functions, including effects on control of hormone release, immune system, vasculature, development, somatosensory thalamic activity and higher-level cognitive functions (Haynes et al., 1999; Kim and Moustaid-Moussa, 2000; Friedman, 2004; Myers et al., 2008; Domingos et al., 2011; Farr et al., 2014; Perissinotti et al., 2018); one of its prominent roles is as effector of the negative feedback loop, supporting homeostatic control of energy and food intake, and adipose tissue mass (Ahima et al., 1996). The majority of neurons in our hypothalamic cultures were leptin-activated, in line with a higher abundance of POMC positive neurons detected by ICC. In these neurons, leptin induces electrical activity and depolarization *via* binding to LRb, activation of Janus tyrosine kinase 2 and the downstream activation of phosphatidylinositol 3 kinase (PI3K), resulting in activation of transient receptor potential cation channel activity (TRPC) (Harvey, 2007; Qiu et al., 2010, 2011, 2014). Indeed, leptin application to cultured hypothalamic neurons *in vitro* also resulted in membrane depolarization and increased neuronal excitability. Treatment with the TRPC channel blocker 2-APB after leptin application produced a decrease in the excitability, which was measured as an increase in the rheobase and a decrease of both the rate of membrane depolarization and the number of spikes. However, we found that in addition to TRPC channel activation, T-type channel activity is also essential in this pathway. Blockade of T-type channels with NNC 55-0396 completely prevented the effect of leptin, even when TRPC channel activity remained intact. Qiu et al. (2010) demonstrated leptin recruits a non-selective Na^+ and Ca^{2+} channel sensitive to SKF96365 and APB and potentiated by lanthanum (La^{3+}), consistent with a TRPC channel complex. Here, we showed T-type channel function is essential in the response to leptin. The leptin-activated current is strongly potentiated by lanthanum (Qiu et al., 2010), a T-type channel blocker more potent than nickel (Mlinar and Enyeart, 1993). Thus, it' is unlikely T-type calcium channels are directly activated by leptin, consistent with our data showing leptin does not directly activate these channels and the steady-state properties of these currents. Instead, leptin induced faster rates of membrane depolarization, which in turn produced less T-type current inactivation prior to activation of an action potential (Gutierrez et al., 2001). Therefore, T-type channels are likely recruited downstream of TRPC channel activation by discrete changes in membrane depolarization induced by TRPC channels and are the final mediator of triggered activity. Insulin and leptin engage a common signaling pathway at the cellular level to activate TRPC5/1 channel complexes and depolarize POMC neurons (Qiu et al., 2014). Interestingly, estradiol-mediated upregulation of Cav3.1 channel rendered POMC neurons more excitable and responsive to insulin-mediated TRPC5 channel activation (Qiu et al., 2018).

Furthermore, we demonstrate TRPC1/C5 channels and $Ca_V3.1$ and $Ca_V3.2$ channels exist in complex. Calcium channels are known to co-exist with other channels in functional complexes (Robitaille et al., 1993; Vivas et al., 2017), notably T-type channels form protein complexes with members of the potassium channel family such as Kv4, KCa3.1, and KCa1.1 (Anderson et al., 2010; Rehak et al., 2013), which ensures rapid potassium channel activation thanks to their proximity with Ca_V3 channels within the microdomain. Furthermore, TRPC channels are known to assemble in multiprotein complexes that include various key Ca^{2+} signaling proteins within Ca^{2+} signaling microdomains (Ambudkar, 2006). For instance, TRPC1, 3, 4, 5, 6, and 7 isoforms can form a macromolecular complex with the α_{1C} subunit of the L-type voltage-gated calcium channel (Cav1.2) in atria and ventricle of developing heart (Sabourin et al., 2011). Here, co-immunoprecipitation experiments show that TRPC5 interacts with $Ca_V3.1$ and $Ca_V3.2$ channels. The functional activity of this complex was corroborated using intracellular calcium chelators; prevention of leptin-induced calcium influx through TRPC channels by intracellular BAPTA (but not EGTA) was sufficient to preclude POMC neuron excitability. Our results agree with those of Qiu et al. (2010), who reported that leptin-induced inward current was reduced by BAPTA but not EGTA. It has been shown that intracellular BAPTA prevents intracellular Ca^{2+}-dependent potentiation of the TRPC channel complex *in vitro*, suggesting that calcium binding to an intracellular site in the TRPC channel complex is necessary for its function (Strübing et al., 2001). However, leptin is capable of recruiting a non-selective Na/Ca current in hypothalamic neurons in the presence of BAPTA, albeit smaller than in control conditions but larger than that observed in the absence of extracellular calcium (Qiu et al., 2010). In line with these results, we show that leptin-induced depolarization can occur even in the presence of either BAPTA or EGTA suggesting that the calcium entry thought to be necessary to self-activate the TRPC1/5 complex is not blocked by the presence of BAPTA in hypothalamic neurons.

T-type Ca^{2+} channels operate in a subthreshold voltage range, with an overlap between steady-state activation and inactivation curves that produces a voltage range where a subset of T-type channels are constitutively open (i.e., steady-state current, I_{stst} or "window current") (Hughes et al., 1999; Crunelli et al., 2005). Furthermore, we observed that the leptin-mediated depolarization of RMP induced a voltage right-shift into the active T-type window current range, resulting in an increase of the steady state T-type calcium current from 40 to 70%; which ultimately affects the intrinsic excitability of POMC neurons. This study was focused on the somatic response of POMC cultured neurons from newborn mice, thus it did not address questions pertaining to the hypothalamic circuit level. However, our results show T-type channel activity is necessary for leptin-mediated effects on hypothalamic POMC neuron excitability and confirms T-type channels as possible additional drug targets for leptin-mediated functions, such as metabolic energy regulation and control of food satiety.

DATA AVAILABILITY STATEMENT

The raw data supporting the conclusions of this article will be made available by the authors, without undue reservation. A previous version of this research is available (https://www.biorxiv.org/content/10.1101/2020.07.21.214296v1).

ETHICS STATEMENT

The animal protocols used in this study were reviewed and approved by an independent Institutional Animal Care and Use Committee at Loyola University Chicago (IACUC 2016032).

AUTHOR CONTRIBUTIONS

EP-R did the conception of research, approved the final version of the manuscript, and supervised the experiments. EP-R, EM-H, and PP designed the experiments, performed experiments, analyzed the data, interpreted results of experiments, and prepared the figures. EP-R and PP wrote the manuscript, edited, and revised the manuscript. All authors contributed to the article and approved the submitted version.

FUNDING

This article was based upon work supported by the National Science Foundation under grant no. 1022075 (EP-R).

ACKNOWLEDGMENTS

We thank all members of the Piedras Laboratory, Drs. O'Connell and Don Carlos for helpful input and comments.

REFERENCES

Ahima, R. S., and Flier, J. S. (2000). Leptin. *Annu. Rev. Physiol.* 62, 413–437. doi: 10.1146/annurev.physiol.62.1.413

Ahima, R. S., Prabakaran, D., Mantzoros, C., Qu, D., Lowell, B., Maratos-Flier, E., et al. (1996). Role of leptin in the neuroendocrine response to fasting. *Nature* 382, 250–252. doi: 10.1038/382250a0

Ambudkar, I. S. (2006). Ca2+ signaling microdomains: platforms for the assembly andregulation of TRPC channels. *Trends Pharmacol. Sci.* 27, 25–32. doi: 10.1016/j.tips.2005.11.008

Anderson, D., Mehaffey, W. H., Iftinca, M., Rehak, R., Engbers, J. D., Hameed, S., et al. (2010). Regulation of neuronal activity by Cav3-Kv4 channel signaling complexes. *Nat. Neurosci.* 13, 333–337. doi: 10.1038/nn.2493

Balasubramanyan, S., Stemkowski, P. L., Stebbing, M. J., and Smith, P. A. (2006). Sciatic chronic constriction injury produces cell-type-specific changes in the electrophysiological properties of rat substantia gelatinosa neurons. *J. Neurophysiol.* 96, 579–590. doi: 10.1152/jn.00087.2006

Baver, S. B., Hope, K., Guyot, S., Bjorbaek, C., Kaczorowski, C., and O'Connell, K. M. (2014). Leptin modulates the intrinsic excitability of AgRP/NPY neurons in the arcuate nucleus of the hypothalamus. *J. Neurosci.* 34, 5486–5496. doi: 10.1523/jneurosci.4861-12.2014

Bean, B. P. (1985). Two kinds of calcium channels in canine atrial cells. differences in kinetics, selectivity, and pharmacology. *J. Gen. Physiol.* 86, 1–30. doi: 10.1085/jgp.86.1.1

Bijlenga, P., Liu, J.-H., Espinos, E., Haenggeli, C.-A., Fischer-Lougheed, J., Bader, C. R., et al. (2000). T-type α1H Ca2+ channels are involved in Ca2+ signaling during terminal differentiation (fusion) of human myoblasts. *Proc. Natl. Acad. Sci. U.S.A.* 97, 7627–7632. doi: 10.1073/pnas.97.13.7627

Bosch, M. A., Hou, J., Fang, Y., Kelly, M. J., and Ronnekleiv, O. K. (2009). 17Beta-estradiol regulation of the mRNA expression of T-type calcium channel subunits: role of estrogen receptor alpha and estrogen receptor beta. *J. Comp. Neurol.* 512, 347–358. doi: 10.1002/cne.21901

Chemin, J., Monteil, A., Perez-Reyes, E., Nargeot, J., and Lory, P. (2001). Direct inhibition of T-type calcium channels by the endogenous cannabinoid anandamide. *EMBO J.* 20, 7033–7040. doi: 10.1093/emboj/20.24.7033

Chorvat, R. J. (2013). Peripherally restricted CB1 receptor blockers. *Bioorg. Med. Chem. Lett.* 23, 4751–4760. doi: 10.1016/j.bmcl.2013.06.066

Cookson, J., and Duffett, R. (1998). Fluoxetine: therapeutic and undesirable effects. *Hosp. Med.* 59, 622–626.

Cowley, M. A., Smart, J. L., Rubinstein, M., Cerdan, M. G., Diano, S., Horvath, T. L., et al. (2001). Leptin activates anorexigenic POMC neurons through a neural network in the arcuate nucleus. *Nature* 411, 480–484. doi: 10.1038/35078085

Crunelli, V., Tóth, T. I., Cope, D. W., Blethyn, K., and Hughes, S. W. (2005). The 'window' T-type calcium current in brain dynamics of different behavioural states. *J. Physiol.* 562, 121–129. doi: 10.1113/jphysiol.2004.076273

Domingos, A. I., Vaynshteyn, J., Voss, H. U., Ren, X., Gradinaru, V., Zang, F., et al. (2011). Leptin regulates the reward value of nutrient. *Nat. Neurosci.* 14, 1562–1568. doi: 10.1038/nn.2977

Farr, O. M., Sloan, D. M., Keane, T. M., and Mantzoros, C. S. (2014). Stress- and PTSD-associated obesity and metabolic dysfunction: a growing problem requiring further research and novel treatments. *Metabolism* 63, 1463–1468. doi: 10.1016/j.metabol.2014.08.009

Friedman, J. M. (2004). Modern science versus the stigma of obesity. *Nat. Med.* 10, 563–569. doi: 10.1038/nm0604-563

Gao, Y., Yao, T., Deng, Z., Sohn, J.-W., Sun, J., Huang, Y., et al. (2017). TrpC5 mediates acute leptin and serotonin effects via Pomc neurons. *Cell Rep.* 18, 583–592. doi: 10.1016/j.celrep.2016.12.072

Gutierrez, C., Cox, C. L., Rinzel, J., and Sherman, S. M. (2001). Dynamics of low-threshold spike activation in relay neurons of the cat lateral geniculate nucleus. *J. Neurosci.* 21, 1022–1032. doi: 10.1523/jneurosci.21-03-01022.2001

Harvey, J. (2007). Leptin regulation of neuronal excitability and cognitive function. *Curr. Opin. Pharmacol.* 7, 643–647. doi: 10.1016/j.coph.2007.10.006

Harvey, J., and Ashford, M. L. (2003). Leptin in the CNS: much more than a satiety signal. *Neuropharmacology* 44, 845–854. doi: 10.1016/S0028-3908(03)00076-5

Haynes, W. G., Morgan, D. A., Djalali, A., Sivitz, W. I., and Mark, A. L. (1999). Interactions between the melanocortin system and leptin in control of sympathetic nerve traffic. *Hypertension* 33(1 Pt 2), 542–547. doi: 10.1161/01.HYP.33.1.542

Hughes, S. W., Cope, D. W., Toth, T. I., Williams, S. R., and Crunelli, V. (1999). All thalamocortical neurones possess a T-type Ca2+ 'window'current that enables the expression of bistability-mediated activities. *J. Physiol.* 517, 805–815. doi: 10.1111/j.1469-7793.1999.0805s.x

Huguenard, J. (1996). Low-threshold calcium currents in central nervous system neurons. *Annu. Rev. Physiol.* 58, 329–348. doi: 10.1146/annurev.ph.58.030196.001553

Kenny, P. J. (2011). Common cellular and molecular mechanisms in obesity and drug addiction. *Nat. Rev. Neurosci.* 12, 638–651. doi: 10.1038/nrn3105

Kim, S., and Moustaid-Moussa, N. (2000). Secretory, endocrine and autocrine/paracrine function of the adipocyte. *J. Nutr.* 130, 3110S–3115S.

Lambert, R. C., Bessaïh, T., Crunelli, V., and Leresche, N. (2014). The many faces of T-type calcium channels. *Pflügers Arch.* 466, 415–423. doi: 10.1007/s00424-013-1353-6

Llinás, R. R. (1988). The intrinsic electrophysiological properties of mammalian neurons: insights into central nervous system function. *Science* 242, 1654–1664. doi: 10.1126/science.3059497

Lu, V. B., Moran, T. D., Balasubramanyan, S., Alier, K. A., Dryden, W. F., Colmers, W. F., et al. (2006). Substantia gelatinosa neurons in defined-medium organotypic slice culture are similar to those in acute slices from young adult rats. *Pain* 121, 261–275. doi: 10.1016/j.pain.2006.01.009

Mlinar, B., and Enyeart, J. (1993). Block of current through T-type calcium channels by trivalent metal cations and nickel in neural rat and human cells. *J. Physiol.* 469, 639–652. doi: 10.1113/jphysiol.1993.sp019835

Myers, M. G., Cowley, M. A., and Munzberg, H. (2008). Mechanisms of leptin action and leptin resistance. *Annu. Rev. Physiol.* 70, 537–556. doi: 10.1146/annurev.physiol.70.113006.100707

Perez-Reyes, E. (2003).). Molecular physiology of low-voltage-activated t-type calcium channels. *Physiol. Rev.* 83, 117–161. doi: 10.1152/physrev.00018.2002

Perissinotti, P. P., Ethington, E. G., Almazan, E., Martínez-Hernández, E., Kalil, J., Koob, M. D., et al. (2015). Calcium current homeostasis and synaptic deficits in hippocampal neurons from Kelch-like 1 knockout mice. *Front. Cell. Neurosci.* 8:444. doi: 10.3389/fncel.2014.00444

Perissinotti, P. P., Ethington, E. G., Cribbs, L., Koob, M. D., Martin, J., and Piedras-Renteria, E. S. (2014). Down-regulation of endogenous KLHL1 decreases voltage-gated calcium current density. *Cell Calcium* 55, 269–280. doi: 10.1016/j.ceca.2014.03.002

Perissinotti, P. P., Rivero-Echeto, M. C., Garcia-Rill, E., Bisagno, V., and Urbano, F. J. (2018). Leptin alters somatosensory thalamic networks by decreasing gaba release from reticular thalamic nucleus and action potential frequency at ventrobasal neurons. *Brain Struct. Funct.* 223, 2499–2514. doi: 10.1007/s00429-018-1645-x

Qiu, J., Bosch, M. A., Jamali, K., Xue, C., Kelly, M. J., and Rønnekleiv, O. K. (2006). Estrogen upregulates T-type calcium channels in the hypothalamus and pituitary. *J. Neurosci.* 26, 11072–11082. doi: 10.1523/jneurosci.3229-06.2006

Qiu, J., Bosch, M. A., Meza, C., Navarro, U.-V., Nestor, C. C., Wagner, E. J., et al. (2018). Estradiol protects proopiomelanocortin neurons against insulin resistance. *Endocrinology* 159, 647–664. doi: 10.1210/en.2017-00793

Qiu, J., Fang, Y., Bosch, M. A., Ronnekleiv, O. K., and Kelly, M. J. (2011). Guinea pig kisspeptin neurons are depolarized by leptin via activation of TRPC channels. *Endocrinology* 152, 1503–1514. doi: 10.1210/en.2010-1285

Qiu, J., Fang, Y., Ronnekleiv, O. K., and Kelly, M. J. (2010). Leptin excites proopiomelanocortin neurons via activation of TRPC channels. *J. Neurosci.* 30, 1560–1565. doi: 10.1523/jneurosci.4816-09.2010

Qiu, J., Zhang, C., Borgquist, A., Nestor, C. C., Smith, A. W., Bosch, M. A., et al. (2014). Insulin excites anorexigenic proopiomelanocortin neurons via activation of canonical transient receptor potential channels. *Cell Metab.* 19, 682–693. doi: 10.1016/j.cmet.2014.03.004

Rehak, R., Bartoletti, T. M., Engbers, J. D., Berecki, G., Turner, R. W., and Zamponi, G. W. (2013). Low voltage activation of KCa1.1 current by Cav3-KCa1.1 complexes. *PLoS One* 8:e61844. doi: 10.1371/journal.pone.0061844

Rivero-Echeto, M. C., Perissinotti, P. P., González-Inchauspe, C., Kargieman, L., Bisagno, V., and Urbano, F. J. (2020). Simultaneous administration of cocaine and caffeine dysregulates HCN and T-type channels. *Psychopharmacology* 238, 787–810. doi: 10.1007/s00213-020-05731-5

Robitaille, R., Garcia, M. L., Kaczorowski, G. J., and Chariton, M. P. (1993). Functional colocalization of calcium and calcium-gated potassium channels in control of transmitter release. *Neuron* 11, 645–655. doi: 10.1016/0896-6273(93)90076-4

Sabourin, J., Robin, E., and Raddatz, E. (2011). A key role of TRPC channels in the regulation of electromechanical activity of the developing heart. *Cardiovasc. Res.* 92, 226–236. doi: 10.1093/cvr/cvr167

Schlick, B., Flucher, B. E., and Obermair, G. J. (2010). Voltage-activated calcium channel expression profiles in mouse brain and cultured hippocampal neurons. *Neuroscience* 167, 786–798. doi: 10.1016/j.neuroscience.2010.02.037

Schneider, C. A., Rasband, W. S., and Eliceiri, K. W. (2012). NIH Image to ImageJ: 25 years of image analysis. *Nat. Methods* 9, 671–675. doi: 10.1038/nmeth.2089

Schwartz, M. W., Woods, S. C., Porte, D. Jr., Seeley, R. J., and Baskin, D. G. (2000). Central nervous system control of food intake. *Nature* 404, 661–671. doi: 10.1038/35007534

Shioda, S., Funahashi, H., Nakajo, S., Yada, T., Maruta, O., and Nakai, Y. (1998). Immunohistochemical localization of leptin receptor in the rat brain. *Neurosci. Lett.* 243, 41–44. doi: 10.1016/S0304-3940(98)00082-2

Sohn, J.-W., Xu, Y., Jones, J. E., Wickman, K., Williams, K. W., and Elmquist, J. K. (2011). Serotonin 2C receptor activates a distinct population of arcuate pro-opiomelanocortin neurons via TRPC channels. *Neuron* 71, 488–497. doi: 10.1016/j.neuron.2011.06.012

Strübing, C., Krapivinsky, G., Krapivinsky, L., and Clapham, D. E. (2001). TRPC1 and TRPC5 form a novel cation channel in mammalian brain. *Neuron* 29, 645–655. doi: 10.1016/s0896-6273(01)00240-9

Takekoshi, K., Ishii, K., Nanmoku, T., Shibuya, S., Kawakami, Y., Isobe, K., et al. (2001). Leptin stimulates catecholamine synthesis in a PKC-dependent manner in cultured porcine adrenal medullary chromaffin cells. *Endocrinology* 142, 4861–4871. doi: 10.1210/endo.142.11.8484

Traboulsie, A., Chemin, J., Kupfer, E., Nargeot, J., and Lory, P. (2006). T-type calcium channels are inhibited by fluoxetine and its metabolite norfluoxetine. *Mol. Pharmacol.* 69, 1963–1968. doi: 10.1124/mol.105.020842

Uebele, V. N., Gotter, A. L., Nuss, C. E., Kraus, R. L., Doran, S. M., Garson, S. L., et al. (2009). Antagonism of T-type calcium channels inhibits high-fat diet-induced weight gain in mice. *J. Clin. Invest.* 119, 1659–1667. doi: 10.1172/jci36954

van den Top, M., Lee, K., Whyment, A. D., Blanks, A. M., and Spanswick, D. (2004). Orexigen-sensitive NPY/AgRP pacemaker neurons in the hypothalamic arcuate nucleus. *Nat. Neurosci.* 7, 493–494. doi: 10.1038/nn1226

Vivas, O., Moreno, C. M., Santana, L. F., and Hille, B. (2017). Proximal clustering between BK and CaV1. 3 channels promotes functional coupling and BK channel activation at low voltage. *Elife* 6:e28029.

Wang, J.-H., Wang, F., Yang, M.-J., Yu, D.-F., Wu, W.-N., Liu, J., et al. (2008). Leptin regulated calcium channels of neuropeptide Y and proopiomelanocortin neurons by activation of different signal pathways. *Neuroscience* 156, 89–98. doi: 10.1016/j.neuroscience.2008.04.079

Wilfong, A. A., and Willmore, L. J. (2006). Zonisamide – a review of experience and use in partial seizures. *Neuropsychiatr. Dis. Treat.* 2, 269–280. doi: 10.2147/nedt.2006.2.3.269

Williams, K. W., and Elmquist, J. K. (2012). From neuroanatomy to behavior: central integration of peripheral signals regulating feeding behavior. *Nat. Neurosci.* 15, 1350–1355. doi: 10.1038/nn.3217

Zhang, C., Bosch, M. A., Rick, E. A., Kelly, M. J., and Rønnekleiv, O. K. (2009). 17β-estradiol regulation of T-type calcium channels in gonadotropin-releasing hormone neurons. *J. Neurosci.* 29, 10552–10562. doi: 10.1523/jneurosci.2962-09.2009

Conflict of Interest: The authors declare that the research was conducted in the absence of any commercial or financial relationships that could be construed as a potential conflict of interest.

frontiers in Neuroscience

ORIGINAL RESEARCH
published: 09 August 2021
doi: 10.3389/fnins.2021.695975

Closed-Loop Fuzzy Energy Regulation in Patients With Hypercortisolism via Inhibitory and Excitatory Intermittent Actuation

Hamid Fekri Azgomi[1], *Jin-Oh Hahn*[2] *and Rose T. Faghih*[1]*

[1] Computational Medicine Lab, Department of Electrical and Computer Engineering, University of Houston, Houston, TX, United States, [2] Department of Mechanical Engineering, University of Maryland, College Park, MD, United States

Hypercortisolism or Cushing's disease, which corresponds to the excessive levels of cortisol hormone, is associated with tiredness and fatigue during the day and disturbed sleep at night. Our goal is to employ a wearable brain machine interface architecture to regulate one's energy levels in hypercortisolism. In the present simulation study, we generate multi-day cortisol profile data for ten subjects both in healthy and disease conditions. To relate an internal hidden cognitive energy state to one's cortisol secretion patterns, we employ a state-space model. Particularly, we consider circadian upper and lower bound envelopes on cortisol levels, and timings of hypothalamic pulsatile activity underlying cortisol secretions as continuous and binary observations, respectively. To estimate the hidden cognitive energy-related state, we use Bayesian filtering. In our proposed architecture, we infer one's cognitive energy-related state using wearable devices rather than monitoring the brain activity directly and close the loop utilizing fuzzy control. To model actuation in the real-time closed-loop architecture, we simulate two types of medications that result in increasing and decreasing the energy levels in the body. Finally, we close the loop using a knowledge-based control approach. The results on ten simulated profiles verify how the proposed architecture is able to track the energy state and regulate it using hypothetical medications. In a simulation study based on experimental data, we illustrate the feasibility of designing a wearable brain machine interface architecture for energy regulation in hypercortisolism. This simulation study is a first step toward the ultimate goal of managing hypercortisolism in real-world situations.

Keywords: closed-loop, energy state, cortisol, hypercortisolism, Bayesian estimation, wearable, fuzzy control

OPEN ACCESS

Edited by:
Lionel Carneiro, The Ohio State University, United States

Reviewed by:
Vincent Wester, Erasmus Medical Center, Netherlands
Margaret F. Keil, Eunice Kennedy Shriver National Institute of Child Health and Human Development (NICHD), United States

***Correspondence:**
Rose T. Faghih
rtfaghih@uh.edu

Specialty section:
This article was submitted to Neuroenergetics, Nutrition and Brain Health, a section of the journal Frontiers in Neuroscience

Received: *22 April 2021*
Accepted: *28 June 2021*
Published: *09 August 2021*

Citation:
Fekri Azgomi H, Hahn J-O and Faghih RT (2021) Closed-Loop Fuzzy Energy Regulation in Patients With Hypercortisolism via Inhibitory and Excitatory Intermittent Actuation. Front. Neurosci. 15:695975. doi: 10.3389/fnins.2021.695975

1. INTRODUCTION

The cortisol hormone is the main stress hormone in an individual's body which is secreted in a pulsatile process (Azgomi and Faghih, 2019; Taghvafard et al., 2019; Wickramasuriya and Faghih, 2019b; Smyth et al., 2020). Cortisol secretion patterns, which are mainly controlled by the hypothalamus, are critical in assessing various functionalities such as regulating blood pressure and adjusting blood glucose levels. So, investigating changes in cortisol secretion would shed some light on one's internal energy state variations (Faghih, 2018; Wickramasuriya and Faghih, 2019b; Smyth et al., 2020). Adrenocorticotrophic hormone (ACTH) (i.e., a tropic hormone) causes the

adrenal cortex to release cortisol in a pulsatile manner (Hakamata et al., 2017; Pednekar et al., 2019, 2020). The hypothalamus employs corticotrophin-releasing hormone (CRH) to stimulate the anterior pituitary to produce ACTH (Faghih, 2014; Faghih et al., 2014). Any irregular patterns in cortisol secretions (e.g., too much cortisol release, which is called hypercortisolism, or not providing a sufficient amount of cortisol, which is called hypocortisolism) may cause the imbalance in internal energy variations (Arnold, 2008; D'Angelo et al., 2015; Harris et al., 2015). These irregularities, which are common among the Cushing's patients who are exposed to the hypercortisolism, lead them to feel fatigue during the daytime and sleep problems at night (Stalder et al., 2016; Vance, 2017). Insufficient release of cortisol early in the morning may result in feeling fatigue during the day. On the other hand, high levels of cortisol in the evening might cause sleep disturbances at night (Dwyer et al., 2019).

While the initial treatment option for Cushing's disease is a surgery with a 78% success rate, evidence shows that the relapse happens in almost 13% of patients (Driessens et al., 2018). For the patients in whom the surgery is not successful or feasible, medical therapy is unavoidable (Pivonello et al., 2015). Due to recent advances in employing novel compounds that can regulate cortisol secretions, medical therapy has attracted more attention (Tritos and Biller, 2017). Nowadays, medical therapy is being suggested in different ways: pre-surgical treatment, post-surgical options for the patients that fail the surgical option, and the primary remedy for those in whom the surgery is not considered as an option (Pivonello et al., 2015).

The clinical observations in Cushing's syndrome patients clearly demonstrate a role for the HPA axis in the regulation of energy balance (Björntorp and Rosmond, 2000; Nieuwenhuizen and Rutters, 2008; Wickramasuriya and Faghih, 2019b). While there exist multiple factors to understand one's energy variations, there is not any specific method to directly infer internal energy state. Hence, it is not possible to present the evidence to show the correlation between energy state and cortisol variations. However, there is evidence that patients with irregular cortisol patterns experience fatigue during day time and disturbed sleep cycles at night. For example, authors in Pednekar et al. (2019, 2020) have shown that the patients with fibromyalgia syndrome, which is also associated with the irregular patterns in cortisol secretions, experience fatigue during the day and sleep disorders at night. Researchers in Crofford et al. (2004) identified lower cortisol levels in the patients with chronic fatigue syndrome. This evidence verifies the potential correlation between cortisol measurements and internal energy state.

As it is discussed, patients with Cushing's syndrome have disturbed circadian rhythm in their sleep cycles. In this regard, medications with inhibitory effects to lower the energy state and help the subjects with more balanced sleep cycles could be helpful. An example of these types of medications could be Melatonin. In the literature, it has been indicated that excessive cortisol secretions associated with Cushing's disease may lead to an irregular Melatonin rhythm (Zisapel et al., 2005; James et al., 2007). So, taking the advantages of Melatonin in improving sleep cycles, we can suggest using this medication for inhibitory effects. Although patients with hypercortisolism usually experience high levels of energy during the evening, they may suffer a lack of sufficient energy levels during the daytime (Pednekar et al., 2019, 2020). As a result, the need for medications to elevate the energy levels is unavoidable. Medications with excitatory effects to enhance energy state and prevent the subjects to feel fatigue during the daytime would be helpful in this regard. An example of these types of medications could be Methylphenidate. As patients with hypercortisolism suffer from not having enough energy levels in the daytime, medications like Methylphenidate could be suggested while implementing the proposed approach in the real world. In literature, it has been validated that taking two doses of Methylphenidate is significantly effective in relieving fatigue (Chaudhuri and Behan, 2004; Blockmans et al., 2006).

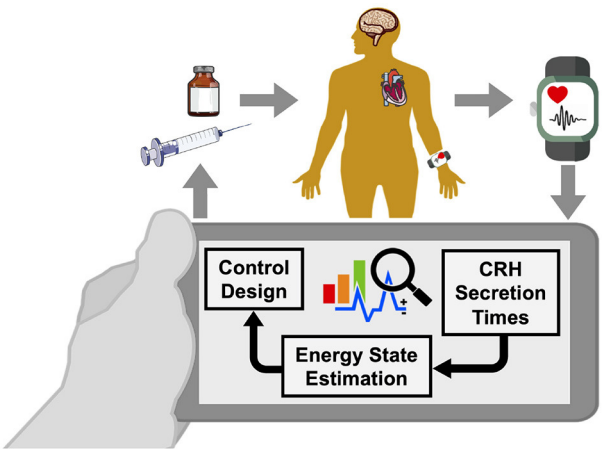

FIGURE 1 | Wearable brain machine interface architecture. Blood cortisol data is being monitored by a wearable-type device. Analyzing the data collected from the human in the loop, we estimate corticotrophin-releasing hormone (CRH) secretion times that result in cortisol secretion. Then, we estimate a hidden energy state. Finally, the designed control algorithm would determine appropriate time and the dosage of medications, and will result in regulating the energy state in patients with hypercortisolism.

Due to the potential medications' side-effects, tolerance, and resistance that a person shows against the use of specific medications, it is highly important to establish a supervision layer that enables automated regulation of medication usage (Fleseriu et al., 2019). We propose our approach by taking the advantages of wearable-type devices capable of monitoring blood cortisol in a non-invasive way as a feedback modality for such supervision. The proposed approach is the first attempt to automate the regulation of medications required to manage the energy levels in patients with hypercortisolism in a closed-loop manner (**Figure 1**).

Recently, there has been an increased interest in employing control theory in advancing modern medication therapies such as goal-directed fluid therapy (Rinehart et al., 2011), cardiopulmonary management (Gholami et al., 2011), fluid resuscitation (Jin et al., 2019), and medically induced coma (Liberman et al., 2013; Yang and Shanechi, 2016). In a similar way, and considering how irregular cortisol secretion patterns affect energy state in patients with hypercortisolism, we leverage

control theory in regulating energy variations in these patients. While there exist medications effective in managing energy levels, there is still a lack of closed-loop and automated architecture for making the decisions on the time and dosage of the medications in real-time. Hence, we construct a virtual patient environment based on the experimental cortisol data for further analysis. Then, we design the control algorithm that can determine the time and dosage of hypothetical simulated medications in a real-time automated fashion.

As someone's energy variations are influenced by changes in their cortisol levels, the objective of this research is to regulate the energy state by monitoring the cortisol secretion patterns. To model the internal energy state and relate it to the cortisol variations, we utilize the state-space model presented in Wickramasuriya and Faghih (2019b). To close the loop, we simulate hypothetical medication dynamics and develop a control system. In the present simulation study, we apply hypothetical medication dynamics as the actuation in a real-time closed-loop brain machine interface architecture (Azgomi and Faghih, 2019; Azgomi et al., 2019). As presented in **Figure 1**, a wearable device measures the cortisol data in a non-invasive manner. We infer the CRH secretion times via a deconvolution algorithm (Faghih, 2014; Faghih et al., 2014; Amin and Faghih, 2018, 2019a,b,c; Pednekar et al., 2019, 2020). We use the state-space approach (Brown et al., 2001; Wickramasuriya and Faghih, 2019b) to link the CRH secretion times, which cause the fluctuations in cortisol levels (Faghih et al., 2015b; Azgomi and Faghih, 2019; Wickramasuriya and Faghih, 2019b, 2020a), to the internal energy state. This state-space representation tracks the internal energy state continuously and provides the capability of utilizing the control systems theory to close the loop. To estimate the hidden cognitive energy-related state in real-time, we employ Bayesian filtering method (Wickramasuriya and Faghih, 2019b). By incorporating hypothetical dynamical system model of medications effective in both decreasing and increasing energy levels (Blockmans et al., 2006; James et al., 2007), and designing a fuzzy controller, we close the loop to regulate the energy state in patients with hypercortisolism in a simulation environment.

In section 2, we explain the steps required for creating the virtual patient environment. We also discuss the state-space model along with the real-time estimation process. We then incorporate the hypothetical medication dynamics and propose a knowledge-based control system to close the loop in real-time. In section 3, we present the outcome of implementing the proposed approach in regulating the energy state in patients with hypercortisolism. More particularly, we present the results on two classes of patients: (1) who do not have the circadian rhythm in their cortisol profiles, and (2) who have the circadian rhythm in their cortisol profiles. The final results demonstrate that our proposed real-time architecture can not only track one's energy state, but also regulate the energy variations in patients with hypercortisolism utilizing the simulated medication dynamics. Section 4 points out the implications of our findings. This simulation study based on the experimental data is the first step toward treating other hormone-related disorders.

2. METHODS

Figure 2 illustrates an overview of the proposed closed-loop architecture. The present study consists of two main parts: the offline process and the real-time closed-loop simulation environment. In the offline part, we first generate multi-day cortisol data for multiple subjects based on their experimental data collected over 24 h. Although there are recent advances in monitoring cortisol levels using wearable devices (Venugopal et al., 2011; Parlak et al., 2018; Parlak, 2021), there is still a lack of technologies for real-time multi-day cortisol data collection. Hence, to design a virtual patient environment, we first follow the results from Wickramasuriya and Faghih (2019b), Brown et al. (2001), and Lee et al. (2016) to simulate cortisol profiles in both healthy subjects and Cushing's patients. To extend our preliminary results presented in Azgomi and Faghih (2019), we simulate data for ten subjects (Faghih, 2014). This offline process enables us to examine the performance of the proposed architecture in multiple cases. By performing deconvolution algorithm, we infer the cortisol secretion times and the circadian upper and lower envelopes. Utilizing Expectation Maximization (EM) approach, we estimate the circadian rhythm forcing function along with model parameters. In the offline stage, we also model dynamical systems for hypothetical medications with both inhibitory (i.e., medications to lower the energy levels) and excitatory (i.e., medications to elevate the energy levels) effects.

As depicted in the bottom section of **Figure 2**, we take the circadian rhythm forcing function in the real-time simulation system and relate the internal energy state to the cortisol secretion times and cortisol upper and lower bound envelopes using the state-space approach. Employing the Bayesian filtering, which uses the estimated model parameters calculated with the offline EM algorithm, we estimate the hidden energy-related state in real-time. Incorporating the dynamical system model of medications and the personalized desired levels of energy, we design a fuzzy controller to close the loop. The deigned control system will take the energy state estimate and determine the time and dosage of each medication as the actuation in the loop. Hence, it controls cortisol variations which will result in energy regulation.

2.1. Data Simulation

Due to the lack of multi-day experimental measurements of healthy subjects and the patients with Cushing's disease, we first simulate multi-day cortisol data profiles (Brown et al., 2001; Faghih, 2014; Lee et al., 2016; Wickramasuriya and Faghih, 2019b). Following Faghih et al. (2014) and Brown et al. (2001), cortisol secretion process could be assumed to follow a second-order stochastic differential equation:

$$\frac{dCort_1(t)}{dt} = -\zeta_1 Cort_1(t) + n(t), \tag{1}$$

$$\frac{dCort_2(t)}{dt} = \zeta_1 Cort_1(t) - \zeta_2 Cort_2(t), \tag{2}$$

where $Cort_1(t)$ and $Cort_2(t)$ are cortisol concentration in adrenal glands and plasma space at time t, respectively (Faghih, 2014).

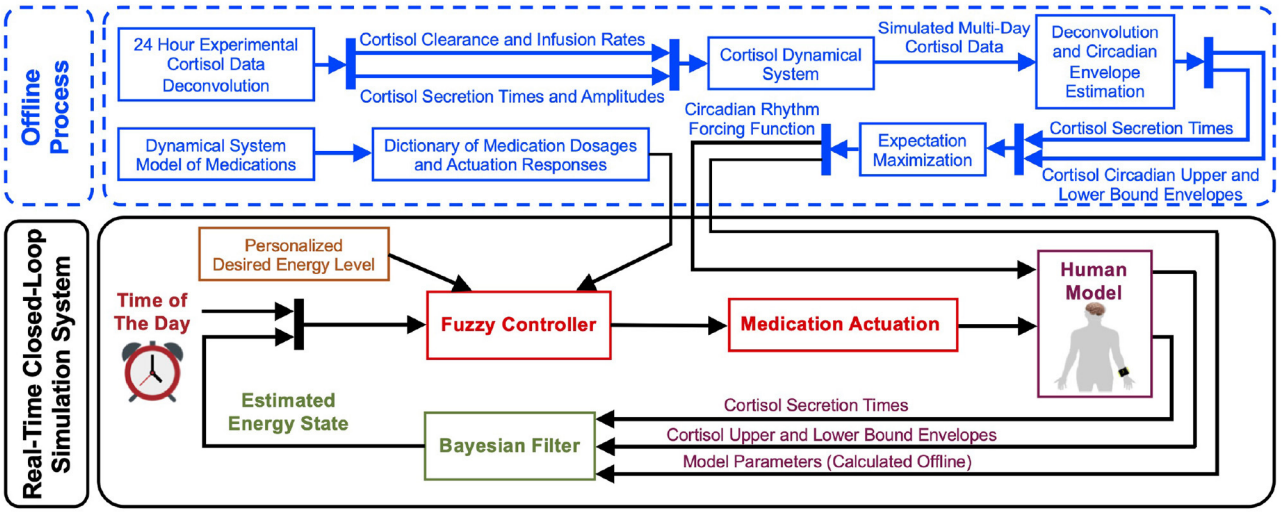

FIGURE 2 | Real-time closed-loop energy regulation. The offline process includes extending the cortisol data profiles for multi-day data creation, simulating the medication dynamics, and estimating the filter parameters required for the closed-loop section. In the real-time closed-loop system, using the state-space representation, the internal energy state gets related to the brain secretion times that result in the cortisol secretions. Then, a Bayesian decoder employs the brain secretion times and the upper and lower cortisol envelopes as the observations to estimate the energy state. Finally, employing the personalized desired energy levels and information regarding the actuation dynamics, a fuzzy controller is generated. The closed-loop system automates the time and dosage of applying simulated medications to regulate the energy state.

Moreover, ζ_1 stands for cortisol infusion rate from adrenal gland to the blood, ζ_2 corresponds to the cortisol clearance rate by the liver (Brown et al., 2001; Faghih et al., 2014). In addition, $n(t)$ represents secretory events (pulses) underlying cortisol release. The output equation $y_k = Cort_2(k) + \psi_k$, where $Cort_2(k)$ is the discretized cortisol concentration in plasma with $\psi_k \sim \mathcal{N}(0, \sigma_\psi^2)$ as the measurement noise with variance σ_ψ^2. We employ estimated model parameters ζ_1 and ζ_2 derived in Faghih et al. (2014). The details of this information are presented in **Supplementary Material**.

To model cortisol secretory events $n(t)$, we follow the approach presented in Brown et al. (2001).

- Healthy Profiles: We use the gamma distribution for pulse inter-arrival times and Gaussian distribution for pulse amplitudes (Brown et al., 2001). The corresponding parameters for gamma distribution are $\alpha = 54$ and $\beta = 39$. The pulse amplitude follows a Gaussian distribution $H_k \sim \mathcal{N}(\mu_k, k_k^2)$, where $\mu_k = 6.1 + 3.93\sin(\frac{2\pi k}{1440}) - 4.75\cos(\frac{2\pi k}{1440}) - 2.53\sin(\frac{4\pi k}{1440}) - 3.76\cos(\frac{4\pi k}{1440})$ and $k_k = 0.1\sqrt{\mu_k}$ (Azgomi and Faghih, 2019; Wickramasuriya and Faghih, 2019b).

To simulate the data for patients with Cushing's disease, we consider two cases: (1) Cushing's patients without circadian rhythms in their cortisol profiles, and (2) Cushing's patients with circadian rhythms in their cortisol profiles. While cortisol variations in patients with Cushing's disease do not follow normal circadian rhythms, at the very early stages of the disease, the circadian rhythms might be slightly dysregulated (Van den Berg et al., 1995; Wickramasuriya and Faghih, 2019b).

- Cushing's patients without circadian rhythm: We follow (Van den Berg et al., 1995; Lee et al., 2016) and consider the inter-arrival times following a gamma distribution that belong to the range of 59 ± 11 min. Regarding the pulse amplitudes, we assume they are within the range of $38 \pm 2.5\ \mu g dL^{-1}\ min^{-1}$, following a Gaussian distribution (Azgomi and Faghih, 2019; Wickramasuriya and Faghih, 2019b),
- Cushing's patients with circadian rhythm: We employ $\mu_k = 38.5 + 1.93\sin(\frac{2\pi k}{1440}) - 1.6\cos(\frac{2\pi k}{1440}) - 1.5\sin(\frac{4\pi k}{1440}) - 3.5\cos(\frac{4\pi k}{1440})$, $k_k = \frac{2.5}{\sqrt{38\mu_k}}$ as the Gaussian distribution parameters in the pulse amplitudes and the same gamma inter-arrival time distribution as described previously for the Cushing's patients with circadian rhythm.

Employing the model parameters ζ_1 and ζ_2 provided in **Supplementary Material** and a vector input of pulse timings and amplitudes $n(t)$ presented above, we simulate the cortisol profiles. We employ coupled differential equations (1) and (2), and add measurement noise to generate cortisol profile data for different subjects in three different situations. More particularly, we simulate the cortisol profiles associated with healthy subjects, Cushing's patients with circadian rhythm in their cortisol profiles and Cushing's patients without circadian rhythm in their cortisol profiles over 5 days for further analysis (Brown et al., 2001; Faghih, 2014, 2018). The resulting multi-day cortisol profiles are presented in **Supplementary Material**. As an example, the results associated with subject 1 are depicted in **Figure 3**.

2.2. State-Space Modeling

Cortisol dynamical system explained above will generate the cortisol observations for our virtual patient environment. We employ the state-space approach presented in Azgomi and Faghih (2019), Wickramasuriya and Faghih (2019b) to relate the hidden cognitive energy-related state to cortisol variations. The

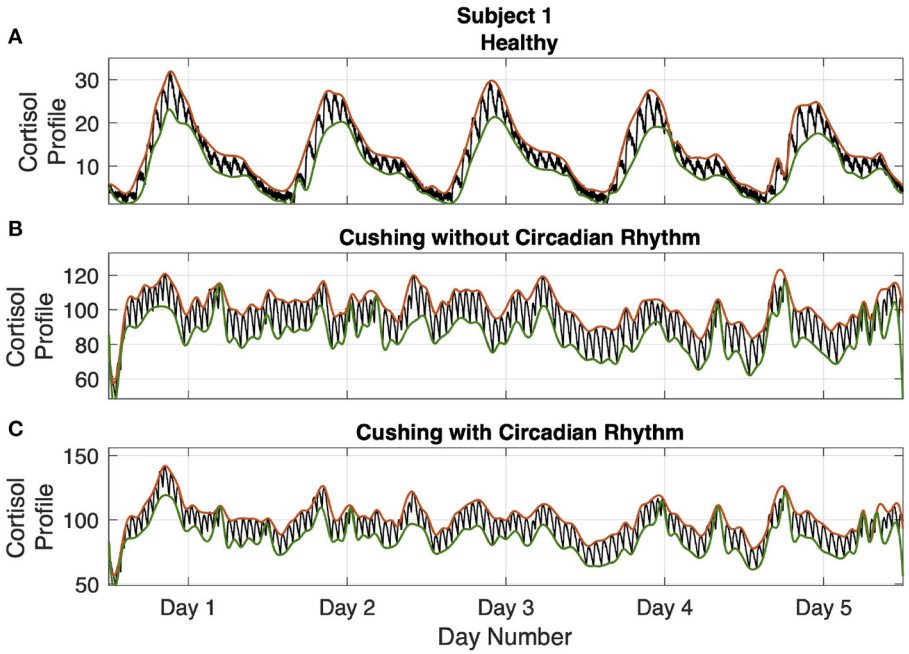

FIGURE 3 | Simulated multi-day cortisol profile - Subject 1. Panel **(A)** displays the healthy profile, panel **(B)** shows the profile associated with the Cushing's patients without circadian rhythm, and panel **(C)** depicts the profiles associated with the Cushing's patients with circadian rhythm. Each panel displays cortisol levels (black curve), upper bound envelopes (orange curve), and lower bound envelopes (green curve).

state-space approach lets us systematically track internal energy state and control it in real-time (Smith et al., 2004). We model the cognitive energy-related state as the following first-order state-space representation:

$$x_k = \rho x_{k-1} + u_k + \epsilon_k + I_k, \tag{3}$$

where x_k is the hidden internal energy-related state, ρ is a person-specific parameter, u_k is the control input, $\epsilon_k \sim \mathcal{N}(0, \sigma_\epsilon^2)$ is the process noise, and I_k is being considered as the forcing function that keeps the energy variations during wakefulness and sleep in 24 h periods. By analyzing the simulated cortisol profiles (Wickramasuriya and Faghih, 2019b), we design the following harmonic forcing function:

$$I_k = \sum_{i=1}^{2} \alpha_i \sin(\frac{2\pi ik}{1440}) + \beta_i \cos(\frac{2\pi ik}{1440}), \tag{4}$$

where the coefficients α_i and β_i along with parameter ρ in (3) for each subject/case are derived using the EM algorithm explained in Wickramasuriya and Faghih (2019b). These parameters are presented in **Supplementary Material**.

Analyzing the discretized cortisol data at a 1 min time resolution, we observe that the presence or absence of the cortisol pulses builds a binary point process (Wickramasuriya and Faghih, 2019b). Hence, we assume the probability of receiving pulses associated with CRH secretion times that results in cortisol secretion, c_k, follows a Bernoulli distribution:

$$P(c_k|p_k) = p_k^{c_k}(1-p_k)^{1-c_k}, \tag{5}$$

where the probability p_k is connected to the energy state x_k by the following sigmoid function:

$$p_k = \frac{1}{1+e^{-(\gamma_0+\gamma_1 x_k)}}. \tag{6}$$

This model relates the probability p_k of observing a CRH pulse event c_k to the energy state x_k through person-specific baseline parameters γ_0 and γ_1 calculated by the offline EM.

In addition to the cortisol secretion times as binary observations, we use the upper and the lower bound envelopes of the blood cortisol measurements as continuous observations to estimate the energy state x_k (Wickramasuriya and Faghih, 2019b). We label these two upper and lower envelopes as R_k and S_k, respectively. Assuming there exists a linear relationship between these envelopes and the corresponding state x_k:

$$R_k = r_0 + r_1 x_k + v_k, \tag{7}$$

$$S_k = s_0 + s_1 x_k + w_k, \tag{8}$$

where $v_k \sim \mathcal{N}(0, \sigma_v^2)$, $w_k \sim \mathcal{N}(0, \sigma_w^2)$, and r_0, r_1, s_0, s_1 are regression coefficients obtained by offline EM algorithm (Prerau et al., 2009; Coleman et al., 2011; Wickramasuriya and Faghih, 2019a).

It is worth mentioning that while there exist recent advances in performing deconvolution methods, there is still lack of real-time deconvolution algorithm. With real-time deconvolution tool, we directly infer the cortisol impulses $n(t)$ in (1) and employ it in further analysis.

2.3. Energy State Estimation

We employ two continuous and one binary observations in the estimation process (Prerau et al., 2009; Coleman et al., 2011; Wickramasuriya and Faghih, 2019a). Taking the CRH pulse events c_k and the upper and lower envelopes R_k and S_k as observations, we perform Bayesian filtering (Coleman et al., 2011; Wickramasuriya and Faghih, 2020b) to estimate the hidden cognitive energy-related state mean x_k and its variance σ_k in two prediction and update steps:

- Prediction step:

$$x_{k|k-1} = \rho x_{k-1|k-1} + I_k + u_k, \tag{9}$$

$$\sigma^2_{k|k-1} = \rho^2 \sigma^2_{k-1|k-1} + \sigma^2_\epsilon. \tag{10}$$

- Update step:

$$A_k = \frac{\sigma^2_{k|k-1}}{\sigma^2_v \sigma^2_w + \sigma^2_{k|k-1}(r_1^2 \sigma^2_w + s_1^2 \sigma^2_v)}, \tag{11}$$

$$\begin{aligned} \hat{x}_k = x_{k|k} = x_{k|k-1} + A_k \Big(& \gamma_1 \sigma^2_v (c_k - p_k) \\ & + r_1^2 \sigma^2_w (R_k - r_0 - r_1 x_{k|k-1}) \\ & + s_1^2 \sigma^2_v (S_k - s_0 - s_1 x_{k|k-1}) \Big), \end{aligned} \tag{12}$$

$$\hat{\sigma}^2_k = \sigma^2_{k|k} = \left(\frac{1}{\sigma^2_{k|k-1}} + \gamma_1^2 p_k (1 - p_k) + \frac{r_1^2}{\sigma^2_v} + \frac{s_1^2}{\sigma^2_w} \right)^{-1}. \tag{13}$$

The p_k presented in (12) is related to the $\hat{x}_k$ by (6). Consequently, the $\hat{x}_k$ is present on both sides of (12) and we employ Newton's method to solve the update equations.

2.4. Dynamic System Model of Medications

The next step in closing the loop and regulating energy-related state is to model the dynamical system of hypothetical medications and include them in control design process. In this research, we focus on the medications that can lead the subjects to reach their desired energy levels (Blockmans et al., 2006; James et al., 2007). In this regard, we consider two classes of medications: (1) for elevating the energy levels required for daily activity (i.e., excitation effect), and (2) for helping the subjects to lower their energy levels in the evening which may help them experience well-ordered sleep cycles at nights (i.e., inhibition effect). To analyze how a specific medication affects one's energy levels and incorporate them in the control design process, we model their dynamics by a second-order state-space representation:

$$\begin{bmatrix} \dot{z}_1(t) \\ \dot{z}_2(t) \end{bmatrix} = \begin{bmatrix} -\theta_{i1} & 0 \\ \theta_{i1} & -\theta_{i2} \end{bmatrix} \begin{bmatrix} z_1(t) \\ z_2(t) \end{bmatrix} + \begin{bmatrix} \eta \\ 0 \end{bmatrix} q(t), \tag{14}$$

where $i = 1, 2$ denotes the type of medications. $y(t) = z_2(t)$ is the estimated energy level and θ_{i1}, θ_{i2} correspond the infusion rate and the clearance rate of each corresponding medication i, respectively. We assume $\boldsymbol{\theta}_i = \begin{bmatrix} \theta_{i1} & \theta_{i2} \end{bmatrix}$. In the state-space representation (14), $q(t) = q_i^* \, \delta(t - \tau_i^*)$ is the actuation input impulses where parameters τ_i^* and q_i^* stand for time and dosage of the corresponding medication i (Faghih, 2014; Faghih et al., 2015a). The η term also determines if the actuation should be excitation (i.e., $\eta = +1$ for elevating the energy level) or inhibition (i.e., $\eta = -1$ for lowering the energy level). With this representation, we analyze how using a specific dosage q_i^* of medication i at time τ_i^* will affect the internal energy levels $z_2(t)$ dynamically. Solving the state-space equation (14) and considering the output equation $y(t) = z_2(t)$, we compute the output at each time step j as:

$$y_j = a_j y_0 + \mathbf{b_j q} + e_j. \tag{15}$$

where $a_j = e^{-\theta_{i2} j}$ and $\mathbf{b_j} = \frac{\theta_{i1}}{\theta_{i1} - \theta_{i2}} \big[(e^{-\theta_{i2} j} - e^{-\theta_{i1} j}) \quad (e^{-\theta_{i2}(j-1)} - e^{-\theta_{i1}(j-1)}) \quad \cdots \quad (e^{-\theta_{i2}} - e^{-\theta_{i1}}) \quad \underbrace{0 \quad \cdots \quad 0}_{N-j} \big]'$. The vector input $\mathbf{q}$ consists of one non-zero element (i.e., $\mathbf{q} = [q_1 \cdots q_N]$, where $q_j = 0, \forall j$ except the one element q_i^* at time τ_i^*) and error term $e_j \sim \mathcal{N}(0, \sigma_e^2)$. Forming the output for the whole time horizon N, we generate the vector representation $\mathbf{y}$ as the observation:

$$\mathbf{y} = \mathbf{A}_\theta y_0 + \mathbf{B}_\theta \mathbf{q} + \mathbf{e}, \tag{16}$$

where $\mathbf{y} = \begin{bmatrix} y_1 \; y_2 \; \cdots \; y_N \end{bmatrix}'$, $\mathbf{A}_\theta = \begin{bmatrix} a_1 \; a_2 \; \cdots \; a_N \end{bmatrix}'$, $\mathbf{B}_\theta = \begin{bmatrix} \mathbf{b_1} \; \mathbf{b_2} \; \cdots \; \mathbf{b_N} \end{bmatrix}'$, and $\mathbf{e} = \begin{bmatrix} e_1 \; e_2 \; \cdots \; e_N \end{bmatrix}'$. To complete the system identification task, we impose the constraint $||\mathbf{q}||_0 = 1$ in the corresponding parameter estimation problem (Dahleh et al., 2004). To find the optimum parameters, we solve the following optimization problem to optimize the error term $J = \mathbf{e}'\mathbf{e}$:

$$\min_{\substack{\boldsymbol{\theta}_i, \mathbf{q} \\ ||\mathbf{q}||_0 = 1}} \; J = \frac{1}{2} ||\mathbf{y} - \mathbf{A}_\theta y_0 - \mathbf{B}_\theta \mathbf{q}||_2^2. \tag{17}$$

Given $\mathbf{y}$, we can estimate $\mathbf{A}_\theta$, $\mathbf{B}_\theta$ (i.e., include $\boldsymbol{\theta}_i$), and $\mathbf{q}$ to obtain the actuation dynamics (Faghih et al., 2015b). As a result of this process, we simulate the way that a specific medication affects the energy levels. In the following part, we explain the control approach and close the loop.

In this *in silico* study, incorporating the hypothetical medication dynamics (14), we design the control strategy to determine the time and the dosage of each medication to regulate the estimated energy state. In the practical case, this system identification step is recommended to be performed in parallel to update the dynamical model parameters in real-time.

2.5. Fuzzy Control System

Fuzzy control, which is known as a knowledge-based control approach, employs the insights about the system, performs the corresponding inference, and makes the control decisions (Garibaldi and Ozen, 2007; Mendes et al., 2019; Yu et al., 2020). As an intelligent approach, it is a powerful bridge from the expertise inference to the real world (Lin et al., 2018; Azgomi

et al., 2019). Any fuzzy controller includes four main parts: rule base, fuzzifier, inference engine, and defuzzifier. In the rule base, we define the rules to achieve our control objective (Zoukit et al., 2019). These IF-THEN rules are derived employing expert knowledge of the system and the corresponding constraints.

In the present study, the estimated cognitive energy-related state and the time of the day are the inputs of the fuzzy controller, and the control output is the time and dosage of the required simulated medications (Azgomi and Faghih, 2019). To design the fuzzy system, we employ information about the personalized levels of energy state and the dictionary of medication dosages and actuation responses (**Figure 2**). We also use two classes of actuation: exciting medications which increase the energy levels, and inhibiting medications which lower the estimated energy levels. The purpose of applying medications with exciting and inhibiting effects is to provide the required energy for daily activity (Pednekar et al., 2020) and lowering the energy-related state to result in a better sleep cycle at nights (Feelders et al., 2019), respectively. Based on the literature and nature of the medications (Blockmans et al., 2006; James et al., 2007), we consider the constraint of applying maximum two medications (i.e., control inputs) per day: one in the morning which increases energy levels, and one in the evening to lower the energy levels. The rule base of the proposed fuzzy controller is presented in **Table 1**.

As an example, to clarify the structure of rules presented in **Table 1**, rule number 1 denotes:

- If the estimated energy state is *High*, and the time is *early in the morning* then the actuation is *positive small*.

To quantify the linguistic variables presented in the rule base, we employ membership functions as the fuzzifiers (Azgomi et al., 2013). Investigating the simulated environment including estimated energy state, hypothetical medication dynamics, personalized levels of energy state, and the rule base, we utilize the appropriate number of relevant membership functions presented in **Figure 4**. As observed in **Figure 4**, we employ six membership functions for time of the day (input 1), three membership functions for estimated energy values (input 2), and seven membership functions for the control output to cover all cases in the rule base (**Table 1**).

We use *Mamdani* inference engine to execute the inference and produce fuzzy outputs (Zulfikar et al., 2018). We employ *minimum* method for both *AND* operation in the fuzzy inputs and implication process for fuzzy output generation. We also use *Maximum* method for rule output aggregation. Consequently, the final fuzzy output will be resulted as:

$$\begin{aligned}\mu_{mamdani}(q) =& \mu_m(q) = \max_j [\mu_j(q)] \\ &= \max_j [min\big(min(\mu_{time}(t), \mu_{state}(x)), \mu_{actuation}(c)\big)] \\ &= \max_j [min(\mu_{time}(t), \mu_{state}(x), \mu_{actuation}(c))].\end{aligned} \tag{18}$$

where j denotes the effective rules at each time step and $\mu_j(q)$ is the resulted fuzzy set. $\mu_{time}(t)$, $\mu_{state}(x)$, and $\mu_{actuation}(c)$ also stand for the membership functions presented in **Figure 4**. To demonstrate the way that this inference engine works, we explain the proposed fuzzy system (18). At each time step, the fuzzy system monitors all the rules presented in **Table 1** and finds the effective rules according to the input membership functions (**Figure 4**). By extracting the corresponding membership degree and executing *AND* operation in each applied rule, it then performs implication between the resulted input fuzzy sets (time and the estimated energy state) and the corresponding output fuzzy membership function (medication actuation). By aggregating results from all applied rules, it generates the final fuzzy output. To produce crisp output out of the generated fuzzy outputs and applying it into the system in real-time, we employ *centroid* defuzzification method:

$$q^* = \frac{\int \mu_m(q).q\ dq}{\int \mu_m(q)\ dq}. \tag{19}$$

At any time step where either the rules with *Zero* actuation output (**Table 1**) are effective, or the output q^* in (19) equals zero, the fuzzy system would determine no need for applied control. At the time t that the fuzzy system results a non-zero output ($q^* \neq 0$), time of actuation would be derived ($\tau^* = t$). Considering the resulted crisp output and constraint to apply maximum two medications per day, the designed control will determine the time and the amplitudes of each medication. Hence, by taking the decisions about the dosage and the desired time of the hypothetical medications [i.e., q^* and τ^* in (14)], the resulted control signal [i.e., u_k in (3)] will be applied to regulate the internal energy state.

TABLE 1 | Fuzzy rule base.

Rule #	Time *(Input 1)*	Energy State *(Input 2)*	Actuation *(Output)*
1	Early morning	High	Positive small
2	Early morning	Low	Positive big
3	Early morning	Medium	Positive medium
4	Late morning	High	Zero
5	Late morning	Low	Positive medium
6	Late morning	Medium	Positive small
7	Early evening	High	Negative medium
8	Early evening	Low	Zero
9	Early evening	Medium	Negative small
10	Late evening	High	Negative big
11	Late evening	Low	Negative small
12	Late evening	Medium	Negative medium

3. RESULTS

In this section, first we present the open-loop results. Then, we present our real-time closed-loop results for two categories of Cushing's diseases: one without circadian rhythm in their cortisol profiles, and another with circadian rhythm in their cortisol profiles. The results associated with ten simulated subjects are presented in **Figures 5–7**.

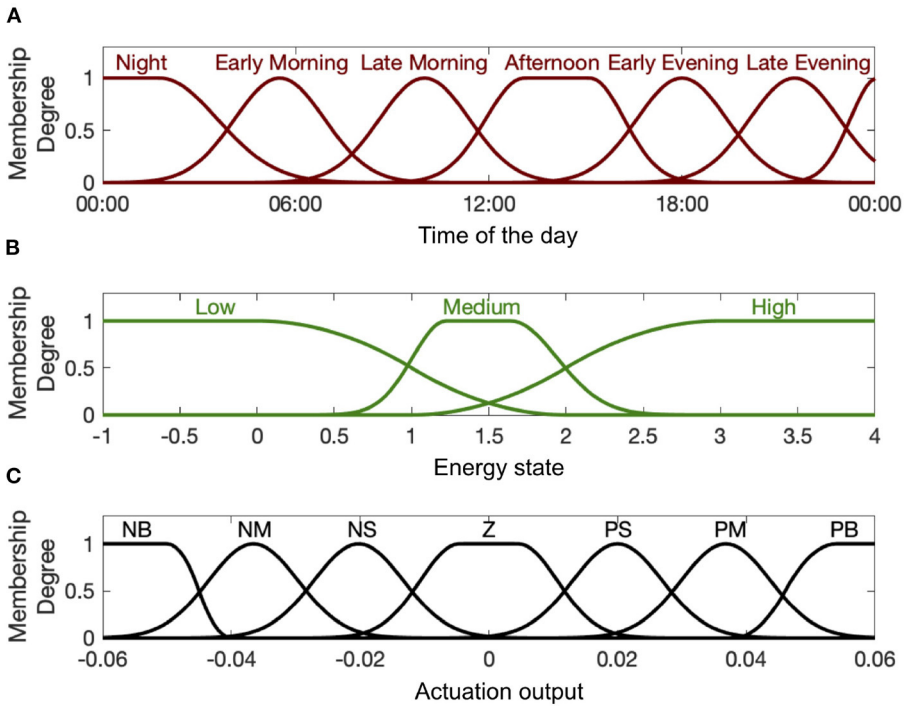

FIGURE 4 | Input and output membership functions. Panel **(A)** shows the first input membership functions describing time of the day. Panel **(B)** shows the input membership functions associated with the estimated energy-related state. Panel **(C)** shows the membership functions for the actuation output (i.e., control signal u_k). The abbreviations P, N, Z, S, M, and B stand for "Positive," "Negative," "Zero," "Small," "Medium," and "Big," respectively.

3.1. Open-Loop (Healthy Subject)

In the first part, we use data associated with healthy subjects to show the tracking performance. As depicted in the left panels of **Figures 5**–**7**, the system tracks the energy state in an open-loop manner. In the middle sub-panel, it is observed that there is not any control in this stage ($u_k = 0$). Top sub-panels show that the estimated energy state has its peak during the daytime (06:00–16:00) and it drops in the evening. It verifies that we successfully track the energy state in the simulated healthy profiles.

3.2. Closed-Loop (Cushing's Patients Without Circadian Rhythm)

In this part, we employ the simulated cortisol data associated with Cushing's patients without circadian rhythm in their cortisol profiles. The results are observed in the middle panels of **Figures 5**–**7**. The white and gray backgrounds correspond to the open-loop and the closed-loop periods, respectively. After day 2, the control is activated and the closed-loop system detects an imbalanced energy state (top sub-panel in the middle panels of **Figures 5**–**7**). Then, the time and dosage of the required simulated medications are produced by the control system (bottom sub-panel in the middle panels of **Figures 5**–**7**). The red pulses stand for the simulated medications with excitation effects, while the blue pulses are associated with the simulated medications with inhibitory effects. Employing the suggested hypothetical medications will lead the generated control input to follow the curves presented in the middle sub-panel of **Figures 5**–**7**. Thereafter, starting day 3 of simulation (once the loop gets closed), the energy state is being regulated.

3.3. Closed-Loop (Cushing's Patients With Circadian Rhythm)

Similar to the previous case, here we investigate the performance of the proposed closed-loop architecture by making use of simulated Cushing's patients' data together with existing circadian rhythm in their cortisol profiles. The results are presented in the right panels of **Figures 5**–**7**. Similarly, the system detects the irregular energy patterns and regulates the energy state variations by designing the corresponding control signals in a closed-loop manner.

4. DISCUSSION AND CONCLUSIONS

Inspired by the fact that CRH plays an undeniable role in internal energy regulation, we proposed our novel approach for regulating the energy-related state using a wearable brain machine interface architecture. In the proposed architecture, we infer one's energy variations by monitoring cortisol data which can be collected using wearable devices in real time (Parlak et al., 2018). We implemented the control algorithm on ten simulated data profiles in healthy subjects and Cushing's patients.

In the offline stage of this research, we simulated the cortisol data for multiple subjects. As it is validated in the literature, we employ stochastic models to simulate multi-day cortisol

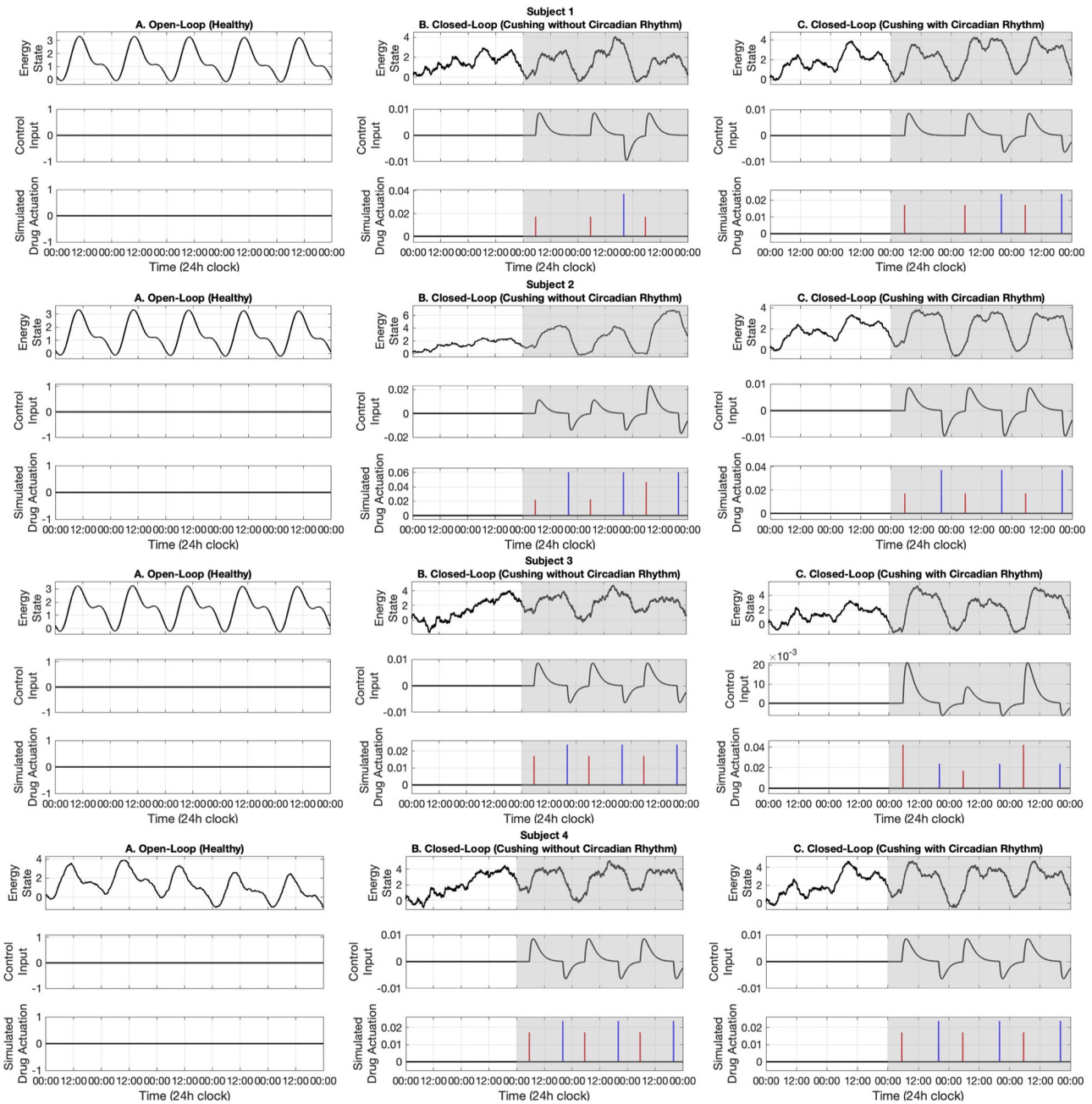

FIGURE 5 | Simulated energy regulation results (Subjects 1–4). For each subject, panel **(A)** displays the open-loop results. Panel **(B)** shows closed-loop results for the Cushing's patients without circadian rhythm, while panel **(C)** shows closed-loop results for the Cushing's patients with circadian rhythm. In each panel: the top sub-panel shows the estimated cognitive energy-related state, the middle sub-panel displays the control input, and the bottom sub-panel depicts the medication injections. Red pulses are related to excitation and the blue pulses are related to inhibition. The white background indicates open-loop simulation (i.e., $u = 0$), while the gray background depicts the closed-loop results.

secretion patterns. Following (Faghih, 2014; Lee et al., 2016; Wickramasuriya and Faghih, 2019b), we consider different gamma distributions for inter-arrival times associated with cortisol secretion impulses. We also assume the pulse amplitudes follow Gaussian distributions. Employing the model parameters that are presented in the manuscript, we simulate cortisol profiles which have day-by-day variability. The stochastic variability existing in model parameters would be viewed as a realistic multi-day case in this *in silico* study. Employing the state-space approach along with EM algorithm, we estimated the model parameters and the forcing circadian function. Using the virtual patient environment, we aimed to track the energy state based

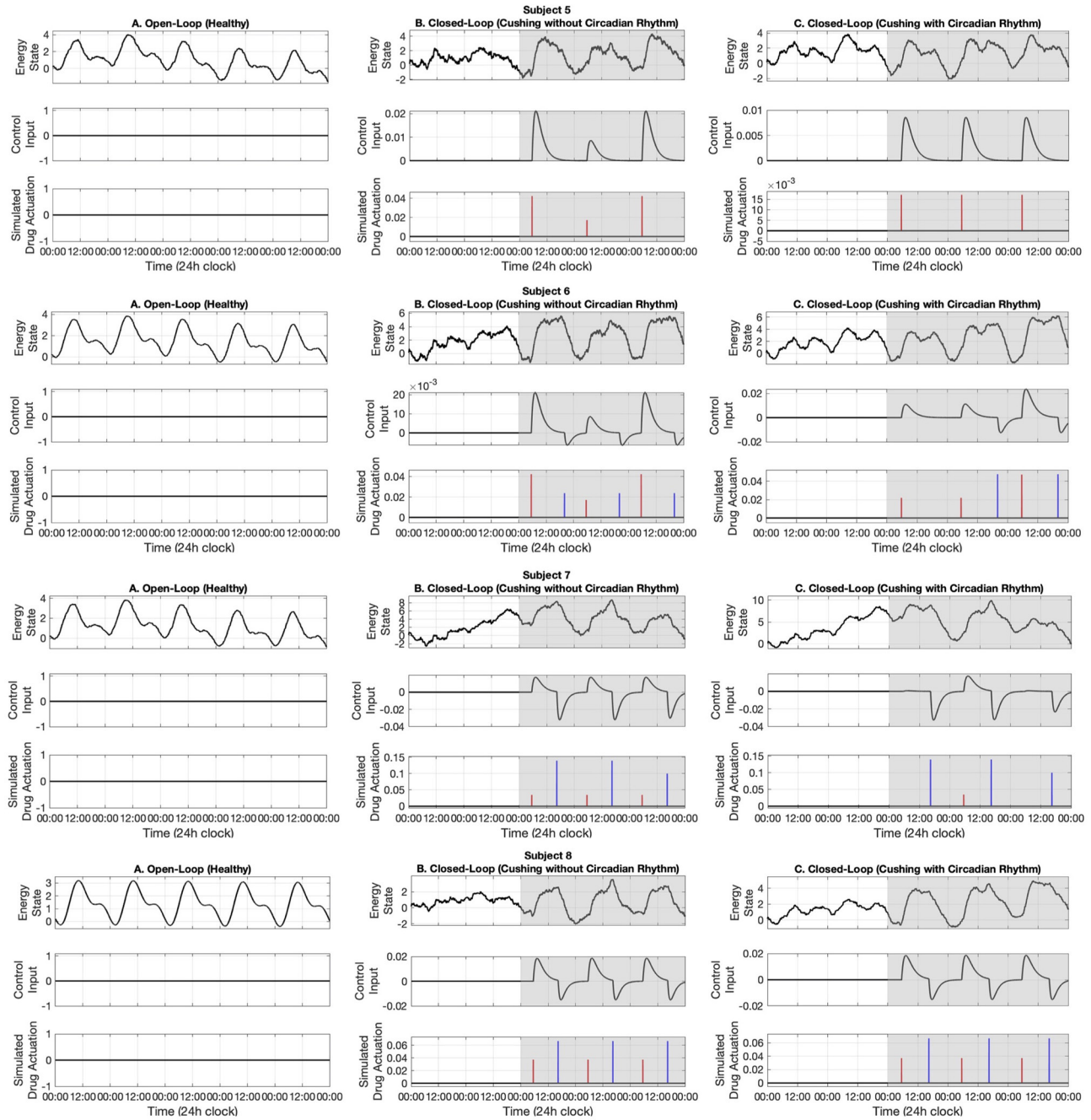

FIGURE 6 | Simulated energy regulation results (Subjects 5–8). For each subject, panel **(A)** displays the open-loop results. Panel **(B)** shows closed-loop results for the Cushing's patients without circadian rhythm, while panel **(C)** shows closed-loop results for the Cushing's patients with circadian rhythm. In each panel: the top sub-panel shows the estimated cognitive energy-related state, the middle sub-panel displays the control input, and the bottom sub-panel depicts the medication injections. Red pulses are related to excitation and the blue pulses are related to inhibition. The white background indicates open-loop simulation (i.e., $u = 0$), while the gray background depicts the closed-loop results.

on the changes in cortisol secretion times and cortisol upper and lower envelopes (see **Figure 2**).

With the goal of tracking the energy state in the proposed architecture, we first simulated a real-time open-loop case. In this part, we used the data associated with healthy subjects. In the present study, due to the lack of real-time deconvolution algorithm, we assume the presence or absence of cortisol secretion forms a binary point process and follows a Bernoulli distribution. Besides, we take the cortisol upper and lower bound envelopes as the continuous observations. Utilizing the EM

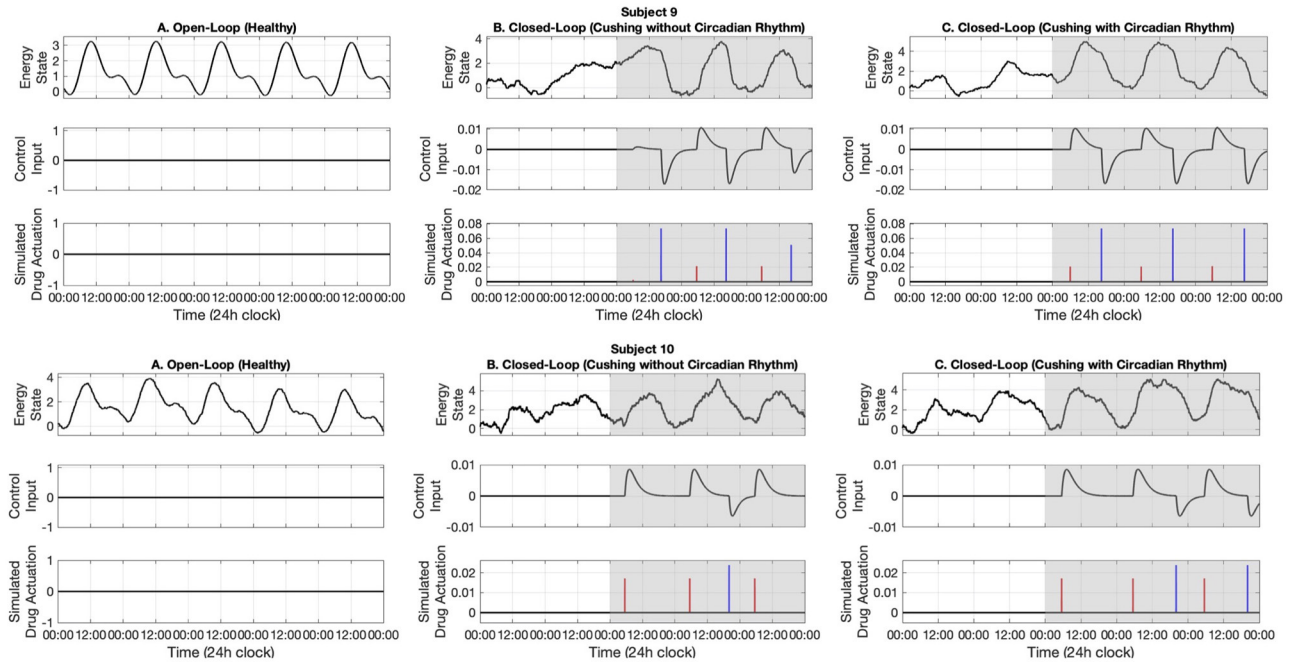

FIGURE 7 | Simulated energy regulation results (Subjects 9 and 10). For each subject, panel **(A)** displays the open-loop results. Panel **(B)** shows closed-loop results for the Cushing's patients without circadian rhythm, while panel **(C)** shows closed-loop results for the Cushing's patients with circadian rhythm. In each panel: the top sub-panel shows the estimated cognitive energy-related state, the middle sub-panel displays the control input, and the bottom sub-panel depicts the medication injections. Red pulses are related to excitation and the blue pulses are related to inhibition. The white background indicates open-loop simulation (i.e., $u = 0$), while the gray background depicts the closed-loop results.

algorithm, we estimated the hidden energy state. As it can be seen in the left panels, with no control implemented (i.e., $u_k = 0$), the energy state variations in simulated healthy profiles are as desired. It is observed that the energy state is at its peak during the daytime and it drops in the evening. It leads to providing enough energy for daily activity and having well-ordered sleep cycles at evening. In fact, this normal condition is because of the well-balanced cortisol secretion patterns in healthy subjects.

In this research, we assumed that including the hypothetical medications would impact the energy state. Hence, we incorporated the simulated medication dynamics as the actuation while closing the loop. In this regard, we first presented the system identification required to design the control system. To incorporate the corresponding medications in real-world implementation of the proposed closed-loop architectures, it is important to pay appropriate attention to medications' half-lives. In the present design, we assumed that the hypothetical medications have prompt effects on one's energy levels. In the case of utilizing long-acting agents, the rules and membership functions should be revised accordingly. While this step is performed in the offline stage of this research, in the practical case, it is recommended to execute it in real-time to update the medication dynamics according to the subject's response. To design the control, we proposed a knowledge-based fuzzy controller. Employing the estimated energy state, personalized desired levels of energy state, and hypothetical medication dynamics we built the rule base, membership functions, and inference engine (see **Figure 2**).

Next, we presented the results of the closed-loop system. In this regard, we employed the cortisol data profiles associated with the Cushing's patients. To depict the performance of the closed-loop system, we assumed the control system gets activated starting day 3, which means the system is open-loop (i.e., $u_k = 0$) in the first 2 days of the simulation. During the open-loop period, we observe that the energy variations do not follow the ideal circadian rhythm. In other words, the patients with hypercortisolism do not have normal cortisol secretion patterns which will cause them to have insufficient energy levels in the day time and experience disturbed sleep cycles at night (Pednekar et al., 2020). Starting day 3, the feedback control system (i.e., $u_k \neq 0$) closes the loop (gray background in **Figures 5**–**7**). In the closed-loop period, the implemented control system detects undesired energy variations and tries to infer the right time and dosage of the simulated medications in real-time. That is to say, the fuzzy structure receives the estimated energy state, employs the rule base (**Table 1**) and membership functions (**Figure 4**), and generates the appropriate control signal. This intermittent control signal is depicted in the bottom sub-panels of **Figures 5**–**7**. When low levels of energy are detected, the red pulses would be generated to adjust the dosage of the required medications with excitation effect to provide required energy levels. On the other hand, once undesired high levels of energy are detected in the evening, the medications with the energy

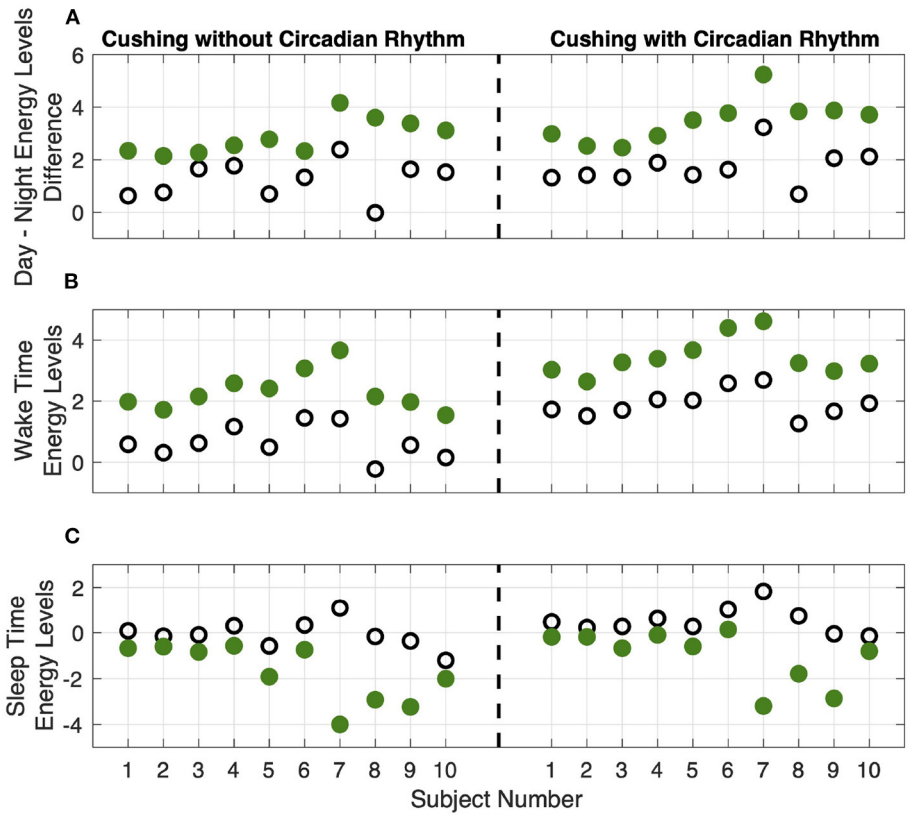

FIGURE 8 | Results analysis. Panel **(A)** shows the difference between average levels of energy in the day and night. Panel **(B)** shows the internal energy growth required for the wake-up time balance. Panel **(C)** shows the decrease in internal energy levels required for sleep time balance. The empty circles and the filled green circles show the results of the open-loop and closed-loop cases, respectively. The left and right sub-panels show the data corresponding to the Cushing patients without and with circadian rhythm in their cortisol profiles, respectively.

lowering effect, i.e., blue pulses, would be suggested to provide the inhibition effect. The required time and dosage of these hypothetical medications are produced by the fuzzy structure. The control actuation signal, which is result of applying these simulated medications, is presented in the middle sub-panels of **Figures 5**–**7**. Considering the constraint of using maximum two medications per day (Bouwer et al., 2000), the energy state is regulated in real-time. It is worth mentioning that in the real-world case, the only needed signal for closing the loop is the time and dosage of required medications. Since this simulation study is the first step to show the feasibility of our proposed approach, we simulated hypothetical medication dynamics to include actuation in the virtual patient environment.

In the final part of our results, we presented the outcomes of our proposed structure on simulated cortisol data profiles associated with the Cushing's patients with circadian rhythm in their profiles. While Cushing's patients do not generally have the required circadian rhythm in their cortisol profiles, there exist some patients with some circadian rhythm in their blood cortisol profiles (Lee et al., 2016). This slight circadian rhythm could be assumed to be available in the patients in their early stages of Cushing's disease. Similar to the results of the Cushing's patients without circadian rhythm, our proposed closed-loop architecture successfully detects the energy irregularities and makes the control decisions in real time.

Analyzing the results of multiple subjects, we observe some interesting outcomes. In the results associated with subjects 1, 5, 6, 7, and 10, we see that for some days no blue pulses (i.e., simulated medications with the inhibition effects) are necessary. It might be because energy levels are already low and would not affect their sleep cycles. In these cases, employing only the medications with excitation effects in the morning may lead to energy regulation in the evening too. These results are shreds of evidence of an intrinsic advantage of our proposed closed-loop architectures which is handling the energy regulation in an automated way and suggesting the medications as needed.

To further depict the efficiency of the proposed closed-loop architecture, we define corresponding metrics (**Figures 8**, **9**). As the first criteria, we analyze the effect of closed-loop system in increasing the difference between average levels of energy in the day and night (top panel of **Figure 8**). As presented, the difference between the average levels of energy in day and night has been increased for all ten simulated subjects in both Cushing's classes (filled green circles compared to the empty circles). As the second criteria, we analyzed the growth of internal energy state in the morning, which will ultimately lead the subjects to wake up with

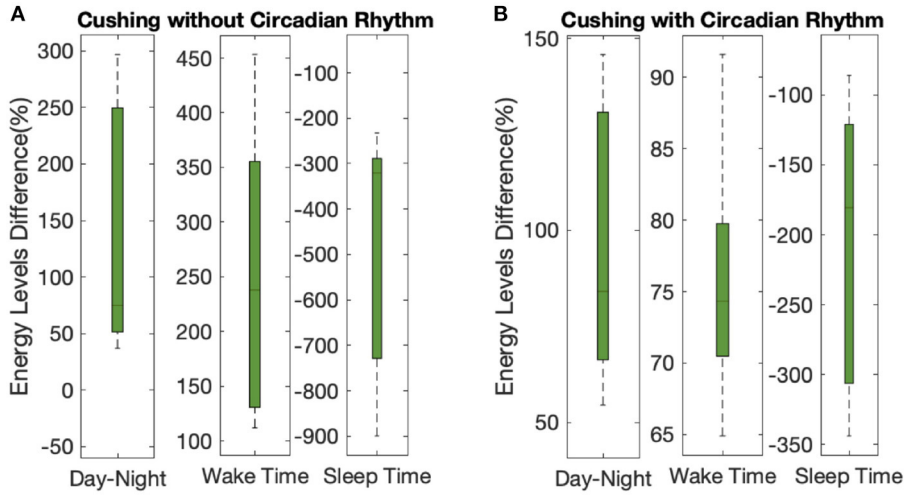

FIGURE 9 | Overall results analysis. The lower- and upper-bounds of the of each box represents the 25th and 75th percentiles of the distribution of each metric for all 10 subjects, and the middle line in each box displays the median. Panels **(A,B)** show the data corresponding to the Cushing patients without and with circadian rhythm in their cortisol profiles, respectively.

higher levels of energy. To do this task, we compared the growth of energy before the start of the day in both open-loop and closed-loop cases (middle panel of **Figure 8**). The observed growth of energy in all simulated subjects will help them to wake up with having more energy required for their daily activities. As the final criteria, we compared the drop of energy levels late at evening (bottom panel of **Figure 8**). It demonstrates how the proposed closed-loop architecture resulted in decreasing the energy levels required for a better sleep cycle. As presented in the bottom panel of **Figure 8**, the internal energy state in patients with Cushing's disease are not decreased sufficiently in the evenings (empty circles). However, in the closed-loop case, by applying the required medications, the simulated energy state has been dropped more efficiently which will further help the subjects to experience more balanced sleep cycle at night.

Analyzing the results on all the simulated subjects, the difference between the average energy levels in day and night in Cushing's patients without and with circadian rhythm in their cortisol profiles is improved by 140% and 97%, respectively (left sub-panels in **Figure 9**). The growth in the energy levels before the wake time in both classes of Cushing's patients is improved by 245% and 75%, respectively (middle sub-panels in **Figure 9**). Similarly, the average drop in the energy levels required for sleep time regulation is improved by 473% and 208% in simulated Cushing's patients without and with circadian rhythm in their profiles has been, respectively (right sub-panels in **Figure 9**). This analysis verify how our proposed architecture is effective in regulating energy levels in a virtual patient environment.

In the offline stage of this research, we simulated multi-day data profiles for healthy subjects and subjects with Cushing's disease. It is worth mentioning that this stage of simulating multi-day data profiles is because of the lack of technology for real-time cortisol measurements. Future advances in wearable technologies would provide the opportunity to continuously monitor the cortisol data and design a system that could take care of inter- and intra-subjects fluctuations. In the present study, we assumed that the suggested medications could be successful in lowering or increasing energy levels. In practical implementation, there exist multiple factors that might cause the proposed architectures (i.e., using suggested medications to regulate internal energy state) to fail and result in less efficiency:

- Diverse sensitivity to glucocorticoid hormones among individuals might prevent to observe similar energy adjustments in response to the medications (Inda et al., 2017).
- Sever dysregulation of the HPA axis, which happens in some endogenous Cushing's syndrome cases, could only be treated by removing the pituitary or adrenal tumor(s) (Nieman et al., 2015).

Implementing the proposed wearable brain machine interface architecture on multiple simulated cortisol profiles, we demonstrated that we can reach energy regulation in hypercortisolism. Simulated results verify that the proposed closed-loop approach has great potential to be utilized in real life. In the prospective practical system, a real-time deconvolution algorithm should be utilized to derive the CRH secretion times. Employing the proposed approach, in addition to taking advantage of wearable devices, which may monitor blood cortisol levels in real-time, the time and dosage of the required medications would be regulated in a closed-loop automated manner. Since the cortisol variations are influenced by a variety of physiological and psychological factors, a future direction of this research could be including additional information from multiple sources while designing the closed-loop system. In the prospective architectures, a multi-input multi-output system will take the information from multiple sources and make the required decisions about taking the medications (i.e., dosage and time). It results in an increase in medications' efficiency and minimize their possible side effects. Future directions of this research could be incorporating all possible medications

and designing the control algorithms with the capability to choose among them. Another possible future direction could be including the system identification process for each medication inside the real-time system. As a result, the way that each specific person responds to a particular medication will be monitored to update the medication dynamics in real-time. Consequently, the personalized control design would be more efficient.

DATA AVAILABILITY STATEMENT

The original contributions presented in the study are included in the article/**Supplementary Material**, further inquiries can be directed to the corresponding author/s.

AUTHOR CONTRIBUTIONS

RF conceived and designed the study. RF and HF developed the algorithms and analysis tools. HF performed the research, analyzed the data, and wrote the manuscript. HF, J-OH, and RF revised the manuscript. All authors contributed to the article and approved the submitted version.

FUNDING

This work was supported in part by NSF Grant 1942585—CAREER: MINDWATCH: Multimodal Intelligent Noninvasive brain state Decoder for Wearable AdapTive Closed-loop arcHitectures, and NSF Grant 1755780—CRII: CPS: Wearable-Machine Interface Architectures.

ACKNOWLEDGMENTS

This paper was presented in part at the proceedings of the Asilomar Conference on Signals, Systems, and Computers (Azgomi and Faghih, 2019).

SUPPLEMENTARY MATERIAL

The Supplementary Material for this article can be found online at: https://www.frontiersin.org/articles/10.3389/fnins.2021.695975/full#supplementary-material

Supplementary Figure 1 | Simulated multi-day cortisol profiles (Subjects 1–4). For each subject, panel **(A)** displays the healthy profile, panel **(B)** shows the profiles associated with the Cushing's patients without circadian rhythm, and panel **(C)** depicts the profiles associated with the Cushing's patients with circadian rhythm. Each panel displays cortisol levels (black curve), upper bound envelops (orange curve), and lower bound envelopes (green curve).

Supplementary Figure 2 | Simulated multi-day cortisol profiles (Subjects 5–8). For each subject, panel **(A)** displays the healthy profile, panel **(B)** shows the profiles associated with the Cushing's patients without circadian rhythm, and panel **(C)** depicts the profiles associated with the Cushing's patients with circadian rhythm. Each panel displays cortisol levels (black curve), upper bound envelops (orange curve), and lower bound envelopes (green curve).

Supplementary Figure 3 | Simulated multi-day cortisol profiles (Subjects 9 and 10). For each subject, panel **(A)** displays the healthy profile, panel **(B)** shows the profiles associated with the Cushing's patients without circadian rhythm, and panel **(C)** depicts the profiles associated with the Cushing's patients with circadian rhythm. Each panel displays cortisol levels (black curve), upper bound envelops (orange curve), and lower bound envelopes (green curve).

Supplementary Table 1 | Infusion and clearance rates associated with the ten simulated cortisol profiles.

Supplementary Table 2 | Parameters used to generate forcing function. ($I_k = \sum_{i=1}^{2} \alpha_i \sin(\frac{2\pi ik}{1440}) + \beta_i \cos(\frac{2\pi ik}{1440})$).

REFERENCES

Amin, M. R., and Faghih, R. T. (2018). "Inferring autonomic nervous system stimulation from hand and foot skin conductance measurements," in *2018 52nd Asilomar Conference on Signals, Systems, and Computers* (Pacific Grove, CA: IEEE), 655–660. doi: 10.1109/ACSSC.2018.8645408

Amin, M. R., and Faghih, R. T. (2019a). Robust inference of autonomic nervous system activation using skin conductance measurements: a multi-channel sparse system identification approach. *IEEE Access* 7, 173419–173437. doi: 10.1109/ACCESS.2019.2956673

Amin, M. R., and Faghih, R. T. (2019b). Sparse deconvolution of electrodermal activity via continuous-time system identification. *IEEE Trans. Biomed. Eng.* 66, 2585–2595. doi: 10.1109/TBME.2019.2892352

Amin, M. R., and Faghih, R. T. (2019c). "Tonic and phasic decomposition of skin conductance data: a generalized-cross-validation-based block coordinate descent approach," in *2019 41st Annual International Conference of the IEEE Engineering in Medicine and Biology Society (EMBC)* (Berlin: IEEE), 745–749. doi: 10.1109/EMBC.2019.8857074

Arnold, L. M. (2008). Understanding fatigue in major depressive disorder and other medical disorders. *Psychosomatics* 49, 185–190. doi: 10.1176/appi.psy.49.3.185

Azgomi, H. F., and Faghih, R. T. (2019). "A wearable brain machine interface architecture for regulation of energy in hypercortisolism," in *2019 53rd Asilomar Conference on Signals, Systems, and Computers* (Pacific Grove, CA: IEEE), 254–258. doi: 10.1109/IEEECONF44664.2019.9049057

Azgomi, H. F., Poshtan, J., and Poshtan, M. (2013). "Experimental validation on stator fault detection via fuzzy logic," in *2013 3rd International Conference on Electric Power and Energy Conversion Systems (EPECS)* (Istanbul: IEEE), 1–6. doi: 10.1109/EPECS.2013.6713039

Azgomi, H. F., Wickramasuriya, D. S., and Faghih, R. T. (2019). "State-space modeling and fuzzy feedback control of cognitive stress," in *2019 41st Annual International Conference of the IEEE Engineering in Medicine and Biology Society (EMBC)* (Berlin: IEEE), 6327–6330. doi: 10.1109/EMBC.2019.8857904

Björntorp, P., and Rosmond, R. (2000). Obesity and cortisol. *Nutrition* 16, 924–936. doi: 10.1016/S0899-9007(00)00422-6

Blockmans, D., Persoons, P., Van Houdenhove, B., and Bobbaers, H. (2006). Does methylphenidate reduce the symptoms of chronic fatigue syndrome? *Am. J. Med.* 119, 167.e23–167.e30. doi: 10.1016/j.amjmed.2005.07.047

Bouwer, C., Claassen, J., Dinan, T. G., and Nemeroff, C. B. (2000). Prednisone augmentation in treatment-resistant depression with fatigue and hypocortisolaemia: a case series. *Depress. Anxiety* 12, 44–50. doi: 10.1002/1520-6394(2000)12:1<44::AID-DA6>3.0.CO;2-C

Brown, E. N., Meehan, P. M., and Dempster, A. P. (2001). A stochastic differential equation model of diurnal cortisol patterns. *Am. J. Physiol. Endocrinol. Metab.* 280, E450–E461. doi: 10.1152/ajpendo.2001.280.3.E450

Chaudhuri, A., and Behan, P. O. (2004). Fatigue in neurological disorders. *Lancet* 363, 978–988. doi: 10.1016/S0140-6736(04)15794-2

Coleman, T. P., Yanike, M., Suzuki, W. A., and Brown, E. (2011). "A mixed-filter algorithm for dynamically tracking learning from multiple behavioral and neurophysiological measures," in *Dynamic Brain: An Exploration of Neuronal Variability and Its Functional Significance* (Oxford Univ. Press), 1–16.

Crofford, L. J., Young, E. A., Engleberg, N. C., Korszun, A., Brucksch, C. B., McClure, L. A., et al. (2004). Basal circadian and pulsatile ACTH and cortisol secretion in patients with fibromyalgia and/or chronic fatigue syndrome. *Brain Behav. Immun*. 18, 314–325. doi: 10.1016/j.bbi.2003.12.011

Dahleh, M., Dahleh, M. A., and Verghese, G. (2004). Lectures on dynamic systems and control. *A A* 4, 1–100. Available online at: https://web.mat.upc.edu/carles.batlle/ioc17013/MIT_6.241/

D'Angelo, V., Beccuti, G., Berardelli, R., Karamouzis, I., Zichi, C., Giordano, R., et al. (2015). Cushing's syndrome is associated with sleep alterations detected by wrist actigraphy. *Pituitary* 18, 893–897. doi: 10.1007/s11102-015-0667-0

Driessens, N., Maiter, D., Borensztein, P., Jaspart, A., Bostnavaron, M., and Beckers, A. (2018). Long-term treatment with metyrapone in four patients with Cushing's disease. *Endocrine Abstracts* 56:GP185. doi: 10.1530/endoabs.56.GP185

Dwyer, R. T., Gifford, R. H., Bess, F. H., Dorman, M., Spahr, A., and Hornsby, B. W. (2019). Diurnal cortisol levels and subjective ratings of effort and fatigue in adult cochlear implant users: a pilot study. *Am. J. Audiol*. 28, 686–696. doi: 10.1044/2019_AJA-19-0009

Faghih, R. T. (2014). *System identification of cortisol secretion: Characterizing pulsatile dynamics* (Ph.D. thesis). Massachusetts Institute of Technology, Cambridge, MA, United States.

Faghih, R. T. (2018). "From physiological signals to pulsatile dynamics: a sparse system identification approach," in *Dynamic Neuroscience*, eds Z. Chen and S. V. Sarma (Springer), 239–265. doi: 10.1007/978-3-319-71976-4_10

Faghih, R. T., Dahleh, M. A., Adler, G. K., Klerman, E. B., and Brown, E. N. (2014). Deconvolution of serum cortisol levels by using compressed sensing. *PLoS ONE* 9:e85204. doi: 10.1371/journal.pone.0085204

Faghih, R. T., Dahleh, M. A., Adler, G. K., Klerman, E. B., and Brown, E. N. (2015a). Quantifying pituitary-adrenal dynamics and deconvolution of concurrent cortisol and adrenocorticotropic hormone data by compressed sensing. *IEEE Trans. Biomed. Eng.* 62, 2379–2388. doi: 10.1109/TBME.2015.2427745

Faghih, R. T., Dahleh, M. A., and Brown, E. N. (2015b). An optimization formulation for characterization of pulsatile cortisol secretion. *Front. Neurosci.* 9:228. doi: 10.3389/fnins.2015.00228

Feelders, R. A., Newell-Price, J., Pivonello, R., Nieman, L. K., Hofland, L. J., and Lacroix, A. (2019). Advances in the medical treatment of Cushing's syndrome. *Lancet Diabetes Endocrinol*. 7, 300–312. doi: 10.1016/S2213-8587(18)30155-4

Fleseriu, M., Petersenn, S., Biller, B. M., Kadioglu, P., De Block, C., T'Sjoen, G., et al. (2019). Long-term efficacy and safety of once-monthly pasireotide in Cushing's disease: a phase III extension study. *Clin. Endocrinol*. 91, 776–785. doi: 10.1111/cen.14081

Garibaldi, J. M., and Ozen, T. (2007). Uncertain fuzzy reasoning: a case study in modelling expert decision making. *IEEE Trans. Fuzzy Syst*. 15, 16–30. doi: 10.1109/TFUZZ.2006.889755

Gholami, B., Bailey, J. M., Haddad, W. M., and Tannenbaum, A. R. (2011). Clinical decision support and closed-loop control for cardiopulmonary management and intensive care unit sedation using expert systems. *IEEE Trans. Control Syst. Technol.* 20, 1343–1350. doi: 10.1109/TCST.2011.2162412

Hakamata, Y., Komi, S., Moriguchi, Y., Izawa, S., Motomura, Y., Sato, E., et al. (2017). Amygdala-centred functional connectivity affects daily cortisol concentrations: a putative link with anxiety. *Sci. Rep*. 7, 1–11. doi: 10.1038/s41598-017-08918-7

Harris, A., Reme, S. E., Tangen, T., Hansen, Å. M., Garde, A. H., and Eriksen, H. R. (2015). Diurnal cortisol rhythm: associated with anxiety and depression, or just an indication of lack of energy? *Psychiatry Res.* 228, 209–215. doi: 10.1016/j.psychres.2015.04.006

Inda, C., Armando, N. G., dos Santos Claro, P. A., and Silberstein, S. (2017). Endocrinology and the brain: corticotropin-releasing hormone signaling. *Endocrine Connect*. 6, R99–R120. doi: 10.1530/EC-17-0111

James, F. O., Cermakian, N., and Boivin, D. B. (2007). Circadian rhythms of melatonin, cortisol, and clock gene expression during simulated night shift work. *Sleep* 30, 1427–1436. doi: 10.1093/sleep/30.11.1427

Jin, X., Bighamian, R., and Hahn, J.-O. (2019). Development and in silico evaluation of a model-based closed-loop fluid resuscitation control algorithm. *IEEE Trans. Biomed. Eng.* 66, 1905–1914. doi: 10.1109/TBME.2018.2880927

Lee, M. A., Bakh, N., Bisker, G., Brown, E. N., and Strano, M. S. (2016). A pharmacokinetic model of a tissue implantable cortisol sensor. *Adv. Healthcare Mater*. 5, 3004–3015. doi: 10.1002/adhm.201600650

Liberman, M. Y., Ching, S., Chemali, J., and Brown, E. N. (2013). A closed-loop anesthetic delivery system for real-time control of burst suppression. *J. Neural Eng.* 10:046004. doi: 10.1088/1741-2560/10/4/046004

Lin, H.-R., Cao, B.-Y., and Liao, Y. Z. (2018). "Fuzzy control," in *Fuzzy Sets Theory Preliminary*, Translated and Compiled by J. Xu; English Proofreading by P-h. Wang (Springer), 73–108. doi: 10.1007/978-3-319-70749-5_3

Mendes, W. R., Araújo, F. M. U., Dutta, R., and Heeren, D. M. (2019). Fuzzy control system for variable rate irrigation using remote sensing. *Expert Syst. Appl*. 124, 13–24. doi: 10.1016/j.eswa.2019.01.043

Nieman, L. K., Biller, B. M., Findling, J. W., Murad, M. H., Newell-Price, J., Savage, M. O., et al. (2015). Treatment of Cushing's syndrome: an endocrine society clinical practice guideline. *J. Clin. Endocrinol. Metab*. 100, 2807–2831. doi: 10.1210/jc.2015-1818

Nieuwenhuizen, A. G., and Rutters, F. (2008). The hypothalamic-pituitary-adrenal-axis in the regulation of energy balance. *Physiol. Behav*. 94, 169–177. doi: 10.1016/j.physbeh.2007.12.011

Parlak, O. (2021). Portable and wearable real-time stress monitoring: a critical review. *Sens. Actuat. Rep*. 3:100036. doi: 10.1016/j.snr.2021.100036

Parlak, O., Keene, S. T., Marais, A., Curto, V. F., and Salleo, A. (2018). Molecularly selective nanoporous membrane-based wearable organic electrochemical device for noninvasive cortisol sensing. *Sci. Adv*. 4:eaar2904. doi: 10.1126/sciadv.aar2904

Pednekar, D. D., Amin, M. R., Azgomi, H. F., Aschbacher, K., Crofford, L. J., and Faghih, R. T. (2019). "A system theoretic investigation of cortisol dysregulation in fibromyalgia patients with chronic fatigue," in *2019 41st Annual International Conference of the IEEE Engineering in Medicine and Biology Society (EMBC)* (Berlin: IEEE), 6896–6901. doi: 10.1109/EMBC.2019.8857427

Pednekar, D. D., Amin, M. R., Azgomi, H. F., Aschbacher, K., Crofford, L. J., and Faghih, R. T. (2020). Characterization of cortisol dysregulation in fibromyalgia and chronic fatigue syndromes: a state-space approach. *IEEE Trans. Biomed. Eng.* 67, 3163–3172. doi: 10.1109/TBME.2020.2978801

Pivonello, R., De Leo, M., Cozzolino, A., and Colao, A. (2015). The treatment of Cushing's disease. *Endocrine Rev*. 36, 385–486. doi: 10.1210/er.2013-1048

Prerau, M. J., Smith, A. C., Eden, U. T., Kubota, Y., Yanike, M., Suzuki, W., et al. (2009). Characterizing learning by simultaneous analysis of continuous and binary measures of performance. *J. Neurophysiol*. 102, 3060–3072. doi: 10.1152/jn.91251.2008

Rinehart, J., Alexander, B., Le Manach, Y., Hofer, C. K., Tavernier, B., Kain, Z. N., et al. (2011). Evaluation of a novel closed-loop fluid-administration system based on dynamic predictors of fluid responsiveness: an *in silico* simulation study. *Crit. Care* 15, 1–12. doi: 10.1186/cc10562

Smith, A. C., Frank, L. M., Wirth, S., Yanike, M., Hu, D., Kubota, Y., et al. (2004). Dynamic analysis of learning in behavioral experiments. *J. Neurosci*. 24, 447–461. doi: 10.1523/JNEUROSCI.2908-03.2004

Smyth, N., Rossi, E., and Wood, C. (2020). Effectiveness of stress-relieving strategies in regulating patterns of cortisol secretion and promoting brain health. *Stress Brain Health* 150:219. doi: 10.1016/bs.irn.2020.01.003

Stalder, T., Kirschbaum, C., Kudielka, B. M., Adam, E. K., Pruessner, J. C., Wüst, S., et al. (2016). Assessment of the cortisol awakening response: expert consensus guidelines. *Psychoneuroendocrinology* 63, 414–432. doi: 10.1016/j.psyneuen.2015.10.010

Taghvafard, H., Cao, M., Kawano, Y., and Faghih, R. T. (2019). Design of intermittent control for cortisol secretion under time-varying demand and holding cost constraints. *IEEE Trans. Biomed. Eng.* 67, 556–564. doi: 10.1109/TBME.2019.2918432

Tritos, N. A., and Biller, B. M. (2017). "Medical therapies in Cushing's syndrome," in *The Hypothalamic-Pituitary-Adrenal Axis in Health and Disease* (Springer), 165–179. doi: 10.1007/978-3-319-45950-9_9

Van den Berg, G., Frölich, M., Veldhuis, J. D., and Roelfsema, F. (1995). Combined amplification of the pulsatile and basal modes of adrenocorticotropin and cortisol secretion in patients with Cushing's disease: evidence for decreased responsiveness of the adrenal glands. *J. Clin. Endocrinol. Metab*. 80, 3750–3757. doi: 10.1210/jcem.80.12.8530629

Vance, M. (2017). "Physical presentation of Cushing's syndrome: typical and atypical presentations," in *Cushing's Disease*, ed E. R. Laws Jr (Elsevier), 57–65. doi: 10.1016/B978-0-12-804340-0.00003-6

Venugopal, M., Arya, S. K., Chornokur, G., and Bhansali, S. (2011). A realtime and continuous assessment of cortisol in isf using electrochemical impedance spectroscopy. *Sens. Actuat. A Phys.* 172, 154–160. doi: 10.1016/j.sna.2011.04.028

Wickramasuriya, D. S., and Faghih, R. T. (2019a). A bayesian filtering approach for tracking arousal from binary and continuous skin conductance features. *IEEE Trans. Biomed. Eng.* 67, 1749–1760. doi: 10.1109/TBME.2019.2945579

Wickramasuriya, D. S., and Faghih, R. T. (2019b). "A cortisol-based energy decoder for investigation of fatigue in hypercortisolism," in *2019 41st Annual International Conference of the IEEE Engineering in Medicine and Biology Society (EMBC)* (Berlin: IEEE), 11–14. doi: 10.1109/EMBC.2019.8857658

Wickramasuriya, D. S., and Faghih, R. T. (2020a). A marked point process filtering approach for tracking sympathetic arousal from skin conductance. *IEEE Access* 8, 68499–68513. doi: 10.1109/ACCESS.2020.2984508

Wickramasuriya, D. S., and Faghih, R. T. (2020b). A mixed filter algorithm for sympathetic arousal tracking from skin conductance and heart rate measurements in pavlovian fear conditioning. *PLoS ONE* 15:e0231659. doi: 10.1371/journal.pone.0231659

Yang, Y., and Shanechi, M. M. (2016). An adaptive and generalizable closed-loop system for control of medically induced coma and other states of anesthesia. *J. Neural Eng.* 13:066019. doi: 10.1088/1741-2560/13/6/066019

Yu, X., He, W., Li, H., and Sun, J. (2020). Adaptive fuzzy full-state and output-feedback control for uncertain robots with output constraint. *IEEE Trans. Syst. Man Cybernet. Syst.* 52, 1–14. doi: 10.1109/TSMC.2019.2963072

Zisapel, N., Tarrasch, R., and Laudon, M. (2005). The relationship between melatonin and cortisol rhythms: clinical implications of melatonin therapy. *Drug Dev. Res.* 65, 119–125. doi: 10.1002/ddr.20014

Zoukit, A., El Ferouali, H., Salhi, I., Doubabi, S., and Abdenouri, N. (2019). "Design of mamdani type fuzzy controller for a hybrid solar-electric dryer: case study of clay drying," in *2019 6th International Conference on Control, Decision and Information Technologies (CoDIT)* (Paris: IEEE), 1332–1337. doi: 10.1109/CoDIT.2019.8820581

Zulfikar, W., Prasetyo, P., Ramdhani, M., and Prasetyo, P. K. (2018). "Implementation of mamdani fuzzy method in employee promotion system," in *IOP Conference Series: Materials Science and Engineering* (IOP Publishing), 012147. doi: 10.1088/1757-899X/288/1/012147

Conflict of Interest: RF is a co-inventor on a provisional patent that designs decoders for estimating energy based on cortisol observations.

The remaining authors declare that the research was conducted in the absence of any commercial or financial relationships that could be construed as a potential conflict of interest.

Publisher's Note: All claims expressed in this article are solely those of the authors and do not necessarily represent those of their affiliated organizations, or those of the publisher, the editors and the reviewers. Any product that may be evaluated in this article, or claim that may be made by its manufacturer, is not guaranteed or endorsed by the publisher.

frontiers in Neuroscience

ORIGINAL RESEARCH
published: 09 September 2021
doi: 10.3389/fnins.2021.718464

Genetic Deletion of KLHL1 Leads to Hyperexcitability in Hypothalamic POMC Neurons and Lack of Electrical Responses to Leptin

Paula P. Perissinotti[1]†, Elizabeth Martínez-Hernández[1]†, Yungui He[2], Michael D. Koob[2] and Erika S. Piedras-Rentería[1]**

[1] Cell and Molecular Physiology Department and Neuroscience Division of the Cardiovascular Research Institute, Loyola University Chicago, Maywood, IL, United States, [2] Institute for Translational Neuroscience and Department of Lab Medicine & Pathology, University of Minnesota, Minneapolis, MN, United States

Kelch-like 1 (KLHL1) is a neuronal actin-binding protein that modulates voltage-gated calcium channels. The KLHL1 knockout (KO) model displays altered calcium channel expression in various brain regions. We analyzed the electrical behavior of hypothalamic POMC (proopiomelanocortin) neurons and their response to leptin. Leptin's effects on POMC neurons include enhanced gene expression, activation of the ERK1/2 pathway and increased electrical excitability. The latter is initiated by activation of the Jak2-PI3K-PLC pathway, which activates TRPC1/5 (Transient Receptor Potential Cation) channels that in turn recruit T-type channel activity resulting in increased excitability. Here we report over-expression of $Ca_V3.1$ T-type channels in the hypothalamus of KLHL1 KO mice increased T-type current density and enhanced POMC neuron basal excitability, rendering them electrically unresponsive to leptin. Electrical sensitivity to leptin was restored by partial blockade of T-type channels. The overexpression of hypothalamic T-type channels in POMC neurons may partially contribute to the obese and abnormal feeding phenotypes observed in KLHL1 KO mice.

Keywords: leptin, Kelch-like 1, $Ca_V3.1$, T-type calcium channels, POMC

OPEN ACCESS

Edited by:
Lionel Carneiro, The Ohio State University, United States

Reviewed by:
Jean-Denis Troadec, Aix-Marseille Université, France
Thomas Alexander Lutz, University of Zurich, Switzerland

***Correspondence:**
Paula P. Perissinotti
peripali@fbmc.fcen.uba.ar
Erika S. Piedras-Rentería
epiedra@luc.edu

†Present address:
Paula P. Perissinotti, Instituto de Fisiología, Biología Molecular y Neurociencias (IFIBYNE, UBA-CONICET), Ciudad Universitaria, Buenos Aires, Argentina
Elizabeth Martínez-Hernández, Department of Physiology and Biophysics, Rush University, Chicago, IL, United States

Specialty section:
This article was submitted to Neuroenergetics, Nutrition and Brain Health, a section of the journal Frontiers in Neuroscience

Received: *31 May 2021*
Accepted: *05 August 2021*
Published: *09 September 2021*

Citation:
Perissinotti PP, Martínez-Hernández E, He Y, Koob MD and Piedras-Rentería ES (2021) Genetic Deletion of KLHL1 Leads to Hyperexcitability in Hypothalamic POMC Neurons and Lack of Electrical Responses to Leptin. Front. Neurosci. 15:718464. doi: 10.3389/fnins.2021.718464

INTRODUCTION

The KLHL1 protein belongs to a family of actin-organizing proteins related to Drosophila Kelch that is expressed primarily in brain tissues, including the cerebral cortex, hippocampus, thalamus, hypothalamus and cerebellum (Nemes et al., 2000; Chen et al., 2008). KLHL1 mRNA is also highly expressed in hypothalamic centers associated with the regulation of energy balance, such as the ventromedial (VMH) and arcuate (ARC) nuclei (Chen et al., 2008). KLHL1 protein modulates voltage-gated calcium channel function among other effects (He et al., 2006). KLHL1 enhances $Ca_V3.2$ T-type function by maintaining the channel at the membrane, it directly interacts with

Abbreviations: AgRP, agouti-related peptide; DIV, days *in vitro*; KLHL1, Kelch-like 1; LRb, leptin receptor; LVA, low-voltage activated; HVA, high-voltage activated, LTS, low-threshold spike, NPY, neuropeptide Y; POMC, hypothalamic proopiomelanocortin positive neurons; TRPC, transient receptor potential cation.

the α_{1H} subunit of the $Ca_V3.2$ channel and promotes its reinsertion into the membrane from the recycling endosome (Aromolaran et al., 2009).

Acute downregulation of KLHL1 using shRNA results in reduced calcium current densities and altered synaptic properties in cultured hippocampal neurons (Perissinotti et al., 2014). KLHL1 KO mice display similar alterations but they also exhibit compensatory expression to sustain calcium current homeostasis in hippocampal neurons, yet they still display synaptic alterations (Perissinotti et al., 2015). Moreover, DRG neurons from KLHL1 KO mice exhibit and uncompensated reduction of $Ca_V3.2$ expression, resulting in reduced neuron excitability and decreased sensitivity to pain (Martínez-Hernández et al., 2020). Thus, deletion of KLHL1 results in differential alteration of calcium currents and neuronal excitability depending on their role in specific nervous system areas.

We recently reported that T-type channels are integral to the signaling cascade that mediates increased excitability in POMC neurons induced by leptin (the Jak2-PI3 kinase-PLCγ pathway). T-type channels ($Ca_V3.1$ or $Ca_V3.2$) exist in a macromolecular complex with TRPC1/5 channels. TRPC1/5 channel activity is recruited by PLCγ, generating membrane depolarization, T-type channel-initiated action potentials and increased excitability (Qiu et al., 2010; Perissinotti et al., 2021).

Here we explored whether genetic ablation of KLHL1 leads to alterations in T-type channel function in the KLHL1 KO hypothalamus. We first assessed the expression levels of TRPC and calcium channels, important targets in the feeding control centers. We found that genetic elimination of KLHL1 resulted over-expression of T-type Cav3.1, increased T-type channel function and neuronal excitability in cultured POMC neurons. Although signaling to the nucleus and Akt/mTOR signal transduction by leptin appear to be normal, the over-expression of Cav3.1 channels circumvented the effect of leptin on POMC neuron excitability, as their basal excitability was already augmented. Leptin sensitivity was restored after partial block of T-type channels with NNC-550396. KLHL1 KO mice displayed adult obesity and abnormal re-feeding after overnight fasting. This work further highlights the importance of T-type channels on the leptin signaling cascade and POMC neuron excitability; abnormally basal hyperexcitability may contribute to the uncharacteristic responses to orexigenic and/or anorexigenic signals observed in KLHL1-KO mice.

MATERIALS AND METHODS

The animal protocols used in this study were reviewed and approved by an independent Institutional Animal Care and Use Committee (IACUC 2016032). KLHL1-knockout (KLHL1-KO) mice were generated in the Laboratory Medicine and Pathology from the University of Minnesota (He et al., 2006). Mixed background WT and KLHL1-KO mice (129S1/Sv-Oca2 C Tyr C Kitl C C57BL/6) and EGFP-POMC$^+$ mice [129S1/Sv-Oca2 C Tyr C Kitl C C57BL/6-Tg (Pomc-EGFP)1Low/J] (The Jackson Laboratory, RRID:IMSR_JAX:009593) were fed *ad libitum* on standard pellet diet. No exclusion criteria were predetermined. Altogether, 15 newborn pups were used for hypothalamic cultures and 34 adult mice (male) for fasting experiments. The study was not pre-registered. Experiments were conducted in the afternoon.

Fasting experiments: Adult male mice (25–31 g, 18–21 weeks old) were housed with *ad libitum* access to both food and water in a controlled environment at 21.5–22.5°C and 12 h light/dark cycles. Experimental manipulations were implemented following IACUC-approved protocols. Mice (WT, $N = 19$; KO, $N = 15$) were fasted with access to water for 20 h (experiments were started at 2 PM) prior to *ad libitum* food access. Pre-fasting, post-fasting and hourly weight after food reintroduction was monitored; weight gain and food consumption were also examined after reintroduction of food.

Cell Culture: Newborn pups (P0, no sex determination) were killed by decapitation after cold-induced anesthesia to abolish perception of pain. Their brains were rapidly removed and whole hypothalami were dissected and cultured as described (Perissinotti et al., 2014) and plated at a density of 25,000–35,000/coverslip and kept in a 5% CO_2 humidified atmosphere at 37°C. Each culture was generated from two independent mice (electrophysiology data was generated from at least three independent batches of cultures, $N = 6$ mice).

Biochemistry: All standard reagents were obtained from Sigma (St. Louis, MO). Crude fractions were extracted from WT or KLHL1-KO whole hypothalamus using standard protocols (Florio et al., 1992). Primary antibody dilutions used: α_{1G} ($Ca_V3.1$), 1:1000 (Millipore, CA); α_{1H} ($Ca_V3.2$), 1:2,000 (Sta. Cruz Biotechnology, CA); TRPC1 (1:200) and TRPC5 (1:200) (Alomone, Israel); Phospho-Stat3 (pSTAT3), 1:500 (Cell Signaling Technology); phosphoinositide 3 phosphate (PI3K), 1:1000 (Cell Signaling Technology); phospho-PI3K (pPI3K), 1:1000 (Cell Signaling Technology); Leptin Receptor (LepRb), 1:1000 (Neuromics). GAPDH, 1:3000 (Enzo Life Science, NY) was used as internal reference to normalize for protein loading unless otherwise noted. Horseradish peroxidase (HRP)-conjugated secondary antibodies were used (1:10,000; Pierce) and developed with Supersignal Femto or West Dura (Pierce, IL) before analysis with a UVP Bioimaging Epichemi3 system (Upland, CA, United States). When necessary, Restore Western Blot Stripping Buffer (Pierce, IL, United States) was used to re-probe membranes.

Immunocytochemistry (IC): WT or KLHL1-KO neurons at 9-11 DIV were prepared as described (Perissinotti et al., 2014). Primary antibody dilutions: $Ca_V3.1$ 1:200 (Alomone) and 1:50 (Millipore); $Ca_V3.2$ 1:5 (supernatant, NeuroMab) and 1:200 (Sta. Cruz); POMC 1:200 (Novus); agouti-related peptide (AgRP), 1:200 (Sta. Cruz). Secondary antibodies: Alexa-594 and –647, 1:2,000 (Molecular Probes, Eugene, OR, United States). Image acquisition was done using a Multiphoton Leica TCS SP5 microscope and analyzed with ImageJ freeware (NIH) (Schneider et al., 2012).

Electrophysiology: Whole-cell patch clamp recordings were performed from WT or KLHL1-KO cultured hypothalamic neurons from 8-10 DIV. Hypothalamic neurons were recorded in external solution containing (in mM) 135 NaCl, 5 KCl, 2 $CaCl_2$, 1 $MgCl_2$, 10 HEPES, 10 glucose and intracellular solution

containing (in mM) 110 K-gluconate, 20 KCl, 2 $MgCl_2$, 1 EGTA, 10 HEPES, 2 ATP-Mg, 0.25 GTP-Li and 10 phosphocreatine-Tris. Pipette resistances were 3.2–4.5 MΩ. Cells with series resistance (R_s) < 20 MΩ were used; R_s was compensated online (>80%). Data was acquired with and analyzed with pClamp 10 software (Molecular Devices). Cell capacitance was measured as described (Perissinotti et al., 2015). Drugs: NNC-550396 dihydrochloride and leptin were purchased from Tocris (Bristol, United Kingdom).

Current-Voltage Relationships (I–V Curves) were performed as described in Perissinotti et al. (2015) and Bean (1985). Briefly, currents were elicited from a holding potential (V_H) = −90 mV (or –50) and depolarized for 150 ms to a test potential (V_T) = −70 to + 60 mV, in 10 mV increments.

Current kinetics: Current activation and inactivation were assessed by stepping the neuron from V_H = −90 mV to V_T = −50 to −20 mV for 150 ms. The rate of activation was estimated from the current rise time from 10 to 90% of its maximum value (rise time 10–90%); these measurements were favored over the calculation of the time constant of activation (τ_{on}) to minimize the contribution of the inactivation process on the activation rate value. Time constant of inactivation (τ_{off}) was obtained from mono-exponential fits. Current deactivation τ was measured by fitting with a mono-exponential function the decaying phase of tail currents elicited from V_H = −90 mV to V_T = −30 mV and back to V_T = −60 to −140 mV.

Steady-state analysis: Steady-state activation (SSA) was analyzed with protocols stepping from V_H = −90 (or –50) mV to V_T = −90 to 0 mV (ΔV = 10 mV) for 12 ms followed by repolarization to –100 mV to evoke inward tail currents. Data were fitted by a single Boltzmann function of the form $I_{max}/[1 + \exp {}^{(V}50^{-V)/k}] + m$, where I_{max} is maximal current, V_{50} is half-voltage of activation, *k* is slope factor, and m is baseline. Steady-state inactivation (SSI) was determined by stepping the membrane potential to various pre-pulse voltage levels (V_{pre} = −110 to 0 mV, 1V = 10 mV) for 1 s before depolarization to a fixed test level (–30 mV) to evoke channel opening. The resulting data were also fitted to a Boltzmann function.

The following equation was used to calculate the theoretical steady-state current (I_{stst}): $I_{stst} = G\ (V_H) * I/I_{max}\ (V_H) * (V_H$ – 50 mV), where I_{stst} is the current in the steady-state or "window current," G is the conductance at holding voltage V_H that was obtained experimentally using the state activation (SSA) protocol and adjusted to a Boltzmann equation (not normalized), I/I_{max} is the fraction of T-type channels available at holding voltage V_H that was obtained experimentally from the steady state inactivation (SSI) protocol and adjusted to a Boltzmann equation, and 50 mV is the estimated reversal potential for calcium (Bijlenga et al., 2000; Lambert et al., 2014; Rivero-Echeto et al., 2021). Reversal potential for Ca^{2+} ions (E_{Ca}) was calculated from current-voltage (I-V) curves.

Recovery from inactivation: T-type channel recovery from inactivation was studied with a paired-pulse protocol. T-type current was inactivated with a 400 ms pulse to −30 mV; a second 50 ms pulse to −30 mV was applied to assess recovery after a variable recovery period at V_H = −90 mV. Data was plotted as recovery time *vs.*% recovery; values were fitted with a double exponential function and a weighted tau (τ_W) was calculated according to: $\tau_W = A^*\tau_1 + B^*\tau_2$, where A and B are preexponential values that refer to the fraction of channels that is recovered with a given τ; A + B = 1.

Calcium influx: Calcium influx was determined by the current integral evoked by an action potential (AP). The AP waveform consisted of a digitized action potential with a resting potential of −70 mV, an upstroke of 116 mV/ms to a peak voltage of +50 mV, followed by a repolarizing slope at −65 mV/ms to a hyperpolarizing potential of −90 mV. The repolarization from after-hyperpolarization slope was 0.78 mV/ms to resting conditions. In a set of experiments (WT or KO-like ramps experiments) the action potential was preceded by a rate of membrane depolarization and a rheobase similar to that recorded in current clamp configuration in WT or KLHL1-KO neurons in response to a ramp rate of 20 pA/s. Influx normalization by capacitance was not necessary as it produced similar results as without normalization. The LVA component was isolated by the subtraction method; these protocols were applied from V_H of −50 or −90 mV prior to clamping the voltage at −70 mV for 10 ms before the triggering of the AP, so no changes in the driving force should be expected.

Resting membrane potential (RMP): RMP was recorded in continuous trace mode without current injection for 20 s and averaged; voltages were corrected for liquid junction potentials.

Spontaneous burst analysis: RMP was recorded for 10 min. and spontaneous APs were identified for burst analysis using the Poisson surprise algorithm with a minimum burst surprise value of 5 to obtain the Poisson surprise value, burst length, spike number ($n > 3$), intra-burst frequency and mean intra-burst interval (Grace and Bunney, 1984; Legendy and Salcman, 1985; Sachdev et al., 1991; Wichmann and Soares, 2006).

Input resistance: Whole cell input resistance (R_{in}) was determined after setting the membrane potential to −60 mV in response to a −60 pA current step.

Membrane excitability: AP discharges were triggered by 3 consecutive depolarizing ramps at rates of 20, 40m and 60 pA/s (1.5 s duration) from a presetting membrane potential of −75 mV (Balasubramanyan et al., 2006; Lu et al., 2006). The rheobase was determined as the minimum amount of current required for firing an action potential.

Shape of single AP: APs were evoked from a presetting voltage of −50 mV (to avoid T-type current activation) by a 3 ms-long rectangular pulse in steps of 50 pA.

Statistical Analysis

These experiments were exploratory with no pre-determined endpoint and no data was excluded from the analyses. No blinding, no randomization, and no sample size calculation were performed. All measurements were done in at least three independent cell cultures. Results are presented as mean ± SEM. The parameter "*n*" indicates number of cells unless otherwise stated and "N" the number of animals. No test for outliers has been applied. The normality of data distribution was assessed by the Kolmogorov-Smirnov test. Statistical analysis was performed with the Sigma Plot 11 Software. Statistical

significance ($P < 0.05$) was determined using either one/two-way analysis of variance (ANOVA) with Fisher LSD's *post hoc* test for comparisons between multiple groups or an independent samples *t*-test for comparisons between two groups. Statistical significance ($P < 0.05$) for two proportions was determined using the Z-test.

RESULTS

KLHL1 Deficiency Leads to Up-Regulation of $Ca_V3.1$ α_{1G} T-Type Channels in the Hypothalamus

The hypothalamus plays an important regulatory role in feeding, TRPC1/5 and $Ca_V3.1/2$ (α_{1G}/α_{1H}) channels are crucial components in the signal transduction pathway induced by leptin that leads to neuronal excitability (**Figure 1A**; Qiu et al., 2010; Perissinotti et al., 2021). We explored the expression levels of these channels in the KLHL1-KO hypothalamus, as this mice model displays compensatory changes in calcium channel expression and excitability in other brain areas. As seen in **Figure 1B**, no changes in TRPC1/5 levels were observed in the KLHL1 KO compared to WT ($P > 0.05$, *t*-test). However, KLHL1-KO mice displayed a considerable increase in $Ca_V3.1$ α_{1G} channel expression and no statistical changes in the levels of $Ca_V3.2$ (**Figure 1B**, $P < 0.05$, *t*-test).

We next explored other key leptin signaling molecules to assess additional leptin intracellular signaling pathways (**Figure 1C**). We probed the expression levels of LRb receptor, as well as STAT3 and PI3K phosphorylation levels as reporters of non-electrical signaling pathways of leptin such as signaling to the nucleus and Akt/mTOR pathway activation (Buettner et al., 2006; Williams et al., 2011). No changes in leptin receptor levels or its downstream effectors were observed in the KLHL1-KO compared to WT hypothalamus (**Figure 1C**, $P > 0.05$, *t*-test).

Larger T-Type Channel Expression in KLHL1-KO Leads to Increased T-Type Current Density

Enhanced T-type channel expression could lead to abnormal oscillatory responses; thus, we characterized and assessed the impact of increased hypothalamic $Ca_V3.1$ protein expression on POMC neuron function and their electrical responses to leptin, which positively regulates these neurons. Cultured hypothalamic neurons were studied from 8-10 days *in vitro* (DIV). Immunocytochemistry analysis from KLHL1-KO ($KLHL1^{-/-}$) cultures yielded similar results to our previous analysis of WT neurons (Perissinotti et al., 2021). From a total of 44 neurons, the distribution of $POMC^+$ *vs.* $AgRP^+$ neurons was 89 *vs.* 11% ($P < 0.05$, Z-test, **Figure 2A**). **Figure 2B** shows a representative bright-field microscopic image of cultured hypothalamic neurons and a representative confocal ICC image, depicting a cluster of POMC-positive neurons in an area of comparable size. **Figures 2C,D** corroborate the expression of $Ca_V3.1$ and $Ca_V3.2$ in KLHL1-KO POMC neurons (no changes in the cellular distribution of channels were observed among WT and KO neurons).

We analyzed the response to leptin in a subset of WT pyramidal neurons using electrophysiology (other neuronal morphologies were not explored); from a total of 19 neurons, 79% responded positively to leptin (excitable), 5% were inhibited and 16% did not respond (**Figure 2E**), as we previously reported (Perissinotti et al., 2021). Neuron cultures from $KLHL1^{-/-}$/EGFP-$POMC^{+/-}$ mice were used to verify the identity of POMC neurons (**Figure 2F**). Ca^{2+} current properties from WT and KLHL1-KO neurons are shown in **Figure 2G**; average traces of low-voltage activated (LVA) and high-voltage activated (HVA) currents were elicited by depolarizing steps from $V_H = -90$ or -50 mV, respectively. Note that LVA currents (red traces) were larger in KLHL1-KO neurons compared to WT, whereas no changes were observed in the HVA component. Overall, total T-type current density was 40% larger in KLHL1-KO neurons (6.2 ± 0.9 *vs.* 8.7 ± 0.8 pA/pF at -30 mV, $P < 0.05$, *t*-test) (**Figure 2E**), corrobating a functional increase in these currents as suggested by the increased protein levels (**Figure 1B**). We defined three distinct groups of neurons according to their I-V curves: neurons that expressed only high-voltage activated (HVA) current ($I_{LVA\ peak} = 0$ pA/pF in the histogram in **Figure 2H**, right), neurons that expressed HVA and low LVA current density levels (LD, $I_{LVA\ peak} < 6$ -pA/pF) and neurons that expressed HVA and high LVA current density (HD, $I_{LVA\ peak}$ from 6 to 20 -pA/pF). The incidence of neurons with HD LVA was much larger in KLHL1-KO neurons (66.7% *vs.* 39.3% in WT; $P < 0.05$, Z-test; **Figure 2I**).

Biophysical analysis of T-type calcium currents (**Figure 3**) depicts changes consistent with an overexpression of the α_{1G} component ($Ca_V3.1$) in KLHL1-KO neurons. As seen in **Figure 3A**, the rise time of activation from –40 to –20 mV was significantly smaller (faster); for instance, the rise time at -40 mV was 10.9 ± 0.9 ms in WT compared to 7.9 ± 0.6 ms in KLHL1-KO neurons ($P < 0.05$, *t*-test). The time constant of inactivation was different at two voltages only (-30 and -40 mV (WT, 33.9 ± 2.7 ms *vs.* KO, 25.5 ± 2.2 ms at -40 mV), **Figure 3B**; $P < 0.05$, *t*-test). Recovery from inactivation (RFI) was faster in KLHL1-KO neurons ($\tau_{W,KLHL1-KO} = 204 \pm 15$ ms *vs.* $\tau_{W,WT} = 305 \pm 33$ ms, $P < 0.05$, *t*-test, **Figure 3C**). The current deactivation time constant was slower in KLHL1-KO neurons (**Figure 3D**) at all ranges tested (e.g., $\tau_{deactivation,-60mV}$ was 4.8 ± 0.4 ms for WT and 6.4 ± 0.5 ms for KLHL1-KO neurons). Lastly, steady-state analysis shows that V_{50} values for activation (SSA) and inactivation (SSI) were both discretely but significantly shifted ~ -2 mV in KLHL1-KO compared to WT neurons (**Figure 3E**; $P < 0.05$, *t*-test). SSA V_{50} was -41.8 ± 0.7 mV in WT (Perissinotti et al., 2021) compared to -44.3 ± 0.9 mV in KLHL1-KO ($P < 0.05$, *t*-test); no change in the slope factor *k* was observed (5.2 ± 0.3 for WT and 5.1 ± 0.3 for KO). Comparably, SSI V_{50} changed from -65.4 ± 1.0 mV in WT (Perissinotti et al., 2021) to -67.5 ± 0.7 mV in KO ($P < 0.05$, *t*-test), and the slope factor *k* changed from 7.1 ± 0.5 to 6.1 ± 0.2 ($P < 0.05$, *t*-test). Accordingly, the changes in the steady-state activation and inactivation curves in KLHL1-KO neurons resulted in a ~ -4 mV shift in the cross point of

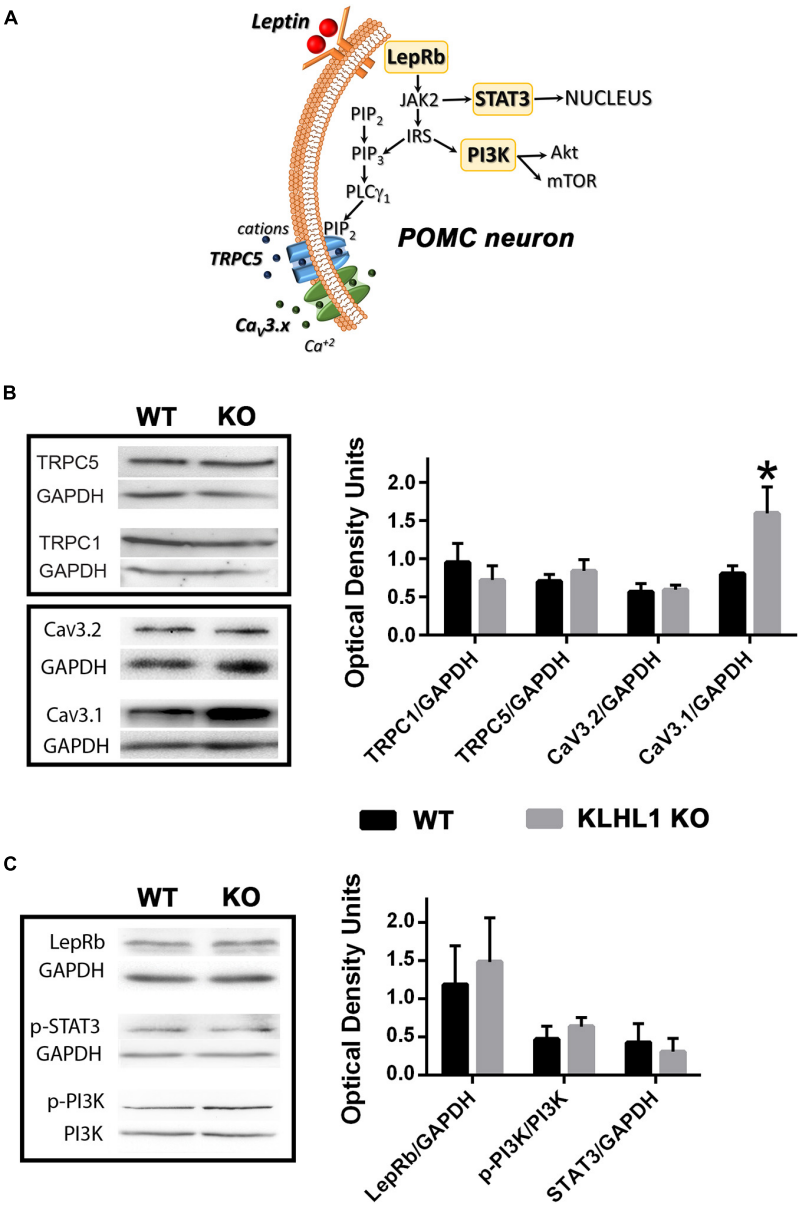

FIGURE 1 | Overexpression of $Ca_V3.1$ T-type calcium channels in KLHL1-KO mice hypothalamus. **(A)** Pleiotropic signaling of leptin in POMC hypothalamic neurons. Leptin binding to its receptor LRb results in the downstream activation of JAK2. STAT3 is subsequently phosphorylated and mobilized to the nucleus resulting in *de novo* gene expression. Activation of insulin receptor substrate (IRS) stimulates Akt- and mTOR pathways *via* activation of phosphorylated PI3K and the production of PIP3. The activation of PLCλ1 by PIP3 mediates the activation of TRPC1/5 channels, recruiting T-type CaV3.1/2 channels thought membrane depolarization. **(B)** Western blot analysis from hypothalamic extracts assessing TRPC1, TRPC5, $Ca_V3.2$ and $Ca_V3.1$ channel levels; $Ca_V3.1$ protein levels are doubled in KLHL1-KO hypothalamus. Bars show densitometric quantification normalized to GAPDH. Data represent means ± S.E.M (TRPC1, $n = 3$ each; TRPC5, $n = 4$ each; $Ca_V3.2$, $n = 5$ each; $Ca_V3.1$, $n = 5$ each). $^*P < 0.05$, *t*-test, $t = 2.230$, df = 8. **(C)** Western blot analysis from hypothalamic extracts assessing LRb, pPI3K and STAT3 levels. Bars show densitometric quantification normalized to GAPDH or PI3K. Data represent means ± SEM ($n = 4$ each; pSTAT3 $n = 3$ each).

the window currents (shaded area under the steady-state curves, **Figure 3D**).

Intrinsic Properties of KLHL1-KO Hypothalamic Neurons

As shown in **Figure 4A**, the RMP of KLHL1-KO neurons was depolarized by ∼2 mV compared to WT ($P < 0.05$, *t*-test). We calculated the T-type window current using the steady-state activation and inactivation curves fitting parameters (Bijlenga et al., 2000; Lambert et al., 2014; Perissinotti et al., 2021; Rivero-Echeto et al., 2021). **Figure 4B** depicts T-type window currents as function of voltage. The superimposed dashed lines show interpolated values for RMP (Y-axis), pinpointing the T-type steady-state current at the respective RMP. Steady-state window currents

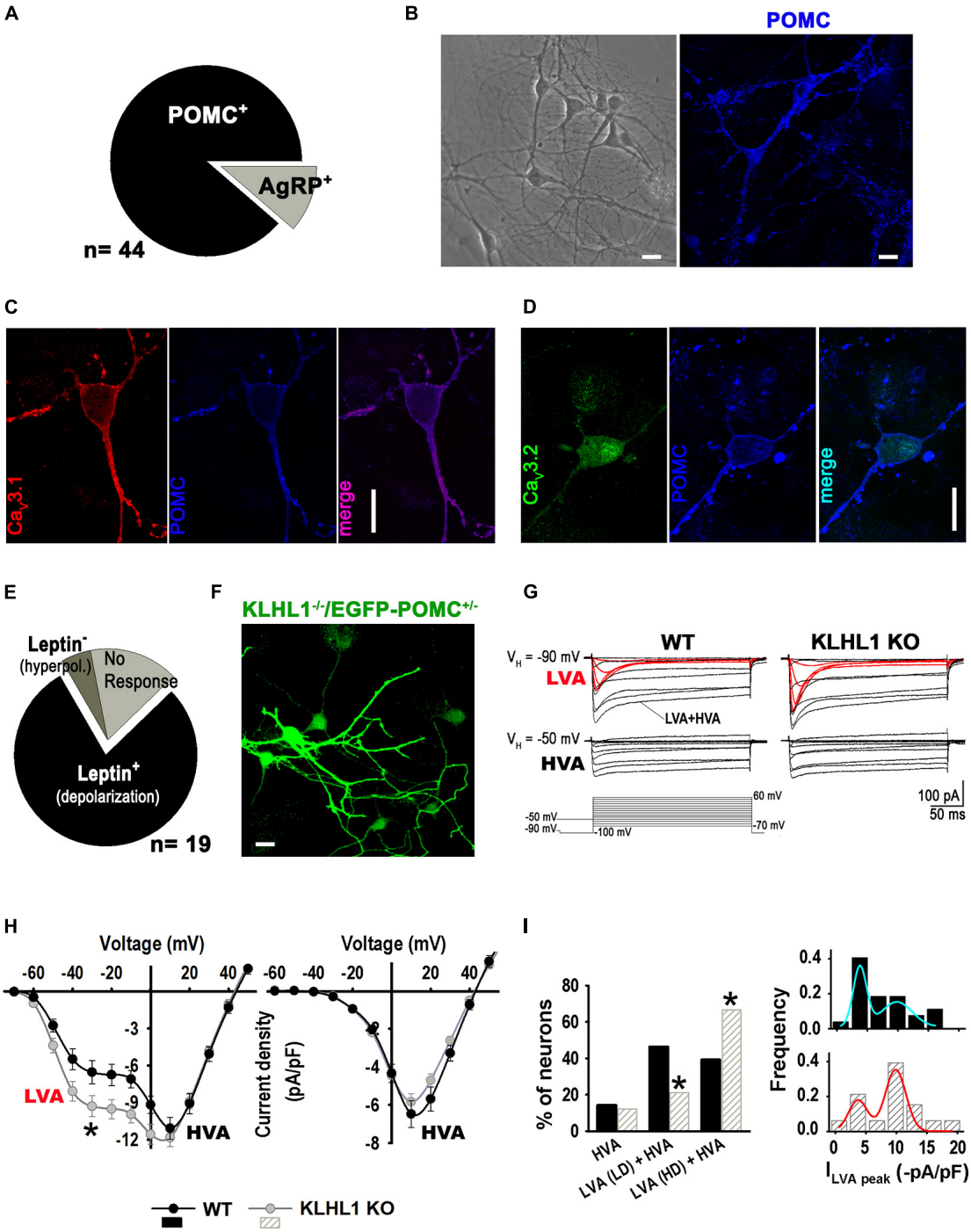

FIGURE 2 | *Up-regulation of T-type current density in KLHL1-KO hypothalamic neurons.* **(A)** Distribution of POMC^{+} and AGRP^{+} neurons in culture (the total neuron number was not assessed). **(B) Left:** Bright-field image of cultured hypothalamic KLHL1-KO neurons at 10 DIV. **Right:** Example of confocal image showing positive POMC^{+} neurons (blue). **(C,D)** Detection of T-type α_{1G} ($Ca_V3.1$, red) and T-type α_{1H} ($Ca_V3.1$, green) in POMC neurons. Bar size, 20 μm. **(E)** Summary of electrophysiology responses in KLHL1 KO hypothalamic cultured neurons. **(F)** Detection of POMC^{+} neurons using neurons from KLHL1 KO mice crossed-bred with mice displaying EGFP^{+} expression driven by the POMC promoter. **(G)** Average current traces obtained using the square voltage protocols shown. LVA refers to low-threshold activated calcium currents (T-type, Ca_V3 channels). HVA refers to high-threshold activated calcium channels. **(H)** Average current-voltage relationship (I-V curve) profiles in WT (n = 26) and KLHL1-KO (n = 28) hypothalamic neurons obtained from V_H of –90 mV (left) or a V_H of –50 mV (right), $^{*}P < 0.05$ (from –60 to 0 mV), t-test; for –30 mV: t = 2.183 (df = 52). **(I) Left:** Comparison of the relative contribution of each neuronal group found: HVA, neurons expressing only high-voltage activated current; LVA (LD) + HVA, neurons expressing HVA and low LVA current density levels (LD, $I_{LVA\ peak}$ < 6 -pA/pF); and LVA (HD) + HVA, neurons expressing HVA and high LVA current density (HD, $I_{LVA\ peak}$ from 6 to 20 -pA/pF). $^{*}P < 0.05$, Z- test. **Right:** LVA current density histogram fitted with superimposed Gaussian functions.

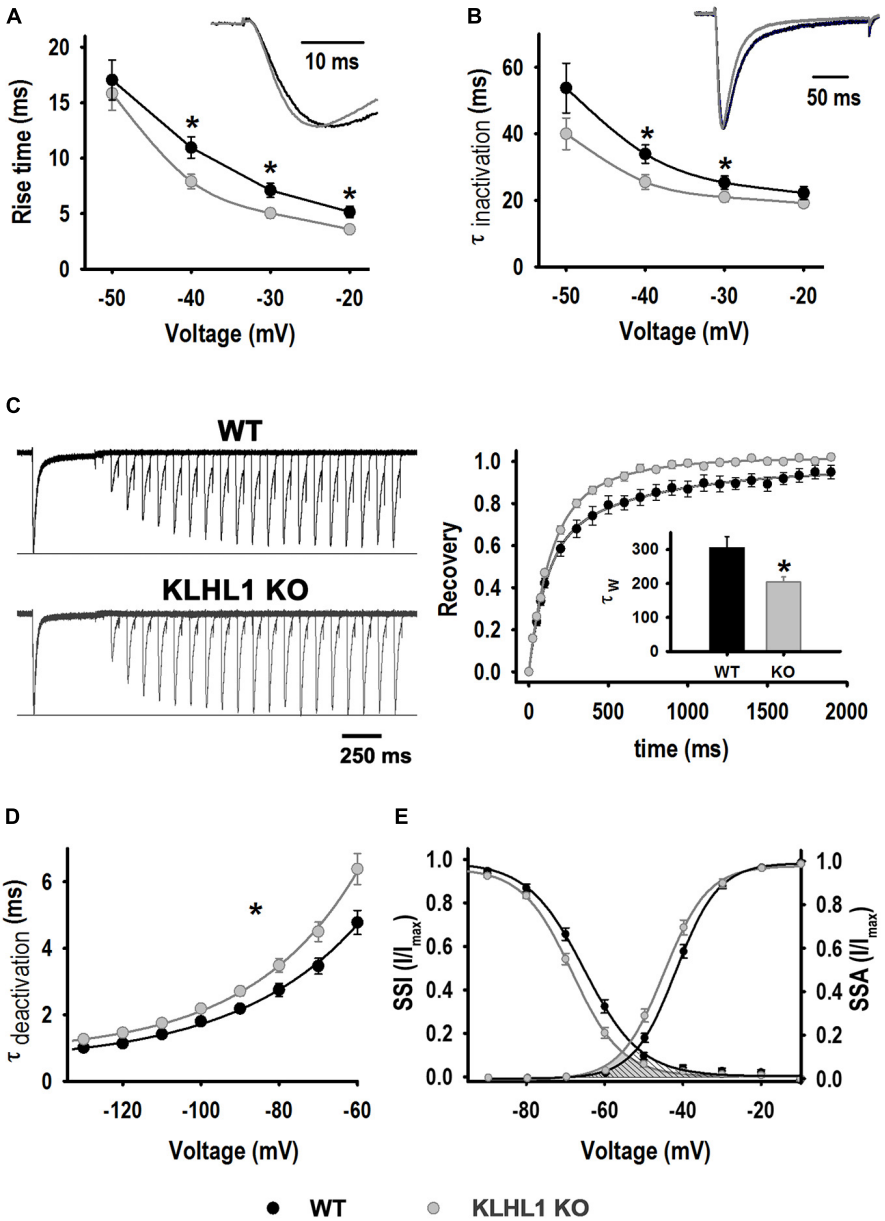

FIGURE 3 | LVA current properties. **(A)** Activation kinetics. Time taken by the current to change from 10% to 90% [Rise time (10–90%)] as function of voltage for WT (n = 21) and K-LHL1-KO (n = 26) neurons. *P < 0.05, t-test, for –40 mV: t = 2.723 (df = 45), for –30 mV: t = 2.743 (df = 45) and for –20 mV: t = 2.735 (df = 45). **(B)** Time constant of inactivation ($\tau_{inactivation}$) as function of voltage for WT (n = 21) and KLHL1-KO (n = 25) neurons. *P < 0.05, t-test, for –40 mV: t = 2.432 (df = 45), for –30 mV: t = 1.807 (df = 45). **(C) Right:** Trace examples of recovery rate from inactivation. **Left:** % recovery *vs.* recovery time (n = 10 for WT and n = 11 for KLHL1 KO). Inset: Recovery time constant (τ_W) values. *P < 0.05, t-test, t = 2.719 (df = 19). **(D)** Time constant of deactivation ($\tau_{deactivation}$) for WT (n = 16) and KO (n = 23) neurons. *P < 0.05 at all voltage tested, t-test: t = 2.515 (–60 mV), t = 2.488 (–70 mV), t = 2.419 (–80 mV), t = 2.666 (–90 mV), t = 2.405 (–100 mV), t = 2.757 (–110 mV), t = 2.837 (–120 mV), t = 2.433 (–130 mV), df = 37. **(E)** SSA and SSI. SSA values obtained for WT: V_{50} = –41.8 ± 0.7 mV and k = 5.2 ± 0.3 (n = 22), KLHL1–KO: V_{50} = –44.3 ± 0.9 mV* and k = 5.1 ± 0.3 (n = 27). *P < 0.05, t-test, t = 2.090 (df = 47). SSI values for WT neurons: V_{50} = –65.4 ± 1.0 mV, k = 7.1 ± 0.5 (WT, n = 21); KLHL1 KO: V_{50} = –67.5 ± 0.7 mV* and k = 6.1 ± 0.2* (n = 27). *P < 0.05, t-test, t = 1.736 for V_{50} and t = 2.251 for k, df = 46.

displayed a leftward shift in KLHL1-KO neurons (P < 0.05, Two-way ANOVA). Noticeably, the steady-state calcium current at the RMP was ∼2.3 times larger for KLHL1-KO than WT neurons.

The presence of window currents is related to spontaneous firing pattern and neuronal excitability; indeed, the percentage of POMC neurons displaying spontaneous firing of action potentials was 31% (10 of 35) in WT compared to 54% (21 of 39) in KLHL1-KO (P < 0.05, Z-test). The firing pattern was different in KO neurons, displaying lower mean-intraburst interval (1.1 ± 0.3 s for WT *vs.* 0.5 ± 0.1 s for KO) and higher intra-burst frequency compared to WT (P < 0.05, t-test). No

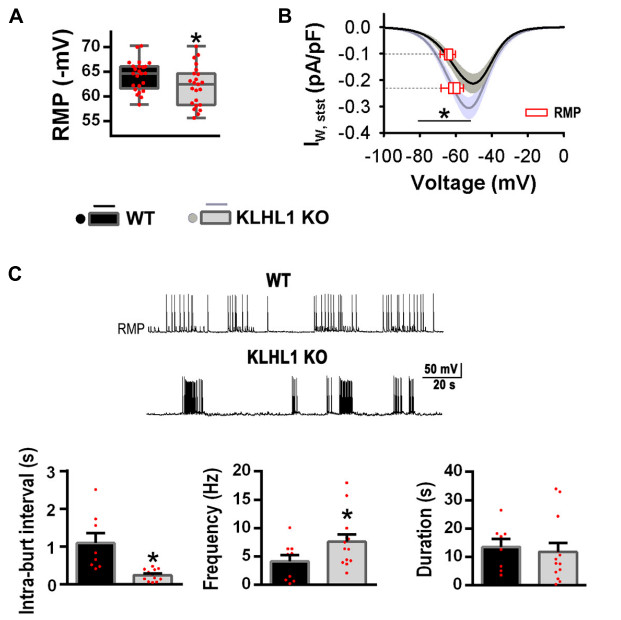

FIGURE 4 | Increased T-type window currents and burst-firing patterns in KLHL1-KO neurons. **(A)** Resting membrane potential (RMP) in WT (n = 24) and KLHL1-KO (n = 23) neurons. *P < 0.05, t-test, t = 2.120 (df = 45). **(B)** T-type steady-state currents in WT (n = 18) and KLHL1-KO (n = 23) neurons. Window currents were calculated for each recording neuron from the SSA and SSI curves fitted to a Boltzmann function; SEM is indicated in gray. The steady-state current at the RMP (empty red box plot) is indicated for both genotypes. *P < 0.05, Two Way ANOVA, $F_{1,139}$ = 13.468 (from –50 to –80 mV). There is a statistically significant interaction between the genotype and the voltage ($F_{11,420}$ = 2.300) (from –20 to –80 mV). **(C) Top:** Example of firing patterns in WT and KLHL1-KO neurons. **Botton:** Mean-intraburst interval, frecuency and duration of the burst activity. *P < 0.05, t-test, t = 3.770 for mean-intraburst interval and t = 1.900 for frequency (df = 18, n = 8 for WT, n = 12 for KLHL1 KO).

TABLE 1 | Passive and active properties of WT and KLHL-1 KO hypothalamic neurons.

	WT	KLHL1 KO
Passive properties		
R_{in} (GΩ)	1.52 ± 0.10(47)	1.40 ± 0.09(45)
C_m (pF)	24.5 ± 2.2(26)	26.8 ± 2.0(28)
Action potential		
Peak (mV)	42.1 ± 3.9(12)	49.5 ± 2.7(12)
Duration at base (ms)	8.3 ± 0.7(12)	10.2 ± 1.4(12)
Rise time (ms)	5.2 ± 0.5(12)	4.9 ± 0.2(12)
Fall time (ms)	3.1 ± 0.3(12)	5.3 ± 1.5(12)
AHP depth below V_m (mV)	5.9 ± 0.8(12)	6.1 ± 1.3(12)
AHP duration to 50% (ms)	72.2 ± 19.0(12)	54.9 ± 15.8(12)

AHP, after-hyperpolarization. The input resistance (R_{in}), the capacitance (C_m) and the shape of single action potential in hypothalamic neurons were not significantly different between genotypes.
P > 0.05, t-test.

significant difference in the burst duration was observed between genotypes (P < 0.05, t-test) (**Figure 4C**).

Membrane excitability was assesed using depolarizing current ramps (20, 40, and 60 pA/s) from a preset membrane potential of ∼–75 mV to circumvent spontaneous firing. Of note, cell capacitance, input resistance and the shape of single APs were indistinguisable between WT and KLHL1-KO neurons (**Table 1**). **Figure 5A** shows examples of the AP firing evoked at 20 and 40 pA/s ramp rates in WT and KLHL1-KO neurons. Note that a large low-threshold spike (LTS) response was elicited by the 20 pA/s ramp rate in KLHL1-KO neurons. In contrast, a faster ramp rate (40 pA/s) was necessary to evoke such response in WT neurons. A LTS response refers to a large membrane depolarization mediated by an increase of T-type calcium conductance. These results are in line with the high T-type current density observed in KLHL1-KO cultures (**Figures 2–4**). To quantitatively analyze the voltage responses to the current ramps, three different measurements were calculated: the rheobase, the number of APs triggered, and the rate of membrane potential depolarization preceding the first AP (i.e., the slope of depolarization, $\Delta V/\Delta t$) (**Figure 5A**) (Perissinotti et al., 2021).

All the data indicates increase excitability in KLHL1 KO neurons. The rheobase was ∼25% lower in KLHL1-KO neurons than WT across all ramp rates tested (P < 0.05, t-test). Similarly, the number of action potentials was increased by ∼50% at ramp rates of 20 and 40 pA/s in KLHL1-KO neurons (P < 0.05, t-test). In addition, the rate of membrane depolarization was ∼2 times faster in KLHL1-KO than WT mice (58.3 ± 5.3 *vs.* 28.0 ± 2.6 mV/s for a ramp rate of 20 pA/s; P < 0.05, t-test).

Due to the unique biophysical properties of T-type currents, their contribution is noticeable during an action potential, as seen in **Figure 5B** (left trace), where the LVA calcium influx in response to an action potential waveform (APW) was 72% larger in KLHL1-KO neurons (P < 0.05, t-test). Faster rates of membrane depolarization favor T-type channel activity because they induce less current inactivation prior to activation of an action potential (Gutierrez et al., 2001). To determine whether differences in the T-type channel recruitment yield the observed alterations in membrane excitability between genotypes, we determined LVA calcium influx in: (1) WT neurons during an AP preceded by a slow rate of membrane depolarization with a rheobase similar to that observed in WT neurons in response to a ramp rate of 20 pA/s ("WT-like ramp," $\Delta V/\Delta t$ ∼30 mV/s, rheobase ∼20 pA), and (2) KLHL1-KO neurons during an AP preceded by a fast rate of membrane depolarization with a rheobase similar to that observed in KLHL1-KO neurons in response to a ramp rate of 20 pA/s ("KO-like ramp," $\Delta V/\Delta t$ ∼60 mV/s, rheobase ∼14 pA) (**Figure 5B**). The KO-like ramp protocol favored T-type channel recruitment (red arrow) and produced greater LVA calcium influx during an action potential in KLHL1-KO neurons. In contrast, a WT-like protocol recruited less T-type channels, producing a small LVA-mediated calcium influx during an action potential in WT neurons. In average, KLHL1-KO neurons displayed ∼4.5 times more LVA calcium influx than WT neurons (P < 0.05, t-test, **Figure 5B**, right panel). Furthermore, application of micromolar concentrations of T-type blocker NNC 55-0396 (10 μM) to KLHL1-KO neurons increased the rheobase level, slowed down the rate of membrane depolarization and reduced the triggered number of APs in

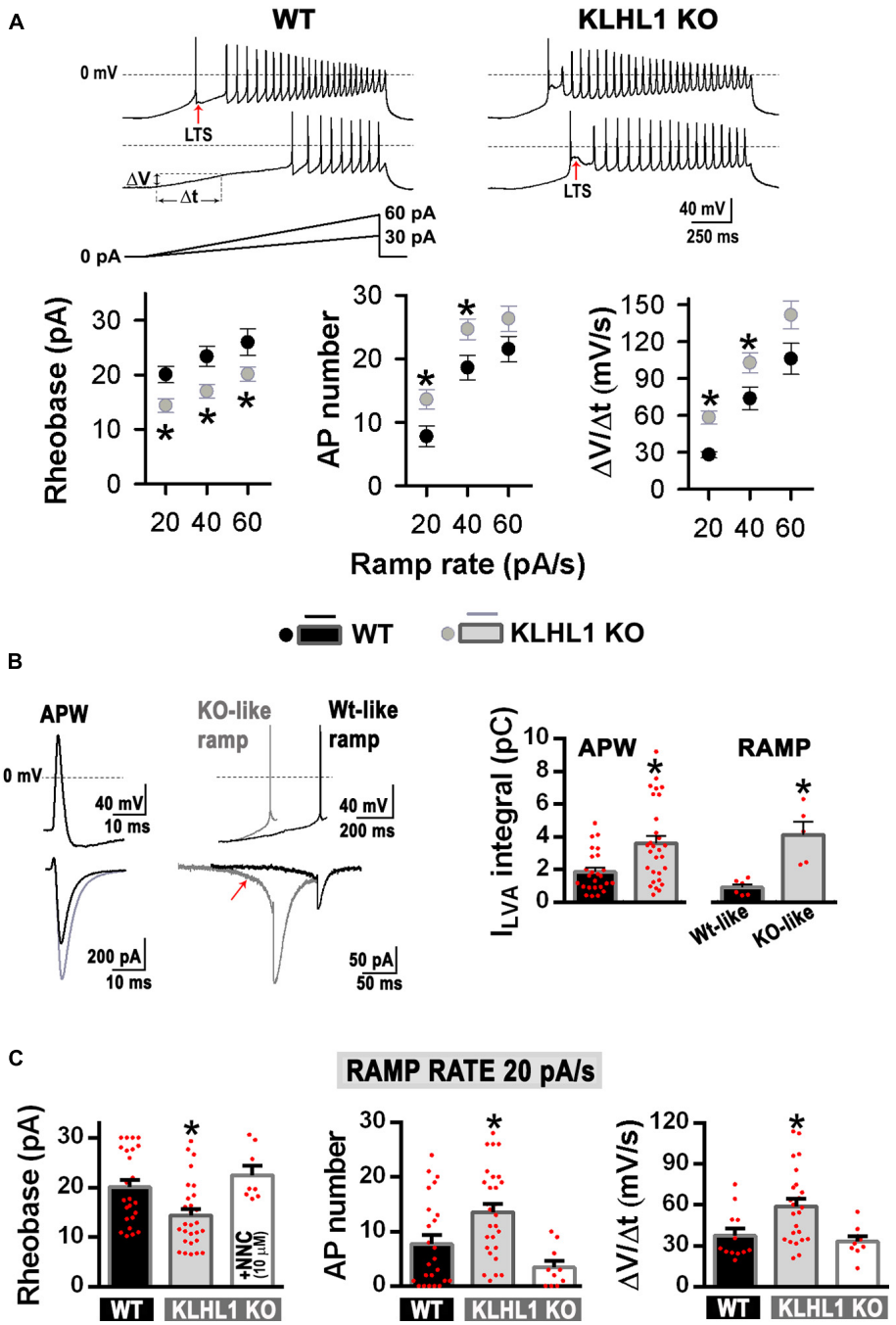

FIGURE 5 | Increased membrane excitability in KLHL1-KO neurons. **(A) Top:** Examples of neuronal firing elicited from V_H = –75 mV by a 20 and 40 pA/s ramps in WT and KLHL1-KO neurons. Red arrows indicate low-threshold spike (LTS) responses. **Bottom:** Rheobase (pA), number of action potentials and rate of membrane potential depolarization (Slope = $\Delta V/\Delta t$, mV/s, see panel A in response to 20, 40 and 60 pA/s ramps) in WT (n = 24, 24, 12) and KLHL1-KO (n = 28, 28, 24) neurons. *$P < 0.05$, t-test. Rheobase: t = 2.924 for 20 pA/s, t = 3.107 for 40 pA/s, t = 2.155 for 60 pA/s, df = 50. AP number: t = 2.607 for 20 pA/s, t = 2.428 for 40 pA/s, df = 50. Slope: t = 2.481 for 20 pA/s, t = 2.108 for 40 pA/s, df = 34. **(B) Left:** Average traces of T-type LVA currents elicited by an action potential waveform ($\Delta V/\Delta t$ = 0 mV/s, APW protocol). **Center:** Isolated LVA component traces elicited by action potentials preceded by a slope and a rheobase representative of either WT (WT-like ramp, $\Delta V/\Delta t$ = 30 mV/s, rheobase = 20 pA) or KLHL1-KO neurons (KO-like ramp, $\Delta V/\Delta t$ = 60 mV/s, rheobase = 14 pA). The KO-like ramp protocol favors T-type channel recruitment (red arrow). **Right:** Average LVA current integral in WT and KLHL1-KO neurons. *$P < 0.05$, t-test. APW protocol: t = 3.241 (df = 52, n = 25 for WT, n = 29 for KLHL1 KO). WT- or KO-like ramp protocols: t = 4.372 (df = 9, n = 6 for WT, n = 5 for KLHL1 KO). **(C)** Quantification of rheobase (pA), number of action potentials and rate of membrane potential depolarization (Slope = $\Delta V/\Delta t$, mV/s) in WT (n = 24, 24, 12), KLHL1-KO (n = 28, 28, 24) and NNC 55-0396 (10 μM)-treated KLHL1-KO (n = 8, 10, 9) neurons in response to 20 pA/s ramps. *Significantly different from WT and NNC-treated KLHL1-KO neurons. $P < 0.05$, ANOVA. Rheobase: $F_{2,57}$ = 6.743, AP number: $F_{2,59}$ = 8.004, Slope: $F_{2,42}$ = 6.029.

response to a ramp rate of 20 pA/s, comparable to WT neurons ($P < 0.05$, t-test, **Figure 5C**).

Leptin Resistance in KLHL1-KO Neurons

So far, we found T-type channel overexpression in KLHL1-KO hypothalamus leads to increases currents and membrane excitability in POMC neurons. It is well-established that POMC neurons increase their excitability in response to administration of nanomolar levels of leptin through the activation of TRPC channels (Qiu et al., 2010, 2011, 2014). We recently reported that TRPC1/5-$Ca_V3.1/2$ complexes mediates leptin-induced excitability in WT POMC neurons (Perissinotti et al., 2021). Therefore, we next analyzed the leptin-mediated effects on membrane excitability on KLHL1-KO hypothalamic neurons.

Leptin induces increased membrane excitability in response to ramp rates of 20, 40 and 60 pA/s in WT neurons (Perissinotti et al., 2021). Remarkably, using the same ramp protocol, no differences in the rheobase, the number of APs and the rate of membrane depolarization were observed between untreated neurons (control) and leptin-treated KLHL1-KO neurons (**Figures 6A,B**); suggesting that the excitability in KLHL1-KO neurons may have reached a plateau under basal conditions. To test this assumption, we studied whether decreasing excitability of KLHL-KO neurons could restore leptin sensitivity. T-type channels were partially inhibited with low concentration of NNC 55-0396 (30 nM) to decrease their membrane excitability. The resulting rheobase, AP number and membrane depolarization rate of KLHL1-KO neurons were indistinguishable from WT neurons ($P > 0.05$, t-test, **Figure 7A**).

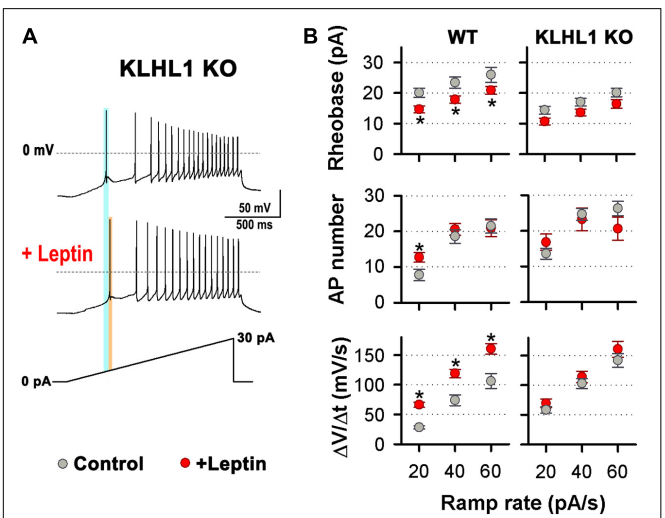

FIGURE 6 | Electrical Resistance to leptin in KLHL1 KO neurons. **(A)** Examples of neuronal firing elicited from V_H = –75 mV by a 20 pA/s ramp in control and leptin-treated (100 nM) KLHL1-KO neurons. Light blue and orange lines indicate the rheobase before and after the addition of leptin, respectively. **(B)** Left: Rheobase (pA), number of action potentials and rate of membrane potential depolarization (Slope = $\Delta V/\Delta t$, mV/s) in response to 20, 40 and 60 pA/s ramps in KLHL1 KO control (n = 28, 28, 25) and leptin-treated (n = 14, 14, 13) neurons. WT neuron behavior is shown for comparison (from Perissinotti et al., 2021). *Significantly different from control, $P < 0.05$, t-test.

Moreover, this partial blockade of T-type currents restored leptin sensitivity to similar levels to those observed in WT neurons ($P < 0.05$, t-test, **Figure 7A**). **Figure 7B** shows leptin effects on membrane excitability in response to ramp rates of 20, 40

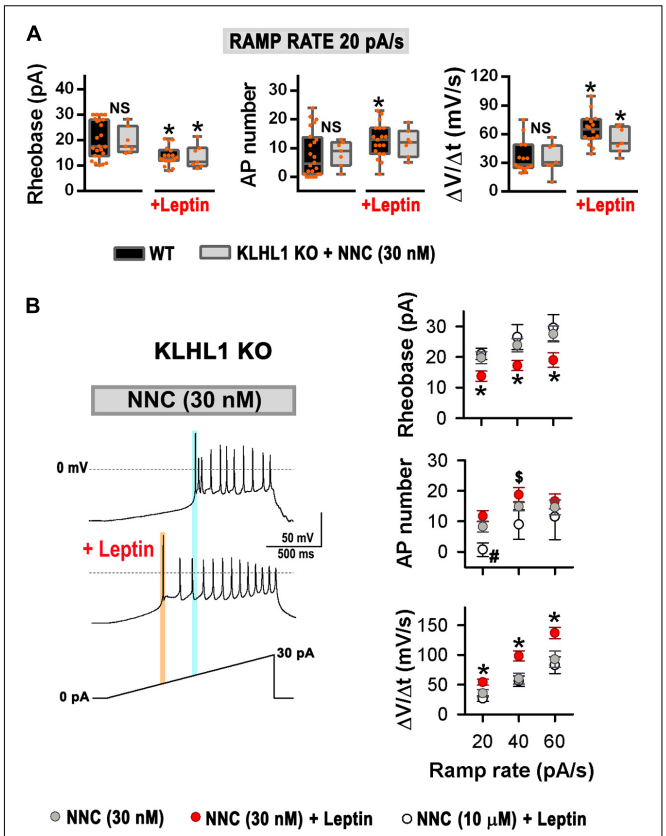

FIGURE 7 | Resistance to leptin in KLHL1 KO neurons is restored by partial blockade of T-type currents. **(A)** Leptin effect on rheobase (pA), number of action potentials and rate of membrane potential depolarization (Slope = $\Delta V/\Delta t$, mV/s) in WT (control, n = 24, 24, 15; + leptin, n = 18, 19, 16) and [NNC (30 nM)]-treated KLHL1-KO (control, n = 7, 7, 7; + leptin, n = 7, 7, 7) neurons in response to a ramp rate of 20 pA/s. NS, no significant difference between WT and [NNC (30 nM)]-treated KLHL1-KO, $P > 0.05$, t-test. *Significantly different from its respective control), $P < 0.05$, t-test. WT: Rheobase: t = 3.285 (df = 40), AP number: t = 2.257 (df = 41), Slope: t = 5.059 (df = 29). [NNC (30 nM)]-treated KLHL1-KO: Rheobase: t = 2.368 (df = 12), Slope: t = 2.362 (df = 12). **(B) Left:** Examples of neuronal firing in KLHL1-KO neurons preincubated with NNC (30 nM) before and after the addition of leptin [NNC (30 nM) + leptin (100 nM)]. V_H = 75 mV, AP triggering was elicited by a 20 pA/s ramp. Light blue and orange lines indicate the rheobase in the NNC treatment and after the addition of leptin ([NNC + leptin] treatment). **Right:** Rheobase (pA), number of action potentials and rate of membrane potential depolarization (Slope = $\Delta V/\Delta t$, mV/s) in response to 20, 40 and 60 pA/s ramps in [NNC (30 nM)]-treated (n = 7), [NNC (30 nM) + leptin]-treated (n = 7) and [NNC (10 μM) + leptin]-treated (n = 5) KLHL1-KO neurons. *Significantly different from NNC (30 nM) and [NNC (10 μM) + leptin]. $^{\#}$Significantly different from NNC (30 nM) and [NNC (30 nM) + leptin]. $^{\$}$Significantly different from [NNC (10 μM) + leptin]. $P < 0.05$, ANOVA. Rheobase: $F_{2,16}$ = 3.867 for 20 pA/s, $F_{2,16}$ = 4.188 for 40 pA/s and $F_{2,16}$ = 3.648 for 60 pA/5. AP number: $F_{2,16}$ = 8.550 for 20 pA/s, $F_{2,16}$ = 4.081 for 40 pA/s. Slope: $F_{2,16}$ = 5.908 for 20 pA/s, $F_{2,16}$ = 6.832 for 40 pA/s, $F_{2,14}$ = 4.770 for 60 pA/s.

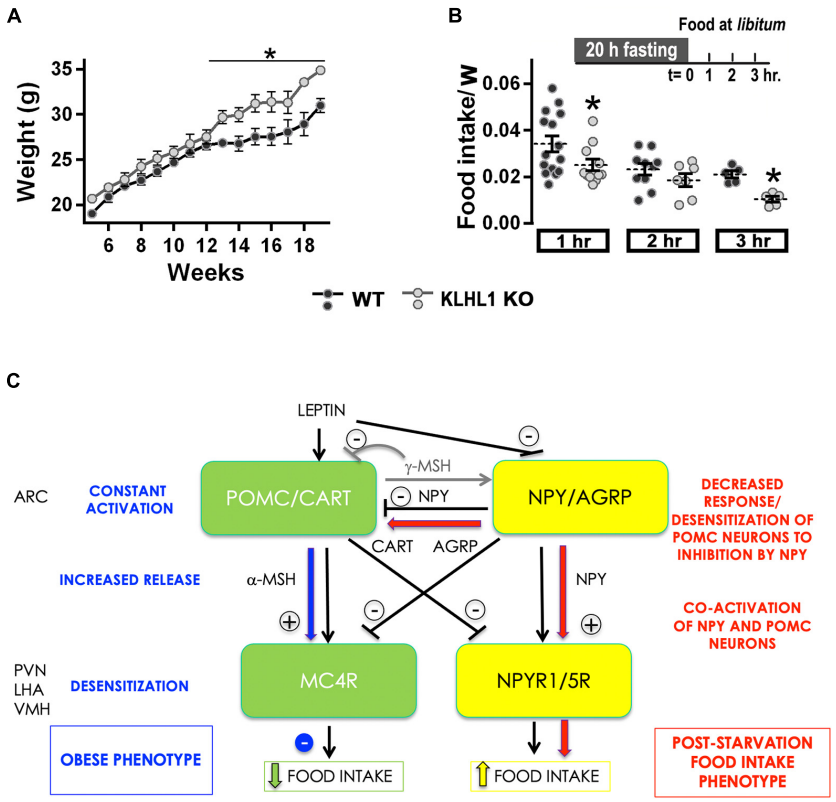

FIGURE 8 | Increased body mass and abnormal fasting response in KLHL1 KO mice. **(A)** Body mass plotted against mice age for WT (black circles, $n = 4–10$) and KLHL1 KO (gray circles, $n = 4–9$). *Significantly different after the 12th week, $P < 0.05$, Two-Way ANOVA, $F_{1,183} = 58.84$. **(B)** Fasting experiment protocol: adult male WT and KLHL1-KO mice were fasted for 20 h. Weight gain and food consumption were examined hourly after food reintroduction ($t = 0$) for three hours. Food intake normalized by weight ratio was calculated after food reintroduction: 1h (WT, KO; $n = 15, 11$), 2h (WT, KO; $n = 10, 7$) and 3h (WT, KO; $n = 5, 5$). *$P < 0.05$, t-test; 1h: $t = 2.004$, df = 24; 3h: $t = 5.451$, df = 8. **(C)** *Reciprocal control of satiety and feeding centers:* The black arrows depict a simplified version of the reciprocal control occurring between the feeding (yellow) and the satiety (green) circuits in hypothalamic nuclei involved in the regulation of energy homeostasis: Arcuate (ARC), paraventricular (PVN) and ventromedial (VMH) and lateral hypothalamic area (LHA). The hyper-excitable and increased depolarized state of POMC neurons could counteract the inhibitory action of NPY, permitting the activation of both satiety and feeding centers, dampening the food intake post-starvation (red). On the other hand, continued hyper-excitability in KLHL1 KO POMC neurons would lead to increased α-MESH release onto MC4R neurons, likely causing long-term desensitization and impairing the satiety response, which would contribute to the obesity phenotype (blue).

and 60 pA/s in [NNC (30 nM)]-treated KLHL1-KO neurons. Leptin increased membrane excitability across all ramps tested. As expected, further application of micromolar concentrations of NNC 55-0396 (10 μM) prevented leptin-mediated effects on membrane excitability, confirming the role of LVA channels in this process. Overall, the data show the electrical efficacy of leptin depends on the neuron's basal excitability level; the larger T-type LVA current activity seen in KLHL1-KO POMC neurons increases their excitability to a plateau level which cannot be further enhanced by the presence of leptin; causing electrical resistance to leptin (i.e., loss of electrical sensitivity lo leptin) that is completely reversible upon partial blockade of T-type channels.

Systemic Deletion of KLHL1 Results in Increased Body Weight and Altered Food Ingestion

Leptin is a key hormone in the regulation of energy balance and plays an essential role in energy homeostasis (Ahima et al., 1996). We assessed the body mass changes of KLHL1-KO mice with age, they displayed significant increases compared to WT after week 12 (**Figure 8A**, $P < 0.05$, Two-way ANOVA) suggesting abnormal energy intake/expenditure balance. We used a starvation-refeeding paradigm as a quick appraisal of whether the mice would respond normally to increased levels of leptin after refeeding. We performed a 20-hr fasting experiment followed by exposure to normal chow at *libitum* (**Figure 8B**; Scott et al., 2009; Liu et al., 2012). Pre-, and post-fasting weight after food reintroduction was monitored for three hours. Both mice cohorts lost similar amounts of weight after fasting (∼10%, not shown). As expected, WT mice displayed sizable food ingestion during the first hour exposed to nourishment, which tapered by the second and third hours exposed to food *ad libitum*, indicating a normal anorexigenic response to leptin. However, when presented with food at *libitum*, food consumption in the KLHL1-KO cohort was slower than in WT mice (**Figure 8B**, $P < 0.05$, t-test), suggesting that KLHL1-KO mice were less sensitive to starvation, displaying abnormal hunger responses.

DISCUSSION

This study provides new insights into the importance of T-type channels in the leptin signaling cascade leading to membrane excitability in POMC hypothalamic neurons. We previously reported that TRPC1/5-$Ca_V3.1/2$ complexes mediate leptin-induced excitability in POMC neurons (Perissinotti et al., 2021), here we show that over-expression of the pore-forming α_{1G} subunit of the T-type $Ca_V3.1$ channel in the KLHL1-KO mice altered their basal excitability, rendering them electrically unresponsive to leptin. Leptin responses were fully restored by partial blockade of T-type channels. Neither leptin receptor (LRb) nor downstream effectors (STAT3, PI3K phosphorylation, TRPC1/5 channels) were altered in the KLHL1-KO hypothalamus.

T-type calcium channels are widely distributed in the hypothalamus (Qiu et al., 2006). mRNA and protein levels of the α_{1G} subunit of the Cav 3.1 channel are highly expressed; whereas α_{1H} and α_{1I} subunits (of Cav 3.2 and Cav 3.3 channels, respectively) are also present but at much lower levels (Craig et al., 1999; Talley et al., 1999). The role of T-type channels is well established, they are expressed in several nuclei and help control neuronal excitability. ARC neurons containing neuropeptide Y (NPY) and agouti-related peptide (AgRP) are conditional pacemakers. T-type currents drive oscillatory activity of NPY/AgRP neurons, in which burst firing frequency is modulated by a transient outwardly rectifying potassium conductance (van den Top et al., 2004). The leptin-dependent inhibition of AgRP/NPY neurons is attributed in part to modulation of K^+ channels such as K_{ATP}, BK and $K_V2.1$ channels (Spanswick et al., 1997; Mirshamsi et al., 2004; Yang et al., 2010; Baver et al., 2014). The orexigenic peptide Ghrelin is reported to directly activate a sustained depolarizing conductance with the pharmacologic properties of SUR1/Trpm4 non-selective cation channels (sulfonylurea receptor 1/transient receptor potential melastatin 4), which activates T- and R-type voltage dependent Ca^{2+} channels in NPY/AgRP neurons (Hashiguchi et al., 2017). Notably, both leptin-dependent activation of POMC neurons and ghrelin-dependent activation of AgRP/NPY neurons involves the subsequent activation of T-type channels to increase neuronal activity (Qiu et al., 2006, 2018; Bosch et al., 2009; Hashiguchi et al., 2017; Perissinotti et al., 2021).

In line with the large hypothalamic $Ca_V3.1$ channel expression, T-type current density was also increased in POMC neurons in KLHL1-KO mice. Biophysical analysis of T-type currents is consistent with overexpression of the α_{1G} component (Perez-Reyes, 2003). Our lab demonstrated that KLHL1 protein positively modulates α_{1H} subunit of the $Ca_V3.2$ channel but it does not affect $Ca_V3.1$ nor $Ca_V3.3$ in the hippocampus (Perissinotti et al., 2015) or in HEK cells that constitutively overexpress these isoforms (Aromolaran et al., 2010). The increased $Ca_V3.1$ expression seen in the hypothalamus is likely the result of homeostatic compensation when KLHL1 is absent, although the molecular mechanisms responsible are currently being investigated.

The biophysical properties of T-type channels permit their stimulation by small depolarizations near the resting potential, rendering them optimal for regulating membrane excitability and burst-firing pattern under physiological conditions near resting state. Accordingly, changes in the steady-state activation and inactivation curves in KLHL1-KO neurons resulted in a ∼-4 mV shift in the window current cross point. This leftwards shift led to a 90% increase of the steady-state calcium current in KLHL1-KO neurons at the resting membrane potential, which was ∼2 mV more depolarized than WT neurons. Intrinsic neuron properties such as the spontaneous firing and the basal excitability are tightly related to T-type "window currents" (Huguenard, 1996; Perez-Reyes, 2003; Crunelli et al., 2005; Molineux et al., 2006; Bayazitov et al., 2013); fittingly, we found increased burst-firing pattern and excitability in POMC neurons from the KLHL1-KO mice. In line with our results, it has been reported that the knockdown of $Ca_V3.1$ calcium channel switch from bursting to tonic firing at thalamocortical projections (Bayazitov et al., 2013). Interestingly, our results demonstrate that changes that alter the basal excitability of POMC neurons, such as over-expression of $Ca_V3.1$ T-type channels, rendered them unresponsive to leptin. Partial blockade of T-type channels brought KLHL1-KO neurons to normal excitability levels, which was sufficient to restore leptin sensitivity in these neurons.

Energy imbalance alters Ca^{2+} handling and excitability of POMC neurons (Paeger et al., 2017). Intracellular Ca^{2+} levels are regulated by several mechanisms including plasma membrane ion channels (e.g., voltage-gated and ligand-gated Ca^{2+} channels), ion exchangers and "pumps," as well as the release from the intracellular Ca^{2+} stores (Verkhratsky and Toescu, 2003). Correspondingly, endoplasmic reticulum (ER) stress was recognized as an important causal factor for the development of leptin resistance induced by diet (Hosoi et al., 2008; Ramírez and Claret, 2015). Diet-induced obesity (DIO) causes increased resting cytosolic Ca^{2+} levels and markedly decreased excitability of anorexigenic POMC neurons, resulting from increased calcium-activated K^+ channel activity (SK channels) (Paeger et al., 2017). The overexpression of $Ca_V3.1$ reported here could lead to increased membrane permeability to calcium at rest due to T-type channel's window current properties (Chemin et al., 2000). However, this is an unlikely scenario (or it is not physiologically relevant in our system), as we have shown that Ca^{2+} influx through T-type channels contributes locally at the submembrane level and not globally to support increased excitability in POMC neurons (Perissinotti et al., 2021).

Although our systemic KLHL1-KO model is not a good model to explore questions regarding obesity and altered starvation responses changes observed in these mice, we examined the possible contribution of the altered molecular mechanisms observed in the KLHL1 KO to these phenotypes. Upregulation of $Ca_V3.1$ channels could contribute to obesity (Kortekaas and Wadman, 1997; Yunker et al., 2003; Aguado et al., 2016). Deletion of $Ca_V3.1$ channels (Cacna1g KO mice) or treated with TTA-A2 (selective blocker of T-type Ca_V3) results in reduced food intake, attenuated weight gain and decreased body fat gain in response to high-fat diet; suggesting a role for $Ca_V3.1$ channels in weight maintenance (Uebele et al., 2009;

Rosenstand et al., 2020). Likewise, ethosuximide, another T -type calcium channel blocker, partially protects against neurosteroid-induced obesity in mice by reducing food intake and body weight (Chidrawar and Ali, 2020); similarly, T-type antagonists prescribed for epilepsy, depression, obsessive-compulsive disorder and bulimia nervosa can cause loss of appetite as a side effect (Cookson and Duffett, 1998; Traboulsie et al., 2006; Willfong and Willmore, 2006). $Ca_V3.1$ channels have been proposed as potential therapeutic targets for the prevention and treatment of obesity (Uebele et al., 2009; Vasconcelos et al., 2016; Chidrawar and Ali, 2020; Zhai et al., 2020).

Furthermore, we found that the fasting-induced response to hunger was abnormal in KLHL1-KO mice, they consumed food at a slower rate than WT mice after twenty hours of food deprivation (short-term). Similarly, mice that exhibit obese phenotypes [ob/ob and diet-induced obesity (DIO)] consumed less food compared to WT mice in response to twenty-four hours food deprivation (Ueno et al., 2007). Factors contributing to the dampened response to hunger in obese mice could be explained by the presence of large readily available fat stores that can be mobilized when food is deprived (Ramirez and Sprott, 1978). Alternatively, it can also be explained by a decreased sensitivity to fasting-induced orexigenic signals or by an increased sensitivity to satiety-induced anorexigenic signals (Ueno et al., 2007). Satiety and anorexigenic signals activate POMC neurons while they inhibit NPY/AgRP neurons; in contrast, starvation and orexigenic signals activate NPY/AgRP neurons and inhibit POMC neurons (**Figure 8C**; Schwartz et al., 1996; Elias et al., 1999; Cowley et al., 2001). The cross-regulation between POMC and AgRP neurons is complex (**Figure 8C**), for instance, the release of alpha-melanocyte stimulating hormone (α-MSH) -a potent anorexigenic in central melanocortin receptor 4 (MC4R) neurons- is promoted by satiety signals, while it is inhibited by starvation signals (reviewed by Minokoshi, 2020). Leptin causes satiety by triggering POMC neuron depolarization and production and release of α-MSH from axon terminals, which activates MC4R neurons and result in suppressed food intake and increased energy expenditure (Cowley et al., 2001; Guo et al., 2004; O'Rahilly et al., 2004; D'Agostino and Diano, 2010; Qiu et al., 2010; Anderson et al., 2016; Baldini and Phelan, 2019). Our data shows this pathway is constitutively activated in cultured KLHL1-KO POMC neurons due to their hyper-excitable basal status and increased burst-firing pattern. Activity patterning is very important in hypothalamic neuron neuropeptide release, and burst firing is a more effective stimulus for peptide release than fast, repetitive firing patterns of activity (Poulain and Wakerley, 1982). Thus, increased spontaneous burst-firing pattern (intra-burst frequency) in KLHL1-KO POMC neurons could enhance basal release of α-MSH from axon terminals, eventually leading to MC4R desensitization and constitutive, partially active satiety responses that would contribute to the obesity phenotype (**Figure 8C**, blue arrows; Gao et al., 2003; Shinyama et al., 2003; Mohammad et al., 2007; McDaniel et al., 2012; Granell et al., 2013).

On the other side, putative $AgRP^+/NPY^+$ neurons from KLHL1 KO mice elicit normal responses to leptin (decreased excitability), thus we hypothesize that activation of the feeding center and NPY release would result in normal food intake post-starvation if successful feedback inhibition of POMC neurons occurred. Application of 100 nM NPY leads to a ∼17 mV average hyperpolarization of POMC neurons, which efficiently prevents triggering of APs (Roseberry et al., 2004). However, the slightly depolarized state of KLHL1 KO POMC neurons and increased T-type channel window current activity could partially counteract the inhibitory effect of NPY, resulting in incomplete activity of the satiety circuit even after food deprivation. Moreover, increased inhibitory stimulus onto POMC neurons by NPY could also lead to long-term desensitization of this inhibitory feedback loop. Here we assessed the acute response of KLHL1 KO mice to starvation; thus, it is possible that activation of the feeding center in parallel to partial activation of the satiety center contributes to the dampened feeding response seen under our experimental conditions (**Figure 8C**, red arrows). Interestingly, Hashiguchi et al. (2017) reported T-type channels as targets in the activation pathway of NPY/AgRP in response to orexigenic signals. Further studies are necessary to determine whether $Ca_V3.1$ channels are upregulated in NPY/AgRP neurons and possible implications on their excitability.

In summary, increased excitability in KLHL1-KO POMC neurons induced the loss of electrical sensitivity lo leptin, contributing to alteration of the hypothalamic feeding and satiety neuron network dynamics that caused dysregulating the energy balance and the body weight. This work corroborates that T-type currents are indispensable in POMC neuron excitability, which is essential for transduction of the leptin cascade. Increased POMC neuron excitability due to increased $Ca_V3.1$ T-type channel activity in the KLHL1-KO mice resulted in electrical resistance to leptin, which could be rescued by simply reducing T-type channel activity.

DATA AVAILABILITY STATEMENT

The raw data supporting the conclusions of this article will be made available by the authors, without undue reservation.

ETHICS STATEMENT

The animal study was reviewed and approved by Institutional Animal Care and Use Committee at Loyola University Chicago (IACUC 2016032).

AUTHOR CONTRIBUTIONS

EP-R conceived of the study, supervised the experiments, and approved the final version of the manuscript.

EP-R, EM-H, and PP designed the experiments, performed the experiments, analyzed the data, interpreted the results of experiments, and prepared the figures. YH and MK generated the KLHL1-knockout mice. EP-R and PP wrote the manuscript, edited and revised the manuscript. All authors contributed to the article and approved the submitted version.

ACKNOWLEDGMENTS

We thank all members of the Piedras laboratory, O'Connell and Don Carlos for helpful input and comments. This paper is based upon work supported by the National Science Foundation under Grant no. 1022075 (EP-R).

REFERENCES

Aguado, C., García-Madrona, S., Gil-Minguez, M., and Luján, R. (2016). Ontogenic changes and differential localization of T-type Ca2+ channel subunits Cav3. 1 and Cav3. 2 in mouse hippocampus and cerebellum. *Front. Neuroanat.* 10:83. doi: 10.3389/fnana.2016.00083

Ahima, R. S., Prabakaran, D., Mantzoros, C., Qu, D., Lowell, B., Maratos-Flier, E., et al. (1996). Role of leptin in the neuroendocrine response to fasting. *Nature* 382, 250–252. doi: 10.1038/382250a0

Anderson, E. J., Çakir, I., Carrington, S. J., Cone, R. D., Ghamari-Langroudi, M., Gillyard, T., et al. (2016). 60 YEARS OF POMC: regulation of feeding and energy homeostasis by α-MSH. *J. Mol. Endocrinol.* 56, T157–T174.

Aromolaran, K. A., Benzow, K. A., Cribbs, L. L., Koob, M. D., and Piedras-Renteria, E. S. (2009). Kelch-like 1 protein upregulates T-type currents by an actin-F dependent increase in alpha(1H) channels via the recycling endosome. *Channels* 3, 402–412. doi: 10.4161/chan.3.6.9858

Aromolaran, K. A., Benzow, K. A., Cribbs, L. L., Koob, M. D., and Piedras-Renteria, E. S. (2010). T-type current modulation by the actin-binding protein Kelch-like 1. *Am. J. Physiol. Cell Physiol.* 298, C1353–C1362.

Balasubramanyan, S., Stemkowski, P. L., Stebbing, M. J., and Smith, P. A. (2006). Sciatic chronic constriction injury produces cell-type-specific changes in the electrophysiological properties of rat substantia gelatinosa neurons. *J. Neurophysiol.* 96, 579–590. doi: 10.1152/jn.00087.2006

Baldini, G., and Phelan, K. D. (2019). The melanocortin pathway and control of appetite-progress and therapeutic implications. *J. Endocrinol.* 241, R1–R33.

Baver, S. B., Hope, K., Guyot, S., Bjorbaek, C., Kaczorowski, C., and O'connell, K. M. (2014). Leptin modulates the intrinsic excitability of AgRP/NPY neurons in the arcuate nucleus of the hypothalamus. *J. Neurosci.* 34, 5486–5496. doi: 10.1523/jneurosci.4861-12.2014

Bayazitov, I. T., Westmoreland, J. J., and Zakharenko, S. S. (2013). Forward suppression in the auditory cortex is caused by the Ca(v)3.1 calcium channel-mediated switch from bursting to tonic firing at thalamocortical projections. *J. Neurosci.* 33, 18940–18950. doi: 10.1523/jneurosci.3335-13.2013

Bean, B. P. (1985). Two kinds of calcium channels in canine atrial cells. Differences in kinetics, selectivity, and pharmacology. *J. Gen. Physiol.* 86, 1–30. doi: 10.1085/jgp.86.1.1

Bijlenga, P., Liu, J.-H., Espinos, E., Haenggeli, C.-A., Fischer-Lougheed, J., Bader, C. R., et al. (2000). T-type α1H Ca2+ channels are involved in Ca2+ signaling during terminal differentiation (fusion) of human myoblasts. *Proc. Natl. Acad. Sci. U.S.A.* 97, 7627–7632. doi: 10.1073/pnas.97.13.7627

Bosch, M. A., Hou, J., Fang, Y., Kelly, M. J., and Ronnekleiv, O. K. (2009). 17Beta-estradiol regulation of the mRNA expression of T-type calcium channel subunits: role of estrogen receptor alpha and estrogen receptor beta. *J. Comp. Neurol.* 512, 347–358. doi: 10.1002/cne.21901

Buettner, C., Pocai, A., Muse, E. D., Etgen, A. M., Myers, M. G. Jr., and Rossetti, L. (2006). Critical role of STAT3 in leptin's metabolic actions. *Cell Metab.* 4, 49–60. doi: 10.1016/j.cmet.2006.04.014

Chemin, J., Monteil, A., Briquaire, C., Richard, S., Perez-Reyes, E., Nargeot, J., et al. (2000). Overexpression of T-type calcium channels in HEK-293 cells increases intracellular calcium without affecting cellular proliferation. *FEBS Lett.* 478, 166–172. doi: 10.1016/s0014-5793(00)01832-9

Chen, W.-L., Lin, J.-W., Huang, H.-J., Wang, S.-M., Su, M.-T., Lee-Chen, G.-J., et al. (2008). SCA8 mRNA expression suggests an antisense regulation of KLHL1 and correlates to SCA8 pathology. *Brain Res.* 1233, 176–184. doi: 10.1016/j.brainres.2008.07.096

Chidrawar, V. R., and Ali, A. (2020). Experimental studies to define the role of Calcium (Ca2+) and Voltage-Gated Calcium Channel Blockers (vCa-CCB) against Neurosteroid Induced Obesity. *J. Pharm. Res. Int.* 32, 60–71. doi: 10.9734/jpri/2020/v32i730461

Cookson, J., and Duffett, R. (1998). Fluoxetine: therapeutic and undesirable effects. *Hosp. Med.* 59, 622–626.

Cowley, M. A., Smart, J. L., Rubinstein, M., Cerdan, M. G., Diano, S., Horvath, T. L., et al. (2001). Leptin activates anorexigenic POMC neurons through a neural network in the arcuate nucleus. *Nature* 411, 480–484. doi: 10.1038/35078085

Craig, P., Beattie, R., Folly, E., Reeves, M., Priestley, J., Carney, S., et al. (1999). Distribution of the voltage-dependent calcium channel α1G subunit mRNA and protein throughout the mature rat brain. *Eur. J. Neurosci.* 11, 2949–2964. doi: 10.1046/j.1460-9568.1999.00711.x

Crunelli, V., Toth, T. I., Cope, D. W., Blethyn, K., and Hughes, S. W. (2005). The 'window'. T-type calcium current in brain dynamics of different behavioural states. *J. Physiol.* 562, 121–129. doi: 10.1113/jphysiol.2004.076273

D'Agostino, G., and Diano, S. (2010). Alpha-melanocyte stimulating hormone: production and degradation. *J. Mol. Med.* 88, 1195–1201. doi: 10.1007/s00109-010-0651-0

Elias, C. F., Aschkenasi, C., Lee, C., Kelly, J., Ahima, R. S., Bjorbaek, C., et al. (1999). Leptin differentially regulates NPY and POMC neurons projecting to the lateral hypothalamic area. *Neuron* 23, 775–786. doi: 10.1016/s0896-6273(01)80035-0

Florio, V., Striessnig, J., and Catterall, W. A. (1992). Purification and reconstitution of skeletal-muscle calcium channels. *Methods Enzymol.* 207, 529–546. doi: 10.1016/0076-6879(92)07037-o

Gao, Z., Lei, D., Welch, J., Le, K., Lin, J., Leng, S., et al. (2003). Agonist-dependent internalization of the human melanocortin-4 receptors in human embryonic kidney 293 cells. *J. Pharmacol. Exp. Ther.* 307, 870–877. doi: 10.1124/jpet.103.055525

Grace, A. A., and Bunney, B. S. (1984). The control of firing pattern in nigral dopamine neurons: burst firing. *J. Neurosci.* 4, 2877–2890. doi: 10.1523/jneurosci.04-11-02877.1984

Granell, S., Molden, B. M., and Baldini, G. (2013). Exposure of MC4R to agonist in the endoplasmic reticulum stabilizes an active conformation of the receptor that does not desensitize. *Proc. Natl. Acad. Sci. U.S.A.* 110, E4733–E4742.

Guo, L., Münzberg, H., Stuart, R. C., Nillni, E. A., and Bjørbaek, C. (2004). N-acetylation of hypothalamic α-melanocyte-stimulating hormone and regulation by leptin. *Proc. Natl. Acad. Sci. U.S.A.* 101, 11797–11802. doi: 10.1073/pnas.0403165101

Gutierrez, C., Cox, C. L., Rinzel, J., and Sherman, S. M. (2001). Dynamics of low-threshold spike activation in relay neurons of the cat lateral geniculate nucleus. *J. Neurosci.* 21, 1022–1032. doi: 10.1523/jneurosci.21-03-01022.2001

Hashiguchi, H., Sheng, Z., Routh, V., Gerzanich, V., Simard, J. M., and Bryan, J. (2017). Direct versus indirect actions of ghrelin on hypothalamic NPY neurons. *PLoS One* 12:e0184261. doi: 10.1371/journal.pone.0184261

He, Y., Zu, T., Benzow, K. A., Orr, H. T., Clark, H. B., and Koob, M. D. (2006). Targeted deletion of a single Sca8 ataxia locus allele in mice causes abnormal gait, progressive loss of motor coordination, and Purkinje cell dendritic deficits. *J. Neurosci.* 26, 9975–9982. doi: 10.1523/jneurosci.2595-06.2006

Hosoi, T., Sasaki, M., Miyahara, T., Hashimoto, C., Matsuo, S., Yoshii, M., et al. (2008). Endoplasmic reticulum stress induces leptin resistance. *Mol. Pharmacol.* 74, 1610–1619. doi: 10.1124/mol.108.050070

Huguenard, J. R. (1996). Low-threshold calcium currents in central nervous system neurons. *Annu. Rev. Physiol.* 58, 329–348. doi: 10.1146/annurev.ph.58.030196.001553

Kortekaas, P., and Wadman, W. J. (1997). Development of HVA and LVA calcium currents in pyramidal CA1 neurons in the hippocampus of the rat. *Dev. Brain Res.* 101, 139–147. doi: 10.1016/s0165-3806(97)00059-x

Lambert, R. C., Bessaïh, T., Crunelli, V., and Leresche, N. (2014). The many faces of T-type calcium channels. *Pflügers Arch.* 466, 415–423. doi: 10.1007/s00424-013-1353-6

Legendy, C. R., and Salcman, M. (1985). Bursts and recurrences of bursts in the spike trains of spontaneously active striate cortex neurons. *J. Neurophysiol.* 53, 926–939. doi: 10.1152/jn.1985.53.4.926

Liu, T., Kong, D., Shah, B. P., Ye, C., Koda, S., Saunders, A., et al. (2012). Fasting activation of AgRP neurons requires NMDA receptors and involves spinogenesis and increased excitatory tone. *Neuron* 73, 511–522. doi: 10.1016/j.neuron.2011.11.027

Lu, V. B., Moran, T. D., Balasubramanyan, S., Alier, K. A., Dryden, W. F., Colmers, W. F., et al. (2006). Substantia Gelatinosa neurons in defined-medium organotypic slice culture are similar to those in acute slices from young adult rats. *Pain* 121, 261–275. doi: 10.1016/j.pain.2006.01.009

Martínez-Hernández, E., Zeglin, A., Almazan, E., Perissinotti, P., He, Y., Koob, M., et al. (2020). KLHL1 Controls CaV3. 2 expression in DRG neurons and mechanical sensitivity to pain. *Front. Mol. Neurosci.* 12:315. doi: 10.3389/fnmol.2019.00315

McDaniel, F. K., Molden, B. M., Mohammad, S., Baldini, G., Mcpike, L., Narducci, P., et al. (2012). Constitutive cholesterol-dependent endocytosis of melanocortin-4 receptor (MC4R) is essential to maintain receptor responsiveness to α-melanocyte-stimulating hormone (α-MSH). *J. Biol. Chem.* 287, 21873–21890. doi: 10.1074/jbc.m112.346890

Minokoshi, Y. (2020). *"Neural Control of Homeostatic Feeding and Food Selection," in New Insights Into Metabolic Syndrome*. Available online at: https://www.intechopen.com/chapters/72998 (accessed July 28, 2021).

Mirshamsi, S., Laidlaw, H. A., Ning, K., Anderson, E., Burgess, L. A., Gray, A., et al. (2004). Leptin and insulin stimulation of signalling pathways in arcuate nucleus neurones: PI3K dependent actin reorganization and K ATP channel activation. *BMC Neurosci.* 5:54. doi: 10.1186/1471-2202-5-54

Mohammad, S., Baldini, G., Granell, S., Narducci, P., Martelli, A. M., and Baldini, G. (2007). Constitutive traffic of melanocortin-4 receptor in Neuro2A cells and immortalized hypothalamic neurons. *J. Biol. Chem.* 282, 4963–4974. doi: 10.1074/jbc.m608283200

Molineux, M. L., Mcrory, J. E., Mckay, B. E., Hamid, J., Mehaffey, W. H., Rehak, R., et al. (2006). Specific T-type calcium channel isoforms are associated with distinct burst phenotypes in deep cerebellar nuclear neurons. *Proc. Natl. Acad. Sci. U.S.A.* 103, 5555–5560. doi: 10.1073/pnas.0601261103

Nemes, J. P., Benzow, K. A., and Koob, M. D. (2000). The SCA8 transcript is an antisense RNA to a brain-specific transcript encoding a novel actin-binding protein (KLHL1). *Hum. Mol. Genet.* 9, 1543–1551. doi: 10.1093/hmg/9.10.1543

O'Rahilly, S., Yeo, G. S., and Farooqi, I. S. (2004). Melanocortin receptors weigh in. *Nat. Med.* 10, 351–352. doi: 10.1038/nm0404-351

Paeger, L., Pippow, A., Hess, S., Paehler, M., Klein, A. C., Husch, A., et al. (2017). Energy imbalance alters Ca2+ handling and excitability of POMC neurons. *eLife* 6:e25641.

Perez-Reyes, E. (2003). Molecular physiology of low-voltage-activated T-type calcium channels. *Physiol. Rev.* 83, 117–161. doi: 10.1152/physrev.00018.2002

Perissinotti, P. P., Ethington, E. G., Almazan, E., Martínez-Hernández, E., Kalil, J., Koob, M. D., et al. (2015). Calcium current homeostasis and synaptic deficits in hippocampal neurons from Kelch-like 1 knockout mice. *Front. Cell. Neurosci.* 8:444. doi: 10.3389/fncel.2014.00444

Perissinotti, P. P., Ethington, E. G., Cribbs, L., Koob, M. D., Martin, J., and Piedras-Renteria, E. S. (2014). Down-regulation of endogenous KLHL1 decreases voltage-gated calcium current density. *Cell Calcium* 55, 269–280. doi: 10.1016/j.ceca.2014.03.002

Perissinotti, P. P., Martínez-Hernández, E., and Piedras-Rentería, E. S. (2021). TRPC1/5-CaV 3 Complex mediates leptin-induced excitability in hypothalamic neurons. *Front. Neurosci.* 15:679078. doi: 10.3389/fnins.2021.679078

Poulain, D., and Wakerley, J. (1982). Electrophysiology of hypothalamic magnocellular neurones secreting oxytocin and vasopressin. *Neuroscience* 7, 773–808. doi: 10.1016/0306-4522(82)90044-6

Qiu, J., Bosch, M. A., Jamali, K., Xue, C., Kelly, M. J., and Rønnekleiv, O. K. (2006). Estrogen upregulates T-type calcium channels in the hypothalamus and pituitary. *J. Neurosci.* 26, 11072–11082. doi: 10.1523/jneurosci.3229-06.2006

Qiu, J., Bosch, M. A., Meza, C., Navarro, U.-V., Nestor, C. C., Wagner, E. J., et al. (2018). Estradiol protects proopiomelanocortin neurons against insulin resistance. *Endocrinology* 159, 647–664. doi: 10.1210/en.2017-00793

Qiu, J., Fang, Y., Bosch, M. A., Rønnekleiv, O. K., and Kelly, M. J. (2011). Guinea pig kisspeptin neurons are depolarized by leptin via activation of TRPC channels. *Endocrinology* 152, 1503–1514. doi: 10.1210/en.2010-1285

Qiu, J., Fang, Y., Ronnekleiv, O. K., and Kelly, M. J. (2010). Leptin excites proopiomelanocortin neurons via activation of TRPC channels. *J. Neurosci.* 30, 1560–1565. doi: 10.1523/jneurosci.4816-09.2010

Qiu, J., Zhang, C., Borgquist, A., Nestor, C. C., Smith, A. W., Bosch, M. A., et al. (2014). Insulin excites anorexigenic proopiomelanocortin neurons via activation of canonical transient receptor potential channels. *Cell Metab.* 19, 682–693. doi: 10.1016/j.cmet.2014.03.004

Ramirez, I., and Sprott, R. L. (1978). Hunger and satiety in genetically obese mice (C57BL/6J-ob/ob). *Physiol. Behav.* 20, 257–264. doi: 10.1016/0031-9384(78)90218-4

Ramírez, S., and Claret, M. (2015). Hypothalamic ER stress: a bridge between leptin resistance and obesity. *FEBS Lett.* 589, 1678–1687. doi: 10.1016/j.febslet.2015.04.025

Rivero-Echeto, M. C., Perissinotti, P. P., González-Inchauspe, C., Kargieman, L., Bisagno, V., and Urbano, F. J. (2021). Simultaneous administration of cocaine and caffeine dysregulates HCN and T-type channels. *Psychopharmacology* 238, 787–810. doi: 10.1007/s00213-020-05731-5

Roseberry, A. G., Liu, H., Jackson, A. C., Cai, X., and Friedman, J. M. (2004). Neuropeptide Y-mediated inhibition of proopiomelanocortin neurons in the arcuate nucleus shows enhanced desensitization in ob/ob mice. *Neuron* 41, 711–722. doi: 10.1016/s0896-6273(04)00074-1

Rosenstand, K., Andersen, K., Terp, R., Gennemark, P., Ellman, D. G., Reznichenko, A., et al. (2020). Deficiency of T-type voltage-gated calcium channels results in attenuated weight gain and improved endothelium-dependent dilatation of resistance vessels induced by a high-fat diet in mice. *J. Physiol. Biochem.* 76, 135–145. doi: 10.1007/s13105-020-00728-2

Sachdev, R. N., Gilman, S., and Aldridge, J. W. (1991). Bursting properties of units in cat globus pallidus and entopeduncular nucleus: the effect of excitotoxic striatal lesions. *Brain Res.* 549, 194–204. doi: 10.1016/0006-8993(91)90458-8

Schneider, C. A., Rasband, W. S., and Eliceiri, K. W. (2012). NIH Image to ImageJ: 25 years of image analysis. *Nat. Methods* 9, 671–675. doi: 10.1038/nmeth.2089

Schwartz, M. W., Seeley, R. J., Campfield, L. A., Burn, P., and Baskin, D. G. (1996). Identification of targets of leptin action in rat hypothalamus. *J. Clin. Invest.* 98, 1101–1106. doi: 10.1172/jci118891

Scott, M. M., Lachey, J. L., Sternson, S. M., Lee, C. E., Elias, C. F., Friedman, J. M., et al. (2009). Leptin targets in the mouse brain. *J. Comp. Neurol.* 514, 518–532.

Shinyama, H., Masuzaki, H., Fang, H., and Flier, J. S. (2003). Regulation of melanocortin-4 receptor signaling: agonist-mediated desensitization and internalization. *Endocrinology* 144, 1301–1314. doi: 10.1210/en.2002-220931

Spanswick, D., Smith, M., Groppi, V., Logan, S., and Ashford, M. (1997). Leptin inhibits hypothalamic neurons by activation of ATP-sensitive potassium channels. *Nature* 390, 521–525. doi: 10.1038/37379

Talley, E. M., Cribbs, L. L., Lee, J.-H., Daud, A., Perez-Reyes, E., and Bayliss, D. A. (1999). Differential distribution of three members of a gene family encoding low voltage-activated (T-type) calcium channels. *J. Neurosci.* 19, 1895–1911. doi: 10.1523/jneurosci.19-06-01895.1999

Traboulsie, A., Chemin, J., Kupfer, E., Nargeot, J., and Lory, P. (2006). T-type calcium channels are inhibited by fluoxetine and its metabolite norfluoxetine. *Mol. Pharmacol.* 69, 1963–1968. doi: 10.1124/mol.105.020842

Uebele, V. N., Gotter, A. L., Nuss, C. E., Kraus, R. L., Doran, S. M., Garson, S. L., et al. (2009). Antagonism of T-type calcium channels inhibits high-fat diet–induced weight gain in mice. *J. Clin. Invest.* 119, 1659–1667. doi: 10.1172/jci36954

Ueno, N., Asakawa, A., and Inui, A. (2007). Blunted metabolic response to fasting in obese mice. *Endocrine* 32, 192–196. doi: 10.1007/s12020-007-9016-z

van den Top, M., Lee, K., Whyment, A. D., Blanks, A. M., and Spanswick, D. (2004). Orexigen-sensitive NPY/AgRP pacemaker neurons in the hypothalamic arcuate nucleus. *Nat. Neurosci.* 7, 493–494. doi: 10.1038/nn1226

Vasconcelos, L. H., Souza, I. L., Pinheiro, L. S., and Silva, B. A. (2016). Ion channels in obesity: pathophysiology and potential therapeutic targets. *Front. Pharmacol.* 7:58. doi: 10.3389/fphar.2016.00058

Verkhratsky, A., and Toescu, E. (2003). Endoplasmic reticulum Ca2+ homeostasis and neuronal death. *J. Cell Mol. Med.* 7, 351–361. doi: 10.1111/j.1582-4934.2003.tb00238.x

Wichmann, T., and Soares, J. (2006). Neuronal firing before and after burst discharges in the monkey basal ganglia is predictably patterned in the normal state and altered in parkinsonism. *J. Neurophysiol.* 95, 2120–2133. doi: 10.1152/jn.01013.2005

Willfong, A., and Willmore, L. (2006). Zonisamide–a review of experience and use in partial seizures. *Neuropsychiatr. Dis. Treat.* 2, 269–280. doi: 10.2147/nedt.2006.2.3.269

Williams, K. W., Sohn, J. W., Donato, J. Jr., Lee, C. E., Zhao, J. J., Elmquist, J. K., et al. (2011). The acute effects of leptin require PI3K signaling in the hypothalamic ventral premammillary nucleus. *J. Neurosci.* 31, 13147–13156. doi: 10.1523/jneurosci.2602-11.2011

Yang, M.-J., Wang, F., Wang, J.-H., Wu, W.-N., Hu, Z.-L., Cheng, J., et al. (2010). PI3K integrates the effects of insulin and leptin on large-conductance Ca2+-activated K+ channels in neuropeptide Y neurons of the hypothalamic arcuate nucleus. *Am. J. Physiol. Endocrinol. Metab.* 298, E193–E201.

Yunker, A., Sharp, A., Sundarraj, S., Ranganathan, V., Copeland, T., and Mcenery, M. (2003). Immunological characterization of T-type voltage-dependent calcium channel CaV3. 1 (alpha1G) and CaV3. 3 (alpha1I) isoforms reveal differences in their localization, expression, and neural development. *Neuroscience* 117, 321–335. doi: 10.1016/s0306-4522(02)00936-3

Zhai, M., Yang, D., Yi, W., and Sun, W. (2020). Involvement of calcium channels in the regulation of adipogenesis. *Adipocyte* 9, 132–141. doi: 10.1080/21623945.2020.1738792

Conflict of Interest: The authors declare that the research was conducted in the absence of any commercial or financial relationships that could be construed as a potential conflict of interest.

Publisher's Note: All claims expressed in this article are solely those of the authors and do not necessarily represent those of their affiliated organizations, or those of the publisher, the editors and the reviewers. Any product that may be evaluated in this article, or claim that may be made by its manufacturer, is not guaranteed or endorsed by the publisher.

frontiers in Neuroscience

REVIEW
published: 13 October 2021
doi: 10.3389/fnins.2021.743546

Oxytocin as an Anti-obesity Treatment

JingJing Niu[1,2], *Jenny Tong*[1,2] *and James E. Blevins*[1,2]*

[1] VA Puget Sound Health Care System, Office of Research and Development, Medical Research Service, Department of Veterans Affairs Puget Sound Health Care System, Seattle, WA, United States, [2] Division of Metabolism, Endocrinology and Nutrition, Department of Medicine, University of Washington School of Medicine, Seattle, WA, United States

Obesity is a growing health concern, as it increases risk for heart disease, hypertension, type 2 diabetes, cancer, COVID-19 related hospitalizations and mortality. However, current weight loss therapies are often associated with psychiatric or cardiovascular side effects or poor tolerability that limit their long-term use. The hypothalamic neuropeptide, oxytocin (OT), mediates a wide range of physiologic actions, which include reproductive behavior, formation of prosocial behaviors and control of body weight. We and others have shown that OT circumvents leptin resistance and elicits weight loss in diet-induced obese rodents and non-human primates by reducing both food intake and increasing energy expenditure (EE). Chronic intranasal OT also elicits promising effects on weight loss in obese humans. This review evaluates the potential use of OT as a therapeutic strategy to treat obesity in rodents, non-human primates, and humans, and identifies potential mechanisms that mediate this effect.

Keywords: obesity, food intake, energy expenditure, oxytocin - therapeutic use, adipose tissue

OPEN ACCESS

Edited by:
Lionel Carneiro, The Ohio State University, United States

Reviewed by:
Susan Erdman, Massachusetts Institute of Technology, United States
Liya Kerem, Hadassah Medical Center, Israel

***Correspondence:**
James E. Blevins
jeblevin@u.washington.edu

Specialty section:
This article was submitted to Neuroenergetics, Nutrition and Brain Health, a section of the journal Frontiers in Neuroscience

Received: *18 July 2021*
Accepted: *16 September 2021*
Published: *13 October 2021*

Citation:
Niu J, Tong J and Blevins JE (2021) Oxytocin as an Anti-obesity Treatment. Front. Neurosci. 15:743546. doi: 10.3389/fnins.2021.743546

SOURCE AND FUNCTIONS OF OXYTOCIN

The obesity epidemic and its associated complications (Eckel et al., 2005; Cornier et al., 2008; Grundy, 2008) increase the risk for cardiovascular disease, cancer, type 2 diabetes (T2D), and death, including that from COVID-19 (Gao et al., 2020; Guo et al., 2020; Jordan et al., 2020; Michalakis and Ilias, 2020; Targher et al., 2020; Zhou et al., 2020) and has become a major health concern (Smyth and Heron, 2006). According to the National Center for Health Statistics, age-adjusted obesity prevalence between 1999–2000 and 2017–2018 has increased in adults from 30.5 to 42.4% (Hales et al., 2020). More than 78 million adults and 12.5 million children and adolescents in the United States are obese (Ogden et al., 2012) and the estimated annual medical cost of obesity is $147 billion in 2008 United States dollars (Finkelstein et al., 2009). Some of the current pharmacologic therapies to treat obesity [i.e., Qsymia (phentermine + topiramate) and Contrave (naltrexone hydrochloride/bupropion hydrochloride)] can worsen sleep disturbance or worsen depression and are not well tolerated (Hollander et al., 2013; Kusminski et al., 2016; Halseth et al., 2018). While major advances in obesity pharmacotherapy have been made with semaglutide, a glucagon-like peptide-1 receptor agonist, which provides significant weight loss of 15% (Wilding et al., 2021), it has been associated with gastrointestinal side effects, including nausea and diarrhea, in overweight and obese adults without diabetes (Rajagopal and Cheskin, 2021). Understanding the unique contributing factors to obesity and designing targeted interventions to lower the disease burden is an urgent need.

While the neurohypophyseal hormone oxytocin (OT) is well recognized for its role in osmoregulation (Verbalis et al., 1995b), prosocial behavior (Striepens et al., 2011; Yamasue et al., 2012) and reproductive behaviors, including lactation (Braude and Mitchell, 1952) and uterine contraction (den Hertog et al., 2001), it is also being tested as a potential therapy to treat post-traumatic stress disorder (van Zuiden et al., 2017; Flanagan et al., 2018), schizophrenia (Striepens et al., 2011; Montag et al., 2012), autism spectrum disorder (Striepens et al., 2011; Yamasue et al., 2012; Miller, 2013; Young and Barrett, 2015), and obesity (Zhang et al., 2013; Lawson et al., 2015; Hsu et al., 2017). This excitement has translated to 535 completed, ongoing, or pending investigations in humans (ClinicalTrials.gov registry, National Institutes of Health). Given the current state of the obesity epidemic and lack of highly effective treatment options, this review focuses on OT as an anti-obesity therapy and mechanisms that contribute to these effects in genetically obese (Kublaoui et al., 2008; Tung et al., 2008; Maejima et al., 2011; Morton et al., 2012; Altirriba et al., 2014) and diet-induced obese (DIO) rodents (Deblon et al., 2011; Maejima et al., 2011, 2017; Zhang and Cai, 2011; Zhang et al., 2011; Morton et al., 2012; Edwards et al., 2021b) as well as in DIO non-human primates (Blevins et al., 2015) and obese humans (Zhang et al., 2013; Lawson et al., 2015; Thienel et al., 2016; Hsu et al., 2017) and assesses the translational and therapeutic potential of OT in humans. Due to the short duration of exposure of OT in the majority of clinical trials, one of the challenges that remains will be to examine the safety, tolerability, and efficacy of chronic intranasal OT use and to identify optimal dosing and frequency of administration to evoke clinically meaningful weight loss in individuals with obesity in the absence of adverse side effects (MacDonald et al., 2011; Tachibana et al., 2013; Zhang et al., 2013; Hsu et al., 2017; Cai et al., 2018). The barriers to the use of chronic treatment include concerns about OT-elicited down-regulation of OT receptors (OTRs) (Insel et al., 1992; Peters et al., 2014; Freeman et al., 2018), the potential for increased anxiety (Peters et al., 2014; Winter et al., 2021), impairments in partner preference (Bales et al., 2013), aggression (Rault et al., 2013), hyponatremia (Bergum et al., 2009; Vallera et al., 2017), adverse cardiovascular effects (Pinder et al., 2002; Vallera et al., 2017; Snider et al., 2019) through interactions with vasopressin receptors (Snider et al., 2019), and feelings of distrust in humans with borderline personality disorder (Bartz et al., 2011) (see Miller, 2013; Leng and Ludwig, 2016a; Leng and Sabatier, 2017, for review).

The majority of central nervous system (CNS) OT is synthesized by magnocellular and parvocellular neurons in the paraventricular nucleus (PVN) as well as the magnocellular neurons in the supraoptic nucleus (SON) in mice (Young et al., 1996; Lein et al., 2007; Blouet et al., 2009; Maejima et al., 2009; Zhang et al., 2011; Sutton et al., 2014), rats (Swaab et al., 1975a,b; Sawchenko and Swanson, 1982; Sawchenko et al., 1984; Rinaman, 1998; Grinevich and Neumann, 2020), non-human primates (Antunes and Zimmerman, 1978; Sofroniew et al., 1981; Kawata and Sano, 1982; Ginsberg et al., 1994; Ragen and Bales, 2013), and humans (Dierickx and Vandesande, 1977; George, 1978; Paulin et al., 1978; Sukhov et al., 1993; Koutcherov et al., 2000) (see Gimpl and Fahrenholz, 2001; Ragen and Bales, 2013, for review). OT is also expressed in magnocellular neurons of the PVN and SON of the prairie vole but it still not clear if OT is expressed in parvocellular PVN neurons or whether OT projections to the nucleus accumbens (NAcc) originate from parvocellular or magnocellular neurons in prairie voles (Ross et al., 2009). In addition to the PVN and SON, OT is found in smaller amounts within magnocellular neurons in the anterior commissural nuclei (mouse) (Castel and Morris, 1988), anterior hypothalamus (mole-rat) (Rosen et al., 2008), accessory nuclei (mouse/rat) (Castel and Morris, 1988; Rinaman, 1998), preoptic area (mole-rat) (Rosen et al., 2008) and periventricular nuclei (mouse) (Castel and Morris, 1988). OT is also expressed in the bed nucleus of the stria terminalis (BNST; mole-rat/rat) (Rinaman, 1998; Rosen et al., 2008), caudal subzona incerta (hamsters) (Vaughan et al., 2011) dorsal hypothalamic area (hamsters) (Shi and Bartness, 2001), mediobasal preoptic area (mouse) (Castel and Morris, 1988), medial amygdala (mole-rat/rat) (Rinaman, 1998; Rosen et al., 2008) and septal region (rat) (Rinaman, 1998).

Mature OT and the carrier neurophysin are processed from the OT/neurophysin 1 prepropeptide (Brownstein et al., 1980) with both being stored in the axon terminals prior to release (Renaud and Bourque, 1991). It appears that the predominant role of neurophysin is to target, package and store OT within secretory granules prior to release (see Gimpl and Fahrenholz, 2001, for review). OT is released both locally from somatodendrites from magnocellular OT neurons in the SON and PVN (Pow and Morris, 1989; Zhang and Cai, 2011; Zhang et al., 2011; Wu et al., 2017) (see Ludwig and Leng, 2006, for review) and distally at axon terminals within the neurohypophysis that originate from magnocellular PVN and SON OT neurons. Recent findings indicate that magnocellular OT neurons also send collateral projections to a number of distal extrahypothalamic sites (Zhang et al., 2021). Magnocellular OT neurons within the PVN appear to send collaterals to the amygdala, caudate putamen and NAcc while those in the SON appear to send collaterals to the caudate putamen, NAcc, piriform cortex and lateral septum (Zhang et al., 2021). In addition, OT is also secreted from axon terminals from parvocellular PVN OT neurons that project to the hypothalamic arcuate nucleus (ARC) (Maejima et al., 2014) (mice), NAcc (Ross et al., 2009, prairie voles)/(Knobloch et al., 2012, rats), midbrain ventral tegmental area (VTA) (Shahrokh et al., 2010), hindbrain parabrachial nucleus (PBN) (Ryan et al., 2017) (mice), dorsal motor nucleus of the vagus (DMV) (Sawchenko and Swanson, 1982; Rinaman, 1998) nucleus tractus solitarius (NTS) (Sawchenko and Swanson, 1982; Rinaman, 1998; Sutton et al., 2014) (rats, mice), and spinal cord (Sawchenko and Swanson, 1982; Sutton et al., 2014) (rats, mice).

The extent to which OT is expressed in outgoing projections from the PVN to hindbrain CNS sites linked to the control of body weight appear to vary based on targets and species. Kirchgessner and Sclafani initially proposed that OT projections from the PVN to hindbrain were important in the control of food intake and body weight based on findings from their lab in which knife cuts that sever PVN-hindbrain projections were found to disrupt OT fibers (Kirchgessner et al., 1988) and result

in hyperphagia and obesity (Kirchgessner and Sclafani, 1988). There is a large body of evidence linking hindbrain NTS OTRs in the control of homeostatic food intake (Kirchgessner and Sclafani, 1988; Kirchgessner et al., 1988; Blevins et al., 2003, 2004; Blouet et al., 2009; Baskin et al., 2010; Ho et al., 2014; Ong et al., 2015, 2017; Roberts et al., 2017; Edwards et al., 2021b). Studies have suggested that OT acts, in part, at NTS OTRs, to enhance the responsiveness of gastrointestinal satiation signals (Olson et al., 1991b; Blevins et al., 2003, 2015; Baskin et al., 2010; Ong et al., 2015, 2017) to limit meal size. More recent studies have implicated NTS OTRs in the control of food motivation and feeding reward (Wald et al., 2020). The role of hindbrain OTRs in the control of energy balance is further reviewed in Blevins and Ho (2013), Lawson et al. (2020), and McCormack et al. (2020) (food intake) and Section "What Receptor Populations Mediate Oxytocin's Effects on Brown Adipose Tissue (BAT) Thermogenesis and Energy Expenditure?". OT has been found to be expressed in up to (1) 6.3–10.1% of neurons with descending projections from the PVN to the dorsal vagal complex (DVC) (Olson et al., 1992) or (2) 11–16% of neurons with descending projections the PVN to the medulla and spinal cord (Sawchenko and Swanson, 1982) (rats). A recent paper found that OT may be found in a substantially higher proportion of neurons that project to the DVC (28.9%) in rats (Maejima et al., 2019). Current findings indicate that species differences (mice vs. rats) could account for the proportion or location where parvocellular PVN OT neurons project to the NTS. Namely, the majority of PVN OT neurons that project to the NTS appear to the reside within the caudal parvocellular PVN in rats (Rinaman, 1998). One recent study by Sutton et al. (2014) determined that there were few OT projections from the rostral parvocellular PVN that terminated within the NTS and that those that did exist were likely fibers of passage. In addition, those OT neurons that are expressed in the rostral PVN appear to project to spinal cord. These findings raise two questions: (1) Do parvocellular PVN OT neurons located within the caudal parvocellular PVN provide the bulk of OT innervation to the NTS in both mice and rats? (2) Is the parvocellular PVN OT projection to the NTS less dense in the mouse model compared to the rat model? Existing findings at least provide indirect evidence in support of a descending PVN to NTS OT projection in a mouse model (Blouet et al., 2009; Matarazzo et al., 2012; Ryan et al., 2017; Wu et al., 2017) and implicate an important role for OTRs within the caudal hindbrain in the control of body weight through reductions of food intake (homeostatic and hedonic) and increases in BAT thermogenesis or core temperature (as surrogate marker of energy expenditure) in both mice (Blouet et al., 2009; Matarazzo et al., 2012; Ryan et al., 2017; Edwards et al., 2021b) and rats (Baskin and Bastian, 2010; Blevins and Ho, 2013; Ho et al., 2014; Ong et al., 2015, 2017; Roberts et al., 2017; Edwards et al., 2021a).

PVN spinally projecting neurons (SPNs) that express OT appear to be involved with modulating cardiovascular function, stress response, thermoregulation and energy expenditure (via BAT thermogenesis) (see Hallbeck et al., 2001; Nunn et al., 2011, for review). Chemogenetic activation of PVN OT neurons, found to send dense projections to thoracic spinal cord in close proximity to choline acetyltransferase (+) (ChAT; marker of cholinergic neurons) neurons, increased energy expenditure (oxygen consumption), tended to increase BAT temperature (P = 0.13) and increased Fos (marker of neuronal activation) within ChAT (+) neurons of the thoracic spinal cord (Sutton et al., 2014) in *Oxytocin-ires-Cre* mice. The proportion of OT found in these PVN SPNs range between 20 and 25% (Cechetto and Saper, 1988) and approximately 40% (Hallbeck et al., 2001) (rats). The lateral parvocellular subdivision contained the highest proportion of PVN OT SPNs (47%), followed by the dorsal parvocellular division (31%) and the medial parvocellular division (24%). It will be helpful to direct future studies to examine the extent to which OTRs within the spinal cord and hindbrain NTS are activated in response to cold and produce overlapping or distinct effects on BAT thermogenesis and energy expenditure.

Data from a combination of pharmacological, microdialysis and/or tract tracing studies suggest that PVN OT neuronal projections to the NAcc are involved with modulating social behavior and feeding reward (Ross et al., 2009; Herisson et al., 2016). Herisson et al. (2016) found that direct injections of OT into the NAcc core reduced intake of palatable sucrose and saccharin solutions, thus providing some of the first evidence linking OTRs within the NAcc core to feeding reward [see Klockars et al., 2015; Lawson et al., 2020 for role of NAcc OTRs in the control of food intake]. Based on the finding by Ross et al. (2009), OT fibers within the NAcc appear to be well conserved in terms of density and distribution in prairie voles, meadow voles, mice and rats. OT has also been found to be expressed in 23% of PVN neurons that project to the NAcc in prairie voles (Ross et al., 2009). In the rat model, the number of fibers (and possibly terminals) found within the NAcc that originate from the PVN appear to vary based on region and if the analysis was done on the side ipsilateral or contralateral to the tracer injection site. Some reports indicate that the NAcc contains only a few OT fibers and/or terminals (Sofroniew, 1983) (not determined if origin was PVN or SON) but other reports that examined only those projections originating from the PVN found there to be up to 50 OT fibers (NAcc core; Knobloch et al., 2012) or >50 OT fibers (NAcc shell; Knobloch et al., 2012) with virtually no projections originating from the SON. These latter findings are consistent with a recent study in mice by Yao et al. (2017), who reported the presence of a low density (∼10–20 fibers) in the NAcc. The reason for the differences in OT fiber density within the NAcc across studies is not clear and may be due, in part, to differences in mouse strain, species and heterogeneity of neuronal projections within a CNS site. A recent study suggests that a subset of these projections may arise from either parvocellular PVN OT neurons or magnocellular PVN or SON neurons. Zhang et al. (2021) determined that a subset of magnocellular OT neurons within the PVN and SON send collateral projections to NAcc. It remains to be determined the extent to which such collateral projections to the NAcc may be important in the control of social behavior and feeding reward.

It is well established that the adiposity signal, leptin, acts, in part, in the ARC to reduce body weight in lean animals by activating anorexigenic [proopiomelanocortin (POMC)] neurons while simultaneously inhibiting orexigenic [neuropeptide Y

(NPY)/agouti-related peptide (AGRP)] neurons (see Schwartz et al., 2000; Woods et al., 2000, for review). Several lines of evidence implicate ARC POMC neurons and the endogenous melanocortin 3/4 receptor (MC3R/MC4R) agonist, alpha-melanocyte stimulating hormone (α-MSH; derivative of POMC), as an important component relaying leptin input from the ARC to PVN OT neurons that are positioned to project to the hindbrain and enhance the hindbrain neuronal and satiety response to cholecystokinin (CCK), ultimately resulting in smaller meals (Seeley et al., 1997; Olszewski et al., 2001; Zhang and Felder, 2004; Blevins et al., 2009; Baskin et al., 2010). What remains unclear is the role of a recently identified OT projection from the PVN or SON to the ARC in the control of energy balance and whether this projection is primarily involved with the control of food intake (Maejima et al., 2014; Liao et al., 2020), energy expenditure, or both. Initially studies found that OT administration into the ARC reduced food intake (Maejima et al., 2014). Furthermore, chemogenetic stimulation of OTR-expressing neurons in the ARC reduced food intake and fasting-elicited refeeding in mice (Fenselau et al., 2017) implicating an important role of endogenous OTR signaling within the ARC in the control of food intake. ARC POMC neurons appear to be downstream targets of OT action as POMC neurons express OTRs and OT stimulates cytosolic Ca (2+) from POMC neurons (Maejima et al., 2014). A complementary study by Fenselau reported that ARC OTR-expressing neurons are glutamatergic and that 50% of ARC OTR-expressing neurons expressed POMC (Fenselau et al., 2017). In addition, bath application of OT stimulated the firing rate of ARC OTR-expressing neurons in Oxtr-Cre:tdTomato mice (Fenselau et al., 2017). Through neuroanatomical tracing studies Maejima found that OT was expressed in 29% and 24% of PVN and SON neurons that project to the ARC, respectively (Maejima et al., 2014). In contrast, Liao et al. (2020) indicated that while there was dense OT fiber innervation of the ARC there appeared to be only "some axon terminals in the arcuate hypothalamus nucleus (Arc)" in OxtCre=C; Z/AP double-heterozygous mice. Yao et al. (2017) examined the density of OT fibers that originate from PVN OT neurons and found that OT fibers were found in medium density (>20 fibers) in the ARC in mice. Fenselau also identified that ARC-OTR expressing neurons also project to the PVN. Furthermore, optogenetic stimulation of terminals that arise from ARC-OTR (+) neurons that innervate the PVN result in the suppression of food intake (Fenselau et al., 2017). Future studies will need to determine the extent to which specific ARC-OTR cell populations may regulate both food intake and energy expenditure.

Existing data suggest that OTRs within the VMH are important in both the control of food intake and energy expenditure (see Sabatier et al., 2007; Sabatier et al., 2013; Lawson, 2017, for review). Noble and Klockars both demonstrated that direct injections of OT into the VMH reduced chow intake but had no effect on more palatable saccharin or sucrose solutions (Klockars O. A. et al., 2017) in rats (Noble et al., 2014; Klockars O. A. et al., 2017). These findings link VMH OTRs more so to the control of homeostatic feeding rather than feeding reward. While OT has been recently described in projections from the PVN to the VMH (Nasanbuyan et al., 2018) in mice existing data suggest that OT fibers within the VMH are likely fibers of passage. These findings are also consistent with a recent report by Yao et al. (2017), who reported the presence of low density of OT fibers (∼10–20 fibers) within the VMH originated from the PVN in mice. While OT fibers were detected within regions of the ventrolateral VMH (Liao et al., 2020) that express OTRs in mice (Nasanbuyan et al., 2018). Liao further determined that there were "almost no axon terminals" within the VMH (Liao et al., 2020). Leng et al. (2008) further commented that there was "virtually complete absence of OT-containing fibres in the VMH" and that "The VMH contains very few fibres that show any immunoreactivity for either OT or vasopressin" and that "it is not known whether the few OT fibres there are 'stray' axons or dendrites of magnocellular neurons or come from parvocellular neurons of the PVN." In addition, Leng commented that "So far, there has been no direct evidence of any projection to or synaptic innervation of VMH neurons by OT neurons from the parvocellular region of the PVN" (Leng et al., 2008). Thus, while there does not appear to be data to support a PVN OT projection to the VMH in mice or rats, direct administration of OT into the VMH reduces food intake (Noble et al., 2014; Klockars O. A. et al., 2017) and increases energy expenditure (Noble et al., 2014). Leng and colleagues have postulated that OT, following somatodendritic release from magnocellular OT neurons (within the SON or PVN), could be an important source of endogenous OT that could reach VMH OTRs by diffusion (1) to the ventricles and subsequent transport through cerebrospinal fluid (CSF) or (2) within the brain (Ludwig and Leng, 2006; Sabatier et al., 2007) (see Leng and Ludwig, 2008; Leng et al., 2008; Sabatier et al., 2013; Leng and Sabatier, 2017, for review). The hypothesis that somatodendritic release of OT acts, in part, at VMH OTRs to suppress food intake is particularly attractive as Leng and Sabatier (2017) indicated that dendritic release is "delayed and long-lasting, potentially contributing to post-prandial satiety." In addition, (1) large amounts of OT are released somatodentrically from magnocellular OT neurons, (2) the SON and PVN are found in close proximity to the VMH, (3) there is robust expression of OTRs within the VMH, and (4) magnocellular OT neurons within the SON and neurons within the VMH are activated in response to food intake (Johnstone et al., 2006). Collectively, these studies have begun to address the potential source of endogenous OT to VMH OTRs and whether this source of endogenous OT to the VMH may also be important in the control of food intake (Leng et al., 2008; see Leng and Ludwig, 2008; Sabatier et al., 2013; Leng and Sabatier, 2017, for review).

The OT projection from the PVN to the VTA has been implicated in the control of social behavior and feeding reward (Mullis et al., 2013; Liu et al., 2020b; Wald et al., 2020) (also see Klockars et al., 2015; Lawson et al., 2020, for additional information on VTA OTRs in the control of food intake). Previous data from Mullis et al. (2013) indicate that direct administration of OT into the VTA reduces consumption of highly palatable 10% sucrose solution. Consistent with these findings, Wald et al. (2020) recently found that OT administration into the VTA reduced bar presses in order to consume palatable sucrose pellets, a finding that suggests OT

decreases the willingness to work to obtain sucrose pellets. In addition, they found that VTA administration of OT also reduced food seeking behavior toward palatable chocolate pellets (Wald et al., 2020). Liu et al. (2020b) subsequently provided mechanistic data using *in vivo* fiber photometry to suggest that OT reduces food cue (sucrose)-elicited activation of dopamine neurons within the VTA suggesting that OT may reduce reward intake, in part, through an inhibitory effect on dopamine neurons and their response to rewarding food cues. Eric Krause and colleagues provided neuroanatomical confirmation that a subpopulation of VTA OTR (+) neurons express dopamine (10%) [in addition to glutamate (≈ 44%)], some of which project to the NAcc (Peris et al., 2016). Recent reports indicate there is a direct projection from the PVN to the VTA in rats (Shahrokh et al., 2010) and Liao indicated there were "some branch-like terminals" within the VTA in OxtCre = C; Z/AP double-heterozygous mice (Liao et al., 2020). Yao et al. (2017) examined the density of OT fibers that originate from PVN OT neurons and found that OT fibers were found in medium density (>20 fibers) in VTA. A separate study found that approximately 20% of PVN OT neurons were found to project to the VTA following green retrobead injections into mice expressing tdTomato under control of the *Oxt* promoter (Xiao et al., 2017). Beier extended these findings and found that approximately 6 and 13% of PVN OT neurons synapsed onto VTA dopamine and GABA neurons in DAT-Cre and GAD2-Cre mice, respectively (Beier et al., 2015). These findings are consistent with those from Peris et al. (2016) who demonstrated that approximately 5% of OTR (+) neurons within the VTA co-localized with tyrosine hydroxylase in OTR-Cre mice.

Data from pharmacological and chemogenetic studies implicate a role for the PVN OT projection to the PBN in the control of fluid intake (Ryan et al., 2017). Ryan et al. (2017) demonstrated that PBN OTR (+) neurons were activated by NaCl or water repletion. In addition, chemogenetic activation of PBN OTRs resulted in a suppression of fluid intake (Ryan et al., 2017). Photostimulation of OT terminals within the PBN also resulted in activation of 22% of PBN OTR (+) neurons (Ryan et al., 2017). Ryan further demonstrated that PBN receives direct innervation from PVN OT neurons (Ryan et al., 2017). It is notable that Sutton et al. (2014) demonstrated very little OT fiber innervation within the PBN that originated from the rostral PVN although it might be possible that OT neurons in more caudal regions of the PVN may innervate the PBN more heavily. Collectively, the findings by Ryan demonstrate that OTR-expressing neurons within the PBN are important in the control of fluid homeostasis.

Similar to the VMH, the raphe pallidus is an area that receives virtually little to no innervation from PVN OT neurons despite receiving dense projections from other neuron subtypes within the PVN (Luo et al., 2019). Sutton et al. (2014) reported the existence of few OT terminals within the raphe pallidus. Despite this, Kasahara et al. (2015) have determined that OTR (+) neurons are activated in response to cold and that increased OTR signaling within the rostral raphe pallidus helps restore deficits in response to cold-induced thermogenesis in OT receptor deficient mice (see sections "Does Endogenous Oxytocin Impact Cold-Induced Thermogenesis and Energy Expenditure?" and "What Receptor Populations Mediate Oxytocin's Effects on Brown Adipose Tissue Thermogenesis and Energy Expenditure?" for additional information).

Data from pharmacological and chemogenetic studies implicate a role for the PVN OT projection to the CeA in the control of fear responses (Knobloch et al., 2012) and food intake (Klockars et al., 2018) (also see Lawson et al., 2020, for additional information on CeA OTRs in the control of food intake). Klockars demonstrated that direct injections of OT into the CeA reduced chow intake but had no effect on more palatable saccharin or sucrose solutions in rats (Klockars et al., 2018) while OT within the basolateral amygdala appeared to reduce intake of both chow and palatable solutions. These findings suggest that OTRs within the CeA may be more involved in the control of homeostatic feeding while those in the basolateral amygdala may participate in both homeostatic and feeding reward. Within the CeA, Yao et al. (2017) examined the density of OT fibers that originate from PVN OT neurons and found a small number of fibers within the CeA (∼0–10 fibers) (mice). In contrast, Liao et al. (2020) identified that there are "many axon terminal branches cover the whole central amygdala region including the central amygdala medial division (CeM), central amygdala lateral division (CeL) and central amygdala capsular part (CeC)" using a $Oxt^{Cre}/^{+}$; Z/AP mice. OT fibers from the PVN are also found to innervate the CeA (∼12–36 fibers/side) and medial amygdala (MeA) (∼30–59 fibers/side) in rats (Knobloch et al., 2012). The reasons for the differences in OT fiber density within the CeA between studies are unclear although differences with respect to mouse strain, species, and heterogeneity of neuronal projections within a CNS site may play a role.

Oxytocin is also expressed in peripheral tissues including the heart (rats; Jankowski et al., 1998) and rat and human gastrointestinal (GI) tract (Ohlsson et al., 2006; Welch et al., 2009; Paiva et al., 2021) (including neurons of myenteric and submucosal plexus of enteric nervous system) (Paiva et al., 2021) as well as the islets of Langerhans of the pancreas and Leydig cells of the testes in rats (Paiva et al., 2021), although the stimuli that impact the release of OT within these areas, where it is released and extent to which these peripheral sources of OT contribute to energy balance is not clear.

OXYTOCIN RECEPTOR EXPRESSION IN CENTRAL NERVOUS SYSTEM SITES ASSOCIATED WITH ENERGY BALANCE IN RODENTS, NON-HUMAN PRIMATES AND HUMANS

There is widespread expression of OTRs in CNS sites that are linked to the control of food intake or BAT thermogenesis based on being anatomically positioned to control sympathetic outflow to interscapular BAT (IBAT) to potentially control energy expenditure. There is wide overlap in OTR distribution in mice and rats in areas that include the forebrain hypothalamus [ARC, MPA, suprachiasmatic nucleus, and VMH]/mouse (Gould and Zingg, 2003; Yoshida et al., 2009; Hidema et al., 2016;

Fenselau et al., 2017; Ryan et al., 2017)/rat (van Leeuwen et al., 1985; Vaccari et al., 1998; Klockars O. A. et al., 2017)] and basal ganglia [e.g., NAcc and CeA/mouse (Yoshida et al., 2009; Hidema et al., 2016; Ryan et al., 2017)/rat (van Leeuwen et al., 1985; Tribollet et al., 1992; Vaccari et al., 1998)], midbrain VTA [mouse (Peris et al., 2017)/rat (Vaccari et al., 1998)] as well as hindbrain PBN [mouse (Ryan et al., 2017)], rostral medullary raphe (raphe pallidus) [mouse (Yoshida et al., 2009; Kasahara et al., 2015; Sun et al., 2019)], AP [mice (Gould and Zingg, 2003; Yoshida et al., 2009; Ryan et al., 2017)], DMV [mouse (Ryan et al., 2017)/rat (Tribollet et al., 1992; Verbalis et al., 1995a; Vaccari et al., 1998)], NTS [mouse (Gould and Zingg, 2003; Yoshida et al., 2009; Sun et al., 2019)/rat (Verbalis et al., 1995b; Baskin and Bastian, 2010; Ong et al., 2015, 2017)] and spinal cord [mouse (Wrobel et al., 2011)/rat (Reiter et al., 1994)]]. OTRs are also found in the SON and PVN in rats (Yoshimura et al., 1993) and subsequent studies identified OTRs on the somata and dendrites of magnocellular OT neurons in lactating female rats but not in male rats (Freund-Mercier et al., 1994) although it is not yet certain if detectability in the female rats is due, in part, to pre-treatment with the OTR antagonist (Freund-Mercier et al., 1994). These autoreceptors are not found in male rats or in untreated lactating rats and have been proposed to contribute to the feed forward effect of OT on its own release during the milk letdown reflex (Freund-Mercier et al., 1994; Freund-Mercier and Stoeckel, 1995). In contrast to rodents, OTRs appear to have a more restricted distribution in CNS sites linked to energy balance within a variety of non-human primate species (cynomolgus, rhesus macaque, and common marmoset) [NAcc, preoptic area, VMH, DMV, and spinal cord (Boccia et al., 2001; Schorscher-Petcu et al., 2009; Freeman et al., 2014)] and humans (CeA, anterior hypothalamus, MPA, PVN, VMH, AP, NTS and spinal cord) (Loup et al., 1989, 1991; Boccia et al., 2013). OT fibers appear to be in proximity of OTR (+) neurons within the ventrolateral VMH in the mouse (Nasanbuyan et al., 2018) (suggesting the presence of synaptic terminals). Similarly, in the rat, the ventrolateral VMH also expresses OT fibers (Daniels and Flanagan-Cato, 2000; Flanagan-Cato et al., 2001) although there appear to be very few OT fibers elsewhere within the VMH of the rat (Caldwell et al., 1988; Jirikowski et al., 1988; Schumacher et al., 1989, see Leng et al., 2008, for review). As mentioned earlier, others have proposed that OT may reach OTRs by diffusion (see Verbalis et al., 1995a; Verbalis, 1999, for review) from magnocellular OT neurons within the SON (see Leng et al., 2008; Sabatier et al., 2013, for review), through the third ventricle (3V) following dendritic release of OT from the PVN or possibly by axonal release within the VMH (Leng et al., 2008). It is important to note that many of the more recent studies have utilized more advanced and complementary screening tools to assess OTR expression in mice compared to the earlier pharmacological and/or antibody screening tools used to identify OTRs in rats in the 1980s and 1990s. Questions about selectivity and specificity of the antibodies and pharmacological tools used in earlier studies limit our ability to more firmly identify species differences, nonetheless, overlapping patterns of OTR distribution within the basal ganglia, hypothalamus, midbrain, hindbrain and spinal cord implicate potentially important roles of these areas in contributing to the control of food intake (homeostatic and hedonic feeding) and energy expenditure that appear to be well conserved across species. OTRs are also found in peripheral sites that include the GI tract (Qin et al., 2009), nodose ganglion (Welch et al., 2009; Brierley et al., 2021), skeletal muscle (Elabd et al., 2014; Gajdosechova et al., 2014, 2015) and bone (Copland et al., 1999; Colucci et al., 2002; Tamma et al., 2009; Colaianni et al., 2012) in rodents as well as white adipocytes or white adipose tissue in both rodents and humans (Muchmore et al., 1981; Schaffler et al., 2005; Tsuda et al., 2006; Altirriba et al., 2014; Gajdosechova et al., 2014, 2015; Yi et al., 2015; Sun et al., 2019). Recent findings by both Sun et al. (2019) and Yuan et al. (2020) have also reported that OTRs are expressed on brown adipocytes or brown adipose tissue. The potential role OTRs on white and brown adipocytes, the GI tract, vagal sensory afferent nerves, skeletal muscle and bone in contributing to the effects of circulating OT in the control of energy balance, muscle maintenance and bone mass is discussed in Section "How Does Oxytocin Impact Body Composition".

IS OXYTOCIN EFFECTIVE AT REDUCING BODY WEIGHT IN RODENT MODELS OF OBESITY?

Previous studies have shown that central, systemic [intraperitoneal (IP), subcutaneous (sc) or intravenous], intraoral (in combination with a proton pump inhibitor) (Maejima et al., 2020) or intranasal administration of OT reduces energy intake, body weight or weight gain in DIO mice and rats (Deblon et al., 2011; Maejima et al., 2011, 2017; Zhang and Cai, 2011; Zhang et al., 2011; Morton et al., 2012; Roberts et al., 2017; Labyb et al., 2018; Seelke et al., 2018; Snider et al., 2019; Edwards et al., 2021b), genetically obese mice and rats [e.g., obese Zucker *fatty* (*fa/fa*) rat, Koletsky (*fak/fak*) rat, *ob/ob*, *db/db and Sim1*$^{\pm}$ mice] (Kublaoui et al., 2008; Maejima et al., 2009; Morton et al., 2012; Altirriba et al., 2014; Iwasaki et al., 2015; Plante et al., 2015; Balazova et al., 2016), ovariectomized rats (Iwasa et al., 2019b), a rat model of dihydrotestosterone-induced polycystic ovary syndrome (PCOS) (Iwasa et al., 2019a), as well as in DIO rhesus monkeys (Blevins et al., 2015).

Numerous findings suggest that OT reduces body weight or weight gain in rodents and non-human primates, in part, by reducing energy intake (see Blevins and Baskin, 2015; Lawson et al., 2020; McCormack et al., 2020, for review). It is well documented that OT reduces food intake (including chow, purified low and high fat diet or sucrose solution) following systemic (Arletti et al., 1989, 1990; Deblon et al., 2011; Maejima et al., 2011, 2015, 2017; Morton et al., 2012; Altirriba et al., 2014; Ho et al., 2014; Blevins et al., 2015; Iwasaki et al., 2015, 2019; Balazova et al., 2016; Klockars A. et al., 2017; Iwasa et al., 2019b, 2020; Erdenebayar et al., 2020), intranasal (Maejima et al., 2015) or CNS administration (Arletti et al., 1989, 1990; Olson et al., 1991a; Lokrantz et al., 1997; Rinaman and Rothe, 2002; Kublaoui et al., 2008; Deblon et al., 2011; Morton et al., 2012; Mullis et al., 2013; Ho et al., 2014; Noble et al., 2014; Ong et al., 2015; Herisson et al., 2016; Klockars O. A. et al., 2017; Klockars et al., 2018; Liu et al., 2020a; Edwards et al., 2021a,b). While many

such investigations have targeted the lateral ventricles, 3V and 4V, which lack the anatomical resolution to differentiate receptor populations, recent findings indicate that OT reduces food intake following direct injections into the ARC (Maejima et al., 2014), CeA (Klockars et al., 2018), basolateral amygdala (Klockars et al., 2018), VMH (Noble et al., 2014; Klockars O. A. et al., 2017), striatum (NAcc core) (Herisson et al., 2016), midbrain VTA (Mullis et al., 2013) and hindbrain NTS (Ong et al., 2015), many of which express OTRs (see section "Oxytocin Receptor Expression in Central Nervous System Sites Associated With Energy Balance in Rodents, Non-human Primates and Humans") and are also innervated by OT neurons within the PVN or SON (see **Figure 1** and see section "Source and Functions of Oxytocin"). Importantly, OT, at doses that reduce food intake when given into the CNS or periphery, is not associated with increased kaolin diet intake (referred to as pica behavior/readout of visceral illness) (Zhang et al., 2011; Blevins et al., 2016; Roberts et al., 2017; Edwards et al., 2021b) or a conditioned taste aversion test (Zhang et al., 2011; Noble et al., 2014; Iwasaki et al., 2015; Blevins et al., 2016) in lean and obese mice (Zhang et al., 2011; Iwasaki et al., 2014; Roberts et al., 2017; Edwards et al., 2021b) and rats (Noble et al., 2014; Blevins et al., 2016; Roberts et al., 2017). Together, these findings suggest that OT, either given alone, or in combination with other drugs, could be an attractive anti-obesity therapy in DIO and genetically obese rodents and DIO non-human primates. In Section "Does Exogenous Oxytocin Increase Energy Expenditure?," we will review the potential role of energy expenditure in contributing to the effects of OT on weight loss in rodents and non-human primates.

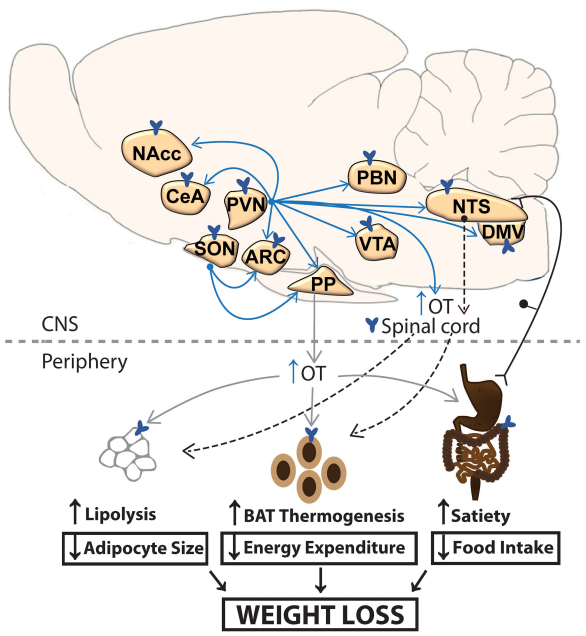

FIGURE 1 | A schematic of circuitry that potentially contributes to the effectiveness of CNS OT on energy homeostasis. OT release within the CNS and spinal cord (shown in blue arrows) or periphery (shown in gray) may impact metabolic processes that result in the reduction of body weight. Dotted arrow represents implicated pathways from NTS to spinal cord and from sympathetic preganglionic neurons in the spinal cord to BAT and WAT. ARC, arcuate nucleus; BAT, brown adipose tissue; CeA, central nucleus of the amygdala; DMV, dorsal nucleus of the vagus; NaCC, nucleus accumbens; NTS, nucleus of the solitary tract; OT, oxytocin; PBN, parabrachial nucleus; PP, posterior pituitary; PVN, paraventricular nucleus; SON, supraoptic nucleus; VTA, ventral tegmental area; WAT, white adipose tissue.

DOES EXOGENOUS OXYTOCIN INCREASE ENERGY EXPENDITURE?

Numerous studies provide both direct and indirect evidence to indicate that OT is important in the control of energy expenditure. Indirect evidence stemming from pair-feeding studies (amount of food given to vehicle-treated animals is equal to that of OT-treated animals) indicate that OT-treated animals lose more weight relative to pair-fed control animals (Deblon et al., 2011; Altirriba et al., 2014; Blevins et al., 2016). These findings were evident following chronic lateral ventricular infusions of OT (16 nmol/day) in high fat diet-fed male rats (weeks 5 to 7 of high fat diet feeding) or chronic sc infusions of OT (50 nmol/day) into male high fat diet-fed rats (weeks 5 to 7 of high fat diet, 45% kcal from fat) (Deblon et al., 2011), male lean standard diet-fed rats (Deblon et al., 2011) as well as in male *ob/ob* mice (Altirriba et al., 2014). Note that it is not clear the extent to which the rats used in the study by Deblon et al. (2011) were DIO without having the body weight and body composition data pre- and post-dietary intervention and they were only maintained on the high fat diet for a relatively short period of time (5 to 7 weeks). However, similar findings have been obtained following a single acute injection of OT (Morton et al., 2012) in male low-fat diet-fed (10% kcal from fat) or high fat diet-fed (45% kcal from fat) Sprague Dawley rats after having been maintained on the respective diets for ∼4 months. These findings suggest that, in addition to reductions of food intake, other mechanisms (including energy expenditure) also contribute to OT-elicited weight loss. In addition, OT infusions over a 14-day period were found to reduce body weight gain despite no changes in cumulative 14-day food intake (Deblon et al., 2011). Furthermore, the findings from long-term administration studies suggest that OT appears to become less effective at reducing food intake despite an unimpaired and persistent reduction of body weight gain or body weight over this period of time (Deblon et al., 2011; Maejima et al., 2011, 2017; Altirriba et al., 2014; Blevins et al., 2016; Roberts et al., 2017).

The most direct evidence in support of an important role for OT in the control of energy expenditure stems from pharmacological studies that included measurements of energy expenditure. Acute administration of OT into the 3V or VMH boosted energy expenditure or oxygen consumption as determined by indirect calorimetry in rodents (Zhang and Cai, 2011; Zhang et al., 2011; Noble et al., 2014). These effects were recapitulated following peripheral administration in a translational DIO non-human primate (rhesus monkey) model (Blevins et al., 2015). In addition, other paradigms in which OT was administered in a paradigm that elicited weight loss, OT was not found to elevate energy expenditure (Blevins et al., 2016).

One explanation for these findings might be that chronic administration of OT could be important in attenuating the counter-regulatory mechanisms that result in weight regain in the setting of prolonged weight loss. Thus, OT, in the setting of weight loss, might prevent the drop in energy expenditure that accompanies prolonged weight loss and restore levels of energy expenditure to that of control animals (Blevins et al., 2016) and mice (Maejima et al., 2011). It is important to acknowledge that energy expenditure was not measured throughout the extent of the treatment period across the chronic treatment studies. We have previously shown that chronic 3V infusions of OT stimulate IBAT temperature during a time that coincides with OT-elicited weight loss (days 2–3 of infusion period) (Roberts et al., 2017) and that 3V OT appeared to maintain IBAT temperature to that of control animals for the remainder of the infusion period (unpublished findings). In addition, following minipump removal and throughout the 4-week washout period, IBAT temperature appeared to be slightly lower in rats that had been previously treated with chronic 3V OT relative to vehicle treated control rats (unpublished findings). It is possible that timing of energy expenditure in relation to OT-elicited weight loss is important and that chronic administration of OT may stimulate BAT thermogenesis and energy expenditure at the onset of OT-elicited weight loss and function, in part, to help maintain weight loss by preventing a drop in BAT thermogenesis and energy expenditure (Blevins et al., 2016) that accompanies prolonged reductions of food intake and weight loss in animals (Fosgerau et al., 2014) and humans (Rosenbaum et al., 2002, 2005, 2010; Schwartz and Doucet, 2010). Current studies are underway to determine the extent to which SNS innervation of BAT is required for OT to increase energy expenditure and elicit weight loss.

Does Exogenous Oxytocin Increase Brown Adipose Tissue Thermogenesis and Browning of White Adipose Tissue?

We know from recent studies that acute forebrain (3V) and hindbrain (4V) injections of OT stimulate IBAT temperature [functional measure of BAT thermogenesis (Song et al., 2008; Leitner and Bartness, 2009; Vaughan et al., 2011)] in both chow-fed and DIO rats and mice (Roberts et al., 2017; Edwards et al., 2021b). In addition, chronic infusions of OT into the 3V stimulates IBAT temperature at the start of OT-elicited reductions of body weight in DIO rats (Roberts et al., 2017) raising the possibility that BAT thermogenesis might contribute to weight loss in response to OT treatment. OT injections into the midbrain (median raphe) or 4V also stimulated core temperature in mice (Yoshida et al., 2009) and rats (Ong et al., 2017). These findings shed light on the potential contribution of OT in stimulating BAT temperature to help maintain body temperature (Cannon and Nedergaard, 2004) particularly during cold stress (Kasahara et al., 2007, 2013, 2015; Xi et al., 2017). In addition to maintaining core temperature during cold challenges, changes in IBAT temperature are often found to precede and contribute to changes in core temperature under conditions of fever and stress (Kataoka et al., 2014).

The majority of studies indicate that the effects of OT on IBAT temperature appear to contribute to non-shivering thermogenesis (mediated by BAT thermogenesis) rather than shivering thermogenesis (generated by movement of skeletal muscle). Namely, chronic administration of OT is not associated with elevations in locomotor activity in rats (Deblon et al., 2011; Blevins et al., 2016; Iwasa et al., 2019b) or mice (Maejima et al., 2011). Data from Carson et al. (2010) indicate that peripheral administration of OT attenuated methamphetamine-elicited increases in locomotor activity in rats. In addition, peripheral administration of OT decreased locomotor activity in rats; central administration of an OTR antagonist also blocked this effect (Angioni et al., 2016). Furthermore, central administration of OT blocked the ability of central delivery of an OT receptor antagonist to stimulate locomotor activity. However, two findings raise the possibility that increased locomotor activity may contribute, in part, to the elevated IBAT temperature. Sutton et al. (2014) found that DREADD-elicited stimulation of PVN OT neurons in *Oxytocin-ires-Cre* mice was associated with a small elevation of locomotor activity, energy expenditure and sc IBAT temperature and a close to significant elevation of sc IBAT temperature ($P = 0.13$). Another study found that VMH administration of OT stimulated short-term physical activity in rats for 1-h post-injection but these effects failed to coincide with the more prolonged effects of 3V or 4V OT on IBAT temperature that we have found in our studies in rats (Roberts et al., 2017) and mice (Roberts et al., 2017; Edwards et al., 2021b). Yuan et al. (2020) recently reported that OT may stimulate markers of thermogenesis in skeletal muscle [including uncoupling protein-3 (UCP-3)] and further work will need to be determined as to what role this mechanism plays in contributing to the effects of OT on energy balance given that OT has been found to have (1) no impact on locomotor activity, (2) reduce locomotor activity, or (3) produce only short-term changes in physical activity that do not coincide with the temporal profile of OT on IBAT temperature.

Previous studies indicate that OT may help stimulate the transformation of white adipocytes to more metabolically active "brown" adipocytes. The process of "browning" (Nedergaard and Cannon, 2014) of WAT may involve the transdifferentiation or *de novo* synthesis of brown adipocytes in white adipose tissue (WAT) culminating with increased expression of uncoupling protein-1 (UCP-1) and the production of heat (Cannon and Nedergaard, 2004). We recently demonstrated that hindbrain (4V) infusions of OT (16 nmol/day) elicit browning of inguinal white adipose tissue (IWAT) (as indicated by increased UCP-1 expression) in the IWAT of chow-fed mice (Edwards et al., 2021b) but not in DIO mice. In addition, chronic sc OT infusions (125 ng/kg/h or $\approx$ 66.2 nmol/day) also appeared to stimulate UCP-1 expression in sc fat of *db/db* mice (Plante et al., 2015) but the UCP-1 staining was not quantified. A more recent study by Yuan et al. (2020) reported that chronic sc OT infusions (100 nmol/day) increased UCP-1 expression in IWAT but not in epididymal WAT (EWAT) of high fat diet-fed mice. It is not clear why Yuan found elevated expression of UCP-1 in IWAT of high fat diet-fed mice while we did not find a significant effect of 4V OT to increase UCP-1 in IWAT from DIO mice in our

study. It is important to note that the dose used in Yuan's study in DIO mice was approximately 6.25-fold higher than that found to be effective following 4V infusions in our study and that higher doses may be required to elicit "browning" of IWAT in DIO mice relative to chow-fed mice. It is difficult to compare across studies as chow-fed mice were also not examined in Yuan's study. Given the existence of outgoing polysynaptic projections from the PVN OT neurons to IWAT (Shi and Bartness, 2001) and EWAT (Shi and Bartness, 2001; Stanley et al., 2010), it is possible that OT acts locally at hindbrain or spinal cord OTRs to elicit browning. In addition, OT may also act peripherally to induce browning of WAT through a direct action on OTRs found on adipocytes (Muchmore et al., 1981; Schaffler et al., 2005; Tsuda et al., 2006; Deblon et al., 2011; Yi et al., 2015) in either IWAT (Gajdosechova et al., 2015) or EWAT depots (Muchmore et al., 1981; Altirriba et al., 2014; Gajdosechova et al., 2014, 2015). Sun et al. (2019) recently found that OT may suppress browning, when it is applied directly to adipocytes *in vitro* as indicated by reduced expression of brown adipocyte specific markers (Cox7a, Cox8b, Cebpb, Retn, and Cidea). Further *in vitro* studies should also include UCP-1 which was not examined in this study. It will be important to determine if the conflicting data are due, in part, to dose, route of administration, acute vs. chronic application, *in vitro* vs. *in vivo* conditions, lack of overlap of brown adipocyte specific markers between studies and if these effects can be blocked by an OTR antagonist. These findings raise the possibility that OT may stimulate energy expenditure through multiple CNS and/or peripheral sites and raise the question as to the extent to which BAT thermogenesis and "browning" of WAT contribute to these effects.

Does Endogenous Oxytocin Impact Cold-Induced Thermogenesis and Energy Expenditure?

Oxytocin receptor or OT deficient mice are associated with adult-onset obesity (Kasahara et al., 2007; Takayanagi et al., 2008; Camerino, 2009; Sun et al., 2019) that appears at 8 (Tamma et al., 2009), 10 (Kasahara et al., 2007) or 16 weeks (Camerino, 2009) in OT null mice and 12 weeks in OTR null mice (Takayanagi et al., 2008). The adult-onset obesity in the OT and OTR null mice is characterized by increased body weight (Kasahara et al., 2007; Takayanagi et al., 2008; Camerino, 2009), fat mass (Sun et al., 2019) and/or fat pad weight (Takayanagi et al., 2008; Camerino, 2009). The finding that this occurs despite having no changes in overall daily food intake (Kasahara et al., 2007; Takayanagi et al., 2008; Camerino, 2009) suggests that other mechanisms (such as impairments in energy expenditure) may contribute to their obesity phenotype. Daily food intake in OT or OT receptor deficient mice is normal regardless of whether the mice were fed chow (Amico et al., 2005; Takayanagi et al., 2008; Camerino, 2009), sucrose-enriched chow (Amico et al., 2005) or high fat diet (Takayanagi et al., 2008). These findings were confirmed in both chow-fed and high fat diet-fed mice with diphtheria toxin-elicited reductions of PVN and SON OT neurons (Wu et al., 2012; Xi et al., 2017). While one other study also reported that OTR deficient mice do not have any overall changes in daily food intake, meal pattern analysis revealed that they have increased meal size during the dark cycle (Yamashita et al., 2013). However, these effects were offset by no change in meal size during the light cycle as well as no change in meal frequency during the light or dark cycle. Collectively, the findings provide strong evidence that the obese phenotype observed in the OT or OT receptor deficient mice can't be explained by impairments in daily food intake.

The obesity phenotype observed in older OT and OTR deficient mice does not appear in younger mice. For example, there is no difference in body weight between OTR null mice and wild-type mice that are younger [6–7 weeks (Welch et al., 2014) or 10 weeks (Takayanagi et al., 2008)]. While Sun et al. (2019) also found no difference in body weight between 12-week-old OTR null mice and wild-type mice, the OTR null mice did have increased fat mass raising the possibility that differences in body weight may have been observed at a subsequent time. Camerino (2009) also found no difference in body weight between OT null and wild type mice at 8 weeks. It is not clear if differences in background strain, housing conditions and/or thermoregulation may have contributed to the differences in obesity phenotype at specific ages between studies.

One factor that seems contrary to the adult-onset obesity phenotype observed at 8, 10 or 16 weeks in OT null mice is that finding that OT null mice tend to have a reduction in muscle regeneration by 12 weeks of age and a significant defect in muscle regeneration and a reduction of both muscle mass and fiber size by 52 weeks of age (Elabd et al., 2014) (characteristic of sarcopenia). These mice tended to have an increased number of adipocytes near the site of muscle regeneration (non-significant) but the hindlimb perimuscular and intramuscular adipose tissue deposition of OT null mice was significantly increased relative to wild-type mice (Elabd et al., 2014). While body weight and body adiposity levels were not reported in these particular mice it is possible that the increase in fat mass compensates for any reduction in lean mass to help maintain the obesity phenotype as OT null mice age and this may help to explain, in part, why the obesity phenotype is not observed in younger OT null mice.

Consistent with a physiological role of endogenous OT in the control of thermogenesis, cold has been found to activate PVN OT neurons (Kasahara et al., 2007) and rostral raphe pallidus OTR (+) cells (Kasahara et al., 2015) as well as to increase expression of OT (hypothalamus) (Yuan et al., 2020) and OTR (BAT and IWAT) (Yuan et al., 2020) and levels of circulating OT (Yuan et al., 2020). One study by Kasahara et al. (2013) reported no change of PVN or SON OT mRNA expression in response to cold but the data were not shown in the study. Mice that lack OT or its receptor do have notable impairments in cold-induced thermogenesis (Kasahara et al., 2007, 2013, 2015; Takayanagi et al., 2008; Xi et al., 2017) and enlarged lipid droplets in IBAT (suggestive of hypo-activity) (Takayanagi et al., 2008) which would potentially contribute to impairments in energy expenditure. Deficits in PVN OT signaling or pharmacological blockage of OT receptors are associated with defects in energy expenditure (Zhang and Cai, 2011; Zhang et al., 2011; Wu et al., 2012). It is well appreciated that BAT thermogenesis is important in the regulation of energy

expenditure (see Cannon and Nedergaard, 2004; Morrison et al., 2014, for review), but it is not clear if OT's effects on energy expenditure result from BAT thermogenesis. One recent report measured both energy expenditure and BAT thermogenesis in mice with diphtheria toxin-elicited reductions of PVN and SON OT signaling and found reductions in both IBAT temperature and core temperature in response to a cold stimulus, both of which were attenuated by OT pre-treatment (1 mg/kg, IP). However, there were no alterations in IBAT temperature, core temperature or energy expenditure in mice that were housed at 20–24°C (Xi et al., 2017). Similar to the findings by Xi et al. (2017), Kasahara et al. (2013) found a reduction in core temperature in OTR deficient mice that were exposed to cold and also no change in energy expenditure between genotypes at room temperature. Whether their findings point to a more important role of endogenous OT in the control of cold-induced thermogenesis and cold-induced elevations of energy expenditure will remain to be determined. It will be important to determine in future studies if mice with global loss of OT or OT receptors have impairments in both BAT thermogenesis and energy expenditure in response to cold exposure and whether pre-treatment with OT rescues both the impairments in BAT thermogenesis and energy expenditure. This could shed light on whether impairments in BAT thermogenesis may also be linked to impairments in energy expenditure in these animals.

What Receptor Populations Mediate Oxytocin's Effects on Brown Adipose Tissue Thermogenesis and Energy Expenditure?

Paraventricular nucleus OT neurons are anatomically positioned to control BAT thermogenesis and energy expenditure through polysynaptic projections to IBAT (Oldfield et al., 2002), stellate ganglia (Jansen et al., 1995) [sympathetic ganglia known to innervate IBAT (Oldfield et al., 2002)], as well as WAT depots [EWAT (Shi and Bartness, 2001; Stanley et al., 2010) and IWAT depots (Shi and Bartness, 2001)]. Oldfield et al. (2002) determined that OT was expressed in approximately 10–15% of PVN neurons that were also co-infected with pseudorabies virus following injections into IBAT. This is in contrast to vasopressin, cocaine and amphetamine-regulated transcript and corticotropin-releasing factor, which were rarely found in PVN OT neurons that were labeled with pseudorabies virus (PRV). Similarly, Jansen et al. (1995) reported that OT was expressed in 10% of PVN neurons that were co-infected with PRV following injections into stellate ganglia and was also found to be more commonly expressed in PRV (+) neurons than vasopressin (2%), CRH (5%) and thyrotropin-releasing hormone (<1%). Shi and Bartness found that 3.49% of PVN OT neurons were co-labeled with PRV following PRV injections into WAT (Shi and Bartness, 2001), higher than vasopressin (1.07%) and tyrosine hydroxylase (2.62%). In a separate study, Stanley et al. (2010) administered PRV into EWAT and determined that up to 17% of neurons that expressed PRV also expressed OT compared to approximately 12, 4 and 26% for vasopressin, TRH and CRH. Collectively, these findings suggest that OT is one of the more predominant peptides found in outgoing projections to IBAT, IWAT and EWAT.

The extent to which specific OTR populations contribute to BAT thermogenesis and energy expenditure have been examined by determining (1) the effects of localized administration of OT on BAT or core temperature, (2) the activation of regions that express OTRs in response to cold and (3) whether deficits in cold-induced thermogenesis in OTR deficient mice can be restored by re-expression of OTRs into specific CNS sites. Central (3V) administration of OT (which does not differentiate forebrain receptor populations or a forebrain vs. hindbrain site of action) has been found to increase BAT temperature in both mice and rats (Roberts et al., 2017). Noble et al. (2014) extended these findings by showing that OT administration into the hypothalamus (VMH) stimulated energy expenditure in rats, thereby providing more direct evidence in support of a role of VMH OTRs in the control of energy expenditure. In addition, Kasahara showed that cold exposure activates both PVN OXT neurons (Kasahara et al., 2007) and neurons within the dorsomedial nucleus (DMN), an area that expresses OTRs) (Kasahara et al., 2013). Kasahara et al. (2013) also noted that cold also stimulated number of c-Fos(+) neurons (marker of neuronal activation) and that this effect was attenuated in OTR deficient mice. Kasahara et al. (2013) further determined the extent to which OTR signaling within the DMH/VMH was sufficient to elicit BAT thermogenesis by measuring BAT thermogenesis in OTR null mice that received adeno-associated viral vector expression of OTRs in DMH/VMH (Kasahara et al., 2013). They found that OTR expression within the DMH/VMH restored deficits in cold-induced thermogenesis and corrected defects in β3- and α2-adrenoceptor mRNA expression in IBAT. Together, these findings indicate that OTR signaling within the DMH and/or VMH is sufficient to elicit BAT thermogenesis.

The role of OTRs within the midbrain raphe nucleus (median raphe) in the control of body temperature has also been explored. Yoshida et al. (2009) found that direct injections of OT into the median raphe increase body temperature supporting a role of OTRs in this region in the regulation of BAT thermogenesis.

In addition to the midbrain raphe and hypothalamic OTRs, several studies have suggested that hindbrain OTRs may also be important in contributing to OT-elicited BAT thermogenesis. Namely, 4V administration (to target hindbrain OTRs) of OT increases BAT temperature in both rats (Roberts et al., 2017) and mice (Edwards et al., 2021b). In addition, Ong et al. (2017) found that 4V administration also increases core temperature in a rat model. Kasahara extended these findings and probed the role of hindbrain OTRs within the rostral raphe pallidus, a region that receives dense innervation from the PVN (Luo et al., 2019), is a component of rostral medullary raphe (RMR) and contains premotor neurons with polysynaptic projections to BAT (Oldfield et al., 2002) and to stellate ganglia that innervate BAT (Jansen et al., 1995). They found that OTR (+) neurons within the rostral raphe pallidus are activated in response to cold exposure (Kasahara et al., 2015). They subsequently addressed if OTRs within the RMR were sufficient to elicit BAT thermogenesis and found that expression of OTRs within the RMR restored deficits in cold-induced thermogenesis and reduced the size of

the lipid droplets in IBAT tissue to that of control mice (Kasahara et al., 2015). Kasahara et al. (2015) also addressed if OTR in the RMR were necessary for thermoregulation by using an AAV-Cre to delete OTR expression from the RMR of $Oxtr^{fx/fx}$ mice. However, AAV-Cre- elicited deletion of OTRs within the RMR was not effective in restoring impairments in core temperature in response to cold stimulus. The NTS is another hindbrain site that expresses OTRs and has outgoing polysynaptic projections to IBAT (Oldfield et al., 2002) and to stellate ganglia that innervate BAT (Jansen et al., 1995). It is not clear if OTR (+) neurons project to rostral raphe pallidus or directly to the spinal cord. Future studies assessing the impact of NTS OTR gain of function and loss of function will help further delineate the role of NTS OTRs in the control of BAT thermogenesis. Together, these findings suggest that OTRs within multiple hindbrain areas may contribute to the effects of OT on BAT thermogenesis.

In addition to acting at OTRs within the brain, OT may also stimulate BAT thermogenesis and energy expenditure through sympathetic pre-ganglionic OTR-expressing neurons within the spinal cord. Chemogenetic stimulation of OT neurons within the rostral PVN, some of which innervate the thoracic spinal cord, increases c-Fos in thoracic spinal cord cholinergic neurons, boosts energy expenditure and tends to elevate IBAT temperature (P = 0.13) (Sutton et al., 2014), although the extent to which these effects are attributed to endogenous OT or another peptide/neurotransmitter within OT neurons has not been determined. Finally, a recent study indicated that OT may also have a direct action through OT on OTRs on brown adipocytes within BAT (Yuan et al., 2020) where OTR expression is found to be upregulated in response to cold (Yuan et al., 2020). Future studies should address if targeted disruption of OTRs within the forebrain hypothalamus, midbrain, hindbrain, spinal cord and BAT decrease both cold-induced thermogenesis and elevations of energy expenditure and elicit adult-onset obesity (similar to that of global OT or OTR deficient mice).

DOES LOCOMOTOR ACTIVITY CONTRIBUTE TO THE ABILITY OF OXYTOCIN TO INCREASE INTERSCAPULAR BROWN ADIPOSE TISSUE TEMPERATURE AND ENERGY EXPENDITURE AND EVOKE WEIGHT LOSS?

In addition to BAT thermogenesis and heat production, increased locomotor activity is another mechanism to stimulate energy expenditure. However, current data suggest that OT's effects on locomotor activity are inconsistent and appear to vary depending on how it was administered (chronic vs. acute) and, in some cases, whether the animals were lean or obese. We and others have also found that chronic infusions of OT into the lateral ventricle or 3V, at a dose that was sufficient to reduce body weight and elevate IBAT temperature (16 nmol/day), had no effect on locomotor activity in DIO rats (Deblon et al., 2011; Blevins et al., 2015; Roberts et al., 2017). In addition, Maejima et al. (2011) have also found that subcutaneous infusion of OT, at a dose that was sufficient to reduce body weight, also had no effect on locomotor activity in DIO mice (1.6 mg/kg/day or ∼56.4 nmol/day). Based on these collective findings, OT-elicited increases in locomotor activity do not appear to be a major contributor to OT-elicited weight loss in DIO models.

Chemogenetic stimulation of PVN OT neurons or acute CNS or systemic administration of OT has been found to either stimulate, reduce or have no effect on locomotor activity. Sutton et al. (2014) found that chemogenetic activation of PVN OT neurons in *Oxytocin-ires-Cre* mice increased locomotor activity and energy expenditure and resulted in a tendency (non-significant) toward an increase in subcutaneous IBAT temperature in animals with transponders implanted above the IBAT depot. A recent study by Zhang et al. (2021) found that chemogenetic activation of magnocellular OT neurons that project to the striatum, results in stimulation of locomotor activity over a 20-min period though an OTR-dependent mechanism. Similar to the forementioned chemogenetic studies, one study found that acute administration of OT into the VMH stimulated physical activity in rats at 1-h post-injection (Noble et al., 2014), but these effects were short-lived and did not following the more prolonged effects of 3V or 4V OT on IBAT temperature in rats (Roberts et al., 2017) and mice (Roberts et al., 2017; Edwards et al., 2021b). Additional findings indicate that systemic OT was found to (1) reduce methamphetamine-elicited elevations in locomotor activity in rats (Carson et al., 2010), (2) reduce locomotor activity in rats in an OTR-dependent manner (Angioni et al., 2016), or (3) have no significant effect on locomotor activity in female ovariectomized (Iwasa et al., 2019b) or perimenopausal rats (Erdenebayar et al., 2020). Consistent with the earlier reports that systemic OT was able to reduce locomotor activity, CNS administration of OT was also found to block the effects of CNS administration of OTR antagonist to increase locomotor activity. Maejima et al. (2015) also found that intranasal OT, at a dose that reduces food intake, had no effect on locomotor activity while systemic (IP) administration reduced locomotor activity but only during the dark cycle (Maejima et al., 2015). Collectively, these studies suggest that OT results in a brief elevation of locomotor activity, has no effect or reduces locomotor activity. In order to assess if locomotor activity may play a role in OT-elicited elevations of IBAT temperature and/or energy expenditure, IBAT temperature, energy expenditure and locomotor activity should be measured in parallel in the same animals under the same conditions.

IS OXYTOCIN EFFECTIVE AT REDUCING BODY WEIGHT IN MALE AND FEMALE RODENTS?

Much of the early historical work regarding the effects of OT in the control of food intake has focused on male rodent models but the few studies that have been completed in female rodents have produced somewhat mixed results. One early study reported that

acute central and peripheral administration of OT reduced food intake similarly in both male and female rats (Benelli et al., 1991). Subsequently, Maejima et al. (2017) examined the effects of OT on body weight and adiposity and found that chronic sc infusions of OT produced similar reductions on body weight and adiposity in male and female DIO C57Bl/6J mice. In addition, central [intracerebroventricular (ICV)] administration of OT was found effective at reducing food intake and weight gain in female genetically obese Sim1 haploinsufficient mice but not in female wild-type counterparts (Kublaoui et al., 2008). A recent study by Seelke et al. (2018) reported that intranasal OT may have a more heightened response to reduce weight gain in female DIO prairie voles but the sample size was small. Iwasa et al. (2019b) reported that chronic systemic OT (1x IP administration over 6 days) treatment reduced food intake and body weight in female ovariectomized rats. One recent study by Liu et al. (2020a) indicate that the effectiveness of central OT (ICV) administration to reduce food intake in female rats is influenced by estrous cycle (particularly proestrous) and that estrogen replacement in ovariectomized rats inhibits OT's effects on food intake. In light of these recent findings and the earlier work by Maejima in DIO mice, it will be important to determine if other routes of administration are as impacted by estrous cycle and whether the ability of chronic central or systemic administration of OT to elicit weight loss in female rodents can be optimized if given intermittently throughout the estrous cycle.

The role of endogenous OT in the control of body weight in female rodent models is not clearly understood due, in part, to inconsistent results and data that has largely been generated in male rodents. Previous studies indicate that male OT null mice develop adult-onset obesity at 10 (Kasahara et al., 2007) or 16 weeks (Camerino, 2009) while OTR receptor null mice develop adult-onset obesity at 12 weeks (Takayanagi et al., 2008). While female OT null mice also develop adult onset obesity (Camerino, 2009; Tamma et al., 2009) as early as 8 weeks (Tamma et al., 2009), female OTR deficient mice fail to develop increased body weight relative to control counterparts (Takayanagi et al., 2008; Sun et al., 2019). However, both male and female OT [3–10 months: females; 8–11 months: males] and OTR null mice [3 months: males and females] develop increased fat mass and/or percent fat (Sun et al., 2019). In contrast to the findings from male and female OT null mice, only male *Oxytocin-IresCre:Rosa26*$^{iDTR/+}$ mice with diphtheria toxin-elicited ablations of PVN OT neurons become obese relative to control *Rosa26*$^{iDTR/+}$ mice (Wu et al., 2012). In contrast to the study from Takayanagi et al. (2008), male OTR$^{-/-}$ mice failed to show increased body weight relative to wild-type controls (Sun et al., 2019) (personal communication with Dr. Tony Yuen and Dr. Mone Zaidi) although it is certainly possible that they would have become obese over time. Further studies will be required in order to provide more clarity on whether differences in genetic background, housing, thermoregulation and/or age might be contributing factors in terms of these apparent differences across studies.

HOW DOES OXYTOCIN IMPACT BODY COMPOSITION?

Oxytocin may impact body composition through a direct effect on OTRs on adipocytes which express OTRs (Muchmore et al., 1981; Schaffler et al., 2005; Tsuda et al., 2006; Altirriba et al., 2014; Gajdosechova et al., 2014, 2015; Yi et al., 2015) or through an indirect effect through outgoing polysynaptic projections from the PVN to both IWAT (Shi and Bartness, 2001) and EWAT (Shi and Bartness, 2001; Stanley et al., 2010).

Chronic administration (repeated injections or minipump infusions) into the CNS (lateral ventricle, 3V) or systemic OT treatment was found to decrease fat mass relative to baseline fat mass (pre-intervention) or decrease fat mass post-treatment in lean (Deblon et al., 2011) and DIO rats (Sprague-Dawley CD® IGS, Long-Evans and Wistar rats) (Deblon et al., 2011; Morton et al., 2012; Blevins et al., 2016; Roberts et al., 2017), DIO C57BL/6J (Roberts et al., 2017) and C57BL/6 mice (Zhang and Cai, 2011; Snider et al., 2019), *db/db* mice (Plante et al., 2015), and *ob/ob* mice (Altirriba et al., 2014) without producing any significant reductions in lean mass. OT (repeated IP administration) was also found to reduce percent fat mass after only 1 week of treatment and these effects were not associated with any effects on lean mass in lean wild-type mice (Sun et al., 2019) (1 μg/mouse, IP, 3x/week). These more selective effects on fat mass in the absence of any adverse effects on lean mass have also been recapitulated following chronic hindbrain (4V) infusions in DIO C57BL/6J mice (Edwards et al., 2021b).

Oxytocin treatment appears to reduce sc (Maejima et al., 2017), mesenteric (Maejima et al., 2011), EWAT (Maejima et al., 2011; Altirriba et al., 2014) and visceral fat (Maejima et al., 2017) in DIO C57Bl/6J (Maejima et al., 2011) and *ob/ob* mice (Altirriba et al., 2014) as well as in female ovariectomized Wistar rats (Iwasa et al., 2019b). In addition, OT reduced adipocyte size across several fat depots including sc (Plante et al., 2015; Iwasa et al., 2019b)/inguinal (Edwards et al., 2021b), visceral (Iwasa et al., 2019b), perirenal (Plante et al., 2015), and epicardial (Plante et al., 2015), EWAT (Eckertova et al., 2011; Maejima et al., 2011; Balazova et al., 2016) and mesenteric (Maejima et al., 2011) depots in C57BL/6J (Maejima et al., 2011) and *db/db* mice (Plante et al., 2015) as well as obese Zucker rats (Balazova et al., 2016) or female ovariectomized Wistar rats (Iwasa et al., 2019b). Chronic sc OT treatment also reduced liver weight and fat in hepatocytes in DIO C57BL/6J mice (Maejima et al., 2011) but was found to have no effect on liver triglyceride content in *ob/ob* mice (Altirriba et al., 2014). In contrast, some studies have reported that chronic systemic or central (4V) OT administration elicited a relative reduction in lean mass compared to vehicle in lean C57BL/6J (Altirriba et al., 2014) and DIO C57BL/6 mice (Snider et al., 2019) as well as in DIO CD IGS rats (Roberts et al., 2017) with or without any relative reductions in fat mass raising the possibility that differential effects may be attributed, in part, to rodent strain, dosing and/or route of administration. While there are exceptions, overall OT treatment

appears to preferentially reduce fat mass while preserving lean mass across rodent models.

More recent studies have found that more translational routes of administration (intranasal) have also yielded promising effects on body composition in rodents and humans. Chronic intranasal administration (8 IU/kg; 1x daily over 7 days) tended to reduce carcass fat mass in DIO prairie voles without negatively impacting lean mass (Seelke et al., 2018). Recent translational studies in humans indicate that chronic intranasal OT (24 IU; 4x daily for 8 weeks) administration also tended to reduce fat mass in obese men and women (Espinoza et al., 2021). Interestingly, it also produced a slight increase in lean mass (Espinoza et al., 2021). These findings are in agreement with previous studies that found both a reduction in relative fat mass (pre- vs. post-intervention) and a slight increase in relative lean mass (pre- vs. post-intervention) following 3V administration (16 nmol/day; ∼3-week body comp measurements) (Blevins et al., 2016) and subcutaneous administration (50 nmol/day) in chow-fed and DIO rats (10-day body comp measurements). Whether these effects on lean mass are due, in part, to OT's effects on muscle mass and/or bone composition merit further investigation and is discussed further in Section "Mechanism of Action Following Peripheral Administration."

Existing data suggest that OT may impact body composition through increased lipolysis or reduced lipogenesis. *In vitro* data indicate that OT stimulates glycerol and free fatty acids and/or reduces triglycerides in 3T3-L1 adipocytes (Deblon et al., 2011; Yi et al., 2015). These findings have been recapitulated *in vivo* in rats (Deblon et al., 2011) and DIO non-human primates (rhesus monkeys) (Blevins et al., 2015). Chronic intranasal OT tended to reduce triglycerides in pre-diabetic obese humans but these effects were not reach statistical significance (Zhang et al., 2013). In addition, chronic ICV infusions of OT (1.6 and 16 nmol/day) increases expression of hormone sensitive lipase (an enzyme linked with lipolysis) in DIO rats (Deblon et al., 2011) in EWAT. In addition, these effects on EWAT were reproduced following chronic sc infusions of OT (50 nmol/day) in *ob/ob* mice (Altirriba et al., 2014) as well as direct application of OT to 3T3-L1 adipocytes (5 μm OT over 24 h) (Deblon et al., 2011). These findings implicate that these pro-lipolytic effects may occur through both a direct and indirect mechanism. OT was also found to decrease expression of fatty acid synthase (an enzyme linked to lipogenesis) in *ob/ob* mice (Altirriba et al., 2014), indicating that OT may also decrease lipogenesis. Existing data from animal models suggest that chronic central or systemic OT infusions reduce respiratory quotient in DIO rats (Deblon et al., 2011) and mice (Maejima et al., 2011) compared to vehicle treatment (Deblon et al., 2011; Maejima et al., 2011) or pair-fed animals (Deblon et al., 2011). These effects were also recently translated to humans as OT was also found to reduce respiratory quotient in lean and obese men (Lawson et al., 2015). Collectively, these findings suggest that OT reduces body adiposity and adipocyte size by increasing lipolysis and lipid utilization or oxidation and reducing lipogenesis.

HOW DOES OXYTOCIN IMPACT MUSCLE MASS AND BONE COMPOSITION?

Effects of Oxytocin on Muscle Mass

Recent studies implicate a role for OT in the control of thermogenesis in skeletal muscle and muscle regeneration. OTR are expressed in skeletal muscle (Elabd et al., 2014; Gajdosechova et al., 2014, 2015) and in C2C12 mouse myoblast cells (Lee et al., 2008). Existing data suggest that OT may elicit direct effects on OTRs in skeletal muscles as (1) OT was found to stimulate intracellular calcium in C2C12 mouse myoblast cells and (2) chronic sc infusions of OT stimulate markers of thermogenesis in skeletal muscle (*UCP-3* and *Atb5a1*) (Yuan et al., 2020). In addition to recently recognized role of skeletal muscle thermogenesis, OT has been found to have an important role in muscle regeneration. Loss of function studies show that OT deficient mice have impairments in muscle regeneration @ 12 months of age, but such impairments were not observed in younger animals (3 months of age) (Elabd et al., 2014). These data are consistent with the finding that OTR deficient mice at 3 months of age do not have any impairments in lean mass relative to age-matched wild-type mice (Sun et al., 2019). In addition, hind limb muscles (gastrocnemius and tibialis anterior) in OT deficient mice are associated with reduced muscle mass. The hind limb muscles (quadriceps, gastrocnemius, and tibialis anterior) in OT deficient mice were found to be associated with increased perimuscular and intermuscular adipose tissue (Elabd et al., 2014), findings which are consistent with increased body weight and/or fat mass in this mouse model (Kasahara et al., 2007; Camerino, 2009; Sun et al., 2019).

Of translational importance is that finding that chronic intranasal OT was found to increase lean mass in senior men and women with sarcopenic obesity (discussed in section "Is Oxytocin Effective at Reducing Body Weight in Male and Female Rodents?"). This is consistent with the finding that positive associations have been observed between overnight serum OT concentrations and lean mass in premenopausal women (Schorr et al., 2017). A separate study using animal models provided potential mechanistic insights into these effects. Systemic (sc) treatment with OT (1 μg/g) was able to improve muscle regeneration in aged mice to a level that as comparable to that of younger mice (Elabd et al., 2014). In these studies, OT was found to increase (1) the proliferative capacity of old satellite myogenic cells to that of young satellite myogenic cells and (2) the proliferation of primary myogenic progenitor cells. The effects of OT on satellite cells were also found to occur through the MAPK/ERK signaling pathway. Collectively, these findings provide supportive data for future mechanistic studies using intranasal OT in humans with sarcopenia.

Effects of Oxytocin on Bone Composition

In animal models, OT has been found to have a critical role in maintaining bone mass in both male and female mice as both OT and OTR null mice develop osteoporosis (Tamma et al., 2009) (see Colaianni et al., 2015; McCormack et al., 2020, for

review). The effects of OT on bone formation are likely due to a direct action of circulating OT as peripheral OTRs as OTRs are expressed on both mouse (Tamma et al., 2009; Colaianni et al., 2012) and human osteoblasts (Copland et al., 1999; Tamma et al., 2009) and osteoclasts (Colucci et al., 2002; Tamma et al., 2009). Furthermore, peripheral administration of OT (two IP injections separated by 12 h; 4 μg/mouse) increased TRAP-positive osteoclast formation while central administration was ineffective (Tamma et al., 2009). Peripheral administration has also been found to increase bone mineral density and osteoblast formation, proliferation and differentiation (Tamma et al., 2009). Sun et al. (2019) recently determined that OTRs on osteoblasts were critically important in bone formation by ablating OTRs in osteoblasts using Col2.3Cre mice. Male and female mice that lack OTRs in osteoblasts were found to have low bone mass that resembled that of the OTR null mice (Sun et al., 2019). Mice that lacked OTRs in osteoclasts also developed high bone mass in Acp5Cre mice suggests an important role of OT to increase osteoclastogenesis. Collectively, the effects of OT on bone are thought to occur through both osteoblast differentiation as well as regulation of osteoclast development and function.

While less is known from a mechanistic standpoint about OT-elicited regulation of bone mass in humans, human studies do reveal that there is a positive association between bone mass and levels of circulating OT in women (Schorr et al., 2017). While Breuil et al. (2015) did not find this positive association in men, it did find a weak negative association between circulating OT and fracture risk. Breuil et al. (2011, 2014) also found that circulating OT levels correlated with osteopenia or osteoporosis in post-menopausal women. In particular, higher circulating levels of OT were associated with high bone mineral density (hip) in women with lower circulating levels of estradiol or higher circulating levels of leptin (Breuil et al., 2014). Similar to what is observed in OT and OTR null mice (Tamma et al., 2009) and in Col2.3Cre mice that lack OTRs in osteoblasts (Sun et al., 2019), humans with low OT serum levels display severe osteoporosis (Breuil et al., 2011). Overall, the effects of OT on bone mineral density in humans appears to be complicated and influenced by sex steroids and metabolic status.

MECHANISM OF ACTION FOLLOWING PERIPHERAL ADMINISTRATION

While systemic administration of OT may impact body adiposity through a direct effect on white and brown adipocytes, it may reduce food intake, in part, through a direct action on peripheral OTRs in the GI tract (Wu et al., 2003, 2008; Monstein et al., 2004; Ohlsson et al., 2006; Qin et al., 2009; Welch et al., 2009), the enteric nervous system (Monstein et al., 2004; Welch et al., 2009), smooth muscle cells (Monstein et al., 2004; Qin et al., 2009) and the vagus nerve (Welch et al., 2009; Brierley et al., 2021) as well as central OTRs (Ring et al., 2006, 2010; Ho et al., 2014; Iwasaki et al., 2019). Peripheral administration of OTR antagonists that are capable of crossing the BBB stimulate food intake in rodents (Olszewski et al., 2010; Zhang and Cai, 2011) which implicate OTRs within either the CNS or periphery in the control of food intake. Subsequent studies showed that peripheral administration of an OTR antagonist that is not thought to readily cross the BBB (L-371,257) produced modest effects to stimulate food intake and body weight gain in chow-fed rats (Ho et al., 2014) suggesting the potential importance of peripheral OTRs in the control of energy balance. Iwasaki et al. (2014, 2019) extended these findings in two separate studies and found that the ability of peripheral administration of OT to reduce food intake and elicit Fos (marker of neuronal activation) in the PVN and hindbrain was either attenuated (0.4 mg/kg, IP) or blocked (0.2 and 0.4 mg/kg, IP) in capsaicin-treated and vagotomized mice. Collectively, these findings suggest that OTR signaling through vagal afferents contributes to the effects of peripheral OT administration to reduce food intake. Furthermore, a recent study found that NTS preproglucagon neurons are critical downstream meditators of the feeding suppression in response to systemic OT (0.4 mg/kg, IP) (Brierley et al., 2021). Together, these findings are consistent with a role of peripheral OTRs in contributing to the effects of systemic OT.

One potential mechanism by which peripheral OT may reduce food intake is through the reduction of gastric emptying. Peripheral OT treatment also decreases gastric emptying in rodents [mice (Welch et al., 2014)/rats (Wu et al., 2003, 2008)] and these effects are attenuated following treatment with an OTR antagonist, Atosiban (Wu et al., 2003, 2008), indicating that these effects are attributed to OTRs. In other cases, systemic administration has been found to have effect on gastric emptying rate [rats (McCann et al., 1989)/humans (Borg et al., 2011)] or a stimulatory effect on gastric motility [rabbits (Li et al., 2007)]. Whether these effects can be attributed, in part, to dosing or species differences awaits further investigation.

Whether the peripheral effects of OT on gastric emptying in rodents is mediated, in part, through activation of peripheral or central OTRs is still not known. CNS administration of OT reduces gastric motility (Rogers and Hermann, 1987; Flanagan et al., 1992) and these effects appear to be mediated by OTRs in the dorsal vagal complex (Rogers and Hermann, 1987). While circulating OT may inhibit gastric motility through a central mechanism these effects may also be mediated through stimulation of OTRs that are expressed in the enteric nervous system (Monstein et al., 2004; Welch et al., 2009) on smooth muscle cells (Monstein et al., 2004; Qin et al., 2009) or nodose ganglion (Welch et al., 2009). As mentioned earlier, systemic OT suppresses food intake, in part, through a vagal mechanism (Iwasaki et al., 2015, 2019) and signaling through NTS preproglucagon (PPG) neurons (Brierley et al., 2021). Future studies that address if the ability of systemic OT to decrease gastric emptying is impaired in capsaicin-treated or vagotomized rodents will help to differentiate a central from peripheral mechanism of action.

Oxytocin may also reduce gastric emptying through the local release of cholecystokinin-8 (CCK-8) and subsequent activation of vagal afferents that innervate the hindbrain. Systemic administration of OT inhibits both gastric emptying and stimulates the release of CCK-8 (Wu et al., 2003, 2008), both of which occur within the time period that peripheral administration of OT reduces food intake (Ho et al., 2014).

In addition, the effects of systemic OT to reduce gastric emptying are blocked by pretreatment with a CCK1 receptor antagonist, devazepide (Wu et al., 2003, 2008). Furthermore, Iwasaki showed that peripheral administration of OT and CCK-8 both activate single vagal afferent neurons (Iwasaki et al., 2014) further supporting both a direct and indirect action of OT to activate vagal relays through activation of CCK1 receptors (Wu et al., 2008). Further studies to determine if the effectiveness of systemic OT to suppress food intake and reduce gastric emptying is attenuated in animals with gastric fistulas that are open (sham feeding; no gastric distension) relative to animals with closed fistulas (real feeding; gastric distension) will be helpful in determining if OT inhibits food intake, in part, by suppressing gastric emptying.

The extent to which circulating OT may inhibit food intake through suppression of the orexigenic signal, ghrelin, is controversial. It has been reported that ghrelin administration centrally can stimulate OT release in rodents (Szabo et al., 2019) and heterocomplex formed by OT receptor and ghrelin receptor can alter OT signaling (Wallace Fitzsimons et al., 2019) (see section "Mechanism of Action Following Peripheral Administration"). One study reported that peripheral OT treatment decreased circulating levels of ghrelin in men (Vila et al., 2009) during a time that is consistent with when OT reduces food intake in rodents (Ho et al., 2014). In contrast, intranasal administration of OT, at a dose that reduced total caloric intake (Lawson et al., 2015), cookie consumption (Ott et al., 2013) and increased circulating levels of OT in other studies (Burri et al., 2008; Striepens et al., 2013), failed to reduce plasma ghrelin. It will be helpful to examine the impact of chronic intranasal OT on circulating levels of ghrelin in the setting of weight loss as this could offer potential mechanistic insights into downstream targets of OT action and additional insights into how OT reduces energy intake in humans, perhaps impacting both homeostatic and reward-based food intake in humans.

EFFECTS OF INTRANASAL OXYTOCIN ON ENERGY HOMEOSTASIS IN RODENT MODELS

The extent to which circulating OT may enter the CNS remains controversial (Mens et al., 1983; Ermisch et al., 1985; Kendrick et al., 1986; Ring et al., 2006, 2010; Neumann et al., 2013; Ho et al., 2014). Circulating OT may have limited or restricted access to the CNS although some studies suggest that OT does cross the BBB (Mens et al., 1983; Ermisch et al., 1985), and CNS sites that are leaky to BBB (e.g., median eminence and area postrema) might serve as sites of OT uptake. It is also unclear whether transport of OT across the BBB could be hampered in the DIO state as has been proposed for other hormones such as leptin (Banks et al., 1999). Leng and Sabatier (2017) have also raised the possibility that with high peripheral doses, "some OT is likely to enter the brain despite the presence of a very effective blood–brain barrier to OT." Consistent with this, Freeman et al. (2016) found elevated levels of OT within the CSF following the highest intravenous dose of OT used in their study (5 IU/kg or ∼29–36.5 IU). Lee et al. (2018) also found that deuterated OT given intravenously at a higher dose (80 IU) also resulted in elevated levels within the CSF of rhesus monkeys. In addition, others found that central administration of a non-penetrant OTR antagonist, L-371,257, was able to block the anxiolytic effects of peripheral administration of OT (Ring et al., 2006). In addition, we have also generated data to suggest that hindbrain OTRs contribute, in part, to the satiety response to peripherally administered OT (Ho et al., 2014). In an effort to target the CNS more directly using a minimally invasive route of administration, the majority of clinical trials have administered OT by the intranasal route of administration.

Intranasal administration enables relatively rapid uptake into the CSF of several neuropeptides and hormones, including insulin, vasopressin, and the melanocyte-stimulating hormone, adrenocorticotrophic hormone (4–10), within 30 min in humans (Born et al., 2002). Intranasal delivery into the cribriform plate rather than the turbinates is one approach that has been proposed to maximize delivery to the CNS and limit uptake into the circulation (Meredith et al., 2015). Intranasal delivery appears to effectively enable OT to enter the CSF in mice, rats, non-human primates and humans within 30–45 min post-treatment (Gossen et al., 2012; Neumann et al., 2013; Chang and Platt, 2014; Monte et al., 2014) although others have found that only aerosolized OT (24 IU) reached the CSF of non-human primates (Modi et al., 2014) while intranasal OT @ 24 IU and IV OT @ 48 IU was ineffective. In addition, the extent to which intranasal OT may reach the parenchyma from the CSF is being debated (see Leng and Ludwig, 2016a,b; Leng and Ludwig, 2016c, for review). As Leng and Ludwig (2016a) stated: "several recent studies have looked at the effects of intranasal application of OT on food intake in man. These involve very high doses of OT that raise plasma concentrations to supraphysiological levels; a small amount of the applied OT probably reaches the brain, but whether it does so in effective amounts is uncertain." In addition, the degree to which the OT measured in CSF in response to intranasal OT is due to elevations of exogenous or endogenous OT is also controversial (Ludwig et al., 2013; Neumann et al., 2013; Lee et al., 2018; Smith et al., 2019). Similar to vasopressin (Gouzenes et al., 1998), OT is one of the few hormones that is can stimulate its own release. This can occur, in part, through magnocellular SON (Yamashita et al., 1987; Moos and Richard, 1989) and PVN (Kendrick, 2000) OT auto-receptors following either central or systemic administration. Systemic OT can do this indirectly by activating vagal afferents (Kendrick, 2000; Iwasaki et al., 2015, 2019) where OTRs are expressed (Welch et al., 2009), increasing Fos within PVN OT neurons (Carson et al., 2010; Hicks et al., 2012; Hayashi et al., 2020) and stimulating release of OT within the CNS (Zhang and Cai, 2011) and likely back into the peripheral circulation. These findings have been recently extended to high fat diet-fed mice where systemic OT treatment was recently shown to increase Fos within PVN OT neurons (Hayashi et al., 2020) and up-regulate hypothalamic OT mRNA. Similarly, chronic CNS infusions of OT can up-regulate hypothalamic OT mRNA and increase OT levels within the circulation (Miller, 2013). The finding that circulating levels of OT are elevated at 15

(Striepens et al., 2013), 30 (Striepens et al., 2013), 40 (Monte et al., 2014), 45 (Striepens et al., 2013), 60 min (Striepens et al., 2013; Kirkpatrick et al., 2014; Lee et al., 2018), or 90 min (Kirkpatrick et al., 2014) following intranasal administration in non-human primates (Monte et al., 2014; Lee et al., 2018) and humans (Striepens et al., 2013; Kirkpatrick et al., 2014) raise the possibility that intranasal OT may be either entering the circulation directly or indirectly following the release of endogenous OT into the CNS and peripheral circulation. To address the possibility that the rise in CNS OT in response to intranasal OT might be a result of endogenous release, Smith, Korgan and Young examined the extent to which intranasal OT entered the CNS in OT null mice (Smith et al., 2019). They found that intranasal OT elevated OT levels within the left amygdala as well as blood (Smith et al., 2019). Collectively, these findings extend the previous findings in rodents, non-human primates and humans and suggest that OT is capable of entering the parenchyma following intranasal delivery.

One question is how translatable are metabolic data that are generated in animal models following central or peripheral administration given that OT is largely being administered intranasally in humans. As previously discussed, OT given by peripheral route of administration is likely to act by both peripheral and central OTRs (particularly at higher doses) to inhibit food intake and potentially stimulate thermogenesis and energy expenditure. There is a very limited amount of metabolic data following intranasal administration in rodent models, but it has been found to largely recapitulate the effects of central and peripheral OT to reduce food intake (Maejima et al., 2015) and/or weight gain (Seelke et al., 2018) in mice and DIO prairie voles, respectively. While additional studies tracking the effects of chronic intranasal administration on food intake, thermogenesis and energy expenditure and weight loss need to be undertaken in the rodent model, the data obtained from both central and peripheral administration in animal models appears to translate well to current findings following intranasal administration in animal models.

EFFECTS OF OXYTOCIN ON DYSLIPIDEMIA AND LIPOLYSIS IN RODENT AND NON-HUMAN PRIMATE MODELS

Both *in vitro* and *in vivo* data suggest that OT reduces dyslipidemia and increases lipolysis in rodent and non-human primate models. OT was found to stimulate glycerol in 3T3-L1 adipocytes (Yi et al., 2015), which express OTRs (Schaffler et al., 2005; Yi et al., 2015), indicating that OT stimulates lipolysis in this model through a direct action. In addition, OT also stimulated glycerol release from epididymal fat pads *ex vivo* (Deblon et al., 2011). ICV OT (1.6 nmol/day) also increased serum glycerol and reduced serum triglycerides following 2-week treatment in rats (Deblon et al., 2011). Chronic 3V infusions (16 nmol/day) over 21–28 days was found to reduce total cholesterol in DIO mice (Roberts et al., 2017) and rats (Blevins et al., 2016; Roberts et al., 2017). Recent findings indicate that in female perimenopausal rats, systemic OT over 12 days was found to reduce triglycerides, LDL and HDL cholesterol (Erdenebayar et al., 2020) raising the possibility that OT could be beneficial in treating hyperlipidemia at the time of menopause or post-menopause. Blevins extended these findings in DIO non-human primates (rhesus monkeys) where chronic 2 × daily subcutaneous injections of OT reduced total cholesterol, Apolipoprotein C-III, high-density lipoprotein, serum triglycerides and increased serum free fatty acids and glycerol following 4-weeks of treatment. It was also associated with a transient reduction of low-density lipoprotein (Blevins et al., 2015). One additional study found that chronic ICV (1.6 nmol/day) infusions of OT stimulated EWAT mRNA expression of lipoprotein lipase (Lpl) and fatty acid transporter (fat) (Deblon et al., 2011), which have both been linked uptake of triglycerides and fatty acids, respectively. While chronic ICV infusions of OT (1.6 nmol/day) did not alter enzymes linked to triglyceride storage or lipogenesis (diacylglycerol *O*-acyltransferase homolog 1, fatty acid synthase, and acetyl-coenzyme A carboxylase alpha), it did stimulate enzymes associated with lipolysis (hormone-sensitive lipase and patatin-like phospholipase domain containing 2) (Deblon et al., 2011). Chronic CNS [ICV, 3V; 16 nmol/day] or systemic OT administration (1.6 mg/kg/day or ∼56.4 nmol/day) is also associated with decreases in respiratory quotient in DIO rats (Deblon et al., 2011; Blevins et al., 2016) and DIO mice (Maejima et al., 2011) relative to vehicle treated animals (Deblon et al., 2011; Maejima et al., 2011; Blevins et al., 2016) or pair-fed control animals (Deblon et al., 2011). Taken together, these findings suggest that OT-elicited lipolysis and lipid oxidation may contribute to OT-elicited weight loss.

OXYTOCIN RECEPTOR DIMERIZATION

The OTR is a G protein-coupled receptor (GPCR) that is coupled to the Gαq alpha subunit (Gαq) or the Gαi alpha subunit (Busnelli and Chini, 2018). Given that the OTR is a GPCR it is prone to the formation of heterodimers with other GPCRs that are in close proximity. These heterodimers can impact intracellular signaling pathways, allosteric interactions, endocytosis, biological function and drug effects (Schellekens et al., 2013; Wallace Fitzsimons et al., 2019). This is of particular interest given that OT and ghrelin have opposing actions on food intake and OTRs and the growth hormone secretagogue receptor (GHS-R1a) have overlapping areas of expression in many CNS sites linked to the control of food intake and/or energy expenditure (including the ARC, VMH, NTS, and VTA) (Abizaid et al., 2006; Zigman et al., 2006). Recent studies have provided strong evidence for cross-talk between both receptors and co-expression of OTR/GHSR resulted in an attenuation of OTR-elicited signaling and potential heterocomplex formation (Wallace Fitzsimons et al., 2019).

In addition to ghrelin, the OTR has been found to form homo- and heterodimers with other receptors. OTRs and vasopressin V1a and V2 receptors also form homo- and heterodimers (Terrillon et al., 2003). In addition, OTR forms heterocomplexes with dopamine D2 receptors which may potentially contribute

to anti-anxiety actions of OT within the CeA (de la Mora et al., 2016). Additional studies provide evidence for the presence of dopamine d2-OTR heteromers located within the ventral and dorsal striatum that may play a role with facilitatory receptor-receptor interactive effects (Romero-Fernandez et al., 2013). Recent studies also indicate that signaling through OT and serotonin 2A receptors appears to be impaired through heteroreceptor formation (Chruscicka et al., 2019). The extent to which these homo- or hetero-complexes may contribute to the effects of OT to reduce both anxiety and feeding reward and potentially explain the ability of OT to produce a more pronounced reduction of energy intake in DIO rodents (Deblon et al., 2011; Maejima et al., 2011; Blevins et al., 2016; Roberts et al., 2017; Edwards et al., 2021b) and obese humans (Thienel et al., 2016) will be important questions for future investigation.

DOES OXYTOCIN REDUCE BODY WEIGHT IN OBESE AND OVERWEIGHT HUMANS?

The beneficial metabolic effects of OT have been recently translated to DIO non-human primates (Blevins et al., 2015) and obese humans (Zhang et al., 2013; Lawson et al., 2015; Thienel et al., 2016). Several small clinical trials conducted in normal weight or overweight/obese men have shown that a single-dose intranasal OT acutely decreased food intake and hedonic eating (Ott et al., 2013; Lawson et al., 2015; Thienel et al., 2016). Large clinical trials of long duration to examine the effectiveness of OT treatment in obesity is lacking but available clinical trial data have revealed beneficial effects of OT on reducing body weight in overweight/obese men and women as well as in an adolescent boy with hypothalamic obesity (Zhang et al., 2013; Hsu et al., 2017). In the first study to show that chronic intranasal OT elicited weight loss in humans, 24 overweight/obese men and women were randomized to receive OT nasal spray 24 international units (IU) four times daily or placebo for 8 weeks (Zhang et al., 2013). OT treatment led to a 8.9 $\pm$ 5.4 kg ($p < 0.001$) weight loss at the end of the trial and the weight reduction was significantly larger than the placebo at the end of the trial. No adverse events (AEs) were reported during the trial. In addition, in a single case study, chronic intranasal OT was found to reduce obesity and food intake in an obese 13-year-old adolescent following removal of a craniopharyngioma (Hsu et al., 2017), which speaks to the generalized energy homeostatic action of OT independent of obesity etiology. A more recent trial found that chronic intranasal OT (24 IU four times daily for 8 weeks) tended to reduce body adiposity and increase lean mass in a group of older adults with sarcopenia and obesity but failed to produce any changes in BMI (Espinoza et al., 2021). While these studies provided preliminary evidence that OT treatment may have promising metabolic benefits, including reduction of adiposity and/or body weight, sufficiently powered and rigorously designed clinical trials are still needed to confirm the effect of OT seen on energy metabolism. In addition to homeostatic food intake, OT has also been associated with limiting consumption of highly palatable foods in rodent and non-human primate models (for review, see Lawson, 2017; McCormack et al., 2020). These findings also have translated to some extent in humans (Lawson et al., 2015). Several labs have reported that intranasal OT reduced chocolate cookie or biscuit consumption (Ott et al., 2013; Thienel et al., 2016; Burmester et al., 2018). In addition, intranasal OT enhances the cognitive control of food craving in women who viewed images of candies and desserts (Striepens et al., 2016). To evaluate the mechanism for these behavioral findings, Plessow et al. (2018) observed that intranasal OT reduced activation of both homeostatic and feeding reward centers in the CNS, in response to images of highly palatable food during functional MRI. While further studies need to be done to clarify if OT modifies macronutrient preference in humans, these findings together suggest that it may play a role in limiting consumption of stress- or emotional-eating of food high in sugar or fat.

Thus, while several small clinical trials conducted in normal weight or overweight/obese men have now shown that a single-dose intranasal OT acutely decreased calorie intake (Lawson et al., 2015; Thienel et al., 2016), hedonic eating (Ott et al., 2013; Lawson et al., 2015; Thienel et al., 2016) and food craving (Striepens et al., 2016) it is still unclear if these findings would hold up in a paradigm of chronic administration or if they would be correlated with clinically meaningful weight loss. While the one study by Zhang et al. (2013) found that chronic intranasal OT elicited weight loss in overweight/obese humans, the mechanism of action of OT remains unexplored (e.g., associated with an increase in energy expenditure and/or decrease in appetite/food intake). Sufficiently powered, rigorously designed clinical trials are needed to examine the efficacy, tolerability and safety of OT use in humans. Based on our preclinical data and available clinical observations, we argue that OT holds promise as an appealing, non-invasive strategy to combat obesity though its CNS action on regulating appetite (Striepens et al., 2013; Freeman et al., 2016) and/or energy expenditure.

TRANSLATIONAL POTENTIAL

Intravenous/intramuscular OT is FDA-approved and has a long track record of clinical use in parturition (Vallera et al., 2017). Intranasal OT has been used clinically for over 50 years (most commonly in the field of psychiatry) and has an excellent safety profile (MacDonald et al., 2011). A systematic review of 38 RTCs conducted between 1990 and 2010 on over 1500 individuals (79% men) showed that OT was not associated with adverse outcomes when delivered at doses of 18–40 IU for short term use in controlled research settings (MacDonald et al., 2011). Mild side effects including drowsiness/sleepiness, calm/relaxed/comfortable, lightheadedness, and feeling of anxious/worried were reported by 279 out of 1529 participants (18%). Since then, longer term studies have been conducted and continued to demonstrate an excellent safety profile of intranasal OT (Tachibana et al., 2013; Zhang et al., 2013; Hsu et al., 2017; Cai et al., 2018). As mentioned earlier, the pharmacokinetics of intranasal OT administration have been investigated. Striepens et al. (2013) showed that, in subjects who received 24 IU of OT intranasally (or placebo), OT levels increased significantly in

plasma at 15, 30, 45, and 60 min after administration, and in cerebrospinal fluid (CSF) at 75 min when the plasma level began to decline. In another study by Gossen et al. (2012), following 26 IU of single intranasal OT administration in eight men plasma OT concentrations increased over a period of 210 min, reaching a peak at 30 min. Lawson et al. (2015) previously showed that a single-dose (24 IU) intranasal OT acutely decreases food intake; Zhang et al. (2013) reported that 24 IU given QID over 8 weeks reduced body weight in overweight/obese men and women. The 40 IU dose has been used in clinical trials for up to approximately 10 weeks at a frequency of once daily and was well tolerated (van Zuiden et al., 2017; Flanagan et al., 2018).

As discussed above, OT may increase BAT thermogenesis through its action in the modulation of CNS sympathetic output and on sympathetic pre-ganglionic OTR-expressing neurons within the spinal cord to increase SNS outflow (see section "Source and Functions of Oxytocin"). Collectively, this may adversely affect cardiac function and hamper its translational potential (Greenfield et al., 2009; Kievit et al., 2013) given the high prevalence of hypertension and cardiovascular disease among individuals who are overweight or obese (Nguyen et al., 2008). However, studies in animals have generated mixed results demonstrating an increase, decrease or no change in blood pressure (Petersson et al., 1996; Nation et al., 2010; Maejima et al., 2011; Ludwig et al., 2013; Yosten and Samson, 2014) or heart rate (Petersson et al., 1996; Yang et al., 2009; Yoshida et al., 2009; Nation et al., 2010; Maejima et al., 2011; Ludwig et al., 2013; Hicks et al., 2014; Plante et al., 2015) depending on route of OT administration and species studied (for review, see Petersson, 2002; Gutkowska and Jankowski, 2012). Studies using intranasal OT in humans have not reported adverse side effects on heart rate (Burri et al., 2008; Kirkpatrick et al., 2014; Lawson et al., 2015), blood pressure (Kirkpatrick et al., 2014; Lawson et al., 2015) or cardiovascular dysfunction (Zhang et al., 2013) in men (Burri et al., 2008; Zhang et al., 2013; Kirkpatrick et al., 2014; Lawson et al., 2015) and non-pregnant women (Zhang et al., 2013; Kirkpatrick et al., 2014). The sample size of these studies was small, and the duration of treatment was short (up to 8 weeks). Therefore, it will be prudent to carefully monitor cardiovascular outcomes such as heart rate and blood pressure with chronic OT treatment in future studies.

CONCLUSION

Pre-clinical data in rodents and non-human primates suggest that OT elicits weight loss, in part, by both central and peripheral mechanisms to reduce food intake (homeostatic and hedonic feeding) and impact energy expenditure in the absence of visceral illness or tolerance. While there is much enthusiasm over the potential use of OT as a therapeutic strategy to treat eating disorders and obesity, we await the results of ongoing clinical trials in obese humans for additional confirmation of its feasibility as a long-term weight loss strategy and assessment of adverse side effects. There is an ongoing need to identify an optimal dose, frequency, and duration of administration and to examine the dose-response effects of intranasal OT on body weight and adiposity in individuals with obesity.

Combination drug treatment has demonstrated impressive efficacy in inducing weight loss [(Frias et al., 2017; Chepurny et al., 2018)] (for review, see Rodgers et al., 2012). We think OT may be more optimal as an adjunct therapy for obesity rather than a monotherapy. It is clear that OT is effective as a monotherapy to elicit weight loss in DIO rodents (Deblon et al., 2011; Maejima et al., 2011, 2017; Zhang and Cai, 2011; Zhang et al., 2011; Morton et al., 2012; Blevins et al., 2016; Roberts et al., 2017; Edwards et al., 2021b), non-human primates (Blevins et al., 2015) and humans (Zhang et al., 2013), but these effects (pre- vs. post-intervention) appear to be modest even after sustained treatments that last 4–8 weeks [$\approx$ 4.9% in DIO mice (Roberts et al., 2017), 8.7% in DIO rats (Roberts et al., 2017), 3.3% in DIO rhesus monkeys (Blevins et al., 2015) and 9.3% humans based on results from a proof of concept study with short duration and small sample size (Zhang et al., 2013)]. The average weight loss with the currently FDA approved medications (i.e., orlistat, liraglutide, naltrexone/bupropion, phentermine/topiramate, semaglutide) ranges between 5 and 14.9% (Allison et al., 2012; Apovian et al., 2015; Bray et al., 2018; Enebo et al., 2021).

Long-term efficacy of OT treatment for obesity remains to be established. The effect of OT on thermogenesis, appetite and stress reduction may offer unique properties that current therapies do not have. OT as an adjunct therapy for obesity is also worth exploring. For instance, pre-clinical and clinical studies indicate that OT in combination with the opioid antagonist, naltrexone, is an effective strategy to reduce food intake (animals, humans) as well as body weight (humans). Peripheral (intravenous) administration of OT and naltrexone was recently found to be effective at reducing palatable 10% sucrose solutions as well as intake of a high fat/high sugar diet in rats (Head et al., 2021). Intranasal OT was also found to be effective at reducing hyperphagia and maintaining weight loss when given in combination with the opioid antagonist, naltrexone, to a 13-year-old adolescent male with craniopharyngioma related hypothalamic obesity (Hsu et al., 2017). Thus, the combination of OT with other therapies that act, in part to reduce food intake (hedonic and/or homeostatic feeding) and increase energy expenditure may act in an additive mechanism to elicit greater weight loss than either treatment alone.

AUTHOR CONTRIBUTIONS

JN helped write and edit the manuscript and she also helped generate **Figure 1**. JT helped write and edit the manuscript. JB provided feedback on the figure and helped write and edit the manuscript. All authors contributed to the article and approved the submitted version.

ACKNOWLEDGMENTS

This material was based upon work supported by the Office of Research and Development, Medical Research Service, Department of Veterans Affairs (VA). This work was also supported by the VA Merit Review Award 5I01BX004102, from the United States Department of Veterans Affairs Biomedical Laboratory Research and Development Service and NIH 5R01DK115976 grant to JB. In addition, we acknowledge JN for her technical assistance with **Figure 1**. The contents do not represent the views of the United States Department of Veterans Affairs or the United States Government.

REFERENCES

Abizaid, A., Liu, Z. W., Andrews, Z. B., Shanabrough, M., Borok, E., Elsworth, J. D., et al. (2006). Ghrelin modulates the activity and synaptic input organization of midbrain dopamine neurons while promoting appetite. *J. Clin. Investig.* 116, 3229–3239. doi: 10.1172/JCI29867

Allison, D. B., Gadde, K. M., Garvey, W. T., Peterson, C. A., Schwiers, M. L., Najarian, T., et al. (2012). Controlled-release phentermine/topiramate in severely obese adults: a randomized controlled trial (EQUIP). *Obesity* 20, 330–342. doi: 10.1038/oby.2011.330

Altirriba, J., Poher, A. L., Caillon, A., Arsenijevic, D., Veyrat-Durebex, C., Lyautey, J., et al. (2014). Divergent effects of oxytocin treatment of obese diabetic mice on adiposity and diabetes. *Endocrinology* 155, 4189–4201. doi: 10.1210/en.2014-1466

Amico, J. A., Vollmer, R. R., Cai, H. M., Miedlar, J. A., and Rinaman, L. (2005). Enhanced initial and sustained intake of sucrose solution in mice with an oxytocin gene deletion. *Am. J. Physiol. Regul. Integr. Comp. Physiol.* 289, R1798–R1806.

Angioni, L., Cocco, C., Ferri, G. L., Argiolas, A., Melis, M. R., and Sanna, F. (2016). Involvement of nigral oxytocin in locomotor activity: a behavioral, immunohistochemical and lesion study in male rats. *Horm. Behav.* 83, 23–38. doi: 10.1016/j.yhbeh.2016.05.012

Antunes, J. L., and Zimmerman, E. A. (1978). The hypothalamic magnocellular system of the rhesus monkey: an immunocytochemical study. *J. Comp. Neurol.* 181, 539–565.

Apovian, C. M., Aronne, L. J., Bessesen, D. H., McDonnell, M. E., Murad, M. H., Pagotto, U., et al. (2015). Pharmacological management of obesity: an endocrine Society clinical practice guideline. *J. Clin. Endocrinol. Metab.* 100, 342–362.

Arletti, R., Benelli, A., and Bertolini, A. (1989). Influence of oxytocin on feeding behavior in the rat. *Peptides* 10, 89–93.

Arletti, R., Benelli, A., and Bertolini, A. (1990). Oxytocin inhibits food and fluid intake in rats. *Physiol. Behav.* 48, 825–830.

Balazova, L., Krskova, K., Suski, M., Sisovsky, V., Hlavacova, N., Olszanecki, R., et al. (2016). Metabolic effects of subchronic peripheral oxytocin administration in lean and obese zucker rats. *J. Physiol. Pharmacol.* 67, 531–541.

Bales, K. L., Perkeybile, A. M., Conley, O. G., Lee, M. H., Guoynes, C. D., Downing, G. M., et al. (2013). Chronic intranasal oxytocin causes long-term impairments in partner preference formation in male prairie voles. *Biol. Psychiatry* 74, 180–188. doi: 10.1016/j.biopsych.2012.08.025

Banks, W. A., DiPalma, C. R., and Farrell, C. L. (1999). Impaired transport of leptin across the blood-brain barrier in obesity. *Peptides* 20, 1341–1345.

Bartz, J., Simeon, D., Hamilton, H., Kim, S., Crystal, S., Braun, A., et al. (2011). Oxytocin can hinder trust and cooperation in borderline personality disorder. *Soc. Cogn. Affect. Neurosci.* 6, 556–563.

Baskin, D. G., and Bastian, L. S. (2010). "Immuno-laser capture microdissection of rat brain neruons for real time quantitative PCR," in *Immunocytochemical methods and protocols, Methods in Molecular Biology*, eds C. Oliver and M. C. Jamur (New York, NY: Humana Press), 219–230. doi: 10.1007/978-1-59745-324-0_23

Baskin, D. G., Kim, F., Gelling, R. W., Russell, B. J., Schwartz, M. W., Morton, G. J., et al. (2010). A new oxytocin-saporin cytotoxin for lesioning oxytocin-receptive neurons in the rat hindbrain. *Endocrinology* 151, 4207–4213. doi: 10.1210/en.2010-0295

Beier, K. T., Steinberg, E. E., DeLoach, K. E., Xie, S., Miyamichi, K., Schwarz, L., et al. (2015). Circuit architecture of VTA dopamine neurons revealed by systematic input-output mapping. *Cell* 162, 622–634. doi: 10.1016/j.cell.2015.07.015

Benelli, A., Bertolini, A., and Arletti, R. (1991). Oxytocin-induced inhibition of feeding and drinking: no sexual dimorphism in rats. *Neuropeptides* 20, 57–62. doi: 10.1016/0143-4179(91)90040-p

Bergum, D., Lonnee, H., and Hakli, T. F. (2009). Oxytocin infusion: acute hyponatraemia, seizures and coma. *Acta Anaesth. Scand.* 53, 826–827. doi: 10.1111/j.1399-6576.2009.01964.x

Blevins, J. E., and Baskin, D. G. (2015). Translational and therapeutic potential of oxytocin as an anti-obesity strategy: insights from rodents, nonhuman primates and humans. *Physiol. Behav.* 152(Pt B), 438–449. doi: 10.1016/j.physbeh.2015.05.023

Blevins, J. E., Eakin, T. J., Murphy, J. A., Schwartz, M. W., and Baskin, D. G. (2003). Oxytocin innervation of caudal brainstem nuclei activated by cholecystokinin. *Brain Res.* 993, 30–41. doi: 10.1016/j.brainres.2003.08.036

Blevins, J. E., Graham, J. L., Morton, G. J., Bales, K. L., Schwartz, M. W., Baskin, D. G., et al. (2015). Chronic oxytocin administration inhibits food intake, increases energy expenditure, and produces weight loss in fructose-fed obese rhesus monkeys. *Am. J. Physiol. Regul. Integr. Comp. Physiol.* 308, R431–R438. doi: 10.1152/ajpregu.00441.2014

Blevins, J. E., and Ho, J. M. (2013). Role of oxytocin signaling in the regulation of body weight. *Rev. Endocrine Metab. Disord.* 14, 311–329.

Blevins, J. E., Morton, G. J., Williams, D. L., Caldwell, D. W., Bastian, L. S., Wisse, B. E., et al. (2009). Forebrain melanocortin signaling enhances the hindbrain satiety response to CCK-8. *Am. J. Physiol. Regul. Integr. Comp. Physiol.* 296, R476–R484. doi: 10.1152/ajpregu.90544.2008

Blevins, J. E., Schwartz, M. W., and Baskin, D. G. (2004). Evidence that paraventricular nucleus oxytocin neurons link hypothalamic leptin action to caudal brain stem nuclei controlling meal size. *Am. J. Physiol. Regul. Integr. Comp. Physiol.* 287, R87–R96. doi: 10.1152/ajpregu.00604.2003

Blevins, J. E., Thompson, B. W., Anekonda, V. T., Ho, J. M., Graham, J. L., Roberts, Z. S., et al. (2016). Chronic CNS oxytocin signaling preferentially induces fat loss in high fat diet-fed rats by enhancing satiety responses and increasing lipid utilization. *Am. J. Physiol. Reg. I* 310, R640–R58. doi: 10.1152/ajpregu.00220.2015

Blouet, C., Jo, Y. H., Li, X., and Schwartz, G. J. (2009). Mediobasal hypothalamic leucine sensing regulates food intake through activation of a hypothalamus-brainstem circuit. *J. Neurosci.* 29, 8302–8311. doi: 10.1523/JNEUROSCI.1668-09.2009

Boccia, M. L., Panicker, A. K., Pedersen, C., and Petrusz, P. (2001). Oxytocin receptors in non-human primate brain visualized with monoclonal antibody. *Neuroreport* 12, 1723–1726. doi: 10.1097/00001756-200106130-00041

Boccia, M. L., Petrusz, P., Suzuki, K., Marson, L., and Pedersen, C. A. (2013). Immunohistochemical localization of oxytocin receptors in human brain. *Neuroscience* 253, 155–164.

Borg, J., Simren, M., and Ohlsson, B. (2011). Oxytocin reduces satiety scores without affecting the volume of nutrient intake or gastric emptying rate in healthy subjects. *Neurogastroenterol. Motil.* 23, 56.e5–61.e5.

Born, J., Lange, T., Kern, W., McGregor, G. P., Bickel, U., and Fehm, H. L. (2002). Sniffing neuropeptides: a transnasal approach to the human brain. *Nat. Neurosci.* 5, 514–516. doi: 10.1038/nn849

Braude, R., and Mitchell, K. G. (1952). Observations on the relationship between oxytocin and adrenaline in milk ejection in the sow. *J. Endocrinol.* 8, 238–241. doi: 10.1677/joe.0.0080238

Bray, G. A., Heisel, W. E., Afshin, A., Jensen, M. D., Dietz, W. H., Long, M., et al. (2018). The science of obesity management: an endocrine society scientific statement. *Endocr. Rev.* 39, 79–132.

Breuil, V., Amri, E. Z., Panaia-Ferrari, P., Testa, J., Elabd, C., Albert-Sabonnadiere, C., et al. (2011). Oxytocin and bone remodelling: relationships with neuropituitary hormones, bone status and body composition. *Joint Bone Spine* 78, 611–615. doi: 10.1016/j.jbspin.2011.02.002

Breuil, V., Fontas, E., Chapurlat, R., Panaia-Ferrari, P., Yahia, H. B., Faure, S., et al. (2015). Oxytocin and bone status in men: analysis of the MINOS cohort. *Osteoporos. Int.* 26, 2877–2882. doi: 10.1007/s00198-015-3201-3

Breuil, V., Panaia-Ferrari, P., Fontas, E., Roux, C., Kolta, S., Eastell, R., et al. (2014). Oxytocin, a new determinant of bone mineral density in post-menopausal women: analysis of the OPUS cohort. *J. Clin. Endocrinol. Metab.* 99, E634–E641. doi: 10.1210/jc.2013-4126

Brierley, D. I., Holt, M. K., Singh, A., de Araujo, A., McDougle, M., Vergara, M., et al. (2021). Central and peripheral GLP-1 systems independently suppress eating. *Nat. Metab.* 3, 258–273.

Brownstein, M. J., Russell, J. T., and Gainer, H. (1980). Synthesis, transport, and release of posterior pituitary hormones. *Science* 207, 373–378.

Burmester, V., Higgs, S., and Terry, P. (2018). Rapid-onset anorectic effects of intranasal oxytocin in young men. *Appetite* 130, 104–109. doi: 10.1016/j.appet.2018.08.003

Burri, A., Heinrichs, M., Schedlowski, M., and Kruger, T. H. (2008). The acute effects of intranasal oxytocin administration on endocrine and sexual function in males. *Psychoneuroendocrinology* 33, 591–600. doi: 10.1016/j.psyneuen.2008.01.014

Busnelli, M., and Chini, B. (2018). Molecular basis of oxytocin receptor signalling in the brain: what we know and what we need to know. *Curr. Top. Behav. Neurosci.* 35, 3–29. doi: 10.1007/7854_2017_6

Cai, Q., Feng, L., and Yap, K. Z. (2018). Systematic review and meta-analysis of reported adverse events of long-term intranasal oxytocin treatment for autism spectrum disorder. *Psychiatry Clin. Neurosci.* 72, 140–151. doi: 10.1111/pcn.12627

Caldwell, J. D., Jirikowski, G. F., Greer, E. R., Stumpf, W. E., and Pedersen, C. A. (1988). Ovarian steroids and sexual interaction alter oxytocinergic content and distribution in the basal forebrain. *Brain Res.* 446, 236–244. doi: 10.1016/0006-8993(88)90882-7

Camerino, C. (2009). Low sympathetic tone and obese phenotype in oxytocin-deficient mice. *Obesity* 17, 980–984. doi: 10.1038/oby.2009.12

Cannon, B., and Nedergaard, J. (2004). Brown adipose tissue: function and physiological significance. *Physiol. Rev.* 84, 277–359.

Carson, D. S., Hunt, G. E., Guastella, A. J., Barber, L., Cornish, J. L., Arnold, J. C., et al. (2010). Systemically administered oxytocin decreases methamphetamine activation of the subthalamic nucleus and accumbens core and stimulates oxytocinergic neurons in the hypothalamus. *Addict. Biol.* 15, 448–463. doi: 10.1111/j.1369-1600.2010.00247.x

Castel, M., and Morris, J. F. (1988). The neurophysin-containing innervation of the forebrain of the mouse. *Neuroscience* 24, 937–966. doi: 10.1016/0306-4522(88)90078-4

Cechetto, D. F., and Saper, C. B. (1988). Neurochemical organization of the hypothalamic projection to the spinal cord in the rat. *J. Comp. Neurol.* 272, 579–604. doi: 10.1002/cne.902720410

Chang, S. W., and Platt, M. L. (2014). Oxytocin and social cognition in rhesus macaques: implications for understanding and treating human psychopathology. *Brain Res.* 1580, 57–68. doi: 10.1016/j.brainres.2013.11.006

Chepurny, O. G., Bonaccorso, R. L., Leech, C. A., Wollert, T., Langford, G. M., Schwede, F., et al. (2018). Chimeric peptide EP45 as a dual agonist at GLP-1 and NPY2R receptors. *Sci. Rep.* 8:3749.

Chruscicka, B., Wallace Fitzsimons, S. E., Borroto-Escuela, D. O., Druelle, C., Stamou, P., Nally, K., et al. (2019). Attenuation of oxytocin and serotonin 2A receptor signaling through novel heteroreceptor formation. *ACS Chem. Neurosci.* 10, 3225–3240. doi: 10.1021/acschemneuro.8b00665

Colaianni, G., Sun, L., Benedetto, A. Di, Tamma, R., Zhu, L. L., Cao, J., et al. (2012). Bone marrow oxytocin mediates the anabolic action of estrogen on the skeleton. *J. Biol. Chem.* 287, 29159–29167. doi: 10.1074/jbc.M112.365049

Colaianni, G., Sun, L., Zaidi, M., and Zallone, A. (2015). The "love hormone" oxytocin regulates the loss and gain of the fat-bone relationship. *Front. Endocrinol.* 6:79. doi: 10.3389/fendo.2015.00079

Colucci, S., Colaianni, G., Mori, G., Grano, M., and Zallone, A. (2002). Human osteoclasts express oxytocin receptor. *Biochem. Biophys. Res. Commun.* 297, 442–445.

Copland, J. A., Ives, K. L., Simmons, D. J., and Soloff, M. S. (1999). Functional oxytocin receptors discovered in human osteoblasts. *Endocrinology* 140, 4371–4374. doi: 10.1210/endo.140.9.7130

Cornier, M. A., Dabelea, D., Hernandez, T. L., Lindstrom, R. C., Steig, A. J., Stob, N. R., et al. (2008). The metabolic syndrome. *Endocrine Rev.* 29, 777–822.

Daniels, D., and Flanagan-Cato, L. M. (2000). Functionally-defined compartments of the lordosis neural circuit in the ventromedial hypothalamus in female rats. *J. Neurobiol.* 45, 1–13.

de la Mora, M. P., Perez-Carrera, D., Crespo-Ramirez, M., Tarakanov, A., Fuxe, K., and Borroto-Escuela, D. O. (2016). Signaling in dopamine D2 receptor-oxytocin receptor heterocomplexes and its relevance for the anxiolytic effects of dopamine and oxytocin interactions in the amygdala of the rat. *Biochim. Biophys. Acta* 1862, 2075–2085. doi: 10.1016/j.bbadis.2016.07.004

Deblon, N., Veyrat-Durebex, C., Bourgoin, L., Caillon, A., Bussier, A. L., Petrosino, S., et al. (2011). Mechanisms of the anti-obesity effects of oxytocin in diet-induced obese rats. *PLoS One* 6:e25565. doi: 10.1371/journal.pone.0025565

den Hertog, C. E., de Groot, A. N., and van Dongen, P. W. (2001). History and use of oxytocics. *Eur. J. Obstetr. Gynecol. Reproduct. Biol.* 94, 8–12.

Dierickx, K., and Vandesande, F. (1977). Immunocytochemical localization of the vasopressinergic and the oxytocinergic neurons in the human hypothalamus. *Cell Tissue Res.* 184, 15–27. doi: 10.1007/BF00220524

Eckel, R. H., Grundy, S. M., and Zimmet, P. Z. (2005). The metabolic syndrome. *Lancet* 365, 1415–1428.

Eckertova, M., Ondrejcakova, M., Krskova, K., Zorad, S., and Jezova, D. (2011). Subchronic treatment of rats with oxytocin results in improved adipocyte differentiation and increased gene expression of factors involved in adipogenesis. *Br. J. Pharmacol.* 162, 452–463. doi: 10.1111/j.1476-5381.2010.01037.x

Edwards, M. M., Nguyen, H. K., Herbertson, A. J., Dodson, A. D., Wietecha, T., Wolden-Hanson, T., et al. (2021b). Chronic hindbrain administration of oxytocin elicits weight loss in male diet-induced obese mice. *Am. J. Physiol. Regul. Integr. Comp. Physiol.* 320, R471–R487.

Edwards, M. M., Nguyen, H. K., Dodson, A. D., Herbertson, A. J., Wietecha, T. A., Wolden-Hanson, T., et al. (2021a). Effects of combined oxytocin and beta-3 receptor agonist (CL 316243) treatment on body weight and adiposity in male diet-induced obese rats. *Front. Physiol.* 12:725912. doi: 10.3389/fphys.2021.725912

Elabd, C., Cousin, W., Upadhyayula, P., Chen, R. Y., Chooljian, M. S., Li, J., et al. (2014). Oxytocin is an age-specific circulating hormone that is necessary for muscle maintenance and regeneration. *Nat. Commun.* 5:4082. doi: 10.1038/ncomms5082

Enebo, L. B., Berthelsen, K. K., Kankam, M., Lund, M. T., Rubino, D. M., Satylganova, A., et al. (2021). Safety, tolerability, pharmacokinetics, and pharmacodynamics of concomitant administration of multiple doses of cagrilintide with semaglutide 2.4 mg for weight management: a randomised, controlled, phase 1b trial. *Lancet* 397, 1736–1748. doi: 10.1016/S0140-6736(21)00845-X

Erdenebayar, O., Kato, T., Kawakita, T., Kasai, K., Kadota, Y., Yoshida, K., et al. (2020). Effects of peripheral oxytocin administration on body weight, food intake, adipocytes, and biochemical parameters in peri- and postmenopausal female rats. *Endocrine J.* 68, 7–16. doi: 10.1507/endocrj.EJ19-0586

Ermisch, A., Barth, T., Ruhle, H. J., Skopkova, J., Hrbas, P., and Landgraf, R. (1985). On the blood-brain barrier to peptides: accumulation of labelled vasopressin, DesGlyNH2-vasopressin and oxytocin by brain regions. *Endocrinol. Exp.* 19, 29–37.

Espinoza, S. E., Lee, J. L., Wang, C. P., Ganapathy, V., MacCarthy, D., Pascucci, C., et al. (2021). Intranasal oxytocin improves lean muscle mass and lowers LDL cholesterol in older adults with sarcopenic obesity: a pilot randomized controlled trial. *J. Am. Med. Dir. Assoc.* 22, 1877.e2–1882.e2. doi: 10.1016/j.jamda.2021.04.015

Fenselau, H., Campbell, J. N., Verstegen, A. M., Madara, J. C., Xu, J., Shah, B. P., et al. (2017). A rapidly acting glutamatergic ARC–>PVH satiety circuit postsynaptically regulated by alpha-MSH. *Nat. Neurosci.* 20, 42–51. doi: 10.1038/nn.4442

Finkelstein, E. A., Trogdon, J. G., Cohen, J. W., and Dietz, W. (2009). Annual medical spending attributable to obesity: payer-and service-specific estimates. *Health Affairs* 28, w822–w831. doi: 10.1377/hlthaff.28.5.w822

Flanagan, J. C., Sippel, L. M., Wahlquist, A., Moran-Santa Maria, M. M., and Back, S. E. (2018). Augmenting Prolonged Exposure therapy for PTSD with

intranasal oxytocin: a randomized, placebo-controlled pilot trial. *J. Psychiatr. Res.* 98, 64–69. doi: 10.1016/j.jpsychires.2017.12.014

Flanagan, L. M., Olson, B. R., Sved, A. F., Verbalis, J. G., and Stricker, E. M. (1992). Gastric motility in conscious rats given oxytocin and an oxytocin antagonist centrally. *Brain Res.* 578, 256–260. doi: 10.1016/0006-8993(92)90255-8

Flanagan-Cato, L. M., Calizo, L. H., and Daniels, D. (2001). The synaptic organization of VMH neurons that mediate the effects of estrogen on sexual behavior. *Hormon. Behav.* 40, 178–182.

Fosgerau, K., Raun, K., Nilsson, C., Dahl, K., and Wulff, B. S. (2014). Novel alpha-MSH analog causes weight loss in obese rats and minipigs and improves insulin sensitivity. *J. Endocrinol.* 220, 97–107. doi: 10.1530/JOE-13-0284

Freeman, S. M., Inoue, K., Smith, A. L., Goodman, M. M., and Young, L. J. (2014). The neuroanatomical distribution of oxytocin receptor binding and mRNA in the male rhesus macaque (*Macaca mulatta*). *Psychoneuroendocrinology* 45, 128–141. doi: 10.1016/j.psyneuen.2014.03.023

Freeman, S. M., Ngo, J., Singh, B., Masnaghetti, M., Bales, K. L., and Blevins, J. E. (2018). Effects of chronic oxytocin administration and diet composition on oxytocin and vasopressin 1a receptor binding in the rat brain. *Neuroscience* 392, 241–251. doi: 10.1016/j.neuroscience.2018.07.037

Freeman, S. M., Samineni, S., Allen, P. C., Stockinger, D., Bales, K. L., Hwa, G. G., et al. (2016). Plasma and CSF oxytocin levels after intranasal and intravenous oxytocin in awake macaques. *Psychoneuroendocrinology* 66, 185–194. doi: 10.1016/j.psyneuen.2016.01.014

Freund-Mercier, M. J., and Stoeckel, M. E. (1995). Somatodendritic autoreceptors on oxytocin neurones. *Adv. Exp. Med. Biol.* 395, 185–194.

Freund-Mercier, M. J., Stoeckel, M. E., and Klein, M. J. (1994). Oxytocin receptors on oxytocin neurones: histoautoradiographic detection in the lactating rat. *J. Physiol.* 480(Pt 1), 155–161.

Frias, J. P., Bastyr, E. J., Vignati, L., Tschop, M. H., Schmitt, C., Owen, K., et al. (2017). The sustained effects of a dual GIP/GLP-1 receptor agonist, NNC0090-2746, in patients with Type 2 diabetes. *Cell Metab.* 26, 343–345. doi: 10.1016/j.cmet.2017.07.011

Gajdosechova, L., Krskova, K., Olszanecki, R., and Zorad, S. (2015). Differential regulation of oxytocin receptor in various adipose tissue depots and skeletal muscle types in obese Zucker rats. *Hormone Metab. Res.* 47, 600–604. doi: 10.1055/s-0034-1395677

Gajdosechova, L., Krskova, K., Segarra, A. B., Spolcova, A., Suski, M., Olszanecki, R., et al. (2014). Hypooxytocinaemia in obese Zucker rats relates to oxytocin degradation in liver and adipose tissue. *J. Endocrinol.* 220, 333–343. doi: 10.1530/JOE-13-0417

Gao, F., Zheng, K. I., Wang, X. B., Sun, Q. F., Pan, K. H., Wang, T. Y., et al. (2020). Obesity is a risk factor for greater COVID-19 severity. *Diabetes Care* 43, e72–e74.

George, J. M. (1978). Immunoreactive vasopressin and oxytocin: concentration in individual human hypothalamic nuclei. *Science* 200, 342–343. doi: 10.1126/science.556308

Gimpl, G., and Fahrenholz, F. (2001). The oxytocin receptor system: structure, function, and regulation. *Physiol. Rev.* 81, 629–683.

Ginsberg, S. D., Hof, P. R., Young, W. G., and Morrison, J. H. (1994). Noradrenergic innervation of vasopressin- and oxytocin-containing neurons in the hypothalamic paraventricular nucleus of the macaque monkey: quantitative analysis using double-label immunohistochemistry and confocal laser microscopy. *J. Comp. Neurol.* 341, 476–491. doi: 10.1002/cne.903410405

Gossen, A., Hahn, A., Westphal, L., Prinz, S., Schultz, R. T., Grunder, G., et al. (2012). Oxytocin plasma concentrations after single intranasal oxytocin administration - a study in healthy men. *Neuropeptides* 46, 211–215. doi: 10.1016/j.npep.2012.07.001

Gould, B. R., and Zingg, H. H. (2003). Mapping oxytocin receptor gene expression in the mouse brain and mammary gland using an oxytocin receptor-LacZ reporter mouse. *Neuroscience* 122, 155–167. doi: 10.1016/s0306-4522(03)00283-5

Gouzenes, L., Desarmenien, M. G., Hussy, N., Richard, P., and Moos, F. C. (1998). Vasopressin regularizes the phasic firing pattern of rat hypothalamic magnocellular vasopressin neurons. *J. Neurosci.* 18, 1879–1885. doi: 10.1523/JNEUROSCI.18-05-01879.1998

Greenfield, J. R., Miller, J. W., Keogh, J. M., Henning, E., Satterwhite, J. H., Cameron, G. S., et al. (2009). Modulation of blood pressure by central melanocortinergic pathways. *N. Engl. J. Med.* 360, 44–52.

Grinevich, V., and Neumann, I. D. (2020). Brain oxytocin: how puzzle stones from animal studies translate into psychiatry. *Mol. Psychiatry* 26, 265–279. doi: 10.1038/s41380-020-0802-9

Grundy, S. M. (2008). Metabolic syndrome pandemic. *Arterioscler. Thromb. Vasc. Biol.* 28, 629–636.

Guo, W., Li, M., Dong, Y., Zhou, H., Zhang, Z., Tian, C., et al. (2020). Diabetes is a risk factor for the progression and prognosis of COVID-19. *Diabetes Metab. Res. Rev.* [Epub ahead of print].

Gutkowska, J., and Jankowski, M. (2012). Oxytocin revisited: its role in cardiovascular regulation. *J. Neuroendocrinol.* 24, 599–608.

Hales, C. M., Carroll, M. D., Fryar, C. D., and Ogden, C. L. (2020). Prevalence of obesity and severe obesity among adults: United States, 2017-2018. *NCHS Data Brief* 360, 1–8.

Hallbeck, M., Larhammar, D., and Blomqvist, A. (2001). Neuropeptide expression in rat paraventricular hypothalamic neurons that project to the spinal cord. *J. Comp. Neurol.* 433, 222–238.

Halseth, K. Shan, Gilder, K., Malone, M., Acevedo, L., and Fujioka, K. (2018). Quality of life, binge eating and sexual function in participants treated for obesity with sustained release naltrexone/bupropion. *Obes. Sci. Pract.* 4, 141–152. doi: 10.1002/osp4.156

Hayashi, R., Kasahara, Y., Hidema, S., Fukumitsu, S., Nakagawa, K., and Nishimori, K. (2020). Oxytocin ameliorates impaired behaviors of high fat diet-induced obese mice. *Front. Endocrinol.* 11:379. doi: 10.3389/fendo.2020.00379

Head, M. A., Levine, A. S., Christian, D. G., Klockars, A., and Olszewski, P. K. (2021). Effect of combination of peripheral oxytocin and naltrexone at subthreshold doses on food intake, body weight and feeding-related brain gene expression in male rats. *Physiol. Behav.* 238:113464. doi: 10.1016/j.physbeh.2021.113464

Herisson, F. M., Waas, J. R., Fredriksson, R., Schioth, H. B., Levine, A. S., and Olszewski, P. K. (2016). Oxytocin acting in the nucleus accumbens core decreases food intake. *J. Neuroendocrinol.* 28:12381. doi: 10.1111/jne.12381

Hicks, C., Jorgensen, W., Brown, C., Fardell, J., Koehbach, J., Gruber, C. W., et al. (2012). The nonpeptide oxytocin receptor agonist WAY 267,464: receptor-binding profile, prosocial effects and distribution of c-Fos expression in adolescent rats. *J. Neuroendocrinol.* 24, 1012–1029. doi: 10.1111/j.1365-2826.2012.02311.x

Hicks, C., Ramos, L., Reekie, T., Misagh, G. H., Narlawar, R., Kassiou, M., et al. (2014). Body temperature and cardiac changes induced by peripherally administered oxytocin, vasopressin and the non-peptide oxytocin receptor agonist WAY 267,464: a biotelemetry study in rats. *Br. J. Pharmacol.* 171, 2868–2887. doi: 10.1111/bph.12613

Hidema, S., Fukuda, T., Hiraoka, Y., Mizukami, H., Hayashi, R., Otsuka, A., et al. (2016). Generation of Oxtr cDNA(HA) -Ires-Cre mice for gene expression in an oxytocin receptor specific manner. *J. Cell. Biochem.* 117, 1099–1111. doi: 10.1002/jcb.25393

Ho, J. M., Anekonda, V. T., Thompson, B. W., Zhu, M., Curry, R. W., Hwang, B. H., et al. (2014). Hindbrain oxytocin receptors contribute to the effects of circulating oxytocin on food intake in male rats. *Endocrinology* 155, 2845–2857. doi: 10.1210/en.2014-1148

Hollander, P., Gupta, A. K., Plodkowski, R., Greenway, F., Bays, H., Burns, C., et al. (2013). Effects of naltrexone sustained-release/bupropion sustained-release combination therapy on body weight and glycemic parameters in overweight and obese patients with type 2 diabetes. *Diabetes Care* 36, 4022–4029. doi: 10.2337/dc13-0234

Hsu, E. A., Miller, J. L., Perez, F. A., and Roth, C. L. (2017). Oxytocin and Naltrexone successfully treat hypothalamic obesity in a boy post-craniopharyngioma resection. *J. Clin. Endocrinol. Metab.* 103, 370-375. doi: 10.1210/jc.2017-02080

Insel, T. R., Winslow, J. T., and Witt, D. M. (1992). Homologous regulation of brain oxytocin receptors. *Endocrinology* 130, 2602–2608.

Iwasa, T., Matsuzaki, T., Mayila, Y., Yanagihara, R., Yamamoto, Y., Kawakita, T., et al. (2019b). Oxytocin treatment reduced food intake and body fat and

ameliorated obesity in ovariectomized female rats. *Neuropeptides* 75, 49–57. doi: 10.1016/j.npep.2019.03.002

Iwasa, T., Matsuzaki, T., Mayila, Y., Kawakita, T., Yanagihara, R., and Irahara, M. (2019a). The effects of chronic oxytocin administration on body weight and food intake in DHT-induced PCOS model rats. *Gynecol. Endocrinol.* 36, 55–60.

Iwasa, T., Matsuzaki, T., Mayila, Y., Kawakita, T., Yanagihara, R., and Irahara, M. (2020). The effects of chronic oxytocin administration on body weight and food intake in DHT-induced PCOS model rats. *Gynecol. Endocrinol.* 36, 55–60.

Iwasaki, Y., Kumari, P., Wang, L., Hidema, S., Nishimori, K., and Yada, T. (2019). Relay of peripheral oxytocin to central oxytocin neurons via vagal afferents for regulating feeding. *Biochem. Biophys. Res. Commun.* 519, 553–558. doi: 10.1016/j.bbrc.2019.09.039

Iwasaki, Y., Maejima, Y., Suyama, S., Yoshida, M., Arai, T., Katsurada, K., et al. (2014). Peripheral oxytocin activates vagal afferent neurons to suppress feeding in normal and leptin-resistant mice: a route for ameliorating hyperphagia and obesity. *Am. J. Physiol. Regul. Integr. Comp. Physiol.* 308, R360–R369. doi: 10.1152/ajpregu.00344.2014

Iwasaki, Y., Maejima, Y., Suyama, S., Yoshida, M., Arai, T., Katsurada, K., et al. (2015). Peripheral oxytocin activates vagal afferent neurons to suppress feeding in normal and leptin-resistant mice: a route for ameliorating hyperphagia and obesity. *Am. J. Physiol. Regul. Integr. Comp. Physiol.* 308, R360–R369.

Jankowski, M., Hajjar, F., Kawas, S. A., Mukaddam-Daher, S., Hoffman, G., McCann, S. M., et al. (1998). Rat heart: a site of oxytocin production and action. *Proc. Natl. Acad. Sci. U.S.A.* 95, 14558–14563. doi: 10.1073/pnas.95.24.14558

Jansen, A. S., Wessendorf, M. W., and Loewy, A. D. (1995). Transneuronal labeling of CNS neuropeptide and monoamine neurons after pseudorabies virus injections into the stellate ganglion. *Brain Res.* 683, 1–24. doi: 10.1016/0006-8993(95)00276-v

Jirikowski, G. F., Caldwell, J. D., Pedersen, C. A., and Stumpf, W. E. (1988). Estradiol influences oxytocin-immunoreactive brain systems. *Neuroscience* 25, 237–248. doi: 10.1016/0306-4522(88)90022-x

Johnstone, L. E., Fong, T. M., and Leng, G. (2006). Neuronal activation in the hypothalamus and brainstem during feeding in rats. *Cell Metab.* 4, 313–321.

Jordan, R. E., Adab, P., and Cheng, K. K. (2020). Covid-19: risk factors for severe disease and death. *BMJ* 368:m1198.

Kasahara, Y., Sato, K., Takayanagi, Y., Mizukami, H., Ozawa, K., Hidema, S., et al. (2013). Oxytocin receptor in the hypothalamus is sufficient to rescue normal thermoregulatory function in male oxytocin receptor knockout mice. *Endocrinology* 154, 4305–4315. doi: 10.1210/en.2012-2206

Kasahara, Y., Takayanagi, Y., Kawada, T., Itoi, K., and Nishimori, K. (2007). Impaired thermoregulatory ability of oxytocin-deficient mice during cold-exposure. *Biosci. Biotechnol. Biochem.* 71, 3122–3126. doi: 10.1271/bbb.70498

Kasahara, Y., Tateishi, Y., Hiraoka, Y., Otsuka, A., Mizukami, H., Ozawa, K., et al. (2015). Role of the oxytocin receptor expressed in the rostral medullary raphe in thermoregulation during cold conditions. *Front. Endocrinol.* 6:180. doi: 10.3389/fendo.2015.00180

Kataoka, N., Hioki, H., Kaneko, T., and Nakamura, K. (2014). Psychological stress activates a dorsomedial hypothalamus-medullary raphe circuit driving brown adipose tissue thermogenesis and hyperthermia. *Cell Metab.* 20, 346–358. doi: 10.1016/j.cmet.2014.05.018

Kawata, M., and Sano, Y. (1982). Immunohistochemical identification of the oxytocin and vasopressin neurons in the hypothalamus of the monkey (*Macaca fuscata*). *Anatom. Embryol.* 165, 151–167. doi: 10.1007/BF00305474

Kendrick, K. M. (2000). Oxytocin, motherhood and bonding. *Exp. Physiol.* 85, 111S–124S. doi: 10.1111/j.1469-445x.2000.tb00014.x

Kendrick, K. M., Keverne, E. B., Baldwin, B. A., and Sharman, D. F. (1986). Cerebrospinal fluid levels of acetylcholinesterase, monoamines and oxytocin during labour, parturition, vaginocervical stimulation, lamb separation and suckling in sheep. *Neuroendocrinology* 44, 149–156. doi: 10.1159/000124638

Kievit, P., Halem, H., Marks, D. L., Dong, J. Z., Glavas, M. M., Sinnayah, P., et al. (2013). Chronic treatment with a melanocortin-4 receptor agonist causes weight loss, reduces insulin resistance, and improves cardiovascular function in diet-induced obese rhesus macaques. *Diabetes* 62, 490–497. doi: 10.2337/db12-0598

Kirchgessner, A. L., and Sclafani, A. (1988). PVN-hindbrain pathway involved in the hypothalamic hyperphagia-obesity syndrome. *Physiol. Behav.* 42, 517–528.

Kirchgessner, A. L., Sclafani, A., and Nilaver, G. (1988). Histochemical identification of a PVN-hindbrain feeding pathway. *Physiol. Behav.* 42, 529–543. doi: 10.1016/0031-9384(88)90154-0

Kirkpatrick, M. G., Francis, S. M., Lee, R., de Wit, H., and Jacob, S. (2014). Plasma oxytocin concentrations following MDMA or intranasal oxytocin in humans. *Psychoneuroendocrinology* 46, 23–31.

Klockars, A., Brunton, C., Li, L., Levine, A. S., and Olszewski, P. K. (2017). Intravenous administration of oxytocin in rats acutely decreases deprivation-induced chow intake, but it fails to affect consumption of palatable solutions. *Peptides* 93, 13–19. doi: 10.1016/j.peptides.2017.04.010

Klockars, A., Levine, A. S., and Olszewski, P. K. (2015). Central oxytocin and food intake: focus on macronutrient-driven reward. *Front. Endocrinol.* 6:65. doi: 10.3389/fendo.2015.00065

Klockars, O. A., Klockars, A., Levine, A. S., and Olszewski, P. K. (2018). Oxytocin administration in the basolateral and central nuclei of amygdala moderately suppresses food intake. *Neuroreport* 29, 504–510. doi: 10.1097/WNR.0000000000001005

Klockars, O. A., Waas, J. R., Klockars, A., Levine, A. S., and Olszewski, P. K. (2017). Neural basis of ventromedial hypothalamic oxytocin-driven decrease in appetite. *Neuroscience* 366, 54–61. doi: 10.1016/j.neuroscience.2017.10.008

Knobloch, H. S., Charlet, A., Hoffmann, L. C., Eliava, M., Khrulev, S., Cetin, A. H., et al. (2012). Evoked axonal oxytocin release in the central amygdala attenuates fear response. *Neuron* 73, 553–566. doi: 10.1016/j.neuron.2011.11.030

Koutcherov, Y., Mai, J. K., Ashwell, K. W., and Paxinos, G. (2000). Organization of the human paraventricular hypothalamic nucleus. *J. Comp. Neurol.* 423, 299–318.

Kublaoui, B. M., Gemelli, T., Tolson, K. P., Wang, Y., and Zinn, A. R. (2008). Oxytocin deficiency mediates hyperphagic obesity of Sim1 haploinsufficient mice. *Mol. Endocrinol.* 22, 1723–1734. doi: 10.1210/me.2008-0067

Kusminski, C. M., Bickel, P. E., and Scherer, P. E. (2016). Targeting adipose tissue in the treatment of obesity-associated diabetes. *Nat. Rev. Drug Discov.* 15, 639–660.

Labyb, M., Chretien, C., Caillon, A., Rohner-Jeanrenaud, F., and Altirriba, J. (2018). Oxytocin administration alleviates acute but not chronic leptin resistance of diet-induced obese mice. *Int. J. Mol. Sci.* 20:88.

Lawson, E. A. (2017). The effects of oxytocin on eating behaviour and metabolism in humans. *Nat. Rev. Endocrinol.* 13, 700–709.

Lawson, E. A., Marengi, D. A., DeSanti, R. L., Holmes, T. M., Schoenfeld, D. A., and Tolley, C. J. (2015). Oxytocin reduces caloric intake in men. *Obesity* 23, 950–956.

Lawson, E. A., Olszewski, P. K., Weller, A., and Blevins, J. E. (2020). The role of oxytocin in regulation of appetitive behaviour, body weight and glucose homeostasis. *J. Neuroendocrinol.* 32:e12805. doi: 10.1111/jne.12805

Lee, E. S., Uhm, K. O., Lee, Y. M., Kwon, J., Park, S. H., and Soo, K. H. (2008). Oxytocin stimulates glucose uptake in skeletal muscle cells through the calcium-CaMKK-AMPK pathway. *Regul. Pept.* 151, 71–74. doi: 10.1016/j.regpep.2008.05.001

Lee, M. R., Scheidweiler, K. B., Diao, X. X., Akhlaghi, F., Cummins, A., Huestis, M. A., et al. (2018). Oxytocin by intranasal and intravenous routes reaches the cerebrospinal fluid in rhesus macaques: determination using a novel oxytocin assay. *Mol. Psychiatry* 23, 115–122. doi: 10.1038/mp.2017.27

Lein, E. S., Hawrylycz, M. J., Ao, N., Ayres, M., Bensinger, A., Bernard, A., et al. (2007). Genome-wide atlas of gene expression in the adult mouse brain. *Nature* 445, 168–176.

Leitner, C., and Bartness, T. J. (2009). Acute brown adipose tissue temperature response to cold in monosodium glutamate-treated Siberian hamsters. *Brain Res.* 1292, 38–51. doi: 10.1016/j.brainres.2009.07.062

Leng, G., and Ludwig, M. (2008). Neurotransmitters and peptides: whispered secrets and public announcements. *J. Physiol.* 586, 5625–5632. doi: 10.1113/jphysiol.2008.159103

Leng, G., and Ludwig, M. (2016a). Intranasal oxytocin: myths and delusions. *Biol. Psychiatry* 79, 243–250. doi: 10.1016/j.biopsych.2015.05.003

Leng, G., and Ludwig, M. (2016b). Reply to: improving research standards to restore trust in intranasal oxytocin. *Biol. Psychiatry* 79, e55–e56. doi: 10.1016/j.biopsych.2015.08.030

Leng, G., and Ludwig, M. (2016c). Reply to: intranasal oxytocin mechanisms can be better understood, but its effects on social cognition and behavior are not to be sniffed at. *Biol. Psychiatry* 79, e51–e52. doi: 10.1016/j.biopsych.2015.06.022

Leng, G., Onaka, T., Caquineau, C., Sabatier, N., Tobin, V. A., and Takayanagi, Y. (2008). Oxytocin and appetite. *Prog. Brain Res.* 170, 137–151.

Leng, G., and Sabatier, N. (2017). Oxytocin - the sweet hormone? *Trends Endocrinol. Metab. TEM* 28, 365–376.

Li, L., Kong, X., Liu, H., and Liu, C. (2007). Systemic oxytocin and vasopressin excite gastrointestinal motility through oxytocin receptor in rabbits. *Neurogastroenterol. Motil.* 19, 839–844. doi: 10.1111/j.1365-2982.2007.00953.x

Liao, P. Y., Chiu, Y. M., Yu, J. H., and Chen, S. K. (2020). Mapping central projection of oxytocin neurons in unmated mice using cre and alkaline phosphatase reporter. *Front. Neuroanat.* 14:559402. doi: 10.3389/fnana.2020.559402

Liu, C. M., Hsu, T. M., Suarez, A. N., Subramanian, K. S., Fatemi, R. A., Cortella, A. M., et al. (2020b). Central oxytocin signaling inhibits food reward-motivated behaviors and VTA dopamine responses to food-predictive cues in male rats. *Hormon. Behav.* 126:104855. doi: 10.1016/j.yhbeh.2020.104855

Liu, C. M., Davis, E. A., Suarez, A. N., Wood, R. I., Noble, E. E., and Kanoski, S. E. (2020a). Sex differences and estrous influences on oxytocin control of food intake. *Neuroscience* 447, 63–73.

Lokrantz, C. M., vnas-Moberg, K. U., and Kaplan, J. M. (1997). Effects of central oxytocin administration on intraoral intake of glucose in deprived and nondeprived rats. *Physiol. Behav.* 62, 347–352. doi: 10.1016/s0031-9384(97)00021-8

Loup, F., Tribollet, E., Dubois-Dauphin, M., and Dreifuss, J. J. (1991). Localization of high-affinity binding sites for oxytocin and vasopressin in the human brain. An autoradiographic study. *Brain Res.* 555, 220–232. doi: 10.1016/0006-8993(91)90345-v

Loup, F., Tribollet, E., Dubois-Dauphin, M., Pizzolato, G., and Dreifuss, J. J. (1989). Localization of oxytocin binding sites in the human brainstem and upper spinal cord: an autoradiographic study. *Brain Res.* 500, 223–230.

Ludwig, M., and Leng, G. (2006). Dendritic peptide release and peptide-dependent behaviours. *Nat. Rev. Neurosci.* 7, 126–136. doi: 10.1038/nrn1845

Ludwig, M., Tobin, V. A., Callahan, M. F., Papadaki, E., Becker, A., Engelmann, M., et al. (2013). Intranasal application of vasopressin fails to elicit changes in brain immediate early gene expression, neural activity and behavioural performance of rats. *J. Neuroendocrinol.* 25, 655–667. doi: 10.1111/jne.12046

Luo, F., Mu, Y., Gao, C., Xiao, Y., Zhou, Q., Yang, Y., et al. (2019). Whole-brain patterns of the presynaptic inputs and axonal projections of BDNF neurons in the paraventricular nucleus. *J. Genet. Genom.* 46, 31–40. doi: 10.1016/j.jgg.2018.11.004

MacDonald, E., Dadds, M. R., Brennan, J. L., Williams, K., Levy, F., and Cauchi, A. J. (2011). A review of safety, side-effects and subjective reactions to intranasal oxytocin in human research. *Psychoneuroendocrinology* 36, 1114–1126. doi: 10.1016/j.psyneuen.2011.02.015

Maejima, Y., Aoyama, M., Sakamoto, K., Jojima, T., Aso, Y., Takasu, K., et al. (2017). Impact of sex, fat distribution and initial body weight on oxytocin's body weight regulation. *Sci. Rep.* 7:8599. doi: 10.1038/s41598-017-09318-7

Maejima, Y., Horita, S., Otsuka, A., Hidema, S., Nishimori, K., and Shimomura, K. (2020). Oral oxytocin delivery with proton pump inhibitor pretreatment decreases food intake. *Peptides* 128:170312. doi: 10.1016/j.peptides.2020.170312

Maejima, Y., Iwasaki, Y., Yamahara, Y., Kodaira, M., Sedbazar, U., and Yada, T. (2011). Peripheral oxytocin treatment ameliorates obesity by reducing food intake and visceral fat mass. *Aging* 3, 1169–1177. doi: 10.18632/aging.100408

Maejima, Y., Kato, S., Horita, S., Ueta, Y., Takenoshita, S., Kobayashi, K., et al. (2019). The hypothalamus to brainstem circuit suppresses late-onset body weight gain. *Sci. Rep.* 9:18360. doi: 10.1038/s41598-019-54870-z

Maejima, Y., Rita, R. S., Santoso, P., Aoyama, M., Hiraoka, Y., Nishimori, K., et al. (2015). Nasal oxytocin administration reduces food intake without affecting locomotor activity and glycemia with c-fos induction in limited brain areas. *Neuroendocrinology* 101, 35–44. doi: 10.1159/000371636

Maejima, Y., Sakuma, K., Santoso, P., Gantulga, D., Katsurada, K., Ueta, Y., et al. (2014). Oxytocinergic circuit from paraventricular and supraoptic nuclei to arcuate POMC neurons in hypothalamus. *FEBS Lett.* 588, 4404–4412. doi: 10.1016/j.febslet.2014.10.010

Maejima, Y., Sedbazar, U., Suyama, S., Kohno, D., Onaka, T., Takano, E., et al. (2009). Nesfatin-1-regulated oxytocinergic signaling in the paraventricular nucleus causes anorexia through a leptin-independent melanocortin pathway. *Cell Metab.* 10, 355–365. doi: 10.1016/j.cmet.2009.09.002

Matarazzo, V., Schaller, F., Nedelec, E., Benani, A., Penicaud, L., Muscatelli, F., et al. (2012). Inactivation of Socs3 in the hypothalamus enhances the hindbrain response to endogenous satiety signals via oxytocin signaling. *J. Neurosci.* 32, 17097–17107. doi: 10.1523/JNEUROSCI.1669-12.2012

McCann, M. J., Verbalis, J. G., and Stricker, E. M. (1989). LiCl and CCK inhibit gastric emptying and feeding and stimulate OT secretion in rats. *Am. J. Physiol.* 256, R463–R468. doi: 10.1152/ajpregu.1989.256.2.R463

McCormack, S. E., Blevins, J. E., and Lawson, E. A. (2020). Metabolic effects of oxytocin. *Endocrine Rev.* 41, 121–145.

Mens, W. B., Witter, A., and van Wimersma Greidanus, T. B. (1983). Penetration of neurohypophyseal hormones from plasma into cerebrospinal fluid (CSF): half-times of disappearance of these neuropeptides from CSF. *Brain Res.* 262, 143–149. doi: 10.1016/0006-8993(83)90478-x

Meredith, M. E., Salameh, T. S., and Banks, W. A. (2015). Intranasal delivery of proteins and peptides in the treatment of neurodegenerative diseases. *AAPS J.* 17, 780–787.

Michalakis, K., and Ilias, I. (2020). SARS-CoV-2 infection and obesity: common inflammatory and metabolic aspects. *Diabetes Metab. Syndr.* 14, 469–471.

Miller, G. (2013). The promise and perils of oxytocin. *Science* 339, 267–269. doi: 10.1126/science.339.6117.267

Modi, M. E., Connor-Stroud, F., Landgraf, R., Young, L. J., and Parr, L. A. (2014). Aerosolized oxytocin increases cerebrospinal fluid oxytocin in rhesus macaques. *Psychoneuroendocrinology* 45, 49–57. doi: 10.1016/j.psyneuen.2014.02.011

Monstein, H. J., Grahn, N., Truedsson, M., and Ohlsson, B. (2004). Oxytocin and oxytocin-receptor mRNA expression in the human gastrointestinal tract: a polymerase chain reaction study. *Regul. Pept.* 119, 39–44.

Montag, C., Brockmann, E. M., Bayerl, M., Rujescu, D., Muller, D. J., and Gallinat, J. (2012). Oxytocin and oxytocin receptor gene polymorphisms and risk for schizophrenia: a case-control study. *World J. Biol. Psychiatry* 14, 500–508.

Monte, O. Dal, Noble, P. L., Turchi, J., Cummins, A., and Averbeck, B. B. (2014). CSF and blood oxytocin concentration changes following intranasal delivery in macaque. *PLoS one* 9:e103677. doi: 10.1371/journal.pone.0103677

Moos, F., and Richard, P. (1989). Paraventricular and supraoptic bursting oxytocin cells in rat are locally regulated by oxytocin and functionally related. *J. Physiol.* 408, 1–18. doi: 10.1113/jphysiol.1989.sp017442

Morrison, S. F., Madden, C. J., and Tupone, D. (2014). Central neural regulation of brown adipose tissue thermogenesis and energy expenditure. *Cell Metab.* 19, 741–756.

Morton, G. J., Thatcher, B. S., Reidelberger, R. D., Ogimoto, K., Wolden-Hanson, T., Baskin, D. G., et al. (2012). Peripheral oxytocin suppresses food intake and causes weight loss in diet-induced obese rats. *Am. J. Physiol. Endoc. M.* 302, E134–E144. doi: 10.1152/ajpendo.00296.2011

Muchmore, D. B., Little, S. A., de Haen, C., and dual, A. (1981). mechanism of action of ocytocin in rat epididymal fat cells. *J. Biol. Chem.* 256, 365–372.

Mullis, K., Kay, K., and Williams, D. L. (2013). Oxytocin action in the ventral tegmental area affects sucrose intake. *Brain Res.* 1513, 85–91. doi: 10.1016/j.brainres.2013.03.026

Nasanbuyan, N., Yoshida, M., Takayanagi, Y., Inutsuka, A., Nishimori, K., Yamanaka, A., et al. (2018). Oxytocin-oxytocin receptor systems facilitate social defeat posture in male mice. *Endocrinology* 159, 763–775. doi: 10.1210/en.2017-00606

Nation, D. A., Szeto, A., Mendez, A. J., Brooks, L. G., Zaias, J., Herderick, E. E., et al. (2010). Oxytocin attenuates atherosclerosis and adipose tissue inflammation in socially isolated ApoE-/- mice. *Psychos. Med.* 72, 376–382. doi: 10.1097/PSY.0b013e3181d74c48

Nedergaard, J., and Cannon, B. (2014). The browning of white adipose tissue: some burning issues. *Cell Metab.* 20, 396–407.

Neumann, I. D., Maloumby, R., Beiderbeck, D. I., Lukas, M., and Landgraf, R. (2013). Increased brain and plasma oxytocin after nasal and peripheral administration in rats and mice. *Psychoneuroendocrinology* 38, 1985–1993. doi: 10.1016/j.psyneuen.2013.03.003

Nguyen, N. T., Magno, C. P., Lane, K. T., Hinojosa, M. W., and Lane, J. S. (2008). Association of hypertension, diabetes, dyslipidemia, and metabolic syndrome with obesity: findings from the National Health and Nutrition Examination Survey, 1999 to 2004. *J. Am. College Surg.* 207, 928–934.

Noble, E. E., Billington, C. J., Kotz, C. M., and Wang, C. (2014). Oxytocin in the ventromedial hypothalamic nucleus reduces feeding and acutely increases energy expenditure. *Am. J. Physiol. Regul. Integr. Comp. Physiol.* 307, R737–R745. doi: 10.1152/ajpregu.00118.2014

Nunn, N., Womack, M., Dart, C., and Barrett-Jolley, R. (2011). Function and pharmacology of spinally-projecting sympathetic pre-autonomic neurones in the paraventricular nucleus of the hypothalamus. *Curr. Neuropharmacol.* 9, 262–277. doi: 10.2174/157015911795596531

Ogden, C. L., Carroll, M. D., Kit, B. K., and Flegal, K. M. (2012). Prevalence of obesity in the United States, 2009-2010. *NCHS Data Brief* 82, 1–8.

Ohlsson, B., Truedsson, M., Djerf, P., and Sundler, F. (2006). Oxytocin is expressed throughout the human gastrointestinal tract. *Regul. Pept.* 135, 7–11.

Oldfield, B. J., Giles, M. E., Watson, A., Anderson, C., Colvill, L. M., and McKinley, M. J. (2002). The neurochemical characterisation of hypothalamic pathways projecting polysynaptically to brown adipose tissue in the rat. *Neuroscience* 110, 515–526. doi: 10.1016/s0306-4522(01)00555-3

Olson, B. R., Drutarosky, M. D., Stricker, E. M., and Verbalis, J. G. (1991b). Brain oxytocin receptor antagonism blunts the effects of anorexigenic treatments in rats: evidence for central oxytocin inhibition of food intake. *Endocrinology* 129, 785–791. doi: 10.1210/endo-129-2-785

Olson, B. R., Drutarosky, M. D., Chow, M. S., Hruby, V. J., Stricker, E. M., and Verbalis, J. G. (1991a). Oxytocin and an oxytocin agonist administered centrally decrease food intake in rats. *Peptides* 1991, 113–118. doi: 10.1016/0196-9781(91)90176-p

Olson, B. R., Hoffman, G. E., Sved, A. F., Stricker, E. M., and Verbalis, J. G. (1992). Cholecystokinin induces c-fos expression in hypothalamic oxytocinergic neurons projecting to the dorsal vagal complex. *Brain Res.* 569, 238–248. doi: 10.1016/0006-8993(92)90635-m

Olszewski, P. K., Klockars, A., Olszewska, A. M., Fredriksson, R., Schioth, H. B., and Levine, A. S. (2010). Molecular, immunohistochemical, and pharmacological evidence of oxytocin's role as inhibitor of carbohydrate but not fat intake. *Endocrinology* 151, 4736–4744. doi: 10.1210/en.2010-0151

Olszewski, P. K., Wirth, M. M., Shaw, T. J., Grace, M. K., Billington, C. J., Giraudo, S. Q., et al. (2001). Role of alpha-MSH in the regulation of consummatory behavior: immunohistochemical evidence. *Am. J. Physiol. Regul. Integr. Comp. Physiol.* 281, R673–R680. doi: 10.1152/ajpregu.2001.281.2.R673

Ong, Z. Y., Alhadeff, A. L., and Grill, H. J. (2015). Medial nucleus tractus solitarius oxytocin receptor signaling and food intake control: the role of gastrointestinal satiation signal processing. *Am. J. Physiol. Regul. Integr. Comp. Physiol.* 308, R800–R806. doi: 10.1152/ajpregu.00534.2014

Ong, Z. Y., Bongiorno, D. M., Hernando, M. A., and Grill, H. J. (2017). Effects of endogenous oxytocin receptor signaling in nucleus tractus solitarius on satiation-mediated feeding and thermogenic control in male rats. *Endocrinology* 158, 2826–2836. doi: 10.1210/en.2017-00200

Ott, V., Finlayson, G., Lehnert, H., Heitmann, B., Heinrichs, M., Born, J., et al. (2013). Oxytocin reduces reward-driven food intake in humans. *Diabetes* 62, 3418–3425.

Paiva, L., Lozic, M., Allchorne, A., Grinevich, V., and Ludwig, M. (2021). Identification of peripheral oxytocin-expressing cells using systemically applied cell-type specific adeno-associated viral vector. *J. Neuroendocrinol.* 33:e12970. doi: 10.1111/jne.12970

Paulin, C., Dubois, P. M., Czernichow, P., and Dubois, M. P. (1978). Immunocytological evidence for oxytocin neurons in the human fetal hypothalamus. *Cell Tissue Res.* 188, 259–264. doi: 10.1007/BF00222635

Peris, J., MacFadyen, K., Smith, J. A., de Kloet, A. D., Wang, L., and Krause, E. G. (2016). Oxytocin receptors are expressed on dopamine and glutamate neurons in the mouse ventral tegmental area that project to nucleus accumbens and other mesolimbic targets. *J. Comp. Neurol.* 525, 1094–1108. doi: 10.1002/cne.24116

Peris, J., MacFadyen, K., Smith, J. A., de Kloet, A. D., Wang, L., and Krause, E. G. (2017). Oxytocin receptors are expressed on dopamine and glutamate neurons in the mouse ventral tegmental area that project to nucleus accumbens and other mesolimbic targets. *J. Comp. Neurol.* 525, 1094–1108.

Peters, S., Slattery, D. A., Uschold-Schmidt, N., Reber, S. O., and Neumann, I. D. (2014). Dose-dependent effects of chronic central infusion of oxytocin on anxiety, oxytocin receptor binding and stress-related parameters in mice. *Psychoneuroendocrinology* 42, 225–236. doi: 10.1016/j.psyneuen.2014.01.021

Petersson, M. (2002). Cardiovascular effects of oxytocin. *Prog. Brain Res.* 139, 281–288.

Petersson, M., Alster, P., Lundeberg, T., and vnas-Moberg, K. U. (1996). Oxytocin causes a long-term decrease of blood pressure in female and male rats. *Physiol. Behav.* 60, 1311–1315.

Pinder, A. J., Dresner, M., Calow, C., Shorten, G. D., O'Riordan, J., and Johnson, R. (2002). Haemodynamic changes caused by oxytocin during caesarean section under spinal anaesthesia. *Int. J. Obstet. Anesth.* 11, 156–159.

Plante, E., Menaouar, A., Danalache, B. A., Yip, D., Broderick, T. L., Chiasson, J. L., et al. (2015). Oxytocin treatment prevents the cardiomyopathy observed in obese diabetic male db/db mice. *Endocrinology* 156, 1416–1428. doi: 10.1210/en.2014-1718

Plessow, F., Marengi, D. A., Perry, S. K., Felicione, J. M., Franklin, R., Holmes, T. M., et al. (2018). Effects of intranasal oxytocin on the blood oxygenation level-dependent signal in food motivation and cognitive control pathways in overweight and obese men. *Neuropsychopharmacology* 43, 638–645. doi: 10.1038/npp.2017.226

Pow, D. V., and Morris, J. F. (1989). Dendrites of hypothalamic magnocellular neurons release neurohypophysial peptides by exocytosis. *Neuroscience* 32, 435–439.

Qin, J., Feng, M., Wang, C., Ye, Y., Wang, P. S., and Liu, C. (2009). Oxytocin receptor expressed on the smooth muscle mediates the excitatory effect of oxytocin on gastric motility in rats. *Neurogastroenterol. Motil.* 21, 430–438. doi: 10.1111/j.1365-2982.2009.01282.x

Ragen, B. J., and Bales, K. L. (2013). "Oxytocin and vasopressin in non-human primates," in *Oxytocin, Vasopressin and Related Peptides in the Regulation of Behavior*, eds E. Choleris, D. W. Pfaff, and M. Kavaliers (Cambridge: Cambridge University Press), 288–306.

Rajagopal, S., and Cheskin, L. J. (2021). In overweight or obese adults without diabetes, semaglutide increased weight loss and GI disorders. *Ann. Intern. Med.* 174:JC80.

Rault, J. L., Carter, C. S., Garner, J. P., Marchant-Forde, J. N., Richert, B. T., and Lay, D. C. Jr. (2013). Repeated intranasal oxytocin administration in early life dysregulates the HPA axis and alters social behavior. *Physiol. Behav.* 112-113, 40–48. doi: 10.1016/j.physbeh.2013.02.007

Reiter, M. K., Kremarik, P., Freund-Mercier, M. J., Stoeckel, M. E., Desaulles, E., and Feltz, P. (1994). Localization of oxytocin binding sites in the thoracic and upper lumbar spinal cord of the adult and postnatal rat: a histoautoradiographic study. *Eur. J. Neurosci.* 6, 98–104. doi: 10.1111/j.1460-9568.1994.tb00251.x

Renaud, L. P., and Bourque, C. W. (1991). Neurophysiology and neuropharmacology of hypothalamic magnocellular neurons secreting vasopressin and oxytocin. *Prog. Neurobiol.* 36, 131–169. doi: 10.1016/0301-0082(91)90020-2

Rinaman, L. (1998). Oxytocinergic inputs to the nucleus of the solitary tract and dorsal motor nucleus of the vagus in neonatal rats. *J. Comp. Neurol.* 399, 101–109. doi: 10.1002/(sici)1096-9861(19980914)399:1<101::aid-cne8>3.0.co;2-5

Rinaman, L., and Rothe, E. E. (2002). GLP-1 receptor signaling contributes to anorexigenic effect of centrally administered oxytocin in rats. *Am. J. Physiol. Regul. Integr. Comp. Physiol.* 283, R99–R106. doi: 10.1152/ajpregu.00008.2002

Ring, R. H., Malberg, J. E., Potestio, L., Ping, J., Boikess, S., Luo, B., et al. (2006). Anxiolytic-like activity of oxytocin in male mice: behavioral and autonomic evidence, therapeutic implications. *Psychopharmacology* 185, 218–225. doi: 10.1007/s00213-005-0293-z

Ring, R. H., Schechter, L. E., Leonard, S. K., Dwyer, J. M., Platt, B. J., Graf, R., et al. (2010). Receptor and behavioral pharmacology of WAY-267464, a non-peptide oxytocin receptor agonist. *Neuropharmacology* 58, 69–77.

Roberts, Z. S., Wolden-Hanson, T. H., Matsen, M. E., Ryu, V., Vaughan, C. H., Graham, J. L., et al. (2017). Chronic hindbrain administration of oxytocin is sufficient to elicit weight loss in diet-induced obese rats. *Am. J. Physiol. Regul. Integr. Comp. Physiol.* 313, R357-R371. doi: 10.1152/ajpregu.00169.2017

Rodgers, R. J., Tschop, M. H., and Wilding, J. P. (2012). Anti-obesity drugs: past, present and future. *Dis. Models Mech.* 5, 621–626.

Rogers, R. C., and Hermann, G. E. (1987). Oxytocin, oxytocin antagonist, TRH, and hypothalamic paraventricular nucleus stimulation effects on gastric motility. *Peptides* 8, 505–513. doi: 10.1016/0196-9781(87)90017-9

Romero-Fernandez, W., Borroto-Escuela, D. O., Agnati, L. F., and Fuxe, K. (2013). Evidence for the existence of dopamine D2-oxytocin receptor heteromers in the ventral and dorsal striatum with facilitatory receptor-receptor interactions. *Mol. Psychiatry* 18, 849–850. doi: 10.1038/mp.2012.103

Rosen, G. J., de Vries, G. J., Goldman, S. L., Goldman, B. D., and Forger, N. G. (2008). Distribution of oxytocin in the brain of a eusocial rodent. *Neuroscience* 155, 809–817.

Rosenbaum, M., Goldsmith, R., Bloomfield, D., Magnano, A., Weimer, L., Heymsfield, S., et al. (2005). Low-dose leptin reverses skeletal muscle, autonomic, and neuroendocrine adaptations to maintenance of reduced weight. *J. Clin. Investig.* 115, 3579–3586. doi: 10.1172/JCI25977

Rosenbaum, M., Kissileff, H. R., Mayer, L. E., Hirsch, J., and Leibel, R. L. (2010). Energy intake in weight-reduced humans. *Brain Res.* 1350, 95–102.

Rosenbaum, M., Murphy, E. M., Heymsfield, S. B., Matthews, D. E., and Leibel, R. L. (2002). Low dose leptin administration reverses effects of sustained weight-reduction on energy expenditure and circulating concentrations of thyroid hormones. *J. Clin. Endocrinol. Metab.* 87, 2391–2394. doi: 10.1210/jcem.87.5.8628

Ross, H. E., Cole, C. D., Smith, Y., Neumann, I. D., Landgraf, R., Murphy, A. Z., et al. (2009). Characterization of the oxytocin system regulating affiliative behavior in female prairie voles. *Neuroscience* 162, 892–903.

Ryan, P. J., Ross, S. I., Campos, C. A., Derkach, V. A., and Palmiter, R. D. (2017). Oxytocin-receptor-expressing neurons in the parabrachial nucleus regulate fluid intake. *Nat. Neurosci.* 20, 1722–1733. doi: 10.1038/s41593-017-0014-z

Sabatier, N., Leng, G., and Menzies, J. (2013). Oxytocin, feeding, and satiety. *Front. Endocrinol.* 4:35. doi: 10.3389/fendo.2013.00035

Sabatier, N., Rowe, I., and Leng, G. (2007). Central release of oxytocin and the ventromedial hypothalamus. *Biochem. Soc. Trans.* 35, 1247–1251.

Sawchenko, P. E., and Swanson, L. W. (1982). Immunohistochemical identification of neurons in the paraventricular nucleus of the hypothalamus that project to the medulla or to the spinal cord in the rat. *J. Comp. Neurol.* 205, 260–272.

Sawchenko, P. E., Swanson, L. W., and Vale, W. W. (1984). Corticotropin-releasing factor: co-expression within distinct subsets of oxytocin-, vasopressin-, and neurotensin-immunoreactive neurons in the hypothalamus of the male rat. *J. Neurosci.* 4, 1118–1129. doi: 10.1523/JNEUROSCI.04-04-01118.1984

Schaffler, N. Binart, Scholmerich, J., and Buchler, C. (2005). Hypothesis paper Brain talks with fat–evidence for a hypothalamic-pituitary-adipose axis? *Neuropeptides* 39, 363–367. doi: 10.1016/j.npep.2005.06.003

Schellekens, H., Dinan, T. G., and Cryan, J. F. (2013). Taking two to tango: a role for ghrelin receptor heterodimerization in stress and reward. *Front. Neurosci.* 7:148. doi: 10.3389/fnins.2013.00148

Schorr, M., Marengi, D. A., Pulumo, R. L., Yu, E., Eddy, K. T., Klibanski, A., et al. (2017). Oxytocin and its relationship to body composition, bone mineral density, and hip geometry across the weight spectrum. *J. Clin. Endocrinol. Metab.* 102, 2814–2824. doi: 10.1210/jc.2016-3963

Schorscher-Petcu, A., Dupre, A., and Tribollet, E. (2009). Distribution of vasopressin and oxytocin binding sites in the brain and upper spinal cord of the common marmoset. *Neurosci. Lett.* 461, 217–222. doi: 10.1016/j.neulet.2009.06.016

Schumacher, M., Coirini, H., Frankfurt, M., and McEwen, B. S. (1989). Localized actions of progesterone in hypothalamus involve oxytocin. *Proc. Natl. Acad. Sci. U.S.A.* 86, 6798–6801. doi: 10.1073/pnas.86.17.6798

Schwartz, A., and Doucet, E. (2010). Relative changes in resting energy expenditure during weight loss: a systematic review. *Obes. Rev.* 11, 531–547. doi: 10.1111/j.1467-789X.2009.00654.x

Schwartz, M. W., Woods, S. C., Porte, D. Jr., Seeley, R. J., and Baskin, D. G. (2000). Central nervous system control of food intake. *Nature* 404, 661–671.

Seeley, R. J., Yagaloff, K. A., Fisher, S. L., Burn, P., Thiele, T. E., van Dijk, G., et al. (1997). Melanocortin receptors in leptin effects. *Nature* 390:349.

Seelke, A. M., Rhine, M. A., Khun, K., Shweyk, A. N., Scott, A. M., Bond, J. M., et al. (2018). Intranasal oxytocin reduces weight gain in diet-induced obese prairie voles. *Physiol. Behav.* 196, 67–77. doi: 10.1016/j.physbeh.2018.08.007

Shahrokh, D. K., Zhang, T. Y., Diorio, J., Gratton, A., and Meaney, M. J. (2010). Oxytocin-dopamine interactions mediate variations in maternal behavior in the rat. *Endocrinology* 151, 2276–2286. doi: 10.1210/en.2009-1271

Shi, H., and Bartness, T. J. (2001). Neurochemical phenotype of sympathetic nervous system outflow from brain to white fat. *Brain Res. Bull.* 54, 375–385. doi: 10.1016/s0361-9230(00)00455-x

Smith, A. S., Korgan, A. C., and Young, W. S. (2019). Oxytocin delivered nasally or intraperitoneally reaches the brain and plasma of normal and oxytocin knockout mice. *Pharmacol. Res.* 146:104324.

Smyth, S., and Heron, A. (2006). Diabetes and obesity: the twin epidemics. *Nat. Med.* 12, 75–80.

Snider, B., Geiser, A., Yu, X. P., Beebe, E. C., Willency, J. A., Qing, K., et al. (2019). Long-acting and selective oxytocin peptide analogs show antidiabetic and antiobesity effects in male mice. *J. Endocrine Soc.* 3, 1423–1444. doi: 10.1210/js.2019-00004

Sofroniew, M. V. (1983). Morphology of vasopressin and oxytocin neurones and their central and vascular projections. *Prog. Brain Res.* 60, 101–114.

Sofroniew, M. V., Weindl, A., Schrell, U., and Wetzstein, R. (1981). Immunohistochemistry of vasopressin, oxytocin and neurophysin in the hypothalamus and extrahypothalamic regions of the human and primate brain. *Acta Histochem. Suppl.* 24, 79–95.

Song, C. K., Vaughan, C. H., Keen-Rhinehart, E., Harris, R. B., Richard, D., and Bartness, T. J. (2008). Melanocortin-4 receptor mRNA expressed in sympathetic outflow neurons to brown adipose tissue: neuroanatomical and functional evidence. *Am. J. Physiol. Regul. Integr. Comp. Physiol.* 295, R417–R428. doi: 10.1152/ajpregu.00174.2008

Stanley, S., Pinto, S., Segal, J., Perez, C. A., Viale, A., DeFalco, J., et al. (2010). Identification of neuronal subpopulations that project from hypothalamus to both liver and adipose tissue polysynaptically. *Proc. Natl. Acad. Sci. U.S.A.* 107, 7024–7029. doi: 10.1073/pnas.1002790107

Striepens, N., Kendrick, K. M., Hanking, V., Landgraf, R., Wullner, U., Maier, W., et al. (2013). Elevated cerebrospinal fluid and blood concentrations of oxytocin following its intranasal administration in humans. *Sci. Rep.* 3:3440.

Striepens, N., Kendrick, K. M., Maier, W., and Hurlemann, R. (2011). Prosocial effects of oxytocin and clinical evidence for its therapeutic potential. *Front. Neuroendocrinol.* 32, 426–450. doi: 10.1016/j.yfrne.2011.07.001

Striepens, N., Schroter, F., Stoffel-Wagner, B., Maier, W., Hurlemann, R., and Scheele, D. (2016). Oxytocin enhances cognitive control of food craving in women. *Hum. Brain Mapp.* 37, 4276–4285. doi: 10.1002/hbm.23308

Sukhov, R. R., Walker, L. C., Rance, N. E., Price, D. L., and Young, W. S. III (1993). Vasopressin and oxytocin gene expression in the human hypothalamus. *J. Comp. Neurol.* 337, 295–306.

Sun, L., Lizneva, D., Ji, Y., Colaianni, G., Hadelia, E., Gumerova, A., et al. (2019). Oxytocin regulates body composition. *Proc. Natl. Acad. Sci. U.S.A.* 116, 26808–26815.

Sutton, A. K., Pei, H., Burnett, K. H., Myers, M. G. Jr., Rhodes, C. J., and Olson, D. P. (2014). Control of food intake and energy expenditure by Nos1 neurons of the paraventricular hypothalamus. *J. Neurosci.* 34, 15306–15318.

Swaab, D. F., Nijveldt, F., and Pool, C. W. (1975a). Distribution of oxytocin and vasopressin in the rat supraoptic and paraventricular nucleus. *J. Endocrinol.* 67, 461–462.

Swaab, D. F., Pool, C. W., and Nijveldt, F. (1975b). Immunofluorescence of vasopressin and oxytocin in the rat hypothalamo-neurohypophypopseal system. *J. Neural Transm.* 36, 195–215. doi: 10.1007/BF01253126

Szabo, R., Menesi, R., Szalai, Z., Daruka, L., Toth, G., Gardi, J., et al. (2019). New metabolic influencer on oxytocin release: the ghrelin. *Molecules* 24:735. doi: 10.3390/molecules24040735

Tachibana, M., Kagitani-Shimono, K., Mohri, I., Yamamoto, T., Sanefuji, W., Nakamura, A., et al. (2013). Long-term administration of intranasal oxytocin is a safe and promising therapy for early adolescent boys with autism spectrum disorders. *J. Child Adolesc. Psychopharmacol.* 23, 123–127. doi: 10.1089/cap.2012.0048

Takayanagi, Y., Kasahara, Y., Onaka, T., Takahashi, N., Kawada, T., and Nishimori, K. (2008). Oxytocin receptor-deficient mice developed late-onset obesity. *Neuroreport* 19, 951–955.

Tamma, R., Colaianni, G., Zhu, L. L., DiBenedetto, A., Greco, G., Montemurro, G., et al. (2009). Oxytocin is an anabolic bone hormone. *Proc. Natl. Acad. Sci. U.S.A.* 106, 7149–7154.

Targher, G., Mantovani, A., Wang, X. B., Yan, H. D., Sun, Q. F., Pan, K. H., et al. (2020). Patients with diabetes are at higher risk for severe illness from COVID-19. *Diabetes Metab.* 46, 335–337.

Terrillon, S., Durroux, T., Mouillac, B., Breit, A., Ayoub, M. A., Taulan, M., et al. (2003). Oxytocin and vasopressin V1a and V2 receptors form constitutive homo- and heterodimers during biosynthesis. *Mol. Endocrinol.* 17, 677–691. doi: 10.1210/me.2002-0222

Thienel, M., Fritsche, A., Heinrichs, M., Peter, A., Ewers, M., Lehnert, H., et al. (2016). Oxytocin's inhibitory effect on food intake is stronger in obese than normal-weight men. *Int. J. Obes.* 40, 1707–1714. doi: 10.1038/ijo.2016.149

Tribollet, E., Dubois-Dauphin, M., Dreifuss, J. J., Barberis, C., and Jard, S. (1992). Oxytocin receptors in the central nervous system. Distribution, development, and species differences. *Ann. N.Y. Acad. Sci.* 652, 29–38.

Tsuda, T., Ueno, Y., Yoshikawa, T., Kojo, H., and Osawa, T. (2006). Microarray profiling of gene expression in human adipocytes in response to anthocyanins. *Biochem. Pharmacol.* 71, 1184–1197. doi: 10.1016/j.bcp.2005.12.042

Tung, Y. C., Ma, M., Piper, S., Coll, A., O'Rahilly, S., and Yeo, G. S. (2008). Novel leptin-regulated genes revealed by transcriptional profiling of the hypothalamic paraventricular nucleus. *J. Neurosci.* 28, 12419–12426. doi: 10.1523/JNEUROSCI.3412-08.2008

Vaccari, C., Lolait, S. J., and Ostrowski, N. L. (1998). Comparative distribution of vasopressin V1b and oxytocin receptor messenger ribonucleic acids in brain. *Endocrinology* 139, 5015–5033. doi: 10.1210/endo.139.12.6382

Vallera, C., Choi, L. O., Cha, C. M., and Hong, R. W. (2017). Uterotonic medications: oxytocin, methylergonovine, carboprost, misoprostol. *Anesthesiol. Clin.* 35, 207–219.

van Leeuwen, F. W., van Heerikhuize, J., van der Meulen, G., and Wolters, P. (1985). Light microscopic autoradiographic localization of [3H]oxytocin binding sites in the rat brain, pituitary and mammary gland. *Brain Res.* 359, 320–325. doi: 10.1016/0006-8993(85)91443-x

van Zuiden, M., Frijling, J. L., Nawijn, L., Koch, S. B. J., Goslings, J. C., Luitse, J. S., et al. (2017). Intranasal oxytocin to prevent posttraumatic stress disorder symptoms: a randomized controlled trial in emergency department patients. *Biol. Psychiatry* 81, 1030–1040.

Vaughan, C. H., Shrestha, Y. B., and Bartness, T. J. (2011). Characterization of a novel melanocortin receptor-containing node in the SNS outflow circuitry to brown adipose tissue involved in thermogenesis. *Brain Res.* 1411, 17–27. doi: 10.1016/j.brainres.2011.07.003

Verbalis, J. G. (1999). The brain oxytocin receptor(s)? *Front. Neuroendocrinol.* 20, 146–156.

Verbalis, J. G., Blackburn, R. E., Hoffman, G. E., and Stricker, E. M. (1995b). Establishing behavioral and physiological functions of central oxytocin: insights from studies of oxytocin and ingestive behaviors. *Adv. Exp. Med. Biol.* 395, 209–225.

Verbalis, J. G., Blackburn, A. N., Hoffman, G. E., and Stricker, E. M. (1995a). "Establishing behavioral and physiological functions of central oxytocin: insights from studies of oxytocin and ingestive behvaviors," in *Oxytocin*, eds R. Ivell and J. Russell (New York, NY: Plenum Press), 209–225.

Vila, G., Riedl, M., Resl, M., van der Lely, A. J., Hofland, L. J., Clodi, M., et al. (2009). Systemic administration of oxytocin reduces basal and lipopolysaccharide-induced ghrelin levels in healthy men. *J. Endocrinol.* 203, 175–179. doi: 10.1677/JOE-09-0227

Wald, H. S., Chandra, A., Kalluri, A., Ong, Z. Y., Hayes, M. R., and Grill, H. J. (2020). NTS and VTA oxytocin reduces food motivation and food seeking. *Am. J. Physiol. Regul. Integr. Comp. Physiol.* 319, R673–R683. doi: 10.1152/ajpregu.00201.2020

Wallace Fitzsimons, S. E., Chruscicka, B., Druelle, C., Stamou, P., Nally, K., Dinan, T. G., et al. (2019). A ghrelin receptor and oxytocin receptor heterocomplex impairs oxytocin mediated signalling. *Neuropharmacology* 152, 90–101. doi: 10.1016/j.neuropharm.2018.12.022

Welch, M. G., Margolis, K. G., Li, Z., and Gershon, M. D. (2014). Oxytocin regulates gastrointestinal motility, inflammation, macromolecular permeability, and mucosal maintenance in mice. *Am. J. Physiol. Gastrointest. Liver Physiol.* 307, G848–G862. doi: 10.1152/ajpgi.00176.2014

Welch, M. G., Tamir, H., Gross, K. J., Chen, J., Anwar, M., and Gershon, M. D. (2009). Expression and developmental regulation of oxytocin (OT) and oxytocin receptors (OTR) in the enteric nervous system (ENS) and intestinal epithelium. *J. Comp. Neurol.* 512, 256–270.

Wilding, J. P. H., Batterham, R. L., Calanna, S., Davies, M., Gaal, L.F. Van, Lingvay, I., et al. (2021). Once-weekly semaglutide in adults with overweight or obesity. *N. Engl. J. Med.* 384:989.

Winter, J., Meyer, M., Berger, I., Royer, M., Bianchi, M., Kuffner, K., et al. (2021). Chronic oxytocin-driven alternative splicing of Crfr2alpha induces anxiety. *Mol. Psychiatry* [Epub ahead of print]. doi: 10.1038/s41380-021-01141-x

Woods, S. C., Schwartz, M. W., Baskin, D. G., and Seeley, R. J. (2000). Food intake and the regulation of body weight. *Annu. Rev. Psychol.* 51, 255–277.

Wrobel, L., Schorscher-Petcu, A., Dupre, A., Yoshida, M., Nishimori, K., and Tribollet, E. (2011). Distribution and identity of neurons expressing the oxytocin receptor in the mouse spinal cord. *Neurosci. Lett.* 495, 49–54. doi: 10.1016/j.neulet.2011.03.033

Wu, C. L., Doong, M. L., and Wang, P. S. (2008). Involvement of cholecystokinin receptor in the inhibition of gastrointestinal motility by oxytocin in ovariectomized rats. *Eur. J. Pharmacol.* 580, 407–415. doi: 10.1016/j.ejphar.2007.11.024

Wu, C. L., Hung, C. R., Chang, F. Y., Pau, K. Y., and Wang, P. S. (2003). Pharmacological effects of oxytocin on gastric emptying and intestinal transit of a non-nutritive liquid meal in female rats. *Naunyn Schmiedebergs Arch. Pharmacol.* 367, 406–413. doi: 10.1007/s00210-003-0690-y

Wu, L., Meng, J., Shen, Q., Zhang, Y., Pan, S., Chen, Z., et al. (2017). Caffeine inhibits hypothalamic A1R to excite oxytocin neuron and ameliorate dietary obesity in mice. *Nat. Commun.* 8:15904. doi: 10.1038/ncomms15904

Wu, Z., Xu, Y., Zhu, Y., Sutton, A. K., Zhao, R., Lowell, B. B., et al. (2012). An obligate role of oxytocin neurons in diet induced energy expenditure. *PLoS One* 7:e45167. doi: 10.1371/journal.pone.0045167

Xi, D., Long, C., Lai, M., Casella, A., O'Lear, L., Kublaoui, B., et al. (2017). Ablation of oxytocin neurons causes a deficit in cold stress response. *J. Endocr. Soc.* 1, 1041–1055. doi: 10.1210/js.2017-00136

Xiao, L., Priest, M. F., Nasenbeny, J., Lu, T., and Kozorovitskiy, Y. (2017). Biased oxytocinergic modulation of midbrain dopamine systems. *Neuron* 95, 368.e5–384.e5. doi: 10.1016/j.neuron.2017.06.003

Yamashita, H., Okuya, S., Inenaga, K., Kasai, M., Uesugi, S., Kannan, H., et al. (1987). Oxytocin predominantly excites putative oxytocin neurons in the rat supraoptic nucleus in vitro. *Brain Res.* 416, 364–368. doi: 10.1016/0006-8993(87)90920-6

Yamashita, M., Takayanagi, Y., Yoshida, M., Nishimori, K., Kusama, M., and Onaka, T. (2013). Involvement of prolactin-releasing peptide in the activation of oxytocin neurones in response to food intake. *J. Neuroendocrinol.* 25, 455–465. doi: 10.1111/jne.12019

Yamasue, H., Yee, J. R., Hurlemann, R., Rilling, J. K., Chen, F. S., Meyer-Lindenberg, A., et al. (2012). Integrative approaches utilizing oxytocin to enhance prosocial behavior: from animal and human social behavior to autistic social dysfunction. *J. Neurosci.* 32, 14109–14117. doi: 10.1523/JNEUROSCI.3327-12.2012

Yang, Z., Han, D., and Coote, J. H. (2009). Cardiac sympatho-excitatory action of PVN-spinal oxytocin neurones. *Auton. Neurosci.* 147, 80–85. doi: 10.1016/j.autneu.2009.01.013

Yao, S., Bergan, J., Lanjuin, A., and Dulac, C. (2017). Oxytocin signaling in the medial amygdala is required for sex discrimination of social cues. *eLife* 6:e31373. doi: 10.7554/eLife.31373

Yi, K. J., So, K. H., Hata, Y., Suzuki, Y., Kato, D., Watanabe, K., et al. (2015). The regulation of oxytocin receptor gene expression during adipogenesis. *J. Neuroendocrinol.* 27, 335–342.

Yoshida, M., Takayanagi, Y., Inoue, K., Kimura, T., Young, L. J., Onaka, T., et al. (2009). Evidence that oxytocin exerts anxiolytic effects via oxytocin receptor expressed in serotonergic neurons in mice. *J. Neurosci.* 29, 2259–2271. doi: 10.1523/JNEUROSCI.5593-08.2009

Yoshimura, R., Kiyama, H., Kimura, T., Araki, T., Maeno, H., Tanizawa, O., et al. (1993). Localization of oxytocin receptor messenger ribonucleic acid in the rat brain. *Endocrinology* 133, 1239–1246.

Yosten, G. L., and Samson, W. K. (2014). Neural circuitry underlying the central hypertensive action of nesfatin-1: melanocortins, corticotropin-releasing hormone, and oxytocin. *Am. J. Physiol. Regul. Integr. Comp. Physiol.* 306, R722–R727. doi: 10.1152/ajpregu.00396.2013

Young, L. J., and Barrett, C. E. (2015). Can oxytocin treat autism? *Science* 347, 825–826.

Young, W. S. III, Shepard, E., Amico, J., Hennighausen, L., Wagner, K. U., LaMarca, M. E., et al. (1996). Deficiency in mouse oxytocin prevents milk ejection, but not fertility or parturition. *J. Neuroendocrinol.* 8, 847–853.

Yuan, J., Zhang, R., Wu, R., Gu, Y., and Lu, Y. (2020). The effects of oxytocin to rectify metabolic dysfunction in obese mice are associated with increased thermogenesis. *Mol. Cell Endocrinol.* 514:110903. doi: 10.1016/j.mce.2020.110903

Zhang, B., Qiu, L., Xiao, W., Ni, H., Chen, L., Wang, F., et al. (2021). Reconstruction of the hypothalamo-neurohypophysial system and functional dissection of magnocellular oxytocin neurons in the brain. *Neuron* 109, 331.e7–346.e7. doi: 10.1016/j.neuron.2020.10.032

Zhang, G., Bai, H., Zhang, H., Dean, C., Wu, Q., Li, J., et al. (2011). Neuropeptide exocytosis involving synaptotagmin-4 and oxytocin in hypothalamic programming of body weight and energy balance. *Neuron* 69, 523–535. doi: 10.1016/j.neuron.2010.12.036

Zhang, G., and Cai, D. (2011). Circadian intervention of obesity development via resting-stage feeding manipulation or oxytocin treatment. *Am. J. Physiol. Endocrinol. Metab.* 301, E1004–E1012.

Zhang, H., Wu, C., Chen, Q., Chen, X., Xu, Z., Wu, J., et al. (2013). Treatment of obesity and diabetes using oxytocin or analogs in patients and mouse models. *PLoS One* 8:e61477. doi: 10.1371/journal.pone.0061477

Zhang, Z. H., and Felder, R. B. (2004). Melanocortin receptors mediate the excitatory effects of blood-borne murine leptin on hypothalamic paraventricular neurons in rat. *Am. J. Physiol. Regul. Integr. Comp. Physiol.* 286, R303–R310. doi: 10.1152/ajpregu.00504.2003

Zhou, F., Yu, T., Du, R., Fan, G., Liu, Y., Liu, Z., et al. (2020). Clinical course and risk factors for mortality of adult inpatients with COVID-19 in Wuhan, China: a retrospective cohort study. *Lancet* 395, 1054–1062. doi: 10.1016/S0140-6736(20)30566-3

Zigman, J. M., Jones, J. E., Lee, C. E., Saper, C. B., and Elmquist, J. K. (2006). Expression of ghrelin receptor mRNA in the rat and the mouse brain. *J. Comp. Neurol.* 494, 528–548.

Conflict of Interest: JB has a financial interest in OXT Therapeutics, Inc., a company developing highly specific and stable analogs of oxytocin to treat obesity and metabolic disease. The authors' interests were reviewed and are managed by their local institutions in accordance with their conflict of interest policies.

The remaining authors declare that the research was conducted in the absence of any commercial or financial relationships that could be construed as a potential conflict of interest.

Publisher's Note: All claims expressed in this article are solely those of the authors and do not necessarily represent those of their affiliated organizations, or those of the publisher, the editors and the reviewers. Any product that may be evaluated in this article, or claim that may be made by its manufacturer, is not guaranteed or endorsed by the publisher.

frontiers in Neuroscience

REVIEW
published: 23 November 2021
doi: 10.3389/fnins.2021.770690

Role of the Autonomic Nervous System in Mechanism of Energy and Glucose Regulation Post Bariatric Surgery

Zhibo An[1†], Haiying Wang[2†] and Mohamad Mokadem[1,3,4,5]*

[1] Division of Gastroenterology and Hepatology, Department of Internal Medicine, Carver College of Medicine, The University of Iowa, Iowa City, IA, United States, [2] Department of Physiology, Basic Medical School of Jining Medical University, Jining, China, [3] Fraternal Order of Eagles Diabetes Research Center, The University of Iowa, Iowa City, IA, United States, [4] Obesity Research and Education Initiative, The University of Iowa, Iowa City, IA, United States, [5] Iowa City Veterans Affairs Health Care System, Iowa City, IA, United States

OPEN ACCESS

Edited by:
Lionel Carneiro, The Ohio State University, United States

Reviewed by:
Yves Borbély, Bern University Hospital, Switzerland
Marcellino Monda, Università degli Studi della Campania Luigi Vanvitelli, Italy

***Correspondence:**
Mohamad Mokadem
mohamad-mokadem@uiowa.edu

[†] These authors have contributed equally to this work

Specialty section:
This article was submitted to Neuroenergetics, Nutrition and Brain Health, a section of the journal Frontiers in Neuroscience

Received: *04 September 2021*
Accepted: *15 October 2021*
Published: *23 November 2021*

Citation:
An Z, Wang H and Mokadem M (2021) Role of the Autonomic Nervous System in Mechanism of Energy and Glucose Regulation Post Bariatric Surgery. Front. Neurosci. 15:770690. doi: 10.3389/fnins.2021.770690

Even though lifestyle changes are the mainstay approach to address obesity, Sleeve gastrectomy (SG) and Roux-en-Y gastric bypass (RYGB) are the most effective and durable treatments facing this pandemic and its associated metabolic conditions. The traditional classifications of bariatric surgeries labeled them as "restrictive," "malabsorptive," or "mixed" types of procedures depending on the anatomical rearrangement of each one of them. This conventional categorization of bariatric surgeries assumed that the "restrictive" procedures induce their weight loss and metabolic effects by reducing gastric content and therefore having a smaller reservoir. Similarly, the "malabsorptive" procedures were thought to induce their main energy homeostatic effects from fecal calorie loss due to intestinal malabsorption. Observational data from human subjects and several studies from rodent models of bariatric surgery showed that neither of those concepts is completely true, at least in explaining the multiple metabolic changes and the alteration in energy balance that those two surgeries induce. Rather, neuro-hormonal mechanisms have been postulated to underly the physiologic effects of those two most performed bariatric procedures. In this review, we go over the role the autonomic nervous system plays- through its parasympathetic and sympathetic branches- in regulating weight balance and glucose homeostasis after SG and RYGB.

Keywords: parasympathetic nervous system, sympathetic nervous system, energy balance, metabolic regulation, bariatric/metabolic surgery

INTRODUCTION

Obesity is associated with several co-morbidities that carry a significant burden on the healthcare system and quality of life of all affected subjects around the world. As of 2014, 13% of adults worldwide were obese, with the most affected region being the American continent, for the prevalence of obesity among adults in the United States increased from 33.7%

in 2007–2008 to 42.4% in 2017–2018 (Hales et al., 2020). Prediction models suggest that the prevalence of overweight condition in the United States will surpass 75% and that of obesity will be ∼50% by the year of 2030 (Wang et al., 2011). The initial and conventional approach for managing obesity involves multiple lifestyle modifications that implement changes in diet, activity and behavior. However, these measures rarely result in durable or drastic weight loss (Wadden et al., 2012). In the face of this raging epidemic, bariatric and metabolic surgery remains the most effective intervention to manage excess body weight and adiposity and it significantly improves most obesity-related morbidities with results lasting more than a decade. Needless to say, because of its invasiveness as well as short and long-term complications (though significantly improved) it is currently offered for selected patients who are morbidly obese and who meet certain specific criteria, after failing conventional therapy. Several types of bariatric surgeries including SG, RYGB, and other forms of gastric bypass, laparoscopic adjustable gastric banding, and duodenal switch with biliopancreatic diversion, are nowadays the most common surgical procedures being offered to patients with obesity (English et al., 2020). Though RYGB was traditionally considered by many to be the gold standard weight loss procedure, SG had become the most commonly performed bariatric surgery since 2013 after its reimbursement was approved by Medicare and Medicaid in 2012 (English et al., 2018). It has been demonstrated that sleeve and RYGB have comparable weight loss outcomes, at least in the short-term (Schauer et al., 2012).

The traditional theory which attributes "restriction" of gastric pouch to reduced caloric consumption and small intestinal bypass to decreased caloric absorption has been repetitively evaluated. It was shown that gastric pouch or sleeve size did not affect meal size or food intake reduction post-bariatric surgery (Topart et al., 2011; McCracken et al., 2018). Additionally, the amount or caloric malabsorption induced by gastric bypass was very modest and cannot explain solely or be responsible for the large amount of weight lost induced by this bariatric procedure (Odstrcil et al., 2010). On the other hand, it was previously shown that alteration in feeding behaviors, bile acid signaling and flow, gut microbiota, as well as several neuro-hormonal effects (through GLP-1, P-YY, Ghrelin, and leptin) play an important role in inducing many of the beneficial effects of bariatric surgery (le Roux et al., 2007; Stefater et al., 2012; Liou et al., 2013; Yan et al., 2014). Obesity was previously reported to be associated with an attenuated vagal tone and a selective increase in sympathetic tone activity specifically to musculoskeletal organs and peripheral arterial bed, predisposing to obesity-associated hypertension (Landsberg, 1986, 2001; Guarino et al., 2017). There is suggestive evidence that RYGB transiently activates the systemic sympathetic nervous system, leading to a subsequent relative enhancement in parasympathetic over sympathetic activity, that seemingly lasts longer (Lips et al., 2013). In addition, other studies suggested that the gut-brain communications via parasympathetic or sympathetic neuron fibers (afferent/sensory or efferent/motor) may also play a differential role in regulating metabolic effects of bariatric surgery (Berthoud, 2008; Ballsmider et al., 2015).

Both arms of the autonomic nervous system have been postulated to play a metabolic regulatory role in bariatric surgery. This review will review go over each system (sympathetic and parasympathetic) in regulating variable metabolic effects of RYGB and SG.

INTRODUCTION OF SYMPATHETIC AND PARASYMPATHETIC NERVES AND THEIR IMPLICATIONS IN METABOLISM

The autonomic neurons of the sympathetic and parasympathetic nervous system innervate multiple organs and regulate their many of their homeostatic functions. The autonomic nervous system often works in a closed-loop feedback mechanism where sensing of variable biological factors is transmitted via afferent neurons to the brain or brain stem. Subsequently, homeostatic centers or nuclei within the central nervous system process these signals and transmit response orders via efferent/motor neurons to target body organs. Both sympathetic and parasympathetic nervous systems maintain whole-body homeostasis (e.g., through their actions on circulation, energy metabolism, thermal situation, respiration, and immunity) in the face of both endogenous and exogenous perturbations (Esler et al., 2003).

An earlier hypothesis postulated that weight gain in obesity is partially due to sympathetic nervous underactivity causing reduction in thermogenesis (Tremblay and Chaput, 2009). However, microneurography and regional noradrenaline spillover measurements in obese individuals have disproven this hypothesis, thus weakening the case for therapeutic use of β3-adrenergic agonists to stimulate thermogenesis (Kamiya et al., 2021). Interestingly, weight loss, secondary to lifestyle interventions such as diet and exercise, improves sympathetic and parasympathetic heart rate variability, which is an index of autonomic control of cardiac activity. Bariatric surgery also improves HRV through weight loss which might also prevent cardiac autonomic neuropathy (CAN) in severe obesity (Williams et al., 2019).

The peripheral nervous system is also involved in direct and indirect regulation of food intake. Vagal afferent neurons in the duodenum and stomach are shown to respond to mechanical stretch by luminal nutrients while also integrating other visceral sensory information along with metabolic, signals, through neuronal projection into brain stem centers. After vagotomy, neuroendocrine signaling pathways from gut hormones, such as ghrelin, are disrupted. Although, celiac branch vagotomy performed concomitantly with RYGB in rat model resulted in a slightly lesser degrees of weight reduction compared to RYGB without vagotomy, this effect seemed to be transient (Hao et al., 2014). Weight loss outcome in human subjects who had RYGB did not seem to be affected by having a vagotomy or not (Okafor et al., 2015). This data suggest that vagal contribution to RYGB-induced weight loss- if present- is already induced at time of surgery, supporting in part the Phantom satiation hypothesis by Gautron (2021). Tracer studies showed that RYGB decreases the density of vagal sensory neurons and also activates

microglia in the NTS, altering neuronal communication – and assumingly energy signaling- between the gut and the CNS (Mulla et al., 2018).

LAPAROSCOPIC SLEEVE GASTRECTOMY AND ROUX-EN-Y GASTRIC BYPASS

Weight Loss

Roux-en-Y gastric bypass, traditionally considered as the gold standard weight loss procedure, has become the second most performed bariatric procedure since 2013. Laparoscopic sleeve gastrectomy (LSG) has become the most performed bariatric procedure worldwide, because of its efficacy in achieving weight loss results and improvements in obesity-associated comorbidities that are comparable to those of RYGB with lower operative and post-operative complications (Rosenthal et al., 2012; Parikh et al., 2013). In comparison with other bariatric surgeries, such as the laparoscopic RYGB, LSG is a shorter and less technically challenging procedure that involves fewer changes in gastrointestinal anatomy. Additionally, the stomach is longitudinally dissected during LSG, with lesser disruption of the distal fibers of gastric vagus, whereas the stomach is transversely transected during RYGB and both the dorsal and the ventral branches of the gastric vagus nerve are disrupted, creating damage to preganglionic efferent and afferent fibers (Berthoud et al., 2011; Saeidi et al., 2012; Browning et al., 2013; Hao et al., 2014).

Glucose Control

Bariatric surgery, including RYGB and LSG, markedly ameliorate glycemic control and may reverse or prevent T2DM in individuals with obesity (Mingrone et al., 2015; Schauer et al., 2017; Borgeraas et al., 2020; McTigue et al., 2020). The metabolic benefits appear to be weight independent as they occur prior to the onset of significant weight loss and are not correlated with weight loss magnitude. The exact underlying mechanisms are still unclear (Mingrone and Cummings, 2016). Multiple pathways have been proposed to be involved in the positive metabolic effects of RYGB, such as adipose function and morphology, glucose turnover in the liver, altered route and timing of food delivery to the small bowel, CNS control of metabolism and nutrient intake, as well as altered hormonal signaling (Batterham and Cummings, 2016). Following RYGB, there is a marked and rapid increase in several gut hormones including glucagon-like peptide-1 (GLP-1), and glucose-dependent insulinotropic peptide (GIP), specifically in the postprandial state- and it is thought the incretin effect of these hormones contributes to improved glycemic control (Falken et al., 2011; Jorgensen et al., 2012). There is also data suggesting that the incretin effect of GLP-1 is not regulated through endocrine pathway via beta cells, supporting the hypothesis that GLP-1 promotes insulin secretions via paracrine and/or neurocrine action (Smith et al., 2014). Rapid delivery to the distal small bowel with ingested nutrients is thought to contribute to the increased GLP-1 response (Salehi et al., 2011). The known incretin effect of GLP-1 along with its central glucoregulatory effects (Parlevliet et al., 2010) and its energy regulatory effect on food intake (Ten Kulve et al., 2017), may partially explain improved glucose profile following RYGB.

Comparing the early weight loss-independent and later weight loss-dependent (after 1 year) glycemic controls of these surgeries, LSG and RYGB showed similar changes on glycemic control, despite lower concentrations of GLP-1 and slightly less BMI reduction following LSG (Wallenius et al., 2018). This is in line with the observation in rodents that even complete absence of GLP-1 does not attenuate the LSG-mediated effects on weight reduction and glucose metabolism (Wilson-Perez et al., 2013).

The increased profile of GLP-1 after bariatric surgeries is thought to be explained by the hind-gut theory, in which stimulation of the distal intestine resulted from rapid nutrient entry further down the gastrointestinal tract such as ileum, where most of L-cells are found (Chambers et al., 2014). In addition, it was suggested that intestinal adaptation following chronic exposure to rapid nutrient delivery may lead to expansion in enteroendocrine cell population or nutrient-sensing capability, which contribute to the exaggerated increase in levels of postprandial GLP-1 after LSG or RYGB. It has to be noted that this observation is more consistent with RYGB than with LSG (Hutch and Sandoval, 2017). Interestingly, there were studies showing that LSG may lead to augmented elevation in postprandial GLP-1 (Ramon et al., 2012; Yousseif et al., 2014) comparable to that of RYGB.

Peptide YY (PYY), an anorexigenic peptide secreted by L-cells mostly located in the ileum and colon, reduces appetite, decreases the contraction of gallbladder, slows gastric emptying, suppresses gastric and pancreatic secretion, and increases nutrient absorption in the ileum. It was demonstrated that reduced PYY secretion in obese patients significantly increases after LSG, comparable to those observed after RYGB (Benaiges et al., 2015).

SYMPATHETIC NERVOUS SYSTEM AND ROUX-EN-Y GASTRIC BYPASS

Bariatric surgery improves metabolic abnormalities in morbidly obese individuals. Hyperlipidemia, hypertension, T2DM, and obstructive sleep apnea are improved substantially following the surgery. Although improved blood pressure following RYGB has been attributed to weight-loss, lower blood pressure can occur before the reduction of body weight (Ahmed et al., 2009). Therefore, the blood pressure -lowering effect secondary to surgery may be weight loss independent. The potential underlying mechanisms of the blood pressure -lowering effects following RYGB include enhanced secretion of incretins, such as GLP-1 and PYY (Ochner et al., 2011), reducing leptin levels (Rodriguez et al., 2012), alerting microbiota in the GI tract (Lin et al., 2019), increasing excretion of urinary sodium

(Docherty et al., 2017), and decreasing sympathetic nervous system activity (Zhang et al., 2014).

It is recognized that obesity is characterized by sympathetic nervous activation which contributes to hypertension associated with obesity. The time course of this change as well as the underlying mechanisms are not completely understood (Lohmeier and Iliescu, 2013). In addition, obesity and overweightness are characterized by sympathetic overactivity which mirrors the severity of the clinical condition and reflects metabolic alterations (Grassi et al., 2019). In the context of obesity, it has been hypothesized that increased resting sympathetic neural activity (tone) occurring following weight gain could be an adaptive mechanism to increase resting energy expenditure therefore reset the body weight back to a given set-point (Landsberg, 1986).

Using microneurography to directly measure sympathetic activity, it was demonstrated that human subjects who had undergone RYGB experience a reduced systemic sympathetic tone, specifically a muscular sympathetic nerve activity contributing (MSNA) to total energy expenditure (Curry et al., 2013).

Endocannabinoids, originally believed to be primarily central neuromodulators, can stimulate autonomic sympathetic pathway, regulate fat intake, and enhance energy expenditure (Quarta et al., 2010; DiPatrizio et al., 2011; Cardinal et al., 2014). Our recent *in vivo* studies with mice suggested that RYGB but not LSG increases splanchnic nerve activity, which induces thermogenesis of visceral fat and enhances resting metabolic rate (Ye et al., 2020). Furthermore, use of an endocannabinoid receptor-1 (CB1) inverse agonist, mirrors RYGB-specific effects on energy expenditure and gut's sympathetic nerve activity. Whereas arachidonoylethanolamide, a CB1 agonist, attenuated the weight loss that was induced by RYGB. Therefore, this "browning" of visceral fat post-RYGB – which is mediated by sympathetic nerve activity- appears to be CB1 signaling dependent. Our findings suggested that CB1 plays a pivotal role in energy balance following RYGB via a pathway that the sympathetic nervous system is involved (Ye et al., 2020).

In summary, obesity seems to be associated with a state of increased sympathetic tone activity (in particular MSNA). RYGB has shown to decrease systemic sympathetic nerve activity (SNA) and likely to increase splanchnic sympathetic nerve activity, selectively, to activate thermogenesis and lipolysis of visceral white adipose tissue.

PARASYMPATHETIC NERVOUS SYSTEM AND ROUX-EN-Y GASTRIC BYPASS

The vagus nerve can act on the stomach and affects weight loss. The gastric sensory input is conveyed to the CNS via gastric vagal afferents, the central terminals of which enter the brainstem via the solitary tract and synapses of neurons on the nucleus tractus solitarius (NTS) (Altschuler et al., 1989; Berthoud and Powley, 1992; Fox et al., 2000; Czaja et al., 2006). ∼70% of vagal afferents innervate the abdominal viscera, mostly the intestines and stomach (Prechtl and Powley, 1990; Berthoud and Powley, 1992; Powley and Phillips, 2002). Abdominal vagal afferent signaling is important in the regulation of food intake following gastrointestinal stimuli (Peters et al., 2005; Campos et al., 2012, 2013). Efferent innervation to the stomach originates from the dorsal motor nucleus of the vagus (Kirchgessner and Gershon, 1989; Berthoud et al., 1991; Moran et al., 1997), which then projects to the myenteric plexus, terminating in the stomach with the highest density of efferent nerves (Berthoud et al., 1991). Furthermore, NTS preganglionic neurons can control the cholinergic excitatory and non-adrenergic non-cholinergic (NANC) inhibitory postganglionic neurons (Broussard and Altschuler, 2000). *In vivo* studies showed that RYGB causes a significant reduction in the weight of rats with T2DM, augmented the concentrations of serum insulin and GLP-1. These metabolic effects following RYGB partially depend on hepatic branch of the vagus nerve, as selective vagotomy of this nerve is associated with weight regain and the relative lower levels of serum GLP-1 and insulin (Qiu et al., 2014).

Ballsmider et al. (2015) found that LSG upregulated, whereas RYGB downregulated the density of the vagal afferents on the NTS in rats. In addition, RYGB, but not LSG, significantly activated microglia in the NTS. These findings suggested that RYGB, but not LSG, leads to vagal microglia activation and remodels gut-brain actions (Ballsmider et al., 2015). In line with this, it was recently demonstrated that subdiaphragmatic vagotomy can remodel central vagal afferent terminals in the NTS (Peters et al., 2013), and activate microglia in the DMV, NTS, and nodose ganglia. This microglia remains markedly activated in the DMV and nodose ganglia for 7 weeks after subdiaphragmatic vagotomy (Gallaher et al., 2012). Based on this delineated role of the vagus nerve mediating gut function and relaying sensory input to feeding centers in the hindbrain, it was speculated that these processes are remodeled after bariatric procedure (Berthoud et al., 2011).

Melanocortin-4 receptors (MC4R) are expressed in the hypothalamus and hindbrain as well as in autonomic neurons including parasympathetic vagal sensory neurons and preganglionic cholinergic motor neurons (parasympathetic and sympathetic). They play an important role in regulation food intake and energy expenditure in response to peripheral energy signals such as micro-nutrients or gut hormones. In line with these observations, severe obesity was found in humans with naturally occurring *Mc4r* mutations and mice with *Mc4r*-deficiency (Huszar et al., 1997; Vaisse et al., 1998). Moreover, MC4Rs appear to be a mechanistic connection between the digestive system, CNS, and autonomic signaling to brown adipose tissue and the abdominal viscera (Zechner et al., 2013).

Furthermore, Zechner et al. (2013) found that MC4Rs in cholinergic preganglionic vagal motor neurons mediated glucose and lipid homeostasis improvements following RYGB and this effect was weight independent. While MC4R signaling in preganglionic cholinergic motor neurons (parasympathetic and sympathetic) is crucial for the increased energy expenditure and weight loss induced by RYGB (Zechner et al., 2013). A rare variant of carriers of MC4R named I251L, was shown

to have enhanced weight loss following RYGB and augmented basal activity *in vitro*, as well as improved early diabetes resolution following surgery that is weight-independent than non-carriers. They suggested that MC4Rs mediated autonomic efferent signaling is key to induce metabolic effects following RYGB, including these weight-independent benefits such as improved glucose profile (Zechner et al., 2013).

An endogenous agonist of the peroxisome proliferator-associated receptor-α (PPAR-α), Oleoylethanolamide (OEA), is produced by enterocytes of the upper small intestine. It was shown that OEA can activate PPAR-α receptors via vagal sensory output to suppress fat intake through striatal (Tellez et al., 2013) and hypothalamic (Gaetani et al., 2010) feeding circuits. Hankir et al. (2017) demonstrated that RYGB stimulated lower small intestine production of OEA, and augmented lipid sensing in the gut through PPAR-α, which subsequently relayed this signal to the CNS via vagal afferents neurons. This vagal signal led to increased dorsal striatal dopamine 1 receptor (D1R) expression/and signaling (Hankir et al., 2017). It was suggested that fat consumption post-RYGB is dependent on local OEA, vagus nerve and dorsal striatal D1R signaling, as interfering with them reversed the metabolic benefits of RYGB on fat preferences and intake (Hankir et al., 2017).

Previous studies have shown a beneficial effect of weight loss primarily on measures of parasympathetic activity after RYGB (Maser et al., 2007; Perugini et al., 2010). Other studies suggested that changes in autonomic tone after RYGB could be secondary to a direct effect of weight loss (Wasmund et al., 2011). It has been previously shown that glucose homeostasis and insulin secretions could be mediated by autonomic nerve system via neurotransmitters and GI peptides, which is thought to be part of the brain-gut signaling pathway that regulate metabolic effects following RYGB. For example, insulin and glucagon release can be regulated by peptides and neurotransmitters released from neurons innervating the islets (Ahren et al., 2006; Sterl et al., 2016). Acetylcholine, pituitary adenylate cyclase activating polypeptide, vasoactive intestinal polypeptide, and gastrin releasing peptide released from parasympathetic neurons all enhance insulin secretion (Bradley et al., 2012). It was shown that patients with T2DM who underwent RYGB, and experienced rapid remission of their diabetes not only had increased actions of GI peptides, but also had increased heart rate variability, particularly the high-frequency component, suggesting an enhanced parasympathetic outflow after RYGB as it has been demonstrated previously (Boido et al., 2015; Katsogiannos et al., 2020). The results support involvement of neuro-hormonal mechanisms in the rapid improvement of glucose metabolism following RYGB in T2DM. This again supports the theory of changes in autonomic nervous system activity following RYGB in modulating the metabolic effects of this surgery.

In summary, there is convincing evidence that the parasympathetic nervous system activity – represented mainly by the vagus nerve- is modulated after RYGB. This alteration in vagal tone has been tightly connected to changes in several gut hormones and early improvement in glucose metabolism post-RYGB.

SYMPATHETIC NERVOUS SYSTEM AND LAPAROSCOPIC SLEEVE GASTRECTOMY

Reduced vagal function and increased sympathetic activity were observed in obese subjects. The improvement in parasympathetic tone following LSG was evidenced by enhanced heart rate variability in women with obesity, as early as the first month after surgery (Ibacache et al., 2020). LSG has shown a greater effect on the parasympathetic tone than RYGB, probably because LSG preserves the vagal trunk at the lesser curvature of stomach (Geronikolou et al., 2017).

Using high-fat diet induced obese mice underwent sham or LSG surgery and implantation of radio telemeters, McGavigan et al. (2017) found LSG decreased blood pressure in LSG-operated mice compared with both sham-operated groups (*ad libitum* and pair feeding), which were associated with a body weight-independent reduction in hypothalamic PERK-mediated ER stress, inflammation of hypothalamus and sympathetic nervous system tone.

The sympathetic nerve system is a key regulator in the production of leptin by white fat. Leptin production is extremely reduced in mice exposed to a cold environment, when sympathetic stimulation of white fat was enhanced. This can also occur after administration of norepinephrine and isoproterenol. Thus sympathetic nerve excitement inhibits the synthesis of leptin (Rayner and Trayhurn, 2001). In contrast, use of methyltyrosine to interfere with catecholamine synthesis can increase leptin levels in experimental animals. The sympathetic nerve system not only regulates leptin production, but also modulates its effects. In a mouse model where, sympathetic nerves are chemically removed, the original leptin effects of increased blood sugar, insulin, and glucagon were altered when exogenous leptin was given to mice (Holzman et al., 1999; Palmen et al., 2001). It was suggested that LSG-induced weight loss results in profound sympathoinhibitor effects, accompanied by a significant and stable attenuation in leptin levels of plasma, while the improved insulin sensitivity was decayed with time regardless (Seravalle et al., 2014).

Laparoscopic sleeve gastrectomy surgery reduces stomach capacity and removes the fundus by excising the larger curvature of the stomach, thereby reducing the level of circulating ghrelin, which is predominantly secreted from the fundus and upper gastric body. As the level of ghrelin is reduced, people are prone to feeling full and reducing food intake, thereby reducing caloric intake (Benaiges et al., 2015). It can also increase insulin secretion to have anti-diabetogenic effects. In addition, the levels of the insulin-promoting hormone GLP-1 and the appetite-suppressing polypeptide PYY3-36 secreted by the gastrointestinal tract are increased after the operation, which promotes the secretion of insulin and increases cellular insulin sensitivity. In addition, LSG surgery regulates blood sugar and triglyceride levels, reduces the secretion of antibiotic peptides such as leptin or monocyte chemoattractant protein 1, and increases anti-inflammatory mediators such as adiponectin.

Sympathetic neuron-associated macrophages (SAMs) are subset of macrophages recently characterized and identified within the white adipose tissue and long the sympathetic fibers innervating fat cells. They express SLC6A2 transporter which is responsible for noradrenaline degradation and consequently decreasing SNS- mediated thermogenesis. SAMs have been observed to be elevated in state of obesity and eliminating them or their degradation enzyme (SCLC6A2) results in activated thermogenesis. We do not know yet, the effect of either RYGB or SG on SAMs level or activity within WAT (Larabee et al., 2020).

In summary, LSG seems to have an early systemic neuro-inhibitory sympathetic effect that might be responsible for the blood pressure, and leptin reduction effects. There is limited proof that LSG (like RYGB) can induce activation of selective autonomic sympathetic nerves or tracts (such as the splanchnic) or augment sympathetic-mediated thermogenesis.

Bariatric surgery might also change taste acuity an/or olfaction, and potentially influence food preference and caloric consumption, which in turn leads to weight loss. Heightened sensitivity to sweetness could also be altered by the increase in GLP-1, P-YY and changes in other regulators hormones (such as insulin, ghrelin and leptin) that occur post RYGB and LSG. Several gut hormones and their receptors are expressed within the taste buds themselves, suggesting a possible role in palatability in addition to their known metabolic functions (Mulla et al., 2018).

PARASYMPATHETIC NERVOUS SYSTEM AND LAPAROSCOPIC SLEEVE GASTRECTOMY

Variable gastrointestinal signaling inputs are thought to be involved in ingestion of food, which can directly- or indirectly-activate vagal afferent nerve endings in a predominantly paracrine fashion to induce gastric relaxation, and pancreatic exocrine secretion. Circulating neurohormones such as CCK and GLP-1 act directly at the brainstem to modulate vagal afferent and efferent activity in addition to their potential actions as neurotransmitters within these neurocircuits (Grayson et al., 2014). One of the hypotheses regarding resolution of T2DM following bariatric procedures (specifically LSG) has been attributed to changes in gut hormone and alteration in anatomy. The rearrangement of gastrointestinal anatomy enhances simultaneous increase of GLP-1, P-YY, adiponectin and post-prandial insulin, and reduction in leptin as a result of fat mass reduction (Borges Mde et al., 2015). Other hypotheses suggest that elevated levels of bile acid, diet-induced thermogenesis, altered gut microbiome, or even changes in energy balance (due to reduction in food intake) per say leads to weight loss and consequently improvement in glucose homeostasis (Pournaras and le Roux, 2013; Hao et al., 2014). Short-term weight loss seems to be comparable between LSG and RYGB (Sjostrom et al., 2012; Boido et al., 2015; Cho et al., 2015), but long term data seems to be in favor of RYGB from the weight loss as well as from the T2DM resolution stand point (O'Brien, 2015). Medications for T2DM and hypertension were decrease or withdrawn for those undergoing bariatric surgery, as early as prior to hospital discharge (Tritsch et al., 2015). In line with this, Ching et al. (2016) found a 60% remission rate of T2DM after LSG that did not correlate with weight loss.

Weight loss and improved glycemic profile following LSG have been attributed to a theory denominating the "gastric hypothesis," which asserts that alterations in the secretion/action of gut hormones such as GLP-1, GIP, leptin, and PYY triggered by direct stomach manipulation are responsible for the rapid restoration of insulin secretion and sensitivity (Yousseif et al., 2014). Ghrelin, released by the gastric fundus, which is normally excised during LSG (de Oliveira et al., 2015; Yang et al., 2015). Thus, decreased levels of ghrelin were also proposed to be one of the mechanisms that result in metabolic benefits following LSG. However, similar weight loss and improved glucose profile following LSG were found in ghrelin-deficient mice that was genetically modified compared to that in wild type mice (Chambers et al., 2013), suggesting that decreased ghrelin is not a critical factor in T2DM remission (Ching et al., 2016).

In summary, glucose regulation after LSG seems to be partially medicated by the changes in gut hormones post-surgery and partially by the weight loss itself. The role of parasympathetic nervous system in regulating glucose homeostasis post-sleeve gastrectomy is less defined or data is lacking at least. It is more likely; however, that the parasympathetic nervous system is more involved (directly or indirectly) in changes in food intake behavior after LSG.

CONCLUSION

Bariatric surgery achieves sustainable improvements in treating metabolic dysfunction related to obesity and improves overall health. The underlying mechanisms by which these procedures cause weight loss and metabolic improvement appear to be diverse and are not yet fully identified. Current evidence suggests that the autonomic parasympathetic nervous system (mainly through its vagus arm) contributes to food intake reduction and improvements in glucose homeostasis following bariatric surgeries. The sympathetic nervous system is also altered after bariatric surgery, with human models showing decrease in systemic tone to the that might correlates with improvement in blood pressure and other homeostatic patterns. Rodent models of RYGB suggest a selective increase in the splanchnic sympathetic nerve activity of the gut, innervating the visceral fat and leading to augmented sympathetic-mediated thermogenesis. Future studies that further unfold details about the underlying molecular mechanisms communicating new energy signals from the gut to the brain along a neuro-hormonal pathway is essential to help us understand how this procedure induces its powerful metabolic effects. Development of effective and less-invasive therapies for weight-management (being surgical or pharmacological) would highly benefit from this information.

AUTHOR CONTRIBUTIONS

MM conceptualized the idea and design of the review and critically revised the manuscript. ZA and HW wrote the first

draft of the manuscript. All authors contributed to the article and approved the submitted version.

FUNDING

This work was supported by the VA Merit Review Program (I01 BX004774), The University of Iowa Department of Internal Medicine, and Fraternal Order of Eagles Diabetes Research Center.

ACKNOWLEDGMENTS

We would like to thank Dr. Karim Noureddine for his critical revision of the manuscript's language and grammatical context.

REFERENCES

Ahmed, A. R., Rickards, G., Coniglio, D., Xia, Y., Johnson, J., Boss, T., et al. (2009). Laparoscopic Roux-en-Y gastric bypass and its early effect on blood pressure. *Obes. Surg.* 19, 845–849. doi: 10.1007/s11695-008-9671-z

Ahren, B., Wierup, N., and Sundler, F. (2006). Neuropeptides and the regulation of islet function. *Diabetes* 55, S98–S107. doi: 10.2337/db06-S013

Altschuler, S. M., Bao, X. M., Bieger, D., Hopkins, D. A., and Miselis, R. R. (1989). Viscerotopic representation of the upper alimentary tract in the rat: sensory ganglia and nuclei of the solitary and spinal trigeminal tracts. *J. Comp. Neurol.* 283, 248–268. doi: 10.1002/cne.902830207

Ballsmider, L. A., Vaughn, A. C., David, M., Hajnal, A., Di Lorenzo, P. M., and Czaja, K. (2015). Sleeve gastrectomy and Roux-en-Y gastric bypass alter the gut-brain communication. *Neural Plast.* 2015:601985. doi: 10.1155/2015/601985

Batterham, R. L., and Cummings, D. E. (2016). Mechanisms of Diabetes Improvement Following Bariatric/Metabolic Surgery. *Diabetes Care* 39, 893–901. doi: 10.2337/dc16-0145

Benaiges, D., Mas-Lorenzo, A., Goday, A., Ramon, J. M., Chillaron, J. J., Pedro-Botet, J., et al. (2015). Laparoscopic sleeve gastrectomy: more than a restrictive bariatric surgery procedure? *World J. Gastroenterol.* 21, 11804–11814. doi: 10.3748/wjg.v21.i41.11804

Berthoud, H. R. (2008). Vagal and hormonal gut-brain communication: from satiation to satisfaction. *Neurogastroenterol. Motil.* 20, 64–72. doi: 10.1111/j.1365-2982.2008.01104.x

Berthoud, H. R., Carlson, N. R., and Powley, T. L. (1991). Topography of efferent vagal innervation of the rat gastrointestinal tract. *Am. J. Physiol.* 260, R200–R207. doi: 10.1152/ajpregu.1991.260.1.R200

Berthoud, H. R., and Powley, T. L. (1992). Vagal afferent innervation of the rat fundic stomach: morphological characterization of the gastric tension receptor. *J. Comp. Neurol.* 319, 261–276. doi: 10.1002/cne.903190206

Berthoud, H. R., Shin, A. C., and Zheng, H. (2011). Obesity surgery and gut-brain communication. *Physiol. Behav.* 105, 106–119. doi: 10.1016/j.physbeh.2011.01.023

Boido, A., Ceriani, V., Cetta, F., Lombardi, F., and Pontiroli, A. E. (2015). Bariatric surgery and prevention of cardiovascular events and mortality in morbid obesity: mechanisms of action and choice of surgery. *Nutr. Metab. Cardiovasc. Dis.* 25, 437–443. doi: 10.1016/j.numecd.2015.01.011

Borgeraas, H., Hofso, D., Hertel, J. K., and Hjelmesaeth, J. (2020). Comparison of the effect of Roux-en-Y gastric bypass and sleeve gastrectomy on remission of type 2 diabetes: a systematic review and meta-analysis of randomized controlled trials. *Obes. Rev.* 21:e13011. doi: 10.1111/obr.13011

Borges Mde, C., Terra, G. A., Takeuti, T. D., Ribeiro, B. M., Silva, A. A., Terra-Junior, J. A., et al. (2015). Immunological evaluation of patients with type 2 diabetes mellitus submitted to metabolic surgery. *Arq. Bras. Cir. Dig.* 28, 266–269. doi: 10.1590/s0102-6720201500040012

Bradley, D., Magkos, F., and Klein, S. (2012). Effects of bariatric surgery on glucose homeostasis and type 2 diabetes. *Gastroenterology* 143, 897–912. doi: 10.1053/j.gastro.2012.07.114

Broussard, D. L., and Altschuler, S. M. (2000). Brainstem viscerotopic organization of afferents and efferents involved in the control of swallowing. *Am. J. Med.* 108, 79S–86S. doi: 10.1016/S0002-9343(99)00343-5

Browning, K. N., Fortna, S. R., and Hajnal, A. (2013). Roux-en-Y gastric bypass reverses the effects of diet-induced obesity to inhibit the responsiveness of central vagal motoneurones. *J. Physiol.* 591, 2357–2372. doi: 10.1113/jphysiol.2012.249268

Campos, C. A., Shiina, H., Silvas, M., Page, S., and Ritter, R. C. (2013). Vagal afferent NMDA receptors modulate CCK-induced reduction of food intake through synapsin I phosphorylation in adult male rats. *Endocrinology* 154, 2613–2625. doi: 10.1210/en.2013-1062

Campos, C. A., Wright, J. S., Czaja, K., and Ritter, R. C. (2012). CCK-induced reduction of food intake and hindbrain MAPK signaling are mediated by NMDA receptor activation. *Endocrinology* 153, 2633–2646. doi: 10.1210/en.2012-1025

Cardinal, P., Andre, C., Quarta, C., Bellocchio, L., Clark, S., Elie, M., et al. (2014). CB1 cannabinoid receptor in SF1-expressing neurons of the ventromedial hypothalamus determines metabolic responses to diet and leptin. *Mol. Metab.* 3, 705–716. doi: 10.1016/j.molmet.2014.07.004

Chambers, A. P., Kirchner, H., Wilson-Perez, H. E., Willency, J. A., Hale, J. E., Gaylinn, B. D., et al. (2013). The effects of vertical sleeve gastrectomy in rodents are ghrelin independent. *Gastroenterology* 144, 50–52.e5. doi: 10.1053/j.gastro.2012.09.009

Chambers, A. P., Smith, E. P., Begg, D. P., Grayson, B. E., Sisley, S., Greer, T., et al. (2014). Regulation of gastric emptying rate and its role in nutrient-induced GLP-1 secretion in rats after vertical sleeve gastrectomy. *Am. J. Physiol. Endocrinol. Metab.* 306, E424–E432. doi: 10.1152/ajpendo.00469.2013

Ching, S. S., Cheng, A. K., Kong, L. W., Lomanto, D., So, J. B., and Shabbir, A. (2016). Early outcomes of laparoscopic sleeve gastrectomy in a multiethnic Asian cohort. *Surg. Obes. Relat. Dis.* 12, 330–337. doi: 10.1016/j.soard.2015.05.009

Cho, J. M., Kim, H. J., Lo Menzo, E., Park, S., Szomstein, S., and Rosenthal, R. J. (2015). Effect of sleeve gastrectomy on type 2 diabetes as an alternative treatment modality to Roux-en-Y gastric bypass: systemic review and meta-analysis. *Surg. Obes. Relat. Dis.* 11, 1273–1280. doi: 10.1016/j.soard.2015.03.001

Curry, T. B., Somaraju, M., Hines, C. N., Groenewald, C. B., Miles, J. M., Joyner, M. J., et al. (2013). Sympathetic support of energy expenditure and sympathetic nervous system activity after gastric bypass surgery. *Obesity* 21, 480–485. doi: 10.1002/oby.20106

Czaja, K., Ritter, R. C., and Burns, G. A. (2006). Vagal afferent neurons projecting to the stomach and small intestine exhibit multiple N-methyl-D-aspartate receptor subunit phenotypes. *Brain Res.* 1119, 86–93. doi: 10.1016/j.brainres.2006.08.042

de Oliveira, L. F., Tisott, C. G., Silvano, D. M., Campos, C. M., and do Nascimento, R. R. (2015). Glycemic behavior in 48 hours postoperative period of patients with type 2 diabetes mellitus and non diabetic submitted to bariatric surgery. *Arq. Bras. Cir. Dig.* 28, 26–30. doi: 10.1590/S0102-67202015005100009

DiPatrizio, N. V., Astarita, G., Schwartz, G., Li, X., and Piomelli, D. (2011). Endocannabinoid signal in the gut controls dietary fat intake. *Proc. Natl. Acad. Sci. U. S. A.* 108, 12904–12908. doi: 10.1073/pnas.1104675108

Docherty, N. G., Fandriks, L., le Roux, C. W., Hallersund, P., and Werling, M. (2017). Urinary sodium excretion after gastric bypass surgery. *Surg. Obes. Relat. Dis.* 13, 1506–1514. doi: 10.1016/j.soard.2017.04.002

English, W. J., DeMaria, E. J., Brethauer, S. A., Mattar, S. G., Rosenthal, R. J., and Morton, J. M. (2018). American Society for Metabolic and Bariatric Surgery estimation of metabolic and bariatric procedures performed in the United States in 2016. *Surg. Obes. Relat. Dis.* 14, 259–263. doi: 10.1016/j.soard.2017.12.013

English, W. J., DeMaria, E. J., Hutter, M. M., Kothari, S. N., Mattar, S. G., Brethauer, S. A., et al. (2020). American Society for Metabolic and Bariatric Surgery 2018 estimate of metabolic and bariatric procedures performed in the United States. *Surg. Obes. Relat. Dis.* 16, 457–463. doi: 10.1016/j.soard.2019.12.022

Esler, M., Lambert, G., Brunner-La Rocca, H. P., Vaddadi, G., and Kaye, D. (2003). Sympathetic nerve activity and neurotransmitter release in humans: translation from pathophysiology into clinical practice. *Acta Physiol. Scand.* 177, 275–284. doi: 10.1046/j.1365-201X.2003.01089.x

Falken, Y., Hellstrom, P. M., Holst, J. J., and Naslund, E. (2011). Changes in glucose homeostasis after Roux-en-Y gastric bypass surgery for obesity at day three, two months, and one year after surgery: role of gut peptides. *J. Clin. Endocrinol. Metab.* 96, 2227–2235. doi: 10.1210/jc.2010-2876

Fox, E. A., Phillips, R. J., Martinson, F. A., Baronowsky, E. A., and Powley, T. L. (2000). Vagal afferent innervation of smooth muscle in the stomach and duodenum of the mouse: morphology and topography. *J. Comp. Neurol.* 428, 558–576. doi: 10.1002/1096-9861(20001218)428:3<558::AID-CNE11>3.0.CO;2-M

Gaetani, S., Fu, J., Cassano, T., Dipasquale, P., Romano, A., Righetti, L., et al. (2010). The fat-induced satiety factor oleoylethanolamide suppresses feeding through central release of oxytocin. *J. Neurosci.* 30, 8096–8101. doi: 10.1523/JNEUROSCI.0036-10.2010

Gallaher, Z. R., Ryu, V., Herzog, T., Ritter, R. C., and Czaja, K. (2012). Changes in microglial activation within the hindbrain, nodose ganglia, and the spinal cord following subdiaphragmatic vagotomy. *Neurosci. Lett.* 513, 31–36. doi: 10.1016/j.neulet.2012.01.079

Gautron, L. (2021). The Phantom satiation hypothesis of bariatric surgery. *Front. Neurosci.* 15:626085. doi: 10.3389/fnins.2021.626085

Geronikolou, S. A., Albanopoulos, K., Chrousos, G., and Cokkinos, D. (2017). Evaluating the homeostasis assessment model insulin resistance and the cardiac autonomic system in bariatric surgery patients: a meta-analysis. *Adv. Exp. Med. Biol.* 988, 249–259. doi: 10.1007/978-3-319-56246-9_20

Grassi, G., Biffi, A., Seravalle, G., Trevano, F. Q., Dell'Oro, R., Corrao, G., et al. (2019). Sympathetic neural overdrive in the obese and overweight state. *Hypertension* 74, 349–358. doi: 10.1161/HYPERTENSIONAHA.119.12885

Grayson, B. E., Fitzgerald, M. F., Hakala-Finch, A. P., Ferris, V. M., Begg, D. P., Tong, J., et al. (2014). Improvements in hippocampal-dependent memory and microglial infiltration with calorie restriction and gastric bypass surgery, but not with vertical sleeve gastrectomy. *Int. J. Obes.* 38, 349–356. doi: 10.1038/ijo.2013.100

Guarino, D., Nannipieri, M., Iervasi, G., Taddei, S., and Bruno, R. M. (2017). The Role of the autonomic nervous system in the pathophysiology of obesity. *Front. Physiol.* 8:665. doi: 10.3389/fphys.2017.00665

Hales, C. M., Carroll, M. D., Fryar, C. D., and Ogden, C. L. (2020). Prevalence of obesity and severe obesity among adults: United States, 2017-2018. *NCHS Data Brief* 360, 1–8.

Hankir, M. K., Seyfried, F., Hintschich, C. A., Diep, T. A., Kleberg, K., Kranz, M., et al. (2017). Gastric bypass surgery recruits a gut PPAR-alpha-striatal D1R pathway to reduce fat appetite in obese rats. *Cell Metab.* 25, 335–344. doi: 10.1016/j.cmet.2016.12.006

Hao, Z., Townsend, R. L., Mumphrey, M. B., Patterson, L. M., Ye, J., and Berthoud, H. R. (2014). Vagal innervation of intestine contributes to weight loss After Roux-en-Y gastric bypass surgery in rats. *Obes. Surg.* 24, 2145–2151. doi: 10.1007/s11695-014-1338-3

Holzman, L. B., St John, P. L., Kovari, I. A., Verma, R., Holthofer, H., and Abrahamson, D. R. (1999). Nephrin localizes to the slit pore of the glomerular epithelial cell. *Kidney Int.* 56, 1481–1491. doi: 10.1046/j.1523-1755.1999.00719.x

Huszar, D., Lynch, C. A., Fairchild-Huntress, V., Dunmore, J. H., Fang, Q., Berkemeier, L. R., et al. (1997). Targeted disruption of the melanocortin-4 receptor results in obesity in mice. *Cell* 88, 131–141. doi: 10.1016/S0092-8674(00)81865-6

Hutch, C. R., and Sandoval, D. (2017). The Role of GLP-1 in the Metabolic Success of Bariatric Surgery. *Endocrinology* 158, 4139–4151. doi: 10.1210/en.2017-00564

Ibacache, P., Carcamo, P., Miranda, C., Bottinelli, A., Guzman, J., Martinez-Rosales, E., et al. (2020). Improvements in heart rate variability in women with obesity: short-term effects of sleeve gastrectomy. *Obes. Surg.* 30, 4038–4045. doi: 10.1007/s11695-020-04721-y

Jorgensen, N. B., Jacobsen, S. H., Dirksen, C., Bojsen-Moller, K. N., Naver, L., Hvolris, L., et al. (2012). Acute and long-term effects of Roux-en-Y gastric bypass on glucose metabolism in subjects with Type 2 diabetes and normal glucose tolerance. *Am. J. Physiol. Endocrinol. Metab.* 303, E122–E131. doi: 10.1152/ajpendo.00073.2012

Kamiya, A., Hiyama, T., Fujimura, A., and Yoshikawa, S. (2021). Sympathetic and parasympathetic innervation in cancer: therapeutic implications. *Clin. Auton. Res.* 31, 165–178. doi: 10.1007/s10286-020-00724-y

Katsogiannos, P., Kamble, P. G., Wiklund, U., Sundbom, M., Espes, D., Hammar, U., et al. (2020). Rapid changes in neuroendocrine regulation may contribute to reversal of type 2 diabetes after gastric bypass surgery. *Endocrine* 67, 344–353. doi: 10.1007/s12020-020-02203-w

Kirchgessner, A. L., and Gershon, M. D. (1989). Identification of vagal efferent fibers and putative target neurons in the enteric nervous system of the rat. *J. Comp. Neurol.* 285, 38–53. doi: 10.1002/cne.902850105

Landsberg, L. (1986). Diet, obesity and hypertension: an hypothesis involving insulin, the sympathetic nervous system, and adaptive thermogenesis. *Q. J. Med.* 61, 1081–1090.

Landsberg, L. (2001). Insulin-mediated sympathetic stimulation: role in the pathogenesis of obesity-related hypertension (or, how insulin affects blood pressure, and why). *J. Hypertens.* 19, 523–528. doi: 10.1097/00004872-200103001-00001

Larabee, C. M., Neely, O. C., and Domingos, A. I. (2020). Obesity: a neuroimmunometabolic perspective. *Nat. Rev. Endocrinol.* 16, 30–43. doi: 10.1038/s41574-019-0283-6

le Roux, C. W., Welbourn, R., Werling, M., Osborne, A., Kokkinos, A., Laurenius, A., et al. (2007). Gut hormones as mediators of appetite and weight loss after Roux-en-Y gastric bypass. *Ann. Surg.* 246, 780–785. doi: 10.1097/SLA.0b013e3180caa3e3

Lin, B. Y., Lin, W. D., Huang, C. K., Hsin, M. C., Lin, W. Y., and Pryor, A. D. (2019). Changes of gut microbiota between different weight reduction programs. *Surg. Obes. Relat. Dis.* 15, 749–758. doi: 10.1016/j.soard.2019.01.026

Liou, A. P., Paziuk, M., Luevano, J. M. Jr., Machineni, S., Turnbaugh, P. J., and Kaplan, L. M. (2013). Conserved shifts in the gut microbiota due to gastric bypass reduce host weight and adiposity. *Sci. Transl. Med.* 5:178ra41. doi: 10.1126/scitranslmed.3005687

Lips, M. A., de Groot, G. H., De Kam, M., Berends, F. J., Wiezer, R., Van Wagensveld, B. A., et al. (2013). Autonomic nervous system activity in diabetic and healthy obese female subjects and the effect of distinct weight loss strategies. *Eur. J. Endocrinol.* 169, 383–390. doi: 10.1530/EJE-13-0506

Lohmeier, T. E., and Iliescu, R. (2013). The sympathetic nervous system in obesity hypertension. *Curr. Hypertens. Rep.* 15, 409–416. doi: 10.1007/s11906-013-0356-1

Maser, R. E., Lenhard, M. J., Irgau, I., and Wynn, G. M. (2007). Impact of surgically induced weight loss on cardiovascular autonomic function: one-year follow-up. *Obesity* 15, 364–369. doi: 10.1038/oby.2007.554

McCracken, J., Steinbeisser, M., and Kharbutli, B. (2018). Does size matter? correlation of excised gastric specimen size in sleeve gastrectomy to postoperative weight loss and comorbidities. *Obes. Surg.* 28, 1002–1006. doi: 10.1007/s11695-017-2975-0

McGavigan, A. K., Henseler, Z. M., Garibay, D., Butler, S. D., Jayasinghe, S., Ley, R. E., et al. (2017). Vertical sleeve gastrectomy reduces blood pressure and hypothalamic endoplasmic reticulum stress in mice. *Dis. Model. Mech.* 10, 235–243. doi: 10.1242/dmm.027474

McTigue, K. M., Wellman, R., Nauman, E., Anau, J., Coley, R. Y., Odor, A., et al. (2020). Comparing the 5-Year diabetes outcomes of sleeve gastrectomy and gastric bypass: the national patient-centered clinical research network (PCORNet) bariatric study. *JAMA Surg.* 155:e200087. doi: 10.1001/jamasurg.2020.0087

Mingrone, G., and Cummings, D. E. (2016). Changes of insulin sensitivity and secretion after bariatric/metabolic surgery. *Surg. Obes. Relat. Dis.* 12, 1199–1205. doi: 10.1016/j.soard.2016.05.013

Mingrone, G., Panunzi, S., De Gaetano, A., Guidone, C., Iaconelli, A., Nanni, G., et al. (2015). Bariatric-metabolic surgery versus conventional medical treatment in obese patients with type 2 diabetes: 5 year follow-up of an open-label, single-centre, randomised controlled trial. *Lancet* 386, 964–973. doi: 10.1016/S0140-6736(15)00075-6

Moran, T. H., Baldessarini, A. R., Salorio, C. F., Lowery, T., and Schwartz, G. J. (1997). Vagal afferent and efferent contributions to the inhibition of food intake by cholecystokinin. *Am. J. Physiol.* 272, R1245–R1251. doi: 10.1152/ajpregu.1997.272.4.R1245

Mulla, C. M., Middelbeek, R. J. W., and Patti, M. E. (2018). Mechanisms of weight loss and improved metabolism following bariatric surgery. *Ann. N. Y. Acad. Sci.* 1411, 53–64. doi: 10.1111/nyas.13409

O'Brien, P. E. (2015). Controversies in bariatric surgery. *Br. J. Surg.* 102, 611–618. doi: 10.1002/bjs.9760

Ochner, C. N., Gibson, C., Shanik, M., Goel, V., and Geliebter, A. (2011). Changes in neurohormonal gut peptides following bariatric surgery. *Int. J. Obes.* 35, 153–166. doi: 10.1038/ijo.2010.132

Odstrcil, E. A., Martinez, J. G., Santa Ana, C. A., Xue, B., Schneider, R. E., Steffer, K. J., et al. (2010). The contribution of malabsorption to the reduction in net energy absorption after long-limb Roux-en-Y gastric bypass. *Am. J. Clin. Nutr.* 92, 704–713. doi: 10.3945/ajcn.2010.29870

Okafor, P. N., Lien, C., Bairdain, S., Simonson, D. C., Halperin, F., Vernon, A. H., et al. (2015). Effect of vagotomy during Roux-en-Y gastric bypass surgery on weight loss outcomes. *Obes. Res. Clin. Pract.* 9, 274–280. doi: 10.1016/j.orcp.2014.09.005

Palmen, T., Ahola, H., Palgi, J., Aaltonen, P., Luimula, P., Wang, S., et al. (2001). Nephrin is expressed in the pancreatic beta cells. *Diabetologia* 44, 1274–1280. doi: 10.1007/s001250100641

Parikh, M., Issa, R., McCrillis, A., Saunders, J. K., Ude-Welcome, A., and Gagner, M. (2013). Surgical strategies that may decrease leak after laparoscopic sleeve gastrectomy: a systematic review and meta-analysis of 9991 cases. *Ann. Surg.* 257, 231–237. doi: 10.1097/SLA.0b013e31826cc714

Parlevliet, E. T., de Leeuw van Weenen, J. E., Romijn, J. A., and Pijl, H. (2010). GLP-1 treatment reduces endogenous insulin resistance via activation of central GLP-1 receptors in mice fed a high-fat diet. *Am. J. Physiol. Endocrinol. Metab.* 299, E318–E324. doi: 10.1152/ajpendo.00191.2010

Perugini, R. A., Li, Y., Rosenthal, L., Gallagher-Dorval, K., Kelly, J. J., and Czerniach, D. R. (2010). Reduced heart rate variability correlates with insulin resistance but not with measures of obesity in population undergoing laparoscopic Roux-en-Y gastric bypass. *Surg. Obes. Relat. Dis.* 6, 237–241. doi: 10.1016/j.soard.2009.09.012

Peters, J. H., Gallaher, Z. R., Ryu, V., and Czaja, K. (2013). Withdrawal and restoration of central vagal afferents within the dorsal vagal complex following subdiaphragmatic vagotomy. *J. Comp. Neurol.* 521, 3584–3599. doi: 10.1002/cne.23374

Peters, J. H., McKay, B. M., Simasko, S. M., and Ritter, R. C. (2005). Leptin-induced satiation mediated by abdominal vagal afferents. *Am. J. Physiol. Regul. Integr. Comp. Physiol.* 288, R879–R884. doi: 10.1152/ajpregu.00716.2004

Pournaras, D. J., and le Roux, C. W. (2013). Are bile acids the new gut hormones? Lessons from weight loss surgery models. *Endocrinology* 154, 2255–2256. doi: 10.1210/en.2013-1383

Powley, T. L., and Phillips, R. J. (2002). Musings on the wanderer: what's new in our understanding of vago-vagal reflexes? I. Morphology and topography of vagal afferents innervating the GI tract. *Am. J. Physiol. Gastrointest. Liver Physiol.* 283, G1217–G1225. doi: 10.1152/ajpgi.00249.2002

Prechtl, J. C., and Powley, T. L. (1990). The fiber composition of the abdominal vagus of the rat. *Anat. Embryol.* 181, 101–115. doi: 10.1007/BF00198950

Qiu, N. C., Zhang, Q., Song, X., Liu, M. E., Li, X. K., Shan, C. X., et al. (2014). Impact of the hepatic branch of the vagus and Roux-en-Y gastric bypass on the hypoglycemic effect and glucagon-like peptide-1 in rats with type 2 diabetes mellitus. *J. Surg. Res.* 191, 123–129. doi: 10.1016/j.jss.2014.03.062

Quarta, C., Bellocchio, L., Mancini, G., Mazza, R., Cervino, C., Braulke, L. J., et al. (2010). CB(1) signaling in forebrain and sympathetic neurons is a key determinant of endocannabinoid actions on energy balance. *Cell Metab.* 11, 273–285. doi: 10.1016/j.cmet.2010.02.015

Ramon, J. M., Salvans, S., Crous, X., Puig, S., Goday, A., Benaiges, D., et al. (2012). Effect of Roux-en-Y gastric bypass vs sleeve gastrectomy on glucose and gut hormones: a prospective randomised trial. *J. Gastrointest. Surg.* 16, 1116–1122. doi: 10.1007/s11605-012-1855-0

Rayner, D. V., and Trayhurn, P. (2001). Regulation of leptin production: sympathetic nervous system interactions. *J. Mol. Med.* 79, 8–20. doi: 10.1007/s001090100198

Rodriguez, A., Becerril, S., Valenti, V., Moncada, R., Mendez-Gimenez, L., Ramirez, B., et al. (2012). Short-term effects of sleeve gastrectomy and caloric restriction on blood pressure in diet-induced obese rats. *Obes. Surg.* 22, 1481–1490. doi: 10.1007/s11695-012-0702-4

Rosenthal, R. J., International Sleeve Gastrectomy Expert Panel, Diaz, A. A., Arvidsson, D., Baker, R. S., and Basso, N. (2012). International Sleeve Gastrectomy Expert Panel Consensus Statement: best practice guidelines based on experience of >12,000 cases. *Surg. Obes. Relat. Dis.* 8, 8–19. doi: 10.1016/j.soard.2011.10.019

Saeidi, N., Nestoridi, E., Kucharczyk, J., Uygun, M. K., Yarmush, M. L., and Stylopoulos, N. (2012). Sleeve gastrectomy and Roux-en-Y gastric bypass exhibit differential effects on food preferences, nutrient absorption and energy expenditure in obese rats. *Int. J. Obes.* 36, 1396–1402. doi: 10.1038/ijo.2012.167

Salehi, M., Prigeon, R. L., and D'Alessio, D. A. (2011). Gastric bypass surgery enhances glucagon-like peptide 1-stimulated postprandial insulin secretion in humans. *Diabetes* 60, 2308–2314. doi: 10.2337/db11-0203

Schauer, P. R., Bhatt, D. L., and Kashyap, S. R. (2017). Bariatric surgery or intensive medical therapy for diabetes after 5 Years. *N. Engl. J. Med.* 376:1997. doi: 10.1056/NEJMc1703377

Schauer, P. R., Kashyap, S. R., Wolski, K., Brethauer, S. A., Kirwan, J. P., Pothier, C. E., et al. (2012). Bariatric surgery versus intensive medical therapy in obese patients with diabetes. *N. Engl. J. Med.* 366, 1567–1576. doi: 10.1056/NEJMoa1200225

Seravalle, G., Colombo, M., Perego, P., Giardini, V., Volpe, M., Dell'Oro, R., et al. (2014). Long-term sympathoinhibitory effects of surgically induced weight loss in severe obese patients. *Hypertension* 64, 431–437. doi: 10.1161/HYPERTENSIONAHA.113.02988

Sjostrom, L., Peltonen, M., Jacobson, P., Sjostrom, C. D., Karason, K., Wedel, H., et al. (2012). Bariatric surgery and long-term cardiovascular events. *JAMA* 307, 56–65. doi: 10.1001/jama.2011.1914

Smith, E. P., An, Z., Wagner, C., Lewis, A. G., Cohen, E. B., Li, B., et al. (2014). The role of beta cell glucagon-like peptide-1 signaling in glucose regulation and response to diabetes drugs. *Cell Metab.* 19, 1050–1057. doi: 10.1016/j.cmet.2014.04.005

Stefater, M. A., Wilson-Perez, H. E., Chambers, A. P., Sandoval, D. A., and Seeley, R. J. (2012). All bariatric surgeries are not created equal: insights from mechanistic comparisons. *Endocr. Rev.* 33, 595–622. doi: 10.1210/er.2011-1044

Sterl, K., Wang, S., Oestricker, L., Wallendorf, M. J., Patterson, B. W., Reeds, D. N., et al. (2016). Metabolic responses to xenin-25 are altered in humans with Roux-en-Y gastric bypass surgery. *Peptides* 82, 76–84. doi: 10.1016/j.peptides.2016.06.001

Tellez, L. A., Medina, S., Han, W., Ferreira, J. G., Licona-Limon, P., Ren, X., et al. (2013). A gut lipid messenger links excess dietary fat to dopamine deficiency. *Science* 341, 800–802. doi: 10.1126/science.1239275

Ten Kulve, J. S., Veltman, D. J., Gerdes, V. E. A., van Bloemendaal, L., Barkhof, F., Deacon, C. F., et al. (2017). Elevated postoperative endogenous GLP-1 levels mediate effects of roux-en-Y gastric bypass on neural responsivity to food cues. *Diabetes Care* 40, 1522–1529. doi: 10.2337/dc16-2113

Topart, P., Becouarn, G., and Ritz, P. (2011). Pouch size after gastric bypass does not correlate with weight loss outcome. *Obes. Surg.* 21, 1350–1354. doi: 10.1007/s11695-011-0460-8

Tremblay, A., and Chaput, J. P. (2009). Adaptive reduction in thermogenesis and resistance to lose fat in obese men. *Br. J. Nutr.* 102, 488–492. doi: 10.1017/S0007114508207245

Tritsch, A. M., Bland, C. M., Hatzigeorgiou, C., Sweeney, L. B., and Phillips, M. (2015). A retrospective review of the medical management of hypertension and diabetes mellitus following sleeve gastrectomy. *Obes. Surg.* 25, 642–647. doi: 10.1007/s11695-014-1375-y

Vaisse, C., Clement, K., Guy-Grand, B., and Froguel, P. (1998). A frameshift mutation in human MC4R is associated with a dominant form of obesity. *Nat. Genet.* 20, 113–114. doi: 10.1038/2407

Wadden, T. A., Webb, V. L., Moran, C. H., and Bailer, B. A. (2012). Lifestyle modification for obesity: new developments in diet, physical activity, and behavior therapy. *Circulation* 125, 1157–1170. doi: 10.1161/CIRCULATIONAHA.111.039453

Wallenius, V., Dirinck, E., Fandriks, L., Maleckas, A., le Roux, C. W., and Thorell, A. (2018). Glycemic Control after Sleeve Gastrectomy and Roux-En-Y Gastric Bypass in Obese Subjects with Type 2 Diabetes Mellitus. *Obes. Surg.* 28, 1461–1472. doi: 10.1007/s11695-017-3061-3

Wang, Y. C., McPherson, K., Marsh, T., Gortmaker, S. L., and Brown, M. (2011). Health and economic burden of the projected obesity trends in the USA and the UK. *Lancet* 378, 815–825. doi: 10.1016/S0140-6736(11)60814-3

Wasmund, S. L., Owan, T., Yanowitz, F. G., Adams, T. D., Hunt, S. C., Hamdan, M. H., et al. (2011). Improved heart rate recovery after marked weight loss induced by gastric bypass surgery: two-year follow up in the Utah Obesity Study. *Heart Rhythm* 8, 84–90. doi: 10.1016/j.hrthm.2010.10.023

Williams, S. M., Eleftheriadou, A., Alam, U., Cuthbertson, D. J., and Wilding, J. P. H. (2019). Cardiac autonomic neuropathy in obesity, the metabolic syndrome and prediabetes: a narrative review. *Diabetes Ther.* 10, 1995–2021. doi: 10.1007/s13300-019-00693-0

Wilson-Perez, H. E., Chambers, A. P., Ryan, K. K., Li, B., Sandoval, D. A., Stoffers, D., et al. (2013). Vertical sleeve gastrectomy is effective in two genetic mouse models of glucagon-like Peptide 1 receptor deficiency. *Diabetes* 62, 2380–2385. doi: 10.2337/db12-1498

Yan, W., Polidori, D., Yieh, L., Di, J., Wu, X., Moreno, V., et al. (2014). Effects of meal size on the release of GLP-1 and PYY after Roux-en-Y gastric bypass surgery in obese subjects with or without type 2 diabetes. *Obes. Surg.* 24, 1969–1974. doi: 10.1007/s11695-014-1316-9

Yang, J., Wang, C., Cao, G., Yang, W., Yu, S., Zhai, H., et al. (2015). Long-term effects of laparoscopic sleeve gastrectomy versus roux-en-Y gastric bypass for the treatment of Chinese type 2 diabetes mellitus patients with body mass index 28-35 kg/m(2). *BMC Surg.* 15:88. doi: 10.1186/s12893-015-0074-5

Ye, Y., Abu El Haija, M., Morgan, D. A., Guo, D., Song, Y., and Frank, A. (2020). Endocannabinoid receptor-1 and sympathetic nervous system mediate the beneficial metabolic effects of gastric bypass. *Cell Rep.* 33:108270. doi: 10.1016/j.celrep.2020.108270

Yousseif, A., Emmanuel, J., Karra, E., Millet, Q., Elkalaawy, M., Jenkinson, A. D., et al. (2014). Differential effects of laparoscopic sleeve gastrectomy and laparoscopic gastric bypass on appetite, circulating acyl-ghrelin, peptide YY3-36 and active GLP-1 levels in non-diabetic humans. *Obes. Surg.* 24, 241–252. doi: 10.1007/s11695-013-1066-0

Zechner, J. F., Mirshahi, U. L., Satapati, S., Berglund, E. D., Rossi, J., Scott, M. M., et al. (2013). Weight-independent effects of roux-en-Y gastric bypass on glucose homeostasis via melanocortin-4 receptors in mice and humans. *Gastroenterology* 144, 580–590.e7. doi: 10.1053/j.gastro.2012.11.022

Zhang, H., Pu, Y., Chen, J., Tong, W., Cui, Y., Sun, F., et al. (2014). Gastrointestinal intervention ameliorates high blood pressure through antagonizing overdrive of the sympathetic nerve in hypertensive patients and rats. *J. Am. Heart Assoc.* 3:e000929. doi: 10.1161/JAHA.114.000929

Conflict of Interest: The authors declare that the research was conducted in the absence of any commercial or financial relationships that could be construed as a potential conflict of interest.

Publisher's Note: All claims expressed in this article are solely those of the authors and do not necessarily represent those of their affiliated organizations, or those of the publisher, the editors and the reviewers. Any product that may be evaluated in this article, or claim that may be made by its manufacturer, is not guaranteed or endorsed by the publisher.

frontiers in Neuroscience

ORIGINAL RESEARCH
published: 29 November 2021
doi: 10.3389/fnins.2021.777572

Compulsive Eating in a Rat Model of Binge Eating Disorder Under Conditioned Fear and Exploration of Neural Mechanisms With *c-fos* mRNA Expression

Zhi Fei Li[1,2,3,4], Sandrine Chometton[3], Geneviève Guèvremont[3], Elena Timofeeva[3†] and Igor Timofeev[4]**

[1] The First Affiliated Hospital, Jinan University, Guangzhou, China, [2] Faculté de Médecine, Département de Médecine Moléculaire, Université Laval, Quebec City, QC, Canada, [3] Centre de Recherche de l'Institut Universitaire de Cardiologie et de Pneumologie de Québec, Quebec City, QC, Canada, [4] Centre de Recherche CERVO, Quebec City, QC, Canada

OPEN ACCESS

Edited by:
Lionel Carneiro, The Ohio State University, United States

Reviewed by:
Roelof Eikelboom, Wilfrid Laurier University, Canada
Elaine Bliley Sinclair, MedStar Georgetown University Hospital, United States

***Correspondence:**
Zhi Fei Li
lizhifei@jnu.edu.cn
Igor Timofeev
igor.timofeev@fmed.ulaval.ca

† *Deceased*

Specialty section:
This article was submitted to Neuroenergetics, Nutrition and Brain Health, a section of the journal Frontiers in Neuroscience

Received: *15 September 2021*
Accepted: *04 November 2021*
Published: *29 November 2021*

Citation:
Li ZF, Chometton S, Guèvremont G, Timofeeva E and Timofeev I (2021) Compulsive Eating in a Rat Model of Binge Eating Disorder Under Conditioned Fear and Exploration of Neural Mechanisms With c-fos mRNA Expression. Front. Neurosci. 15:777572. doi: 10.3389/fnins.2021.777572

Compulsive eating is the most obstinate feature of binge eating disorder. In this study, we observed the compulsive eating in our stress-induced binge-like eating rat model using a conflicting test, where sucrose and an aversively conditioned stimulus were presented at the same time. In this conflicting situation, the binge-like eating prone rats (BEPs), compared to the binge-like eating resistant rats (BERs), showed persistent high sucrose intake and inhibited fear response, respectively, indicating a deficit in palatability devaluation and stronger anxiolytic response to sucrose in the BEPs. We further analyzed the neuronal activation with *c-fos* mRNA *in situ* hybridization. Surprisingly, the sucrose access under conditioned fear did not inhibit the activity of amygdala; instead, it activated the central amygdala. In the BEPs, sucrose reduced the response of the paraventricular hypothalamic nucleus (PVN), while enhancing activities in the lateral hypothalamic area (LHA) to the CS. The resistance to devaluating the palatable food in the BEPs could be a result of persistent Acb response to sucrose intake and attenuated recruitment of the medial prefrontal cortex (mPFC). We interpret this finding as that the reward system of the BEPs overcame the homeostasis system and the stress-responding system.

Keywords: binge eating disorder, compulsive eating, reward devaluation, *c-fos* expression, fear conditioning, nucleus accumbens

INTRODUCTION

Binge eating disorder (BED) is characterized by discrete episodes of overeating within a short period of time, usually less than 2 h, even when not feeling hungry (Bogduk, 2013). People with BED will continuously eat until physically feeling uncomfortable. In humans, negative consequences associated with overeating include social impairment, emotional disturbances, psychiatric disorders, and life-threatening medical conditions associated with weight gain (Moore et al., 2017).

Stress is one of the main inducers of BED in human patients. Evidence from both human and animal studies revealed that stress could have bidirectional influence on feeding behaviors, either

inhibiting or stimulating food intake (Maniam and Morris, 2012). The direction of this changing effect of stress on feeding is dependent on the palatability of the food following stress (Pecoraro et al., 2004). A variety of rodent models of the BED have been developed by using food deprivation and/or stress. Our lab previously developed a binge-like eating rat model through intermittent foot shock stress followed by 1-h sucrose access (Calvez and Timofeeva, 2016). In this model, the binge-eating prone rats (BEPs) consume more sucrose solution than the binge-eating resistant rats (BERs) both in normal condition and after stress, and the BEPs further increase their sucrose intake after the stress stimulation.

Another hallmark of the BED is the compulsive eating, demonstrated as repetitively returning into engorging unhealthy food with full knowledge of the hazardous physical and psychological consequences. Both our BED rat model and the animal models stated in other literature noticed compulsive eating, in a modified Light/Dark box test (Calvez and Timofeeva, 2016) and unconditioned stimulus (US) such as foot shock (Oswald et al., 2011), respectively. The BEPs consumed larger amount of sucrose than the BERs in the intensively illuminated light box. In response to stress, the BEPs demonstrated a hyporeactivity of the hypothalamic–pituitary–adrenal (HPA) axis compared with the BERs (Calvez et al., 2016).

To gain a better understanding of the compulsive eating in the BED, we adopted the fear conditioning paradigm. Aversively conditioned stimuli have an inhibitory effect on the feeding behavior, and this effect can be abolished by lesions of the central nucleus but not the basolateral nucleus of the amygdala (Petrovich et al., 2009). Thus, the first objective of this study is to observe compulsive eating in our BED rat model by creating a conflicting situation with simultaneous presence of a 10% sucrose solution and an aversively conditioned stimulus. Based on that, we hypothesized that (1) the abnormally intense motivation for palatable food in the BEPs would attenuate the inhibitory effect of the CS on feeding, and (2) the BEPs would show less fear response to the CS because of a stronger anxiolytic effect of palatable food on the BEPs relative to BERs. The second objective is to explore the underlying neural mechanisms *via* analyzing the *c-fos* mRNA expression in different brain regions related to feeding, reward processing, and stress responding. The *c-fos* gene is one of the immediate early genes widely used as a marker of early neuronal activation (Kovács, 1998), because its expression is correlated with the functional activation of neurons. As a result, we hypothesized that different levels of *c-fos* mRNA expression in brain regions underlying food intake and stress response would be observed between the BEPs and BERs after fear conditioning test.

MATERIALS AND METHODS

Animals

Young (PD 45, 151–175 g) female Sprague Dawley rats ($n = 170$) were purchased from Charles River. All rats were individually housed in transparent plastic cages, lined with wood shavings and crinkle paper. The rats were maintained on a 12-h light/dark cycle (lights on from 2:00 to 14:00), and provided with *ad libitum* access to standard laboratory rat chow (Teklad Global 18% Protein Rodent Diet; 3.1 kcal/g, Harlan Teklad, Montreal, QC, Canada) and tap water, unless noted otherwise. All rats were acclimated to the housing conditions and handling procedures for at least 1 week prior to the experiments.

Classification of the Binge-Like Eating Prone Rats and Binge-Like Eating Resistant Rats

Rats were classified as the BERs or the BEPs according to the procedures previously described (Calvez and Timofeeva, 2016). All rats were given a 24-h access to a 10% sucrose solution in their home cages to decrease their neophobia to sucrose. Then, we assessed the consumption of 10% sucrose solution (0.4 kcal/ml) during several intermittent 1-h sessions starting from the beginning of the dark phase in home cages, with random intertrial intervals (ITIs) of 1 or 2 days. When the sucrose intake became stable for three consecutive No Stress sessions, three Stress sessions were conducted with intervals of 2 or 3 days. In the Stress sessions, 1-h sucrose access was provided in home cages immediately after four rounds of mild foot shock in a procedure room (0.6 mA DC impulse, 3 s duration, with inter-shock intervals of 15 s). The second and third Stress sessions were separated by a No Stress session to prevent the rats from associating the sucrose access with foot shock. The food pellets were removed during sucrose access in home cages, and put back immediately after each session ended. Sucrose intake of all animals in each Stress session was divided into high, intermediate, and low intake tertiles. Rats with sucrose intake in the high tertiles at least twice and never in the low tertiles were sorted as binge-like eating prone, while rats with sucrose intake in the low tertiles at least twice and never in the high tertiles were classified as binge-like eating resistant. After the phenotyping, 42 rats were categorized into the BEP group and 44 rats into the BER group. In order to keep this animal model consistent with our previously published studies, sucrose intake without normalization by body weight was used for the phenotyping.

The Fear Conditioning Test

The fear conditioning test was composed of three parts: Habituation and Appetitive sessions, Fear Conditioning sessions, and the Test session (**Figure 1A**). All sessions lasted for 15 min, and were videotaped (Logitech HD Webcam C270) from the top of the sound-attenuating cubicle (Med Associates inc.; ENV-022V, 55.9 cm × 38.1 cm × 35.6 cm) containing the behavioral test chamber (Med Associates inc.; ENV-007-VP, 30.5 cm × 24.1 cm × 29.2 cm). The test chamber had a grid floor and aluminum sides, and there were Plexiglas in the front and the top sides, except for the back side. The test chamber was illuminated with a light (4 W) placed 25 cm above the floor. A speaker (Med Associates inc.; ENV-224AM) was installed on the left wall, 20 cm above the floor. Two photobeam lickometers (Med Associates inc.; ENV-251L) were installed on the front and back parts of the right wall, 3 cm above the floor, supplied with a bottle of 10% sucrose solution and water, respectively. A door

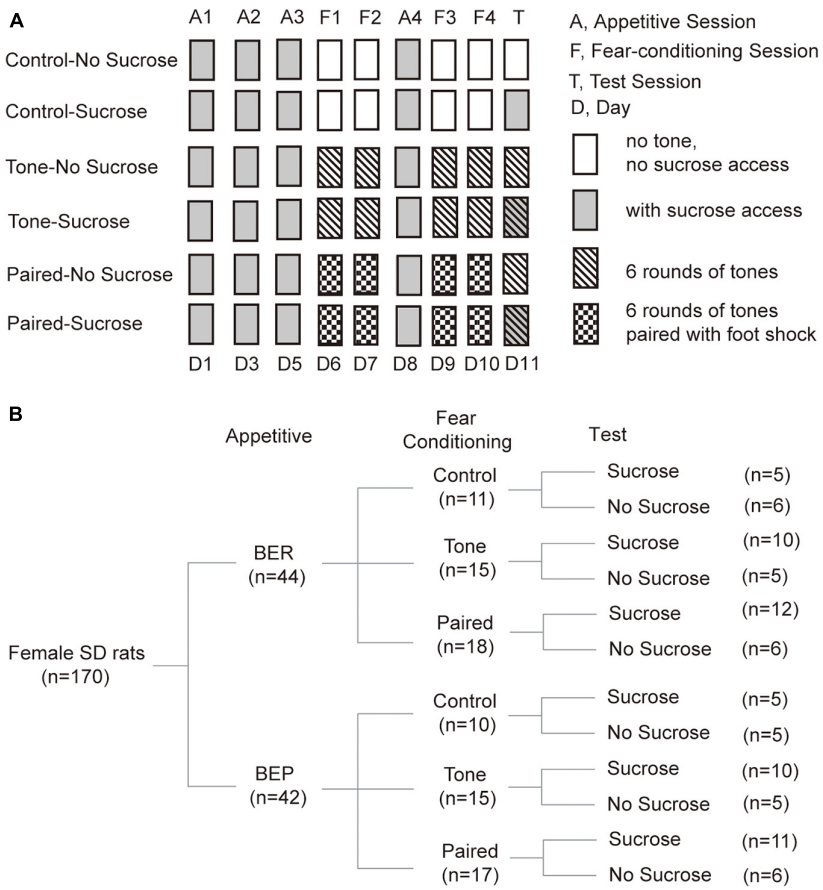

FIGURE 1 | Diagram of treatments and groups in the Fear Conditioning test. **(A)** Diagram of fear conditioning test procedures. **(B)** Number of animals in each group at each step during the fear conditioning test.

in front of the sucrose lickometer was controlled by a custom-designed program (Med-PC V, Med Associates inc.) to start and end the sucrose access.

Habituation and Appetitive Sessions

For the Habituation and Appetitive sessions, the test chamber was arranged as context A. In this context, a white plastic panel was installed on the grid floor and apple-scented beads were placed in the sound attenuating box. The light was placed on the top right corner of the left wall. Furthermore, the test chamber was cleaned with Percept cleaner between each rat, and the animals were transported from the housing room to the test room on a cart. In this context, the rats were habituated to drink 10% sucrose solution in the behavioral test chamber with ITIs of 1 or 2 days at random, until the sucrose intake became stable for three sessions. Thus, the last three sessions during which the sucrose intake of BER and BEP groups showed no significant changes were defined as Appetitive sessions (**Figure 1A**).

Fear Conditioning Sessions

In Fear Conditioning sessions, the behavioral cage was modified into context B to be different from the context of Appetitive sessions. The plastic floor and apple-scented beads were removed. The light was moved to the top right corner of the right wall. A piece of curved white plastic board was placed to serve as the back and sidewalls of the test chamber and there was neither sucrose nor water access for the rats. The test chamber was cleaned with Citrosol cleaner between each rat and the BEPs and BERs were transported by the experimenter. In this stage, we divided rats of both phenotypes into three groups (Control, Tone, and Paired groups; **Figure 1B**).

(a) For the Paired groups, a mild foot shock (1 s, 0.6 mA, DC impulses) was delivered through the grid floor during the last second of each of the six tones (the first tone started 20 s after the onset of the trial, 20 s, 2 kHz, 75 dB), separated by 125-s no-stimulus periods.
(b) For the Tone groups, the same condition was applied, but no foot shock was delivered in these sessions.
(c) For the Control groups, no tone or foot shock was applied during each 15-min Fear Conditioning session.

Between the second and third Fear Conditioning sessions, an Appetitive session was inserted to prevent the rats from losing their phenotype (**Figure 1A**). In this Appetitive session, the behavioral cage was arranged as context A.

The Test Session

The test cage was arranged as context A in the Test session. During the Test session, context A was used as in the Appetitive session. We divided rats of each group in the Fear Conditioning sessions into two groups (No Sucrose and Sucrose; **Figure 1B**). Sucrose groups had access to 10% sucrose solution throughout the Test session, while the No Sucrose groups did not. For the Tone and Paired groups, six rounds of the same tones as in Fear Conditioning sessions were presented, but without foot shock stimulus (**Figure 1A**).

During the Appetitive sessions and the Test session, sucrose intake was assessed by weighing the bottle before and after the experiment, and the licking events were detected by the lickometer and recorded with a multichannel system (Tucker-Davis Technologies) and the Med Associates system (Med Associates inc.). Freezing behavior of the Paired groups was observed on video and quantified by the experimenter during the tones in Fear Conditioning sessions and the Test session.

Licking Microstructure Analyses

The licking events were analyzed in all 12 groups (**Figure 1B**). In No Sucrose groups, the licks were too scarce for licking microstructure analysis and further statistical analysis, which was the reason that these licking misstructure results were absent for these groups in the Test session. The first lick latency was defined as the time in seconds between the beginning of the session, and the first lick of sucrose solution. A licking cluster was defined as a burst of three or more licks with inter-cluster intervals of 500 ms or longer. The meal duration was calculated as the total duration in seconds of all clusters during the 15-min access to sucrose solution. The cluster size was defined as the average number of licks per cluster, and the cluster duration was defined as the average duration of all clusters in seconds. The total number of licks, meal duration, number of clusters, cluster size, cluster duration, and first lick latency were computed for each session with a customized MATLAB script (R2014a, The MathWorks, inc.).

Brain Preparation

Immediately after the Test session, each rat was returned to its home cage, with access to neither chow nor water for 30 min. Then, the rats were anesthetized with a mixture of ketamine (60 mg/kg) and xylazine (7.5 mg/kg) and intracardially perfused with ice-cold saline followed by 4% paraformaldehyde (PFA) in phosphate buffer. The brains were removed from the skulls and fixed in 4% PFA for 1 week before being transferred to a PFA (4%)/sucrose (20%) solution. After freezing, brains were conserved in −80°C. Each brain was cut into 30-μm coronal sections using a microtome (Histoslide 2000, Reichert Jung, Heidelberger, Germany). All sections from each brain were distributed into a 24-well plate filled with a cold sterile cryoprotecting solution containing ethylene glycol (30%), glycerol (20%), and sodium phosphate buffer (50 mM, pH 7.2), and stored at −30°C.

In situ Hybridization for *c-fos* mRNA

The protocol of *in situ* hybridization we used to localize the *c-fos* mRNA in this study was largely adapted from the method described by Simmons et al. (1989). The procedures have been described in detail previously (Poulin and Timofeeva, 2008). Briefly, brain sections were mounted onto poly-L-lysine-coated slides and conserved in 100% ethanol. After the slides dried up, they were successively fixed in 4% PFA for 20 min, digested with proteinase K (0.01 mg/ml) at 37°C for 25 min, acetylated with acetic anhydride (0.25% in 0.1 M triethanolamine, pH 8.0), and dehydrated through ethanol gradient (50, 70, 95, and 100%). After the slides dried up, 90 μl of the hybridization solution containing a ^{35}S labeled antisense cRNA probe against *c-fos* mRNA (De Ávila et al., 2018) was spread on each slide. All slides were then covered with coverslips and incubated overnight in a slide warmer at 60°C. After the coverslips were removed, the slides were rinsed four times with 4 × saline sodium citrate buffer (SSC, 0.6 M NaCl, 60 mM trisodium citrate buffer, pH 7.0), digested with RNase-A (20 μg/ml in 10 mM Tris–500 mM NaCl containing 1 mM EDTA) for 30 min at 37°C, rinsed in SSC with descending concentrations (2×, 1×, 0.5×, and 0.1×), and finally dehydrated through ethanol gradient. Thereafter, the slides were defatted in toluene, dipped in nuclear emulsion (Kodak), and exposed for 7 days before being developed in the developer (Kodak) and fixed in rapid fixer (Kodak). Finally, slides were rinsed in running cold tap water for 1 h, stained with thionin, dehydrated through an ethanol gradient, cleared in toluene, and coverslipped with DPX.

Relative *c-fos* mRNA Expression Analyses

The slides were analyzed under a light microscope (Olympus) equipped with a camera coupled to a computer with Stereo Investigator software (v1103). The luminosity of the system was set to the maximum. To avoid saturation, the exposure time for each region was adjusted with the section that had the strongest hybridization signal. For every area of interest, two photos were taken under both bright-field and dark-field illumination without moving the slides at a magnification of 4×. Thus, the position of the area of interest on both images are exactly the same. When the borders of the area of interest were not clear on the dark-field images, the light-field images were used to assist drawing the contours on the dark-field image.

There are many brain regions related to BED. In this study, we want to explore the neural mechanism of compulsive property of binge eating. For this purpose, we created a conflicting situation and allowed the stress-induced binge-like eating rats to make the decision between responding to stress or palatable food. Thus, we examined the *c-fos* mRNA expression in brain regions closely related to stress responding, food intake regulation, and decision-making, namely, the amygdala (2.16–3.48 mm caudal to the bregma), the paraventricular hypothalamic nucleus (PVN, 1.56–1.80 mm caudal to the bregma), the lateral hypothalamic area (LHA, 2.28–3.48 mm caudal to the bregma), the nucleus accumbens (Acb, 2.28–1.08 mm rostral to the bregma), the bed nucleus of the stria terminalis (BNST, 0.36 mm rostral to 0.36 mm

caudal to the bregma), and the medial prefrontal cortex (mPFC, 3.72–2.52 mm rostral to the bregma).

The area of interest was outlined on each photo by the experimenter with Stereo Investigator. The hybridization signal was quantified by calculating the optical density (OD) in the contour on the dark-field image with a customized MATLAB script (R2014a, The MathWorks, inc.). The OD of each area of interest was corrected by subtracting the background signal, which was determined by three small contours on the unlabeled areas around the area of interest.

Brain slices from different brain regions were labeled in different batches of *in situ* hybridization. Moreover, the exposure parameters were constant only for slices from the same brain region, while different from region to region. Thus, the optical densities were comparable only between images from the same brain region, but not between different brain regions.

Statistical Analyses

Results are presented as mean ± standard deviation (SD). The phenotype effects on first lick latency in Appetitive sessions and the Test session were analyzed using one-way ANOVA. Two-way ANOVA with Bonferroni *post hoc* test was used for all other statistical analyses. A difference was considered significant when p-values < 0.05. Statistical analyses were performed using the Prism 6.04 (GraphPad Software inc., La Jolla, CA, United States), and graphs were made with Prism 6.04 and arranged into figures with Adobe Illustrator® CS.

RESULTS

Classification of the Binge-Like Eating Resistant Rats and Binge-Like Eating Prone Rats

The difference in sucrose intake between the BEPs and BERs during the phenotyping in our study was similar to previously published results (Calvez and Timofeeva, 2016). The BEPs had significantly higher sucrose intake than the BERs both in the non-stressful situation ($p < 0.0001$) and after foot shock stress ($p < 0.0001$). Moreover, the BEPs consumed even more sucrose after stress ($p < 0.0001$), but the stress showed no significant impact on the sucrose intake of the BERs ($p = 0.998$). Two-way ANOVA assessed the effect of stress ($F_{1,168} = 24.530$, $p < 0.0001$), phenotype ($F_{1,168} = 168.400$, $p < 0.0001$), and their interaction ($F_{1,168} = 25.220$, $p < 0.0001$) on the 1-h sucrose intake in both non-stressful and after stress situations (data not shown).

Sucrose Intake Behavior During the Appetitive and Test Sessions

There was no significant difference in the body weight between BER and BEP rats throughout the fear conditioning test (data not shown). Anyway, to eliminate the potential influence of body weight on the sucrose intake, the quantity of sucrose intake during Appetitive and Test sessions of each rat was calculated as the energy of the consumed sucrose normalized by its body weight (kcal/kg body weight). As the BEPs and BERs were accommodated in the behavioral test chamber, the 15-min sucrose intake of both phenotypes gradually reached a plateau. The last three sessions with stable sucrose consumption of the BEPs and BERs were defined as the Appetitive sessions (**Figure 2A**). Two-way ANOVA revealed a significant effect of phenotype on the sucrose intake in the Appetitive sessions. The BEPs took more sucrose than the BERs in all Appetitive sessions, which is consistent with their phenotypes in the home cage during the binge eating classification (**Figure 2A**). Analysis of the microstructure of licking events showed that the total number of licks was significantly higher in the BEPs than the BERs for the three Appetitive sessions (**Figure 2B**). The meal duration was also significantly higher in the BEPs than the BERs in the first and second sessions, and close to the significance in the third (**Figure 2C**). The number of clusters (**Figure 2D**), cluster size (**Figure 2E**), and cluster duration (**Figure 2F**) were not significantly different between the BEPs and BERs. Finally, the BEPs showed significantly lower average first lick latency in three Appetitive sessions than the BERs rats (two-tailed unpaired t-test, $p = 0.003$, data not shown).

In the Test session, because of the scarcity of licks in the no-sucrose groups, we only considered the sucrose intake of the groups with sucrose access. To diminish the individual differences, we normalized the sucrose intake/body weight of each rat to its average sucrose intake/body weight in the Appetitive sessions. Two-way ANOVA revealed a significant effect of stress ($F_{2,47} = 14.180$, $p < 0.0001$) on the sucrose intake in the Test session, and a close to significant effect of its interaction with phenotype ($F_{2,47} = 3.117$, $p = 0.054$) but not of the phenotype itself ($F_{1,47} = 0.481$, $p = 0.491$). The result demonstrated that the unconditioned tones failed to change the sucrose intake of either the BEPs or the BERs (**Figure 3A**). When the tones were previously associated with foot shocks, they prominently decreased the sucrose intake of the BER-Paired-Sucrose group compared with the BER-Control-Sucrose group and the BER-Tone-Sucrose group (**Figure 3A**). The aversive CS slightly decreased the sucrose intake of BEPs, but without reaching a significant level (**Figure 3A**). We also analyzed the first lick latency in the Test session showing that the conditioned fear significantly increased the first lick latency of BER-Paired rats ($n = 18$) compared with the BEP-Paired rats ($n = 17$) (two-tailed unpaired t-test, $p = 0.047$, data not shown).

Next, we analyzed the licking microstructures during tones and between tones separately, in Tone and Paired groups. During tones, two-way ANOVA revealed a substantial effect of the CS on all licking microstructures, namely, the number of licks, licking duration ($F_{1,31} = 20.280$, $p < 0.001$), number of clusters ($F_{1,39} = 0.038$, $p = 0.003$), cluster size, and cluster duration, without the effect of phenotype or their interaction. Between tones, the CS only showed a significant effect on the number of licks and licking duration, while the interaction between CS and phenotype displayed a major influence on the number of licks, licking duration, cluster size, and cluster duration. For the BERs, both during tones and between tones, the conditioned fear significantly decreased the number of licks (**Figures 3B,C**), licking duration (**Figures 3D,E**), cluster size (**Figures 3H,I**), and cluster duration (**Figures 3J,K**). The number of clusters

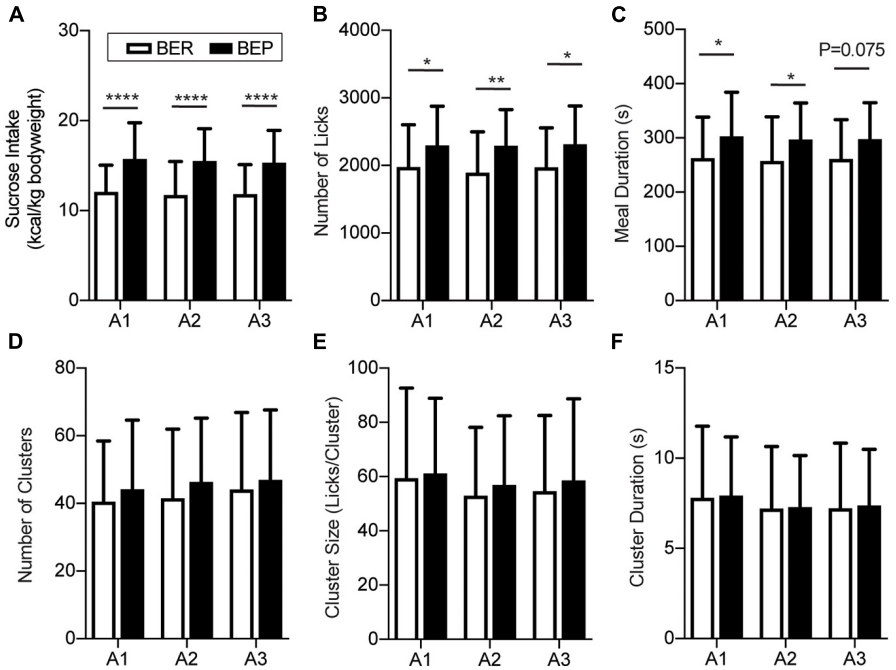

FIGURE 2 | Feeding behavior during appetitive sessions. Binge-like eating prone (BEP) rats showed constant higher sucrose intake during the Appetitive sessions compared to binge-like eating resistant (BER) rats. **(A)** Sucrose intake normalized to body weight. Licking microstructures during the Appetitive sessions: total number of licks **(B)**, meal duration **(C)**, number of clusters **(D)**, cluster size **(E)**, and cluster duration **(F)**. *Significantly different ($p < 0.05$) between the BEP group and BER group. **$p < 0.01$, ****$p < 0.0001$.

only decreased during tones (**Figures 3F,G**). In the BEPs, the conditioned fear only decreased the number of licks (**Figure 3B**) and the licking duration (**Figure 3D**) during tones, and the other analyzed licking microstructures were not significantly changed by the conditioned fear.

Freezing Behavior During Fear Conditioning Sessions and the Test Session

The fear response of each rat was measured as the average freezing time during six tones in each session. In the Fear Conditioning sessions, the BER-Paired and BEP-Paired groups had similar acquisition efficiency and showed no phenotype difference throughout all four sessions (**Figure 4A**). The freezing time significantly increased in the second Fear Conditioning session compared with the first and became relatively stable afterward. Two-way ANOVA revealed a significant effect of the session number ($F_{3,99} = 23.750$, $p < 0.0001$) on the freezing behavior, but not the phenotype ($F_{1,33} = 0.365$, $p = 0.550$) or their interaction ($F_{3,99} = 0.659$, $p = 0.579$).

Again, to diminish individual differences, we normalized the freezing time of each rat in the Test session to its average freezing time of the last three Fear Conditioning sessions (**Figure 4B**). With the absence of foot shock during the Test session, the BER-Paired-No Sucrose and BEP-Paired-No Sucrose rats slightly reduced their freezing behavior in response to the CS, and no significant difference between phenotypes was detected. The presence of sucrose decreased the freezing behavior in both BER-Paired-Sucrose and BEP-Paired-Sucrose rats compared with the No Sucrose groups, but only the diminution in BEP-Paired rats was statistically significant. Moreover, the freezing time of BEP-Paired-Sucrose rats was significantly different compared with BER-Paired-Sucrose rats. Two-way ANOVA revealed the significant effect of the sucrose ($F_{1,31} = 15.170$, $p = 0.001$) on the freezing behavior, but not the phenotype ($F_{1,31} = 2.928$, $p = 0.097$) or their interactions ($F_{1,31} = 1.429$, $p = 0.241$).

c-fos Analyses in Different Brain Regions Involved in Feeding, Stress, and Reward

The *c-fos* mRNA expression was detected by *in situ* hybridization and quantified as the OD. To simplify the presentation, we reduced the number of groups by combining the Control and Tone groups into Non-Paired ones for each phenotype when analyzing the correlation between sucrose intake and *c-fos* mRNA expression.

Activation of the Amygdala by the CS Was Not Inhibited by Sucrose Intake

It has long been known that the amygdala plays an important role in the fear conditioning learning and expressing process. The basolateral amygdala (BLA) is the primary site where the association between the CS and US is formed, while the output projections from the central amygdala (Ce) control the freezing behavior and feeding inhibition in response to an aversive CS. Two subregions of the amygdala were analyzed: the Ce and BLA.

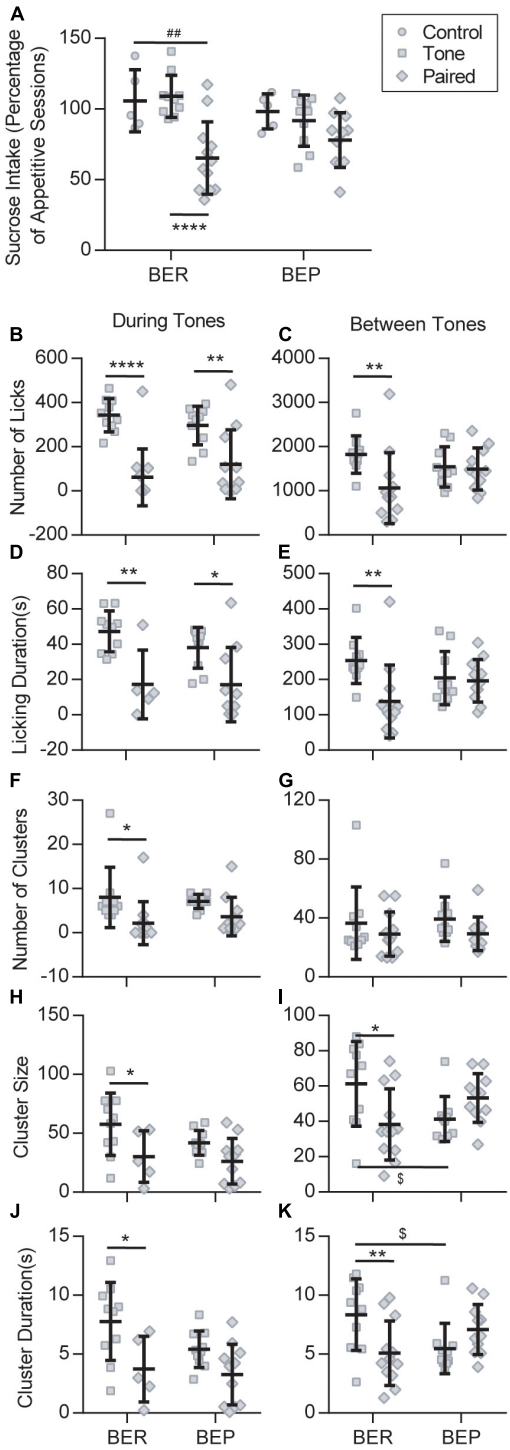

FIGURE 3 | Feeding behavior during the Test session. **(A)** Sucrose intake during the Test session normalized to the average intake of each animal during all appetitive sessions. $^{\#\#}$Significantly different ($p < 0.01$) from the BER-Control group. ****Significantly different ($p < 0.0001$) from the BER-Tone group. Licking microstructures during the Test session: number of licks **(B,C)**, licking duration **(D,E)**, number of clusters **(F,G)**, cluster size **(H,I)**, and cluster duration **(J,K)**. *Significantly different ($p < 0.05$) from the Tone group with the same phenotype. **$p < 0.01$, ****$p < 0.0001$. $^{\$}$Significantly different ($p < 0.05$) from the BER-Tone group.

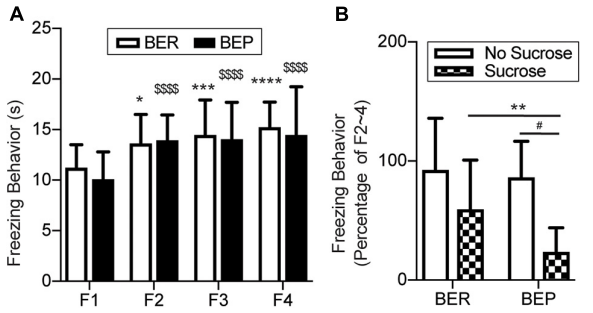

FIGURE 4 | Conditioned fear response in training sessions and the test session. **(A)** Freezing behavior during the Training sessions. *Significantly different ($p < 0.0.5$) from the F1 session within the BER group. ***$p < 0.001$; ****$p < 0.0001$. $^{\$\$\$\$}$Significantly different ($p < 0.0001$) from the F1 session within the BEP group. **(B)** Freezing behavior during the Training sessions normalized to the average freezing behavior of each animal during F2–4. F1–4, Fear Conditioning sessions 1–4. **Significantly ($p < 0.05$) different from the BER-Sucrose group. $^{\#}$Significantly ($p < 0.01$) different from the BEP-No Sucrose group.

In both Ce and BLA of both BEPs and BERs, the *c-fos* mRNA expression was more prominent in Paired groups compared with Non-Paired groups, as shown in the representative photos (**Figure 5A**). Statistical analysis revealed that the Paired groups had higher *c-fos* mRNA expression than the Control and Tone groups in the BLA (**Figure 5B**) and Ce (**Figure 5C**) of both phenotypes whether or not there was sucrose access.

The Lateral Hypothalamic Area Was Activated by the CS

The LHA is located anterior to the ventral tegmental area (VTA), and posterior to the preoptic area. It integrates information from cortical and subcortical regions, such as the amygdala and basal forebrain networks, and consequently mediates some specific behaviors *via* projecting to downstream circuits involved in reward (e.g., the VTA) and feeding regulation (e.g., brain stem motor pattern generator). Two subregions of the LHA were analyzed: the perifornical part (PeFLH) and the posterior lateral part (PLH). In both subregions of both BEPs and BERs, the *c-fos* mRNA expression was higher in the Paired groups than the Non-Paired groups (**Figure 5D**), whether or not there was sucrose access. The *c-fos* mRNA levels in the PLH (**Figure 5E**) and the PLH (**Figure 5F**) demonstrated a significant increase in the Paired groups compared with Non-Paired groups in both phenotypes, whether or not there was sucrose access in the Test session.

The Activation of the Paraventricular Hypothalamic Nucleus by the CS Was Inhibited by Sucrose Intake in the Binge-Like Eating Prone Rats

The PVN is the initiating site of the HPA axis, and neurosecretory neurons in the parvocellular PVN (PVNp) are mainly responsible for the release of corticotropin-releasing factor (CRF) through median eminence in response to stress. The magnocellular component of the PVN (PVNm) releases vasopressin and oxytocin into the systemic circulation upon stress exposure. Two

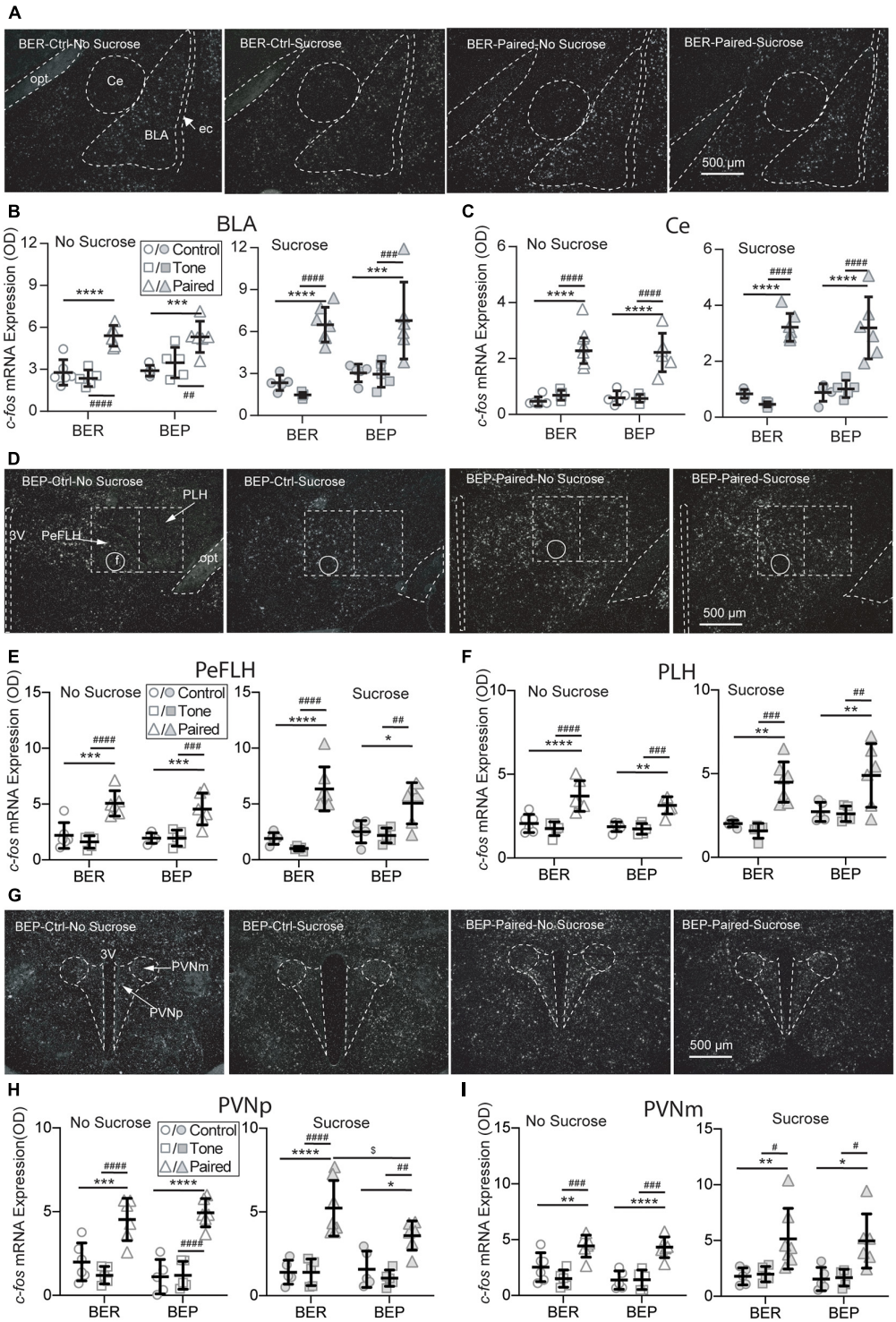

FIGURE 5 | Effects of fear conditioning on the *c-fos* mRNA expression in the amygdala, LHA, and PVN. Representative images of the *c-fos* mRNA *in situ* hybridization signals in the central amygdala (Ce), basal lateral amygdala (BLA), perifornical (PeFLH), and peduncular part (PLH) of the lateral hypothalamus, and parvocellular part (PVNp) and magnocellular part (PVNm) of the paraventricular hypothalamic nucleus marked with broken contours **(A,D,G)**. Relative *c-fos* mRNA expression of No Sucrose and Sucrose groups in the amygdala **(B,C)**, LHA **(E,F)**, and PVN **(H,I)** of BERs and BEPs. 3V, 3rd ventricle; ec, external capsule; f, fornix; opt, the optic tract; rf, rhinal fissure. *Significantly different ($p < 0.05$) from the Control group within the same phenotype. **$p < 0.01$, ***$p < 0.001$, ****$p < 0.0001$. #Significantly different ($p < 0.05$) from the Tone group within the same phenotype. ##$p < 0.01$, ###$p < 0.001$, ####$p < 0.0001$. $Significantly different ($p < 0.05$) from the BER group with the same treatment.

subregions of the PVN were analyzed: the PVNp and PVNm. In both subregions of both BEPs and BERs, the *c-fos* mRNA expression was obviously higher in Paired groups compared with Non-Paired groups, as shown in the representative photos (**Figure 5G**). Regardless of sucrose access, the *c-fos* mRNA expression in the PVNp (**Figure 5H**) and the PVNm (**Figure 5I**) displayed a significant increase in the Paired groups in both phenotypes. With the access to sucrose, the BEP-Paired-Sucrose group had lower *c-fos* mRNA expression than the BER-Paired-Sucrose group in the PVNp (**Figure 5H**-right), while sucrose did not significantly change *c-fos* mRNA expression in the PVNm (**Figure 5I**-right).

Persistent Acb Response to Sucrose in the Binge-Like Eating Prone Rats Under Conditioned Fear

The dorsal striatum is the central component in the neural circuit of processing the information about the contingencies of the reward stimulus and controlling goal-directed learning process, such as instrumental conditioning. It integrates and processes all reward-related information and subsequently optimizes the reward-related responses. As part of the ventral striatum, the Acb makes the outcome-based predictions. It is responsible for predicting the error-based outcome and constantly updating the predictions about reward and punishment. Two subregions of the Acb were analyzed: the core part (AcbC) and the shell part (AcbSh) of the Acb (**Figure 6A**). Without sucrose access, the BEP-Non-Paired group had higher *c-fos* mRNA expression in the AcbC and AcbSh than the BER-Non-Paired group. Moreover, the CS pointedly decreased the *c-fos* mRNA expression in the AcbC and AcbSh of the BEP-Paired group compared with the BEP-Control group (AcbC: $p < 0.001$; AcbSh: $p = 0.007$; **Figures 6B,C**). With the presence of the CS, the BEP-Paired-Sucrose group had significantly lower *c-fos* mRNA expression in the AcbC and AcbSh than the BER-Paired-Sucrose group (**Figure 6B**-right, **Figures 6C**-right).

The mPFC Was Less Recruited in Response to the CS in Binge-Like Eating Prone Rats With Access to Sucrose

The choice of appropriate defensive behavior (e.g., fight/flight) in a dangerous situation is very important for a better chance of surviving. It has been found that the medial prefrontal cortex is involved in shifting from one strategy to another in various kinds of tasks, including selecting proper defensive responding strategies in stressful situations. Two subregions of the mPFC were analyzed: the prelimbic part (PrL) and the infralimbic part (IL) (**Figure 6D**). Without access to sucrose, the *c-fos* mRNA expression in both PrL and IL of the BER-Tone-No Sucrose group was significantly lower than the BER-Control-No Sucrose and BER-Paired-No Sucrose groups (**Figures 6E,F**).

The Bed Nucleus of the Stria Terminalis Responded to the CS Only in the Binge-Like Eating Prone Rats

The BNST is composed of a large number of subregions with different functions in stress responding. For example, the anteroventral BNST is highly involved in HPA axis activation. Lesions of this subregion diminish the PVN activation and compress the HPA axis response to restrain the impacts of stress. The anterolateral BNST CRF-expressing neurons project to the PVN, indicating a central modulation action of CRF on the HPA axis. Two subregions of the BNST were analyzed: the dorsal part (STD) and the ventral part (STV) (**Figure 6G**). The BEP-Paired groups showed significantly lower *c-fos* mRNA expression in the STD (**Figure 6H**) and STV (**Figure 6I**) than the BEP-Control groups, regardless of sucrose access.

Sucrose Showed Differentiated Effects on the Neural Activities Between Binge-Like Eating Resistant Rats and Binge-Like Eating Prone Rats

Sucrose intake had a tendency to increase *c-fos* mRNA expression in the Ce of both BEPs ($p = 0.060$) and BERs ($p = 0.060$) under conditioned fear (**Figure 7A2**), but this tendency was not as obvious in the BLA (**Figure 7A1**) as in the Ce. Therefore, the amygdala only responded to the CS, and it was not influenced by the phenotype or sucrose intake. The LHA has long been known as a feeding regulation center. Under conditioned fear, the BEPs responded to sucrose access with increased *c-fos* mRNA expression in the PLH ($p = 0.046$), which was not found in the BERs (**Figure 7B2**). This differentiation between BERs and BEPs was not observed in the PeFLH (**Figure 7B1**). Moreover, sucrose intake decreased the *c-fos* mRNA expression in response to the CS in the BEPs relative to the BERs in the PVNp (**Figure 7C1**), but not in the PVNm (**Figure 7C2**).

The BEP-Paired group responded to sucrose with significantly lower *c-fos* mRNA expression in the AcbC and AcbSh compared with the BER-Paired group (**Figures 7D1**, D2). Moreover, sucrose access decreased the *c-fos* mRNA expression in the BEP-Paired-Sucrose group relative to the BEP-Paired-No Sucrose group in the PrL ($p = 0.028$; **Figure 7E1**), but not in the IL (**Figure 7E2**). Finally, the sucrose did not change the *c-fos* mRNA expression in the STD and STV of both phenotypes (data not shown).

DISCUSSION

Compulsive Eating Was Confirmed in Our Binge-Like Eating Rat Model

In this study, a conflicting situation was created with an aversive CS and palatable food. Consistent with our first hypothesis in the Section "Introduction," the BEPs showed higher sucrose consumption and lower fear response relative to the BER rats in the presence of the CS during the Test session. However, there actually existed two possible explanations for this result: (1) The higher sucrose intake in BEPs relative to BERs was a result of lower sensitivity to the CS in BEPs. (2) The BEPs had higher motivation for sucrose than the BERs, which overcame the fear for the CS and sucrose had a stronger anxiolytic effect on the BEPs relative to the BERs, which diminished their fear response to the CS. The second explanation was exactly our hypothesis. To confirm our hypothesis, we had to exclude the possibility of the first explanation. To solve this problem, we set the No Sucrose groups as a control. We can see that the freezing behavior was

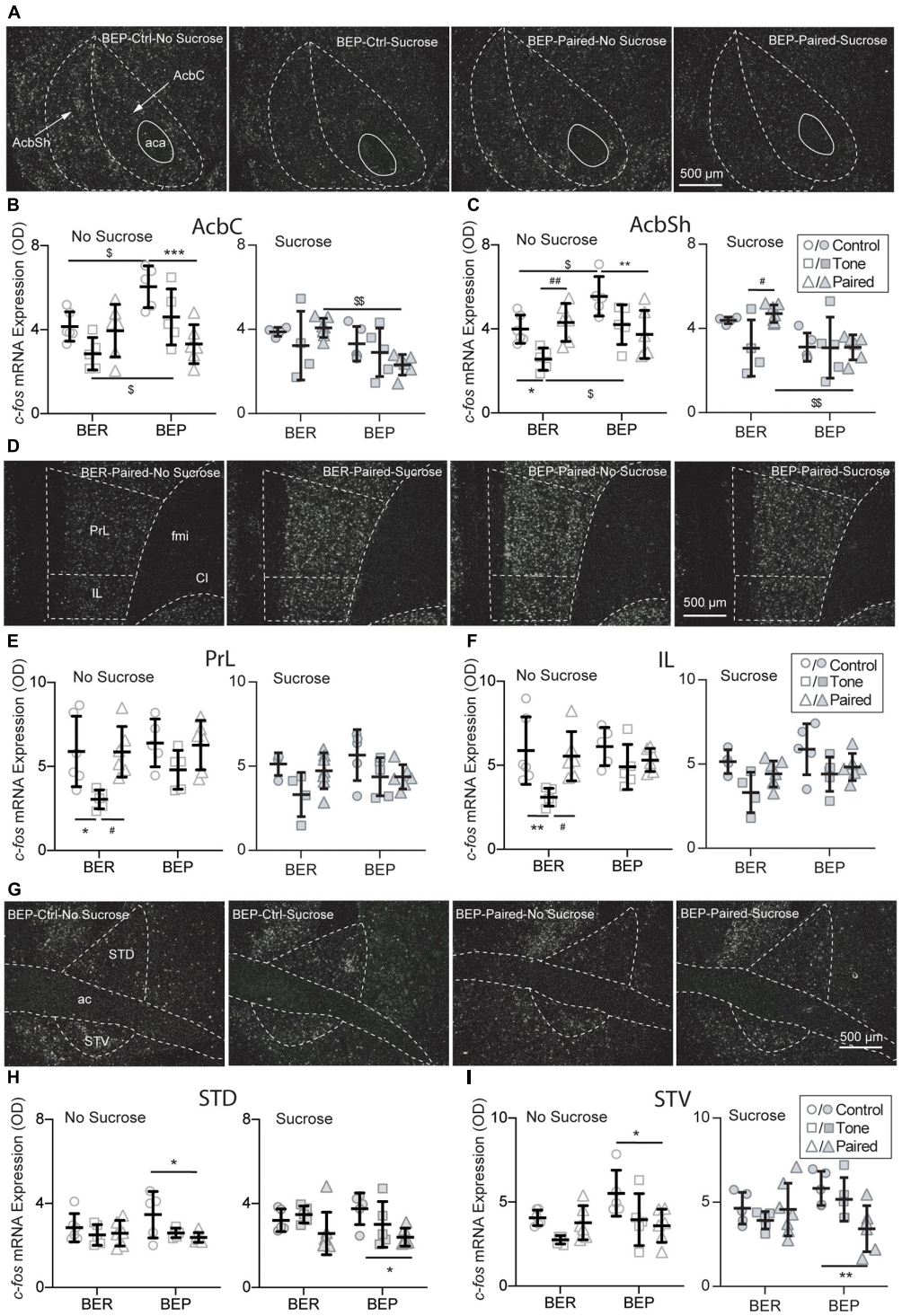

FIGURE 6 | Effects of fear conditioning on the *c-fos* mRNA expression in the Acb, mPFC, and BNST. Representative images of the *c-fos* mRNA *in situ* hybridization signals with the core (AcbC) and shell (AcbSh) part of the nucleus accumbens (Acb), the prelimbic part (PrL), and infralimbic (IL) part of the medial prefrontal cortex (mPFC), and the dorsal part (STD) and ventral (STV) part of the bed nucleus of stria terminalis (BNST) marked with broken contours **(A,D,G)**. Relative *c-fos* mRNA expression of No Sucrose and Sucrose groups and Paired groups in the Acb **(B,C)**, mPFC **(E,F)**, and BNST **(H,I)** of BERs and BEPs. ac, anterior commissure; aca, anterior part of the anterior commissure; LV, lateral ventricle; ic, internal capsule; fmi, forceps minor of the corpus callosum; CI, claustrum. *Significantly different ($p < 0.05$) from the Control group with the same phenotype. **$p < 0.01$, ***$p < 0.001$. #Significantly different ($p < 0.05$) from the Tone group with the same phenotype. ##$p < 0.01$. $Significantly different ($p < 0.05$) from the BER group with the same treatment. $$$p < 0.01$.

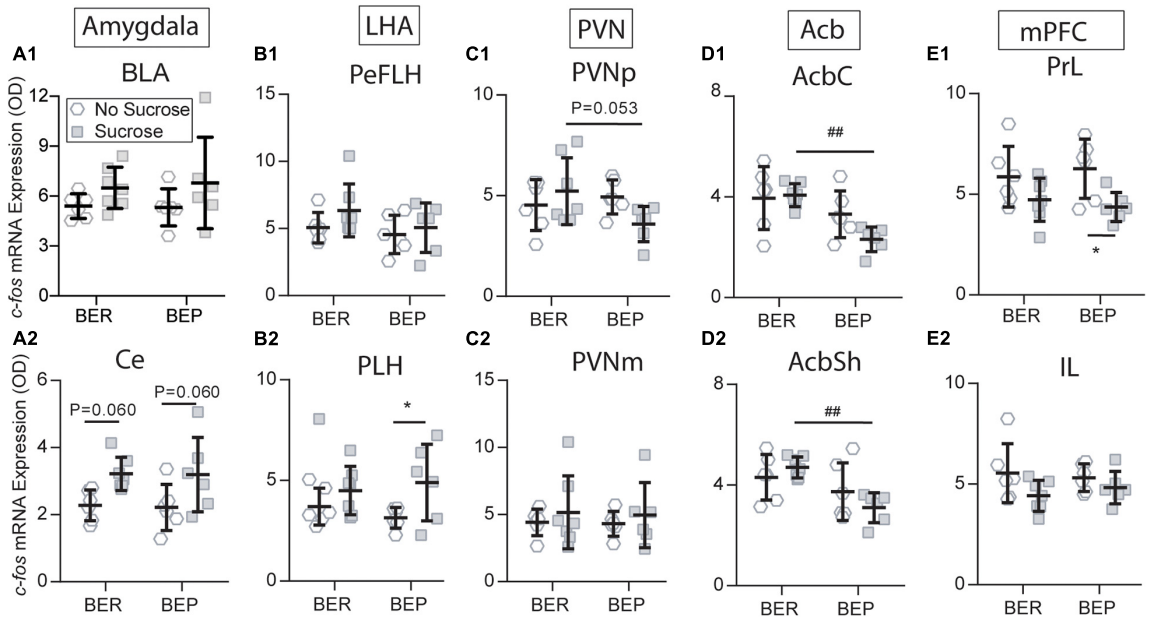

FIGURE 7 | Sucrose changed the *c-fos* expression in response to the fear conditioning in the amygdala **(A1,A2)**, LHA **(B1,B2)**, PVN **(C1,C2)**, Acb **(D1,D2)**, and mPFC **(E1,E2)**. Acb, nucleus accumbens; AcbC, nucleus accumbens core; AcbSh, nucleus accumbens shell; BLA, basolateral amygdala; Ce, central amygdala; IL, infralimbic mPFC; LHA, lateral hypothalamus; mPFC, medial prefrontal cortex; PeFLH, perifornical part of the lateral hypothalamus; PLH, peduncular part of the lateral hypothalamus; PrL, prelimbic mPFC; *significantly different ($p < 0.05$) from the BEP-No Sucrose group. ##Significantly different ($p < 0.01$) from the BER-Sucrose group.

comparable between BEPs and BERs when they had no access to sucrose during both Fear Conditioning training sessions and the Test session. This finding perfectly confirmed that BERs and BEPs had comparable sensitivity to the CS and that the attenuated effects of the CS were indeed a result of abnormally high motivation for sucrose in the BEPs. Combined with the decreased freezing behavior in BEP-Paired-Sucrose rats, it also indicated a stronger anxiolytic effect of sucrose on the BEPs relative to the BERs.

Until now, we have observed all aspects of compulsive eating in the BEPs in our BED rat model: habitual overeating in the Appetitive sessions, as well as overeating to relieve negative sensation and overeating despite aversive consequences in the Test session. In an acute stressful environment, the animals have to recruit their energy and attention for a swift and proper response, and concurrently inhibit other housekeeping activities such as food intake, digestion, and reproduction. In the BERs, the conditioned fear inhibited the licking behavior not only during tones but also between tones, a relatively less stressful but uncertain situation. In the BEPs, the licking behavior was not affected between tones, suggesting a deficiency of devaluating the palatable food when confronted with potential dangers. Similarly, both humans and animals with eating disorders appear to have some struggles in suppressing food-seeking and -taking in an emergent situation (Oswald et al., 2011). Overeating of palatable food despite aversive consequence happens when an abnormally high motivation for palatable food inhibits the normal function of the stress-responding system (Voon, 2015).

Exploration of Neural Mechanisms Underlying the Compulsive Eating

To understand the neural mechanisms underlying the different feeding and freezing behavior under conditioned fear, we analyzed the *c-fos* mRNA expression in brain regions involved in stress responding, feeding regulation, and reward processing. In **Figures 5**, **6**, we tested two factors, phenotype and fear conditioning, to see whether the analyzed brain regions of BER and BEP respond differently to fear conditioning when they had no access to sucrose, or when they had access to sucrose. In this way, we can know if there is a difference between BER and BEP rats in their brain activities in response to fear conditioning, without considering the effect of sucrose access. In **Figure 7**, we put together all four Paired groups and tested two other factors, phenotype and sucrose, to see if sucrose can change the brain activities in response to fear conditioning and if this effect is different between BER and BEP rats. Consistent with our second hypothesis in the Section "Introduction," we found different neuronal activities in many brain regions between BERs and BEPs that could be underlying their different sucrose consumption and freezing behavior under conditioned fear.

The Acb, Medial Prefrontal Cortex, and Lateral Hypothalamic Area Were Possibly Underlying the Abnormally High Motivation for Sucrose in the Binge-Like Eating Prone Rats

Higher tonic Acb activity might be underlying the habitual overeating of the BEPs. Distinct cell types and input projections

in the Acb are in charge depending on the availability of palatable food, representing productive and unproductive rewarding seeking (Lafferty et al., 2020). A popular hypothesis is that the hyperpolarization of medial spinal neurons (MSNs) in the Acb is primarily underlying the appetitive motivation (wanting), and inhibition of these GABAergic neurons can disinhibit the downstream targets, such as the ventral pallidum, VTA, and LHA, and promote hedonic responses (liking) and continuation of feeding behaviors (Castro et al., 2015). Extended access to palatable food can induce hyperphagia and compulsive eating in rats, accompanied by gradually worsened responsiveness of reward system, decreased baseline extracellular dopamine in the Acb (van de Giessen et al., 2014), and downregulated striatal dopamine D2 receptors (D2Rs) (Johnson and Kenny, 2010). Considering the inhibitory function of the D2Rs, these changes could decrease the tonic inhibition of the Acb, and possibly contributed to the higher baseline Acb activity in the BEPs.

Consistently, without the stimulation of CS and sucrose, the BEPs showed a higher baseline activity in the Acb compared with the BERs, indicating a stronger motivation for palatable food in an environment where sucrose was usually available. Thus, we propose that tonic reward response was diminished in the BEPs, and consequently, they had to eat more and faster to activate the reward system. It could drive a higher motivation and expectation for sucrose in the BEPs, which could explain the shorter first lick latency of the BEPs when they got access to sucrose. We hypothesize that the hyperactivity of the Acb of BEPs in "resting state" reflected higher motivation (wanting) for sucrose when it is unavailable (unproductive seeking), while the larger amplitude of decrease of the Acb activation might exaggerate hedonic rewarding value of sucrose (liking) in BEPs.

The persistent hedonic response in the Acb and diminished recruitment of the mPFC in the presence of palatable food in the BEPs were possibly underlying their deficient devaluation of palatable food in face of aversive consequences. It is also well known that inhibition of the Acb increased, and stimulation decreased, intake of food (Chometton et al., 2020; Yang, 2021). Under conditioned fear, the sucrose failed to significantly inhibit the activity of the Acb in BERs. It indicates that the dynamic function of the Acb depends on the current salience of stimuli and that the hedonic value of sucrose for BER decreased in the face of the CS. We can comprehend this disrupted hedonic response as an evidence of devaluation of palatable food in the presence of aversive stimuli. Increased activity of the projection from the AcbSh D1R (dopamine type 1 receptor expressing) MSNs to the LHA GABA neurons has been proven underlying the inhibition of feeding behavior by salient external stimuli (O'Connor et al., 2015). On the contrary, the CS did not change the pattern of responding to sucrose in the BEPs, suggesting a resistance to the devaluation of palatable food by potential aversive consequences.

Considering its reciprocal connections with the amygdala and dense projections to the LHA and Acb, the mPFC may also play an important role in devaluating the palatable food under a stressful situation, and modulating value-based decision-making. A recent study (Christoffel et al., 2021) found that anterior paraventricular thalamus (aPVT) and mPFC projections to the Acb differentially regulate the rewarding properties of high-fat food. Inhibition of the glutamatergic mPFC-Acb projection promotes the acquisition of binge eating on high-fat food, while stimulating the same project would suppress the hedonic feeding. Consistently, the BEPs in this study displayed inhibited PrL activity with access to sucrose under conditioned fear, but not the BERs. This decreased PrL activity in the BEPs was very likely responsible for their deficient decision-making adjustment and persistent sucrose intake under the conditioned fear.

The PVNp Was Likely an Important Target of Sucrose for Its Stronger Anxiolytic Effects on the Binge-Like Eating Prone Rats

The amygdala and BNST were not likely the target of sucrose for its anxiolytic effects. For many years, the amygdala has been considered as the emotional center, especially for coding the conditioned fear response. Consistent with the functions of the BLA and Ce in the fear conditioning acquisition and expression, respectively, the CS activated both of them without any difference between the BERs and BEPs. This is consistent with the comparable fear response of the BEPs and BERs in Fear Conditioning sessions and the Test session when they had no access to sucrose. Petrovich previously showed that lesions of the Ce, not the BLA, abolished the feeding-inhibiting effect of an aversive CS (Petrovich et al., 2009). Consistent with this special function of the Ce, this study found that the Ce further increased its activity in response to sucrose access in the presence of an aversive cue, compared with the cue itself. It indicated the involvement of the Ce in the devaluation of palatable food in face of potential aversive consequences. Surprisingly, compared with Paired-No Sucrose groups, the activities of the BLA and Ce in Paired-Sucrose groups of BER and BEP rats were not inhibited by sucrose intake in this study, suggesting that the amygdala is not likely the functioning site of the anxiolytic effects of palatable foods, or at least indicating that we need to look into the activities of subtypes of neurons for the underlying mechanisms.

The BNST is part of the "extended amygdala," along with the Ce and caudal Acb. Substantial evidence supports the involvement of the BNST in the fear and anxiety response to conditioned and unconditioned stimuli. The BNST controls the stress-induced seeking and consumption of drugs and palatable food by receiving stress information from the Ce (Erb et al., 2001) and projecting to the VTA (Kudo et al., 2012). In human patients, the severe obsessive–compulsive disorder could be alleviated by electrical deep brain stimulation in the BNST (Luyten et al., 2016).

In this study, sucrose intake inhibited the *c-fos* mRNA expression in the Acb of the BEPs, but not in the BERs. The BEPs showed decreased BNST activity in response to the CS, but not BERs. Lesions of the BNST did not affect the fear response to an aversively conditioned sound, but decreased the response to another unconditioned sound, indicating a fear-generalization function of the BNST (Duvarci et al., 2009). Considering this discrimination inhibitory effect of the BNST, its lower activity in the BEPs during the Test session might explain the unaffected licking behavior of BEP-Paired rats between tones compared with BER-Paired rats. This different BNST response to the CS between

the BEPs and the BERs was observed even without sucrose access, suggesting different stress responding strategies between phenotypes, which might be involved in the development of stress-induced overeating in BEPs. Anyway, the sucrose access failed to induce significant change in the activity of the BNST in BERs and BEPs under conditioned fear, excluding it as a direct functioning site of sucrose for an anxiolytic effect.

The enhanced anxiolytic effect of sucrose on the BEPs was regulated by diminished PVNp response to the CS by sucrose access. As part of the HPA axis, the neuroendocrine neurons of the PVN are responsible for the secretion of CRF and vasopressin in response to stress stimuli. Not surprisingly, in Paired groups, the CS significantly upregulated the *c-fos* mRNA expression in the PVN of both BEPs and BERs, which is consistent with many previous IEG-based (immediate early gene-based) mapping studies (Honkaniemi et al., 1994). It is also known that palatable food, such as sucrose and lard, could attenuate the stimulating effect of stress on the HPA axis (Foster et al., 2008). In this study, sucrose ingestion attenuated the PVNp response to stress in the BEPs compared with the BERs. This result is consistent with the freezing behavior. However, similar to the amygdala, there is no evidence showing that the PVNp directly controls the freezing behavior. Nevertheless, we can still hypothesize that sucrose has a stronger anxiolytic effect on the BEPs than the BERs, which can also explain the higher sucrose intake of the BEPs during the phenotype classification. Decreased HPA axis response to stress in the BEPs has been observed in another study with the BED rat model, demonstrating as attenuated plasm corticosterone, and CRF mRNA expression in the PVN in response to the foot shock stress (Calvez et al., 2016). The parvocellular part of the PVN sends glutamatergic projections to the Acb, and pharmacogenetic stimulation of the PVN–Acb projections can decrease the intake of highly palatable food (Smith et al., 2020). These findings are consistent with results in this study. In conclusion, the hedonic value of palatable food has strong anxiolytic effect *via* inhibiting the PVN activity; conversely, the mental status regulates the hedonic value of palatable food *via* the PVN–Acb pathway.

The Feeding Center Lateral Hypothalamic Area Was Possibly an Integrating Site of Rewarding and Stress Responding Information to Regulate the Compulsive Eating in the Binge-Like Eating Prone Rats

Studies with the retrograde tracing technique revealed that the BLA and Ce send projections to the ventral and dorsal LHA, respectively (Reppucci and Petrovich, 2016). Noxious stimulation increases *c-fos* expression in the LHA (Bullitt, 1990), and lesions of the LHA significantly decrease arterial pressure response to a CS (LeDoux et al., 1988). The activation of the LHA by CS in this study was likely induced by activating projections from the amygdala and might play a role in the devaluation of sucrose by projecting to the ventral tegmental area (VTA) (Nieh et al., 2015, 2016). Moreover, the LHA is recognized as the feeding center, and it receives the leptin information from the arcuate nucleus (ARC) and changes the hedonic value of the nutrition, which is important for the regulation of homeostatic feeding, *via* projections to the reward areas, such as the VTA (Domingos et al., 2013). The post-ingestive rewarding effect of sucrose might be the response for the increase of PLH activity of the BEPs under conditioned fear that likely contributed to the inhibiting effect of sucrose on the freezing behavior. Thus, we conclude that the CS also had a strong impact on the activity of the LHA, and under the conditioned fear, the abnormally higher PLH activity in the BEPs finally drove their compulsive eating.

In conclusion, the response of Acb and mPFC to the palatable food is dynamically modulated by the current value of the food and that the Acb and mPFC participate in coding for the devaluation of palatable food in the face of potential aversive consequences. The compulsive eating observed in the BEPs was likely facilitated by deficits in devaluating the rewarding effects of sucrose, represented by attenuated recruitment of the mPFC, persistent Acb response to sucrose intake, and increased LHA activity in stressful situations. The interaction between the rewarding system and the stress responding system facilitates the development of the BEP phenotype, leading to abnormally high motivation for binging on high-sugar and high-fat diet over healthier food. When the hedonic system hijacks the homeostatic system and the stress-responding system, compulsive eating will attenuate the normal response to potential aversive consequences.

Drawbacks of This Study

This study used female rats, rather than male rats, because the prevalence of the BED is higher in women compared to men (Cossrow et al., 2016). However, this choice leads to an inevitable problem—the estrus cycle and hormone fluctuations in female animals. The fear response and food intake of the female rats in this study might have been influenced by the estrous phase of individual animals in the Test session. Unfortunately, the estrous phase was not taken into consideration in this study, because excluding some animals from each group, especially the control groups, or separating them into subgroups according to their estrous phases would make the sample size too small for statistical analysis. Future studies with a larger number of animals are necessary to solve this problem.

Fear Conditioning Test as a Good Paradigm for Analyzing Compulsive Eating

To our knowledge, this is the first study that combined the fear conditioning and binge eating animal model to observe the impulsivity of binge eating, and explored the neuronal activities underlying the regulation of feeding behavior, fear response, and compulsive eating under a stressful situation. The fear conditioning paradigm has many advantages over direct foot shock. For example, if we want to do some electrophysiological recording during the aversive stimulus, the foot shock will generate noise in the signals, and even damage the amplifiers, which can be avoided with the conditioned cues, such as light and sound. Our findings indicate some potential targets for the treatment of the BED. For example, we can suppress the craving for palatable food by decreasing the baseline activity of the Acb and enhance the devaluation of palatable food by increasing the recruitment of the mPFC, and modifying the Acb response

to palatable food. The conflicting test with fear conditioning paradigm developed in this study can provide a useful tool to explore the brain and endocrine mechanisms of the occurrence of the BED, and may provide a platform to test and compare the pharmacotherapies to suppress the compulsive eating of palatable foods.

DATA AVAILABILITY STATEMENT

The original contributions presented in the study are included in the article/supplementary material, further inquiries can be directed to the corresponding authors.

ETHICS STATEMENT

The animal study was reviewed and approved by the institutional Université Laval Animal Care Committee, Laval University, Quebec, Canada. The ethics number is 2017-013-1.

AUTHOR CONTRIBUTIONS

All authors listed have made a substantial, direct, and intellectual contribution to the work, and approved it for publication.

FUNDING

This project was financially supported by the Canadian Institutes of Health Research (CIHR, IC094843). ZL receives a scholarship from the China Scholarship Council (CSC).

ACKNOWLEDGMENTS

The authors acknowledge Christophe Lenglos for the MATLAB scripts for analyzing the optical density of *c-fos in situ* hybridization signals. Thanks to Yusang Liu for revising the manuscript.

REFERENCES

Bogduk, N. (2013). "Diagnostic and statistical manual of mental disorders," in *Encyclopedia of Pain*, eds B. N. L. Elbow, M. Johnson, and N. Bogduk (Berlin: Springer), 979–982.

Bullitt, E. (1990). Expression of c-fos-like protein as a marker for neuronal activity following noxious stimulation in the rat. *J. Comp. Neurol.* 296, 517–530. doi: 10.1002/cne.902960402

Calvez, J., and Timofeeva, E. (2016). Behavioral and hormonal responses to stress in binge-like eating prone female rats. *Physiol. Behav.* 157, 28–38. doi: 10.1016/j.physbeh.2016.01.029

Calvez, J., De Ávila, C., Guèvremont, G., and Timofeeva, E. (2016). Stress differentially regulates brain expression of corticotropin-releasing factor in binge-like eating prone and resistant female rats. *Appetite* 107, 585–595. doi: 10.1016/j.appet.2016.09.010

Castro, D. C., Cole, S. L., and Berridge, K. C. (2015). Lateral hypothalamus, nucleus accumbens, and ventral pallidum roles in eating and hunger: interactions between homeostatic and reward circuitry. *Front. Syst. Neurosci.* 9:90. doi: 10.3389/fnsys.2015.00090

Chometton, S., Guèvremont, G., Seigneur, J., Timofeeva, E., and Timofeev, I. (2020). Projections from the nucleus accumbens shell to the ventral Pallidum are involved in the control of sucrose intake in adult female rats. *Brain Struct. Funct.* 225, 2815–2839. doi: 10.1007/s00429-020-02161-z

Christoffel, D. J., Walsh, J. J., Heifets, B. D., Hoerbelt, P., Neuner, S., Sun, G., et al. (2021). Input-specific modulation of murine nucleus accumbens differentially regulates hedonic feeding. *Nat. Commun.* 12:2135. doi: 10.1038/s41467-021-22430-7

Cossrow, N., Pawaskar, M., Witt, E. A., Ming, E. E., Victor, T. W., Herman, B. K., et al. (2016). Estimating the prevalence of binge eating disorder in a community sample from the United States: comparing DSM-IV-TR and DSM-5 criteria. *J. Clin. Psychiatry* 77, e968–e974. doi: 10.4088/JCP.15m10059

De Ávila, C., Chometton, S., Lenglos, C., Calvez, J., Gundlach, A. L., and Timofeeva, E. (2018). Differential effects of relaxin-3 and a selective relaxin-3 receptor agonist on food and water intake and hypothalamic neuronal activity in rats. *Behav. Brain Res.* 336, 135–144. doi: 10.1016/j.bbr.2017.08.044

Domingos, A. I., Sordillo, A., Dietrich, M. O., Liu, Z.-W., Tellez, L. A., Vaynshteyn, J., et al. (2013). Hypothalamic melanin concentrating hormone neurons communicate the nutrient value of sugar. *Elife* 2:e01462. doi: 10.7554/eLife.01462

Duvarci, S., Bauer, E. P., and Paré, D. (2009). The bed nucleus of the stria terminalis mediates inter-individual variations in anxiety and fear. *J. Neurosci.* 29, 10357–10361. doi: 10.1523/JNEUROSCI.2119-09.2009

Erb, S., Salmaso, N., Rodaros, D., and Stewart, J. (2001). A role for the CRF-containing pathway from central nucleus of the amygdala to bed nucleus of the stria terminalis in the stress-induced reinstatement of cocaine seeking in rats. *Psychopharmacology* 158, 360–365. doi: 10.1007/s002130000642

Foster, M. T., Warne, J. P., Ginsberg, A. B., Horneman, H. F., Pecoraro, N. C., Akana, S. F., et al. (2008). Palatable foods, stress, and energy stores sculpt corticotropin-releasing factor, adrenocorticotropin, and corticosterone concentrations after restraint. *Endocrinology* 150, 2325–2333. doi: 10.1210/en.2008-1426

Honkaniemi, J., Kononen, J., Kainu, T., Pyykönen, I., and Pelto-Huikko, M. (1994). Induction of multiple immediate early genes in rat hypothalamic paraventricular nucleus after stress. *Mol. Brain Res.* 25, 234–241. doi: 10.1016/0169-328x(94)90158-9

Johnson, P. M., and Kenny, P. J. (2010). Dopamine D2 receptors in addiction-like reward dysfunction and compulsive eating in obese rats. *Nat. Neurosci.* 13, 635–641. doi: 10.1038/nn.2519

Kovács, K. J. (1998). Invited review c-Fos as a transcription factor: a stressful (re) view from a functional map. *Neurochem. Int.* 33, 287–297. doi: 10.1016/s0197-0186(98)00023-0

Kudo, T., Uchigashima, M., Miyazaki, T., Konno, K., Yamasaki, M., Yanagawa, Y., et al. (2012). Three types of neurochemical projection from the bed nucleus of the stria terminalis to the ventral tegmental area in adult mice. *J. Neurosci.* 32, 18035–18046. doi: 10.1523/JNEUROSCI.4057-12.2012

Lafferty, C. K., Yang, A. K., Mendoza, J. A., and Britt, J. P. (2020). Nucleus accumbens cell type-and input-specific suppression of unproductive reward seeking. *Cell Rep.* 30, 3729–3742.e3723. doi: 10.1016/j.celrep.2020.02.095

LeDoux, J. E., Iwata, J., Cicchetti, P., and Reis, D. (1988). Different projections of the central amygdaloid nucleus mediate autonomic and behavioral correlates of conditioned fear. *J. Neurosci.* 8, 2517–2529. doi: 10.1523/JNEUROSCI.08-07-02517.1988

Luyten, L., Hendrickx, S., Raymaekers, S., Gabriëls, L., and Nuttin, B. (2016). Electrical stimulation in the bed nucleus of the stria terminalis alleviates severe obsessive-compulsive disorder. *Mol. Psychiatry* 21:1272. doi: 10.1038/mp.2015.124

Maniam, J., and Morris, M. J. (2012). The link between stress and feeding behaviour. *Neuropharmacology* 63, 97–110. doi: 10.1016/j.neuropharm.2012.04.017

Moore, C. F., Sabino, V., Koob, G. F., and Cottone, P. (2017). Neuroscience of compulsive eating behavior. *Front. Neurosci.* 11:469. doi: 10.3389/fnins.2017.00469

Nieh, E. H., Matthews, G. A., Allsop, S. A., Presbrey, K. N., Leppla, C. A., Wichmann, R., et al. (2015). Decoding neural circuits that control compulsive sucrose seeking. *Cell* 160, 528–541. doi: 10.1016/j.cell.2015.01.003

Nieh, E. H., Vander Weele, C. M., Matthews, G. A., Presbrey, K. N., Wichmann, R., Leppla, C. A., et al. (2016). Inhibitory input from the lateral hypothalamus to the ventral tegmental area disinhibits dopamine neurons and promotes behavioral activation. *Neuron* 90, 1286–1298. doi: 10.1016/j.neuron.2016.04.035

O'Connor, E. C., Kremer, Y., Lefort, S., Harada, M., Pascoli, V., Rohner, C., et al. (2015). Accumbal D1R neurons projecting to lateral hypothalamus authorize feeding. *Neuron* 88, 553–564. doi: 10.1016/j.neuron.2015.09.038

Oswald, K. D., Murdaugh, D. L., King, V. L., and Boggiano, M. M. (2011). Motivation for palatable food despite consequences in an animal model of binge eating. *Int. J. Eat. Disord.* 44, 203–211. doi: 10.1002/eat.20808

Pecoraro, N., Reyes, F., Gomez, F., Bhargava, A., and Dallman, M. F. (2004). Chronic stress promotes palatable feeding, which reduces signs of stress: feedforward and feedback effects of chronic stress. *Endocrinology* 145, 3754–3762. doi: 10.1210/en.2004-0305

Petrovich, G. D., Ross, C. A., Mody, P., Holland, P. C., and Gallagher, M. (2009). Central, but not basolateral, amygdala is critical for control of feeding by aversive learned cues. *J. Neurosci.* 29, 15205–15212. doi: 10.1523/jneurosci.3656-09.2009

Poulin, A.-M., and Timofeeva, E. (2008). The dynamics of neuronal activation during food anticipation and feeding in the brain of food-entrained rats. *Brain Res.* 1227, 128–141. doi: 10.1016/j.brainres.2008.06.039

Reppucci, C. J., and Petrovich, G. D. (2016). Organization of connections between the amygdala, medial prefrontal cortex, and lateral hypothalamus: a single and double retrograde tracing study in rats. *Brain Struct. Funct.* 221, 2937–2962. doi: 10.1007/s00429-015-1081-0

Simmons, D. M., Arriza, J. L., and Swanson, L. (1989). A complete protocol for in situ hybridization of messenger RNAs in brain and other tissues with radiolabeled single-stranded RNA probes. *J. Histotechnol.* 12, 169–181. doi: 10.1179/014788889794651870

Smith, A. E., Ogunseye, K. O., Debenedictis, J. N., Peris, J., Kasper, J. M., and Hommel, J. D. (2020). Glutamatergic projections from homeostatic to hedonic brain nuclei regulate intake of highly palatable food. *Sci. Rep.* 10:22093. doi: 10.1038/s41598-020-78897-9

van de Giessen, E., Celik, F., Schweitzer, D. H., Van Den Brink, W., and Booij, J. (2014). Dopamine D2/3 receptor availability and amphetamine-induced dopamine release in obesity. *J. Psychopharmacol.* 28, 866–873. doi: 10.1177/0269881114531664

Voon, V. (2015). Cognitive biases in binge eating disorder: the hijacking of decision making. *CNS Spectr.* 20, 566–573. doi: 10.1017/S1092852915000681

Yang, B. (2021). When to stop eating: an auxiliary brake on food consumption from the nucleus accumbens. *J. Neurosci.* 41, 1847–1849. doi: 10.1523/JNEUROSCI.1666-20.2020

Conflict of Interest: The authors declare that the research was conducted in the absence of any commercial or financial relationships that could be construed as a potential conflict of interest.

Publisher's Note: All claims expressed in this article are solely those of the authors and do not necessarily represent those of their affiliated organizations, or those of the publisher, the editors and the reviewers. Any product that may be evaluated in this article, or claim that may be made by its manufacturer, is not guaranteed or endorsed by the publisher.

frontiers in Neuroscience

ORIGINAL RESEARCH
published: 30 November 2021
doi: 10.3389/fnins.2021.748186

Ontogeny of the Projections From the Dorsomedial Division of the Anterior Bed Nucleus of the Stria Terminalis to Hypothalamic Nuclei

*Marc Lanzillo†, Manon Gervais† and Sophie Croizier**

Center for Integrative Genomics, University of Lausanne, Lausanne, Switzerland

OPEN ACCESS

Edited by:
Claude Knauf,
Université Toulouse III Paul Sabatier, France

Reviewed by:
Carmelo Quarta,
Institut National de la Santé et de la Recherche Médicale (INSERM), France
Lionel Carneiro,
The Ohio State University, United States

***Correspondence:**
Sophie Croizier
sophie.croizier@unil.ch

† These authors have contributed equally to this work

Specialty section:
This article was submitted to Neuroenergetics, Nutrition and Brain Health, a section of the journal Frontiers in Neuroscience

Received: *27 July 2021*
Accepted: *27 October 2021*
Published: *30 November 2021*

Citation:
Lanzillo M, Gervais M and Croizier S (2021) Ontogeny of the Projections From the Dorsomedial Division of the Anterior Bed Nucleus of the Stria Terminalis to Hypothalamic Nuclei. Front. Neurosci. 15:748186. doi: 10.3389/fnins.2021.748186

The bed nucleus of the stria terminalis (BNST) is a telencephalic structure well-connected to hypothalamic regions known to control goal-oriented behaviors such as feeding. In particular, we showed that the dorsomedial division of the anterior BNST innervate neurons of the paraventricular (PVH), dorsomedial (DMH), and arcuate (ARH) hypothalamic nuclei as well as the lateral hypothalamic area (LHA). While the anatomy of these projections has been characterized in mice, their ontogeny has not been studied. In this study, we used the DiI-based tract tracing approach to study the development of BNST projections innervating several hypothalamic areas including the PVH, DMH, ARH, and LHA. These results indicate that projections from the dorsomedial division of the anterior BNST to hypothalamic nuclei are immature at birth and substantially reach the PVH, DMH, and the LHA at P10. In the ARH, only sparse fibers are observed at P10, but their density increased markedly between P12 and P14. Collectively, these findings provide new insight into the ontogeny of hypothalamic circuits, and highlight the importance of considering the developmental context as a direct modulator in their proper formation.

Keywords: DiI-based tract tracing, ontogeny, bed nuclei of the stria terminalis, PVH, DMH, ARH, LHA

INTRODUCTION

The bed nucleus of the stria terminalis (BNST), a complex forebrain structure, has long been involved in stress- and anxiety-related behaviors (Walker et al., 2003). The BNST receives strong connections from the prefrontal cortex and the amygdala (Dong et al., 2001), and project in turn onto hypothalamic nuclei that mediate goal-oriented behaviors (Dong and Swanson, 2006; Barbier et al., 2021). Indeed, the dorsomedial part of the anterior BNST strongly projects onto the paraventricular (PVH), the dorsomedial (DMH), the arcuate (ARH) nuclei, and the lateral hypothalamic area (LHA). In particular, nociceptin-expressing neurons of the dorsomedial part of the BNST control feeding throughout arcuate AgRP neurons (Smith et al., 2019). In addition, corticotropin-releasing hormone (CRH)- and cholecystokinin (CCK)-expressing neurons of the dorsal part of the anterior BNST regulate aversive and appetitive behaviors via neurons of the

LHA, including Orexin-expressing neurons (Jennings et al., 2013; Giardino et al., 2018). While we start to know more about the anatomy and the functional role of these projections, when the projections from the dorsomedial part of the anterior BNST to the aforementioned hypothalamic nuclei develop is still unknown.

Our work highlighted a postnatal formation of the neurocircuits arising from the dorsomedial part of the anterior BNST and innervating the PVH, DMH, ARH, and LHA. This study will serve as a developmental basis to further evaluate long-lasting functions supported by these neuronal networks, and how alteration of maternal environment can precipitate the onset of metabolic and anxiety-related disorders in adulthood.

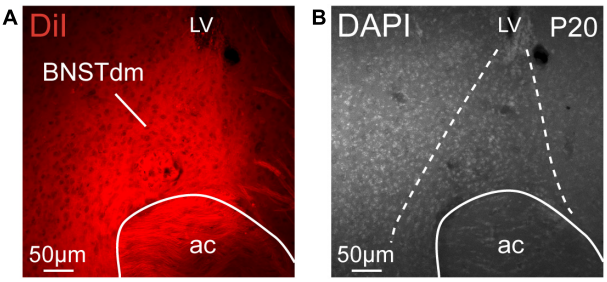

FIGURE 1 | (A) Low magnification confocal image showing the distribution of DiI in the dorsomedial part of the anterior BNST (BNSTdm) of a P20 male mouse. **(B)** Low magnification image of a DAPI staining showing the cytoarchitectonic purposes of the BNSTdm. Dashed lines indicate the limit of the BNSTdm. ac, anterior commissure; LV, lateral. Scale bars are shown in the figure.

MATERIALS AND METHODS

Animals and Tissue Preparation

All experimental procedures were approved by the Veterinary Office of Canton de Vaud (#VD3193). Mice were housed in individual cages and maintained in a temperature-controlled room with a 12 h light/dark cycle and provided *ad libitum* access to water and standard laboratory chow (Kliba Nafag). C57Bl6/J neonatal mice (Charles River) were anesthetized with sodium pentobarbital (150 mg/kg) and perfused on P4, P8, P10, P12, P14, P16, P18, P20, and P22 with 4% paraformaldehyde solution in phosphate buffer (Applichem, PFA), pH 7.4. The brains were then embedded in 3% agarose, and sectioned from rostral to caudal to expose the anterior BNST without affecting the hypothalamic nuclei. Each brain block was stained with 2% Chicago Blue to visualize anatomic features. A small cristal of DiI (SantaCruz Biotechnology) was placed into the dorsomedial part of the anterior BNST under binocular loup (Zeiss). After implantation, brains were stored in 4% PFA for 6 weeks in the dark at 37°C. There were 70 µm-thick sections that were then cut through the hypothalamus using a vibratome. Sections were mounted on Superfrost slides and cover slipped with DAPI-Fluoromount (SouthernBiotech).

Analysis

Confocal images of DiI-labeled fibers were observed and/or acquired through the hypothalamus of P4 (n = 4), P8 (n = 3–4), P10 (n = 3–4), P12 (n = 3–6), P14 (n = 4–6), P16 (n = 3–8), P18 (n = 3–7), P20 (n = 3–6), and P22 (n = 3–6) male mice using a Zeiss LSM 710 confocal microscope equipped with a 20X objective. Brains were collected from 2 to 4 independent litters. The following regions were analyzed: (1) the neuroendocrine PVH, (2) the autonomic posterior PVH, (3) dorsomedial (DMHdm) and ventrolateral (DMHvl) parts of the DMH, (4) dorsomedial (ARHdm) and ventromedial (ARHvm) parts of the ARH, and (5) LHA (perifornical area) at the level of the DMH and ARH. DAPI-labeled nuclei allowed a clear morphological delimitation. For the quantification of DiI-positive fiber density, each image was binarized and integrated intensity (total numbers of pixels) was then calculated for each image using Image J (NIH). For this purpose, regions of interest (ROI) with the following dimensions were centered over each region studied: 150 × 150 µm for the neuroendocrine PVH; 243 × 70 µm for the posterior PVH; 115 × 115 µm for the DMHdm and DMHvl; 90 × 90 µm for the ARHdm and ARHvm; and 100 × 100 µm for the LHA (perifornical area). These ROI have been chosen based on the size of the ARH in early ages, and to be able to compare fiber density in both ARHdm and ARHvm.

Statistics

Statistical analyses were conducted using GraphPad Prism (version 9). Statistical significance was determined using one-way ANOVA and two-way ANOVA followed by Tukey's *post hoc* test. $P \leq 0.05$ was considered statistically significant. Graphs have been generated using Prism 9 software and all values were represented as mean ± SEM.

RESULTS

To examine the development of projections from the dorsomedial division of the anterior BNST to hypothalamic nuclei in male mice, we used the well-described DiI lipophilic fluorescent tracer. A representative injection site into the dorsomedial division of the anterior BNST is shown in **Figure 1**. Correct injection sites were obtained in 49 cases from P4 to P22 in which DiI crystal was centered in the dorsomedial division of the anterior BNST. Descending projections from the dorsomedial division of the anterior BNST follow distinct trajectories to reach several hypothalamic nuclei mostly localized in periventricular zone, but not exclusively. From the dorsomedial division of the anterior BNST, DiI-positive fibers follow a periventricular route, and travel ventrally and caudally to reach the PVH, and then the ARH as described in rats (Dong and Swanson, 2006; Barbier et al., 2021). To reach the LHA, fibers can either extend from the DMH that does not display clear neuroanatomic border with the LHA, or follow the medial forebrain bundle in very lateral parts of the LHA to reach the caudal part of the brainstem (Dong and Swanson, 2006; Barbier et al., 2021).

While DiI tracer is known to mostly display anterograde diffusion, it has already been described to diffuse from terminals to cell bodies. In our samples, we observed retrogradely labeled

neurons, notably in the PVH (**Figure 2A**), and in the ARH (**Figure 3A**), but this was in a very limited number of samples, and it concerned only a few neurons.

Development of the Projections From the Dorsomedial Division of the Anterior Bed Nucleus of the Stria Terminalis to the Paraventricular Nucleus of the Hypothalamus

The PVH is composed of a rostral division that mostly contains neuroendocrine neurons, and one caudal part where the majority of intermediolateral column-projecting neurons are found (Biag et al., 2012). Both are innervated by fibers arising from the dorsomedial division of the anterior BNST (Dong and Swanson, 2006; Barbier et al., 2021). We thus assessed the ontogeny of fibers coming from the dorsomedial division of the anterior BNST by quantifying the DiI-positive fiber density in both PVH divisions (**Figure 2**).

Regardless the PVH subdivisions, this nucleus is among the first studied hypothalamic nuclei to receive inputs from the dorsomedial division of the anterior BNST (**Figure 2**). At P4, no DiI-positive fibers were observed in the PVH. At P8, only a few DiI-positive fibers were observed in the rostral part of the PVH (**Figures 2A–C**), while none were seen in the autonomic part at more posterior level (postPVH) (**Figures 2D–F**). At P10, the density of DiI-positive fiber substantially increased in the rostral part (**Figure 2C**, 96.7-fold-change between P8 and P10), and rapidly reached a plateau as we only observed a twofold change between P10 and P22 (**Figure 2C**). On the contrary, DiI-positive fiber density was gradually increasing between P10 and P20-P22 in the autonomic part of the PVH (**Figure 2F**, 25.6-fold change between P10 and P22).

Development of the Projections From the Dorsomedial Division of the Anterior Bed Nucleus of the Stria Terminalis to the Dorsomedial Nucleus of the Hypothalamus

The DMH can be subdivided in dorsomedial and ventrolateral parts, and we recently showed that the ventrolateral part received greater inputs from the dorsomedial division of the anterior BNST compared to the dorsal part (Barbier et al., 2021). We quantified the DiI-positive fiber density in both dorsomedial and ventrolateral parts of the DMH (**Figure 3**). Like the PVH, at P4, no DiI-positive fibers were observed in the DMH but this nucleus also appears as being among the first studied hypothalamic nuclei to receive projections from the dorsomedial division of the anterior BNST (**Figure 3**). At P8, we did not detect fibers coming from the dorsomedial division of the anterior BNST in both studied parts of the DMH (**Figure 3C**). While the projections into the dorsomedial part gradually increased from P10 to P22 (**Figures 3A,C**, 3.2-fold change between P10 and P22), the first DiI-positive fibers were observed at P10 in the ventrolateral part and reached a plateau from P12 until P22 (**Figure 3C**, ranging from 88 552 AU at P10, to 320 334 AU and 341 676 AU at P12 and P22, respectively, corresponding to a 3.6-fold change between P10 and P12).

Development of the Projections From the Dorsomedial Division of the Anterior Bed Nucleus of the Stria Terminalis to the Lateral Hypothalamic Area

LHA extends from anterior hypothalamus in PVH-containing sections until the posterior part of the tuberal hypothalamus (Franklin and Paxinos, 2008). In this study, we chose to specifically assess DiI-positive fiber density in perifornical area (at the level of the ARH and DMH corresponding to Bregma -1.7 mm in adult), as abundant fibers coming from the dorsomedial division of the anterior BNST are observed, particularly dorsally to the fornix (Dong and Swanson, 2006; Barbier et al., 2021). At P4, no fibers coming from the dorsomedial division of the anterior BNST were observed in the LHA. At P8, only a few fibers were detected in some cases, and substantially increased at P10 (**Figure 4C**, 106.9-fold change between P8 and P10), to reach a plateau around P12 (**Figure 4C**, DiI-fiber density was comprised between 171 479 AU and 140 694 AU, at P12 and P22).

Development of the Projections From the Dorsomedial Division of the Anterior Bed Nucleus of the Stria Terminalis to the Arcuate Nucleus of the Hypothalamus

Out of the studied hypothalamic nuclei, the ARH is the last nucleus that received projections from the dorsomedial part of the anterior BNST (**Figures 5**, **6**). However, like PVH, DMH, and LHA, no DiI-positive fibers were observed at P4, as well as at P8 (**Figure 5C**). A 2-day delay was observed in the DiI-positive fiber detection between the dorsomedial and ventromedial part of the ARH with only a few fibers observed in the dorsomedial part at P10, and almost none in the ventromedial part of the ARH at the same age (**Figures 5A,C**). Between P12-P14, fibers coming from the dorsomedial part of the BNST first enter dorsally into the ARH by following a periventricular route (**Figure 5A**), and gradually increased until P20 to reach a postnatal peak of intensity (**Figures 5A,C**, 15.2-fold change between P12 and P20). At P22, the dorsomedial part of the ARH showed less DiI-positive fibers than observed at P20. This was not the case in the ventromedial division of the ARH. We used the same surface area to quantify DiI-positive fiber densities in both ARH parts (**Figure 5B**), and the density observed in dorsomedial part compared to ventromedial part was 2.8-fold lower at P22 (**Figures 5A,C**).

Control Injections

For each crystal we implanted, we assessed the final localization, and we only used those that were DiI crystal which was restricted to the dorsomedial part of the anterior BNST for quantification. In these cases, and as we already described (Barbier et al., 2021), the VMH was devoid of DiI-positive fibers (data not shown). In some cases, the dorsomedial part of the anterior BNST was missed, and DiI crystal was observed

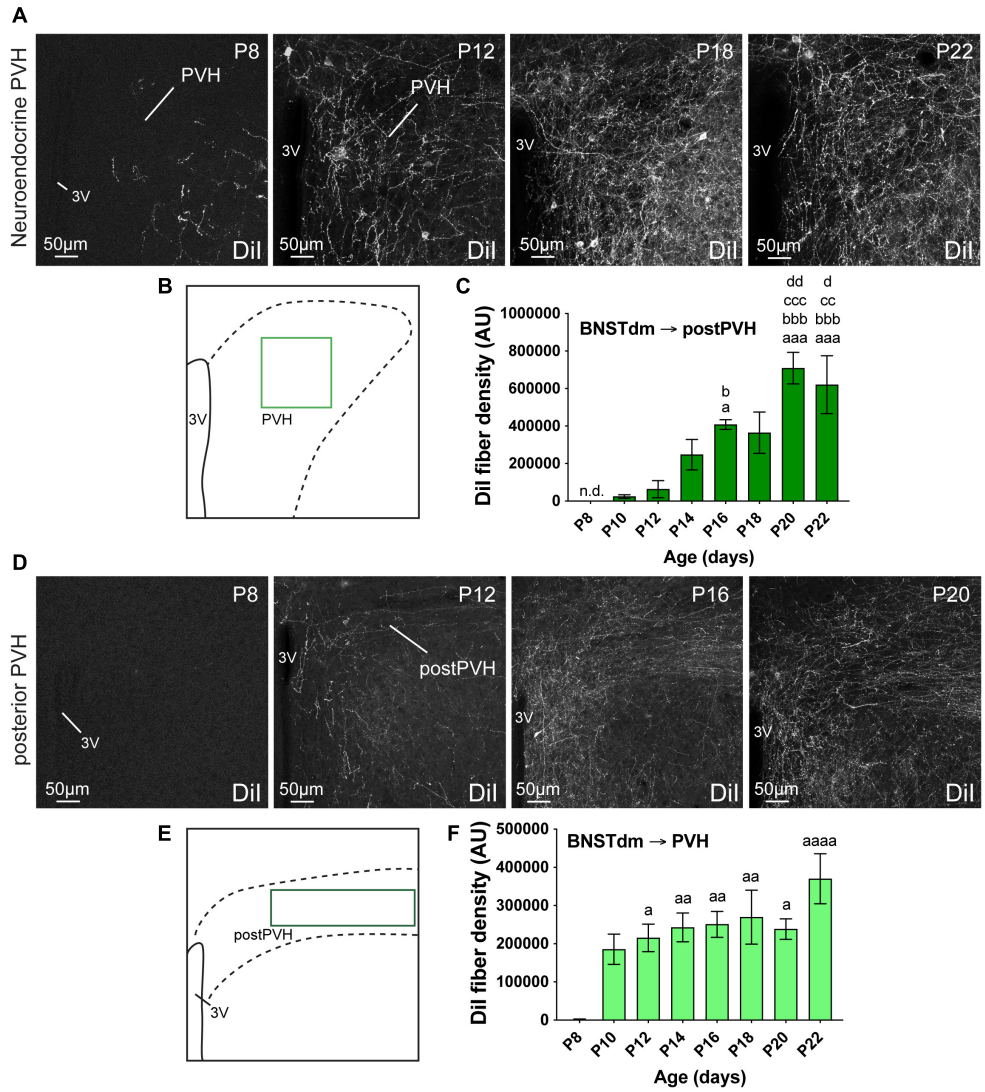

FIGURE 2 | (A) Confocal images showing DiI-positive fibers in the neuroendocrine part of the PVH of P8, P12, P18, and P22 male mice. **(B)** Scheme illustrating the region of interest (ROI in light green, 150 × 150 µm) used to quantify the DiI-positive fiber density in the neuroendocrine part of the PVH. **(C)** Quantification of DiI-positive fiber density is summarized in the graph. **(D)** Confocal images showing DiI-positive fibers in the posterior part of the PVH of P8, P12, P16, and P20 male mice. The density of DiI-positive fibers gradually increases over postnatal ages. **(E)** Scheme illustrating the region of interest (ROI in dark green, 243 × 70 µm) used to quantify the DiI-positive fiber density in the autonomic part of the PVH. **(F)** Quantification of DiI-positive fiber density is summarized in the graph. 3V, third ventricle. Scale bars are shown in the figure. Values are shown ± SEM. Statistical significance was determined using one-way ANOVA **(C,F)**. $^{a}P \leq 0.05$, $^{aa}P \leq 0.01$, $^{aaa}P \leq 0.001$, $^{aaaa}P \leq 0.0001$ vs. P8; $^{b}P \leq 0.05$, $^{bbb}P \leq 0.001$ vs. P10; $^{cc}P \leq 0.01$, $^{ccc}P \leq 0.001$ vs. P12; $^{d}P \leq 0.05$, $^{dd}P \leq 0.01$ vs. P14.

in the adjacent septohypothalamic nucleus (ventral part of the lateral septum). In these cases, DiI-positive fibers were also observed in the PVH, ARH, DMH, and LHA, as described in rats (Risold and Swanson, 1997).

DISCUSSION

BNST is usually considered as a hub for the integration of stress- and anxiety-related behaviors (Walker et al., 2003; Daniel and Rainnie, 2016). Its strong connections to hypothalamic nuclei known to control goal-oriented behaviors (Dong and Swanson, 2006; Boutrel et al., 2010; Bi et al., 2012; Diniz and Bittencourt, 2017; Timper and Brüning, 2017; Smith et al., 2019; Barbier et al., 2021) revealed putative functions of these circuits in the stress-related control of feeding. Whereas we recently described the anatomy of the projections from the dorsomedial part of the anterior BNST to hypothalamic nuclei such as the PVH, DMH, ARH, and LHA (Barbier et al., 2021), there is no evidence on the developmental period in which these circuits develop. In this study, we focused our interest only in males, but we are currently assessing the sexually dimorphic aspect of these circuits using both developmental and functional approaches. Here, by using the well-described DiI-based tract

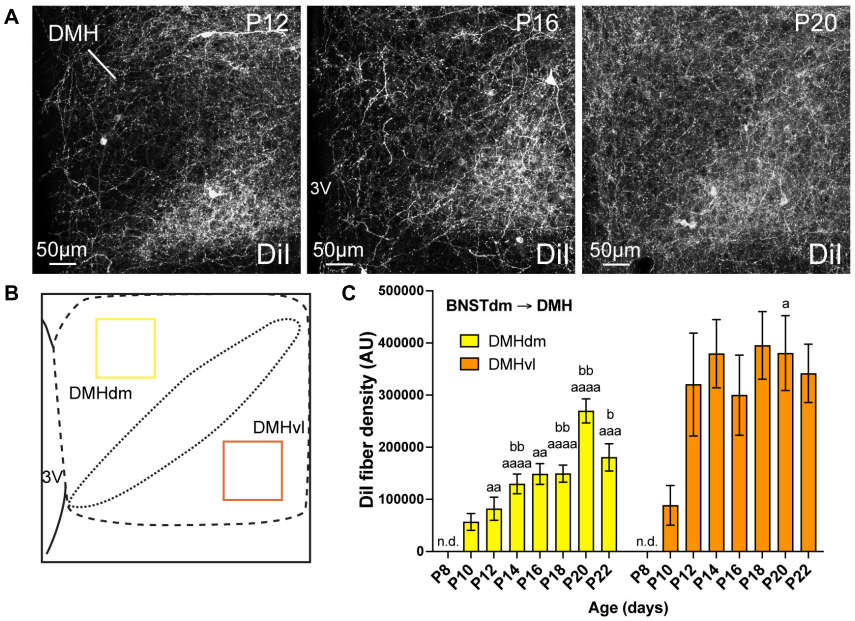

FIGURE 3 | (A) Confocal images showing DiI-positive fibers in the DMH of P12, P16, and P20 male mice. The density of DiI-positive fibers gradually increases over postnatal ages. **(B)** Scheme illustrating the regions of interest (ROI, 115 × 115 μm) used to quantify the DiI-positive fiber density in the dorsomedial part (DMHdm, yellow) and in the ventrolateral part (DMHvl, orange) of the DMH. **(C)** Quantification of DiI-positive fiber density is summarized in the graph. fx, fornix; 3V, third ventricle. Scale bars are shown in the figure. Values are shown ± SEM. Statistical significance was determined using two-way ANOVA **(C)**. $^{a}P \leq 0.05$, $^{aa}P \leq 0.01$, $^{aaa}P \leq 0.001$, $^{aaaa}P \leq 0.0001$ vs. P8; $^{b}P \leq 0.05$, $^{bb}P \leq 0.01$ vs. P10.

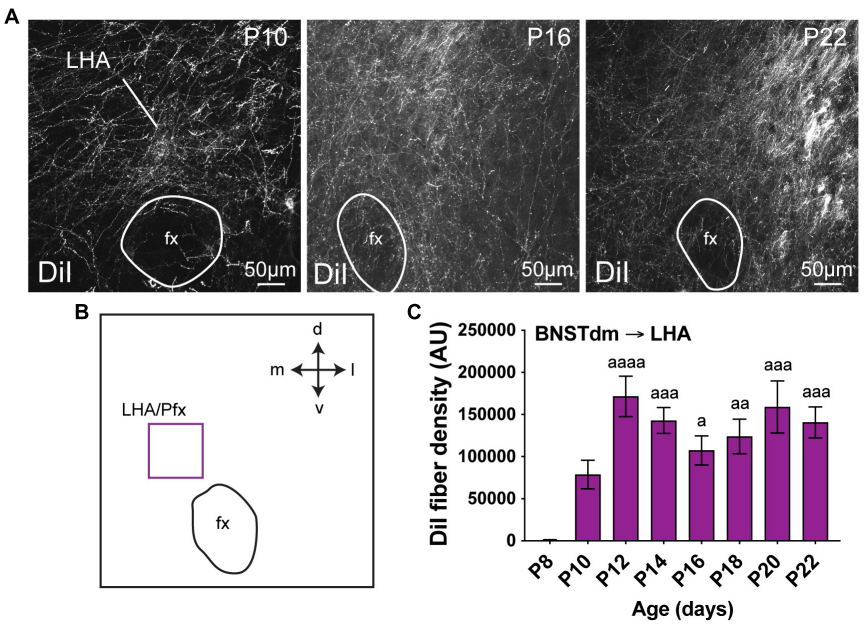

FIGURE 4 | (A) Confocal images showing DiI-positive fibers in the LHA of P10, P16, and P22 male mice. **(B)** Scheme illustrating the regions of interest (ROI in purple, 100 × 100 μm) used to quantify the DiI-positive fiber density in the perifornical area (Pfx) of the LHA. **(C)** Quantification of DiI-positive fiber density is summarized in the graph. fx, fornix. Scale bars are shown in the figure. Values are shown ± SEM. Statistical significance was determined using one-way ANOVA **(C)**. $^{a}P \leq 0.05$, $^{aa}P \leq 0.01$, $^{aaa}P \leq 0.001$, $^{aaaa}P \leq 0.0001$ vs. P8.

tracing approach we showed that these projections, immature at birth, develop progressively during postnatal life (**Figure 6**) to form similar neurocircuits to that described in adult male mice. Despite DiI molecules are known to diffuse in the lipidic layer of the axonal membrane in both anterograde and retrograde direction (Makarenko, 2014), our data support the predominant

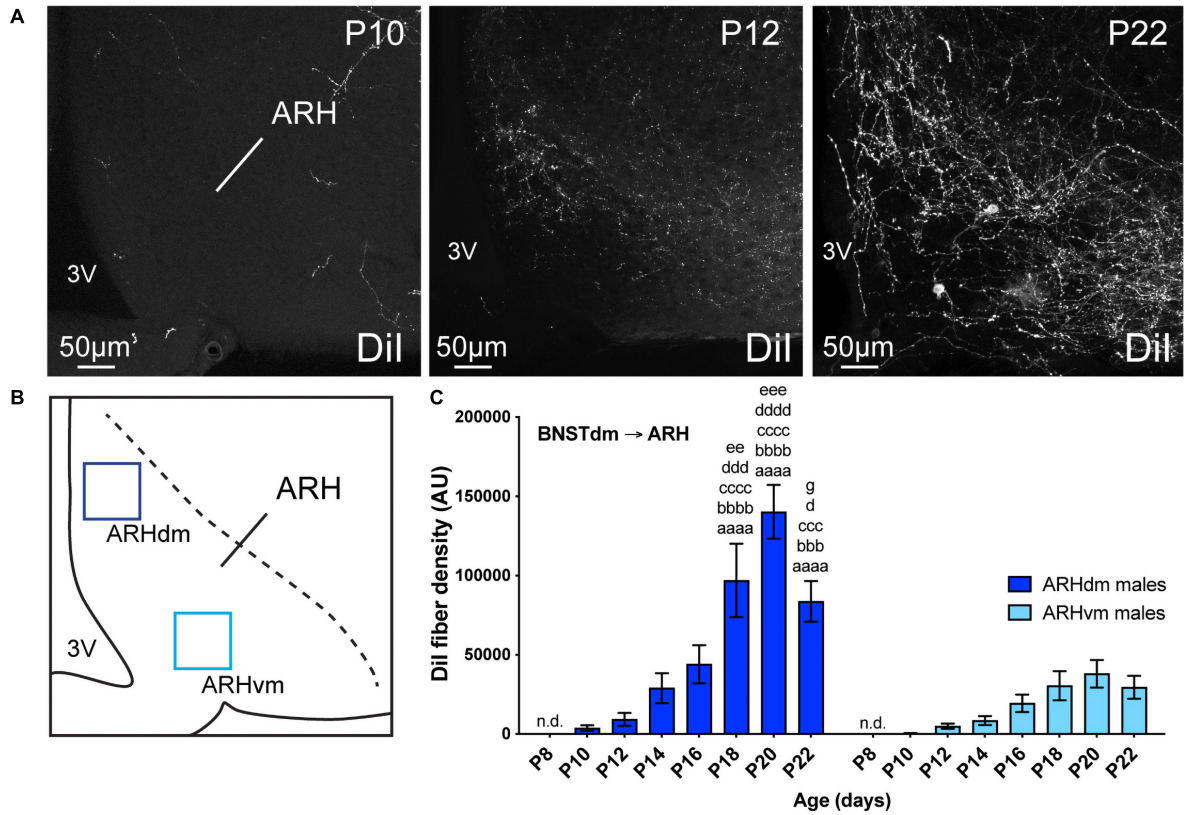

FIGURE 5 | (A) Confocal images showing DiI-positive fibers in the ARH of P10, P12, and P22 male mice. The density of DiI-positive fibers gradually increases over postnatal ages. **(B)** Scheme illustrating the regions of interest (ROI, 90 × 90 µm) used to quantify the DiI-positive fiber density in the dorsomedial part (ARHdm, dark blue) and in the ventromedial part (ARHvm, light blue) of the ARH. **(C)** Quantification of DiI-positive fiber density is summarized in the graph. 3V, third ventricle. Scale bars are shown in the figure. Values are shown ± SEM. Statistical significance was determined using two-way ANOVA **(C)**. $^{aaaa}P \leq 0.0001$ vs. P8; $^{bbb}P \leq 0.001$, $^{bbbb}P \leq 0.0001$ vs. P10; $^{ccc}P \leq 0.001$, $^{cccc}P \leq 0.0001$ vs. P12; $^{d}P \leq 0.05$, $^{ddd}P \leq 0.001$, $^{dddd}P \leq 0.0001$ vs. P14; $^{ee}P \leq 0.01$, $^{eee}P \leq 0.001$ vs. P16; $^{g}P \leq 0.05$ vs. P20.

anterograde property of the DiI. Indeed, in our materiel we observed intense DiI-positive fibers in the PVH, DMH, ARH, and LHA, and only a few retrogradely labeled neurons. Some studies limited the retrograde property of the DiI to the absence of reciprocal projections (Makarenko, 2014), it is clearly not the case in our study as it has been clearly established that the anterior part of the BNST receive reciprocal connections from the ARH (Bouret et al., 2004a; Betley et al., 2013; Steculorum et al., 2016), and the DMH (Thompson et al., 1996) where we observed only a few retrogradely labeled neurons.

In this study, we analyzed the DiI fiber density only every 2 days from P4 to P22, and we are aware that the described developmental time-course could present a 1-day delay/bias. Thus, out of the four studied areas, the projections from the dorsomedial division of the anterior BNST first reach the more dorsal structures of the hypothalamus including the PVH, DMH, and LHA at P10–P12. Later, the projections reach ventral hypothalamic structures following a periventricular route and enter the dorsal part of the ARH (P12–P14) to finally reach its ventral part (P14–P16). These dorsal to ventral gradient and time-course are consistent with the path followed by the projections coming from the dorsomedial part of the anterior BNST (Dong and Swanson, 2006; Barbier et al., 2021) to reach the PVH, DMH, ARH, and LHA.

In rodents, the formation of long projections has been primarily thought of as developing during embryonic life, when the brain is smaller, and local and shorter projections developing during postnatal ages. The formation of short intrahypothalamic projections is not necessarily consistent with this description as previous studies in rodents have shown that a few intrahypothalamic circuits are already developed at birth (Polston and Simerly, 2006) while others are still immature, notably the projections from the ARH to the PVH, DMH, and LHA (Bouret et al., 2004a). In our study, we showed that longer BNST to ARH projections were also immature at birth and precede the development of the reciprocal ARH to anterior BNST projections (Bouret et al., 2004a), and could serve as scaffold for the development of ARH to BNST projections by following this breadcrumb trail. Finally, other studies have shown that extrahypothalamic projections can form during embryonic life, notably the projections from the LHA to the posterior part of the brain (Croizier et al., 2011), and from the ARH to the

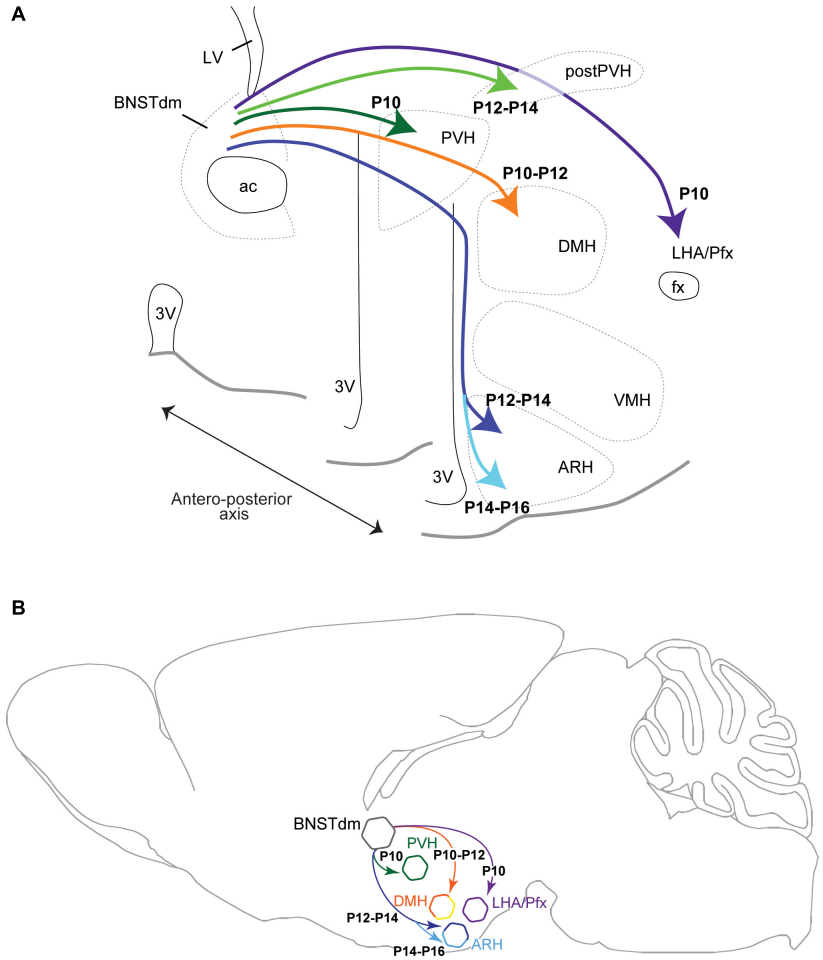

FIGURE 6 | Brain coronal **(A)** and sagittal **(B)** section views showing the developmental time-course during postnatal ages of projections coming from the dorsomedial part of the anterior BNST (BNSTdm) to innervate several hypothalamic nuclei including the neuroendocrine and autonomic parts of the PVH, the DMH, the perifornical area (Pfx)/LHA and the ARH. The projections first reach dorsal parts of the hypothalamus to innervate the PVH, DMH, and LHA, to reach later the ARH by taking a periventricular and dorsal route.

upper thoracic spinal cord (personal data not shown). These data suggest no clear rules in the timing of the establishment of hypothalamic circuits *per se*, but could reflect the involvement of other factors such as the level of circulating hormones with leptin (Bouret et al., 2004b; Croizier et al., 2016), and ghrelin (Steculorum et al., 2015), or testosterone that directly influences the development of neuronal circuits and structures, notably the formation and differentiation of the sexually dimorphic BNST (Chung et al., 2002).

Developing environment is critical for the overall formation of neurocircuits, and this extended developmental window may increase the vulnerability of key hypothalamic circuits, and subsequently long-lasting neuronal functions. Here, all studied projections from the dorsomedial part of the anterior BNST to hypothalamic area develop when pups are on lactation as the switch from suckling to solid food occurs around P17 in mice (König and Markl, 1987). When lactating dams are fed a high fat diet, milk is enriched in insulin, leptin, glucose, and free fatty acids (Vogt et al., 2014), and the development of hypothalamic circuits is altered in offspring (Vogt et al., 2014; Park et al., 2020). Such changes in developing environment and in milk content in particular, could directly affect the expression of key guidance proteins, and subsequently the formation of hypothalamic circuits. However, while alteration of maternal metabolism and nutrition with maternal obesity, and maternal exposure to high fat diet interfere with the proper formation of the ARH to hypothalamic nuclei projections, including the PVH (Vogt et al., 2014; Park et al., 2020), there is no clear evidence on how maternal stress can impinge on the development of hypothalamic circuits and in particular, the BNST to ARH projections. Based on the literature, we can suspect that alteration of maternal environment notably maternal stress and early life stress could trigger developmental outcomes leading to metabolic dysfunctions and anxiety-like behaviors in the offspring (Delpierre et al., 2016; Derks et al., 2016; Romaní-Pérez et al., 2017). Regarding the physiological role of the anterior

BNST projections to key hypothalamic circuits, deciphering how and when these circuits develop is a step forward toward a better understanding of the developmental origin of metabolic diseases.

DATA AVAILABILITY STATEMENT

The raw data supporting the conclusions of this article will be made available by the authors, without undue reservation.

ETHICS STATEMENT

The animal study was reviewed and approved by the Veterinary Office of Canton de Vaud (#VD3193).

AUTHOR CONTRIBUTIONS

SC conceived the project, designed the experiments, analyzed the data, and wrote the manuscript. ML, MG, and SC performed all experiments. All authors contributed to the article and approved the submitted version.

FUNDING

This work was supported by a grant from the Swiss National Science Foundation (PZ00P3_167934/1) and the Novartis Foundation for medical-biological research (19B145) (SC). The latter funder was not involved in the study design, collection, analysis, interpretation of data, the writing of this article or the decision to submit it for publication.

ACKNOWLEDGMENTS

We thank CIG Animal Facility for their assistance with animal housing.

REFERENCES

Barbier, M., González, J. A., Houdayer, C., Burdakov, D., Risold, P. Y., and Croizier, S. (2021). Projections from the dorsomedial division of the bed nucleus of the stria terminalis to hypothalamic nuclei in the mouse. *J. Comp. Neurol.* 529, 929–956. doi: 10.1002/cne.24988

Betley, J. N., Cao, Z. F., Ritola, K. D., and Sternson, S. M. (2013). Parallel, redundant circuit organization for homeostatic control of feeding behavior. *Cell* 155, 1337–1350. doi: 10.1016/j.cell.2013.11.002

Bi, S., Kim, Y. J., and Zheng, F. (2012). Dorsomedial hypothalamic NPY and energy balance control. *Neuropeptides* 46, 309–314. doi: 10.1016/j.npep.2012.09.002

Biag, J., Huang, Y., Gou, L., Hintiryan, H., Askarinam, A., Hahn, J. D., et al. (2012). Cyto- and chemoarchitecture of the hypothalamic paraventricular nucleus in the C57BL/6J male mouse: a study of immunostaining and multiple fluorescent tract tracing. *J. Comp. Neurol.* 520, 6–33. doi: 10.1002/cne.22698

Bouret, S. G., Draper, S. J., and Simerly, R. B. (2004a). Formation of projection pathways from the arcuate nucleus of the hypothalamus to hypothalamic regions implicated in the neural control of feeding behavior in mice. *J. Neurosci.* 24, 2797–2805. doi: 10.1523/JNEUROSCI.5369-03.2004

Bouret, S. G., Draper, S. J., and Simerly, R. B. (2004b). Trophic action of leptin on hypothalamic neurons that regulate feeding. *Science* 304, 108–110. doi: 10.1126/science.1095004

Boutrel, B., Cannella, N., and de Lecea, L. (2010). The role of hypocretin in driving arousal and goal-oriented behaviors. *Brain Res.* 1314, 103–111. doi: 10.1016/j.brainres.2009.11.054

Chung, W. C., De Vries, G. J., and Swaab, D. F. (2002). Sexual differentiation of the bed nucleus of the stria terminalis in humans may extend into adulthood. *J. Neurosci.* 22, 1027–1033. doi: 10.1523/JNEUROSCI.22-03-01027.2002

Croizier, S., Amiot, C., Chen, X., Presse, F., Nahon, J. L., Wu, J. Y., et al. (2011). Development of posterior hypothalamic neurons enlightens a switch in the prosencephalic basic plan. *PLoS One* 6:e28574. doi: 10.1371/journal.pone.0028574

Croizier, S., Prevot, V., and Bouret, S. G. (2016). Leptin controls parasympathetic wiring of the pancreas during embryonic life. *Cell Rep.* 15, 36–44. doi: 10.1016/j.celrep.2016.02.088

Daniel, S. E., and Rainnie, D. G. (2016). stress modulation of opposing circuits in the bed nucleus of the stria terminalis. *Neuropsychopharmacology* 41, 103–125. doi: 10.1038/npp.2015.178

Delpierre, C., Fantin, R., Barboza-Solis, C., Lepage, B., Darnaudéry, M., and Kelly-Irving, M. (2016). The early life nutritional environment and early life stress as potential pathways towards the metabolic syndrome in mid-life? A lifecourse analysis using the 1958 British birth Cohort. *BMC Public Health* 16:815. doi: 10.1186/s12889-016-3484-0

Derks, N. A., Krugers, H. J., Hoogenraad, C. C., Joëls, M., and Sarabdjitsingh, R. A. (2016). Effects of early life stress on synaptic plasticity in the developing hippocampus of male and female rats. *PLoS One* 11:e0164551. doi: 10.1371/journal.pone.0164551

Diniz, G. B., and Bittencourt, J. C. (2017). The melanin-concentrating hormone as an integrative peptide driving motivated behaviors. *Front. Syst. Neurosci.* 11:32. doi: 10.3389/fnsys.2017.00032

Dong, H. W., Petrovich, G. D., and Swanson, L. W. (2001). Topography of projections from Amygdala to bed nuclei of the stria terminalis. *Brain Res. Brain Res. Rev.* 38, 192–246. doi: 10.1016/s0165-0173(01)00079-0

Dong, H. W., and Swanson, L. W. (2006). Projections from bed nuclei of the stria terminalis, anteromedial area: cerebral hemisphere integration of neuroendocrine, autonomic, and behavioral aspects of energy balance. *J. Comp. Neurol.* 494, 142–178. doi: 10.1002/cne.20788

Franklin, K., and Paxinos, G. (2008). *The Mouse Brain in Stereotaxic Coordinates, Compact*, 3rd Edn. Cambridge, MA: Academic Press.

Giardino, W. J., Eban-Rothschild, A., Christoffel, D. J., Li, S. B., Malenka, R. C., and de Lecea, L. (2018). Parallel circuits from the bed nuclei of stria terminalis to the lateral hypothalamus drive opposing emotional states. *Nat. Neurosci.* 21, 1084–1095. doi: 10.1038/s41593-018-0198-x

Jennings, J. H., Rizzi, G., Stamatakis, A. M., Ung, R. L., and Stuber, G. D. (2013). The inhibitory circuit architecture of the lateral hypothalamus orchestrates feeding. *Science* 341, 1517–1521. doi: 10.1126/science.1241812

König, B., and Markl, H. (1987). Maternal care in house mice. *Behav. Ecol. Sociobiol.* 20, 1–9. doi: 10.1007/BF00292161

Makarenko, I. G. (2014). DiI tracing of the hypothalamic projection systems during perinatal development. *Front. Neuroanat.* 8:144. doi: 10.3389/fnana.2014.00144

Park, S., Jang, A., and Bouret, S. G. (2020). Maternal obesity-induced endoplasmic reticulum stress causes metabolic alterations and abnormal hypothalamic development in the offspring. *PLoS Biol.* 18:e3000296. doi: 10.1371/journal.pbio.3000296

Polston, E. K., and Simerly, R. B. (2006). Ontogeny of the projections from the anteroventral periventricular nucleus of the hypothalamus in the female rat. *J. Comp. Neurol.* 495, 122–132. doi: 10.1002/cne.20874

Risold, P. Y., and Swanson, L. W. (1997). Connections of the rat lateral septal complex. *Brain Res. Brain Res. Rev.* 24, 115–195. doi: 10.1016/s0165-0173(97)00009-x

Romaní-Pérez, M., Lépinay, A. L., Alonso, L., Rincel, M., Xia, L., Fanet, H., et al. (2017). Impact of perinatal exposure to high-fat diet and stress on responses to nutritional challenges, food-motivated behaviour and mesolimbic dopamine function. *Int. J. Obes.* 41, 502–509. doi: 10.1038/ijo.2016.236

Smith, M. A., Choudhury, A. I., Glegola, J. A., Viskaitis, P., Irvine, E. E., de Campos Silva, P. C. C., et al. (2019). Extrahypothalamic GABAergic nociceptin–expressing neurons regulate AgRP neuron activity to control feeding behavior. *J. Clin. Investig.* 130, 126–142. doi: 10.1172/JCI130340

Steculorum, S. M., Collden, G., Coupe, B., Croizier, S., Lockie, S., Andrews, Z. B., et al. (2015). Neonatal ghrelin programs development of hypothalamic feeding circuits. *J. Clin. Investig.* 125, 846–858. doi: 10.1172/JCI73688

Steculorum, S. M., Ruud, J., Karakasilioti, I., Backes, H., Engström Ruud, L., Timper, K., et al. (2016). AgRP neurons control systemic insulin sensitivity via myostatin expression in brown adipose tissue. *Cell* 165, 125–138. doi: 10.1016/j.cell.2016.02.044

Thompson, R. H., Canteras, N. S., and Swanson, L. W. (1996). Organization of projections from the dorsomedial nucleus of the hypothalamus: a PHA-L study in the rat. *J. Comp. Neurol.* 376, 143–173. doi: 10.1002/(SICI)1096-9861(19961202)376:1<143::AID-CNE9<3.0.CO;2-3

Timper, K., and Brüning, J. C. (2017). Hypothalamic circuits regulating appetite and energy homeostasis: pathways to obesity. *Dis. Model. Mech.* 10, 679–689. doi: 10.1242/dmm.026609

Vogt, M. C., Paeger, L., Hess, S., Steculorum, S. M., Awazawa, M., Hampel, B., et al. (2014). Neonatal insulin action impairs hypothalamic neurocircuit formation in response to maternal high-fat feeding. *Cell* 156, 495–509. doi: 10.1016/j.cell.2014.01.008

Walker, D. L., Toufexis, D. J., and Davis, M. (2003). Role of the bed nucleus of the stria terminalis versus the amygdala in fear, stress, and anxiety. *Eur. J. Pharmacol.* 463, 199–216.

Conflict of Interest: The authors declare that the research was conducted in the absence of any commercial or financial relationships that could be construed as a potential conflict of interest.

Publisher's Note: All claims expressed in this article are solely those of the authors and do not necessarily represent those of their affiliated organizations, or those of the publisher, the editors and the reviewers. Any product that may be evaluated in this article, or claim that may be made by its manufacturer, is not guaranteed or endorsed by the publisher.

frontiers in Neuroscience

REVIEW
published: 27 January 2022
doi: 10.3389/fnins.2021.767405

Nutritional Impact on Metabolic Homeostasis and Brain Health

Lionel Carneiro[1] and Luc Pellerin[2]*

[1] Department of Biological Chemistry and Pharmacology, Ohio State University, Columbus, OH, United States, [2] Inserm U1082, Université de Poitiers and CHU de Poitiers, Poitiers, France

Aging in modern societies is often associated with various diseases including metabolic and neurodegenerative disorders. In recent years, researchers have shown that both dysfunctions are related to each other. Although the relationship is not fully understood, recent evidence indicate that metabolic control plays a determinant role in neural defects onset. Indeed, energy balance dysregulation affects neuroenergetics by altering energy supply and thus neuronal activity. Consistently, different diets to help control body weight, blood glucose or insulin sensitivity are also effective in improving neurodegenerative disorders, dampening symptoms, or decreasing the risk of disease onset. Moreover, adapted nutritional recommendations improve learning, memory, and mood in healthy subjects as well. Interestingly, adjusted carbohydrate content of meals is the most efficient for both brain function and metabolic regulation improvement. Notably, documented neurological disorders impacted by specific diets suggest that the processes involved are inflammation, mitochondrial function and redox balance as well as ATP production. Interestingly, processes involving inflammation, mitochondrial function and redox balance as well as ATP production are also described in brain regulation of energy homeostasis. Therefore, it is likely that changes in brain function induced by diets can affect brain control of energy homeostasis and other brain functions such as memory, anxiety, social behavior, or motor skills. Moreover, a defect in energy supply could participate to the development of neurodegenerative disorders. Among the possible processes involved, the role of ketone bodies metabolism, neurogenesis and synaptic plasticity, oxidative stress and inflammation or epigenetic regulations as well as gut-brain axis and SCFA have been proposed in the literature. Therefore, the goal of this review is to provide hints about how nutritional studies could help to better understand the tight relationship between metabolic balance, brain activity and aging. Altogether, diets that help maintaining a metabolic balance could be key to both maintain energy homeostasis and prevent neurological disorders, thus contributing to promote healthy aging.

Keywords: nutrition, aging, neurological disorder, nutrient sensing, cognition, metabolism

OPEN ACCESS

Edited by:
Jong-Min Kim,
Seoul National University Bundang Hospital, South Korea

Reviewed by:
João M. N. Duarte,
Lund University, Sweden
Han Kyoung Choe,
Daegu Gyeongbuk Institute of Science and Technology (DGIST), South Korea

****Correspondence:***
Lionel Carneiro
lionel.carneiro@inserm.fr

Specialty section:
This article was submitted to Neuroenergetics, Nutrition and Brain Health, a section of the journal Frontiers in Neuroscience

Received: *30 August 2021*
Accepted: *13 December 2021*
Published: *27 January 2022*

Citation:
Carneiro L and Pellerin L (2022) Nutritional Impact on Metabolic Homeostasis and Brain Health. Front. Neurosci. 15:767405. doi: 10.3389/fnins.2021.767405

INTRODUCTION

Modern societies experience a surge in their aging population due to improved medicine that led to extended life expectancy. However, in parallel with aging of the population, age-related disorders are also on the rise (Thane, 2013; Vilić, 2017). Those age-related disorders include notably metabolic and neurodegenerative disorders as well as cancer (Finkel et al., 2007; Wyss-Coray, 2016;

Meldrum et al., 2017). Interestingly, recent research has demonstrated the key role of metabolic regulations on both neurological disorders and cancer. Moreover, the aging process appears to be affected by metabolic control (Yates et al., 2012; World Health Organization [WHO], 2015; Luengo et al., 2017). Therefore, diet is a key element in healthy living and healthy diet as defined by WHO[1] is of great importance for global health. Hence, it is now admitted that healthy aging can be promoted by a balanced energy homeostasis that can be defined by an equilibrium between energy intake and energy expenditures that allows body weight and internal parameters (glycemia, temperature, pH) to remain constant. In support of this concept, different types of diet have been linked to healthy living. For instance, Japanese and Mediterranean diets are found in populations known for their lower metabolic disorders' incidence or a higher life expectancy (Martinez-Gonzalez and Martin-Calvo, 2016; Poli et al., 2019; Tomata et al., 2019). Noteworthily, these benefits are well known examples described not only in scientific journals but emerging also among the lay public communication media. Other diet changes for lipid, carbohydrates or protein content or caloric supply, or special diets s (e.g., ketopgenic diet, medium Chain triglycerides diet, caloric restrictions, intermittent fasting. . .) have been developed to prevent or treat certain disorders including cancer, as well as metabolic or neurodegenerative disorders (Amine et al., 2003; World Health Organization [WHO], 2003; Moynihan and Petersen, 2004; Gano et al., 2014; D'Alessandro et al., 2016; Billingsley et al., 2018; Duan et al., 2018; Reddavide et al., 2018; Klement and Pazienza, 2019; Mittelman, 2020). Ketogenic diet (KD), low glycemic index diet (LGI), or adjusted diets (for polyunsaturated fatty acids, medium chain triglycerides or other, proteins. . .) are the most documented (Apekey et al., 2009; Kanoski and Davidson, 2011; Paoli, 2014; Sanders, 2014; Vergati et al., 2017; Abdelhamid et al., 2018; Dohrmann et al., 2019; Włodarek, 2019; Carneiro and Leloup, 2020; van Name et al., 2020). However, little is known about the mechanisms involved in the beneficial effects of diets on health. Of note, neurological disorders are often targeted by diet interventions. Therefore, diet utilization in neurological conditions has led to numerous publications on the putative role of diets. Such an observation is of interest since the brain is the highest energy consumer of the body. Indeed, at least 20% of the total body glucose consumption at rest occurs in the brain for its normal activity. In addition, the brain can rapidly adjust energy supply to keep a constant level of nutrient availability (Peters, 2011; Pellerin and Magistretti, 2012). Overall, it appears clear that brain activity and energy homeostasis of the body are tightly linked. Hence, brain 60 disorders are associated with dysregulated energy balance. In addition, obesity or diabetes have been 61 shown to contribute to brain disorders development (Murakami et al., 2010; Val-Laillet et al., 2011; Castanon et al., 2015; Bogdanov et al., 2020; Bremner et al., 2020; Tanaka et al., 2020). In fact, neurological disorders studies provided interesting mechanistic hypotheses thanks to the disease mechanisms knowledge (Gómez-Pinilla, 2008; Gano et al., 2014; Li et al., 2017, 2020; Williams and Cervenka, 2017; Gomez-Pinilla et al., 2021). These observations reinforced the relationship between aging and associated disorders with metabolic regulation. Furthermore, it also indicates that metabolic balance is a key component of healthy aging. It is worth to note that the hypothesized mechanisms involved in the beneficial effect of diets on brain function have also been described in the brain control of energy homeostasis (Carneiro and Leloup, 2020). Therefore, it is likely that disturbed energy balance will contribute to dysfunction of brain control of energy homeostasis. In turn, this dysregulated brain energy homeostasis control would alter brain metabolism and participate to brain disorders. Hence, it is important to fully understand the mechanisms involved in dietary beneficial effects on brain activity to better understand brain control of energy homeostasis as well as brain function and diseases.

In this review, we thus aim to summarize the recent knowledge about the impact of diet on neurological function and disorders. The putative mechanisms at play will be presented, and the relationships with brain regulation of energy homeostasis will be discussed.

DIET AND BRAIN FUNCTION OF HEALTHY POPULATIONS

Cognitive responses are dependent on adequate brain function. Exposure to a high fat diet (HFD) has been described to decrease cognitive performances in various tests probing different aspects including working and spatial memory, mood, or spatial memory (Cordner and Tamashiro, 2015). Similarly, a high sucrose diet has also negative impact on cognitive responses (Davis et al., 2020). Therefore, these studies have permitted to demonstrate the deleterious effect of non-healthy diets on cognition. Altogether, obesogenic/diabetogenic diets induce a negative alteration of cognitive functions. However, it remains difficult to discriminate the cognitive decline from obesity or diabetes development. Therefore, to determine the impact of a diet on cognitive function independently of any other metabolic effect, it is necessary to study first the impact of healthy diets on healthy populations.

Among the so-called healthy diets, the Mediterranean diet is described to prevent cognitive decline during aging (Safouris et al., 2015; Aridi et al., 2017). However, these studies only report a decreased risk of developing dementia, and thus a decline in cognitive functions (Safouris et al., 2015; Charisis et al., 2021). In contrast, little is known of the effect of a healthy diet in young healthy people and their cognitive functions. In fact, attempts to determine the impact of a Mediterranean diet on young adult's cognitive performances led to interesting results (McMillan et al., 2011). In their study, McMillan et al. (2011), gave a specific diet regimen to one group while the control group had no diet changes from their habits. In their study, the authors report an improvement in reaction time during a spatial memory test as well as an increase of accuracy scores. However, other cognitive tests did not show any change after the Mediterranean diet. This restricted impact makes it difficult to conclude on a clear effect of the diet on cognitive function. One possible pitfall is the duration of diet exposure in the study of McMillan et al. (2011).

[1]https://www.who.int/news-room/fact-sheets/detail/healthy-diet

Indeed, in this study, the Mediterranean diet was given for a short period of 10 days. Therefore, a longer term follow up must be done to clearly address the impact of the Mediterranean diet on cognition of healthy adults. In addition, in their study, McMillan et al. (2011) observed a significant improvement of mood. This strong effect following short-term exposure to a diet in a relatively small group of subjects supports the idea of a potentially larger impact of healthy diets on brain function. Altogether, while encouraging, this study needs to be pursued with a larger group and on a longer period. It would be also of interest to compare different dietary habits to identify the factors involved in the putative improvements. Therefore, retrospective and intervention studies could help to determine specific diet composition patterns. Prospective studies would also help to determine chronic effects of diet on health during aging. Indeed, healthy aging could be defined as aging without loss of autonomy due to a disease as oppose to unhealthy aging when a disorder development leads to a loss of independence due to treatments and the need of assistance. Indeed, it is unlikely that aging with complete absence of disease could be considered. However, it is worth to note that healthy aging according to such a definition would be hard to achieve. Nevertheless, a delay in the onset of certain diseases would still help people live longer in healthy conditions. In addition to clearly address the diet effect and test the putative role of specific nutrients or foods, an experimentally controlled diet should be provided to both control and treated groups. Therefore, intervention studies are also necessary.

In another study, the Christian Orthodox Church (COC) fasting diet led to significant results on health and cognition. This specific diet implies a limited intake of animal-based products and a significant increase in fruit and vegetables. Such a nutrient composition makes the diet enriched in fibers and folates while the amount of saturated fatty acids is significantly lowered (Rodopaios et al., 2019). Spanaki et al. (2021) evaluated the cognitive profile of people following the COC fasting diet *vs* a group not adhering to it. The authors reported decreased levels of anxiety and depression and better cognitive performances in the COC fasting diet group. This result supports a beneficial effect of a healthy diet on healthy populations. Indeed, the COC fasting diet is an isocaloric diet, derived from the Mediterranean diet. In addition to prioritizing healthy nutrients (unsaturated fatty acids, complex sugars, fibers. . .), the COC fasting diet is also classified as an intermittent fasting. Intermittent fasting has been described for its potent impact on metabolic improvements and global health benefits (Mattson et al., 2017, 2018; Mattson, 2019). The study of Spanaki et al. (2021) on COC fasting diet resumes the intermittent fasting benefits while also providing evidence for a cognitive improvement even in healthy people.

On the other hand, other studies of intermittent fasting habits failed to report any positive role on cognition. Thus, studies of individuals that follow Ramadan practices (a fasting during daylight period followed during 28 consecutive days with no food or drink consumption) do not report cognitive improvement although sleep and arousal are positively affected (Dolu et al., 2007; Tian et al., 2011; Meo and Hassan, 2015; Chamari et al., 2016). Nevertheless, few of the studies related to Ramadan fasting focused on cognitive function including memory, attention, or test accuracy for instance. In addition, it is worth to note that the population studied often includes athletes and thus, the effect of exercise and training could mask the impact of diet. Finally, it is important to note that this religious practice of intermittent fasting only lasts one month. Hence, it is possible that significant effects on cognition would only appear after a longer period. Indeed, other intermittent fasting studies show that neurogenesis and brain plasticity, two mechanisms highly involved in cognition, are significantly affected. However, it is important to recall that studies on healthy populations are rare, which makes it difficult to clearly conclude on intermittent fasting and cognition interaction.

In fact, there is very few studies really testing cognitive function in relation with the diet in healthy adults. However, schoolchildren are a healthy population whose cognitive function has been tested in relation with the diet. Interestingly, in these schoolchildren, the diet appears to significantly affect cognitive results (Naveed et al., 2020). Several studies in adolescents show a positive relationship between a low glycemic index breakfast and learning, attention, stress, and even mood (Micha et al., 2010, 2011; Cooper et al., 2011, 2012, 2015; Edefonti et al., 2014). Noteworthily, when compared to adolescents without breakfast, both low and high glycemic index breakfast provide a beneficial impact on cognition. Such an observation indicates that cognitive improvement needs a high energy amount (Cooper et al., 2011). However, the fact that the low glycemic index breakfast is more beneficial indicates that the quality of the nutrients ingested has also a significant impact on brain activity. Thus, low glycemic index foods containing fibers or non-digestible carbohydrates, or low carbohydrates seems to have a better impact. This result supports a role for products of gut metabolism for the non-digestible carbohydrates or from other sources of energy than glucose: SCFA and ketone bodies that we will discuss in section "Putative Mechanisms at Play to Explain the Beneficial Roles of Certain Diets on Brain Function."

Overall, it is difficult to clearly address whether diet can affect cognitive function in healthy populations after adolescence. On the other hand, there is no doubt that unhealthy dietary habits induce cognitive decline during aging and increase the risk of dementia and age-related neurological disorders. In this regard, a better knowledge of the effects of healthy diets on cognition in healthy adults becomes necessary. Such understanding would help to make better dietary recommendations toward the prevention of age-related disorders. In addition, schoolchildren studies indicate that the diet can significantly affect school performances. Hence, it should be of interest to determine whether such a role is specific to learning processes in young populations or can also influence cognitive performances in adults. It is of interest to note the results obtained on mood improvement as well. Indeed, mood disorders represent an increasing concern in modern societies and working environment (Kessler, 2006; Woo and Postolache, 2008; Hannerz et al., 2009; Firth et al., 2020). Thus, dietary improvements could be an important step to prevent the onset of depression and anxiety symptoms and contribute to better life conditions in a large part of the population.

HEALTHY DIETS AND BRAIN DISORDERS

A certain number of brain disorders have been targeted by specific dietary interventions since decades and even centuries. For instance, the ketogenic diet (KD) is given to epileptic patients since more than 100 years (Williams and Cervenka, 2017). Furthermore, treatment for several other brain conditions now include dietary interventions (Carneiro and Leloup, 2020). Noteworthily, the knowledge of mechanisms disrupted in the disorders studied have led to several hypotheses on the diet induced mechanisms at play in the beneficial effects observed. In this section, we will describe recent research on brain disorders and the impact of food on the symptoms, progress, and outcome of the diseases. The putative mechanisms will be presented as well as the diet composition with the most significant impact.

Epilepsy is a neurological condition characterized by recurrent spontaneous seizures. These seizure episodes result from hypersynchronous discharges of neurons (Thijs et al., 2019). Notably, epileptic persons have been treated with ketogenic diets for more than 100 years with significant decreases in seizure events (Williams and Cervenka, 2017). This beneficial effect is of particular interest in drug resistant patients. Indeed, ketogenic diet intervention is associated with up to a 60% decrease of seizures in drug resistant individuals (Levy et al., 2012; Sharma and Jain, 2014a; Martin et al., 2016). Ketogenic diets have been initially used as a replacement for a fast (Wheless, 2004). Indeed, the classical ketogenic diet is a very high fat content diet (70% and above of energy from fats) and low protein and carbohydrate (10% or less). Therefore, the limited availability of sugars as energy source forces the body to use fat as the primary source of energy as it would happen during a fasting period. In the liver, this metabolic shift leads to the formation of ketone bodies from β-oxidation. However, this diet also produces long term side effects including ketoacidosis, liver lipid accumulation in long term diet, weight loss, diminished growth, kidney stones, increased blood cholesterol and fatty acid levels, while it also bears disadvantages such as a poor taste and thus aversive effects, among others. To counter those effects, several modified ketogenic diets have now been developed. Although these diets still induce ketogenesis, most of the negative effects can be dampened (Sharma and Jain, 2014b). For instance, a modified Atkins diet (the other name for the ketogenic diet), a low glycemic index diet, and medium chain triglycerides diets have also been tested with good results on epileptic patients. Although less restrictive on carbohydrates, all these modified ketogenic diets still lead to increased circulating ketone bodies levels (Verrotti et al., 2020). Mostly, these modified ketogenic diets include higher amounts of carbohydrates although still at very low levels compared to a normal diet (up to 20% instead of 55%). In addition, protein levels are less restricted and medium chain triglycerides are preferred. Overall, the amount of sugars as well as their type (complex sugars are not absorbed, but metabolized by the microbiota, therefore making glucose availability limited for host cells) appear to be key in the effect of the ketogenic diet to obtain a positive outcome on epileptic populations. These ketogenic diets have provided significant results on epileptic individuals in multiple clinical studies. Notably, the results presented show beneficial effects of the diets in a wide range of populations. Indeed, this is the case for epileptic children, adults, but also patients with GLUT1 deficiency syndrome or pyruvate dehydrogenase deficiency (both diseases are associated with seizures) (D'Andrea Meira et al., 2019). Finally, it is worth to note that if ketogenic diets are used on drug resistant patients, in regard of the significantly positive effects measured, it would be of interest to expand the ketogenic diet use to all categories of epileptic patients. However, one limitation to this global use is the poor understanding of the mechanisms involved. In addition, the ketogenic diet presents numerous negative effects that need to be considered (migraines, keto-acidosis, liver steatosis, fatigue, but also poor taste).

Interestingly, many other brain disorders have been shown to improve in patients following a similar low carbohydrate availability induced by diet strategies. Such observations support the idea of a brain metabolic shift that would compensate for decreased glucose supply.

First, high fat diet has been previously described as increasing the risk of brain stroke (Haley et al., 2019). In accordance, adjustments of the diet composition would prevent the occurrence of stroke. Thus, some studies have attempted to determine the impact of a healthy diet on stroke prevention but also during recovery. Results of such investigations clearly support a beneficial effect of adjusted diet on stroke events. Interestingly, as observed for epilepsy, low carbohydrate, ketogenic, or low glycemic index diets led to the most significant benefits (Ayuso et al., 2017). Here though, a high fructose diet is also described as a potent enhancer of stroke risk. This observation suggests that blood glucose level alone is highly important in stroke prevention. Therefore, diets with a lowering effect on glycemia or lipidemia would be beneficial for stroke prevention. In addition, the importance of a low level of blood glucose is also supported by the impact of low carbohydrate, or low glycemic index diets since they are expected to only slightly alter blood glucose levels. Accordingly, the Mediterranean diet is shown to promote stroke prevention, as well as reduce severity (Psaltopoulou et al., 2013; Lakkur and Judd, 2015; Tuttolomondo et al., 2015). Further, the vegetarian diet, a low glycemic index diet, is also associated with a decreased risk of stroke (Chiu et al., 2020). Finally, the ketogenic diet that limits the use of sugars as energy source, is described as participating to the improvement of the outcome following a stroke (Shaafi et al., 2014, 2019).

Overall, since high blood glucose is linked to an earlier stroke onset and worst outcome, a diet intervention targeting glycemia would be of interest in stroke management. Further, dietary habits that limit blood glucose increase would also help prevent stroke accidents. Hence, more research on the role of diets in stroke outcome and prevention is required. Indeed, currently, only descriptive studies have been performed. Notably, no mechanistic studies have really permitted to identify the cellular pathways involved in the positive role of healthy diets. Furthermore, in addition to diet intervention, the description of the mechanisms could help identify better pharmacological targets to improve stroke recovery.

When considering age-related disorders in general, Alzheimer's disease (AD) is the most common cause of dementia (García-Casares et al., 2021). More recently, AD has been linked to metabolic disorders. Notably, individuals with type 2 diabetes or obesity present a higher risk of AD (Sims-Robinson et al., 2010). In addition, AD patients are characterized by a glucose uptake defect in brain cells. Interestingly, a lower risk of AD development is associated with the Mediterranean diet (Scarmeas et al., 2007). In another study, Gu et al. (2010) assessed the association of different nutrients with the prevention of AD. The authors described the putative role of ω3 and 6 polyunsaturated fatty acids (PUFA), Vitamin E and folates in the protective role of the Mediterranean diet (Gu et al., 2010). Interestingly, here, the lipid profile seems to play a key role. However, it is worth to note that the low glycemic index of such a diet could still be involved in the protective effect. Nevertheless, these results strongly support a role of brain energetics. Indeed, ω3 and 6 are well known for their role in brain activity (Yehuda, 2003). Thus, here PUFA could act as alternative energy sources for the brain in a diet limiting glucose availability. Similarly, Bayer-Carter et al. (2011), demonstrated a strong relationship between diet composition and both risk and progress of AD. As observed before, the low saturated fat diet is beneficial here as well. In addition, the authors also showed that the low fat associated to a low glycemic index diet displays the best results on cognition and AD markers measured (Bayer-Carter et al., 2011).

Similar observations can be found for Parkinson's disease (PD) (Maraki et al., 2019). Furthermore, diet-induced hyperketonemia was described as providing benefits to PD patients (VanItallie et al., 2005). Such results confirm a key role of low glucose for brain disorders improvement. Interestingly, the Mediterranean diet is also known to decrease the risk of PD (Jackson et al., 2019). It is interesting to note the beneficial effect of the Mediterranean diet on such a wide range of brain disorders. Overall, it suggests that common mechanisms are most likely involved in the development of cognitive deficits, and putatively in aging, affecting important metabolic processes for general brain function. In support of this hypothesis, mood disorders also can be addressed through a nutritional approach showing here as well a tight relationship with metabolic control (Pervanidou et al., 2013; Hajebrahimi et al., 2016). Thus, high glycemic index diets are correlated with an increased risk of depressive disorder as well as to an increased severity of the disease (Salari-Moghaddam et al., 2019). Autism Spectrum disorder (ASD) is another neurological disorder with both behavioral and metabolic dysregulations since obesity and type 2 diabetes during pregnancy represent risk factors for this disease (Lyall et al., 2011; Krakowiak et al., 2012). Furthermore, ASD risk is expected to increase with a high glycemic index diet while a low glycemic index should decrease this risk (Currais et al., 2016; Carneiro and Leloup, 2020). After birth, dietary intervention in ASD affected newborns have shown good results. For instance, in rodent models, a ketogenic diet improves social interactions and dampens repetitive behaviors (Ruskin et al., 2013). Noteworthily, low glycemic index diets also improved ASD behaviors. Such an effect involved a change in gut microbiota which is known to be associated with ASD (van de Sande et al., 2014; Berding and Donovan, 2020; Kandeel et al., 2020).

The benefits of a low glycemic index ketogenic diet on brain function are not limited to neurodegeneration, stroke or ASD that are associated with cell death and/or cell dysfunctions. Indeed, mood disorders can also be improved by dietary interventions (Arab et al., 2019). In this situation, carbohydrates levels appear as key in the effect of the diet (Firth et al., 2020). Therefore, a long-term low carbohydrate diet exhibits positive effects on mood and cognition (Brinkworth et al., 2009).

Overall, it is interesting to note that many brain disorder conditions can be targeted by imposing a particular diet to improve the symptoms, help recovery, or prevent the onset of the disease. In addition, it appears clear that the impact of a diet on glycemia will have strong effects on brain function. However, such a result is not surprising since the brain represents at least 20% of the total body glucose consumption at rest. Hence, it is interesting to note that decreasing the availability of glucose has a positive impact on brain function in pathological conditions. Knowledge of the mechanisms at play would provide a better understanding of the diet effect but also of the disease itself. Furthermore, it could also provide a better understanding of the relationship between brain function and metabolic regulations and disorders. Furthermore, it is interesting to note that gut-brain communication seems to be central to the interaction brain function-metabolism. Indeed, several studies report the involvement of gut products in brain function and disease.

Among the different types of diet, it is interesting to note that low glycemic index (GI) diets are described as the most beneficial on health (Carneiro and Leloup, 2020). Such diets are enriched in foods with low GI, meaning that the effect on blood glucose is limited. Noteworthily, Mediterranean diet, ketogenic diet and modified ketogenic diets are all considered as low GI. Furthermore, among the diets described in the literature, these diets are the most frequently used. In fact, those diets present similar metabolic effects including gut microbiota changes favoring short Chain Fatty Acids (SCFA) production, and liver ketogenesis. Altogether, the mechanisms involved are linked to the action of these molecules in the body that will affect brain function.

PUTATIVE MECHANISMS AT PLAY TO EXPLAIN THE BENEFICIAL ROLES OF CERTAIN DIETS ON BRAIN FUNCTION

Studies made in the context of epilepsy have led to several hypotheses about the mechanisms involved in the effect of the ketogenic diet to reduce seizures. Some suggested mechanisms directly involve the end product of lipid oxidation, whose synthesis is stimulated by the decrease in carbohydrate availability: ketone bodies (Guzmiirp and Geefen, 1993; Gano et al., 2014). In addition, mitochondria and gene regulation are also expected to be involved.

Inflammation

Inflammation is a common marker found in many brain disorders including epilepsy, stroke, AD and PD. ASD is also

considered at higher risk for the fetus in women suffering from inflammatory diseases during pregnancy (Theoharides et al., 2016; Raj et al., 2017; Siew et al., 2019). Interestingly, ketone bodies that are produced under most diets used in clinical studies have been demonstrated to present anti-inflammatory properties. This direct effect has been demonstrated in ischemia-induced seizures. Here, the activation by ketone bodies of the GPR109 receptor located on infiltrated macrophages in brain, stimulates the production of prostaglandins. In turn, this induces an anti-inflammatory response that protects against seizures (Rahman et al., 2014; Vezzani et al., 2016). Further, Youm et al. (2015) also observed a reduction in ischemic seizures in mice fed a ketogenic diet or receiving a brain infusion of ketone bodies. In addition, they also demonstrated that ketone bodies inhibit the assembly of NLRP3 inflammasomes by blocking the K^+ efflux (Youm et al., 2015).

Alzheimer's disease is also linked with inflammation (Hascup et al., 2019). Indeed, the accumulation of Aβ stimulates the recruitment of microglia and astrocytes. In parallel, interferon gamma (IFNγ), interleukin 1β (IL1β), and tumor necrosis factor α (TNF α) are secreted leading to a local inflammation (Sastre et al., 2006; Tan et al., 2013). Since microglial cells are from the same lineage than macrophages, therefore it is possible that a direct mechanism as described for stroke could also occur in AD. In fact, high caloric diets known to induce inflammation are also described to exacerbate AD. In addition, since healthy diets can decrease the Aβ accumulation, it is expected that inflammation will also be lower by dampening the recruitment of immune cells (Samadi et al., 2019). However, it is worth to note that in this case, the effect seems indirect. Thus, as suggested by Samadi et al. (2019), the effect of a normal diet compared to a healthy diet (such as Mediterranean diet) should be studied to clearly address the issue of the impact of a healthy diet independently of the high caloric negative effect already described. Autism is a neurological disorder whose risk for the offspring is increased by obesity or diabetes during pregnancy (Lyall et al., 2011; Krakowiak et al., 2012). In fact, the chronic inflammation induced by these metabolic disorders plays an important role in the increased risk of autism (Vargas et al., 2005; Patterson, 2009; Michel et al., 2012). Interestingly, this inflammatory grade can be decreased by a low glycemic index diet while a high glycemic index diet is shown to participate to the inflammatory processes (Fleming et al., 2011; Neuhouser et al., 2012; Uchiki et al., 2012). Again, in mouse models, a ketogenic diet was able to improve social behaviors (Ruskin et al., 2013). In addition, gluten-free food was shown to decrease the inflammatory grade and improved autism symptoms (Karhu et al., 2020; Sumathi et al., 2020).

However, it is difficult to clearly identify the mechanisms regulating inflammation. Indeed, the diets used in the studies differ widely, which makes it difficult to attribute the effects to ketone bodies only. Furthermore, some studies described direct effects while others indicated an indirect action of ketone bodies. Therefore, further investigations are essential to demonstrate the interactions between inflammation and diet since it is clear that the inflammatory grade plays an important role in neurological disorders (**Figure 1**).

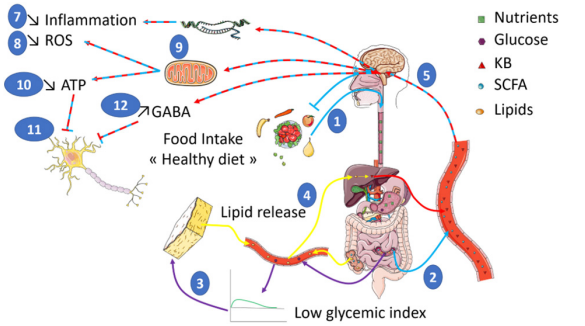

FIGURE 1 | Food intake of a diet rich in low glycemic index food is shown to have a positive impact on health (1). The composition of such a diet enriched in non-digestible fibers leads to the production of SCFA (Short Chain Fatty Acids) by gut bacteria (2). In addition, the low impact on glycemia (3) will trigger an increase in KB (Ketone Bodies) production through the induced lipid oxidation increase (4). In turn, both ketone bodies and SCFA are expected to act on brain function (5) by stimulating the transcription of genes (6) involved in the reduction of inflammation (7) and ROS production (8). SCFA and KB also modulate mitochondrial activity (9) to reduce ROS production. In addition, the reduced mitochondrial respiration will diminish ATP levels (10) that would inhibit neuronal activity (11). Finally, other studies indicate increased GABA levels also contribute to the inhibition of neuronal activity (12). Altogether, such a global effect on brain bioenergetics could participate to brain benefits of healthy diet in the context of brain disorders whose neuronal function is altered.

Redox Balance Regulation

Oxidative stress is often found in brain areas affected in the different aforementioned brain disorders (Frustaci et al., 2012; Pearson-Smith and Patel, 2017; Carneiro and Leloup, 2020). Interestingly, reactive oxygen species (ROS) production can vary depending on nutrient fluxes (Leloup et al., 2011). Therefore, not surprisingly, several studies suggested that the impact of a diet on neurological disorders involves changes in the Redox balance that could participate in the positive outcome.

Ketone bodies in particular can alter the Redox balance since they can directly enter mitochondria where a large amount of ROS can be produced within cells. In mitochondria, ketone bodies stimulate mitochondrial respiration and NADH oxidation. This in turn reduces ROS production while increasing ATP synthesis (Izzo et al., 2016). These events will prevent the mitochondrial permeability transition (mPT) and thus prevent cell death (Kim et al., 2015). Since ketone bodies affect mPT, this mechanism could participate to the anti-epileptic effect of the ketogenic diet. Indeed, mouse models of epilepsy present an increase in the threshold of mPT. In addition, mPT prevention involves modulation of cyclophilin D. Finally, in these mice it is observed a decrease of long-term potentiation and of learning and memory capacities, supporting a role in cognition (Zhou et al., 2018).

Another possible regulatory mechanism of ROS production can be due to the improved mitochondrial activity induced by ketone bodies (Cooper et al., 2018). Noteworthily, mitochondrial activity is associated with neuronal function and diseases. In addition, mitochondria are a main contributor of ROS production within cells. Therefore, the ability of ketogenic diets

to decrease mitochondrial ROS production when compared to a normal chow diet is of great interest. This antioxidant property appears to come from changes in the expression of genes coding for the oxidative pathway. In addition, the NAD/NADH ratio is increased by ketone bodies. This increased ratio will in turn reduce ROS production in mitochondria and participate to the improvement of epilepsy management (Pearson-Smith and Patel, 2017).

In fact, ketone bodies can directly increase O_2 consumption at the mitochondrial respiratory chain level. This O_2 consumption increase will reduce ROS production. Therefore, the decrease oxidative stress associated with a lower ROS level is likely to be at play in the improvement of epilepsy observed following a ketogenic diet. Indeed, oxidative stress is associated with epileptic seizures, and therefore a decrease in oxidative stress should also help decrease the frequency of seizures (Knowles et al., 2018). In addition of decreasing ROS production, it has been also shown that a ketogenic diet stimulates the expression level of catalase. Catalase is the main antioxidant enzyme and thus participate to convert ROS into non-reactive species. Catalase expression is stimulated by the transcription factor peroxisome proliferator activated receptor γ2 (PPARγ2) (Knowles et al., 2018). In fact, in this study the authors demonstrated a regulation of the PPAR gene through histone hyper-acetylation. More precisely, it is suggested that ketone bodies inhibited histone deacetylases. In turn, PPAR upregulates antioxidant genes and downregulates pro-inflammatory genes (NFKappaB, cyclooxygenase 2, and iNOS). This hypothesis is supported by the successful use of histone deacetylase inhibitors as anti-inflammatory and anti-epileptogenic molecules (Jeong et al., 2011; Shimazu et al., 2013; Damaskos et al., 2017; Simeone et al., 2017a,b).

Stroke studies have also demonstrated the increased risk as well as the negative impact on recovery caused by high glycemia and therefore diabetes (Sander and Kearney, 2009; Lee et al., 2018). Oxidative stress is also associated with diabetes (Leloup et al., 2011). Furthermore, hyperglycemia-induced oxidative stress is expected to participate to the poor outcome following stroke. Thus, a well-balanced blood glucose level is important in the treatment and prevention of stroke (Robbins and Swanson, 2014). In this regard, diets that help maintain a low level of blood glucose contribute to a better outcome in patients with acute ischemic stroke independently of diabetes (Song et al., 2018). In the same study however, the authors suggested that chronic hyperglycemia is the main cause of stroke as it was previously proposed (Kamouchi et al., 2011; Luitse et al., 2017). Although no direct evidence related to the Redox balance is provided, it is worth to note that chronic hyperglycemia is expected to induce a chronic increase in ROS production. On the other hand, a better control of glucose levels would prevent an excessive ROS increase. Therefore, ROS levels could likely participate in the observed effects.

Finally, a similar involvement of ROS level regulation can be found in AD (Prins, 2008; Achanta and Rae, 2017). Several reports suggest that ROS production could be inhibited by an increased expression level of uncoupling proteins (U) as previously shown independently of the diet (Sullivan et al., 2004; Klaus and Ost, 2020). Therefore, the expression level of UCPs needs to be determined in healthy diets fed individuals to evaluate whether it could be another player involved in the beneficial effect of such diets. Alternatively, the ketogenic diet could also participate in the reduction of ROS production by upregulating the expression of antioxidant proteins (MnSOD, Glutathione, and Nrf2) (Taylor et al., 2019). Lastly, the decrease in neuronal activity induced by a lower energy amount provided by the diet is also hypothesized to contribute to lower ROS production and thus potentially neuroprotection (Ma et al., 2007; **Figure 1**).

Blood Glucose Level

Aside end products of metabolism such as ketone bodies, the blood glucose level appears to play an important role in diseases' risk, progress, and outcome. In fact, a rapid rise in glycemia is associated with increased oxidative stress as well as endothelial dysfunction in diabetes (Ceriello et al., 2008). Even more than hyperglycemia, excessive blood glucose level variations are more deleterious. Such high variability is one of the consequences of high glycemic index foods that induce a rapid increase in glycemia but only transiently since it is quickly regulated to reestablish a normal glycemia. This rapid rise is shown as negative for stroke recovery due to endothelial dysfunction (Santos-García et al., 2009). Furthermore, high glycemic index diets are responsible for insulin resistance that will increase serum levels of fibrinogen and von Willebrand factor involved in endothelial function, which will contribute to increase the risk of stroke (Meigs et al., 2000; Raynaud et al., 2000; Schothorst et al., 2009). In fact, a high glycemic index diet induces hypercoagulability associated with increased thrombosis risk. In parallel, small vessel diseases are also increased and participate to a negative outcome after a stroke (Song et al., 2018). Interestingly, the low glycemic index Mediterranean diet is linked to a lower risk of stroke (Spence, 2019). It was also shown that chronic episodes of hyperglycemia are associated with a decrease in cognitive function recovery. In this context, diets limiting the amplitude of glycemic variations are more beneficial on both vascular and cognitive function recovery following stroke (Lim et al., 2018).

Neuronal Activity

Neurological disorders can be defined as brain diseases affecting neuronal activity. Such disorders are often associated with a decrease of glucose utilization. Since glucose is the main energy source for brain cells, it is thus not surprising that brain function will be altered. Therefore, diets providing ketone bodies could partly compensate this decreased glucose utilization. Indeed, it was previously observed that during glucose utilization limitation, ketone bodies can be used by the brain as an alternative energy source (Mergenthaler et al., 2013). More precisely, ketone bodies reaction with oxaloacetate produces acetyl-coA that will then stimulates the Krebs cycle. In turn, the Krebs cycle activity will increase the production of α-ketoglutarate. Then α-ketoglutarate reaction consumes aspartate, whose level is decreased in cells, and produces large amounts of glutamate. This glutamate is then decarboxylated by a glutamic acid decarboxylase which results in the synthesis of GABA (γ-aminobutyric acid), the inhibitory neurotransmitter found in the brain (Hartman et al., 2007). This metabolic loop might be very interesting in the context of stroke or epilepsy since GABA is a known anti-seizure substance targeted by some

drugs that enhance GABA action (Petroff et al., 1996; Homanics et al., 1997; Olsen and Avoli, 1997; Treiman, 2001; Chuang and Reddy, 2020; Sills and Rogawski, 2020). This mechanism of action is strongly supported by the finding of high levels of GABA in the cerebrospinal fluid of children treated with low carbohydrate diets (Dahlin et al., 2005).

In addition to this indirect mechanism, ketone bodies are also expected to directly enter mitochondria and the tricarboxylic acid cycle (TCA) where they will be oxidized and thus stimulate oxidative phosphorylation. This in turn inhibits phosphofructokinase 1 and glycolysis, decreasing ATP production. A decreased ATP level will lead then to the opening of ATP-sensitive potassium channels (K_{ATP}) and thus a decrease of neuronal activity (Ma et al., 2007). Such a hypothesis has been tested in a genetic model of drosophila presenting seizure-like activity when mechanically stimulated. This fly displays decreased seizures when given ketone bodies. Furthermore, the blockade of K_{ATP} channels or administration of a GABA antagonist partially reverses decreased seizure induced by ketone bodies (Li et al., 2017). However, this partial recovery suggests that other mechanisms are at play as well. Among possible mechanisms, blockade of the transfer of the vGLUT transporter (vesicular glutamate transporter) to the synapse by ketone bodies is suggested by some studies. Such a transfer inhibition would cause a decrease in glutamate excitatory activity, and thus neuronal activity inhibition (Juge et al., 2010; Omote et al., 2011). Another possible mechanism could involve the synaptic vesicle recycling. In fact, the authors showed that mice treated with ketone bodies present a reduction of both endocytosis and exocytosis combined with a misbalance between endocytosis and exocytosis. This effect is hypothesized by the authors to participate to the anticonvulsant activity of the ketogenic diet in epilepsy (Hrynevich et al., 2016; **Figure 1**).

Short Chain Fatty Acids

Lastly, it is interesting to note that if most research results suggest a role for ketone bodies in the beneficial effects provided by low carbohydrate diets, other factors have more recently been suggested to play a key role as well. Therefore, microbiota has been shown to interact with brain function through the metabolism of dietary fibers in certain bacteria that produce propionate or butyrate, two SCFA (short-chain fatty acids). In fact, these SCFA exert various actions in the brain by regulating histone deacetylases, transcription factors, and antioxidant regulations. Noteworthily, all of these processes have been described to play a role in neuronal function regulation and neurodegenerative disorders. The healthy diets providing the most benefits in the context of neurological disorders are adjusted for carbohydrate contents and often enriched in dietary fibers. Therefore, it is expected that such diets could involve SCFA positive regulations while processed foods and non-healthy diets would rather have a negative impact. Indeed, many diets in industrialized countries contain high amounts of processed food, and also lead to a decrease in the number of bacteria producing SCFA. These diets are also known for their negative impact on neurodegeneration (Martínez Leo and Segura Campos, 2020). In addition, highly processed foods are likely to have a high glycemic index and therefore induce large rises in blood glucose when ingested. On the other hand, dietary fibers are low glycemic index carbohydrates which support a protective role of low glycemic index foods against neurodegenerative diseases.

In addition to neurodegenerative disorders, the gut-brain axis related to nutrition has been shown to participate in the pathophysiology of Autism, suggesting a role for the gut in general brain function and diseases (van de Sande et al., 2014; Berding and Donovan, 2020; Kandeel et al., 2020). For instance, dietary fibers induced SCFA production in the

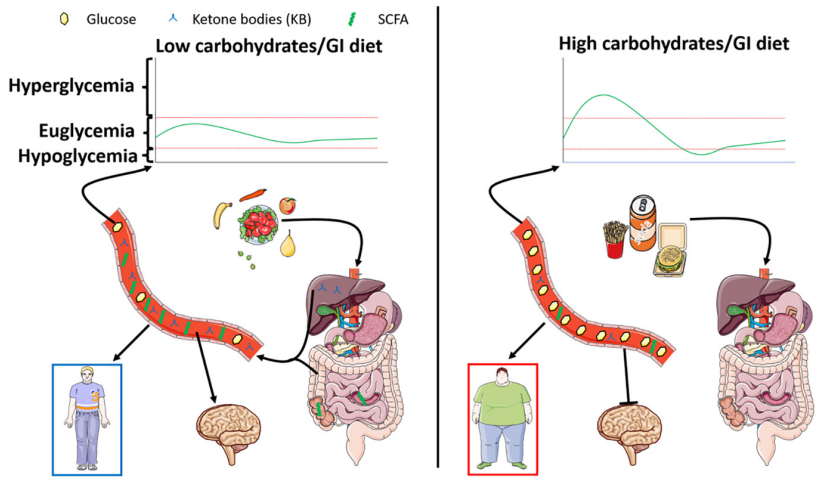

FIGURE 2 | Left panel represents the effect of a low carbohydrate/glycemic index diet known for its beneficial impact on energy homeostasis. The low levels of digestible sugars are responsible for increased SCFA produced within the gut, paralleled by stimulated lipid oxidation leading to the production of ketone bodies. Both nutrients exhibited a putative beneficial role on metabolism and brain function leading to the prevention of cognitive deficits. On the other hand, represented in the right panel, a high carbohydrate/glycemic index diet will favor obesity and associated metabolic disorders. Interestingly, such diets dampen the production of ketone bodies and SCFA and are associated with decreased cognitive function.

Mediterranean diet is believed to participate in the protection against Parkinson's disease. First, SCFA can improve insulin sensitivity and reduce inflammation while stimulating BDNF (brain-derived neurotrophic factor) production. All of these factors contribute to the protection against Parkinson's disease. The antioxidant properties of the Mediterranean diet are also expected to participate to this protection since antioxidant products can stimulate SCFA production (Jackson et al., 2019).

Nevertheless, despite several encouraging results linking gut microbiota, SCFA and brain, no clear pathway and/or mechanisms have been identified. However, it is worth to note that most of the hypotheses come back to inflammation, Redox balance or epigenetic gene regulations that have been strongly suggested as involved in the nutritional benefits to brain function and diseases. Thus, it appears worthwhile to pursue research efforts in this direction to putatively identify possible therapies or so-called "nutri-therapies."

Gut Microbiota

It is worth to note that diet change will affect gut microbiota composition. In recent years, many reports have highlighted the role of the microbiota on brain function and notably during brain disorders. Mediterranean diet for instance which is enriched in plant foods will likely modify the microbiome to favor fiber processing bacteria (*Akkermansia municiphilla, Ruminococcus bromii, Faecalibacterium prausnitzii, Eubacterium rectale, Eubacterium hallii, and R. bromii. . .)* (Morrison and Preston, 2016; Harris et al., 2021) and therefore produce SCFA. Similarly, low GI diet is a diet containing a high number of fibers. This specific composition will also favor fiber processing bacteria that will again release SCFA. Thus, the shift toward a SCFA producing microbiome would likely be beneficial in a context of neurological disorders as discussed above. Bile acids are also products affected by food composition. Briefly, high fat content increases bile acid production. These biliary acids can then be transformed by bacteria from the gut producing molecules that can interact with specific receptors found in brain to modulate satiety. Interestingly, studies have also suggested that bile acids can display antioxidant and anti-inflammatory properties. Thus, we cannot exclude a putative role of bile acids and gut microbiome in the dietary effect (Huang et al., 2022). Finally, microbiota can also produce tryptophan whose anti-inflammatory action has also been demonstrated. Overall, it is thus very likely that other factors produced by the new microbiome selected by the diet could impact brain health.

Hence, although largely studied now, the role of microbiota on brain disorders would need further attention especially in the context of diet intervention. Moreover, a specific review of the literature would be needed to extensively present the recent progress made on this topic (Yu et al., 2016; Barber et al., 2020; Beam et al., 2021; Huang et al., 2022).

CONCLUSION

Altogether, it is rather likely that nutritional approaches could be significantly beneficial in a wide range of brain disorders. However, although a quite large number of studies suggests effects involving inflammation, Redox balance and mitochondrial activity, gene regulations, and neuronal activity regulation, no direct demonstration has been made so far. Furthermore, it appears that ketone bodies and SCFA produced in response to specific diets, are at the origin of the beneficial effects. However, it is important to stay cautious since ketone bodies impact on health is still not completely understood. Particularly, discrepancies exist in the literature about their positive or negative impact on metabolism. Among the putative explanations for these contradictory results, the amount of ketone bodies could play a role. In fact, a dose-dependent effect is among the hypotheses to be tested. Therefore, with the current understanding of ketone bodies effect on physiological processes, it is not possible to target the biological pathways involving ketone bodies. Nevertheless, ketogenic diets or low glycemic index diets are widely used with little side effects. Thus, focusing on the clinical outcome following such diets for individuals suffering from neurological disorders could be an interesting future research axis. Furthermore, a better understanding of the negative effects on the risks for certain disorders is also of great importance. This knowledge would be needed in order to adapt nutritional facts especially regarding sugars to improve health of aging populations in our societies (**Figure 1**).

Finally, although promising, the use of diets against diseases is also to be consider with care. Indeed, diets described in this review can also be associated with negative side effects to be taken into account. Among those negative effects, sarcopenia, weight loss, ketoacidosis, fatigue are well known. Ketogenic diets are especially known for those effects that need to be carefully controlled. In this regard, modified ketogenic diets have been recently developed to include higher amounts of carbohydrates in order to limit some of the side effects. Metabolic overload or nutritional biases are also to be mentioned when looking at these specific diets. Indeed, the high amount of fats associated with decreased carbohydrates can be either regarded as unbalanced diets. In fact, these "healthy" diets are biased since they force the organism to switch to an unnatural metabolism. Lastly, it is worth to note the aversive effect of such diets due to a low amount of carbohydrate. Indeed, taste and hedonic aspects of food intake are both part of a normal healthy feeding behavior. Therefore, use of such diets come along with increased use of non-caloric sweeteners whose effects on health are still poorly documented. Altogether, research is needed not only to completely understand the mechanisms at play in healthy diet benefits, but also to clearly determine the balance between positive and negative effects of such dietary changes in populations either healthy as preventive action, or unhealthy to provide a reduction of symptoms (**Figure 2**).

AUTHOR CONTRIBUTIONS

Both authors wrote the manuscript, contributed to the article, and approved the submitted version.

REFERENCES

Abdelhamid, A. S., Martin, N., Bridges, C., Brainard, J. S., Wang, X., Brown, T. J., et al. (2018). Polyunsaturated fatty acids for the primary and secondary prevention of cardiovascular disease. *Cochrane Database Syst. Rev.* 2018:CD012345. doi: 10.1002/14651858.CD012345.pub2

Achanta, L. B., and Rae, C. D. (2017). β-hydroxybutyrate in the brain: one molecule, multiple mechanisms. *Neurochem. Res.* 42, 35–49. doi: 10.1007/s11064-016-2099-2

Amine, E. K., Baba, N. H., Belhadj, M., Deurenberg-Yap, M., Djazayery, A., Forrestre, T., et al. (2003). Diet, nutrition and the prevention of chronic diseases. *World Health Organ. Tech. Rep. Ser.* 916, i–viii,1–149. doi: 10.1093/ajcn/60.4.644a

Apekey, T. A., Morris, A. J. E., Fagbemi, S., and Griffiths, G. J. (2009). Effects of low-fat and low-GI diets on health. *Nutr. Food Sci.* 39, 663–672. doi: 10.1108/00346650911002995

Arab, A., Mehrabani, S., Moradi, S., and Amani, R. (2019). The association between diet and mood: a systematic review of current literature. *Psychiatry Res.* 271, 428–437. doi: 10.1016/j.psychres.2018.12.014

Aridi, Y. S., Walker, J. L., and Wright, O. R. L. (2017). The association between the mediterranean dietary pattern and cognitive health: a systematic review. *Nutrients* 9:674. doi: 10.3390/nu9070674

Ayuso, M. I., Gonzalo-Gobernado, R., and Montaner, J. (2017). Neuroprotective diets for stroke. *Neurochem. Int.* 107, 4–10. doi: 10.1016/j.neuint.2017.01.013

Barber, T. M., Kabisch, S., Pfeiffer, A. F. H., and Weickert, M. O. (2020). The health benefits of dietary fibre. *Nutrients* 12, 1–17. doi: 10.3390/nu12103209

Bayer-Carter, J. L., Green, P. S., Montine, T. J., Van-Fossen, B., Baker, L. D., Watson, G. S., et al. (2011). Diet intervention and cerebrospinal fluid biomarkers in amnestic mild cognitive impairment. *Arch. Neurol.* 68, 743–752. doi: 10.1001/archneurol.2011.125

Beam, A., Clinger, E., and Hao, L. (2021). Effect of diet and dietary components on the composition of the gut microbiota. *Nutrients* 13, 1–15. doi: 10.3390/nu13082795

Berding, K., and Donovan, S. M. (2020). Dietary patterns impact temporal dynamics of fecal microbiota composition in children with autism spectrum disorder. *Front. Nutr.* 6:193. doi: 10.3389/fnut.2019.00193

Billingsley, H. E., Carbone, S., and Lavie, C. J. (2018). Dietary fats and chronic noncommunicable diseases. *Nutrients* 10:1385. doi: 10.3390/nu10101385

Bogdanov, V. B., Bogdanova, O. V., Dexpert, S., Delgado, I., Beyer, H., Aubert, A., et al. (2020). Reward-related brain activity and behavior are associated with peripheral ghrelin levels in obesity. *Psychoneuroendocrinology* 112:104520. doi: 10.1016/j.psyneuen.2019.104520

Bremner, J. D., Moazzami, K., Wittbrodt, M. T., Nye, J. A., Lima, B. B., Gillespie, C. F., et al. (2020). Diet, stress and mental health. *Nutrients* 12:2428. doi: 10.3390/nu12082428

Brinkworth, G. D., Buckley, J. D., Noakes, M., Clifton, P. M., and Wilson, C. J. (2009). Long-term effects of a very low-carbohydrate diet and a low-fat diet on mood and cognitive function. *Arch. Internal Med.* 169, 1873–1880. doi: 10.1001/archinternmed.2009.329

Carneiro, L., and Leloup, C. (2020). Mens sana in corpore sano: does the glycemic index have a role to play? *Nutrients* 12:2989. doi: 10.3390/nu12102989

Castanon, N., Luheshi, G., and Layé, S. (2015). Role of neuroinflammation in the emotional and cognitive alterations displayed by animal models of obesity. *Front. Neurosci.* 9:229. doi: 10.3389/fnins.2015.00229

Ceriello, A., Esposito, K., Piconi, L., Ihnat, M. A., Thorpe, J. E., Testa, R., et al. (2008). Oscillating glucose is more deleterious to endothelial function and oxidative stress than mean glucose in normal and type 2 diabetic patients. *Diabetes* 57, 1349–1354. doi: 10.2337/db08-0063

Chamari, K., Briki, W., Farooq, A., Patrick, T., Belfekih, T., and Herrera, C. P. (2016). Impact of Ramadan intermittent fasting on cognitive function in trained cyclists: a pilot study. *Biol. Sport* 33, 49–56. doi: 10.5604/20831862.1185888

Charisis, S., Ntanasi, E., Yannakoulia, M., Anastasiou, C. A., Kosmidis, M. H., Dardiotis, E., et al. (2021). Mediterranean diet and risk for dementia and cognitive decline in a Mediterranean population. *J. Am. Geriatr. Soc.* 69, 1548–1559. doi: 10.1111/jgs.17072

Chiu, T. H. T., Chang, H. R., Wang, L. Y., Chang, C. C., Lin, M. N., and Lin, C. L. (2020). Vegetarian diet and incidence of total, ischemic, and hemorrhagic stroke in 2 cohorts in Taiwan. *Neurology* 94, 1112–1121. doi: 10.1212/WNL.0000000000009093

Chuang, S. H., and Reddy, D. S. (2020). Isobolographic analysis of antiseizure activity of the GABA Type A receptor-modulating synthetic neurosteroids brexanolone and ganaxolone with tiagabine and midazolam. *J. Pharmacol. Exp. Ther.* 372, 285–298. doi: 10.1124/jpet.119.261735

Cooper, M. A., McCoin, C., Pei, D., Thyfault, J. P., Koestler, D., and Wright, D. E. (2018). Reduced mitochondrial reactive oxygen species production in peripheral nerves of mice fed a ketogenic diet. *Exp. Physiol.* 103, 1206–1212. doi: 10.1113/EP087083

Cooper, S. B., Bandelow, S., and Nevill, M. E. (2011). Breakfast consumption and cognitive function in adolescent schoolchildren. *Physiol. Behav.* 103, 431–439. doi: 10.1016/j.physbeh.2011.03.018

Cooper, S. B., Bandelow, S., Nute, M. L., Morris, J. G., and Nevill, M. E. (2012). Breakfast glycaemic index and cognitive function in adolescent school children. *Br. J. Nutr.* 107, 1823–1832. doi: 10.1017/S0007114511005022

Cooper, S. B., Bandelow, S., Nute, M. L., Morris, J. G., and Nevill, M. E. (2015). Breakfast glycaemic index and exercise: combined effects on adolescents' cognition. *Physiol. Behav.* 139, 104–111. doi: 10.1016/j.physbeh.2014.11.024

Cordner, Z. A., and Tamashiro, K. L. K. (2015). Effects of high-fat diet exposure on learning & memory. *Physiol. Behav.* 152, 363–371. doi: 10.1016/j.physbeh.2015.06.008

Currais, A., Farrokhi, C., Dargusch, R., Goujon-Svrzic, M., and Maher, P. (2016). Dietary glycemic index modulates the behavioral and biochemical abnormalities associated with autism spectrum disorder. *Mol. Psychiatry* 21, 426–436. doi: 10.1038/mp.2015.64

D'Alessandro, A., de Pergola, G., and Silvestris, F. (2016). Mediterranean diet and cancer risk: an open issue. *Int. J. Food Sci. Nutr.* 67, 593–605. doi: 10.1080/09637486.2016.1191444

D'Andrea Meira, I., Romão, T. T., do Prado, H. J. P., Krüger, L. T., Pires, M. E. P., and da Conceição, P. O. (2019). Ketogenic diet and epilepsy: what we know so far. *Front. Neurosci.* 13:5. doi: 10.3389/fnins.2019.00005

Dahlin, M., Elfving, Å, Ungerstedt, U., and Åmark, P. (2005). The ketogenic diet influences the levels of excitatory and inhibitory amino acids in the CSF in children with refractory epilepsy. *Epilepsy Res.* 64, 115–125. doi: 10.1016/j.eplepsyres.2005.03.008

Damaskos, C., Valsami, S., Kontos, M., Spartalis, E., Kalampokas, T., Kalampokas, E., et al. (2017). Histone deacetylase inhibitors: an attractive therapeutic strategy against breast cancer. *Anticancer Res.* 37, 35–46. doi: 10.21873/anticanres.11286

Davis, J. A., Paul, J. R., McMeekin, L. J., Nason, S. R., Antipenko, J. P., Yates, S. D., et al. (2020). High-fat and high-sucrose diets impair time-of-day differences in spatial working memory of male mice. *Obesity* 28, 2347–2356. doi: 10.1002/oby.22983

Dohrmann, D. D., Putnik, P., Bursać Kovačević, D., Simal-Gandara, J., Lorenzo, J. M., and Barba, F. J. (2019). Japanese, mediterranean and argentinean diets and their potential roles in neurodegenerative diseases. *Food Res. Int.* 120, 464–477. doi: 10.1016/j.foodres.2018.10.090

Dolu, N., Yüksek, A., Sizer, A., and Alay, M. (2007). arousal and continuous attention during ramadan intermittent fasting. *J. Basic Clin. Physiol. Pharmacol.* 18, 315–322. doi: 10.1515/JBCPP.2007.18.4.315

Duan, Y., Zeng, L., Zheng, C., Song, B., Li, F., Kong, X., et al. (2018). Inflammatory links between high fat diets and diseases. *Front. Immunol.* 9:2649. doi: 10.3389/fimmu.2018.02649

Edefonti, V., Rosato, V., Parpinel, M., Nebbia, G., Fiorica, L., Fossali, E., et al. (2014). The effect of breakfast composition and energy contribution on cognitive and academic performance: a systematic review. *Am. J. Clin. Nutr.* 100, 626–656. doi: 10.3945/ajcn.114.083683

Finkel, T., Serrano, M., and Blasco, M. A. (2007). The common biology of cancer and ageing. *Nature* 448, 767–774. doi: 10.1038/nature05985

Firth, J., Firth, J., Gangwisch, J. E., Gangwisch, J. E., Borisini, A., Wootton, R. E., et al. (2020). Food and mood: how do diet and nutrition affect mental wellbeing? *BMJ* 369:m2382. doi: 10.1136/bmj.m2382

Fleming, T. H., Humpert, P. M., Nawroth, P. P., and Bierhaus, A. (2011). Reactive metabolites and AGE/RAGE-mediated cellular dysfunction affect the aging process – A mini-review. *Gerontology* 57, 435–443. doi: 10.1159/000322087

Frustaci, A., Neri, M., Cesario, A., Adams, J. B., Domenici, E., Dalla Bernardina, B., et al. (2012). Oxidative stress-related biomarkers in autism: systematic

review and meta-analyses. *Free Rad. Biol. Med.* 52, 2128–2141. doi: 10.1016/j.freeradbiomed.2012.03.011

Gano, L. B., Patel, M., and Rho, J. M. (2014). Ketogenic diets, mitochondria, and neurological diseases. *J. Lipid Res.* 55, 2211–2228. doi: 10.1194/jlr.R048975

García-Casares, N., Gallego Fuentes, P., Barbancho, M. Á, López-Gigosos, R., García-Rodríguez, A., and Gutiérrez-Bedmar, M. (2021). Alzheimer's disease, mild cognitive impairment and mediterranean diet. A systematic review and dose-response meta-analysis. *J. Clin. Med.* 10:4642. doi: 10.3390/jcm10204642

Gómez-Pinilla, F. (2008). Brain foods: the effects of nutrients on brain function. *Nat. Rev. Neurosci.* 9, 568–578. doi: 10.1038/nrn2421

Gomez-Pinilla, F., Cipolat, R. P., and Royes, L. F. F. (2021). Dietary fructose as a model to explore the influence of peripheral metabolism on brain function and plasticity. *Biochim. Biophys. Acta Mol. Basis Dis.* 1867:166036. doi: 10.1016/j.bbadis.2020.166036

Gu, Y., Nieves, J. W., Stern, Y., Luchsinger, J. A., and Scarmeas, N. (2010). Food combination and alzheimer disease risk: a protective diet. *Arch. Neurol.* 67, 699–706. doi: 10.1001/archneurol.2010.84

Guzmiirp, M., and Geefen, M. J. (1993). Regulation of fatty acid oxidation in mammalian liver. *Biochim. Biophys. Acta* 1167, 227–241.

Hajebrahimi, B., Kiamanesh, A., Asgharnejad Farid, A. A., and Asadikaram, G. (2016). Type 2 diabetes and mental disorders; A plausible link with inflammation. *Cell. Mol. Biol.* 62, 71–77. doi: 10.14715/cmb/2016.62.13.13

Haley, M. J., Krishnan, S., Burrows, D., de Hoog, L., Thakrar, J., Schiessl, I., et al. (2019). Acute high-fat feeding leads to disruptions in glucose homeostasis and worsens stroke outcome. *J. Cereb. Blood Flow Metab.* 39, 1026–1037. doi: 10.1177/0271678X17744718

Hannerz, H., Tüchsen, F., Pedersen, B. H., Dyreborg, J., Rugulies, R., and Albertsen, K. (2009). Work-relatedness of mood disorders in Denmark. *Scand. J. Work Environ. Health* 35, 294–300. doi: 10.5271/sjweh.1329

Harris, H. C., Morrison, D. J., and Edwards, C. A. (2021). Impact of the source of fermentable carbohydrate on SCFA production by human gut microbiota in vitro - a systematic scoping review and secondary analysis. *Crit. Rev. Food Sci. Nutr.* 61, 3892–3903. doi: 10.1080/10408398.2020.1809991

Hartman, A. L., Gasior, M., Vining, E. P. G., and Rogawski, M. A. (2007). The neuropharmacology of the ketogenic diet. *Pediatr. Neurol.* 36, 281–292. doi: 10.1016/j.pediatrneurol.2007.02.008

Hascup, E. R., Broderick, S. O., Russell, M. K., Fang, Y., Bartke, A., Boger, H. A., et al. (2019). Diet-induced insulin resistance elevates hippocampal glutamate as well as VGLUT1 and GFAP expression in AβPP/PS1 Mice HHS Public Access. *J. Neurochem.* 148, 219–237. doi: 10.13140/RG.2.2.11180.10888

Homanics, G. E., Delorey, T. M., Firestone, L. L., Quinlan, J. J., Handforth, A., Harrison, N. L., et al. (1997). Mice devoid of-aminobutyrate type A receptor 3 subunit have epilepsy, cleft palate, and hypersensitive behavior (gene targetingbenzodiazepineAngelman syndromeanesthesia). *Neurobiology* 94, 4143–4148.

Hrynevich, S. V., Waseem, T. V., Hébert, A., Pellerin, L., and Fedorovich, S. V. (2016). β-Hydroxybutyrate supports synaptic vesicle cycling but reduces endocytosis and exocytosis in rat brain synaptosomes. *Neurochem. Int.* 93, 73–81. doi: 10.1016/j.neuint.2015.12.014

Huang, F., Pariante, C. M., and Borsini, A. (2022). From dried bear bile to molecular investigation: a systematic review of the effect of bile acids on cell apoptosis, oxidative stress and inflammation in the brain, across pre-clinical models of neurological, neurodegenerative and neuropsychiatric disorders. *Brain Behav. Immun.* 99, 132–146. doi: 10.1016/j.bbi.2021.09.021

Izzo, V., Bravo-San Pedro, J. M., Sica, V., Kroemer, G., and Galluzzi, L. (2016). Mitochondrial permeability transition: new findings and persisting uncertainties. *Trends Cell Biol.* 26, 655–667. doi: 10.1016/j.tcb.2016.04.006

Jackson, A., Forsyth, C. B., Shaikh, M., Voigt, R. M., Engen, P. A., Ramirez, V., et al. (2019). Diet in Parkinson's disease: critical role for the microbiome. *Front. Neurol.* 10:1245. doi: 10.3389/fneur.2019.01245

Jeong, E. A., Jeon, B. T., Shin, H. J., Kim, N., Lee, D. H., Kim, H. J., et al. (2011). Ketogenic diet-induced peroxisome proliferator-activated receptor-γ activation decreases neuroinflammation in the mouse hippocampus after kainic acid-induced seizures. *Exp. Neurol.* 232, 195–202. doi: 10.1016/j.expneurol.2011.09.001

Juge, N., Gray, J. A., Omote, H., Miyaji, T., Inoue, T., Hara, C., et al. (2010). Metabolic control of vesicular glutamate transport and release. *Neuron* 68, 99–112. doi: 10.1016/j.neuron.2010.09.002

Kamouchi, M., Matsuki, T., Hata, J., Kuwashiro, T., Ago, T., Sambongi, Y., et al. (2011). Prestroke glycemic control is associated with the functional outcome in acute ischemic stroke: the fukuoka stroke registry. *Stroke* 42, 2788–2794. doi: 10.1161/STROKEAHA.111.617415

Kandeel, W. A., Meguid, N. A., Bjørklund, G., Eid, E. M., Farid, M., Mohamed, S. K., et al. (2020). Impact of clostridium bacteria in children with autism spectrum disorder and their anthropometric measurements. *J. Mol. Neurosci.* 70, 897–907. doi: 10.1007/s12031-020-01482-2

Kanoski, S. E., and Davidson, T. L. (2011). Western diet consumption and cognitive impairment: links to hippocampal dysfunction and obesity. *Physiol. Behav.* 103, 59–68. doi: 10.1016/j.physbeh.2010.12.003

Karhu, E., Zukerman, R., Eshraghi, R. S., Mittal, J., Deth, R. C., Castejon, A. M., et al. (2020). Nutritional interventions for autism spectrum disorder. *Nutr. Rev.* 78, 515–531. doi: 10.1093/nutrit/nuz092

Kessler, R. (2006). Prevalence and effects of mood disorders on work performance in a nationally representative sample of U.S. Workers. *Am. J. Psychiatry* 163, 1561–1568. doi: 10.1176/appi.ajp.163.9.1561

Kim, D. Y., Simeone, K. A., Simeone, T. A., Pandya, J. D., Wilke, J. C., Ahn, Y., et al. (2015). Ketone bodies mediate antiseizure effects through mitochondrial permeability transition. *Ann. Neurol.* 78, 77–87. doi: 10.1002/ana.24424

Klaus, S., and Ost, M. (2020). Mitochondrial uncoupling and longevity – A role for mitokines? *Exp. Gerontol.* 130:110796. doi: 10.1016/j.exger.2019.110796

Klement, R. J., and Pazienza, V. (2019). Impact of different types of diet on gut microbiota profiles and cancer prevention and treatment. *Medicina (Lithuania)* 55:84. doi: 10.3390/medicina5504008

Knowles, S., Budney, S., Deodhar, M., Matthews, S. A., Simeone, K. A., and Simeone, T. A. (2018). Ketogenic diet regulates the antioxidant catalase via the transcription factor PPARγ2. *Epilepsy Res.* 147, 71–74. doi: 10.1016/j.eplepsyres.2018.09.009

Krakowiak, P., Walker, C. K., Bremer, A. A., Baker, A. S., Ozonoff, S., Hansen, R. L., et al. (2012). Maternal metabolic conditions and risk for autism and other neurodevelopmental disorders. *Pediatrics* 129, 1121–1128. doi: 10.1542/peds.2011-2583

Lakkur, S., and Judd, S. E. (2015). Diet and stroke: recent evidence supporting a mediterranean-style diet and food in the primary prevention of stroke. *Stroke* 46, 2007–2011. doi: 10.1161/STROKEAHA.114.006306

Lee, K. J., Lee, J. S., and Jung, K. H. (2018). Interactive effect of acute and chronic glycemic indexes for severity in acute ischemic stroke patients. *BMC Neurol.* 18:105. doi: 10.1186/s12883-018-1109-1

Leloup, C., Casteilla, L., Carrière, A., Galinier, A., Benani, A., Carneiro, L., et al. (2011). Balancing mitochondrial redox signaling: a key point in metabolic regulation. *Antioxid. Redox Signal.* 14, 519–530. doi: 10.1089/ars.2010.3424

Levy, R. G., Cooper, P. N., Giri, P., and Weston, J. (2012). Ketogenic diet and other dietary treatments for epilepsy. *Cochrane Database Syst. Rev.* 2012, 1–54. doi: 10.1002/14651858.CD001903.pub2

Li, J., O'Leary, E. I., and Tanner, G. R. (2017). The ketogenic diet metabolite beta-hydroxybutyrate (β-HB) reduces incidence of seizure-like activity (SLA) in a K atp- and GABA b-dependent manner in a whole-animal Drosophila melanogaster model. *Epilepsy Res.* 133, 6–9. doi: 10.1016/j.eplepsyres.2017.04.003

Li, R. J., Liu, Y., Liu, H. Q., and Li, J. (2020). Ketogenic diets and protective mechanisms in epilepsy, metabolic disorders, cancer, neuronal loss, and muscle and nerve degeneration. *J. Food Biochem.* 44:e13140. doi: 10.1111/jfbc.13140

Lim, J. S., Kim, C., Oh, M. S., Lee, J. H., Jung, S., Jang, M. U., et al. (2018). Effects of glycemic variability and hyperglycemia in acute ischemic stroke on post-stroke cognitive impairments. *J. Diabetes Complications* 32, 682–687. doi: 10.1016/j.jdiacomp.2018.02.006

Luengo, A., Gui, D. Y., and vander Heiden, M. G. (2017). Targeting metabolism for cancer therapy. *Cell Chem. Biol.* 24, 1161–1180. doi: 10.1016/j.chembiol.2017.08.028

Luitse, M. J. A., Velthuis, B. K., Kappelle, L. J., van der Graaf, Y., and Biessels, G. J. (2017). Chronic hyperglycemia is related to poor functional outcome after acute ischemic stroke. *Int. J. Stroke* 12, 180–186. doi: 10.1177/1747493016676619

Lyall, K., Pauls, D. L., Santangelo, S., Spiegelman, D., and Ascherio, A. (2011). Maternal early life factors associated with hormone levels and the risk of having a child with an autism spectrum disorder in the nurses health study II. *J. Autism Dev. Disord.* 41, 618–627. doi: 10.1007/s10803-010-1079-7

Ma, W., Berg, J., and Yellen, G. (2007). Ketogenic diet metabolites reduce firing in central neurons by opening KATP channels. *J. Neurosci.* 27, 3618–3625. doi: 10.1523/JNEUROSCI.0132-07.2007

Maraki, M. I., Yannakoulia, M., Stamelou, M., Stefanis, L., Xiromerisiou, G., Kosmidis, M. H., et al. (2019). Mediterranean diet adherence is related to reduced probability of prodromal Parkinson's disease. *Mov. Disord.* 34, 48–57. doi: 10.1002/mds.27489

Martin, K., Jackson, C. F., Levy, R. G., and Cooper, P. N. (2016). Ketogenic diet and other dietary treatments for epilepsy. *Cochrane Database Syst. Rev.* 2016, 1–54. doi: 10.1002/14651858.CD001903.pub3

Martínez Leo, E. E., and Segura Campos, M. R. (2020). Effect of ultra-processed diet on gut microbiota and thus its role in neurodegenerative diseases. *Nutrition* 71:110609. doi: 10.1016/j.nut.2019.110609

Martinez-Gonzalez, M. A., and Martin-Calvo, N. (2016). Mediterranean diet and life expectancy; Beyond olive oil, fruits, and vegetables. *Curr. Opin. Clin. Nutr. Metab0 Care* 19, 401–407. doi: 10.1097/MCO.0000000000000316

Mattson, M. P. (2019). An evolutionary perspective on why food overconsumption impairs cognition. *Trends Cogn. Sci.* 23, 200–212. doi: 10.1016/j.tics.2019.01.003

Mattson, M. P., Longo, V. D., and Harvie, M. (2017). Impact of intermittent fasting on health and disease processes. *Ageing Res. Rev.* 39, 46–58. doi: 10.1016/j.arr.2016.10.005

Mattson, M. P., Moehl, K., Ghena, N., Schmaedick, M., and Cheng, A. (2018). Intermittent metabolic switching, neuroplasticity and brain health. *Nat. Rev. Neurosci.* 19, 81–94. doi: 10.1038/nrn.2017.156

McMillan, L., Owen, L., Kras, M., and Scholey, A. (2011). Behavioural effects of a 10-day Mediterranean diet. Results from a pilot study evaluating mood and cognitive performance. *Appetite* 56, 143–147. doi: 10.1016/j.appet.2010.11.149

Meigs, J. B., Mittleman, M. A., Nathan, D. M., Tofler, G. H., Singer, D. E., Murphy-Sheehy, P. M., et al. (2000). Hyperinsulinemia, hyperglycemia, and impaired hemostasis the framingham offspring study. *JAMA* 283, 221–228.

Meldrum, D. R., Morris, M. A., and Gambone, J. C. (2017). Obesity pandemic: causes, consequences, and solutions—but do we have the will? *Fertil. Steril.* 107, 833–839. doi: 10.1016/j.fertnstert.2017.02.104

Meo, S. A., and Hassan, A. (2015). Physiological changes during fasting in Ramadan. *J. Pakistan Med. Assoc.* 65, S6–S13.

Mergenthaler, P., Lindauer, U., Dienel, G. A., and Meisel, A. (2013). Sugar for the brain: the role of glucose in physiological and pathological brain function. *Trends Neurosci.* 36, 587–597. doi: 10.1016/j.tins.2013.07.001

Micha, R., Rogers, P. J., and Nelson, M. (2010). The glycaemic potency of breakfast and cognitive function in school children. *Eur. J. Clin. Nutr.* 64, 948–957. doi: 10.1038/ejcn.2010.96

Micha, R., Rogers, P. J., and Nelson, M. (2011). Glycaemic index and glycaemic load of breakfast predict cognitive function and mood in school children: a randomised controlled trial. *Br. J. Nutr.* 106, 1552–1561. doi: 10.1017/S0007114511002303

Michel, M., Schmidt, M. J., and Mirnics, K. (2012). Immune system gene dysregulation in autism and schizophrenia. *Dev. Neurobiol.* 72, 1277–1287. doi: 10.1002/dneu.22044

Mittelman, S. D. (2020). The role of diet in cancer prevention and chemotherapy efficacy. *Annu. Rev. Nutr.* 40, 273–297. doi: 10.1146/annurev-nutr-013120-041149

Morrison, D. J., and Preston, T. (2016). Formation of short chain fatty acids by the gut microbiota and their impact on human metabolism. *Gut Microbes* 7, 189–200. doi: 10.1080/19490976.2015.1134082

Moynihan, P., and Petersen, P. E. (2004). Diet, nutrition and the prevention of dental diseases. *Public Health Nutr.* 7, 201–226. doi: 10.1079/phn2003589

Murakami, K., Miyake, Y., Sasaki, S., Tanaka, K., Fukushima, W., Kiyohara, C., et al. (2010). Dietary glycemic index is inversely associated with the risk of Parkinson's disease: a case-control study in Japan. *Nutrition* 26, 515–521. doi: 10.1016/j.nut.2009.05.021

Naveed, S., Lakka, T., and Haapala, E. A. (2020). An overview on the associations between health behaviors and brain health in children and adolescents with special reference to diet quality. *Int. J. Environ. Res. Public Health* 17:953. doi: 10.3390/ijerph17030953

Neuhouser, M. L., Schwarz, Y., Wang, C., Breymeyer, K., Coronado, G., Wang, C. Y., et al. (2012). A low-glycemic load diet reduces serum C-reactive protein and modestly increases adiponectin in overweight and obese adults. *J. Nutr.* 142, 369–374. doi: 10.3945/jn.111.149807

Olsen, R. W., and Avoli, M. (1997). GABA an d Epileptogenesis. *Epilepsia* 38, 399–407.

Omote, H., Miyaji, T., Juge, N., and Moriyama, Y. (2011). Vesicular neurotransmitter transporter: bioenergetics and regulation of glutamate transport. *Biochemistry* 50, 5558–5565. doi: 10.1021/bi200567k

Paoli, A. (2014). Ketogenic diet for obesity: friend or foe? *Int. J. Environ. Res. Public Health* 11, 2092–2107. doi: 10.3390/ijerph110202092

Patterson, P. H. (2009). Immune involvement in schizophrenia and autism: etiology, pathology and animal models. *Behav. Brain Res.* 204, 313–321. doi: 10.1016/j.bbr.2008.12.016

Pearson-Smith, J. N., and Patel, M. (2017). Metabolic dysfunction and oxidative stress in epilepsy. *Int. J. Mol. Sci.* 18:2365. doi: 10.3390/ijms18112365

Pellerin, L., and Magistretti, P. J. (2012). Sweet sixteen for ANLS. *J. Cereb. Blood Flow Metab.* 32, 1152–1166. doi: 10.1038/jcbfm.2011.149

Pervanidou, P., Bastaki, D., Chouliaras, G., Papanikolaou, K., Laios, E., Kanaka-Gantenbein, C., et al. (2013). Circadian cortisol profiles, anxiety and depressive symptomatology, and body mass index in a clinical population of obese children. *Stress* 16, 34–43. doi: 10.3109/10253890.2012.689040

Peters, A. (2011). The selfish brain: competition for energy resources. *Am. J. Hum. Biol.* 23, 29–34. doi: 10.1002/ajhb.21106

Petroff, O. A. C., Rothman, D. L., Behar, K. L., and Mattson, R. H. (1996). Low brain GABA level is associated with poor seizure control. *Ann. Neurol.* 40, 908–911. doi: 10.1002/ana.410400613

Poli, A., Agostoni, C., Graffigna, G., Bosio, C., Donini, L. M., and Marangoni, F. (2019). The complex relationship between diet, quality of life and life expectancy: a narrative review of potential determinants based on data from Italy. *Eat. Weight Disord.* 24, 411–419. doi: 10.1007/s40519-018-0582-2

Prins, M. L. (2008). Cerebral metabolic adaptation and ketone metabolism after brain injury. *J. Cereb. Blood Flow Metab.* 28, 1–16. doi: 10.1038/sj.jcbfm.9600543

Psaltopoulou, T., Sergentanis, T. N., Panagiotakos, D. B., Sergentanis, I. N., Kosti, R., and Scarmeas, N. (2013). Mediterranean diet, stroke, cognitive impairment, and depression: a meta-analysis. *Ann. Neurol.* 74, 580–591. doi: 10.1002/ana.23944

Rahman, M., Muhammad, S., Khan, M. A., Chen, H., Ridder, D. A., Müller-Fielitz, H., et al. (2014). The b-hydroxybutyrate receptor HCA 2 activates a neuroprotective subset of macrophages. *Nat. Commun.* 5:3944. doi: 10.1038/ncomms4944

Raj, D., Yin, Z., Breur, M., Doorduin, J., Holtman, I. R., Olah, M., et al. (2017). Increased white matter inflammation in aging- and alzheimer's disease brain. *Front. Mol. Neurosci.* 10:206. doi: 10.3389/fnmol.2017.00206

Raynaud, E., Pérez-Martin, A., Brun, J.-F., Aïssa-Benhaddad, A., Fédou, C., and Mercier, J. (2000). Relationships between fibrinogen and insulin resistance. *Atherosclerosis* 150, 365–370.

Reddavide, R., Rotolo, O., Caruso, M. G., Stasi, E., Notarnicola, M., Miraglia, C., et al. (2018). The role of diet in the prevention and treatment of inflammatory bowel diseases. *Acta Biomed.* 89, 60–75. doi: 10.23750/abm.v89i9-S.7952

Robbins, N. M., and Swanson, R. A. (2014). Opposing effects of glucose on stroke and reperfusion injury: acidosis, oxidative stress, and energy metabolism. *Stroke* 45, 1881–1886. doi: 10.1161/STROKEAHA.114.004889

Rodopaios, N. E., Mougios, V., Konstantinidou, A., Iosifidis, S., Koulouri, A. A., Vasara, E., et al. (2019). Effect of periodic abstinence from dairy products for approximately half of the year on bone health in adults following the Christian Orthodox Church fasting rules for decades. *Arch. Osteopor.* 14:68. doi: 10.1007/s11657-019-0625-y

Ruskin, D. N., Svedova, J., Cote, J. L., Sandau, U., Rho, J. M., Kawamura, M., et al. (2013). Ketogenic diet improves core symptoms of autism in BTBR Mice. *PLoS One* 8:e65021. doi: 10.1371/journal.pone.0065021

Safouris, A., Tsivgoulis, G., Sergentanis, T., and Psaltopoulou, T. (2015). Mediterranean diet and risk of dementia. *Curr. Alzheimer Res.* 12, 736–744. doi: 10.2174/1567205012666150710114430

Salari-Moghaddam, A., Saneei, P., Larijani, B., and Esmaillzadeh, A. (2019). Glycemic index, glycemic load, and depression: a systematic review and meta-analysis. *Eur. J. Clin. Nutr.* 73, 356–365. doi: 10.1038/s41430-018-0258-z

Samadi, M., Moradi, S., Moradinazar, M., Mostafai, R., and Pasdar, Y. (2019). Dietary pattern in relation to the risk of Alzheimer's disease: a systematic review. *Neurol. Sci.* 40, 2031–2043. doi: 10.1007/s10072-019-03976-3

Sander, D., and Kearney, M. T. (2009). Reducing the risk of stroke in type 2 diabetes: pathophysiological and therapeutic perspectives. *J. Neurol.* 256, 1603–1619. doi: 10.1007/s00415-009-5143-1

Sanders, T. A. B. (2014). Protective effects of dietary PUFA against chronic disease: evidence from epidemiological studies and intervention trials. *Proc. Nutr. Soc.* 73, 73–79. doi: 10.1017/S0029665113003789

Santos-García, D., Blanco, M., Serena, J., Arias, S., Millán, M., Rodríguez-Yáñez, M., et al. (2009). Brachial arterial flow mediated dilation in acute ischemic stroke. *Eur. J. Neurol.* 16, 684–690. doi: 10.1111/j.1468-1331.2009.02564.x

Sastre, M., Klockgether, T., and Heneka, M. T. (2006). Contribution of inflammatory processes to Alzheimer's disease: molecular mechanisms. *Int. J. Dev. Neurosci.* 24, 167–176. doi: 10.1016/j.ijdevneu.2005.11.014

Scarmeas, N., Luchsinger, J. A., Mayeux, R., and Stern, Y. (2007). Mediterranean diet and Alzheimer disease mortality. *Neurology* 69, 1084–1093. doi: 10.1212/01.wnl.0000277320.50685.7c

Schothorst, E. M., Bunschoten, A., Schrauwen, P., Mensink, R. P., and Keijer, J. (2009). Effects of a high-fat, low- versus high-glycemic index diet: retardation of insulin resistance involves adipose tissue modulation. *FASEB J.* 23, 1092–1101. doi: 10.1096/fj.08-117119

Shaafi, S., Mahmoudi, J., Pashapour, A., Farhoudi, M., Sadigh-Eteghad, S., and Akbari, H. (2014). Ketogenic diet provides neuroprotective effects against ischemic stroke neuronal damages. *Adv. Pharm. Bull.* 4, 479–481. doi: 10.5681/apb.2014.071

Shaafi, S., Sharifi-Bonab, M., Ghaemian, N., Mokhtarkhani, M., and Akbari, H. (2019). Early motor-behavioral outcome of ischemic stroke with ketogenic diet preconditioning: interventional animal study. *J. Stroke Cerebrovasc. Dis.* 28, 1032–1039. doi: 10.1016/j.jstrokecerebrovasdis.2018.12.024

Sharma, S., and Jain, P. (2014a). The ketogenic diet and other dietary treatments for refractory epilepsy in children. *Ann. Indian Acad. Neurol.* 17, 253–259. doi: 10.4103/0972-2327.138471

Sharma, S., and Jain, P. (2014b). The modified atkins diet in refractory epilepsy. *Epilepsy Res. Treat.* 2014:404202. doi: 10.1155/2014/404202

Shimazu, T., Hirschey, M. D., Newman, J., He, W., Shirakawa, K., Le Moan, N., et al. (2013). Suppression of oxidative stress by β-hydroxybutyrate, an endogenous histone deacetylase inhibitor. *Science* 339, 211–214. doi: 10.1126/science.1227166

Siew, J. J., Chen, H. M., Chen, H. Y., Chen, H. L., Chen, C. M., Soong, B. W., et al. (2019). Galectin-3 is required for the microglia-mediated brain inflammation in a model of Huntington's disease. *Nat. Commun.* 10:3473. doi: 10.1038/s41467-019-11441-0

Sills, G. J., and Rogawski, M. A. (2020). Mechanisms of action of currently used antiseizure drugs. *Neuropharmacology* 168:107966. doi: 10.1016/j.neuropharm.2020.107966

Simeone, T. A., Matthews, S. A., Samson, K. K., and Simeone, K. A. (2017a). Regulation of brain PPARgamma2 contributes to ketogenic diet anti-seizure efficacy. *Exp. Neurol.* 287, 54–64. doi: 10.1016/j.expneurol.2016.08.006

Simeone, T. A., Simeone, K. A., and Rho, J. M. (2017b). Ketone bodies as anti-seizure agents. *Neurochem. Res.* 42, 2011–2018. doi: 10.1007/s11064-017-2253-5

Sims-Robinson, C., Kim, B., Rosko, A., and Feldman, E. L. (2010). How does diabetes accelerate Alzheimer disease pathology? *Nat. Rev. Neurol.* 6, 551–559. doi: 10.1038/nrneurol.2010.130

Song, T. J., Chang, Y., Kim, A. R., Kim, Y., and Kim, Y. J. (2018). High dietary glycemic load was associated with the presence and burden of cerebral small vessel diseases in acute ischemic stroke patients. *Nutr. Res.* 51, 93–101. doi: 10.1016/j.nutres.2017.12.009

Spanaki, C., Rodopaios, N. E., Koulouri, A., Pliakas, T., Papadopoulou, S. K., Vasara, E., et al. (2021). The christian orthodox church fasting diet is associated with lower levels of depression and anxiety and a better cognitive performance in middle life. *Nutrients* 13:627. doi: 10.3390/nu13020627

Spence, J. D. (2019). Nutrition and risk of stroke. *Nutrients* 11:647. doi: 10.3390/nu11030647

Sullivan, P. G., Rippy, N. A., Dorenbos, K., Concepcion, R. C., Agarwal, A. K., and Rho, J. M. (2004). The Ketogenic diet increases mitochondrial uncoupling protein levels and activity. *Ann. Neurol.* 55, 576–580. doi: 10.1002/ana.20062

Sumathi, T., Manivasagam, T., and Thenmozhi, A. J. (2020). "The role of gluten in autism," in *Personalized Food Intervention and Therapy for Autism Spectrum Disorder Management. Advances in Neurobiology*, Vol. 24, eds M. Essa and M. Qoronfleh (Cham: Springer), 469–479. doi: 10.1007/978-3-030-30402-7_14

Tan, M. S., Yu, J. T., Jiang, T., Zhu, X. C., and Tan, L. (2013). The NLRP3 inflammasome in Alzheimer's disease. *Mol. Neurobiol.* 48, 875–882. doi: 10.1007/s12035-013-8475-x

Tanaka, H., Gourley, D. D., Dekhtyar, M., and Haley, A. P. (2020). Cognition, brain structure, and brain function in individuals with obesity and related disorders. *Curr. Obesity Rep.* 9, 544–549. doi: 10.1007/s13679-020-00412-y

Taylor, M. K., Swerdlow, R. H., and Sullivan, D. K. (2019). Dietary neuroketotherapeutics for Alzheimer's disease: an evidence update and the potential role for diet quality. *Nutrients* 11, 1–24. doi: 10.3390/nu11081910

Thane, P. (2013). The ageing of modern societies: crisis or opportunity? *Historia* 396, 333–349.

Theoharides, T. C., Tsilioni, I., Patel, A. B., and Doyle, R. (2016). Atopic diseases and inflammation of the brain in the pathogenesis of autism spectrum disorders. *Transl. Psychiatry* 6:e844. doi: 10.1038/tp.2016.77

Thijs, R. D., Surges, R., O'Brien, T. J., and Sander, J. W. (2019). Epilepsy in adults. *Lancet* 393, 689–701. doi: 10.1016/S0140-6736(18)32596-0

Tian, H. H., Aziz, A. R., Png, W., Wahid, M. F., Yeo, D., and Png, A. L. C. (2011). Effects of fasting during Ramadan month on cognitive function in Muslim athletes. *Asian J. Sports Med.* 2, 145–153. doi: 10.5812/asjsm.34753

Tomata, Y., Zhang, S., Kaiho, Y., Tanji, F., Sugawara, Y., and Tsuji, I. (2019). Nutritional characteristics of the Japanese diet: a cross-sectional study of the correlation between Japanese Diet Index and nutrient intake among community-based elderly Japanese. *Nutrition* 57, 115–121. doi: 10.1016/j.nut.2018.06.011

Treiman, D. M. (2001). GABAergic mechanisms in epilepsy. *Epilepsia* 42, 8–12. doi: 10.1046/j.1528-1157.2001.042Suppl.3008.x

Tuttolomondo, A., Casuccio, A., Buttà, C., Pecoraro, R., di Raimondo, D., della Corte, V., et al. (2015). Mediterranean Diet in patients with acute ischemic stroke: relationships between Mediterranean Diet score, diagnostic subtype, and stroke severity index. *Atherosclerosis* 243, 260–267. doi: 10.1016/j.atherosclerosis.2015.09.017

Uchiki, T., Weikel, K. A., Jiao, W., Shang, F., Caceres, A., Pawlak, D., et al. (2012). Glycation-altered proteolysis as a pathobiologic mechanism that links dietary glycemic index, aging, and age-related disease (in nondiabetics). *Aging Cell* 11, 1–13. doi: 10.1111/j.1474-9726.2011.00752.x

Val-Laillet, D., Layec, S., Guérin, S., Meurice, P., and Malbert, C. H. (2011). Changes in brain activity after a diet-induced obesity. *Obesity* 19, 749–756. doi: 10.1038/oby.2010.292

van de Sande, M. M. H., van Buul, V. J., and Brouns, F. J. P. H. (2014). Autism and nutrition: the role of the gut-brain axis. *Nutr. Res. Rev.* 27, 199–214. doi: 10.1017/S0954422414000110

van Name, M. A., Savoye, M., Chick, J. M., Galuppo, B. T., Feldstein, A. E., Pierpont, B., et al. (2020). A low ω-6 to ω-3 PUFA ratio (n-6:n-3 PUFA) diet to treat fatty liver disease in obese youth. *J. Nutr.* 159, 2314–2321. doi: 10.1093/jn/nxaa183

VanItallie, T. B., Nonas, C., di Rocco, A., Boyar, K., Hyams, K., and Heymsfield, S. B. (2005). Treatment of Parkinson disease with diet-induced hyperketonemia: a feasibility study. *Neurology* 64, 728–730. doi: 10.1212/01.WNL.0000152046.11390.45

Vargas, D. L., Nascimbene, C., Krishnan, C., Zimmerman, A. W., and Pardo, C. A. (2005). Neuroglial activation and neuroinflammation in the brain of patients with autism. *Ann. Neurol.* 57, 67–81. doi: 10.1002/ana.20315

Vergati, M., Krasniqi, E., Monte, G. D., Riondino, S., Vallone, D., Guadagni, F., et al. (2017). Ketogenic diet and other dietary intervention strategies in the treatment of cancer. *Curr. Med. Chem.* 24, 1170–1185. doi: 10.2174/0929867324666170116122915

Verrotti, A., Iapadre, G., di Francesco, L., Zagaroli, L., and Farello, G. (2020). Diet in the treatment of epilepsy: what we know so far. *Nutrients* 12:2645. doi: 10.3390/nu12092645

Vezzani, A., Lang, B., and Aronica, E. (2016). Immunity and inflammation in epilepsy. *Cold Spring Harb. Perspect. Med.* 6, 1–22. doi: 10.1101/cshperspect.a022699

Vilić, D. (2017). Causes and consequences of increased aging trend in modern society. *Sociol. Discours.* 6, 5–34. doi: 10.7251/socen1712005v

Wheless, J. W. (2004). "History and Origin of the Ketogenic Diet," in *Epilepsy and the Ketogenic Diet*, eds C. E. Stafstrom and J. M. Rho (Totowa, NJ: Humana Press), 31–50. doi: 10.1007/978-1-59259-808-3_2

Williams, T. J., and Cervenka, M. C. (2017). The role for ketogenic diets in epilepsy and status epilepticus in adults. *Clin. Neurophysiol. Pract.* 2, 154–160. doi: 10.1016/j.cnp.2017.06.001

Włodarek, D. (2019). Role of ketogenic diets in neurodegenerative diseases (Alzheimer's disease and parkinson's disease). *Nutrients* 11:169. doi: 10.3390/nu11010169

Woo, J. M., and Postolache, T. T. (2008). The impact of work environment on mood disorders and suicide: evidence and implications. *International Journal on Disability and Human Development* 7, 185–200. doi: 10.1515/IJDHD.2008.7.2.185

World Health Organization [WHO] (2003). Diet, nutrition and the prevention of chronic diseases. Report of a Joint WHO/FAO expert consultation. *WHO Tech. Rep. Ser.* 916, 1–148.

World Health Organization [WHO] (2015). *World Report on Ageing and Health*. Geneva: WHO, 1–260.

Wyss-Coray, T. (2016). Ageing, neurodegeneration and brain rejuvenation. *Nature* 539, 180–186. doi: 10.1038/nature20411

Yates, K. F., Sweat, V., Yau, P. L., Turchiano, M. M., and Convit, A. (2012). Impact of metabolic syndrome on cognition and brain: a selected review of the literature. *Arterioscler. Thromb. Vasc. Biol.* 32, 2060–2067. doi: 10.1161/ATVBAHA.112.252759

Yehuda, S. (2003). Omega-6/omega-3 ratio and brain-related functions. *World Rev. Nutr. Diet.* 92, 37–56. doi: 10.1159/000073791

Youm, Y. H., Nguyen, K. Y., Grant, R. W., Goldberg, E. L., Bodogai, M., Kim, D., et al. (2015). The ketone metabolite β-hydroxybutyrate blocks NLRP3 inflammasome-mediated inflammatory disease. *Nat. Med.* 21, 263–269. doi: 10.1038/nm.3804

Yu, D., Zhang, X., Shu, X. O., Cai, H., Li, H., Ding, D., et al. (2016). Dietary glycemic index, glycemic load, and refined carbohydrates are associated with risk of stroke: a prospective cohort study in urban Chinese women. *Am. J. Clin. Nutrit.* 104, 1345–1351. doi: 10.3945/ajcn.115.129379

Zhou, Z., Austin, G., Young, L., Johnson, L., and Sun, R. (2018). Mitochondrial metabolism in major neurological diseases. *Cells* 7, 229–254. doi: 10.3390/cells7120229

Conflict of Interest: The authors declare that the research was conducted in the absence of any commercial or financial relationships that could be construed as a potential conflict of interest.

Publisher's Note: All claims expressed in this article are solely those of the authors and do not necessarily represent those of their affiliated organizations, or those of the publisher, the editors and the reviewers. Any product that may be evaluated in this article, or claim that may be made by its manufacturer, is not guaranteed or endorsed by the publisher.

Advantages of publishing in Frontiers

OPEN ACCESS
Articles are free to read for greatest visibility and readership

FAST PUBLICATION
Around 90 days from submission to decision

HIGH QUALITY PEER-REVIEW
Rigorous, collaborative, and constructive peer-review

TRANSPARENT PEER-REVIEW
Editors and reviewers acknowledged by name on published articles

Frontiers
Avenue du Tribunal-Fédéral 34
1005 Lausanne | Switzerland

Visit us: www.frontiersin.org
Contact us: frontiersin.org/about/contact

REPRODUCIBILITY OF RESEARCH
Support open data and methods to enhance research reproducibility

DIGITAL PUBLISHING
Articles designed for optimal readership across devices

FOLLOW US
@frontiersin

IMPACT METRICS
Advanced article metrics track visibility across digital media

EXTENSIVE PROMOTION
Marketing and promotion of impactful research

LOOP RESEARCH NETWORK
Our network increases your article's readership